The University Of Sheffield.

Durability and Long-term Structural Performance of GFRP Bars in Concrete

By:

Hamed A. Fergani

A thesis submitted in partial fulfilment of the requirements for the degree of Doctor of Philosophy

The University of Sheffield
Faculty of Engineering
Department of Civil and Structural Engineering

October 2017

ABSTRACT

Although glass fibre reinforced polymer (GFRP) bars do not corrode in the same way as conventional steel reinforcement, their physical and mechanical properties are prone to degradation following exposure to a variety of aggressive environments. Despite the relatively large amount of research on durability of FRP reinforcement in concrete environments, the available design models are still not able to account for all of the most typical in-service conditions, especially the effect of sustained stress on long-term properties. Thus, there is a need to develop a reliable prediction model to estimate the rate of degradation of GFRP bars and long-term performance in real structural applications.

A comprehensive test programme was carried out on 348 GFRP specimens subjected to different environments (concrete, alkali solution and tap water), different temperature levels (20, 40, 60°C) and two different levels of sustained stress. The mechanical performance of the GFRP specimens, as well as their physical and chemical characteristics, were evaluated through the implementation of a complementary set of techniques, including direct tension test, flexural tests, inter-laminar shear tests, moisture absorption, SEM-EDX, FTIR, and DMA. The material tests were complemented by accelerated tests on GFRP RC tension ties and small-scale beams to examine the effect of the studied environments on the long-term bond and flexural behaviour of GFRP RC members under service conditions. While no significant reduction was observed in the elastic modulus of the tested GFRP bars, tensile strength, flexural strength and transfer properties (ILSS) were found to be affected by the conditioning environment. The most significant cause of GFRP bar degradation in concrete was found to be driven by chemical reactions, which tend to be accelerated by a range of physical processes, with elevated temperatures playing a key role in triggering and accelerating the development of critical degradation mechanisms.

The test results on the long-term performance of GFRP bars in concrete showed that stressed specimens conditioned in a wet environment underwent a reduction in tension stiffening response as a result of bond degradation and a reduced stress transfer from the bar to the surrounding concrete. The results also indicated that the accelerated aging conditions affected overall flexural behaviour and led to overall higher deflections and larger crack widths.

A new framework, based on the implementation of the Arrhenius principle and a TSF concept, was developed to account for the effects of exposure temperature, moisture, sustained stress and service life on residual long-term properties of GFRP bars in concrete. A modified design equation was developed and proposed, along with a revised set of environmental reduction factors

RESEARCH CONTRIBUTION

The candidate has carried out experimental and analytical study on durability and long-term behaviour of concrete members reinforced with glass fibre reinforced polymer (GFRP) bars and has contributed to the activities of Task Group 5.1 (formerly 9.3) of the International Federation for Structural Concrete and COST Action TU1207. As a result of the work presented here, the following papers and reports were published or submitted for publication:

Journal Papers

1. H Fergani, M Di Benedetti, C Miàs Oller, C Lynsdale, M Guadagnini. *Durability and degradation mechanisms of GFRP reinforcement subjected to severe environments and sustained stress.* Published in Construction and Building Materials Journal.
2. H Fergani, M Di Benedetti, C Miàs, C Lynsdale, M Guadagnini. *Long-term performance of GFRP bars RC member under loading condition and severe environments.* Published in to Composite Structures Journal.
3. H Fergani, M Di Benedetti, C Miàs, C Lynsdale, M Guadagnini. *Durability and service life prediction of GFRP bars embedded in concrete under sustained stress.* To be submitted to Composites Part B: Engineering International Journal.

Conference Papers

1. H Fergani, M Guadagnini, C Lynsdale, C Miàs.,(2015) *'Durability of GFRP bars in concrete beams'*, FRPRCS-12, APFIS-2015, Nanjing, China.
2. Mias, C., Guadagnini, M., Torres, L., Barris, C., And Fergani, H.,(2015) *'Strength of GFRP RC beams after sustained loading'*, FRPRCS-12, APFIS-2015, Nanjing, China.
3. Di Benedetti, M, Cholostiakow, S, Fergani, H, Zappa. E, Cigada, A, and Guadagnini, M, (2015). *3D-DIC for strain measurement in small scale GFRP RC specimens*. Third Conference on Smart Monitoring, Assessment and Rehabilitation of Civil Structures, Antalya, Turkey
4. Fergani, H., Di Benedetti, M., Mias, C., Lynsdale, C. and Guadagnini, M.,(2016). *Long-term performance of GFRP bars under the combined effects of sustained load and severe*

environments. In Proceedings The 8th International Conference on Fibre-Reinforced Polymer (FRP) Composites in Civil Engineering, Hong Kong, China

5. Fergani, H., Di Benedetti, M., Mias, C., Lynsdale, C. and Guadagnini, M.,(2017). *Characterization and durability study of GFRP bars exposed to severe environments and under sustained loads*. In Proceedings The 5th International Conference on Durability of Fibre Reinforced Polymer (FRP) Composites for Construction and Rehabilitation of Structures, Sherbrooke, Canada
6. Fergani, H., Di Benedetti, M., Mias, C., Lynsdale, C. and Guadagnini, M.,(2017). *long-term behaviour of GFRP reinforced concrete beams under sustained loads and aggressive environment.* In Proceedings The 5th International Conference on Durability of Fibre Reinforced Polymer (FRP) Composites for Construction and Rehabilitation of Structures, Sherbrooke, Canada
7. Fergani, H., Di Benedetti, M., Mias, C., Lynsdale, C. and Guadagnini, M.,(2017). *Long-term flexural behaviour of GFRP RC members under sustained loads and aggressive environment* In Proceedings COST Action TU1207 Next Generation Design Guidelines for Composites in Construction, Budapest, Hungary
8. Fergani, H., Di Benedetti, M., Mias, C., Lynsdale, C. and Guadagnini, M.,(2017). *Experimental investigation of tension stiffening in GFRP RC tensile members exposed to severe environments under sustained load*. In Proceedings of Advanced Composites in Construction (ACIC) 2017 Conference, Sheffield, UK

ACKNOWLEDGEMENTS

First and foremost, I would like to express my deepest gratitude and appreciation to my supervisor Dr. Maurizio Guadagnini for his great commitment to my research and for his support, at both the professional and personal level. Thanks for your guidance and your time during these last four years.

I would also like to express my appreciation to my co-supervisor Dr Cyril Lynsdale for his support and encouraging attitude toward my research.

My sincere gratitude and respect are extended to Dr. Matteo Di Benedetti and Dr. Cristina Miàs for their genuine help and guidance while I have been conducting this PhD research.

I would also like to thank all the technical staff in our Laboratories for their technical support; particular thanks go to Don, Robin, Shane, Paul, Kieran, Chris and Glen.

Furthermore, I would like to warmly thank all friends in the concrete group who I have met during my years in Sheffield.

I would like to express my gratitude to my brothers and sisters and extended family for giving me constant support and encouragement throughout my study.

I am also very grateful to my daughters, Rawan, Mariam, Alla, Jana and Rana, for their support, understanding and patience throughout this thesis work.

Finally, the patience, support, encouragement and love of my wife cannot be praised enough; to her this thesis is dedicated.

TABLE OF CONTENTS

LIST OF FIGURES

LIST OF TABLES

CHAPTER 1

1 INTRODUCTION

The use of fibre reinforced polymer (FRP) bars as primary reinforcement in concrete structures to resolve corrosion related issues has received a great deal of attention in the civil engineering industry, and is becoming increasingly accepted [1]. The superior mechanical and physical properties of FRP composites, such as their high tensile strength, corrosion resistance and low weight, make FRP bars a viable alternative to conventional steel reinforcement in concrete structures such as marine structures and seawalls, as well as pavements, superstructures and bridge decks that are subjected to de-icing salts. [1-4]. In addition, some types of FRP bars (e.g. glass FRP), as a result of their nonconductive properties, are used as reinforcement for concrete structures supporting equipment that is sensitive to electromagnetic fields, such as railway magnetic levitation systems and magnetic resonance imaging units. Among the various types of FRP bars, glass fibre reinforced polymer (GFRP) bars are most widely used in the construction industry due to their low cost [4]. However, the lack of reliable data on their long-term in-service performance still presents a significant obstacle to their widespread use in concrete structure applications [5]. Moreover, the corrosion processes of GFRP bars in concrete are very different in nature from those of steel reinforcement. The physical and mechanical properties of GFRP bars can be degraded over time due to fatigue, creep, exposure to moisture, high temperature, alkalinity [6,7]. The deterioration of GFRP bars in concrete could result from resin matrix degradation, fibre-resin matrix interface debonding, or fibre degradation [8,9]. All potential sources of degradation should be taken into account when using GFRP bars as main reinforcement. Long-term durability and performance are probably the most significant reasons for using GFRP bars for the aforementioned applications. However, the lack of reporting of reliable durability data on field applications of GFRP bars has made the durability and long-term performance of GFRP bars in concrete structures a very complicated topic, and difficult to address. Thus, great concern has arisen in the construction industry regarding the safety of using GFRP bars as main reinforcement in reinforced concrete (RC) structures. Therefore, in recent years, the long-term performance and durability of GFRP bars in concrete has become a pressing issue and an area of research activity in several countries around the world. In order to ensure the long-term safety of GFRP bar RC structures, the different design codes and guidelines [10-13] for GFRP RC concrete structures

have specified environmental reduction factors associated with the tensile strength of GFRP bars and associated limitation levels for sustained stress. These environmental reduction factors are generally applied as a single factor that is very general in nature and does not take into account the variations of significant parameters that have been identified in the literature, such as moisture, temperature, alkali environment of the concrete and exposure time, which can affect GFRP bars' performance and durability in concrete. This in turn can lead to over conservative or unsafe design for the different application conditions, e.g. humid and dry regions, hot and cold countries [14]. To achieve an optimised design in terms of cost and structure integrity, there is a need to develop more accurate and refined environmental reduction factors for GFRP bars used as reinforcements for concrete structures.

1.1 AIMS AND OBJECTIVES

The main aim of this research is to examine and develop an in depth understanding of the degradation mechanisms of GFRP bars in a concrete environment exposed to high temperature, and under different levels of sustained stress. This work will be instrumental in enabling more reliable assessment of the long-term performance of GFRP bars and GFRP reinforced concrete members and estimation of service life of FRP RC structures exposed to a variety of different environments.

1.1.1 Research Objectives

In order to achieve the main aim of this research the following specific objectives are identified:

1- To review the existing literature on durability and long-term performance of GFRP bars in concrete environments.
2- To simulate the prolonged exposure of GFRP bars to different real life environments using accelerated controlled environments.
3- To determine the residual mechanical, chemical and physical properties (strength, stiffness, microstructure, chemical composition, and bond to concrete) of GFRP bars after exposure to the identified environments.
4- To examine the effect of sustained stress on the long-term behaviour of GFRP bars.
5- To evaluate the performance of GFRP reinforced concrete elements exposed to different environments and subjected to different levels of sustained stress.
6- To understand the degradation mechanisms of GFRP.

7- To identify a reliable correlation between accelerated aging (laboratory aging) and natural exposure (actual field exposures)
8- To develop model to predict the long-term performance of FRP bars in a concrete environment.
9- To assess the environmental reduction factors recommended in the existing design codes/guidelines and the predictive models recommended by fib TG 9.3.
10- To develop a new durability approach for GFRP bars reinforced concrete members and propose more accurate and refined environmental reduction factors compared to those factors recommended in the existing design codes/guidelines, for GFRP bars used as main reinforcement of concrete, which could result in optimised design of GFRP bar reinforced concrete structures in different environmental conditions.

1.2 STRUCTURE OF THE DISSERTATION

This thesis consists of seven chapters.

1.2.1 Chapter 1

Provides background; identifies the problem, purpose and research significance; in addition, the overall methodology and layout of the thesis are briefly summarised

1.2.2 Chapter 2

In this chapter, a detailed literature review is presented and the following key issues are discussed:

- mechanical and physical properties of FRP reinforcement for concrete
- parameters affecting durability of reinforced concrete structures
- the concrete environment and degradation mechanisms of GFRP in concrete
- long-term performance of concrete elements reinforced with GFRP bars: bond and flexural behaviour
- design for durability and environmental reduction factors presented in the existing design codes/guidelines
- existing service life prediction models for GFRP bars under environmental exposure

1.2.3 Chapter 3

This chapter describes: the methodology adopted to investigate the durability of GFRP in concrete; the multi-scale experimental programme carried on small GFRP sections, GFRP bars, GFRP RC prisms and beams.

1.2.4 Chapter 4

Durability and degradation mechanisms of GFRP reinforcement subjected to severe environments and sustained stress

The content of this Chapter was published in the Journal of Construction and Building Materials

This chapter deals with the experimental investigation of the mechanical, physical and chemical properties of GFRP and provides a better understanding of the long-term performance of GFRP bars by employing accelerated conditioning methodologies that more closely reflect the in-service conditions of GFRP RC members, including alkaline and moist environments as well as sustained stresses.

1.2.5 Chapter 5

Long-term performance of GFRP bars in concrete elements under sustained load and environmental actions

The content of this Chapter was published in Composite Structures.

This paper presents an experimental programme aimed at investigating the long-term tension stiffening and flexural behaviour of concrete elements reinforced with glass fibre reinforced polymer (GFRP) bars subjected to accelerated aging conditions. The effects of the long-term exposure to sustained stress and environmental actions on flexural behaviour are discussed. Analytical comparisons between the experimental results and *fib* Model Code 2010 and Eurocode 2 prediction models are presented and analysed.

1.2.6 Chapter 6

Durability and service life prediction of GFRP bars embedded in concrete under sustained stress

The content of this Chapter has been prepared for submission as a paper to Composites Part B: Engineering.

This chapter discusses the existing design approaches for using GFRP bars as main reinforcement for concrete structures and proposes a new approach to predict the long-term strength behaviour of GFRP bars reinforced concrete structures exposed to different environmental conditions. The model is based on proper understanding of degradation mechanisms of GFRP bars in concrete structures in service.
The newly developed approach is based on *fib* TG9.3-2007 associated with the implementation of time shift factors (TSF) to incorporate the effects of exposure to temperature, moisture, sustained stress and time. On the same basis, a new equation to predict the design strength retention of GFRP bars in reinforced concrete members for different applications is developed by incorporating the effects of the relative humidity, temperature, the design life and sustained stress. Finally, a new series of tensile strength reduction factors for different environmental exposures and applications are proposed.

1.2.7 Chapter 7

This chapter includes a summary of results, followed by recommendations for further studies.

1.3 REFERENCES

1. Nkurunziza, G., Debaiky, A., Cousin, P. and Benmokrane, B., (2005). Durability of GFRP bars: a critical review of the literature. *Progress in structural engineering and materials*, 7(4), pp.194-209.
2. Benmokrane, B. and Mohamed, H.M., (2013), J. Durability issues of FRP for civil infrastructure. In *11th international symposium on fiber reinforced polymers for reinforced concrete structures (FRPRCS11). Guimaraes*.
3. Micelli, F. and Nanni, A., (2004). Durability of FRP rods for concrete structures. *Construction and Building materials*, *18*(7), pp.491-503.
4. Nanni, A., Claure, G., y Basalo, F.J.D.C. and Gooranorimi, O., (2016). Concrete and Composites Pedestrian Bridge. Concrete International, 38(11), pp.57-63.

5. Davalos, J.F., Chen, Y. and Ray, I., (2012). Long-term durability prediction models for GFRP bars in concrete environment. *Journal of Composite Materials*, 46(16), pp.1899-1914.

6. Robert, M., Wang, P., Cousin, P. and Benmokrane, B., (2010). Temperature as an accelerating factor for long-term durability testing of FRPs: Should there be any limitations?. *Journal of Composites for Construction*, *14*(4), pp.361-367.

7. Dejke, V. and Tepfers, R., (2001), July. Durability and service life prediction of GFRP for concrete reinforcement. In *Proc., 5th Int. Conf. on Fiber-Reinforced Plastics for Reinforced Concrete Structures (FRPRCS-5)* (Vol. 1, pp. 505-516). London: Thomas Telford.

8. Fergani, H., Di Benedetti, M., Mias, C., Lynsdale, C. and Guadagnini, M.,(2017). Characterization and durability study of GFRP bars exposed to severe environments and under sustained loads. *In Proceedings The 5th International Conference on Durability of Fibre Reinforced Polymer (FRP) Composites for Construction and Rehabilitation of Structure*s, Sherbrooke, Canda

9. Chen, Y., Davalos, J.F., Ray, I. and Kim, H.Y., (2007). Accelerated aging tests for evaluations of durability performance of FRP reinforcing bars for concrete structures. *Composite Structures*, 78(1), pp.101-111.

10. Norway Standard NS 3473 (1998), Norwegian Council for Building Standardization, Norway.

11. ACI ,(2006), Guide for the Design and Construction of Concrete Reinforced with FRP Bars, American Concrete Institute, Committee 440. Farmington Hills, MI, USA.

12. CHBDC ,(2006), *Canadian Highway Bridge Design Code*, Canadian Standards Association International, Toronto, Ontario, Canada.

13. JSCE ,(1997), Recommendation for Design and Construction of Concrete Structures Using Continuous Fiber Reinforcing Materials, Research Committee on Continuous Fiber Reinforcing Materials, *Japan Society of Civil Engineers*, Tokyo, 325 p.

14. Huang, J. and Aboutaha, R., (2010). Environmental reduction factors for GFRP bars used as concrete reinforcement: New scientific approach. *Journal of Composites for Construction*, *14*(5), pp.479-486.

CHAPTER 2

2 LITERATURE REVIEW

2.1 COMPOSITES IN CIVIL ENGINEERING APPLICATIONS

Composite materials consist of two or more constituent materials. In this research the expression 'composite' applies to fibre reinforcement polymer, also known as FRP. Generally FRP consists of continuous fibres embedded in a polymer resin matrix, see Figure. 2.1. The essential role of the fibres is to provide strength and stiffness to the composites. The polymer matrix binds the fibres together, protects them from erosion and corrosion, and provides stress transfer between the longitudinal fibres [1]. The most common types of fibres used to manufacture FRP composites are Carbon, Glass, Aramid and most recently Basalt. GFRP composites are more widely used than others in civil engineering applications due to their lower production costs.

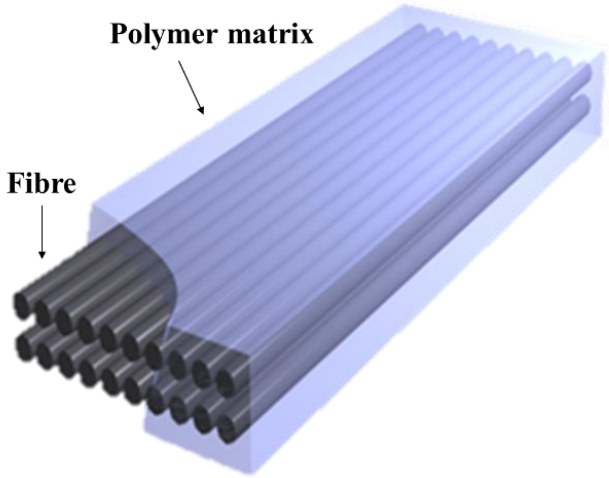

Figure 2. 1: Schematic diagram of a Fibre Reinforced Polymer composite

2.2 FIBRES

Four different types of fibre are most commonly used in FRP bars for concrete structures, namely Aramid, Basalt, Carbon and Glass [2]. These types of fibre under tensile loading show a linear elastic behaviour up to failure without exhibiting any yield [3]. Aramid and carbon fibre are anisotropic with different values of thermal and mechanical properties in the longitudinal direction, while basalt and glass fibre are isotropic [4]. Because of the low cost of GFRP bars, it has become more popular for concrete structure application than other types of fibre. Table 2.1 shows the mechanical and physical properties of different fibres for FRP composites.

Table 2. 1: Typical properties of fibres for FRP composites [5]

Characteristic of fibres	Basalt	E-glass	S-glass	Carbon	Aramid
Tensile Strength (MPa)	4840	3100~3800	4020~4650	3500~6000	2900~3400
Elongation at break (mm)	3.1	4.7	5.3	1.5~2.0	2.8~3.6
Elastic modulus (GPa)	79.3~93.1	72.5~75.5	83~86	230~600	70~140
Temperature of use (°C)	-260~+500	-50~+380	-50~+300	-50~+700	-50~+290
Thermal expansion Coefficient (10^{-6}/°C)	8	5	2.9	-1.2…-0.2	-2 longitudinal 59 radial
Poisson`s coefficient	_____	0.22	0.22	0.2	_____

2.2.1 Aramid Fibres

Aramid fibres, which are formed from aromatic polyamide and known commercially as poly paraphenylene terephthalamide (PPD-T), were first produced in the early 1960s [1]. Today, aramid fibres are manufactured by Akzo Nobal (Twaron), Dupont (Kevlar), Teijin (Technora), and SVM aramid fibres are made in Russia. Aramid fibres are produced from polymer materials and sensitive to moisture diffusion [6]. It is also important to mention that aramid fibres have very poor resistance to elevated temperature compared to glass and carbon and basalt fibres [7]. Several studies have shown that elevated temperature increases the rate of absorption of moisture, and at saturated state, the aramid/epoxy composites have shown high reduction in flexural capacity [8]. Furthermore, aramid fibres are considered to be materials with poor resistance to ultraviolet rays

[7]. However, Kevlar aramid fibre has excellent fatigue resistance and exhibits low creep under loading. Moreover, under loading condition aramid fibre behaves linearly up to failure, even at high temperature [8]. Finally, this type of fibre is rarely used in concrete structures due to the significantly higher production cost compared with GFRP fibres.

2.2.2 Basalt Fibres

The term 'basalt' commonly refers to a type of igneous rock. The production process for basalt fibres is much easier than for glass fibres, although the production costs of the two are similar. Due to advances in production of Basalt fibres they are now considered to have very good fire resistance, to be durable materials in chemically active environments and good materials for vibration isolation and acoustic insulation applications [5]. However, the potential of using basalt fibre in civil engineering applications is still at the investigation and development stage.

2.2.3 Carbon fibres

Carbon fibres (CFRP) are produced from either coal pitch or petroleum and polyacrylonitrile. In general, these types of fibres exhibit higher tensile strength and stiffness compared to other types of fibre which makes them quite attractive for use in the aerospace industry. These fibres, contrary to other fibres, have high tensile strength and tensile modulus but as the stiffness increases the ultimate tensile strength and failure elongation decrease [5].These mechanical properties of carbon fibres remain stable as the temperature increases and this fibre material has excellent resistance to most aggressive environments [5]. However, the high cost of CFRP has been a major obstacle to its use in the civil engineering industry [5].

2.2.4 Glass fibres

Glass fibres are the most generally used to produce fibres for FRP composites. These fibres are produced by dragging molten glass through apertures of 1-3 mm at a speed of 200 mph [9]. The fibres are then cooled down from a temperature of 1200°C to 20°C temperature within 10-5 seconds. Usually the diameter of these fibres ranges from 4 micron to 30 micron [9]. The most common types of glass fibres are E-Glass, S-2 Glass, AR- Glass, A- Glass, C-Glass, D-Glass, R-Glass and ECR-Glass. These fibres usually are categorised and named based on their chemical structure [10)]. The main advantages of using glass fibres are their excellent properties such as high tensile strength, corrosion resistance, low cost, and very good insulating properties. Whereas, disadvantages that limit their application are very low stiffness, sensitivity to deterioration and damage during processing, and high hardness [9]. Among the different types of glass fibres,

electrical grade glass or E-Glass is the most widely used for GFRP bars due to its good mechanical properties and low cost of production. S-2 Glass fibres are more expensive than E-Glass fibres but their mechanical properties are better than those of E-Glass fibres. AR glass fibres (Alkali-resistances fibres) help to prevent degradation due to alkali attack in concrete environments. This type is produced by adding zirconium to the chemical composition of the glass [5]. However, the mechanical properties of glass fibre, in general, deteriorate in water and alkaline environments and it is more susceptible to stress corrosion than other fibres. This issue will be treated in more detail in this chapter, literature review section. Some mechanical and physical properties of different types of glass fibres are presented in Table 2.2

Table 2. 2: Mechanical properties of different types of glass fibres [11]

Glass designation	Type	Tensile Strength (MPa)	Elastic modulus (GPa)	Ultimate strain (%)	Density (g/cm3)
E-Glass	Standard conventional glass	3400	73	<4.8	2.6
S-Glass	High strength glass	4400	86	<4.6	2.53
C-Glass	Chemical resistant glass	2400	70	<4.8	2.52
ECR-Glass	Chemically resistant to conventional glass	3440	73	<4.8	2.72
AR- Glass	Alkali resistant glass	3000	73	<4.4	2.68

2.3 RESIN MATRIX

Since the resin matrix has a significant role in achieving the durability and long-term performance of FRP bars, optimum selection of this matrix is very important. Its binder role needs to be considered due to its significant effect on the transfer properties of the composite product. Matrices can be produced from polymeric, ceramic or metallic materials. According to the literature, FRP bars are formed from two main types of polymer matrices: thermoset (polyester, vinyl ester, and epoxy) and thermoplastic (polyurethanes, polyethylene teraphthalate, polypropylene and nylon). The polymer resin matrix does not provide much strength in a composite system, since most of the applied load is carried by the fibres [5]. The prime role of the resin matrix is to transfer the load onto the fibres [12]. Furthermore, the resin matrix provides some degree of protection for the surface of the fibres against aggressive environments and physical abrasion [13].

2.3.1 Polyester Resins

The main advantages of the polyester resins matrix are low cost, fast cure time and low viscosity. Unsaturated polyester resins are the most widely used resins, due to their relatively low cost. Hence, polyester resins now account for about 75% of the total thermoset resins used in the composite market. The main disadvantage of polyester resin matrices is their high volumetric shrinkage behaviour of around (5% - 12%). This behaviour can be controlled by adding a small portion of low-shrinkage polyester resin that has a thermoplastic component [9]. The commercially available types of unsaturated polyester resins matrix in the market include Iso Polyester, Orthophthalic Polyester, Chlorendics and Bisphenol A Furmerates.

2.3.2 Epoxy Resins

These types of resin matrix offer excellent mechanical properties and good resistance to corrosive liquids in alkaline and acidic environments [10]. In general, epoxy resins have higher viscosity and are more expensive compared with most polyester resins. Owing to their higher viscosity properties epoxy resins are more difficult to use [10]. The main advantages of epoxy resins compared with other types of resin matrices are their wide range of good physical and mechanical properties, low shrinkage, especially during the curing process, their high resistance to solvent materials and their excellent bonding to a wide range of filler (fibres, nano-substrates) materials [9].

2.3.3 Vinyl ester Resins

Vinyl ester resins are used in GFRP bars for concrete structures to resist the degradation in alkaline environments and to achieve high mechanical properties. Vinyl ester resins have higher fracture toughness compared with epoxy resins, without the processing difficulties encountered with epoxy resins in shape fabrication and handling [10]. This type of resin also has lower viscosity, and lower curing time compared with polyester resins. However, vinyl ester resins have the major disadvantages of high volume of shrinkage after the curing process, of around 5% - 10%. It is also worthy of mention that using heat-resistant epoxy resins along with vinyl ester resins can enhance the mechanical properties of the matrix at high temperature and its thermal stability [9].

2.3.4 Polyurethanes

The thermoplastic resins generally are softened from solid state to be formed and shaped before being cooled down [14]. Polyurethane resins are produced from primary constituents, polyol and

poly isocyanate, using a process called "Reaction Injection Moulding" (RIM). The high viscosity exhibited by polyurethane resins during the processing procedure is considered as one of their disadvantages. However, different properties can be incorporated into this type of polymer resin, depending on the constituents used, which can enable the final product to be flexible or rigid [10]. Approximate properties of the resins matrix are presented in Table 2.3

Table 2. 3: Approximate properties of the resins matrix [15]

Type	Tensile strength (MPa)	Elastic modulus (GPa)	Ultimate strain (%)	Density (g/cm^3)
Polyester	65	4.0	2.5	1.2
Epoxy	90	3.0	8.0	1.2
Vinyl ester	80	3.5	6.0	1.12
Polyurethane	70	2.9	5.9	varies

2.4 MANUFACTURING PROCESS

Various fabrication techniques have been used to manufacture FRP composites products, such as filament winding, pultrusion, vacuum compaction, bag moulding, etc. Each method of manufacturing offers a better solution for a specific FRP composites product; however, most FRP bars for concrete structures are manufactured by the pultrusion process see Figure. 2.2.

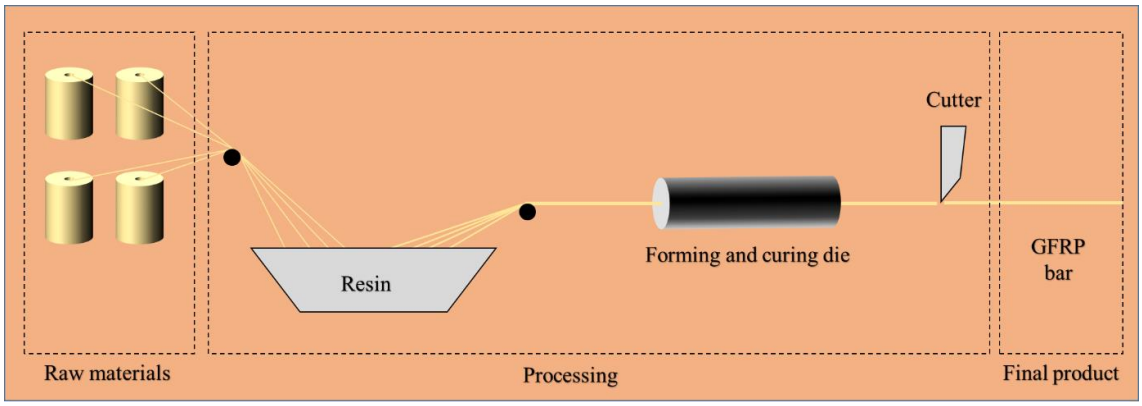

Figure 2. 2: Pultrusion process

2.5 ADVANTAGES AND DISADVANTAGES OF FRP

2.5.1 Advantages

FRP bars have a great many advantages compared with conventional steel reinforcements. The use of FRP bars enables contracting companies to facilitate and expedite the installation process, thereby reducing the application time and cost [16]. In terms of physical and mechanical

properties, FRP composites have advantages such as high strength, high specific stiffness, low specified weight, non-corrosive nature, fatigue resistance and excellent durability in various environments [17]. The advantages of FRP composites materials [16] are summarised as the following:

1- High tensile strength

2- Lightweight compared to steel bars

3- Fast installation

4- Non-corrosive nature

5- Excellent durability in several environments

6- High fatigue resistance, especially CFRP

7- Flexibility to be formed into different shapes.

2.5.2 Disadvantages

Despite their various advantages over conventional steel rebars, FRP bars have a number of disadvantages which should be considered carefully, such as high initial cost of materials, lack of design standards, uncommon design method, lack of long-term performance record, durability issues, and others. The most serious obstacles to the use of FRP bars in a wide range of civil engineering applications in the construction industry are the initial cost and lack of long-term information. The following points summarise the main disadvantages of using FRP composites [16] in concrete structures:

1- High materials cost

2- Low modulus of elasticity can result in large deflections and wide cracks

3- Low shear strength

4- De-bonding or peeling off at crack locations

5- Tendency to creep under sustained stress

6- Lack of experience in using new materials for civil engineering applications

7- Lack of lifespan records

8- Durability issues

9- Lack of unified design code standards and methods for making and testing long-term predictions

2.6 APPLICATIONS OF FRP BARS IN CIVIL ENGINEERING

FRP bars have been used in various types of concrete structures, especially in the following cases:

- In concrete where reinforcement is subjected to aggressive environments such as construction in the chemical industry, road bridges where reinforcements are exposed to de-icing salts, and marine structures in hot weather conditions
- In medical facilities where concrete members are subjected to electromagnetic waves from MRI equipment and the presence of steel reinforcement in the surrounding concrete would obstruct the equipment's performance
- For lightweight concrete requirements
- For secondary load bearing members

2.7 DURABILITY OF GFRP COMPOSITES

Durability of FRP, in general, can be defined as its ability to retain its original properties over time under given mechanical and environmental in-service conditions. This entails its ability to resist cracking, oxidation, chemical degradations, de-bonding and wearing [18]. The long-term behaviour of the material is one of the most important concerns when a new product is being developed for structural applications. The use of FRP products is increasing as more understanding of his performance is known and less expensive manufacturing techniques are becoming available. However, the available data on durability of FRP materials in structural concrete applications are limited and in some cases contradictory. These contradictions may be due to the fact that, as of yet, there are no universally accepted testing methodologies, and research has been conducted on a variety of different FRP reinforcing bars that were manufactured using different fabrication processes as well as different types of fibres/resin systems. Although carbon, glass, basalt and aramid FRP bars are commercially available for use in infrastructure applications, GFRP bars are the most widely used due to their good mechanical performance and low cost of production . Many factors that can affect the durability of GFRP bars in a concrete environment have been investigated during the last three decades, and are discussed in detail in this section. The discussion highlights the factors with the most significant effects on durability according to available research. Based on these research studies, the factors illustrated in Figure. 2.3 should be taken into account when assessing the durability of GFRP bars in concrete. Potential

synergies should also be given serious consideration regarding the combination of environmental effects and physical effects [19].

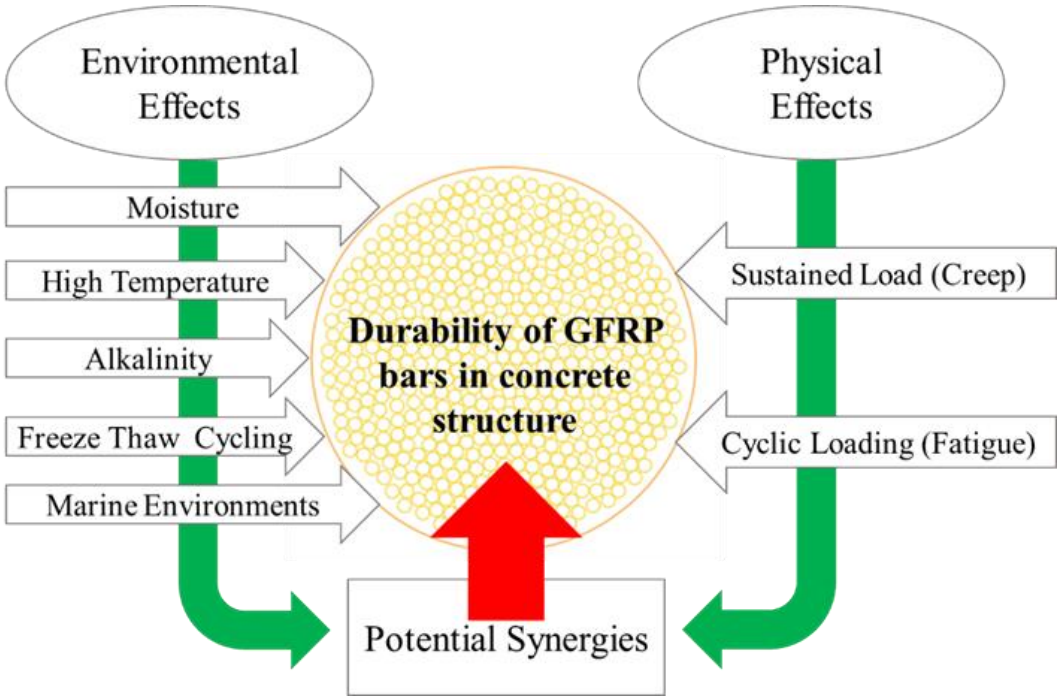

Figure 2. 3: Potentially harmful effects of GFRP bars in civil engineering application [19]

Various models have been suggested for predicting the long-term performance of FRP reinforcement based on tests results obtained from different accelerated aging methods [20, 21] and will be discussed in detail in Section 2.10.2. Exposure to various types of solution (alkaline solution, deionised water, tap water, saline solution) at high temperature have been used to accelerate the degradation mechanism [13, 22-24]. Although tensile strength and modulus of elasticity are most frequently used as indications of long-term durability [25], there have been many studies focusing on other mechanical properties, including interlaminar shear strength and flexural strength [26]. The measurement of retention of mechanical properties after conditioning is often complemented by physical, microstructure and chemical investigations [5], which can lead to the determination of the relevant degradation mechanisms. For example, researchers have used analytical techniques such as Mobile Microscopy, Scanning Electron Microscopy (SEM), Energy Dispersive X-ray Analyses (EDX), Dynamic Mechanical Analysis (DMA), Thermo Gravimetric Analysis (TGA), Differential Scanning Calorimetry (DSC), and Fourier Transform Infrared Spectroscopy (FTIR) to achieve a more fundamental understanding of GFRP bars' long-term behaviour [25,27].

Given the many available techniques for both mechanical and physical characterisation, along with the fact that there is no international agreement on standardised durability tests for FRP bars and the uncertainty over the correlation between accelerated aging and long-term conditioning in real applications, comparing findings obtained from different studies is generally complex. Different research groups have used different experimental procedures and examined different parameters such as non-accelerated or accelerated aging, duration of aging, different alkaline solution compositions to simulate the concrete environment, different loading conditions during aging, conditioning of bare bars or bars embedded in concrete, and various test methods to evaluate the influences of exposure. Moreover, variations in the fabrication methods of FRP reinforcement and quality of production add additional complications. All of the factors discussed above are examined in the following sections and should be considered carefully when interpreting and comparing the available test results.

2.8 CHEMICAL, PHYSICAL AND MECHANICAL FACTORS AFFECTING DURABILITY OF FRP REINFORCEMENT

2.8.1 Effect of moisture absorption

The effects of moisture uptake on the durability of GFRP composites have been investigated by numerous researchers [28-30]. One of the most significant aspects to study in terms of the effect of moisture on GFRP composites, in addition to the polymer's moisture absorption, is the susceptibility of glass fibre to water [6]. A combination of water and elevated temperature is frequently used for accelerating the diffusion and chemical reaction between water component and chemical composition of the composites and to determine the synergistic influence of moisture and high temperature [6]. In general, all polymer materials absorb moisture [31]. The molecules of moisture diffuse through the resin matrix [22] and act as a plasticizer to weaken the Van der Walls' bonds between the polymer chains and cause softening in the resin matrix [6]. Matrix softening can lead to reduction in mechanical properties (strength and stiffness), also encouraging creep and stress relaxation to take place. The effects of moisture absorption become more serious with increasing of exposure temperature, especially with temperatures close to glass transition value [32]. In regard to the fibre-matrix interface, this layer, which has a thickness of a few micrometres, serves the purpose of transferring the load between fibre and matrix [33]. The layer consists of a coupling agent in the form of saline materials, which can dissolve in water.

Thus, the presence of moisture damages the interface layer and destroys the bond between the fibre and the matrix. Glass fibres are also susceptible to moisture absorption [34]. Moisture attacks the surface of the glass fibre, with the free hydroxides ions causing further breakage in the silica chain structure. This chemical reaction leads to breakage of the bond of silicon oxygen and subsequent conversion to hydrosilanes [35]. The degradation mechanism of glass fibres in water is attributed to leaching of the alkali ions out of the glass structure by reaction with hydroxide ions according to the following Eq 2.1 [22]:

$$S_i - \overset{\uparrow}{O}Na + H_2O \longrightarrow S_i OH + OH^- \tag{2.1}$$

(Dissolution of glass fibre in water)

The chemical interaction often involves two stages. The first stage is a reaction between the water and the alkali silicate glass, which is often considered as an exchange between hydrogen ions from the water and alkali ions from the glass chain structure, followed by a hydrolysis reaction, as illustrated in the following equations:

$$S_i - ONa + H_2O \longrightarrow S_i - OH + NaOH \tag{2.2}$$

$$S_i - O - S_i + OH^- \longrightarrow S_i - OH + S_i - O^- \tag{2.3}$$

$$S_i - O^- + H_2O \longrightarrow S_i - OH + OH^- \tag{2.4}$$

These reactions cause flaw formation on glass fibres surfaces and strength reduction. The surface of glass fibre can also be dissolved in water according to the following equations [36, 37]:

$$H_2O + S_i - O - S_i \longrightarrow S_iOH + HOS_i \tag{2.5}$$

$$S_iO_2 + 2H_2O \longrightarrow H_4S_iO_4 \tag{2.6}$$

2.8.1.1 Changing of mechanical properties in water

The physical and mechanical properties of GFRP bars are functions of the material properties of the fibres and matrix. However, the onset of damage in one of these constituents can initiate degradation processes over time. A critical factor promoting the degradation rate in GFRP is the

rate at which water molecules are transported into the GFRP reinforcing bar. Several research studies have been carried out to measure the residual mechanical properties of GFRP bars exposed to water at various temperatures ranging between 20-80 °C [6,30,38]. Moisture absorption rate is generally measured by weight gain of bars immersed in water. Often, the bars have been dried before immersion in water to determine the original moisture content. The same principle has been used for other solutions and conditions. These investigations provide valuable data on the general mechanisms of degradation and degradation rate of GFRP bars in water as a function of time. Bank et al. (1998) determined the reduction in mechanical properties of E-glass /vinyl ester bars after immersion in water at 23-80°C for 224 days [6]. The residual flexural properties for the bars aged at 40 and 80°C were around 86% and 55% respectively, whereas no significant reduction was found in flexural properties for bars aged at 23°C. The inter-laminar shear strength (ILSS) was not dramatically affected. No change was recorded in the flexural modulus of the aged bars, thus leading to the conclusion that the modulus, in contrast to the strength, is not significantly affected by local damage. In this research it was noticed that the glass transition temperature (Tg) increased for bars aged at 80°C but not for those aged at lower temperatures. Bank et al. [6] found that E-glass/vinyl ester bars immersed in water for up to 6 months at 60°C exhibited an 85% reduction in flexural strength. Also, Nishizaki and Meiarashi [38], who exposed GFRP specimens to water at 60°C for more than 400 days, reported that the specimens exhibited a rate of 38% retention in flexural strength. In another research, Hayes et al. [39] aged glass/vinyl ester composites in wet/dry cycles at 45°C for a month and found that the measured reduction in tensile strength and modulus of elasticity was about 26% for both properties [39]. Nishizaki and Meiarashi [38] evaluated the effect of exposure to water and moist environments at temperatures of 40°C and 60°C. The researchers reported that higher temperature exposure resulted in higher reductions in bending strength. The authors concluded that the critical factors in determining the durability of GFRP are water absorption and high temperature. Dejke [8] conducted tests on four different types of GFRP bars. Specimens were exposed to water at 20, 40, 60 and 80°C. After 540 days of conditioning at 60°C the reduction in tensile strength was 59% for bars supplied by FIBERBAR (E-glass/Vinyl ester), 43% for the bars supplied by Hughes Bros. (E-glass/Vinyl ester), 25% for AR-glass/vinyl ester and 32% for AR-glass/polyester. However, no significant change in the modulus of elasticity was observed. In addition, Nkurunziza et al. [28] evaluated the performance of GFRP specimens that were subjected to sustained exposure to a level of stress corresponding to 30% of the ultimate tensile strength, and exposure to deionised water at 70 °C temperature for 60 days. The researchers found that the reduction in tensile strength was about 4% of the original value. Helbling and Karbhari [29], on the other hand, investigated the influence

of deionized water on GFRP composites properties. The specimens were immersed in deionized water for up to 340 days. The specimens showed strength reduction of 12.5 %, 34% and 51 % at 22 °C, 40 °C and 60 °C respectively. Kotani et al. [30] examined GFRP laminates. The GFRP samples were tested to assess their tensile properties after hydrothermal aging. The specimens were exposed to deionised water at temperatures of 40, 80 and 95 °C. The strength of the woven GFRP decreased with increase in temperature. The reductions in tensile strength were 86%, 53% and 50% at 40, 80 and 95 °C respectively. Hongseob et al. [40] evaluated the deterioration of three differently produced GFRP bars exposed to distilled water at 40°C for 60 days. The reduction in ILSS was 11 % for (AR-glass/ epoxy) bars, 16 % for (50%E-glass/50% epoxy) bars and 10% for (20%E-glass/80% epoxy) bars.

2.8.1.2 Moisture uptake process and moisture content

The effects of temperature on moisture uptake and the diffusion rate have been investigated by a number of researchers. Verghese et al. [41] carried out moisture absorption research on vinyl ester resin, and glass fibre composite with vinyl ester [41]. The authors claim that moisture absorption kinetics in polymer or composites can be categorised into three stages as follows:

Stage 1: Fickian moisture absorption

This is marked as an initial absorption process which follows Fick's 2nd law. This process exhibits linear behaviour and is described as a quick process. The diffusion rate in this stage is controlled due to the equilibrium of moisture concentration gradients between the surrounding environment and material. Therefore, any environmental change corresponding to change in diffusion rate, for instance change in temperature, results in an increase or decline in absorption rate.

Stages 2: Transition region

This can be described as non-linear behaviour of the absorption rate. This stage is differentiated by prolonged equilibration of concentration gradients as a result of the material's saturation. This stage, therefore, is characterised as a transition stage from the conventional controlled diffusion process to a chemical equilibrium process. This chemical equilibrium is established between the liquid phase and the polymer, if the chemical structure of the chemical allows for chemical interactions with moisture. Thus in this stage the material becomes extremely susceptible to aspects of the surrounding environment, such as temperature.

Stage 3: Non-Fickian behaviour

This stage is crucial for long-term performance of the composites. In this stage deviation from Fickian behaviour occurs due to micro damage induced and accumulated by chemical interaction, with additional moisture absorption in the case of a long period of exposure. After a very long time of exposure, the glass fibres may start to degrade, which could enable more discrepancies to occur. The Verghese investigation [41] proposed a model for polymer moisture absorption based on Fick's second law. The diffusion rates were obtained for various temperatures ranging from 25 to 84°C. The dependence of the diffusion rate on measured temperature was found to be in agreement with the Arrhenius principle. The activation energy for diffusion was calculated using an Arrhenius plot. Zheng et al. (1993) applied the same principle to determine the diffusion rate from weight gain measurements [42]. The specimens of net resin and composites were immersed in water. Similarity was observed between the activation energy obtained from the net resin and composite, indicating that moisture diffusion in resins or composites takes place only by diffusion through the matrix and/or fibre-resin interface. Saadatmanesh et al. [43] and Chin et al. [44] obtained similar findings. Saadatmanesh adopted Fick's law to measure the intrusion depth of moisture and to predict strength reduction associated with intrusion of agent to the composite. It was also concluded that vinyl ester resin is less permeable than polyester. Bank et al. [6] performed gain weight measurements on E-glass/Vinyl ester bars. According to their finding, the temperature impacts the moisture content at saturation stage. However, it seemed that the saturation state could not be achieved. This phenomenon was attributed to the increase of voids as a result of the material's degradation during conditioning time and a consequent increase in moisture content.

2.8.2 An alkaline environment

It has been reported in the literature that an alkaline environment is a major degradation source for GFRP bars and causes a reduction in mechanical properties [24]. The alkaline agents contact and ingress the reinforced GFRP bars from chemical solutions or water penetrating through the concrete pores. Chen et al. [45] stated that alkaline solutions with pH value of 13.6 can be more aggressive on FRP composites than real concrete due to the greater mobility of OH^- ions in these solutions . Yilmaz [46] proposed that GFRP composites in concrete deteriorate due to chemical attack in the alkaline environment and growth of hydration products between the fibre filaments. Prolonged interaction may cause the fibres to be dragged away from the resin and also contribute to the development of micro cracks inside the fibres [47]. A chemical attack from the alkaline environment can contribute to surface loss of matrix and deep etching in the glass fibre, causing

a reduction in mechanical properties of the fibre and thus of the composite [35]. In addition, combined with chemical attack, a high level of sustained mechanical loading increases the degradation of the fibres/matrix interface [28]. Robust evidence has been provided of extensive deterioration in mechanical properties, particularly with exposure to a combination of an alkaline environment at high temperature and high sustained stress, which are considered as the most severe conditions [48].

2.8.2.1 Use of alkaline solution to simulate concrete pore solutions

Deterioration of GFRP composites due to an alkali environment has been widely investigated in the field of GFRP durability. It has been identified that resin matrices are particularly susceptible to alkali attacks. The alkaline environment causes a hydrolysis reaction in the ester chain of the resin matrix and this is the typical mode of resin degradation [7]. More specifically, the free hydroxide ions (OH^-) attack the polymer matrix and the long molecular chains break by hydrolysis reaction, promoting the ingress of more (OH^-) ions and water molecules (H_2O) Eq. (2.7). These, in turn, can break the polymer-polymer chain secondary bond, creating localised voids (increase in free volume) and ultimately decreasing physical and mechanical properties of the GFRP matrix (i.e. plasticization) [22].

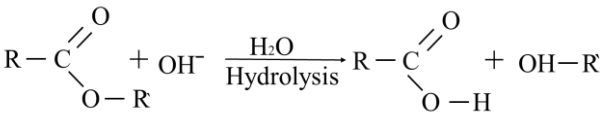

(2.7)

It has also been well documented that glass fibre is susceptible to alkaline ions attack [49]. It has been claimed that GFRP bars are degraded by attack from alkaline ions produced by the alkaline environment of cement components and or by growth of hydration products between the glass fibre filaments [46]. Degradation of fibres in alkali solutions is usually due to a combination of chemical interaction between water molecules and glass chemical components and leaching of alkali (Na^+, Ca^+, K^+ and Al^+ ions) out of the fibre. As the process continues, the dissolved alkali from the glass increase the pH level, thereby acting as catalysts for chemical reactions. The alkali ions in the solution attack the silica network in the glass fibre and break the silica chain bonds Si-O [50]. This chemical process can lead to both bar skin loss and deep pitting in the glass fibre, resulting in reduction in the mechanical properties of the fibre and then of the composite [51]. The methods for testing the effects of alkali on GFRP bars vary due to the absence of standardised international agreements on durability test procedure for GFRP bars. GFRP bars have been tested through exposure to accelerated and non-accelerated conditions. Usually the GFRP bars are

immersed in an artificial alkaline solution to simulate concrete pore solution (with and without sustained stress) at different temperature levels for different periods of time [22, 24, 52]. The temperature range of 20-60°C is usually used [53], and an alkaline solution with pH of 12.7-13.5 [54]. A number of researchers have applied sustained stress during exposure time to investigate the stress corrosion resistance of GFRP bars. The residual mechanical properties are often examined as indications of degradation and degradation rate. The chemical and microstructural properties for aged bars have been investigated by diffusion testing [6, 27, 55] and by using scanning electron microscopy (SEM), energy dispersive x-ray analyses (EDX), dynamic mechanical analysis (DMA), thermogravimetric analysis (TGA), differential scanning calorimetry (DSC) and Fourier transform infrared spectroscopy (FTIR). Usually, results obtained from accelerated exposure and non-accelerated exposure are compared to produce a lifetime predictive model. Extensive degradation of mechanisms and processes in mechanical properties has been documented.

2.8.2.2 Investigation of change in mechanical properties by simulating pore solution

Katsuki and Uomoto [56] investigated the effect of alkali attack on glass fibre woven with vinyl-ester resin. In this investigation, samples were immersed for 120 days in 1.0 mol/liter aqueous sodium hydroxide (NaOH) solutions at 40°C to accelerate the degradation. It was documented that the reduction in the tensile strength was as much as 60% after aging. The authors claimed that the thickness of the resin matrix should be controlled to protect the glass fibre from alkali ion attack [56]. Bakis et al. [57] exposed three different types of GFRP bars to Calcium Hydroxide Ca $(OH)_2$ at 80°C for 28 days. All aged bars showed a reduction in tensile strength. The bars produced with a 100% vinyl ester matrix exhibited lower reduction in mechanical properties due to exposure than the bars with matrices that were part polyester or part vinyl ester. Coomarasamy [58] carried out a durability study on GFRP bars by subjecting the bars to an alkaline solution with pH level of 13.5 at 60°C for 6 months. The aged bars exhibited about a 30% drop in tensile strength . Another durability study was carried out by Alsayed and Alhozaimy [59] on two types of GFRP bars, both of which were exposed to water and alkaline solution for 120 days at ambient temperature. The reduction for the first type of GFRP bar (60% urethane modified vinyl ester and 40% unsaturated polyester, coated with cement paste) when immersed in alkaline solution was 30% in tensile strength, whereas for the second type of GFRP bar (resin matrix not declared) the reduction was almost zero. It was concluded from this study that the resin matrix type and quality control are the key factors for durability of GFRP bars. Micelli and Nanni [60] carried out accelerated tests to evaluate the residual mechanical properties of E-glass fibres fabricated with

polyester and thermoplastic resin matrices. The GFRP bars were subjected to a simulated pore solution with pH level of 12.6 at 60°C. The measured reductions in tensile strength of GFRP bars containing polyester resin after 500 hr and 1000 hr conditioning in alkaline solution were 30% and 40% respectively of the ultimate strength. No significant reduction was reported in the GFRP bars fabricated with thermoplastic resins and exposed to alkaline solution. It was also concluded that the resin matrix properties have significant effects on the durability of GFRP bars, and polyester resin does not offer good protection against alkali attack and reduction in tensile strength. However, in the research carried out by Sheared et al. [61] on pull-out specimens reinforced by GFRP bars exposed to various alkaline solutions, it was reported that no physical or mechanical evidence of any degradation was observed after 12 months of exposure. Chen et al. [45] conducted accelerated tests on two types of GFRP bars that were exposed to two simulated alkaline pore solution types, normal and high performance concrete, at 60°C . The deterioration of the GFRP bars was accelerated by using elevated temperatures. The interlaminar shear strength (ILSS) of the GFRP bars was measured before and after exposure, and this was considered to be an evaluation of durability of GFRP. The results showed that after 45 days aging in Solution 2 at 60 °C, in GFRP bars type one there was a reduction in ILSS of 8%, while in the type two GFRP bars a reduction of about 20% was observed. Hongseob et al. [40] evaluated the degradation rate of three differently produced GFRP bars exposed to alkaline solution at 40°C for 60 days. The reduction in ILSS was 16 % for (AR-glass/ epoxy) bars, 19 % for the (50%E-glass/50% epoxy) bars and 16% for the (20%E-glass/80% epoxy) bars. Al Salloum et al. [24] examined the effects on GFRP bars of exposure to several severe environmental conditions, including alkaline solution at room temperature and 50°C for 6, 12 and 18 months . The tensile strength retention for these durations were 85, 80 and 75% respectively. Sawpan et al. [27] immersed GFRP bars in simulated alkaline solution at 60°C for up to 24 months to measure their durability in a concrete environment. Moisture absorption of the tested GFRP rebar was found to be about 0.76%. It was also reported that the reductions in both the glass transition temperature (Tg) and the ILSS were about 8%. No degradation of the GFRP composites was evident in chemical analysis based on Fourier transform infrared spectroscopy (FTIR) results as supported by scanning electron micrography (SEM). It was also reported that moisture diffusion was the key factor that controlled the long-term mechanical and thermal properties of GFRP composites.

2.8.3 Real concrete

It has been suggested that an alkaline solution of pH 13.6 can be more aggressive on GFRP bars than the real concrete environment [45]. This is attributed to the fact that the degradation

mechanisms in the alkaline solution require lower activation energy due to restriction of the mobility of hydroxide ions and water molecules in concrete [45]. Since GFRP bars have been used as internal reinforcement for concrete structures, it is very important to study the degradation of GFRP bars when embedded in real concrete environments. A number of researchers [35,63,64] reported that, when a GFRP bar consisting of E-glass and vinyl ester is embedded in concrete, plasticization of the resin matrix takes place, along with a combination of the above mentioned chemical reactions for glass fibres. In general, concrete is a highly alkaline environment [65]. Alkaline constituents become concentrated in the residual water ("pore solution") through a hydration reaction. Alkali ions (Na^+ and K^+ ions) in cement are dissoluble in the water pore solution, while Calcium Hydroxide Ca $(OH)_2$ is mostly crystallized in the concrete paste [65,66]. Throughout the hydration process the hardened concrete consists of some very poorly crystallised hydrates of different cement compounds, termed as gel, and of $Ca(OH)_2$ crystals [67]. At the early stage of C3S hydration the formed Calcium Hydroxide $Ca(OH)_2$ dissolves in water. The decay of C3S to form C-S-H slows down and finally stops when the OH- ions cannot accommodate any more Calcium Hydroxide $Ca(OH)_2$. Then, the concentration of calcium hydroxide $Ca(OH)_2$ in the pore solution becomes high. Due to the calcium hydroxide $Ca(OH)_2$ and the presence of soluble potassium and sodium hydroxides a highly alkaline environment with pH of >12 becomes existent in the concrete pore solution. When GFRP bars are embedded in concrete, the moist and highly alkaline environment of the concrete pore solution, at the first stages of hydration, deteriorate the resin matrix. This makes it easier for alkaline components such as (Na^+, Ca^+, OH^-) of the concrete pore solution to ingress through the matrix and reach the resin matrix/fibre interface, see Figure. 2.4.

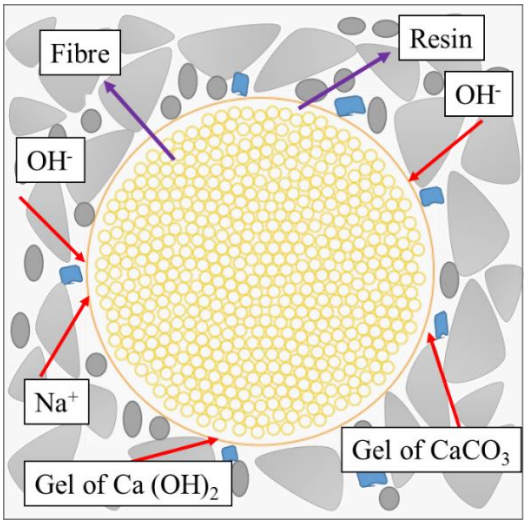

Figure 2. 4: Degradation of the GFRP bar in concrete

Calcium hydroxide ions diffuse through the resin matrix to reach the glass fibres [63,68]. In some cases it has been observed that glass acts as a nucleation site for $Ca(OH)_2$ in concrete pastes [63,64]. Calcium hydroxide crystals precipitate on the surface of GFRP bars [68,69]. Tested GFRP bars embedded in concrete in these researches revealed deterioration at the fibre matrix interface and at the fibre surface, as a result of nucleation of calcium hydroxide crystals on the glass fibre surface that initiated embrittlement of the fibre. De-bonding between fibre and matrix can occur, accompanied by pitting on the fibre skin, and cracking and notching of glass fibres.

2.8.3.1 Change of mechanical properties in real concrete

A number of studies have evaluated the effects of the concrete pore solution on the mechanical properties of GFRP reinforcement. Almusallam et al. [70] determined the tensile strength of GFRP bars embedded in stressed concrete in different environments for 120 days. The maximum reduction in tensile capacity was about 10 % for unstressed GFRP bars and up to 27.9 % reduction in tensile strength for stressed bars. Giernacky et al. [71] examined GFRP bars embedded in concrete under service for 6 months and reported that the reduction in tensile strength of the GFRP bars was almost 20 % . Svecova et al. [72] also examined GFRP bars embedded in concrete beams immersed in tap water at 60°C. The authors reported significant reductions in tensile strength of about 36% to 53%. Dejke [8] assessed the durability of GFRP bars from different manufacturers. The GFRP bars were embedded in concrete and exposed to 100 % relative humidity at 20, 60, 80°C for 600 days. It was reported that the reductions in tensile strength were about 25% and 42% at 20°C and 60 °C respectively after 600 days, whereas for the same bars the reduction reached 50% after less than 250 days at 80°C. It was also reported that another manufacturer's GFRP bars exhibited reductions of around 15% and 56 % in their tensile strength when exposed to 20°C, 60 °C for 520 days respectively. Mukherjee and Arwikar [73] reported that GFRP bars embedded in concrete beams and subjected to outdoors conditions for 18 and 30 months exhibited a reduction in tensile strength of approximately 39%. Bakis et al. [74] studied the difference in the degradation rate of GFRP bars between simulated alkaline solution and real concrete environments. GFRP bars with E-glass and vinyl ester resin matrix were embedded in concrete beams. The beams were pre-cracked and exposed to four environmental conditions for one year. After aging, the bars were extracted and tested to examine their tensile properties. The reduction in tensile strength of bars embedded in real concrete environments was about 2.5 %. However, reduction in tensile strength of GFRP bars immersed in alkaline solution was approximately 25 %. It was reported that the reduction in the tensile properties in the real concrete environment is much lower than the reduction with alkaline solution. Mufti et al. [55] studied the durability of GFRP bars embedded

in concrete in several structures across Canada for up to 8 years. The main objective of the investigation was to provide the civil engineering industry with results on the performance of GFRP materials that have been exposed to real concrete. The authors concluded that GFRP bars are durable and should be permitted for use as primary reinforcements in concrete. Almusallam et al. [75] studied the durability of GFRP bars embedded in concrete prisms and subjected to different environmental conditions for 6, 12, and 18 months. The aging environments included ordinary tap water and seawater at 20°C, 50°C dry/wet cycles in seawater and in alkaline solution at 50 °C. In addition, samples were also exposed to two typical field environments in the Kingdom of Saudi Arabia (Riyadh area and coast area). Tensile properties were evaluated to examine the long-term performances of the GFRP bars. Scanning electron microscopy was also used to investigate the degradation of GFRP bars in such environments. The tensile test results showed that after 18 months of exposure, the specimens subjected to tap water and the alkaline solution at 50°C exhibited the maximum reduction in their tensile strength properties, whereas almost no degradation was observed in the two field conditions. He and Yang [76] studied the durability performance of GFRP bars embedded in concrete beams under stress and exposed to tap water at 23°C and alkaline solution at 60°C for up to 18 months [76]. Maximum tensile strength losses of 15.8% and 24.6% were observed in specimens aged in tap water at 23°C and alkaline solution at 60°C respectively.

2.8.4 Effect of marine environments on the durability of GFRP bars

GFRP bars in civil engineering applications may be exposed to a marine environment, which may present aggressive agents to GFRP composites, very often salts. Salt attack generally occurs because of the presence of free chloride ions in the saline solution surrounding GFRP materials. Tannous and Saadatmanesh [77] reported that CI^- ions cause the same damage as OH^- ions. CI^- ions penetrate the resin matrix, inducing micro-cracks and resulting in debonding of fibres and accelerated moisture uptake, leading to reductions in mechanical properties of the GFRP bar. Durability of GFRP bars in contact with saline environments is typically measured by examining the change in mechanical properties after exposing the naked bars to saline solutions at different temperature levels for a long period of time [13]. In addition, the long-term performances of GFRP bars in concrete in saline environments were also examined by embedding the bars in concrete beams or in pull-out specimens and exposing them to saline solution [11, 52, 78]. A saline solution with high salt concentration and elevated temperature was used to accelerate the tests [52]. Usually, sodium chloride, magnesium chloride and calcium chloride are used to simulate seawater [78]. Field exposure (non-accelerated environment) tests of GFRP bars have

been carried out to assess the durability of GFRP bars in saline environments [24]. The results usually vary and no observations have been carried out to differentiate between degradation as a result of chloride and concomitant degradation due to moisture absorption and/or alkali attack of the glass fibres. Gangarao and Vijay [79] carried out accelerated tests on GFRP plates by exposing polyester and vinyl ester to a saline environment at 21°C for 240 days. A tensile strength reduction of up to 17% was observed. The authors concluded that the degradation rate for GFRP plates can be calculated by the following formula:

$$\sigma_t = \sigma_0 \, e^{-\lambda t} \tag{2.8}$$

where

σ_t is tensile strength at time t, λ is a constant and equal to 0.0015 and t is predicted time.

Steckel et al. [49] assessed the effect of a saline environment on 3 different E-glass FRP composites (containing polyester resin, epoxy and vinyl ester). After 3000 hr of conditioning in saline solution at 23°C no significant degradation in mechanical properties was observed. Vijay and Gangarao [80] studied sand coated GFRP bars. The bars were immersed in a 3% sodium chloride solution at 20°C temperature. The reductions in tensile strength after 15 and 30 months of exposure were 18.5% and 24.5% respectively. Vijay and Gangarao [81] exposed GFRP RC beams to saline solution at ambient temperature for 1 year. The reduction in flexural capacity was around 18.4%. The reduction was, however, attributed to degradation caused by the concrete environment rather than to degradation caused by salt. Vijay and Gangarao [82] carried out a durability study on sand coated GFRP bars, in which they exposed the bars to 3% sodium chloride solution under sustained stress, with 27% of the ultimate stress applied for up to 8 months. The GFRP bars exhibited a 22.9% reduction in tensile strength. Tannous and Saadatmanesh [77] also examined GFRP bars embedded in concrete beams and exposed to saline solutions with concentration of 7% (2:1 NaCl +$MgCl_2$) and (2:1 NaCl +$CaCl_2$) for 1 year. The durability of the GFRP bars was evaluated by measuring the reduction in flexural capacity as a result of the bars' degradation. The loss in flexural capacity was 11% and 9% for the two solutions respectively. The same GFRP bars showed a reduction in tensile strength of around 30% when exposed directly to the solutions. The authors claimed that the concrete limits the effect of exposure to de-icing salts. Spainhour and Thompson [83] examined concrete beams reinforced by GFRP composites. The stressed and unstressed beams were exposed to artificial seawater subjected to wet dry cycling. The stressed beams lost their strength after 6 months of exposure, whereas the unstressed beams lost their strength after 15 months. Mukhopadhyaya et al. [84] observed degradation in

GFRP plates in externally reinforced concrete elements subjected to wet and dry cycles in a 5% sodium solution (NaCl). Adimi et al. [85] examined the fatigue behaviour of GFRP RC beams exposed to saline solution (NaCl) at different levels of concentration from 1% to 10%. The fatigue test conditions were α=0.043 to 0.43 (R=0.1, at 4Hz). The authors concluded that the effect of salinity on the fatigue life of GFRP materials is negligible. Wu et al. [86] studied the effects of seawater on GFRP composites with E-glass fibres and vinyl ester resin matrix. The specimens were exposed to seawater (with pH of 8.24), de-ionized water (with pH of 6.95), and saline solution (with pH of 8.24) at 23°C for periods of up to 365 days. After 365 days of exposure, the reduction in tensile strength was almost the same for all environments at around 13.5%. Alsayed et al. [87] studied the effect of seawater on tensile strength of GFRP bars and weight gain . The conditioned bars were bare bars and bars embedded in cement paste (low and high alkali cement) that were immersed in seawater at temperature levels of 23, 35, 50ºC for 180 days. The maximum reduction in the tensile strength and the highest weight gain were recorded at 50ºC in specimens coated in high alkalinity cement paste. The reduction in tensile strength was 12%, while the reduction was 3% for bars embedded in low alkalinity cement paste. Chen et al. [45] studied the durability of GFRP bars for concrete structures. Bare GFRP bars and GFRP bars embedded in concrete were exposed to saline solution at temperatures of 40 and 60°C for 70 days. The reductions in tensile strength were 2% and 26% respectively. Almusallam and Al-Salloum [88] studied the effect of seawater on the long-term behaviour of GFRP bars in concrete beams subjected to sustained loads. Concrete beams reinforced with GFRP bars were subjected to a certain sustained stress level and immersed in seawater at 40°C for 480 days. The long-term behaviour of the GFRP bars was measured through change in the tensile strength of the GFRP bars. The results exhibited a significant reduction of around 20% in the tensile strength of GFRP bars when subjected to sustained stress. This can be attributed to the stress opening up micro cracks in the bars and an increase in the moisture diffusion rate rather than salinity effects. Al-Zahrani [89] examined the effects of salinity on E glass fibres embedded in three different types of resin matrix (vinyl ester, modified vinyl ester and polyurethane). The reductions in tensile strength after 720 days of exposure to seawater at 30 °C were 35%, 12% and 21% respectively. Kim et al. [90] carried out short-term durability tests for types of E-glass/vinyl ester bars exposed to seawater at 25, 40, 80°C for up to 132 days. The reductions in tensile strength were 11%, 16%, 22% respectively. Al-Salloum et al. [24] examined the durability of GFRP bars . The bars were embedded in concrete prisms and exposed to seawater at 50°C for 18 months and some specimens subjected to a wet/dry cycle. Test results showed that the reduction in tensile strength was 16% for immersed bars and 9% for bars subjected to the wet/dry cycle. Robert and Benmokrane [51]

conducted a study on the durability of GFRP reinforcing bars embedded in concrete and exposed to saline solutions at 23, 40, 60°C temperatures for 1 year [52]. The losses in tensile strength were 8%, 9%, 11% respectively. In general, the previous researches indicate that there is considerable degradation of GFRP bars exposed to saline solution. However, this degradation is not attributed only to salt attack but is accompanied by other reactions, such as plasticization by the diffusion of water molecules and or alkali ions attacking glass fibres from the concrete pore solution [79]. Some researches indicated that saline solution has a slightly more severe effect than fresh water [89]. Alsayed et al. [87] observed that the loss in strength was less when GFRP composites were exposed to saline solution rather than water. Results also expressed that the vinyl ester resin matrix showed lower diffusivity and better resistance to salt attack than the polyester resin matrix.

2.8.5 Thermal Aging

2.8.5.1 Effects of Elevated Temperature

Long-term or short term exposure to elevated temperatures can cause irreversible physical and chemical changes within GFRP materials. Elevated temperature accelerates most of the degradation mechanisms that can occur in polymers, such as oxidation, mechanical creep, and fatigue. Oxidation reaction is usually considered to be the main obstacle to using polymers at high temperatures [91]. The effect of thermal action on the oxidation processes depends on the chemical structure of the polymer chain. Thermo-oxidation is started by the reaction of oxygen with free radicals R^* to form peroxide radicals:

$$R^* + O_2 \longrightarrow ROO^* \qquad (2.9)$$

In general, all polymers contain free radicals due to their polymerisation and curing history. Once formed the peroxide radicals undergo slower propagation reactions that break down the polymer chains. The overall degradation mechanism usually requires quite a long induction period to produce a little degradation [91]. At the end of this period there is a quick increase in degradation leading to a significant loss in the mechanical properties of the polymer. During this induction period the polymer is highly susceptible to temperature. Therefore, the polymer matrix properties of GFRP composites are more affected by increase in temperature than by the glass fibre properties. As the resin matrix plays a crucial role in the stress distribution between the GFRP bars and concrete elements, it can be expected that the bond between the concrete and the GFRP bars is the first parameter to be damaged when the temperature rises significantly [92,93]. In general, in short term testing the mechanical properties of GFRP bars (strength and modulus) under loading remain unchanged with increase in temperature, until the transverse properties of

the matrix are decreased when the temperature approaches the glass transition temperature (Tg). In such tests, elevated temperatures of between 30 and 40°C have almost no effect on the elastic modulus or the strength of the majority of available commercial fibres [94]. However, long-term thermal aging at a high temperature combined with sustained loading can cause more degradation in the properties of the matrix [95]. Wang et al. (2007) carried out a study on the tensile properties of GFRP bars subjected to elevated temperature [96]. The test results show that the stress–strain curves of GFRP bars continued almost linearly until failure at elevated temperatures. However, there was a dramatic lessening in the failure load of GFRP bars at elevated temperatures, reaching zero at 500 °C. The elastic modulus of the GFRP bars remained almost unaffected until 300–400 C. Beyond this range of temperature, there was a dramatic reduction in the elastic modulus. Robert et al. (2010) examined GFRP bars subjected to low temperatures ranging from 0 to 100°C [97]. Variations in the mechanical properties (flexural, tensile and shear) of sand coated GFRP reinforcing bars due to thermal exposure were evaluated. Microstructural analysis was also carried out using scanning electron microscopy (SEM) and physical measurement using thermo-gravimetric analysis (TGA), and differential scanning calorimetry (DSC) to observe any change in the fibres, matrix, and the fibre/matrix interface due to exposure to extreme temperatures. The authors observed enhancement of mechanical properties that they attributed to matrix stiffness at lower temperatures. However, at temperatures approaching the (Tg) of the resin matrix, the mechanical properties, especially tensile strength and stiffness, were reduced considerably. Other degradation in GFRP composites due to thermal aging possibly occurred as the result of the different thermal expansion coefficients for each component of the GFRP composites. In GFRP reinforced concrete, thermal expansion incompatibility has been found not only between fibres and resin but also between concrete and GFRP composites, see Table 2.4. In GFRP reinforced concrete elements exposed to prolonged high temperature, transverse thermal expansion of the GFRP bars is very significant since this expansion may lead to cracks occurring along the bars in the concrete cover and then cause bond failure. Gentry and Husain (1999) performed a theoretical analysis of cracks in concrete due to thermal expansion of FRP reinforcement [98]. Based on this study it seems likely that cracks can be generated due to this mechanism. Moreover, this study indicated that the helical wrapping texture used with some commercial types of FRP to improve the bond, may to some extent reduce the thermal transverse expansion of FRP bars. El-badry et al. (2000) carried out a study on the effects of cracks in concrete due to the transverse expansion of GFRP on the performance of GFRP RC concrete [99]. The authors concluded that cracks induced by transverse expansion lead to a reduction in tension stiffening behaviour, thus increasing deflection in GFRP RC beams. Katz et al. (1998) investigated the effects of elevated

temperatures on bond strength between concrete and FRP bars [93]. The bars were exposed to temperatures of up to 250 ℃ and tested for pull-out strength. The test results showed that with exposure to temperatures of up to 100°C, the reduction in bond is similar to the bond reduction occurring in traditional steel rebars. However, at higher temperatures the bond strength of GFRP bars was reduced dramatically. The residual bond strength at 200-220°C was about 10% compared to the bond strength at 20°C temperature. The authors concluded that high reduction in bond strength is associated with temperature exceeding Tg value for the resin matrix of FRP bars.

Table 2. 4: Thermal expansion coefficients [100]

Materials	Coefficient of thermal expansion ($x10^{-6}$ 1/K)	
	Longitudinal	Transverse
Glass fibres	5 to 15	5 to 15
Resins	60 to 140	
GFRP	7 to 12	9 to 20
Concrete	6 to 13	

A sudden change in temperature generally causes damage to brittle materials, and if that variation in temperature continues in a cyclic form at the surface of the bars, fatigue may occur [101]. That process can lead to high radial pressures on the surface of the reinforcement [101], the formation of cracks along the bars in the concrete cover, and lead to bond deterioration. Adimi and Boukhili [34] carried out fatigue tests on three types of GFRP bars, with polyester, epoxy and vinyl ester. The test results showed that the fatigue life for GFRP bars with vinyl ester and epoxy can be reduced by a factor of 100 at a test temperature of 100°C relative to a test at room temperature. GFRP bars with a polyester resin matrix were not tested at elevated temperature as the Tg of these materials was found to be very low, at around 80°C, whereas for the tested GFRP bars with epoxy and vinyl ester the Tg was found to be 165 and 145℃ respectively. Variation in temperature exposure can induce residual stresses in GFRP composites due to the differences in longitudinal thermal expansion coefficients between the fibre and resin matrix [102]. In cold regions, differences in the curing and operating temperatures of a composite material can reach 93°C, which can lead to residual stresses inducing micro cracks within the resin matrix and or causing de-bonding between the fibre/matrix interfaces [103]. Grammatikos et al. [104] examined the influences of thermal cycles on the structural integrity of GFRP composites [104]. Two identical GFRP profiles were subjected, dry or immersed in distilled water, to freeze–thaw at temperatures between 20°C and -10 ℃ for a total of 300 cycles. Computed Tomography scanning (CT-scan) was used to evaluate the microstructural changes due to freeze thaw cycling. After conditioning, the GFRP specimens showed a slight decrease in Tg that indicated minor structural degradation. In the dry specimens, changes observed in either the in-plane shear or tensile properties were

negligible, whereas the immersed specimens exhibited significant degradation of their shear strength and tensile properties. However, the stiffness of the immersed samples remained unaffected as a result of the potentially reversible nature of plasticization, which plays a role in increasing the material's molecular mobility. Therefore, despite their initial moisture uptake, the immersed specimens subsequently recovered when they lost moisture due to freeze–thaw cycling.

2.8.5.2 Thermal and moisture effects on GFRP bars and composites

Generally, thermal aging influences the diffusion rate of moisture and then affects the mechanical properties of GFRP composites [95]. The tensile strength, shear strength and stiffness of GFRP composites decrease when the material is exposed to moisture and elevated temperatures of 40° to 80°C. An increase in aging temperature can induce creep and stress relaxation [105]. The reduction in mechanical properties of GFRP composites exposed to cold weather is not critical compared to the severity of hot weather [103]. Variations in strength and stiffness both increase and decrease, reliant on the temperature range observed in polymeric materials exposed to low temperatures, resulting in precocious brittle failure. The toughness and flexibility of polymers at low temperatures are linked to their glassy state of molecular movement [106-108]. Reduction in the exposure temperature can cause an increment in mechanical properties and also fatigue and creep resistances. However, this reduction can also lead to possible decreases in deflection, elongation, fracture toughness and compressive strength. Grammatikos et al. [104] studied the influence of hydrothermal aging on the durability of GFRP pultruded flat sheet, exposed to distilled water at 25 °C, 40 °C, 60 °C or 80 °C for 224 days. The authors concluded that elevated temperature significantly increases the diffusion rate. The tensile strength and stiffness remained unaffected by conditioning, and whereas there was a slight drop in shear strength, this recovered after further hydrothermal aging. It was also observed that the visco elastic properties changed due to plasticization and additional cross-linking. Optical microscopy showed cracking in the resin matrix in specimens aged at 80 °C for 112 days.

2.8.6 Effect of stress

The tensile strength of GFRP reinforcement decreases when subjected to environmental conditions associated with sustained load. Water molecules contribute as an active agent for fibre/resin matrix debonding, and the rate of degradation is accelerated by sustained stress and temperature [109]. Vijay and GangaRao [82] carried out a study on the effects on GFRP bars of exposure to alkane solutions with different pH under different levels of sustained stress for 30 months. The maximum tensile strength reduction in the GFRP bars after 30 months of aging at

22°C temperature was 30%, whereas the specimens under sustained stress exhibited a reduction in tensile strength of about 25.2% after just 10 months. Based on these observations it was concluded that the matrix/fibre interface layer plays an important role in the durability of GFRP bars. The interface layer controls the diffusion rate of moisture, thus controlling the rate of stress corrosion of the fibres. Chateauminois et al. [110] identified the damage in GFRP composites induced by imposing sustained load. The damage starts with random fractures of fibres causing relaxation in the resin matrix around those fractures and leading to reduction in the elastic modulus. The second phase involves micro cracking of the resin matrix, debonding in the interface layer, and further fibre breakages, leading to a rapid decrease in the elastic modulus. The sequence of these phases leads to total failure due to stress rupture. These degradation mechanisms are quite similar to that of cyclic fatigue [111,112]. The time to total failure is strongly reliant on the initial imposed strain and a minimum strain can cause fracture onset. Clarke and Sheard [113] conducted a study on the durability of GFRP-reinforced concrete in alkali, wet/dry conditions at different temperatures and stress levels. They suggested a 100-year life threshold stress limit of about 25% for E-glass, 50% for aramid, and 75% for carbon fibre. Almusallam et al. [88] examined the long-term behaviour of GFRP bars embedded in moist concrete at elevated temperature and subjected to a certain level of sustained stress. The test results indicated that the GFRP bars subjected to sustained stress underwent a significant reduction in tensile strength for all exposure conditions. Nkurunziza et al. [114] evaluated the long-term performance of GFRP bars in different environments and under sustained stress for up to 10000hr at ambient temperature. The GFRP bars were subjected to two different levels of sustained strain of 4000 and 6000 με. The test results exhibited that the GFRP bars under the considered loading and environmental conditions performed very well and the reduction in tensile strength was still within the limitations imposed by the design code of practice [115]. However, it was observed that there was no significant reduction in the stiffness of any of the tested bars. Bakis [116] carried out a durability study on GFRP bars. The bars were embedded in concrete beams subjected to sustain stress. The sets of beams were exposed to different environments for three years: stressed beams at ambient temperature, stressed beams aged outdoors in central Pennsylvania, saline solution at 60°C, and stressed beams immersed in water subjected to freeze–thaw cycling with temperatures between 20°C and -17 °C. The conditioned beams were examined to investigate cracks in the bond and mechanical properties of bars extracted from the beams. After elapse of the aging time, the crack widths had increased by up to 75% and the local bond strength had remained almost constant or slightly increased. However, the tensile strength of GFRP bars aged in moist environment at high temperature had decreased by as much as 25%,

while the tensile properties of GFRP bars aged indoors or outdoors had remained almost constant. Xiongjun et al. [117] examined the effects of different environmental conditions on GFRP bars embedded in pre-cracked concrete beams under sustained stress. The beams were exposed to alkaline solution at elevated temperature and the same specimens were exposed to tap water subjected to freeze/thaw cycles. The test results for extracted bars showed that the reduction in tensile stress due only to sustained stress was higher, 10.5% in the bars embedded in concrete in dry conditions. However, the bars aged in beams under sustained stress and exposed to saline solution at 60℃ exhibited a reduction in tensile strength of about 17%, while there was a tensile reduction of about 8% due to the freezing and thawing cycle. Wang et al. [118] studied the durability of glass fibre reinforced polymer composites under sustained loads and simultaneously immersed in either tap water or saline solution. The mechanical properties of the specimens before and after aging were examined along with their moisture absorption behaviour to assess the long-term performances of the GFRP composites under combined effects. The moisture absorption curves for both conditions showed a two stage diffusion process. The first stage followed Fickian behaviour, while during the second stage the curves fluctuated due to occurrence of mass loss with increasing immersion time that was attributed to hydrolysis of the resin. It was observed that the absorption rates of GFRP composites in saline solution were higher than those in tap water. Stressed specimens showed similar trends compared with unstressed samples and had a higher absorption rate. It was noticed that immersion in solutions caused some enhancement of the tensile properties (strength and elastic modulus) of GFRRP composites in the early stages. This phenomenon can be attributed to post curing taking place.

2.9 GFRP BARS AS REINFORCEMENT OF CONCRETE STRUCTURES

To serve their purpose as reinforcement in concrete structures, GFRP bars should fulfil two basic requirements: 1) the bars should have enough tensile strength to enable the concrete member to carry the applied stress, and 2) the bond stress between the GFRP bars and concrete should be sufficient to transfer the tensile stress in the bar to the concrete. The durability of a GFRP RC member can be defined as the duration of time until its tensile strength or bond strength becomes degraded to the point where it is no longer able to play its role in the concrete structure. In GFRP bars different properties are controlled by different components of the composites. Therefore, the tensile or bond properties that control the long-term performances of GFRP RC elements depend on the rate at which parts of the bars deteriorate. Thus, for long-term prediction, both the bond strength and tensile strength of GFRP bars in concrete elements must be taken into consideration.

2.9.1 Synergic degradation of GFRP bars in RC concrete elements

The long-term performances of GFRP RC element bars can be controlled by bond or tensile failure. Often the failure mode relies on the degradation mode of the GFRP bars, which in turn depends on the exposure to surrounding environments and loading conditions. As discussed earlier in this chapter, three types of essential chemical attack take place (oxidation, hydrolysis, alkaline ions) in GFRP bars at the resin matrix, matrix/fibre interface and fibres. It is possible that one of these types of chemical attack may control the overall course of degradation of GFRP bars and consequently one of the bar's constituents becomes the weakest link in terms of the bar's durability. The long-term performances of GFRP bar constituents can vary among available GFRP bar products and depend on their diffusion resistance properties and the resistance of the GFRP bars' constituents to degradation of each GFRP product. The three following degradation modes are supposed to control the long-term performance of GFRP in concrete:

Degradation mode A:

Alkaline ions from concrete pore solution causing deterioration only on the bar surfaces.

Degradation mode B:

Penetration of alkaline ions and water molecules through the outer layer of the bar

Degradation mode C:

Water molecules dissolve the interface the double agent bond layer and associate with alkaline ions to attack the glass fibre.

2.9.2 Degradation mode A:

Degradation occurs at the surface of the bar that is considered as the contact layer with the concrete. This layer plays the role of transferring the stress in the GFRP reinforcement to the concrete. The layer mainly consists of resin that can be degraded by alkali ions attack from the concrete pore solution. If this layer turns out to be the weakest link in the composites system then bond failure will take place. Bars surface configurations differ among GFRP bars products. Some GFRP bar products are made with a helical wrap along a sand coating to enhance their bond with concrete. Other GFRP bar products have a rough resin texture to enable the GFRP bars to form a sufficient bond with the surrounding concrete. As the surface parts of the bar will be in direct with high alkalinity concrete pore solution, it is clear that these parts should have high alkaline

resistance and retain sufficient ILLS capacity for the entire lifetime of the bar. A new generation of GFRP bars is being produced with spiral wrap which provides the bars with a deformed profile. Such surface texture should make the bond of the bar with the concrete sufficiently strong to avoid being affected by surface deterioration. Finally, it can be presumed that degradation mode A can affect long-term performance if high reduction in bond strength is experienced due to exposure, while there is no reduction in tensile strength. It is worthy of mention that this mode does not involve moisture diffusion into the bar.

2.9.3 Degradation mode B:

In this mode, the degradation occurs at the surfaces of the bar and is due to ingress of alkaline ions and water molecules inside the rich resin layer that induces damage at the outer layer and fibre/ matrix interface. This can result in a reduction in both capacity and tensile strength. Thus, the bond or tensile properties should be considered in relation to the ability of the affected layer to transfer the stress to the inner unaffected core of the GFRP bar. In real concrete elements exposure to harmful agents is likely to be different along the bar. For example, the parts close to a crack have a higher probability of exposure to moisture than other parts. In such circumstances, the GFRP bars are likely to deteriorate in small areas, resulting in the occurrence of tensile failure rather than bond failure. Katsuki and Uomoto [119] suggested that this mode of failure occurs in GFRP bars embedded in concrete structures. They and other researchers therefore developed predictive models for service life based on this failure mode.

2.9.4 Degradation mode C:

In GFRP bars where the diffusion of the water molecules and alkaline ions reaches into deeper layers and to the glass fibre layers, the degradation rate is likely to be lower than with modes A and B. The fibre orientation decreases the resin's exposed area and creates an obstacle to moisture diffusion. At this stage, therefore, the chemical reaction and the concentration of water molecules and alkaline ions, rather than the diffusion mechanisms, control the degradation rate. Despite the low rate of degradation in this stage, the chemical reaction can result in the degradation of a whole cross section materials of the composite. This degradation mode can cause a reduction in both ILSS and tensile strength of GFRP bars, resulting in the possibility of both bond and tensile failure taking place. As with mode B tensile failure is most likely to take place if the environmental exposure varies along the bar. However, bond failure may occur if the GFRP RC elements are exposed to an environmental condition under loading conditions. It is clear that bond failure is possible in all cases and this issue should therefore be considered carefully.

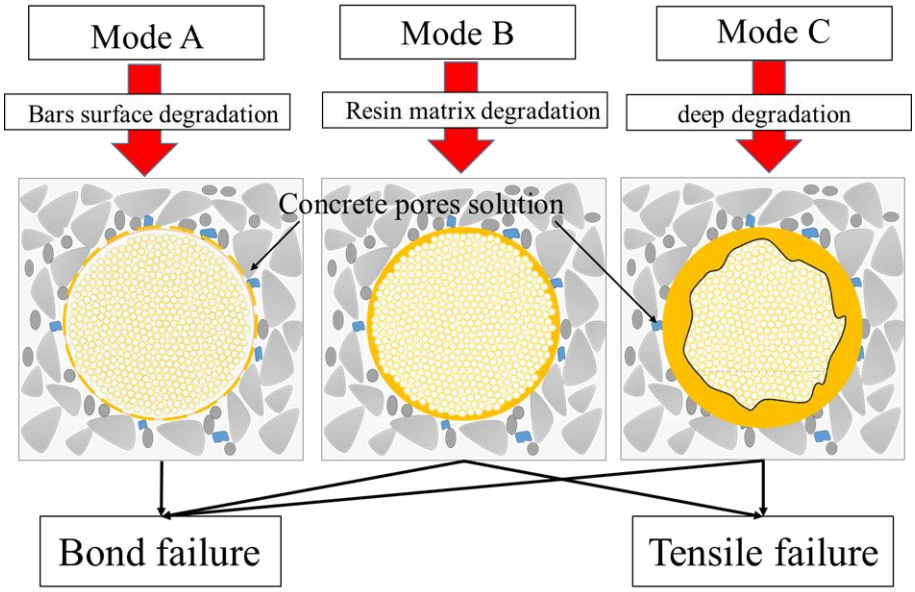

Figure 2. 5: Possible modes of failure of GFRP bars in concrete

2.10 DEGRADATION PREDICTION TECHNIQUES AND STRENGTH PREDICTION MODELS FROM THE LITERATURE

Several predictive models for the residual tensile and bond strength of GFRP bars in the concrete environment are currently available in the literature, most of which, due to lack of long-term durability data, are based on accelerated conditions tests. Typically, the service life of materials used in the construction industry is in the range of 50 to 100 years, whereas GFRP bars have been used in civil engineering applications for less than 30 years. The majority of researchers have used elevated temperature associated with moisture to speed up the degradation process. They have then used different approaches to transform or translate the data obtained under accelerated conditions to develop predicted models for the long-term performances of GFRP bars in real applications [26, 50, 120-122]. In general, Fick's law and the Arrhenius principle have been used to model the degradation rate and predict the long-term performance of FRP bars embedded in concrete. The models based on Fick's law use moisture diffusion or alkaline penetration to obtain the degradation rate of composites and to predict service life. Meanwhile, the models developed using the Arrhenius principle rely on the fact that the diffusion rate increases with increasing the temperature and is directly linked to the rate of transport of the aggressive compound through the composites. These principles are relied upon to develop accelerated tests and speed up the degradation of composites by exposing them to moisture, high temperature and under sustained stress.

2.10.1 Accelerated aging tests for long-term performance of GFRP bars in concrete:

2.10.1.1 Accelerated procedure using alkaline solution

A significant factor affecting the mechanical degradation of GFRP composites is the rate at which the type of solution is diffused into the GFRP composite. The deterioration takes place in one component (resin matrix, the interface layer, and glass fibre) of the composite and then causes a reduction in all of the composite's properties. Katsuki and Uomoto [119] investigated alkali diffusion into GFRP bars with vinyl-ester resin. The specimens were exposed to alkaline solution at 40°C for 120 days to accelerate the degradation mechanisms. It was reported that the reduction in ultimate tensile strength was around 60 %. Porter and Barnes [120] carried out accelerated test procedures to study the durability of GFRP composites. The outcome of this research was that the predicted long-term performances of GFRP composites based on testing samples exposed to the alkaline solution at elevated temperature achieved good correlation with aging due to real weathering. Accelerated conditions significantly influenced the mechanical properties of the GFRP composites. It was stated that immersion in alkaline solution with pH of 13 at 60°C for 90 days was equivalent to 50 years of real weathering conditions. Micelli and Nanni [60] applied accelerated testing procedure on GFRP bars with thermoplastic and polyester resin matrix to examine their durability. The GFRP bars made with thermoplastic and polyester resins matrix were immersed in alkaline solution with pH of 12.6 at 60°C. The tensile strength of the specimens was tested after 21 and 42 days of exposure. The reductions in ultimate tensile strength of GFRP bars fabricated with polyester resin were around 30% and 40% respectively, whereas, no significant reductions were observed in the GFRP bars produced with thermoplastic resin matrix. Nkurunziza et al. [28] evaluated the durability of GFRP using an accelerated test procedure that included exposure to high alkaline solution combined with various sustained stress levels. The authors concluded that the imposed stresses on the specimens at high temperatures during aging can induce cracks in the resin matrix and accelerate the diffusion of alkali ions through the resin, thereby causing chemical degradation of the glass fibres. It was recommended that the accelerated procedure should include sustained stress to reflect the real conditions for GFRP bars in service.

2.10.1.2 Accelerated procedure using concrete

With a view of providing more meaningful experimental data on the performance of GFRP reinforcement in structural concrete elements, a number of researchers have carried out durability investigations on GFRP bars embedded in real concrete environments [74, 88, 123, 124]. Almusallam et al. [88] performed an investigation of the long-term durability performances of

GFRP bars embedded in concrete beams under sustained stress. The bars were embedded in concrete beams and immersed in water and saline solution at 40°C. The beams were subjected to a sustained stress of about 25% of the ultimate tensile strength of the GFRP bars. The bars were then extracted from the concrete and tested in direct tension after 16 months of exposure. The loss of tensile strength for unloaded and loaded bars was 16.3% and 47% in tap water and 19.6% and 48 % in saline solution, respectively. The test results showed that sustained load has a significant effect on the degradation of GFRP bars. Bakis et al. [74] studied the difference in the degradation rate of GFRP bars exposed to alkaline solution and real concrete under loads for 1 year. After completion of the conditioning period, the GFRP bars were extracted and tested for tension. The bars embedded in concrete exhibited a 2.5% reduction in tensile strength compared with the unconditioned bars, whereas the bars aged in simulated pore solution showed a reduction of 25%. The authors stated that the loss of tensile strength in real concrete is much lower than the reduction in alkaline solution. Mufti et al. [124] carried out a field study to investigate the degradation of GFRP bars embedded in real structures for 5 to 8 years. GFRP bars exposed to different environmental conditions were extracted from five different bridges located in North America. The mechanical, physical properties and chemical composition were examined by different techniques. The test findings showed that no degradation had taken place in any of the specimens. Zhou et al. [23] performed an investigation of the durability of bonding of GFRP bars to concrete under an acid environment. The degradation processes were accelerated by immersing the specimens in acid solutions with different concentrations. Pull-out tests were carried out for 120 specimens to study the effect of acidic environment on bonding strength of GFRP to concrete. The tests results showed that after 75 days of exposure, the maximum bond strength reductions were 11%, 22%, 17.2% and 14% for the environments of tap water, pH = 2, pH = 3, and pH = 4 environments, respectively. The long-term performances of bond strength of GFRP bars for similar environments were determined using an Arrhenius equation and time shift method (TSF). Davalos et al. [125] carried out a durability study on glass fibre reinforced polymer (GFRP) bars within a concrete environment using accelerated aging methods, to formulate and validate the master curves for long-term predictions. The GFRP bars were embedded in concrete beams and immersed in water under stress at elevated temperature. After aging, the GFRP bars were tested for residual tensile strength, which was used as an indication of durability performance. Based on test results and microstructure investigation, the authors claimed that the degradation of the fibre/resin matrix interface governs the degradation mechanism for GFRP bars in the concrete environment. A prediction model was developed based on the Arrhenius principle and correlations were drawn with other studies and real field data.

2.10.2 Prediction models for long-term performance of GFRP bars in concrete

2.10.2.1 Tensile models

A number of researchers have attempted to evaluate the performance and deterioration of GFRP embedded in concrete. Most of the results showed clearly that GFRP bars' constituent materials along with the short and long-term loading and exposure conditions play a crucial role in the long-term performance of GFRP bars. Based on existing experimental data, a number of predictive models for long-term performance have been developed. These models offer the designer a tool to predict the residual strength of FRP bars over time [5, 8, 48, 77, 82, 126, 127, 128]. A review of the most cited models is provided in the following section. In general, Fick's law and the Arrhenius principle have been used to model the degradation rate and predict the long-term performance of FRP bars embedded in concrete. The diffusion of moisture into the resin and the fibre/matrix interface for a short term of exposure follows the Fickian diffusion path. Fickian diffusion vs temperature curves has also been clearly represented by the Arrhenius principle [129]. Shen and Springer [130] suggested that the diffusion coefficient according to Fick's law can be obtained by using the following equation:

$$D = \frac{\pi r^2}{16}\left(\frac{M_2 - M_1}{M_m}\right)^2 \left(\frac{1}{\sqrt{t_2} - \sqrt{t_1}}\right)^2 \qquad (2.10)$$

where

D is the diffusion coefficient; M_1, M_2, and M_m are the moisture contents of the bar (in percent) at time t_1, t_2, and at saturation, respectively; r is radius of the bar.

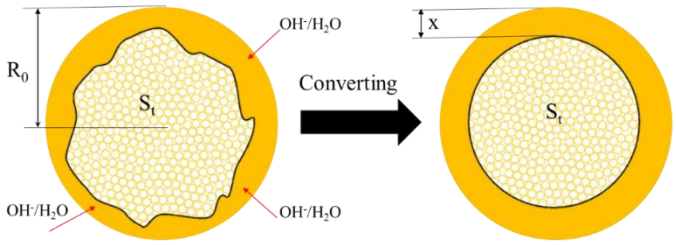

Figure 2. 6: Simple model for predicting alkali penetration [119]

Katsuki and Uomoto [119] suggested a predictive model for tensile strength retention according to Fick's law. The residual tensile strength of the FRP bar, based on this model, can be obtained by determining the amount of alkaline penetration into the bar and the authors proposed the following equation for calculating the depth of penetration:

$$x = \sqrt{2.D.C.t} \tag{2.11}$$

where

x is the depth of penetration starting from the bar surface; *D* is the diffusion coefficient; *C* is the alkaline solution concentration in (percent); *t* is the conditioning time.

Based on the assumption that the strength at the unaffected zone is the same as that before exposure and the affected area no longer contributes to the bar's strength capacity, the strength at a certain age after exposure can be calculated according to Eq 2.10.

$$\sigma_0 = \frac{P_0}{S_0} = \frac{P_t}{S_t} \rightarrow P_t = S_t \times \sigma_0 \rightarrow \sigma_t = \frac{P_t}{S_0} \tag{2.12}$$

where:

σ_0, σ_t are the tensile strength before immersing and the residual strength at t; P_0, P_t are the failure load before immersing and at t; S_0, $S_t$are the initial sectional area of the bar and the unaffected area at t (time of immersion).

The authors assumed that the glass fibre exposed to alkaline solution diffusion no longer contributes to the tensile capacity. Based on this hypothesis the authors recommended the following equation to estimate the residual strength:

$$\sigma_t = \frac{P_t}{S_0} = \sigma_0 \times \frac{S_t}{S_0} = \sigma_0 \times \frac{\pi(R_0 - x)^2}{\pi {R_0}^2} \tag{2.13}$$

Then the residual tensile strengths can be:

$$\sigma_{t=} \left(1 - \frac{\sqrt{2.\mathrm{D.C.t}}}{R_0}\right)^2 . \sigma_0 \tag{2.14}$$

σ_t is the residual tensile strength; σ_0 is initial tensile strength; R_0 is the radius of the FRP bar.

Tannous and Saadatmanesh [77] also suggested an approach based on Fick's law that uses the same assumption to predict the residual tensile strength. The diffusion coefficient and residual tensile strength can be determined using a moisture absorption test.

Trejo et al. [126] stated that the hypothesis of the complete loss of strength capacity of aging glass fibre has been overestimated. The authors suggested associating an exposure factor, λ, to take into account the time-dependent deterioration of the bond between the glass and resin. The recommended modified formula is as follows:

$$\sigma_t = \left(1 - \frac{\sqrt{2.D.\lambda.t}}{R_\circ}\right)^2 . \sigma_0 \tag{2.15}$$

Also, Katsuki and Uomoto [119] stated that the Arrhenius principle can provide a good correlation between the temperature and the rate of diffusivity of moisture and chemical reaction. The Arrhenius equation is as follows:

$$K = A\ exp\left(-\frac{E_a}{RT}\right) \tag{2.16}$$

K is the chemical rate of constant; *A* is the frequency factor; E_a is activation energy [KJ]; *R* is the universal gas constant*; T* is the absolute temperature [K].

Thus the proposed formula to determine the effect of temperature on diffusion rate is as follows:

$$D_{at} = D_{a0} e^{-\frac{E_a}{RT}} \tag{2.17}$$

where:

D_{at} is the diffusion coefficient at temperature *t*; D_{a0} is constant rate which is the diffusion coefficient at reference temperature.

Dejke [8] used the previous approach to produce a relative time shift factor *TSF*. The author used the *TSF* to transform the time in the accelerated test to actual service life for the GFRP reinforcement and the following equation was proposed to determine the *TSF*:

$$TSF = \frac{t_1}{t_2} = \frac{c/k_1}{c/k_2} = \frac{\mathrm{A.e}^{-\frac{\mathrm{E_a}}{\mathrm{RT_2}}}}{\mathrm{A.e}^{-\frac{\mathrm{E_a}}{\mathrm{RT_1}}}} = \mathrm{e}^{\frac{\mathrm{E_a}}{\mathrm{R}}\left(\frac{1}{\mathrm{T_1}} - \frac{1}{\mathrm{T_2}}\right)} \tag{2.18}$$

where

T_1 is the temperature [K]; T_2 is the selected reference temperatures [K];t_1 and t_2 are the times required for a certain decrease in residual strength at T_1 and T_2, respectively.

Vijay and GangaRao, [80] also developed a model using the Arrhenius relationship to correlate the accelerated aging tests results from the laboratory with real field performance as follows:

$$\frac{N}{C} = 0.098 \cdot e^{0.0558 \cdot T} \tag{2.19}$$

Similar attempts by Gremel et al. [122] on other types of GFRP bars led to generation of a similar equation with little change in parameters to predict long-term performances of GFRP bars in concrete:

$$\frac{N}{C} = 0.2 \cdot e^{0.052 \cdot T} \tag{2.20}$$

where

N is the age in-service field in days; C is the age accelerated exposure in days; T is temperature exposure

This developed correlation model was based on climate conditions in the North-eastern United States, with the assumption that the average annual temperature was11.7°C.

2.10.2.1.1 Bond strength models

A number of bond predictive models have been proposed based on significant experimental work data [23, 92, 131, 132]. Nanni et al. [131] proposed a predictive model for bond strength degradation of FRP embedded in concrete. The model generated was based also on the Arrhenius principle.

$$Bond\ reduction\ (\%) = 100\left(24755 - 8.62 \cdot e^{\frac{-1572}{T}} . t^{0.382}\right) \cdot \frac{100}{24755} \tag{2.21}$$

Where

T is the absolute temperature of the environment in Kelvin*; t* is the exposure time in days.

This model was said to be able to predict adequately the degradation of the bond strength of FRP bars in concrete structures in Pennsylvania, United States of America for a period of 50 years. Katz and Berman [92] carried out in-depth analysis of bond strength of different types of GFRP bars with concrete at various temperature levels. This investigation produced a semi-empirical model to describe the increment of reduction in bond strength, as temperature increases. A linear regression analysis was performed on the obtained experimental data and the following formula (2.22) was proposed.

$$y = a \cdot tanh[-b \cdot (x - k_1 \cdot c)] + d \qquad (2.22)$$

The authors identified unknown parameters (a, b, c, k_1 and d) that related to the GFRP bars' properties. The following predictive model for bond strength was derived for any GFRP bar configurations at high temperature:

$$\tau = 0.5 \cdot (1 - \tau_r^*) \cdot tanh\left\{-\frac{0.02}{C_r}\left[T - k_1\left(T_g \frac{k_1}{0.02} C_r\right)\right]\right\} + 0.5 \cdot (1 + \tau_r^*) \qquad (2.23)$$

where

τ_r^* is the normalized residual bond strength*;* T is the exposure temperature; C_r is the degree of crosslinking of the resin matrix; T_g is the glass transition temperature of the resin matrix at the surface of the bar

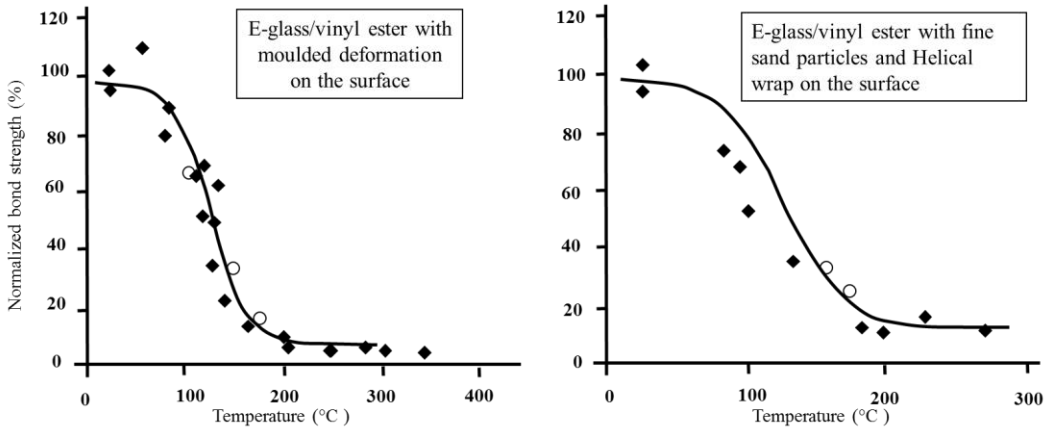

Figure 2. 7: Comparison of predicted and experimental results [92]

The authors used this formula to assess the experimental tests results from their work and previous studies on bond strength under exposure to elevated temperature. The authors stated that the model gives a good agreement between the theoretical and empirical values of bond strength, regardless of the different properties of the GFRP bars, the type of materials and the surface texture of the bar.

2.10.3 Design requirements for durability

Due to the change in material properties with time as a result of environmental and loading conditions, most of the published design guidelines on using FRP in concrete structures apply a partial reduction in tensile properties of FRP reinforcement. This partial reduction should reflect severe environmental exposure, sustained load and variation of materials to ensure an acceptable level of safety. The imposed factors must be associated with the original material properties to give a total level of safety that ensures an acceptable long-term performance of the bars in a concrete structure [28]. In general terms, the design value of tensile strength can be obtained by multiplying the characteristic tensile strength with an environmental reduction factor 'n_{env}'[5].

$$f_{ftd=f_{ftc}} \cdot n_{env} \tag{2.24}$$

Table 2. 5: Stress reduction factors according to international design codes

Factor	ACI 440.1R-15	NS3473	JSCE	CHBDC	IStructE
Reduction for environmental deterioration (ULS)	C_E "environmental reduction factor" GFRP:0.70-0.80 AFRP:0.80-0.90 CFRP:0.90-1.00	η_{env} "conversion factor" GFRP:0.50 AFRP:0.90 CFRP:1.00	$1/\gamma_{fm}$ "material factor" GFRP:0.77 AFRP:0.87 CFRP:0.87	Φ_{FRP} "resistance factor" GFRP:0.75 AFRP:0.85 CFRP:0.85	$1/\gamma_m$ "material factor"
Reduction for sustained stress (ULS)	Pending	η_{lt} "conversion factor" GFRP:0.8-1.0 AFRP:0.7-1.0 CFRP:0.9-1.0		F "Factor" GFRP:0.8-1.0 AFRP:0.5-1.0 CFRP:0.9-1.0	GFRP:0.3 AFRP:0.5 CFRP:0.6
Total strength reduction for environmental actions (SLS)	Including GFRP:0.39-0.52 AFRP:0.44-0.59 CFRP:0.50-0.65	GFRP:0.4-0.5 AFRP:0.6-0.9 CFRP:0.9-1.0	GFRP:0.77 AFRP:0.87 CFRP:0.87	GFRP:0.6-0.7 AFRP:0.4-0.8 CFRP:0.7-0.8	GFRP:0.3 AFRP:0.5 CFRP:0.6
Stress limits for permanent load (SLS)	GFRP:0.14-0.16 AFRP:0.24-0.27 CFRP:0.44-0.50	Reduction for modulus stress limits not specified	0.8x"creep failure strength" not more than 0.7 GFRP:≤0.7 AFRP:≤0.7 CFRP≤0.7	GFRP:0.6-0.7 AFRP:0.4-0.8 CFRP:0.7-0.8	Stress limits not specified

It can be seen from Table 2.5 that there are disagreements between codes regarding the value of reduction safety factors and there is no recognisable impact of different environmental conditions on the value of strength reduction factors, which causes them to give imprecise values. In order to resolve these issues a refined approach on durability of FRP has been proposed by *fib* TG 9.3 (2007) that takes into account the most significant environmental degradation parameters affecting FRP's durability in concrete according to the literature. According to the approach put forward by *fib* TG 9.3 Bulletin 40 [5], the characteristic strength of FRP bars for specific environmental exposure can be calculated with the following equation:

$$f_{fk,t} = f_{fk1000h} / \eta_{env,t} \quad (2.25)$$

Expanded to:

$$f_{fk,t} = f_{fk1000h} ((100 - R_{10})/100)^{n} \quad (2.26)$$

where:

$f_{fk,t}$ is the characteristic tensile strength at proposed design time; $f_{fk1000h}$ is the residual strength of FRP bars after conditioning 1000h; $\eta_{env,t}$ is the environmental tensile strength reduction factor;

R_{10} is the standard reduction of tensile strength in percentage per logarithmic decade of exposure; n is the environmental exponent given as the sum of all environmental degradation parameters (e.g. temperature, moisture) by Eq 2.27

$$n = n_{mo} + n_T + n_{SL} + n_d \quad (2.27)$$

where:

n_{mo} is the term for moisture condition; n_T is the term for temperature, n_{SL} is the term for desired service life; n_d is the term for diameter correction. The four degradation parameters are presented in the following tables [5]

Table 2. 6: Environmental factors as presented in (*fib* TG 9.3, 2007)

Environmental factor	Range	Term
Moisture, n_{mo}	Dry	-1
	Out doors	0
	Wet	1
Temperature, n_T	10 °C	0
	20 °C	0.5
	25 °C	0.75
	30 °C	1
	40 °C	1.5
	50 °C	2.5
	60 °C	3.5
Service life in years, n_{SL}	100	3
	50	2.7
	20	2.3
	10	2
	5	1.7
	1	1
	0.1	0
Diameter correction factor, n_d	Same as tested	0
	75% of tested	0.5
	50% of tested	1

It is clear from Eq. 2.27 that the sustained stress parameter (e.g. at service level) is not included even though this may also have an impact on the long-term mechanical properties. The performance of FRP bars in concrete subjected to coupled environmental and mechanical loads is still not well understood, although both initiation and development of degradation mechanisms are considered to be affected significantly [48]. It is hoped that the efforts made in this research to investigate the effect of sustained stress associated with various forms of environmental exposure on the durability of GFRP bars will calibrate further the environmental reduction factors

for GFRP bars in concrete structures. This would help the designer to apply more accurate safety factors based on the type of GFRP reinforcement used, the service life of the planned structure, the exposure environment of the design, and the stress conditions. Furthermore, consideration should be given to the effects of bond degradation within the design requirements for durability of GFRP RC elements.

2.11 LONG-TERM BOND PERFORMANCE OF GFRP BARS

GFRP materials are classified as anisotropic and categorised as materials with high tensile strength in the longitudinal direction. Furthermore, the resin matrix has a coefficient of thermal expansion (CTE) that is up to three to six times greater than the thermal expansion coefficient of concrete. This difference in expansion behaviour between concrete and GFRP bars can affect the long-term bond performance of GFRP bars in concrete and these behaviours should be considered carefully [62]. The long-term bond behaviour plays a significant role in the long-term performance of GFRP reinforcement concrete structures [133]. Several studies have been conducted on the long-term bond behaviour of GFRP bars embedded in concrete. These studies have demonstrated that bond performance and strength can vary due to differences in material composition and properties of GFRP bars and have also tested various assessment methods. Porter and Barnes [120] carried out pull-out bond tests to investigate long-term performances of GFRP bars in the concrete. Specimens were exposed to saline solution at 60°C for 90 days. The tests results indicated that there was no reduction in bond strength of aged specimens. Bakis et al. [134] performed another bond durability study on GFRP bars embedded in concrete. The specimens were immersed and saturated in $Ca(OH)_2$ for 28 days at 80 °C, followed by 5 days of drying. The tests result showed no reduction in bond strength, although degradation in microstructure level was observed in the GFRP bars. Shahidi et al. [135] investigated the long-term bond strength for different types of FRP bars embedded in concrete and subjected to sustained load. The specimens were tested in pull-out for both short-term and long-term behaviour for specimens under sustained stress. The aged specimens were subjected to different levels of sustained stress of up to 70% of ultimate bond strength and the end slip of the specimens was monitored during the tests. The test results revealed a significant reduction in long-term bond performances of GFRP bar specimens. The bond slip was increased by 75 % compared with short term test. Davalos et al. [133] aged pull-out specimens with GFRP reinforcement in water at 20°C, 60°C for 45 days. The test results exhibited a significant reduction in bond strength, which was about 20% for specimens

conditioned in water at 60°C. Robert et al. [136] carried out tests of long-term bond strength performances of GFRP bars embedded in concrete and immersed in water at various temperature levels. The authors found that the long-term performances of bond strength of GFRP bars embedded in moist concrete decreased as the duration of conditioning increased. However, the reduction in bond strength was minor around 7% even for specimens conditioned at the high temperature of 50°C. Belarbi et al. [78] carried out an investigation on the long-term bond performances of GFRP/fibre-reinforced concrete (FRC). The specimens were subjected to a combination of environmental conditioning, de-icing saline solution, including freeze-thaw cycles and elevated temperature. The tests results exhibited, after aging, a reduction in ultimate bond strength in plain concrete. However, adding polypropylene fibres to the concrete resulted in improvement in bond strength and restriction of cracking behaviour. Based on some studies, it is noted that the long-term bond behaviour of GFRP bars is highly affected by the surface geometry of the GFRP bar and transverse properties of rich resin outer layer of the bar [57]. Furthermore, imposing prolonged sustained stress results in a bond degradation that then also affects the long-term bond performance of the GFRP reinforcement in a concrete structure.

2.12 LONG-TERM FLEXURAL PERFORMANCE OF GFRP BARS IN CONCRETE BEAMS UNDER SUSTAINED LOAD

GFRP bars have been used in a wide range of concrete structures as a main reinforcement [137]. In general, GFRP bars have higher tensile strength than conventional steel rebars. However, owing to the relatively low stiffness of GFRP bars, GFRP RC members exhibit larger deflections and larger crack widths compared to the concrete member reinforced with conventional steel rebars [138]. These larger crack widths can considerably affect the long-term performance of GFRP RC structures, increasing deformations with time due to the change in GFRP RC materials' properties as a result of the material degradation [139]. Therefore, the design of GFRP RC members is often controlled by limiting deflection and crack width at service loads (i.e. serviceability limit state - SLS). In experimental studies performed by Brown [140] and Brown and Bartholomew [141] on long-term behaviour of GFRP RC beams in comparison with beams reinforced with steel rebars, the test results showed a similar trend of long-term performances between steel and GFRP bars. The authors concluded that the same fundamental methods for long-term deflection prediction can be used if some modification factors are added. Liew and Tan [142] investigated the accelerated environmental conditions effects of tropical climate on RC beams strengthened with GFRP laminates. The authors reported that the beams bonded with

GFRP-laminates exhibited a similar failure mode to conventional RC beams. However, exposure to tropical climate conditions for 9 months resulted in a 2% reduction in flexural capacity. Furthermore, exposure to the same conditions for up to 6 years resulted in a reduction in flexural strength capacity of 15%, which was attributed to deterioration of the bond between GFRP and concrete. Saha and Tan [143] carried out an investigation on RC beams strengthened with GFRP laminate exposed to tropical weathering and subjected to sustained stress for six months. The examined beams were studied for long-term deflection performance and cracking at different time points, and after the planned exposed time the beams were unloaded and tested to failure. The test results showed that the beams exposed to tropical weathering conditions for six months underwent higher deflection and exhibited wider crack width compared to control beams that were kept under ambient conditions, recording figures of about 8% and 15% respectively. Also, the reduction in flexural capacity was about 17% compared to that of the unconditioned control beams. The authors reported that the failure mode after weathering exposure changed from concrete crushing to GFRP rupture, which gives an indication on GFRP laminate deterioration. They also indicated that the effect of weathering exposure was more severe in the presence of sustained stress. Almusallam and Al-Salloum [88] carried out a study to investigate the effect of different environmental conditions on the long-term performances of GFRP bars in concrete beams under sustained stress. These GFRP RC beams were subjected to a certain stress level around 25% of the ultimate load capacity of the beam and immersed in tap water and saline solution at elevated temperature. Test results were recorded in terms of tensile strength of the GFRP bars and load–deflection responses of both unstressed and stressed beams. The results showed that for all the considered environments there was a significant reduction in tensile strength of the GFRP bars when they were subjected to sustained stress. The flexural test results showed a reduction in ultimate failure loads. The reductions in failure loads after 8 months of exposure in tap water, saline solution and saline solution (wet and dry cycle) were 12.5, 26.4, and 20.8%, respectively. For beams under stress, the reductions were 30.6, 25.0, and 33.3% for the considered environmental conditions. Laoubi et al. [144] conducted an investigation on the effects of freeze/thaw cycles and sustained stresses on the long-term behaviour of GFRP RC beams. The GFRP reinforced beams were subjected to 100, 200 and 360 freeze/thaw cycles (-20 °C to +20 °C) either for unstressed beams or beams under stress of around 27% of the ultimate tensile strength of the GFRP bar. The test results showed that the single or compound action of freeze/thaw cycles and sustained stresses had no significant influence on the long-term behaviour of the GFRP RC beams in terms of load-deflections responses, strains, and load capacity of the beams. The authors also mentioned that they considered the long-term deflections responses and

the creep strain limits applied by ACI 440.1R-06 to be conservative [145]. Almusallam performed a study to investigate the durability of RC beams strengthened with GFRP laminates [146]. The long-term performance of these specimens was evaluated through examining load deflection response and flexural capacity after exposing them to different environments. The beams were exposed to different aging conditions, namely, hot–dry field conditions, wet–dry in tap water environment, wet–dry in saline solution environment, and wet–dry in high alkaline environment, for up to 2 years. The test results showed that after 2 years of exposure to different environmental conditions, none of the considered environmental conditions had a noticeable effect on the flexural strength capacity of the tested beams. Gross et al. [15] carried out an experimental investigation to examine the long-term performances of GFRP bars in concrete beams subjected to sustained service load for up to 3 years. It was observed that the crack widths in GFRP RC beams under stress increased about twofold over one year of loading. This increase in crack widths for GFRP RC beams was higher than for the steel-reinforced beams. Miàs et al. [139] carried out an experimental study to evaluate the long-term performance of GFRP RC beams under service sustained load at ambient temperature for 250 days. Two levels of reinforcement ratios and two levels of sustained load were examined. The test results revealed no significant effects of the considered sustained load levels. Park et al. [11] studied the long-term behaviour of concrete beams reinforced by two types of GFRP bars (i.e. helically wrapped, sand-coated surface). The beams were exposed to accelerated aging conditions (i.e., 80% relative humidity at 47 °C) and subjected to sustained loads for 300 days. The test results indicated that the environmental exposure caused a reduction in the ultimate flexural capacity of the RC-GFRP specimens reach to 20% approximately..

2.13 CONCLUSIONS

This chapter has discussed the durability of GFRP bars in concrete environments and their long-term performance in concrete structures. The purpose was to review and summarise the current knowledge and research to identify the areas where further research is still required. A number of aggressive agents that affect the durability of GFRP bars used in civil engineering applications were identified and presented. Although it is widely known that GFRP rebars have different advantages in terms of mechanical characteristics compared to conventional steel reinforcement, the influence of potential synergies on the mechanical properties of loading and environmental exposure in real environments needs further investigation. Exposure to high alkalinity of concrete, moisture and under loading conditions at elevated temperature was identified as the most harmful

form of synergy affecting the lifetime of GFRP bars in concrete structures. Current results indicate that GFRP bars are prone to degradation in alkaline environments due to the presence of hydroxide ions and water molecules [147]. The diffusion of these hydroxide ions and water molecules into the rich resin layer of the bars can have adverse influences on long-term durability of GFRP bars in concrete elements; hence it is necessary to understand fully the long-term durability and performance of GFRP bars in order to have confidence in using these bars in concrete. Although the resin matrix in GFRP bars around individual filaments is expected to protect the glass fibres from attack by harmful agents, the alkaline pore solution in the surrounding concrete can expedite the degradation process of resins, resulting in significant reductions in tensile strength and degradation in the concrete/GFRP reinforcement bond. The factors that were identified as affecting this degradation are matrix type, fibre type, manufacturing processes, installation procedures and the short- and long-term loading and exposure condition (physical and chemical). The resins matrix on GFRP bars, in general, plays an important role in protecting glass fibres from moisture ingress and transferring the load to glass fibres. However, moisture diffusion into the resins matrix of GFRP bars subjected to stress at different temperature levels with respect to solution concentrations has not been comprehensively assessed and its deterioration effects on the bond behaviour with surrounding concrete have not been evaluated so far. In this context, the bond degradation of GFRP bars under sustained stress and subjected to different environmental conditions needs to be examined to provide a safe design. However, the long-term performances of GFRP in concrete structures under loading conditions generally have not been extensively investigated and are not fully understood. Potential synergies of sustained stress, high alkalinity and elevated temperature associated with moisture can have significant effects on degradation mechanisms of GFRP materials. It is therefore important to evaluate their influence on the long-term properties of materials in order to prevent undesirable outcomes in the structure's lifetime. No study has been carried out on degradation mechanisms of GFRP bars subject to various combinations of different sustained stress, different alkaline environments and different temperatures associated with wet environments for gaining comprehensive understanding of degradation processes. The rates of degradation of mechanical properties (tensile properties, flexural properties, transfer properties) are also not available to designer engineers, either in the form of tables or design charts, with respect to the expected environmental exposure and loading conditions. Gaining this knowledge requires in-depth investigation of the changes that occur in chemical, physical and microstructural properties before and after aging.

After reviewing the literature on durability testing approaches, it was observed that there is no unified standard method to use as guidance. Each investigation or research study has used its own

experimental method to produce experimental data for modelling potential GFRP bars degradation. Correlations between accelerated aging (laboratory aging) and natural exposure have been derived by using different models. Most of these models were generated based on Fick's law or the Arrhenius principle or by simple regression analysis. Through reviewing previous work for measuring the durability of GFRP, it was decided to design an experimental programme, based on accelerated test methods (see Chapters 3-5). The selected accelerated test methods included high alkalinity environments, wet environments, elevated temperature associated with sustained stress, since the potential synergies of these parameters were identified as the most aggressive agents affecting the durability of GFRP bars in concrete structures. Different combinations and scenarios of these parameters were therefore proposed to study the change over time of the bars' mechanical properties (i.e. tensile strength, flexural strength, bond strength and modulus of elasticity). In an attempt to achieve a more fundamental understanding of their long-term behaviour, several techniques were proposed to investigate the changes in chemical, physical and microstructural properties using moisture absorption tests, Fourier transform infrared spectroscopy (FTIR), scanning electron microscopy (SEM), energy dispersive x-ray analysis (EDX) and dynamic mechanical analysis (DMA). As criteria for assessing the long-term performances of GFRP in concrete structures, their bond performances with concrete and the flexural behaviour of GFRP RC beams were selected. It is also worth mentioning that the available information in the literature addressing the long-term performance of GFRP bars in concrete elements is very limited in terms of the conditions considered in this research.

It appears that by understanding the degradation mechanisms of GFRP bars in concrete environments under loading conditions and by accumulating and analysing the experimental results, the model originally proposed in *fib* Bulletin 40 [5] can be modified and improved to predict long-term mechanical performances of GFRP bars in multiple environments under loading conditions which represent the exposure conditions of GFRP RC structures in service. This model could enable structural engineers to predict long-term degradation of GFRP bars, in the form of tensile strength reduction and or bond strength reduction, without resorting to running a long-term and costly testing program.

2.14 REFERENCES

1. Astrom, B.T., (1997). Manufacturing of polymer composites. CRC Press.
2. Wallenberger, F.T. and Weston, N.E., (2001). Glass fibres from high and low viscosity melts. *In MRS Proceedings* (Vol. 702, pp. U5-3). Cambridge University Press.
3. Hollaway, L., (1993). Polymer composites for civil and structural engineering. Blackie Academic.
4. Gay, D., (2014). Composite materials: design and applications. *CRC press*.
5. *fib* TG 9.3, Bulletin 40. FRP reinforcement in RC structures. (2007): Lausanne, Switzerland
6. Bank, L.C., Gentry, T.R. and Barkatt, A. (1995). Accelerated test methods to determine the long-term behaviour of FRP composite structures: environmental effects. *Journal of Reinforced Plastics and Composites*, 14(6), pp.559-587.
7. Machida, A., 1993. State-of-the-art report on continuous fibre reinforcing materials. Second Research Committee on CFRM, *Japan Society of Civil Engineers*: Concrete Engineering Series, 3.
8. Dejke, V. ,(2001). Durability of FRP reinforcement in concrete: literature review and experiments, Ph.D. dissertation, Chalmers University of Technology, Goteborg, Sweden
9. Mallick, P.K., Fiber-Reinforced Composites Materials, Manufacturing, and Design (1993). *Marcel Decker*, Inc, New York, p.74
10. Composites Institute of the Society of the Plastics (1992) Industry Inc. (CISPI). "Introduction to Composites" technical report
11. Park, Y., (2014) Long-term performance of GFRP reinforced concrete beams and bars subjected to aggressive environments, Ph.D. dissertation, The University of Texas
12. Ehrenstein, G.W.(2007) Expert Report – GFRP – Reinforcing Bars "ComBAR"" Report No: STN Report Erlangen 2007 01 EN (2007).
13. Vijay, P.V. and GangaRao, H.V.S., (1999). Development of fiber reinforced plastics for highway application: aging behavior of concrete beams reinforced with GFRP bars. *CFC-WVU Report*, (99-265).
14. McKague, L. (2001), Thermoplastic Resins, Composites, *ASM Handbook Volume 2 Composites,* ASM International, Material Park, Ohio, p 133–140.

15. Huang, J. (2010) "Durability design of GFRP bar reinforced concrete members: A new approach", Ph.D. dissertation, Syracuse University
16. Zaneldin and EL-Ariss. (2010). Fibre Reinforced Polymer Materials in Construction Applications. *Journal of Civil Engineering and Science.*
17. Kong, S. and Frangopol, M. (2003), Life-cycle reliability-based maintenance cost optimization of deteriorating structures with emphasis on bridges," *Journal of Structural Engineering*, 129(6), 818-828.
18. Karbhari and Vistasp, M. (2003). Durability of FRP composites for civil infrastructure myth, mystery or reality. *Advances in Structural Engineering*, 6, 243-255.
19. Youssef, T. (2010). Time-dependent behaviour of fibre reinforced polymer (FRP) bars and FRP reinforced concrete beams under sustained load", Ph.D. dissertation, University of Sherbrooke
20. Chen, Y., Davalos, J.F. and Ray, I. (2006). Durability prediction for GFRP reinforcing bars using short-term data of accelerated aging tests. *Journal of Composites for Construction*, 10(4), pp.279-286.
21. Carra, G. and Carvelli, V. (2015). Long-term bending performance and service life prediction of pultruded Glass Fibre Reinforced Polymer composites. *Composite Structures*, 127, pp.308-315.
22. Chen, Y., Davalos, J.F., Ray, I. and Kim, H.Y. (2007). Accelerated aging tests for evaluations of durability performance of FRP reinforcing bars for concrete structures. *Composite Structures*, 78(1), pp.101-111.
23. Zhou, J., Chen, X. and Chen, S. (2011). Durability and service life prediction of GFRP bars embedded in concrete under acid environment. *Nuclear Engineering and Design*, 241(10), pp.4095-4102.
24. Al-Salloum, Y.A., El-Gamal, S., Almusallam, T.H., Alsayed, S.H. and Aqel, M. (2013). Effect of harsh environmental conditions on the tensile properties of GFRP bars. *Composites Part B: Engineering*, 45(1), pp.835-844.
25. Benmokrane, B., Elgabbas, F., Ahmed, E.A. and Cousin, P. (2015). Characterization and comparative durability study of glass/vinyl ester, basalt/vinyl ester, and basalt/epoxy FRP bars. *Journal of Composites for Construction*, 19(6), p.04015008.
26. Micelli, F., and Tegola, A. L. (2004) Durability of GFRP Rods in Water and Alkaline Solution. *Proceedings of the First International Conference on Innovative Materials and Technologies for Construction and Restoration*, Lence, June 6-9, pp 365-374.

27. Sawpan, M.A., Mamun, A.A. and Holdsworth, P.G. (2014). Long-term durability of pultruded polymer composite rebar in concrete environment. Materials & Design, 57, pp.616-624
28. Nkurunziza, G., Benmokrane, B., Debaiky, A.S. and Masmoudi, R., (2005). Effect of sustained load and environment on long-term tensile properties of glass fibre-reinforced polymer reinforcing bars. *ACI structural journal*, 102(4), p.615.
29. Helbling, C. and Karbhari, V.M., (2005). Durability assessment of combined environmental exposure and bending. *ACI Special Publication*, 230, pp.1397-1418.
30. Kotani, M., Yasufuku, Y., Tamaishi, Y. and Kawada, H. (2010). Study of strength degradation mechanism of woven GFRP in water environment. *Journal of Solid Mechanics and Materials Engineering*, 4(11), pp.1574-1584.
31. Karbhari, V.M., Chin, J., Hunston, D., Benmokrane, B., Juska, T., Morgan, R., Lesko, J.J., Sorathia, U. and Reynaud, D., (2003). Durability gap analysis for fibre-reinforced polymer composites in civil infrastructure. *Journal of composites for construction*, 7(3), pp.238-247.
32. Taly, N. and Gangarao, H.V.S. (2001). Bond behaviour of FRP reinforcing bars- the-state-of-the-art. Society for the Advancement of Material and Process Engineering, 2001: A *Materials and Processes* Odyssey, pp.1784-1796.
33. Thomason, J.L., (1995). The interface region in glass fibre-reinforced epoxy resin composites: 2. Water absorption, voids and the interface. *Composites*, 26(7), pp.477-485.
34. Adimi, R., and Boukhili, R. (1998). Influence of Resin and Temperature on the Interlaminar Shear Fatigue of Glass Fibre Reinforced Composite Rods. Durability of Fibre Reinforced Polymer (FRP) *Composites for Construction*, Proceeding of the First International Conference (CDCC' 98), August, pp 681-690.
35. Chu, W. and Karbhari, V. M. (2005). Effect of Water Sorption on Performance of Pultruded E-Glass/Vinyl ester Composites. *Journal of Materials in Civil Engineering*, January/February, pp 63-71.
36. Do Remus, R.H., Mehrotra, Y., Lanford, W.A. and Burman, C., (1983). Reaction of water with glass: influence of a transformed surface layer. Journal of Materials Science, 18(2), pp.612-622
37. Perera, G., Doremus, R. H. & Lanford, W. (1991). Dissolution Rates of Silicate Glasses in Water at pH 7. *Journal of the American Ceramic Society*, 74, 1269-1274.

38. Nishizaki, I. and Meiarashi, S. (2002). Long-Term Deterioration of GFRP in Water and Moist Environment. *Journal of Composites for Construction*, 6, 21-27.
39. Hayes, M. D., Garcia, K., Verghese, N., Lesko, J.J. (1998). The Effect of Moisture on the Fatigue Behaviour of a Glass Vinyl Ester Composite, *Second international Conference on Composites in Infrastructure*, lCCl 98, USA.
40. OH, H. S., Moon, D. Yand Kim, S. D. (2011). An Investigation on Durability of Mixture of Alkali-Resistant Glass and Epoxy for Civil Engineering Application. *Procedia Engineering*, 14, 2223-2229.
41. Varghese, N.E., Hayes, M., Garrier, C., Wood, J. and Lesko,J.J.(1998), Tempererture sequencing during hygrothermal aging of polymer and polymer matrix composites: the reverse thermal effect, *proceeding of the 2nd international conference on fibre composites in infrastructure ICCI`98*, Vol. 2, 720-739
42. Zheng, Q. and Morgan, R. J. (1993). Synergistic Thermal-Moisture Damage Mechanisms of Epoxies and Their Carbon Fiber Composites. *Journal of Composite Materials*, 27, 1465-1478.
43. Saadatmanesh, H. and Tannous, F., (1997). Durability of FRP rebars and tendons. In *Proceedings of the 3rd International Symposium on Non-Metallic (FRP) Reinforcement for Concrete Structures* (Vol. 2, pp. 147-154).
44. Chin, J.W., Nguyen, T. and Aouadi, K. (1997). Effects of environmental exposure on fibre-reinforced plastic (FRP) materials used in construction. *Journal of Composites*, Technology and Research, 19(4), pp.205-213.
45. Chen, Y., Davalos, J. F., Ray, I., and Kim, H. Y. (2005) "Accelerated Aging Tests for Evaluation of Durability Performance of FRP Reinforcing Bars for Concrete Structures" *Composite Structures*, Vol. 29, September, pp 1-11.
46. Yilmaz, V. T. (1992) Chemical Attack on Alkali-Resistant Fibres in a Hydrated Cement Matrix: Characterisation of Corrosion Products." *Journal of Non-Crystalline Solids*, Vol. 151, pp 236-244.
47. Kajorncheappunngam, S., Gupta, R. K., and Gangarao, H. V. S. (2002) "Effect of Aging Environment on Degradation of Glass-Reinforced Epoxy." *Journal of Composites for Construction*, February, pp 61-69.
48. Serbescu, A., Guadagnini, M. and Pilakoutas, K. (2014). Mechanical characterization of basalt FRP rebars and long-term strength predictive model. *Journal of Composites for Construction*, 19(2), p.04014037.

49. Steckel, G. L., Hawkins, G. F., and Bauer, J. L. (1998) Environmental Durability of Composites for Seismic Retrofit of Bridge Columns." Fibre Composites in Infrastructure, *Proceedings of the Second International Conference on Fibre Composites in Infrastructure ICCI'98*, Vol. 2, Tucson, pp. 460-475.
50. Almenara, P. C., and Thornburrow, P. (2004) A New Glass Fibre Reinforcement for Anti Corrosion Composites. Advanced Polymer *Composites for Structural Applications in Construction* – ACIC, Edited by Hollaway, L. C., and Chryssanthopoulos, M. K., Woodhead Publishing, Cambridge, pp 319-326.
51. Chu, W., Wu, L. and Karbhari, V. M. (2004) Durability Evaluation of Moderate Temperature and E-glass/vinylester Systems. *Composite Structures*, 66, pp 367-376.
52. Robert, M. and Benmokrane, B. (2013). Combined effects of saline solution and moist concrete on long-term durability of GFRP reinforcing bars. *Construction and Building Materials*, 38, pp.274-284.
53. Robert, M., Cousin, P. and Benmokrane, B., (2009). Durability of GFRP reinforcing bars embedded in moist concrete. *Journal of Composites for Construction*, 13(2), pp.66-73.
54. Kamal, A.S.M. and Boulfiza, M., (2010). Durability of GFRP rebars in simulated concrete solutions under accelerated aging conditions. *Journal of Composites for Construction*, 15(4), pp.473-481.
55. Mufti, A.A., Onofrei, M., Benmokrane, B., Banthia, N., Boulfiza, M., Newhook, J., Bakht, B., Tadros, G. and Brett, P., (2005). Report on the studies of GFRP durability in concrete from field demonstration structures. *In Proceedings of the Conference on Composites in Construction* (pp. 11-13).
56. Katsuki, F., and Uomoto, T. (1995). Prediction of Deterioration of FRP Rods due to Alkali Attack. *Proceedings of the Second International RILEM Symposium (FRPRCS-2)*, Non-Metallic (FRP) Reinforcement for Concrete Structures, L. Taerwe, ed., E&FN Spon, London, pp. 83-89.
57. Bakis, C. E., Freimanis, A. J., Gremel, D., and Nanni, A. (1998) Effect of Resin Material on Bond and Tensile Properties of Unconditioned and Conditioned FRP Reinforcement Rods. Durability of Fibre Reinforced Polymer (FRP) Composites for Construction, *Proceeding of the First International Conference (CDCC' 98*), August, pp 525-535.
58. Coomarasamy, A. and Ip, A. K. C. (1998) Evaluation of Fibre Reinforced Plastic (FRP) Materials for Long-term Durability in Concrete Structures." *Proceedings of the First*

International conference on durability of fibre reinforced polymer (FRP) composites for construction, Sherbrooke, August, pp 325-336.

59. Alsayed, S., and Alhozaimy, A. (1998). Effect of High Temperature and Alkaline Solutions on the Durability of GFRP Bars. *Proceedings of the First International Conference on Durability of Fibre Reinforced Polymer (FRP) Composites for Construction*, Sherbrooke, August, pp 623-634.
60. Micelli, F. and Nanni, A. (2004). Durability of FRP rods for concrete structures. *Construction and Building materials*, 18(7), pp.491-503.
61. Sheard, P., Clarke, J. L., Dill, M., Hammersley, G., and Richardson, D. (1997) "Eurocrete - Taking Account of Durability for Design of FRP Reinforced Concrete Structures." Non-Metallic (FRP) Reinforcement for Concrete Structures, *Proceeding of the Third International Symposium*, Vol. 2, October, pp 75-82.
62. Masmoudi, R., Masmoudi, A., Ouezdou, M.B. and Daoud, A. (2011). Long-term bond performance of GFRP bars in concrete under temperature ranging from 20 C to 80 C. *Construction and Building Materials*, 25(2), pp.486-493.
63. Mills, R. H. (1981) "Preferential Precipitation of Calcium Hydroxide on Alkali-Resistant Glass Fibres" *Cement and Concrete Research*, Vol. 11, pp. 689-697.
64. Yilmaz, V. T., and Glasser, F. P. (1991) Reaction of Alkali-Resistant Glass Fibres with Cement. Part 2. Durability in Cement Matrices Conditioned with Silica Fume." Glass Technology, Vol. 32, No. 4, August, pp 138-147.
65. Lea, F. M. (2001) "The Chemistry of Cement and Concrete." London, Arlond.
66. Andersson, K., Allard, B., Bengtsson, M., and Magnusson, B. (1989) Chemical Composition of Cement Pore Solutions." *Cement and Concrete Research*, Vol. 19, pp 327-332.
67. Taylor, H. F. W. (1990) "Cement Chemistry" Thomas Telford, 2nd Edition.
68. Karbhari, V.M., (2002). Response of fibre reinforced polymer confined concrete exposed to freeze and freeze-thaw regimes. *Journal of composites for construction*, 6(1), pp.35-40.
69. Al-Cheikh, A., and Murat, M. (1988). Kinetics of Non-Congruent Dissolution of E-Glass in Saturated Calcium Hydroxide Solution. *Cement and Concrete Research*, Vol. 18, No. 6, pp 943-950.
70. Almusallam, T.H., Al-Salloum, Y.A., Alsayed, S.H. and Alhozaimy, A.M., (2002). Tensile strength of GFRP bars in concrete beams under sustained loads at different

environments. In Second International Conference on Durability of Fiber Reinforced Polymer (FRP) *Composites for Construction* (pp. 29-31).

71. Giernacky, R. G., Bakis, C. E., Mostoller, J. D., Boothby, T. E., and Mukherjee, A. (2002). Evaluation of Concrete Beams Reinforced with Internal GFRP Bars: A Long-Term Durability Study. *Second International Conference on Durability of Fiber Reinforced Polymer (FRP) Composites for Construction (CDCC 02)*, Montreal, Quebec, Canada, May, pp. 39-45.
72. Svecova, D., Rizkalla, S., Vogel, H. and Jawara, A., (2002). Durability of GFRP in low-heat high performance concrete. *In 2nd International Conference on Durability of Fiber Reinforced Polymer (FRP) Composites for Construction* (pp. 29-31).
73. Mukherjee, A. and Arwikar, S. J. (2005). Performance of Glass Fibre Reinforced Polymer Reinforcing Bars in Tropical Environments - part I: Structural scale tests." *ACI Structural Journal*, 102(5), pp. 745-753.
74. Bakis, C. E., Boothby, T. E., Schaut, R. A., and Pantano, C. G. (2005). Tensile Strength of GFRP Bars under Sustained Loading in Concrete Beams. *Proceedings of the 7th International Symposium. Fibre Reinforced Polymer Reinforcement for Concrete Structures, FRPRCS-7,* American Concrete Institute, pp. 1429-1446.
75. Almusallam, T.H., Al-Salloum, Y.A., Alsayed, S.H., El-Gamal, S. and Aqel, M., (2013). Tensile properties degradation of glass fiber-reinforced polymer bars embedded in concrete under severe laboratory and field environmental conditions. *Journal of Composite Materials*, 47(4), pp.393-407.
76. He, X.J., Dai, L. and Yang, W.R., (2017). Durability and degradation mechanism of GFRP bars embedded in concrete beams with cracks. Plastics, *Rubber and Composites*, 46(1), pp.17-24.
77. Tannous, F.E. and Saadatmanesh, H., (1999). Durability of AR glass fibre reinforced plastic bars. *Journal of Composites for Construction*, 3(1), pp.12-19.
78. Belarbi, A. and Wang, H. (2011). Bond durability of FRP bars embedded in fibre-reinforced concrete. *Journal of Composites for Construction*, 16(4), pp.371-380.
79. Gangarao, H.V.S. and Vijay, P.V. (1997). Aging of structural composites under varying environmental conditions. *Proc. 3rd Intl. Sym. Non-Metallic (FRP) Reinforcement for Concrete Structures (FRPRCS-3)*, Sapporo, Japan, October 14–16, Vol. 2, pp. 91–98.
80. Vijay P.V. and GangaRao, H.V.S. (1998). Accelerated aging and durability of GFRP bars. *CDCC '98*, Sherbrooke, Canada, August.

81. Vijay P.V. and GangaRao, H.V.S. (1998), "Creep behavior of concrete beams reinforced with GFRP bars," *CDCC '98*, to be held in August, Sherbrooke, Canada.
82. Vijay, P.V. and GangaRao, H.V.S., (1999). Accelerated and natural weathering of glass fiber reinforced plastic bars. *Special Publication*, 188, pp.605-614.
83. Spainhour, L.K. and Thompson, I. (1998). Effect of carbon fibre jackets on reinforced concrete columns exposed to a simulated tidal zone. *In Second International Conference on Fibre Composites in Infrastructure* (Vol. 1).
84. Mukhopadhyaya, P., Swamy, R.N. and Lynsdale, C.J., (1998). Influence of aggressive exposure conditions on the behaviour of adhesive bonded concrete–GFRP joints. *Construction and Building Materials*, 12(8), pp.427-446.
85. Adimi, R., Rahman, H., Benmokrane, B. and Kobayashi, K., (1998). Durability of FRP reinforcements under tension axial cyclic loading. In first International Conference on durability of fibre reinforced polymer (FRP) composites for construction, Sherbrook, pp 635-647.
86. Wu, L., Murphy, K., Karbhari, V.M. and Zhang, J.S., (2002). Short-term effects of sea water on E-glass/vinylester composites. Journal of applied polymer science, 84(14), pp.2760-2767.
87. Alsayed, S.H., Alhozaimy, A.M., Al-Salloum, Y.A. and Almusallam, H. (2002). Durability of the new generation of GERP rebars under severe environments.
88. Almusallam, T.H. and Al-Salloum, Y.A., (2006). Durability of GFRP rebars in concrete beams under sustained loads at severe environments. *Journal of composite materials*, 40(7), pp.623-637.
89. Al-Zahrani, M. (2007). Tensile strength degradation of glass fibre reinforced polymer bars in aggressive solutions both as stand-alone and cast-in-concrete. *In Proceedings of the eighth International Conference on FRP reinforcement for concrete structures* (pp. 16-18).
90. Kim, H.Y., Park, Y.H., You, Y.J. and Moon, C.K., (2008). Short-term durability test for GFRP rods under various environmental conditions. *Composite structures*, 83(1), pp.37-47.
91. Wright, D., (2001). Failure of plastics and rubber products: causes, effects and case studies involving degradation. *iSmithers Rapra* Publishing.
92. Katz, A. and Berman, N., (2000). Modeling the effect of high temperature on the bond of FRP reinforcing bars to concrete. *Cement and Concrete Composites*, 22(6), pp.433-443.

93. Katz, A., Berman, N. and Bank, L.C., (1999). Effect of high temperature on bond strength of FRP rebars. *Journal of Composites for Construction*, 3(2), pp.73-81.
94. Mallick, P.K., (2007). Fibre-reinforced composites: materials, manufacturing, and design. CRC press.
95. Katz, A., Berman, N. and Bank, L.C., (1998). Effect of cyclic loading and elevated temperature on the bond properties of FRP rebars. *In International Conference on the Durability of Fiber Reinforced Polymer (FRP) Composites for Construction*, Sherbrooke, Québec (pp. 403-413).
96. Wang, Y.C., Wong, P.M.H. and Kodur, V. (2007). An experimental study of the mechanical properties of fibre reinforced polymer (FRP) and steel reinforcing bars at elevated temperatures. *Composite Structures*, 80(1), pp.131-140.
97. Robert, M., Wang, P., Cousin, P. and Benmokrane, B., (2010). Temperature as an accelerating factor for long-term durability testing of FRPs: Should there be any limitations?. *Journal of Composites for Construction*, 14(4), pp.361-367.
98. Gentry, T.R. and Husain, M., (1999). Thermal compatibility of concrete and composite reinforcements. *Journal of Composites for Construction*, 3(2), pp.82-86.
99. Elbadry, M.M., Abdalla, H. and Ghali, A., (2000). Effects of temperature on the behaviour of fiber reinforced polymer reinforced concrete members: experimental studies. Canadian *Journal of Civil Engineering*, 27(5), pp.993-1004.
100. Balázs, G.L. and Borosnyói, A., 2001. Long-term behavior of FRP. In Composites in Construction: A Reality (pp. 84-91).
101. Halliwell, S.M., (2000). Polymer composites in construction. CRC.
102. Gentry, T.R. and Hudak, C.E. (1996). Thermal compatibility of plastic composite reinforcement and concrete. *Advanced Composite Materials in Bridges and Structures*, MM El-Badry, ed., Canadian Society for Civil Engineering, Montreal, Quebec, pp.149-156.
103. Dutta, P.K., Hui, D., and Prasad, Y. (1994), Influence of subfreezing temperatures on the flexural behaviour of thick composites, *2nd Biennial European Joint Conf. Eng. Sys. Des. Analy. (ESDA)*, Queen Mary and Westfield College, University of London
104. Grammatikos, S. A., R. G. Jones, M. Evernden and J. R. Correia (2016). Thermal cycling effects on the durability of a pultruded GFRP material for off-shore civil engineering structures. *Composite Structures* 153: 297-310.

105. Benmokrane, B. and Mohamed, H.M. (2013). June. Durability issues of FRP for civil infrastructure. *In 11th International Symposium on Fibre Reinforced Polymers for Reinforced Concrete Structures (FRPRCS11)*. Guimaraes2013 (pp. 11-4).
106. Allred, R.E. (1981). The effect of temperature and moisture content on the flexural response of Kevlar/epoxy laminates: Part II. [±45, 0/90] filament orientation. *Journal of Composite Materials*, 15(2), pp.117-132.
107. Kumar, S.V. and GangaRao, H.V. (1998). Fatigue response of concrete decks reinforced with FRP rebars. Journal of Structural Engineering, 124(1), pp.11-16.
108. Kelen, T., 1983. Polymer degradation. Van Nostrand Reinhold Co
109. Lagrange, A., Melennec, C. and Jacquemet, R. (1990). Influence of various stress conditions of the moisture diffusion of composites in distilled water and in natural sea-water. Durability of polymer based composite systems for structural applications, pp.385-392.
110. Chateauminois, A., Chabert, B., Soulier, J.P., and Vincent, L.(1993). Effects of hygrothermal aging on the durability of glass/epoxy composites. Physico-chemical analysis and damage mapping in static fatigue, *Proc. ICCM* '93, 1993.
111. GangaRao, H.V.S., Vijay, P.V., Gupta, R.K., and Barbero, E.(2001) Mechanical-hygrotheramal responses and predictive models for FRP composites-state-of-the-art review submitted to US Army Corps of Engineers, *Engineer Research and Development Centre, Construction Engineering Research Laboratory*, CFC-Report No. 02-100,01.
112. Leu, B.L., Dolan, C.W. and Hundley, A. (1997). Creep-rupture of fiber reinforced plastics in a concrete environment (Vol. 2, p. 187). *FRPRCS-3*.
113. Clarke, J.L. and Sheard, P., (1998). Designing durable FRP reinforced concrete structures. *In Proceedings of the 1st International Conference on Durability of Fibre Reinforced Polymer (FRP) Composite for Construction*. Sherbrooke, Quebec, Canada (pp. 13-24).
114. Nkurunziza, G., Cousin, P., Masmoudi, R. and Benmokrane, B., (2003). Effect of sustained tensile stress and temperature on GFRP composite bars properties: 1. Preliminary experiment in deionised water and alkaline solution. *International Journal of Materials and Product Technology*, *19*(1-2), pp.15-27.
115. ACI Committee 440 (2003). Guide for the Design and Construction of Concrete Reinforced with FRP Bars (ACI 440.1R-03), *American Concrete Institute*, Farmington Hills, Michigan, 42 pp

116. Bakis, C.E., (2011). Durability of GFRP reinforcement bars. *In Advances in FRP Composites in Civil Engineering* (pp. 33-36). Springer Berlin Heidelberg.
117. He, X., Yang, J. and Bakis, C.E., (2013). Tensile strength characteristics of GFRP bars in concrete beams with work cracks under sustained loading and severe environments. *Journal of Wuhan University of Technology-Mater*. Sci. Ed., 28(5), pp.934-937
118. Wang, J., GangaRao, H., Liang, R., Zhou, D., Liu, W. and Fang, Y. (2015). Durability of glass fiber-reinforced polymer composites under the combined effects of moisture and sustained loads. *Journal of Reinforced Plastics and Composites*, 34(21), pp.1739-1754.
119. Katsuki, F. and Uomoto, T., (1997). Evaluation of alkali resistance of GFRP Rods. Concrete library international, (29), pp.283-292.
120. Porter, M. L., and Barnes, B. A. (1998) Accelerated Durability of FRP Reinforcement for Concrete Structures. Durability of Fibre Reinforced Polymer (FRP) Composites for Construction, *Proceeding of the First International Conference (CDCC' 98)*, August, pp 191-201.
121. Khelifi, O., and Nanni, A. (2004) Effects of Different Coatings on the Durability of Thermoplastic E-glass FRP Bar. *Proceedings of the First International Conference on Innovative Materials and Technologies for Construction and Restoration*, Lence, June 6-9, pp 210-222.
122. Gremel, D., Galati, N., and Stull, J. (2005) Method for Screening Durability and Constituent Materials in FRP Bars *Proceedings of the Seventh International Symposium on Fibre-Reinforced Polymer (FRP) Reinforcement for Concrete Structures* (SP-230-9), pp 153-164.
123. Benmokrane, B., Rahman, H., Ton-That, M. T., and Robert, J. F. (1998). Improvement of the Durability of FRP Reinforcements for Concrete Structures." *Proceedings of the First International Conference on Durability of Fibre Reinforced Polymer (FRP) Composites for Construction*, Sherbrooke, August, pp 571-
124. Mufti, A. A., Onofrei, M., Benmokrane, B., Banthia, N., Boulfiza, M., Newhook, J. P., Bakht, B., Tadros, G. S., and Brett, P. (2007). "Field Study of Glass-Fibre-Reinforced Polymer Durability in Concrete." *Canadian Journal of Civil Engineering*, 34(3), pp. 355-366.
125. Davalos, J.F., Chen, Y. and Ray, I., (2012). Long-term durability prediction models for GFRP bars in concrete environment. *Journal of Composite Materials*, 46(16), pp.1899-1914.

126. Trejo, D., Aguiniga, F., Yuan, R., James, R. W., and Keating, P. B. (2005). Characterization of Design Parameters for Fiber Reinforced Polymer Composite Reinforced Concrete Systems, *Texas Transportation Institute Research Report* 9-1520-3.
127. Weber, A. and Jütte, B., (2007) how to determine safe design values for FRP reinforcement in different exposure conditions?. *Technical report*.
128. Weber, A., (2013). From national approval to an European standard-Ways to a safer and wider application of FRP rebars. Univ. of Minho, Guimaraes, Portugal.
129. Phifer, S. and Lesko, J.J., (2002). Moisture absorption and strength characterization of hygrothermally aged neat and clay filled vinyl ester and pultruded vinyl ester e-glass laminates. In Proc., *2nd Int. Conf. on Durability of Fibre Reinforced Polymer (FRP) Composites for Construction (CDCC'02*) (pp. 485-497).
130. Shen, C.H. and Springer, G.S. (1976). Moisture absorption and desorption of composite materials. *Journal of Composite Materials*, 10(1), pp.2-20.
131. Nanni, A., Bakis, C. E., and Mathew, J. A. (1998) "Acceleration of FRP Bond Degradation." Proceedings from *the First International Conference on Durability of Fibre Reinforced Polymer (FRP) Composites for Construction*, Sherbrooke, August, pp 45-56.
132. Tighiouart, B., Benmokrane, B., and Gao, D. (1998) Investigation of Bond in Concrete Member with Fibre Reinforced Polymer (FRP) Bars." *Construction and Building Materials*, Vol. 12, pp 453-462.
133. Davalos, J.F., Chen, Y. and Ray, I., (2008). Effect of FRP bar degradation on interface bond with high strength concrete. *Cement and Concrete Composites*, 30(8), pp.722-730.
134. Bakis, C.E., Al-Dulaijan, S.U., Nanni, A., Boothby, T.E. and Al-Zahrani, M.M., (1998). Effect of cyclic loading on bond behavior of GFRP rods embedded in concrete beams. *Journal of Composites*, Technology and Research, 20(1), pp.29-37.
135. Shahidi, F., Wegner, L.D. and Sparling, B.F. (2006). Investigation of bond between fibre-reinforced polymer bars and concrete under sustained loads. *Canadian Journal of Civil Engineering*, 33(11), pp.1426-1437.
136. Robert, M., and Benmokrane, B., (2010).Effect of aging on bond of GFRP bars embedded in concrete, *Cement and concrete composites*, 2010, v32, pp.461-467.
137. GangaRao, H.V., Taly, N. and Vijay, P.V., (2006). Reinforced concrete design with FRP composites. CRC press.

138. Mias, C., Torres, L., Guadagnini, M. and Turon, A. (2015). Short and long-term cracking behaviour of GFRP reinforced concrete beams. *Composites Part B: Engineering*, 77, pp.223-231.
139. Mias, C., Torres, L., Turon, A. and Sharaky, I.A. (2013). Effect of material properties on long-term deflections of GFRP reinforced concrete beams. *Construction and Building Materials*, 41, pp.99-108.
140. Brown, V. (1997). October. Sustained load deflections in GFRP-reinforced concrete beams. *In Proceedings of the Third Int. Symposium on Non-Metallic (FRP) Reinforcement for Concrete Structures (FRPRCS-3)* (Vol. 2, pp. 495-502).
141. Brown, V.L. and Bartholomew, C.L. (1996). January. Long-term deflections of GFRP-reinforced concrete beams. *In first international conference on composites in infrastructure*.
142. Liew, Y.S. and Tan, K.H. (2003). Durability of GFRP Composites under Tropical Climate. *In Fibre-Reinforced Polymer Reinforcement for Concrete Structures*: (In 2 Volumes) (pp. 769-778).
143. Saha, M.K. and Tan, K.H. (2005), October. GFRP-Bonded RC beams under sustained loading and tropical weathering. *In 7th International Symposium on FRP Reinforcement for Concrete Structures (FRPRCS-7)* Kansas City, MO, USA (pp. 1379-1396).
144. Laoubi, K., El-Salakawy, E. and Benmokrane, B. (2006). Creep and durability of sand-coated glass FRP bars in concrete elements under freeze/thaw cycling and sustained loads. *Cement and Concrete Composites*, 28(10), pp.869-878.
145. ACI ,2006, Guide for the Design and Construction of Concrete Reinforced with FRP Bars, American Concrete Institute, Committee 440. Farmington Hills, MI, USA.
146. Almusallam, T.H., (2006). Load–deflection behaviour of RC beams strengthened with GFRP sheets subjected to different environmental conditions. *Cement and Concrete Composites*, 28(10), pp.879-889.
147. Nkurunziza, G., Debaiky, A., Cousin, P. & Benmokrane, B. (2005). Durability of GFRP bars: A critical review of the literature. *Progress in Structural Engineering and Materials*, 7, 194-209.

CHAPTER 3

3 EXPERIMENTAL METHODOLOGY

3.1 INTRODUCTION

The experimental programme was designed to quantify the long-term deterioration in mechanical properties due to environmental exposure and sustained loading. A complementary set of physical, chemical and mechanical tests was carried out to enable a more comprehensive assessment of the different time-dependant degradation processes. Figure 3.1 presents a flow chart summarising the entire experimental programme, including the type of tests conducted in this study, the parameters examined through each of these tests, and the main objective of the study, which is the development of a comprehensive predictive model. The different tests are presented in turn in this chapter, along with the initial characterization of the materials investigated in this work.

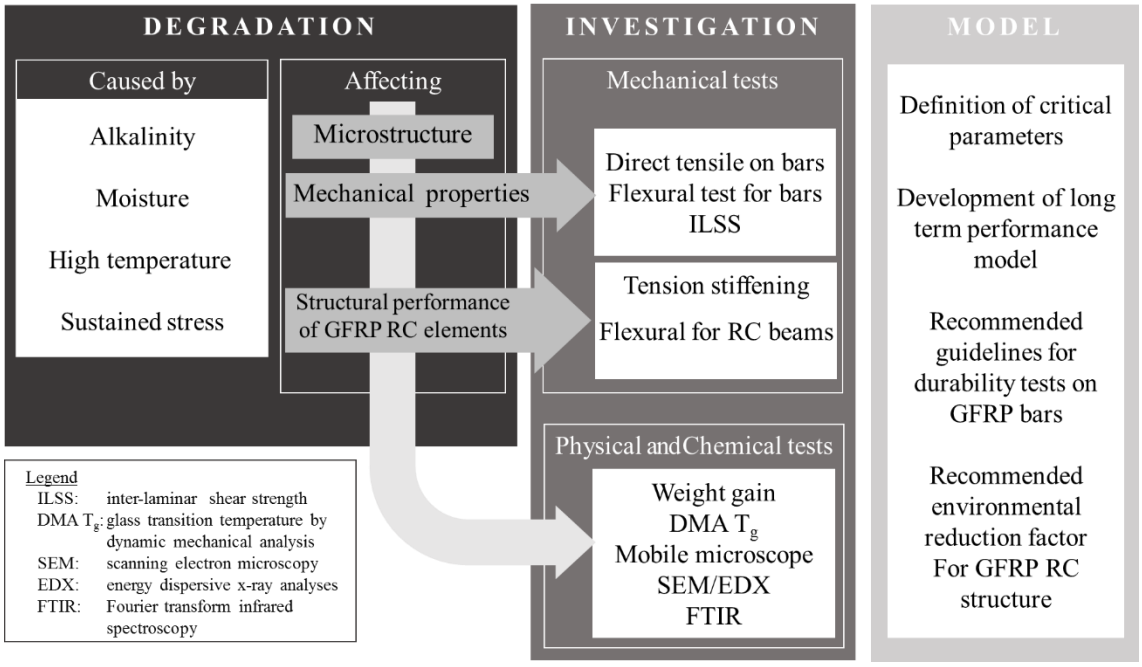

Figure 3. 1: Overview of the experimental program

3.2 TEST SPECIMENS

3.2.1 GFRP bars

The GFRP bars used in this research (ComBAR®) were made of continuous longitudinal E-CR glass fibres (alkali free with high acid corrosion resistance) impregnated in vinyl ester resin with a glass fibre content of 75% by volume and 88% by weight. The bars were manufactured by Schöck using a pultrusion process and had a nominal diameter of 8mm. The bars had a ribbed surface to improve their bond with the surrounding concrete. Table 3.1 summarises averages and standard deviations of ultimate tensile strength, f_{fu}, modulus of elasticity, E_f, and failure strain (ε) obtained from direct tension tests conducted on five specimens according to [1]. Nominal manufacturer values, when available, are also provided in brackets.

Table 3. 1: Reinforcement material properties

Reinforcement		**E_f [GPa]**		**ε [%]**		**f_{fu} [MPa][1]**	
Material	**Size [mm]**	**Avg.**	**St.D.**	**Avg.**	**St.D.**	**Avg.**	**St.D.**
GFRP	Ø8	57 (60)*	1.5	2.8	0.9	1542 (1000)*	28

*Value provided by manufacture in brackets; [1] determined using the nominal diameter as given by the manufacturer

Figure 3. 2: GFRP bars

3.3 CONDITIONING ENVIRONMENT

Non-accelerated as well as accelerated aging tests were conducted by conditioning the specimens in three different environments, simulating alkali pore solution, water and real concrete. The environments used are describe in the following sections.

3.3.1 Alkali solution

Alkali solution was chosen to simulate the concrete pore solution and accelerate aging of the GFRP specimens. The alkaline solution comprised 118.5 g of $Ca(OH)_2$, 0.9 g of NaOH and 4.2 g of KOH dissolved in 1 litre of deionised water, giving a pH value of around 13.5 as recommended by ACI 440.3R-04 [1]. The boxes containing alkaline solution were covered with plastic lids and sealed to avoid pH level reduction as a result of evaporation. The pH level of the alkaline solution was checked periodically using a HI8424 pH meter and it was found to be in the range of 13 to 13.5.

Figure 3. 3 : Equipment used and pH measurments

3.3.2 Tap water

A tap water environment was chosen as the bench mark environment to determine the effect of moisture on the deterioration processes of GFRP materials, and gain comparative data against alkaline exposure. The chemical composition of used tap water is presented in Table 3.2.

Table 3. 2: Tap water chemical compositions and properties

Calcium (mg/l)	Magnesium (mg/l)	Fluoride (mg/l)	Aluminium (µg/l)	Iron (µg/l)	Nitrate (mg/l)	Sodium (mg/l)	Copper (mg/l)	pH
3.60	2.20	0.05	33	29.20	1.68	31.40	.01	8.5

Figure 3. 4:Aging specimens in water

3.3.3 Concrete

The beam specimens (BM) were cast using ready mixed concrete provided by a local concrete plant, whilst the concrete used for the specimens to be tested in tension stiffening (TS) and direct tension (DT) was mixed in the laboratory following the same mix design. The concrete mixes were produced using 358 kg/m^3 of cement type CEM I, 1000 kg/m^3 of coarse aggregate with a maximum size of 10 mm, 817 kg/m^3 of sand and 225 kg/m^3 of water. The mechanical properties of the concrete used in this study are summarised in Table 3.3. The average compressive strength of each mix of concrete was evaluated by testing three standard 100mm cubes at the age of 28 days. Meanwhile, the conditioned specimens were cured under the same conditions as the beam specimens and tested on the same day of the first beam test. Some specimens were stored in standard laboratory conditions (about 23°C, 40%RH) , whilst the remainder of the specimens were aged under accelerated conditions, moist environments and at different temperatures ranging from 20°C to 60°C, to expedite the degradation process and to evaluate the acceleration level for the different temperatures. The bars subjected to direct tensile tests were extracted from the concrete after the specified exposure time.

Table 3. 3: Concrete properties

Sample	Conditioning			F_c (MPa)		E_c(GPa)		F_{ct} (MPa)	
	Environment	Temperature	Time (days)	Ave	St.D	Ave	St.D	Ave	St.D
BM	Moist	20°C	28	55	1.4	33	___	3.2	___
TS/DT	Moist	20°C	28	60	5.2	33	___	3.6	___

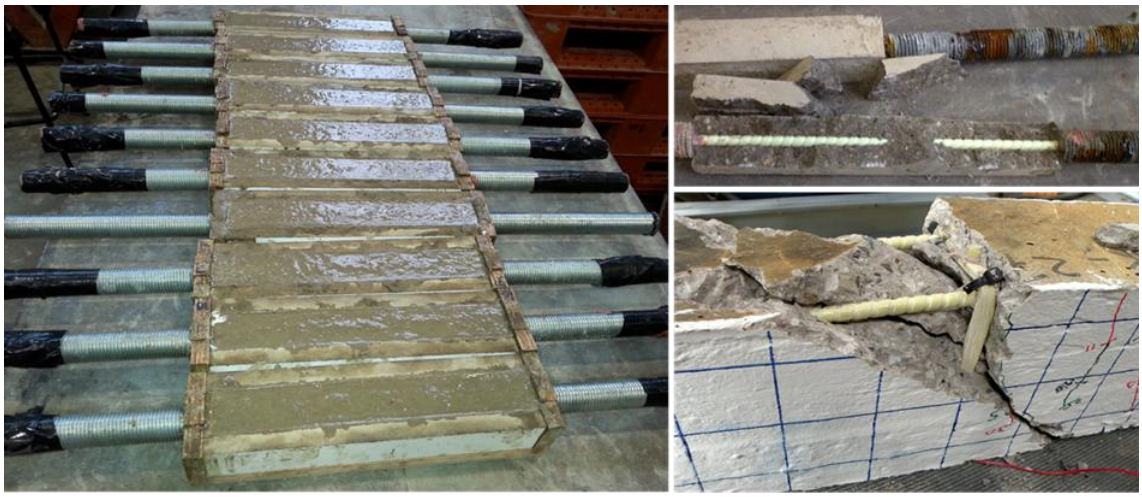

Figure 3. 5: GFRP bars embedded in concrete

3.3.4 Sustained stress

The sustained stress to induce the desired level of tensile strain during conditioning time was applied using three different configurations (Figure. 3.6 1-3): 1) for bare bars the sustained strain was imposed by tying pairs of specimens at the two ends, with a wedge interposed at mid-length to impose the required curvature; 2) for tension stiffening specimens the load was applied via a spring of adequate stiffness mounted in a stiff pre-tensioning rig. Prior to any conditioning, all samples were fitted with appropriate end anchors (threaded steel hollow tubes) filled with epoxy resin that can be mounted directly in the tensile testing machine or in a bespoke pre-tensioning rig. The required sustained strain was imposed by compressing the steel springs by the desired amount (Figure. 3.6); 3) the beams were clamped in pairs back to back using an external rigid frame consisting of transverse steel bolts and steel springs sandwiched between two steel plates as shown in (Figure. 3.6).

A sustained stress inducing a tensile strain of 3000 με was selected as representative of in-service conditions (SLS), while a higher stress inducing a strain of 5000 με was examined to assess the effect of less stringent serviceability limits.

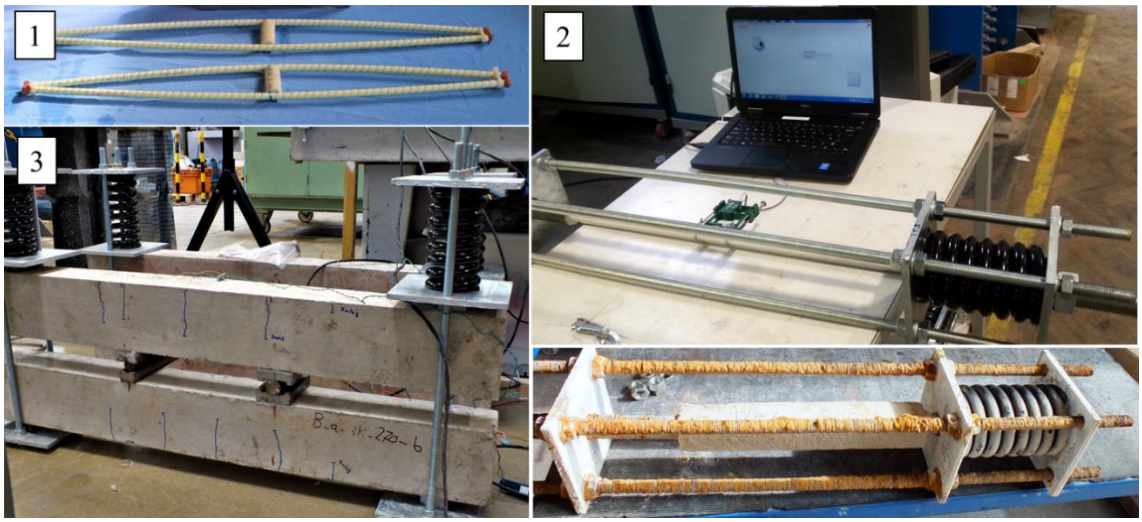

Figure 3. 6: Sustained stress configurations in different tests: 1) water absorption; 2) direct tension; 3) FRP RC beams.

3.3.5 Conditioning temperatures

Three conditioning tanks were used to condition the GFRP bars and GFRP RC specimens at 20°C, 40°C and 60°C respectively. The range of temperatures was chosen so that it represents the real life as well as accelerates the degradation mechanisms. The 20°C represents the average service life temperature of GFRP bars in the internal application. Whereas the 60°C was chosen as it is high enough to accelerate the degradation process yet still below the glass transition temperature expected of GFRP bars. While the 40°C has been chosen to produce the intermediate temperature and to gain additional insight into the effect of temperature on the degradation mechanisms. This temperature is relatively high but below the glass transition of the resins matrix. The length of exposure was also chosen on the basis of previous research employing accelerated tests and it was found to be appropriate to enable the onset and stabilisation of the main degradation processes [2, 3]. Fifteen polypropylene boxes with lids were used to accommodate the specimens conditioned in alkaline solution in these tanks. Each tank contained a heater and water pump to ensure good circulation of water and uniform heat distribution. Before storing the specimens in the tanks, each tank was filled with water up to the desired level and checks were carried out to ensure it was heated to the required temperature. All tanks were insulated on all sides with insulation sheets of 40mm thickness to minimise the heat loss. The temperature of the conditioning tank was checked periodically. After piling the specimens and boxes on the rack in the tank (Figure. 3.3), the top of each tank was covered with a polypropylene lid, so as to minimise heat and moisture loss. The

main objective of aging the specimens at different temperature levels was to determine the degradation rates for a range of temperatures, and their correlation.

3.4 TEST METHODS

The mechanical, physical and chemical properties of conditioned GFRP bars were examined to evaluate how environmental exposure and sustained stress influence GFRP materials. Structural tests on beam and tension tie specimens were also carried out to examine long-term performance of GFRP RC elements (namely in terms of bending and bond performance). In addition, moisture absorption tests were conducted on specimens exposed to tap water and alkaline solution, in some cases under sustained stress. DMA (Dynamic Mechanical Analysis) was performed to determine changes in the glass transition temperature of the GFRP composite over time. Specimens were also investigated using SEM/EDX (Scanning Electron Microscopy/Electron Dispersive X-ray) and FTIR (Fourier transform infrared spectroscopy analysis) to detect signs of physical deterioration or chemical change in the composite material (resin matrix, resin/fibre interface, glass fibre).

3.4.1 Moisture absorption tests

3.4.1.1 Test purpose

To determine the relative rate of absorption of moisture by GFRP bars subjected to aging and exposure conditioning.

3.4.1.2 Specimen preparation

Prior to conditioning, the specimens were dried in an oven at 55°C for 24hr. The unstressed specimens were 300 mm long and the stressed samples 350 mm, with the two ends sealed using Chemfix epoxy to prevent absorption through the sawn ends. The sustained stress to induce the desired level of tensile strain during conditioning time was imposed by tying pairs of specimens at the two ends, with a wedge interposed at mid-length to impose the required curvature. The moisture uptake was monitored monthly using a digital scale with accuracy of 0.001 g. For each set of measurements, the specimens were removed from their respective conditioning environments at the same time, their surface was wiped dry with a cloth, and weighed immediately

3.4.1.3 Set-up

The moisture uptake was monitored monthly using a digital scale with accuracy of 0.001 g. Moisture absorption measurements were carried out periodically according to [4] and the weights

of the GFRP samples were measured monthly to examine the increase due to fluid uptake after exposure. The percentage weight gain was calculated with Eq. 3.1

$$W\% = \frac{(W_{cond} - W_{dry})}{W_{dry}} * 100 \quad (3.1)$$

where

$W\%$=weight gain percentage by total weight due to moisture uptake; W_{cond}=weight of the specimen after its conditioning; and W_{dry}=weight of the dried specimen before conditioning

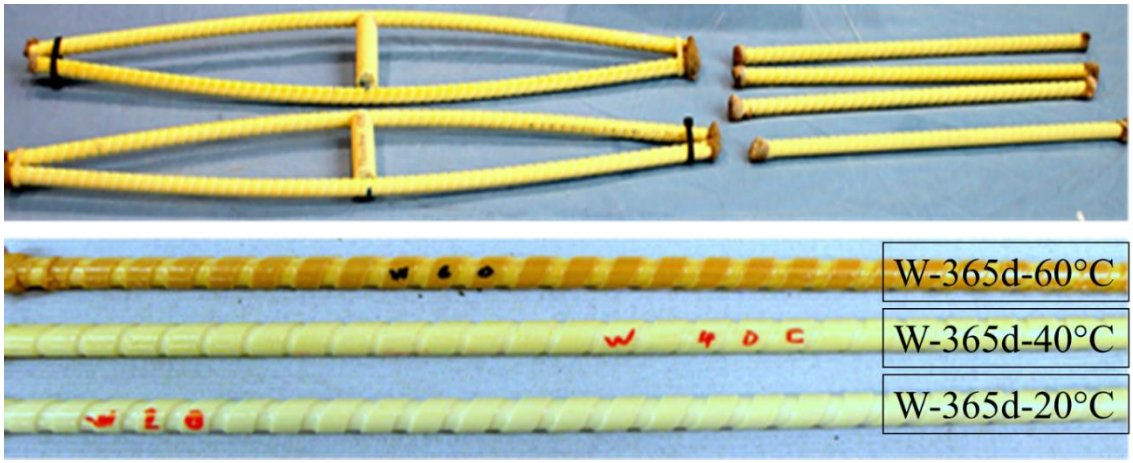

Figure 3. 7: Specimens for the moisture absorption test

3.4.2 Tensile test

3.4.2.1 Test purpose

To determine tensile properties of GFRP bars subject to aging and exposure conditioning, including modulus of elasticity, ultimate tensile stress and ultimate tensile strain (elongation).

3.4.2.2 Specimens preparation

All samples were prepared in accordance to available standards (e.g. American Concrete Institute -ACI 440.3R-04). Prior to any conditioning, all specimens were fitted with appropriate end anchors filled with epoxy resin that could be mounted directly in the tensile testing machine or in a bespoke pre tensioning rig (Figure. 3.8).

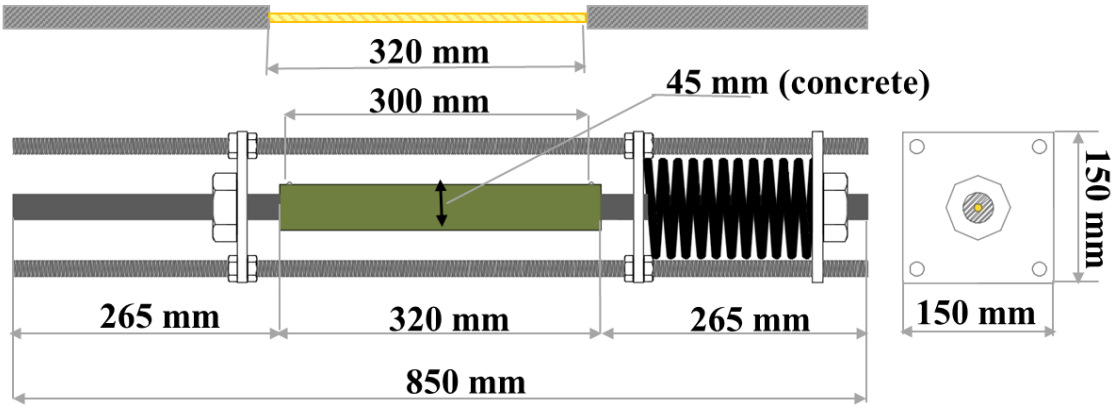

Figure 3. 8: Details of the tensile strength specimens and pre tensioning rig

3.4.2.3 Set-up

Uniaxial tensile loading was applied to all specimens. Testing was performed using a hydraulic universal testing machine with maximum capacity of 1000 kN. The extension (elongation) of the specimen was measured using a clip-on extensometer placed at the mid-length of the specimen. The extensometer was removed after reaching about 50-60% of the expected maximum load to avoid damage of the instrument. The extensometer had a gage length of 51 mm and accuracy of 0.025 mm. The tests were carried out in displacement control at a rate of 1.5 mm/min. The applied load and bar elongation were recorded during the test using a control data acquisition system. The complete stress-strain curves were not available over the entire load history as a result of removing the extensometer before failure. The linear part of the stress-strain curve is used to estimate the elastic modulus of the bar and also extrapolated to determine the corresponding ultimate strain. The test set-up is shown in Figure (3.9).

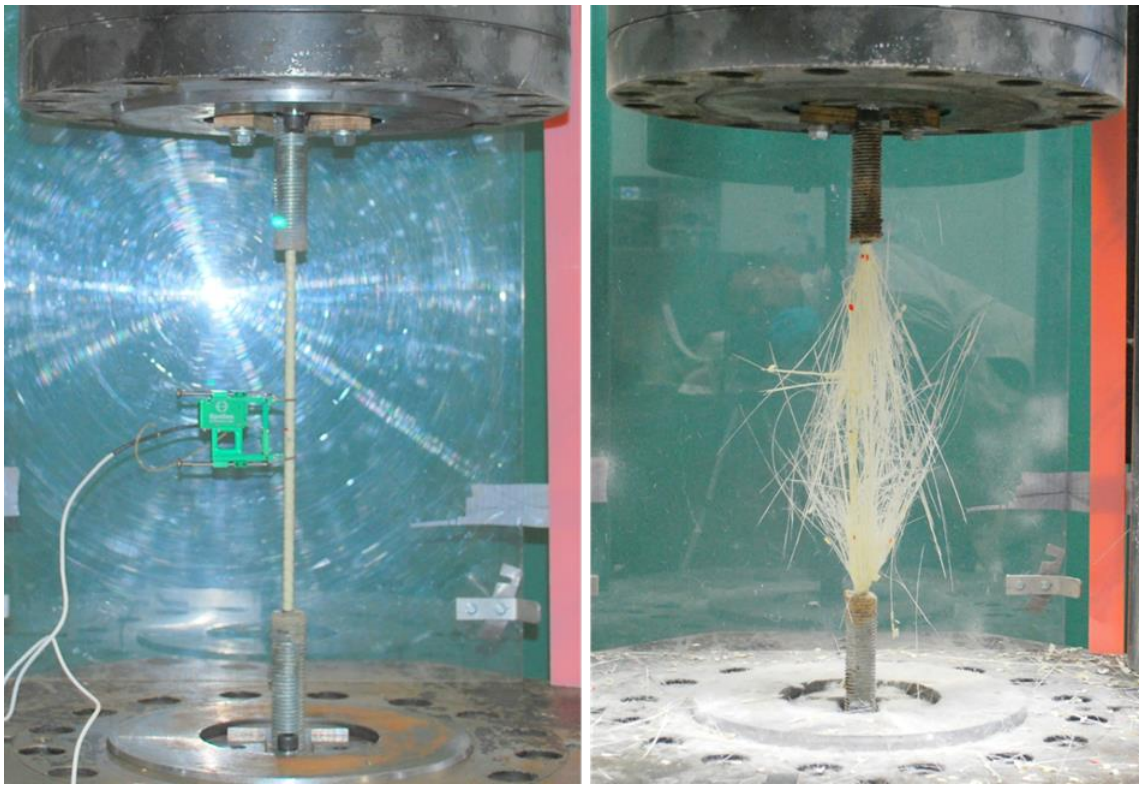

Figure 3. 9: Details of the tensile test set-up and failure mode

3.4.3 Inter-laminar shear test (ILSS)

3.4.3.1 Test purpose

To determine the transverse properties of the resin matrix of FRP rods after aging and exposure conditioning. Average properties including experimental inter-laminar shear strength (ILSS) and failure load (maximum recorded load) [5] were tested.

The *ILSS* was calculated using the following equation:

$$ILSS = 0.849 * \frac{P}{d^2} \quad (3.2)$$

Where

P is the failure load and d is the diameter of the FRP bar.

3.4.3.2 Specimens preparation

Samples were obtained from FRP bars (exposed to all combinations of temperature, aging, exposure and sustained load) so as to have a clear span of 30 mm and a sufficient overhanging

portion. This span was selected in order to obtain the desired inter laminar shear failure All specimens showed the desired failure mode, that is the development of a crack perpendicular to the direction of application of the load. A schematic representation of the ILSS test apparatus is shown in Figure. 3.10.

3.4.3.3 Set-up

The tests were performed in displacement control using a universal testing machine. The load capacity of the machine was 10 kN and the displacement rate of crosshead motion was 1.0 mm/min.

Figure 3. 10: Inter-laminar shear test

3.4.4 Flexural test: FRP bars

3.4.4.1 Test purpose

To determine the flexural properties of FRP bars subject to aging and exposure conditioning, including flexural strength (f_u), flexural modulus of elasticity (E) and maximum tensile strain (ε_u) [ASTM Standard D4476, 2014].

The flexural strength (N/mm^2) was calculated using the following equation:

$$f_u = \frac{P \cdot L \cdot C}{4I} \tag{3.3}$$

where

P is the failure load (N) and *L* is the clear span (mm), *C* is the distance of centroid from extremities (mm) and *I* is the moment of inertia of the bar (mm^4).

The flexural modulus of elasticity (N/mm^2) was calculated using the following equation:

$$E = \frac{PL^3}{48\, I \cdot d} \tag{3.4}$$

where

d is the mid-span deflection at load *P* (mm).

The maximum outer fibre strain (ε_u) was calculated with the following equation:

$$\varepsilon_u = \frac{f_u}{E} \tag{3.5}$$

3.4.4.2 Specimens preparation

Tests were carried out on simply supported specimens with a clear span equal to 16 times the bar diameter (~130 mm Figure. 3.11).

3.4.4.3 Set-up

The tests were performed in displacement control using a universal testing machine. The load capacity of the machine was 10 kN and the displacement rate of crosshead motion was 2.0 mm/min.

Figure 3. 11: Test set-up for flexural test on FRP bars

3.4.5 Glass transition (Tg) temperature

The mechanical properties of FRP materials are highly influenced by their thermal properties. The glass transition temperature (T_g) of FRPs can be defined as the temperature at which the polymer state changes from vitreous to viscoelastic. At this temperature, the mechanical properties decrease as a result of polymer softening. With regards to GFRPs, reduction of the T_g can be caused by rupture of the polymeric chain as a result of hydrolysis in the presence of alkalis and also by the plasticizing impact due to the presence of moisture.

3.4.5.1 Test purpose

To determine the glass transition temperature (T_g) of FRPs subjected to aging and exposure conditioning [7].

3.4.5.2 Specimens preparation

The samples were obtained by cutting the FRP bars to the dimensions recommended by the standard [7] using a high precision diamond blade.

3.4.5.3 Set-up

A Dynamic Mechanical Analyser (DMA) was used to apply a forced oscillation with constant amplitude to the test samples at a fixed frequency. Change in the storage modulus with increasing temperature was obtained by analysis of the flexural mechanical response. The test set-up is shown in Figure. 3.12.

Figure 3. 12: Details of glass transition test using a DMA machine

3.4.6 Scanning Electron Microscopy and Energy-dispersive X-ray spectroscopy (SEM/EDX)

3.4.6.1 Test purpose

To investigate the microstructural and chemical changes in GFRP bars before and after conditioning.

3.4.6.2 Specimens preparation

10 mm-long GFRP bars were cut using low speed diamond blades. The samples were placed vertically in moulds, cast in cold mounting epoxy resin and cured for 24 hours at room temperature. The flat surfaces were first ground using sand papers of decreasing roughness (400 to 1200 grit), and then polished by means of polishing cloths and water and oil diamond pastes (6 and 1 µm). The polishing speed used was about 150 rpm for 5 minutes. Finally, the specimens were coated with carbon. The carbon coating was using to make the specimens conductive to enable and improve the imaging of samples in the electron microscope technique

3.4.6.3 Set-up

SEM/EDX analysis was performed using a focused scanned electron beam from a high magnification microscope (Phillips XL30 SEM) to produce images of the sample at 20Kv.

Figure 3. 13: Details of (Phillips XL30 SEM/EDX) machine

3.4.7 Fourier transform infrared spectroscopy (FTIR)

Hydrolysis is a chemical reaction that can lead to the formation of new hydroxyl groups. In turn, the formation of a hydroxyl chain affects the polymeric chain and weakens the GFRP materials as the resin in the matrix is then unable to transfer the stress to the fibres.

3.4.7.1 Test purpose

To verify by FTIR analysis whether hydrolysis occurs in the resin by measuring the amount of hydroxide groups before and after conditioning.

3.4.7.2 Specimens preparation

Samples to examine the external surface of the GFRP bar were prepared by cutting 30-mm-long samples longitudinally from the bars up to a maximum depth of 3 mm, whilst samples to analyse the internal layers were prepared by grinding the GFRP bars into a fine powder (approximately 2 mg). The milled samples were pressed into a disc after being mixed with approximately 200 mg of anhydrous Potassium Bromide (KBr) (see Figure 3.14). The KBr was used as it does not contain bands in the mid-IR region of the spectrum and it has a transmittance of 100 % in the range of wave number (4000-400 cm-1).

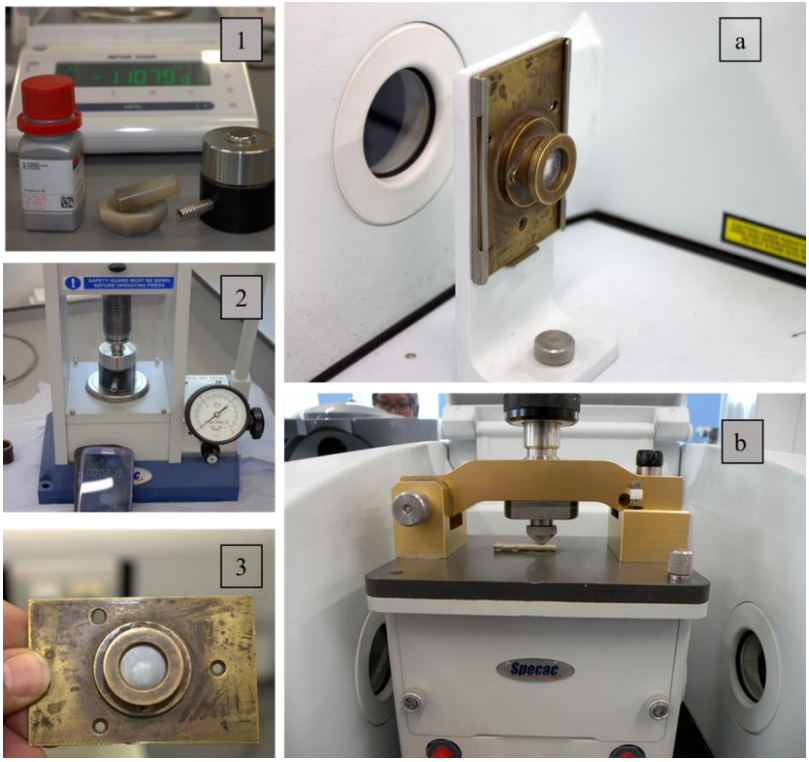

Figure 3. 14: (1, 2, and 3) Preparation of specimens extracted from internal layers, (a) scanning of prepared samples (b) scanning of the external surface of the GFRP bars.

3.4.8 Tension stiffening test

3.4.8.1 Test purpose

To determine the bond properties of GFRP bars with concrete after aging in different exposure conditions as well as to investigate the influence of changing the bond properties on tension stiffening behaviour of GFRP RC elements. The specimen preparation and set-up (Figure 3.15) for this test are discussed in more detail in Chapter 5.

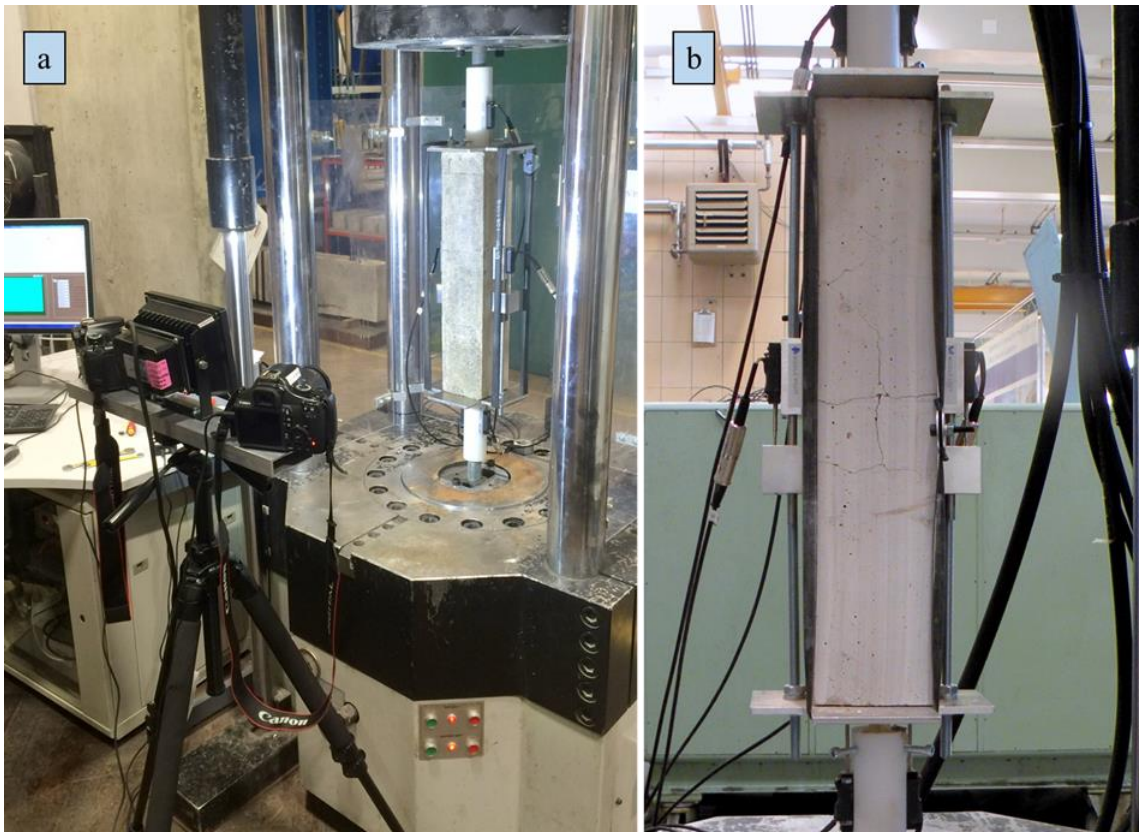

Figure 3. 15: Test set-up for tension stiffening test on GFRP RC specimens (a) DIC measurement (b) measurement by potentiometers.

3.4.9 Flexural test for GFRP RC beam

3.4.9.1 Test purpose

To determine flexural properties of FRP RC members subject to aging and exposure conditioning and sustained stress in order to represent long-term behaviour of GFRP RC in service. Average

properties including experimental mid-span deflection, crack width and moment capacity were examined. The test set-up (Figure 3.16) and loading protocol are explained in detail in Chapter 5.

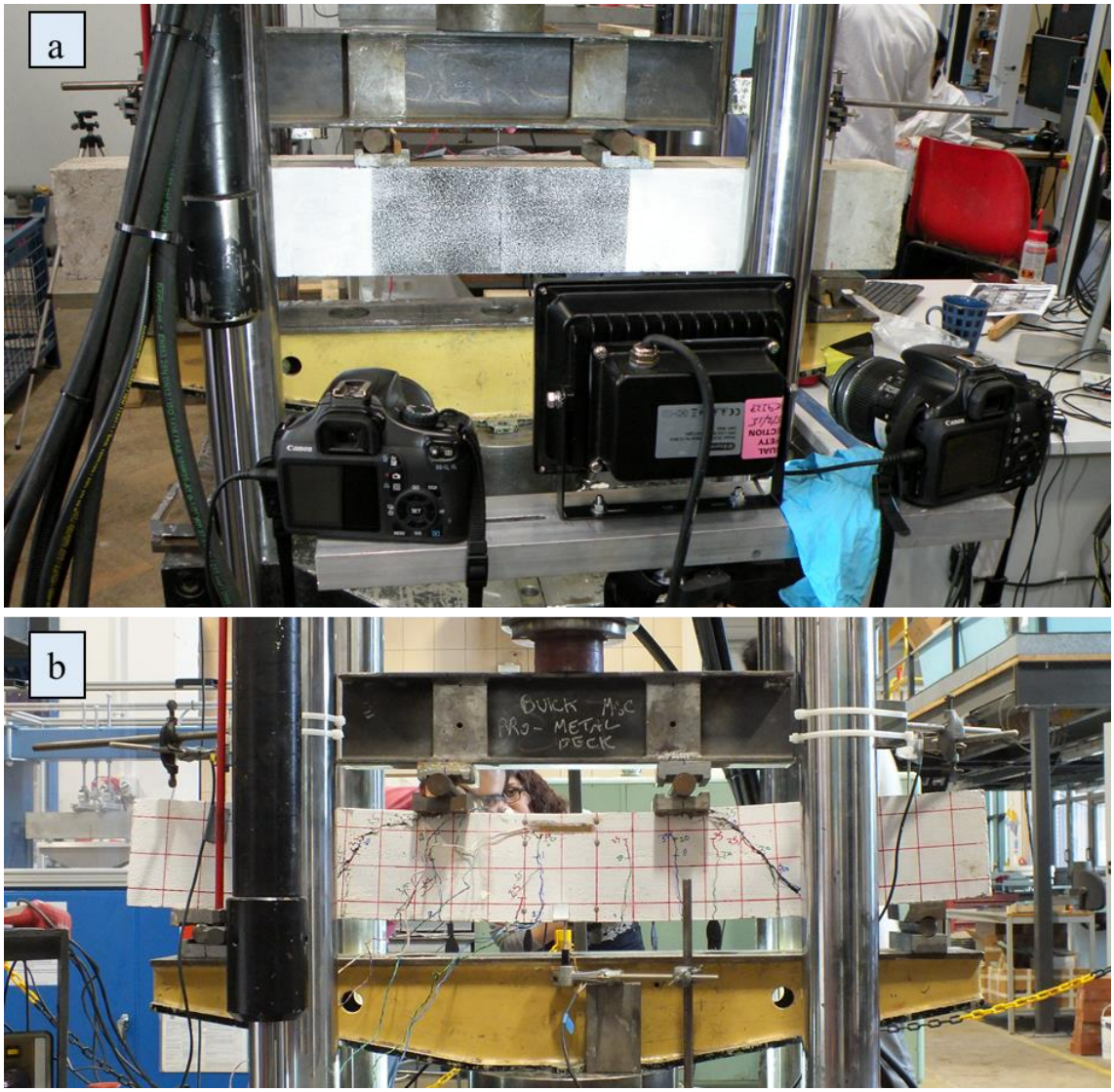

Figure 3. 16: Test set-up for flexural test on GFRP RC specimens (a) DIC measurement (b) traditional measurement.

3.5 SUMMARY

The methodology adopted in this study was illustrated in detail. The entire test matrix (Table 3.4) consisted of 348 GFRP specimens exposed to different environmental conditions. The program included tests on: unconditioned reference specimens (REF); unstressed and stressed bare bars conditioned in alkaline solution (K and K S3) or tap water (W and W S3) at 20, 40 and 60°C; unstressed and stressed bars embedded in concrete (i.e. moist and alkali environment) at ambient temperature (CON) and immersed in tap water (M CON, M CON S3 and M CON S5) at 20, 40

and 60°C. The exposure durations taken into account varied from 1000 hr (~42 days) to 8760 hr (1 year).

Additional information on the various tests are discussed in more detail in Chapters 4 and 5, along with the relevant tests results. The insights gained through the implementation of the described testing methodology are then used to assist the development of a design model for predicting long-term properties (Chapter 6).

Table 3. 4: Test matrix

	Conditioning		**Test method**								
Exposures	**Temp**	**Time**	**MAb**	**TNS**	**ILSS**	**FLX**	**DMA**	**FTIR**	**SEM/EDX**	**T.S**	**FLXC**
	(°C)	(hr)	(Nº)	(Nº)	(Nº)	(Nº)	(Nº)	(Nº)	(Nº)	(Nº)	(Nº)
REF	20	0		5	5	5	3	5	5	2	2
K	20	1000, 2000, 6480, 8760	3	9	3	3	1	3	2		
	40		3	9	3	3	1	3	2		
	60		3	9	3	3	1	3	2		
K-S3	20	1000, 2000, 6480, 8760	4	9	3	3		3	2		
	40		4	9	3	3	N.A.	3	2		
	60		4	9	3	3		3	2		
W	20	1000, 2000, 6480, 8760	3		3	3	1	3	2		
	40		3	N.A.	3	3	1	3	2		
	60		3		3	3	1	3	2		
W-S3	20	1000, 2000, 6480, 8760	4		3	3		3	2		
	40		4	N.A.	3	3	N.A.	3	2		
	60		4		3	3		3	2		
CON	20	2000, 6480, 8760	N.A.	9	N.A.	N.A.	N.A.	N.A.	N.A.		2
M-CON	20	1000, 2000, 6480	N.A.	9	N.A.	N.A.	N.A.	N.A.	N.A.		
	40			9							
	60			9						2	
M-CON-S3	20	1000, 2000, 6480	N.A.	9	N.A.	N.A.	N.A.	N.A.	N.A.		
	40			9							
	60			9						2	2
M-CON-S5	60	42, 90, 270	N.A.	9	N.A.	N.A.	N.A.	N.A.	N.A.		2

Note: TNS, tensile test; MAb, water absorption test; ILSS, inter-laminar shear strength; FLX, flexural tests; DMA, T_g by dynamic mechanical analysis; FTIR, Fourier transform infrared spectroscopy; SEM, scanning electron microscopy; EDX, energy dispersive x-ray analyses; T.S, tension stiffening test; FLXC, flexural tests for concrete beams; REF, reference samples; K, alkaline solution; W, tap water; M, moisture; CON, concrete; S3 and S5 sustained stress at 3000 με and 5000 με, respectively.

3.6 REFERENCES:

1. ACI, A., 2004. 440.3 R-04: Guide Test Methods for Fiber-Reinforced Polymers (FRPs) for Reinforcing or Strengthening Concrete Structures. *American Concrete Institute, Farmington Hills, USA*.
2. Robert, M., Wang, P., Cousin, P. and Benmokrane, B., 2010. Temperature as an accelerating factor for long-term durability testing of FRPs: Should there be any limitations?. *Journal of Composites for Construction*, 14(4), pp.361-367.
3. Davalos, J.F., Chen, Y. and Ray, I., 2012. Long-term durability prediction models for GFRP bars in concrete environment. *Journal of Composite Materials*, 46(16), pp.1899-1914.
4. ASTM Standard D570,1998(2010), "Test Method for Water Absorption of Plastics, ", ASTM International. West Conshohocken, PA.
5. ASTM Standard D4475,2002(2016), "Test Method for Apparent Horizontal Shear Strength of Pultruded Reinforced Plastic Rods By the Short-Beam Method". ASTM International, West Conshohocken, PA.
6. ASTM Standard D 4476, 2003(2014), "Test Method for Flexural Properties of Fiber Reinforced Pultruded Plastic Rods,". ASTM International. West Conshohocken, PA.
7. ASTM Standard D7028,2007(2015),"Test Method for Glass Transition Temperature (DMA Tg) of Polymer Matrix Composites by Dynamic Mechanical Analysis (DMA) ", ASTM International. West Conshohocken, PA.

CHAPTER 4

4 DURABILITY AND DEGRADATION MECHANISMS OF GFRP REINFORCEMENT SUBJECTED TO SEVERE ENVIRONMENTS AND SUSTAINED STRESS

ABSTRACT

Despite the large amount of research that has been carried out to date on the use of glass fibre reinforced polymer (GFRP) bars in concrete, one factor still hindering their widespread use in civil engineering applications is the lack of comprehensive data on their long-term in-service performance. This chapter presents the test results of an experimental study investigating the physical and mechanical properties of GFRP bars exposed to severe environments and subjected to different levels of sustained load. The test environments included moist concrete, alkaline solution and tap water, with temperatures varying from 20°C to 60°C. The mechanical properties of the bars were characterized through direct tension, flexural and inter-laminar shear tests, while the physical and chemical properties were determined through the implementation of a series of complementary techniques, including moisture absorption measurements, scanning electron microscope (SEM), Fourier Transform Infrared Spectroscopy (FTIR) and Energy dispersive x-ray analyses (EDX). The test results showed that the elevated temperatures play a key role in triggering and accelerating the development of critical degradation mechanisms. The reduction in the tensile strength of all conditioned samples subjected to a sustained stress equivalent to 3000 με was always within the limits recommended in existing codes for high durability bars, while a lower average strength retention was observed for higher levels of sustained stress (equivalent to 5000 με). Finally, it can be conclude that the long-term mechanical properties of the tested GFRP bars appeared to be mainly affected by moisture diffusion through the resin rich layer and debonding at the fibre/matrix interfaces due to the dissolution of the saline coupling agents.

4.1 INTRODUCTION

Corrosion of steel reinforcement is one of the main causes of degradation of reinforced concrete (RC) structures. In order to reduce the high maintenance cost associated with this problem, alternative reinforcing materials, such as Fibre Reinforced Polymer (FRP) reinforcements, have been investigated over the past three decades [1-4]. Despite the large amount of research that has been carried out on the use of FRP in concrete, the lack of comprehensive data on their long-term in-service performance [3, 5] still hinders the widespread use of FRP bars in civil engineering applications.

The durability of Glass FRP (GFRP) bars in concrete has usually been evaluated by using accelerated test methods that expose the bars to environments harsher than those they may encounter in service and by studying the change with time of their mechanical properties (i.e. tensile strength, bond strength and modulus of elasticity) [2, 6-10]. In an attempt to achieve a more fundamental understanding of their long-term behaviour, several researchers also investigated changes in physical, chemical and microstructural properties using scanning electron microscopy (SEM) [4,11], energy dispersive x-ray analyses (EDX) [11,12], dynamic mechanical analysis (DMA) [13], thermogravimetric analysis (TGA) [13,14], differential scanning calorimetry (DSC) [10,14] and Fourier transform infrared spectroscopy (FTIR) [10,15].

Among the conditioning environments examined in the literature, moist and alkaline environments have been reported to be the most detrimental for the GFRP matrix and the fibres [6, 16-19]. In particular, in moist environments the free hydroxide ions (OH^-) attack the polymer matrix and the long molecular chains are disassembled by hydrolysis, promoting the ingress of more OH^- ions and water molecules (H_2O) Eq. 4.1. These, in turn, can break the polymer-polymer chain secondary bond, creating localized voids (increase in free volume) and ultimately affecting the physical and mechanical properties of the GFRP matrix (i.e. plasticization) [6]. The presence of water can also lead to the degradation of glass fibres through dissolution (i.e. leaching) according to Eq. 4.2. This process, which consists in the extraction of alkalis from the glass structures, continues until alkalis become available. The hydroxide produced by the leaching process Eq. 4.2 increases the pH of the solution and, as the pH exceeds the threshold value of 9, the Si networks are affected (i.e., silica dissolution in alkaline environment, Eq. 4.3). [19]

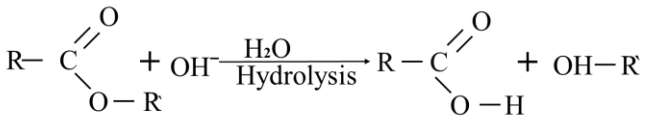

(4.1)

$$\text{Si—O—Na} + \text{H}_2\text{O} \longrightarrow \text{Si—OH} + \text{OH}^- \tag{4.2}$$

$$\text{Si—O—Si} + \text{OH}^- \longrightarrow \text{Si—OH} + \text{Si—O}^- \tag{4.3}$$

While direct submersion of bare bars in an alkaline and water solution at elevated temperature is recommended by current standards to accelerate aging [20-22], previous studies [11, 18, 19] have shown that these environments are excessively harsh and cause premature deterioration of GFRP bars, consequently lead to conservative predictions of service life. As a result, researchers attempted to evaluate the performance of GFRP bars by embedding them directly into concrete and exposing the specimens to high temperatures to accelerate reaction rates, yet subjecting them only to the inherent alkaline and moist environment provided by the concrete surrounding the bars [9,18,23].

In addition to the exposure environment, the presence of sustained stress might generate stress concentrations around the micro-imperfections present in the matrix (e.g. pores) and accelerate the propagation of micro cracks [24]. This, in turn, would ease the ingress of the surrounding media (e.g. alkali solution and water) and have a possible detrimental impact on the durability of the fibres [25]. Only a limited number of studies have examined the influence of sustained stress on the long-term properties of FRP and concluded that low values of sustained stress (20% of the ultimate strength or less) did not significantly affect the residual mechanical properties. Such studies, however, only examined the performance of bare composite specimens [26], or were limited to relatively low values of sustained stress (equivalent to a strain level of about 2000με) and did not include any chemical/physical analysis of the microstructure [27].

4.2 RESEARCH SIGNIFICANCE

This study aims to provide a better understanding of the long-term performance of GFRP bars by employing accelerated conditioning methodologies that more closely reflect the in-service conditions of GFRP RC members including alkaline and moist environments as well as sustained stresses. A comprehensive experimental programme was designed to study the degradation mechanisms at both micro (chemical properties) and macro levels (physical and mechanical properties). Ultimately, the goal of this research is to develop an effective model to assess and predict the durability of GFRP bars, which in turn, would directly assist in the development of more reliable and less conservative design tools for GFRP RC members.

4.3 EXPERIMENTAL PROGRAMME

"The author apologies for some repetition in experimental work program as this chapter has been published as journal paper".

Figure. 4.1 presents a flow chart summarizing the complementary experimental program carried out in this research. The flow chart is divided in three sections: Section 1 – Degradation; Section 2 – Investigation; and Section 3 – Model. Section 1 shows the conditioning parameters (i.e. moist and alkali environments, high temperature and sustained stress) considered in this research and the GFRP bar properties that are affected (at both the macro level - tensile and bond properties - as well as at the micro level). Section 2 summarizes the tests used to assess the investigated material properties. The use of this complementary set of tests was implemented to enable a more comprehensive assessment of the degradation processes based not only on the outcomes of the mechanical tests but also on the results of the physical and chemical tests. Section 3 is presented in the chart as the logical convergence of this study, and the resulting durability model will be discussed in chapter 6.

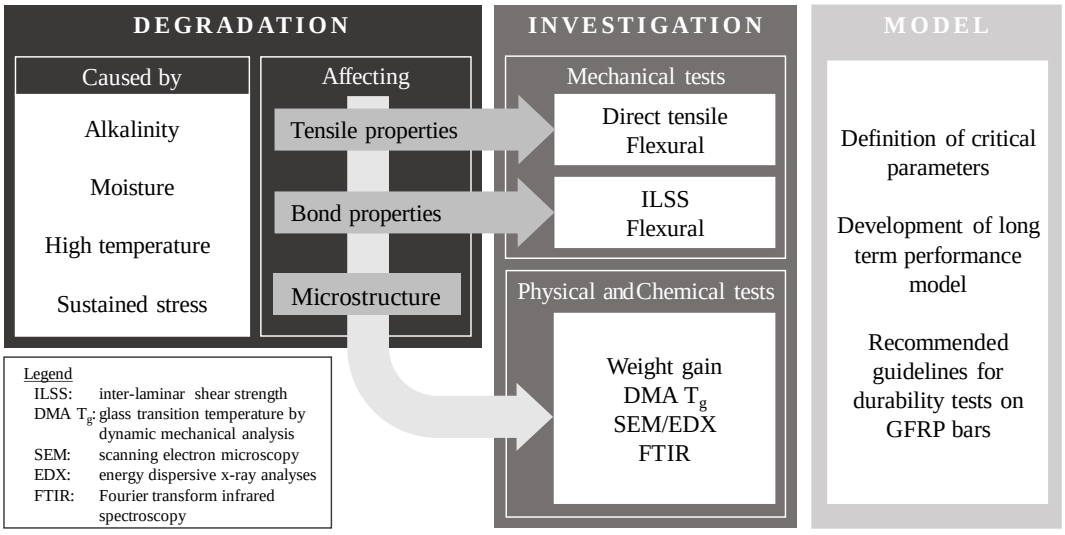

Figure 4. 1: Overview of experimental program.

4.3.1 Test Matrix

The test matrix (Table 4.1) consisted of 334 GFRP samples obtained from bars with a nominal diameter of 8 mm, made of continuous E Glass fibres impregnated in a vinyl ester resin and manufactured using the pultrusion process. The program included tests on: unconditioned reference specimens (REF); unstressed and stressed bare bars conditioned in alkaline solution (K and K-S3) or tap water (W and W-S3) at 20, 40 and 60°C; unstressed and stressed bars embedded

in concrete (i.e. moist and alkali environment) at ambient temperature (CON) and immersed in tap water (M-CON, M-CON-S3 and M-CON-S5) at 20, 40 and 60°C. The exposure durations taken into account varied from 1000 hr (~42 days) to 8760 hr (1 year).

Although it has been shown in previous research that direct exposure of GFRP to alkaline solution is undoubtedly more aggressive than any realistic civil engineering application, such condition has been included as it is recommended in current testing guidelines [21, 22]. The alkaline solution was prepared according to the recommendations of the ACI 440 committee [22] using 118.5 g of $Ca(OH)_2$, 0.9 g of NaOH and 4.2 g of KOH in 1 litre of deionised water. The pH level of this solution was periodically controlled and kept at about 12.7, which is a representative value for a mature concrete pore solution [28].

A sustained stress inducing a tensile strain of 3000 με (micro-strain) was applied to the FRP bars as recommended in ACI 440.3R and CAN/CSA-S806 [22,21], while a higher stress inducing a strain of 5000 με was examined to assess the effect of less stringent serviceability limits (corresponding to larger allowable crack widths and deflections) [29]. The sustained stress inducing the desired level of tensile strain was applied using two different configurations: via a spring of adequate stiffness mounted in a stiff pre-tensioning rig (Figure. 4.2-a); or by tying pairs of specimens at the two ends with a wedge interposed at mid-length to impose the required curvature (Figure.4.2-b). During the conditioning period, the strain level of the bars was measured periodically using a caliper and demec gauge system. The length of the steel springs used in the loading system were also checked regularly using a digital caliper with an accuracy of 0.02mm to assure that the load was maintained constant.

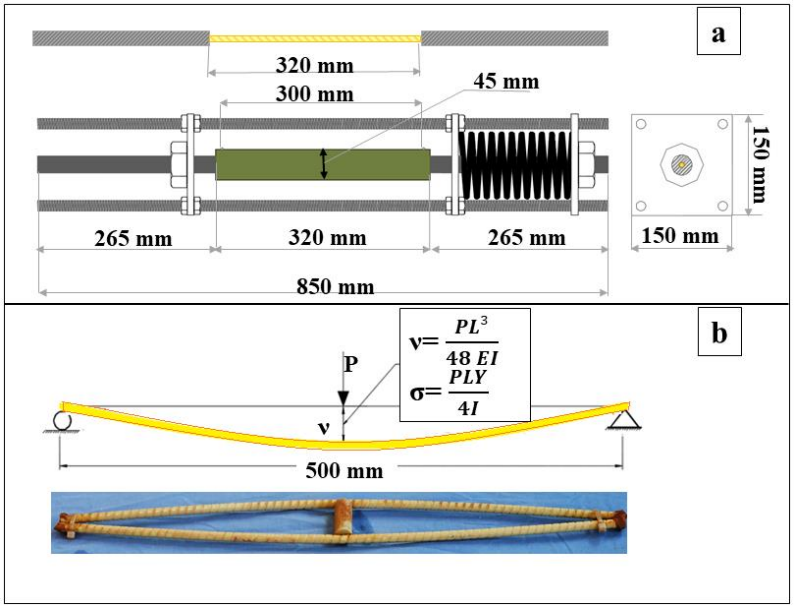

Figure 4. 2: Sketch illustrating the methods of application of sustained stress for (a) tensile and (b) moisture absorption test specimens.

Table 4. 1: Test Matrix

Exposures	Conditioning		Test method						
	Temp (°C)	Time (hr)	MAb (Nº)	TNS (Nº)	ILSS (Nº)	FLX (Nº)	DMA (Nº)	FTIR (Nº)	SEM/EDX (Nº)
REF	20	0		5	5	5	3	5	5
K	20	1000, 2000, 6480, 8760	3	9	3	3	1	3	2
	40		3	9	3	3	1	3	2
	60		3	9	3	3	1	3	2
K-S3	20	1000, 2000, 6480, 8760	4	9	3	3	N.A.	3	2
	40		4	9	3	3		3	2
	60		4	9	3	3		3	2
W	20	1000, 2000, 6480, 8760	3	N.A.	3	3	1	3	2
	40		3		3	3	1	3	2
	60		3		3	3	1	3	2
W-S3	20	1000, 2000, 6480, 8760	4	N.A.	3	3	N.A.	3	2
	40		4		3	3		3	2
	60		4		3	3		3	2
CON	20	2000, 6480, 8760	N.A.	9	N.A.	N.A.	N.A.	N.A.	N.A.
M-CON	20	1000, 2000, 6480	N.A.	9	N.A.	N.A.	N.A.	N.A.	N.A.
	40			9					
	60			9					
M-CON-S3	20	1000, 2000, 6480	N.A.	9	N.A.	N.A.	N.A.	N.A.	N.A.
	40			9					
	60			9					
M-CON-S5	60	42, 90, 270	N.A.	9	N.A.	N.A.	N.A.	N.A.	N.A.

Note: TNS, tensile test; MAb, water absorption test; ILSS, inter-laminar shear strength; FLX, flexural tests; DMA, T_g by dynamic mechanical analysis; FTIR, Fourier transform infrared spectroscopy; SEM, scanning electron microscopy; EDX, energy dispersive x-ray analyses; REF, reference samples; K, alkaline solution; W, tap water; M, moisture; CON, concrete; S3 and S5 sustained stress at 3000 με and 5000 με, respectively.

4.3.2 Test methodology

Direct tensile tests (TNS) [22], inter-laminar shear strength tests (ILSS) [30] and flexural tests (FLX) [31] were carried out to evaluate the mechanical properties. All tests were performed in displacement control using hydraulic and mechanical actuators with a maximum capacity of 1000 kN (TNS) and 10 kN (ILSS and FLX), respectively. Data were recorded at 1 Hz using an NI LabVIEW data acquisition system. Details of the set-up of each test are shown in. Figure. 4.3.

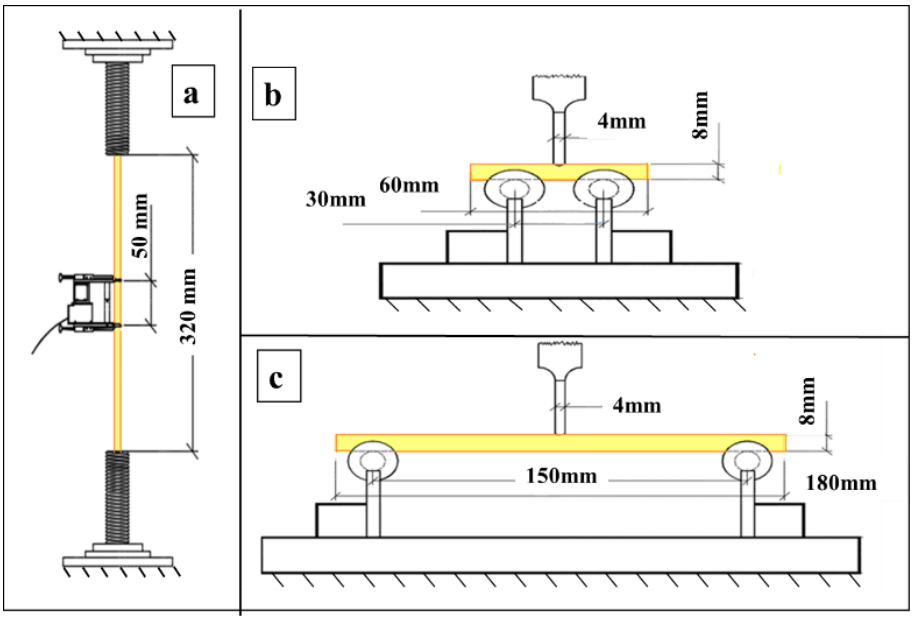

Figure 4. 3: Set-up for (a) tensile, (b) inter-laminar shear strength and (c) flexural tests.

A series of tests on the physical and chemical properties of the samples was also carried out to investigate the microstructure and the integrity of the GFRP material before and after exposure. Standard test methods were implemented to measure the glass transition temperature (T_g) by dynamic mechanical analysis (DMA) [32] (Figure. 4.4-a) as well as moisture absorption (MAb) [33]. DMA was performed using a Mettler Toledo DMA/SDTA861e machine while moisture absorption was assessed monthly by measuring the weight gain due to fluid uptake into 300-mm-long (unstressed) and 450-mm-long (stressed) GFRP samples with the two ends sealed using epoxy to prevent absorption from the cut edges. In addition, scanning electron microscopy (SEM), energy dispersive x-ray analyses (EDX) and Fourier transforms infrared spectroscopy analysis (FTIR) were carried out following procedures available in the literature [12, 34] (Figure. 4. 4-b).

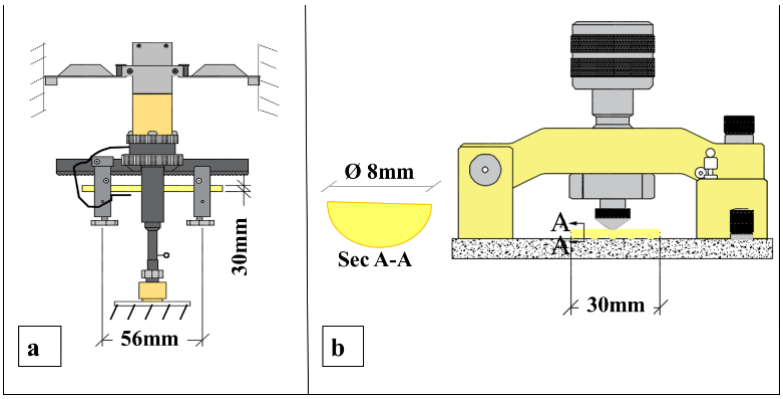

Figure 4. 4: Set-up for (a) T_g and (b) FTIR tests.

SEM and EDX were performed using a high magnification microscope (Phillips XL30 SEM) which uses a focussed scanned electron beam to produce images of the sample. Prior to the analysis, 10-mm-long samples were cut from the GFRP bars using a low speed diamond blade. The samples were subsequently placed vertically in moulds, cold-mounted in epoxy resin and cured for 24 hr at room temperature. The cross sections were then grinded using sand paper of increasing grit (400, 600, 800 and 1200) and polished with 6 μm and 1 μm diamond pastes. The specimens were then carbon coated and analysed. Finally, FTIR analyses were performed using an FTIR spectrometer to investigate the external surface and the internal layers of the GFRP bars. In the former case, 30-mm-long samples were cut longitudinally from the bars up to a maximum depth of 3 mm, while in the latter the samples were prepared by grinding the GFRP bars into a fine powder (approximately 2 mg). The milled samples were pressed into a disc after being mixed with approximately 200 mg of anhydrous Potassium Bromide (KBr). The disc analysis was carried out by treating the KBr as the background reference. In both configurations, 32 scans were routinely obtained with an optical retardation of 0.25 cm to yield a resolution of 4 cm^{-1}. Typical characteristic absorption bands available in the literature are reported in Table 4.2. Past studies on FRP examining civil engineering applications specifically focused on spectral zones in the band between 3600-2900 cm^{-1} including the stretching mode of the hydroxyl group OH (3450 cm^{-1}) and of the carbon-hydrogen group CH (2928 cm^{-1}) [12, 34]. In this research the acquisition of the spectra was performed ranging from 4000 to 600 cm^{-1}, so as to include the stretching modes of C-O and C=C (1295 cm^{-1} and 920 cm^{-1} respectively).

Table 4. 2: Assignments of the main absorption bands of the FTIR spectra

Absorption bands (cm^{-1})	Assignment
3400	O-H bending vibration
3026	C-H stretch of the benzene
2960, 2928, 2871	CH, CH_2, CH_3 stretch
1722	C=O- Stretching vibration in saturated aldehyde, ketone or acid
1608, 1510	C=C- Stretching vibration of skeleton in benzene ring
1295	C-O stretch
1160	C-CO-C stretch
920	C=C stretch

4.4 RESULTS AND DISCUSSION

The results of the experimental programme are presented in this section. Firstly, the results from the moisture absorption tests, which can be used to investigate changes in the diffusion

mechanism of water and alkaline solutions, are reported and used to support the results of physical and chemical tests, which assessed the deterioration of the micro structure (i.e., matrix, fibres and interface layer). Finally, the data acquired from all tests is utilized to discuss the changes in mechanical properties at the macro scale.

4.4.1 Moisture absorption properties

Figure. 4.5 shows the absorption rate of stressed (S3) and unstressed GFRP bars in water (W) and alkaline (K) environment against the square root of the exposure time. The absorption rate was calculated as the ratio between the average moisture uptake and the initial weight.

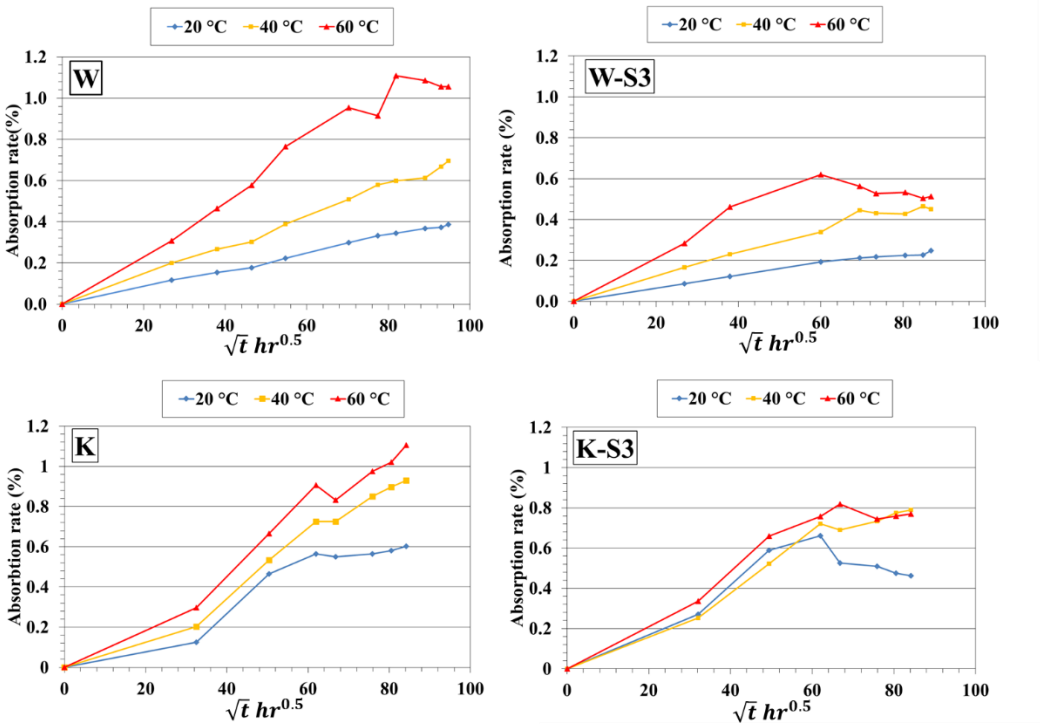

Figure 4. 5: Moisture absorption rate of unstressed and stressed (S3) GFRP bars immersed in water (W) and alkaline solution (K) at different temperature.

In all samples, weight increased gradually with respect to the exposure time, following the Fick's law up to about 4500 hr (~67 √hr). At this stage, the diffusion mechanism started to become unstable (non-Fickian behaviour) resulting in absorption rate curves characterized by portions of weight loss, due to the degradation of the outer layer leading to material loss, and by portions of weight gain, possibly due to the filling of new or pre-existing voids and micro cracks. While no saturation was reached at the end of the considered ageing period (8760 hr - ~93 √hr), stressed samples consistently showed a lower moisture uptake than unstressed ones. This phenomenon could be attributed to the method used to stress the samples (i.e. bending, Figure.4 2b) which

reduces the number of open pores in the portion of the bar in compression. This is discussed further in section 4.2.2. In addition, the exposure temperature played a critical role on the absorption process. The measured data showed that the higher the temperature the higher the absorption rate. This can be attributed to an increase in the chemical reactions rate as well as to a higher void pressure resulting from an increase in the volume of gases as temperature rises. This pressure build-up favoured the propagation of micro cracks and consequently increased the free volumes within the bars that could be filled by the surrounding solution.

It can be finally observed that, for all temperatures, specimens exposed to alkali solution showed slightly higher moisture uptake than those exposed to tap water as the former contains more free hydroxide ions (OH^-), which work as a solvent for the polymer, thus promoting the solution ingress.

4.4.1.1 Chemical and physical degradation of GFRP bars in wet environments

4.4.1.1.1 Effects on Matrix

The effect of the different conditioning environments, temperatures and applied stress levels, on the GFRP matrix was studied at different depths of the samples. In particular, the external surface was analysed using both SEM images and FTIR. FTIR was also employed to examine an inner portion of the bars, yet still sufficiently close to the surface, while the core of the samples was analysed using DMA.

FTIR was employed to detect possible chemical changes in the polymeric chain after conditioning. Intensity changes in the hydroxyl group (OH) (Eq.4.1) and in the stretching bands of C=O and C-O were investigated to verify that hydrolysis and oxidation reactions took place. Since the intensity of a FTIR spectrum can be affected by several parameters, it is customary [19] to quantify the changes in a given band as a ratio with the variations of the aromatic group CH, which is very stable and does not easily break apart and react with other substances. Thus, changes in the OH/CH and C=O/CH ratios as well as in the C-O/CH ratio can be used to gage hydrolysis and oxidation reactions, respectively. Similarly, changes in the C=C peak, also referred to as curing index [35], were monitored to gain information on the curing process.

The FTIR spectra were calculated on the surface of control (REF), unstressed (W and K) and stressed (W-S3 and K-S3) samples (Figure.4.6-a) as well as on a deeper portion of control (REF) and unstressed (W and K) samples (Figure.4.6-b, grinded samples). All samples were conditioned for 8760 hr at 60ºC.

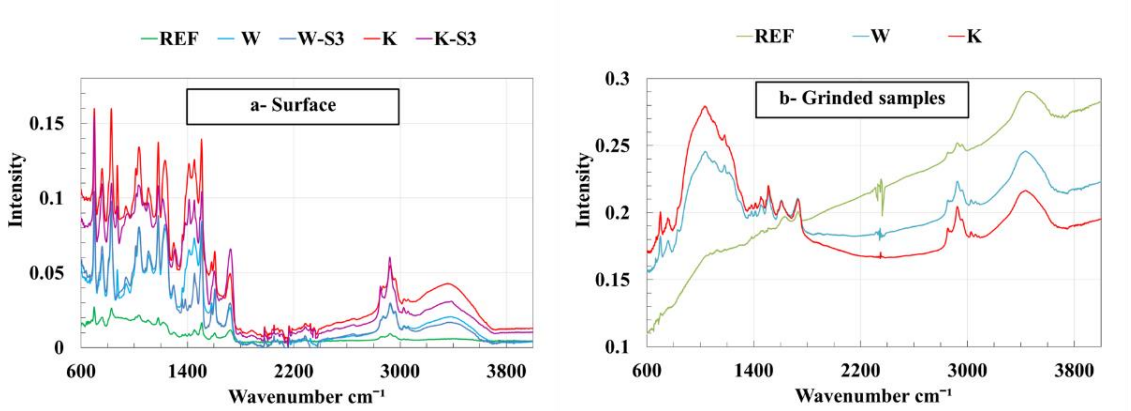

Figure 4. 6: FTIR spectra for the resin matrix on (a) the surface of GFRP bars and on (b) grinded samples. Results for unstressed and stressed (S3) specimens conditioned in water (W) and alkali solution (K) at 60°C for 8760 hr are compared to benchmark samples (REF).

The results of the FTIR analysis on the surface of the samples (Table 4.3) showed that all the OH/CH ratios increased with respect to REF and that such increase was more marked in unstressed samples than in stressed ones. This directly confirms that moisture entered the polymer matrix promoting the hydrolysis reaction and it also implies that stressed samples had lower chemical interaction (i.e., lower hydrolysis). As the intensity of OH was similar for unstressed samples (W and K), the C=O/CH ratio was used as an additional indicator of the hydrolysis reaction taking place and to assess the effect of the conditioning environment. The reduction in C=O/CH was due to the breakage of the end of the vinyl ester chain and, as suggested by the lower value, the alkaline solution seemed to cause more breakage of the ester chain than water (i.e. more hydrolysis). Conversely, while oxidation occurred in all samples as all the C-O/CH ratios increased with respect to REF, this reaction was more evident in stressed samples than unstressed ones and in water rather than alkaline solution.

Table 4. 3: Band ratios results for FTIR analysis on the outer surface of the samples

Samples	OH/C-H (1)		C=O/C-H (2)		C-O/C-H (3)		C=C/C-H (4)		C=C/C-H (5)	
	Value	(%)	Value	(%)	Value	(%)	Value	(%)	Value	(%)
REF	1.05	-	2.07	-	1.79	-	1.49	-	3.45	-
W	1.40	1.33	1.82	0.88	2.80	1.56	2.47	1.66	2.92	0.85
W-S3	1.16	1.10	2.10	1.01	2.94	1.64	2.73	1.83	3.32	0.96
K	1.32	1.26	1.52	0.73	2.16	1.21	1.98	1.33	2.89	0.84
K-S3	1.16	1.10	2.46	1.19	2.46	1.37	1.87	1.26	3.36	0.97

Table 4.4 shows that, for all grinded deeper samples, there was a small reduction of the OH/CH ratio and a negligible variation of the C=O/CH ratio with respect to the REF samples, suggesting

that no hydrolysis reaction occurred in this portion of the bar. The test results also showed an increase in the ratio of C-O/CH ratio in both K and W samples due to the oxidation of the methylene group (CH_2) at the end of the vinyl ester chain.

Table 4. 4: Band ratios results for FTIR analysis on a grinded portion of the inner layer of the samples

Samples	OH/C-H (1)		C=O/C-H (2)		C-O/C-H (3)		C=C/C-H (4)		C=C/C-H (5)	
	Value	(%)	Value	(%)	Value	(%)	Value	(%)	Value	(%)
REF	1.17	-	0.57	-	0.70	-	0.79	-	0.62	-
W	1.13	0.97	0.57	1.00	1.00	1.43	0.98	1.24	1.08	1.74
K	1.13	0.97	0.57	1.00	1.19	1.70	1.11	1.41	1.41	2.27

For both surface and grinded specimens, an increase in the C=C/CH ratio with respect to REF was observed (column 4 in Table 4.3). This may be attributed to additional repeating unit connecting to the backbone chain and increasing the number of benzene rings and consequently the stiffness of the resin.

Additional evidence of matrix deterioration (i.e. cracks, voids and de-bonding from the fibres) was provided by the SEM images of the outer layers of GFRP bars conditioned in water (W) and alkaline solution (K) at 60°C for 8760 hr (Figure.4.7)

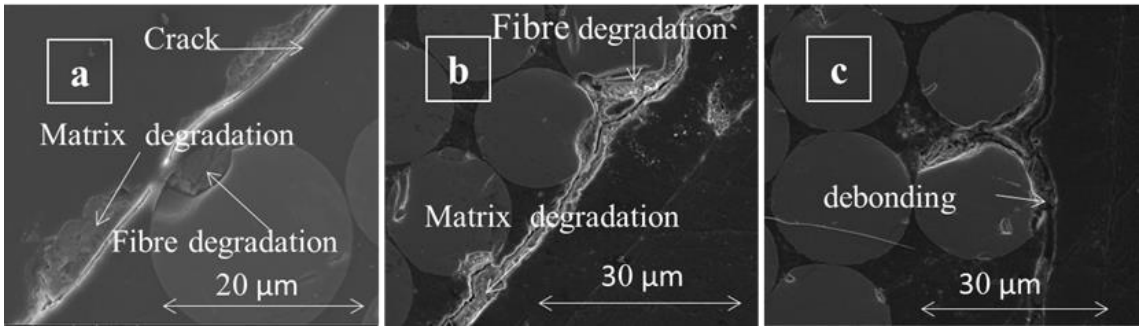

Figure 4. 7: SEM images of the cross-sections of specimen conditioned in (a) water and (b and c) alkaline solution at 60°C for 8760 hr.

The analysis of the innermost part of the GFRP bars was carried out by determining the glass transition temperature (T_g) of samples obtained from the core of specimens aged for 8760 hr in water (W) and alkaline solution (K) at 20°C, 40°C and 60°C. After the specimens were removed from the conditioning environment, they were stored in sealed plastic bags up to the time of testing. The values of Tg were determined according to the storage modulus (E') method. Figure. 4.8 shows that the change in T_g was negligible for low temperatures, while a reduction of more than 5% was observed at 60°C for both environments. Since a reduction in T_g indicates a reduction

of cohesive forces between polymer chains, it can be concluded that, at least at elevated temperatures, the matrix in the core of the specimens had deteriorated.

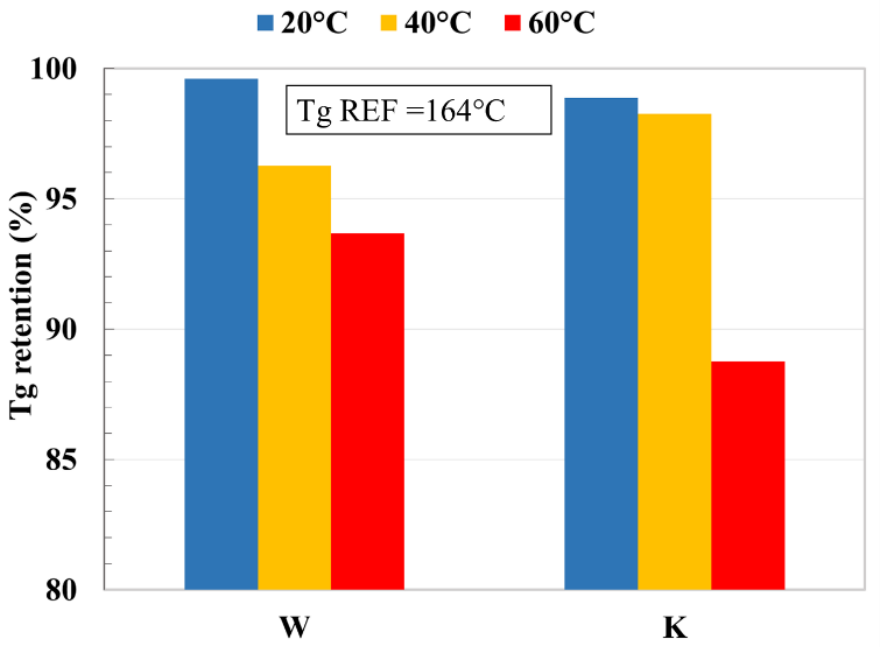

Figure 4. 8: Change in glass transition temperature (Tg) for specimens conditioned in water (W) and alkaline solution (K) at different temperatures for 8760 hr.

All the results confirm that the higher the conditioning temperatures the higher the deterioration of the resin matrix and indicate that the polymer chain undergoes disruption (hydrolysis) and reconstruction (oxidation) of the bond links with possible repercussion on the physical and mechanical properties of the polymer matrix.

4.4.1.1.2 Effects on matrix/fibre interface

The interface between the matrix and the fibres is a very thin layer (approximately1 μm) of coupling agent, consisting of a saline-based material susceptible to moisture and alkaline environments. The assessment of the deterioration of such a thin layer was only possible by using highly magnified SEM images.

Figure. 4.9 shows, at the top, the typical crack pattern observed in the cross-section of unstressed (left) and stressed (right) samples, as well as the approximate locations where the SEM images (a, b, c and d) were taken. As no significant deterioration was seen in samples conditioned at low temperatures, only images of samples conditioned in water and alkaline solution at 60°C for 8760 hr are presented. These results confirm that moisture dissolved the saline substances at the interface causing local loss of bond between fibres and matrix (i.e., cracks and debonding). In

addition, it can be noticed that for the unstressed sample the cracks tend to propagate circumferentially around the outermost layer of fibres, while the cracks are concentrated on the tension side of the stressed samples and propagate both radially and circumferentially as a result of the three-point bending set-up used to stress the specimens (Figure. 4.2-b).

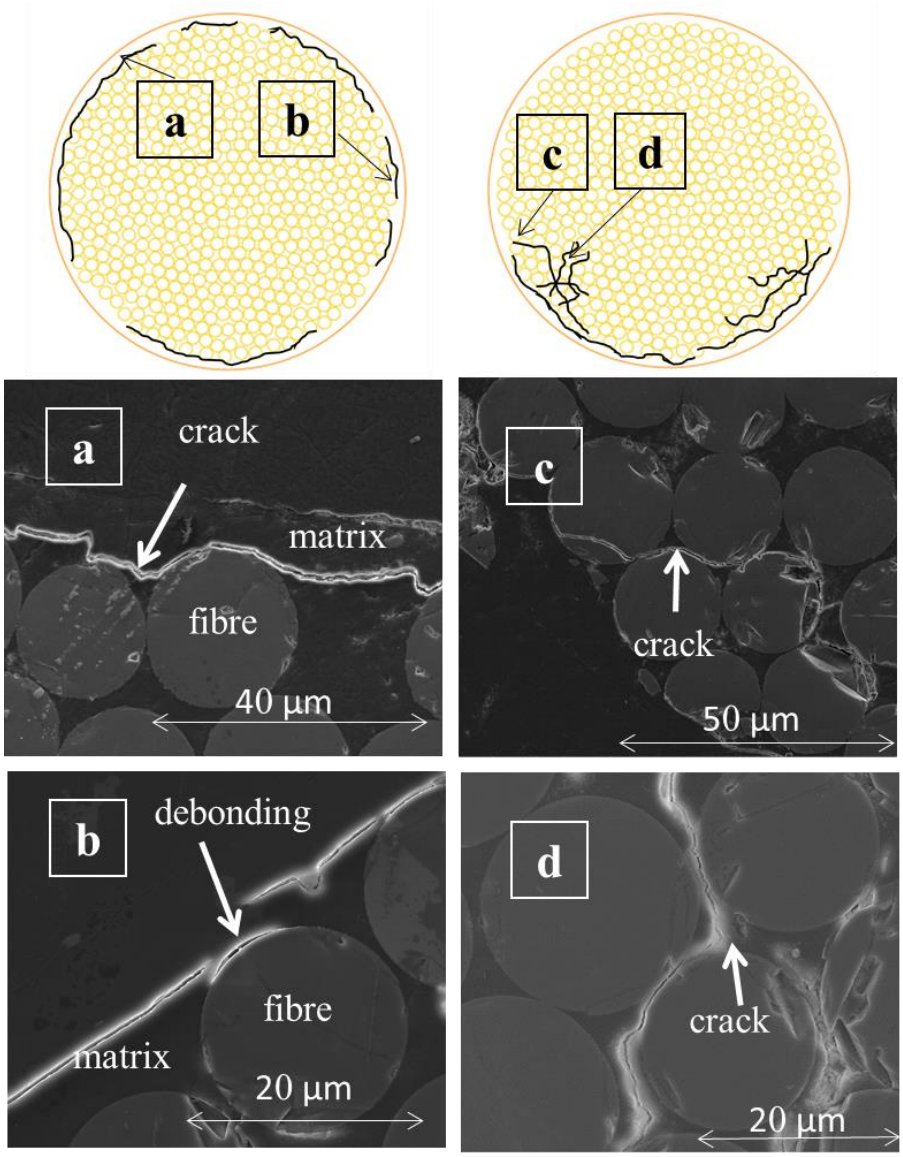

Figure 4. 9: SEM images of the cross sections of unstressed specimen (left) and stressed specimens (right) conditioned in water at 60°C for 8760 hr.

4.4.1.1.3 Effects on glass fibres

Highly magnified SEM images were used to study the degradation of the glass fibres in water and alkaline solution (Eq. 4.2 and Eq. 4.3). In addition, as silica (Si), aluminium (Al) and calcium (Ca) are not chemical elements present in an epoxy matrix, a precise elemental analysis using

EDX was carried out to detect the presence of such elements as a result of the glass fibres dissolution.

The results of the EDX analysis carried out on the matrix and the fibres of a reference sample (Figure. 4.10-a and Figure. 4.10-b, respectively) and on the matrix of samples conditioned in water and alkaline solution at 60°C for 8760 hr (Figure. 4.10-c and Figure. 4.10-d, respectively) are presented in the form of the spectra displaying the concentration (peaks) of each chemical element identified in the analysis.

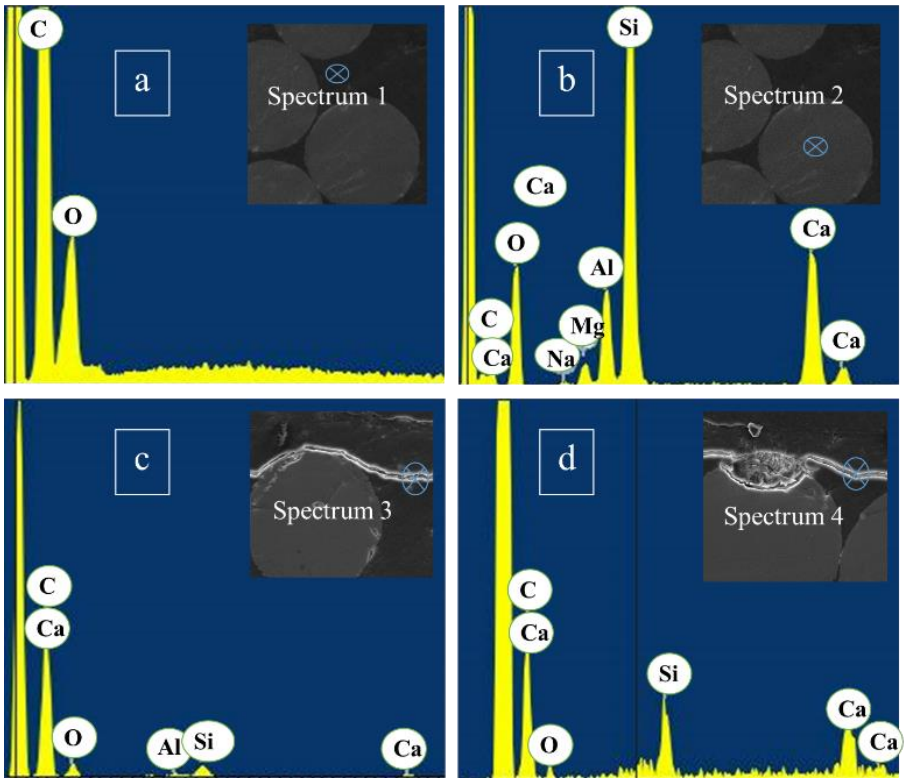

Figure 4. 10: Results of EDX scans for specimens conditioned (c) in water and (d) alkaline solution at 60°C for 8760 hr are compared to benchmark samples for (a) matrix and (b) fibres.

In all figures, the location where the analysis was performed is indicated by a target. The EDX analysis detected the aforementioned chemical elements in the resin matrix near to the fibre/matrix interface both for specimens conditioned in water (W, Figure. 4.10-c) and alkaline solution (K, Figur.e 4.10-d). This confirmed that water molecules and hydroxide ions, through micro-cracks in the matrix, reached the glass fibres deteriorating them. Additional evidence of the fibre deterioration was provided by SEM images as shown in Figure. 4.11.

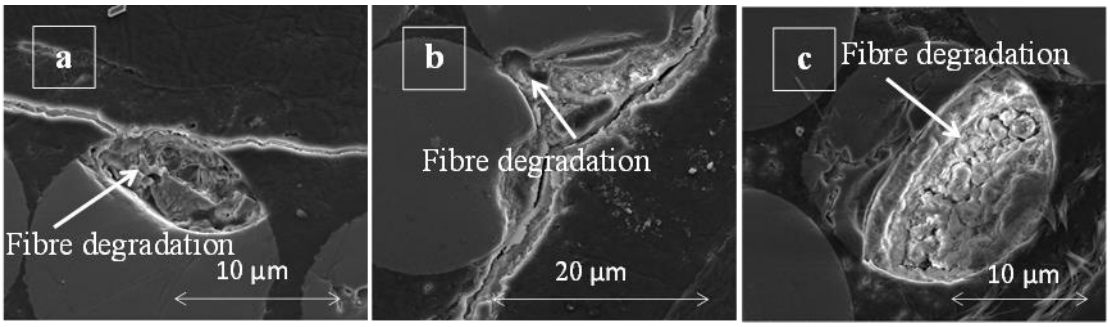

Figure 4. 11: SEM images showing the degradation in glass fibres after conditioning in alkaline solution at 60°Cfor 8760 hr

4.4.1.2 Mechanical degradation of GFRP bars in wet environments under sustained stress

4.4.1.2.1 Tensile properties

The results of the tensile tests are summarized in Table 4.5, including average (Avg) tensile strength and modulus of elasticity, their coefficients of variation (COV) and their retention calculated as percentage of results for REF. The tensile strength was calculated using a nominal diameter of 8 mm while the modulus of elasticity was calculated as the slope of the stress-strain curve between 20% and 60% of the ultimate tensile strength.

Table 4. 5: Tensile test results

Conditioning			Tensile Strength			Modulus of Elasticity		
Exposures	Temp	Time	Avg	COV	Retention	Avg	COV	Retention
	(°C)	(hr)	(MPa)	(%)	(%)	(GPa)	(%)	(%)
REF	20	0	1542	1.8	100	56.1	2.7	100
K	20	1000	1472	0.3	95	56.7	0.7	101
	20	2000	1454	0.2	94	53.6	0.6	96
	20	6480	1498	n.a.*	97	58.5	n.a.*	104
	40	1000	1407	1.9	91	57.5	4.0	102
	40	2000	1390	1.3	90	57.0	4.5	102
	40	6480	1310	n.a.*	84	60.4	n.a.*	108
	60	1000	1310	3.1	84	59.2	6.2	106
	60	2000	1139	11.6	73	58.0	1.7	103
	60	6480	997	n.a.*	64	66.4	n.a.*	118
K-S3	60	1000	1327	5.4	86	58.9	4.4	105
	60	2000	1164	4.5	75	56.1	4.2	100
CON	20	6480	1540	0.7	100	56.7	6.4	101
M-CON	20	2000	1421	5.3	92	55.3	3.4	99
	20	6480	1392	6.9	90	55.5	3.5	99
	40	1000	1458	1.4	95	56.5	0.1	101
	40	2000	1370	1.0	89	57.5	1.9	102
	40	6480	1148	18.0	74	58.4	5.4	104
	60	1000	1244	5.9	80	59.8	6.0	107
	60	2000	1227	1.1	79	58.8	4.2	105
	60	6480	917	1.4	59	55.4	1.9	99
M-CON-S3	20	1000	1473	0.2	96	57.6	1.0	103
	20	2000	1416	1.8	92	61.6	6.5	110
	20	6480	1365	11.5	89	55.5	3.0	99
	40	1000	1228	17.0	87	58.5	0.3	104
	40	2000	1335	3.6	87	57.0	4.2	102
	40	6480	1177	3.6	76	57.2	2.7	102
	60	1000	1233	2.4	82	58.3	2.8	104
	60	2000	1073	11.0	74	58.8	2.7	105
	60	6480	919	4.2	59	61.1	3.4	109
M-CON-S5	60	1000	1190	14.0	77	59.4	2.2	106
	60	2000	1023	0.6	66	59.9	0.9	107
	60	6480	971	4.8	63	58.3	5.0	104

* COV not available since only one specimen was tested.

Figure. 4.12 shows the tensile strength and moisture absorption rate over the conditioning time for unstressed and stressed specimens exposed to moist concrete (M-CON, M-CON-S3, and M-CON-S5) and alkaline solution (K and K-S3) at 20, 40 and 60°C. The results indicate that tensile strength decreased as moisture uptake increased and these effects were accelerated by increasing the temperature.

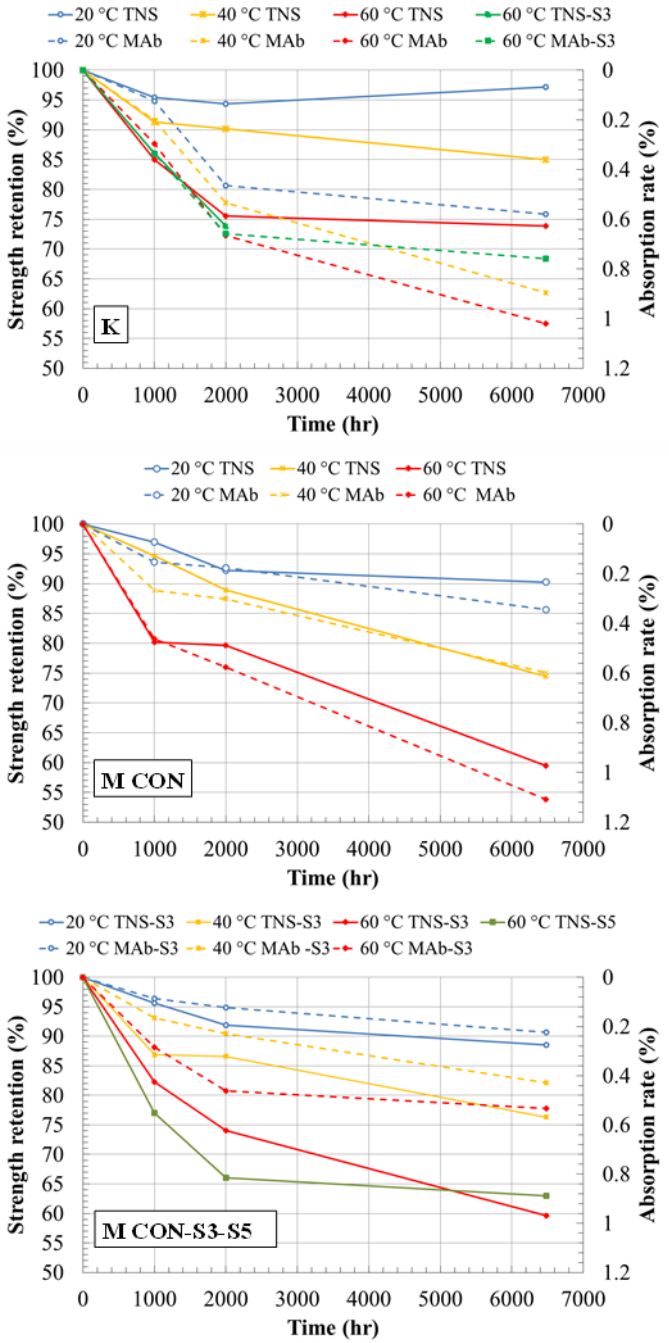

Figure 4. 12: Tensile strength (TNS) retention and moisture absorption (MAb) over time for unstressed and stressed (S3 and S5) bars conditioned in alkaline solution (K) and concrete (M-CON).

The reduction in tensile properties of GFRP bars can be interpreted in light of the results obtained by FTIR and SEM/EDX. The deterioration of the matrix allowed the ingress of hydroxide ions with a two-fold effect: 1) causing de-bonding between fibres and matrix, consequently reducing the GFRP ability to transfer effectively the load from the matrix to the fibres; 2) dissolving the glass fibres, thus resulting in a local reduction of the number of fibres effectively contributing to carry the load.

In addition, even if the test results showed that the changes in the average tensile modulus of elasticity of most conditioned specimens is negligible, as it varied within the variability of the experimental data, a small increase in stiffness can be noticed. The degree of post-curing of the matrix that was also captured by FTIR analysis both on the surface and in the inner layers of the bar might have also contributed to the observed increase in stiffness. .The majority of the tensile strength reduction occurred within the first 2000 hr for all environments, with a slightly higher degradation rate being observed for the specimens conditioned in alkaline solution (K). The unstressed specimens embedded in concrete (M-CON), exhibited a slightly higher retention rate up to 2000 hr but their strength at 6480 hr was overall lower than that of specimens immersed in alkaline solution. This can be attributed to the formation of salt barriers on the surface of the K specimens that inhibited further diffusion and damage to the microstructure. The application of a sustained stress during conditioning, equivalent to 3000 με and 5000 με, affected slightly only the tensile strength, possibly because the level of imposed strain was small compared to the ultimate strain of the REF samples (i.e., 27000με). Finally, it can be stated that the reduction in tensile strength due to chemical reaction of these materials in aforementioned environment takes very short time to occur and stabilize. Therefore, the adopted duration and environments by this research (i.e, moist concrete at elevated temperature) can be implemented to examine the durability of GFRP and their long term properties. While, the correlation of the presented measurements to a real condition can be obtained by using the developed predictive models in this study or by using other published models. However, for a more accurate correlation and calibration of these models, field studies on GFRP bars used in real structural applications for a prolong used time should be carried out.

4.4.1.2.2 Flexural properties and inter-laminar shear strength

Table 4.6 summarizes the results of flexural (flexural strength and modulus of elasticity) and inter-laminar shear tests (ILSS) in terms of average values, coefficients of variation and retention

for unstressed and stressed bars directly exposed to water (W and W-S3) and alkaline solution (K and K-S3) at 20, 40 and 60°C for 6480 hr.

Table 4. 6: The results of flexural (flexural strength and modulus of elasticity) and inter-laminar shear tests (ILSS)

Conditioning		**Flexural Strength**			**Modulus of Elasticity**			**ILLS**		
Exp.	T	Avg	COV	Retention	Avg	COV	Retention	Avg	COV	Retention
	(°C)	(MPa)	(%)	(%)	(GPa)	(%)	(%)	(MPa)	(%)	(%)
REF	20	1368	7.1	100	55.6	1.5	100	73	2.5	100
W	20	1360	4.0	99	59.5	1.3	107	66	4.8	90
	40	1326	4.3	97	62.4	0.7	112	63	3.3	86
	60	1124	4.0	82	56.2	1.0	101	55	5.4	75
W-S3	20	1331	6.6	97	56.1	1.7	101	65	3.8	89
	40	1054	8.2	77	65.4	4.6	115	64	3.7	87
	60	1054	5.0	77	58.2	2.7	104	63	4.0	86
K	20	1203	1.6	88	57.8	0.2	103	70	1.6	95
	40	1296	3.5	94	57.9	0.3	103	68	3.5	93
	60	1143	4.0	83	55.8	0.2	100	54	4.0	74
K-S3	20	1306	7.9	95	55.8	2.2	100	66	6.2	90
	40	1157	3.9	84	57.4	2.3	103	64	1.7	87
	60	1145	2.2	83	52.92	2.2	95	61	1.3	85

The retention of mechanical properties is also shown in Figure.4.13 and Figure. 4.14 along with the moisture absorption (MAb) rate results to illustrate the effects of moisture ingress on flexural and inter-laminar properties.

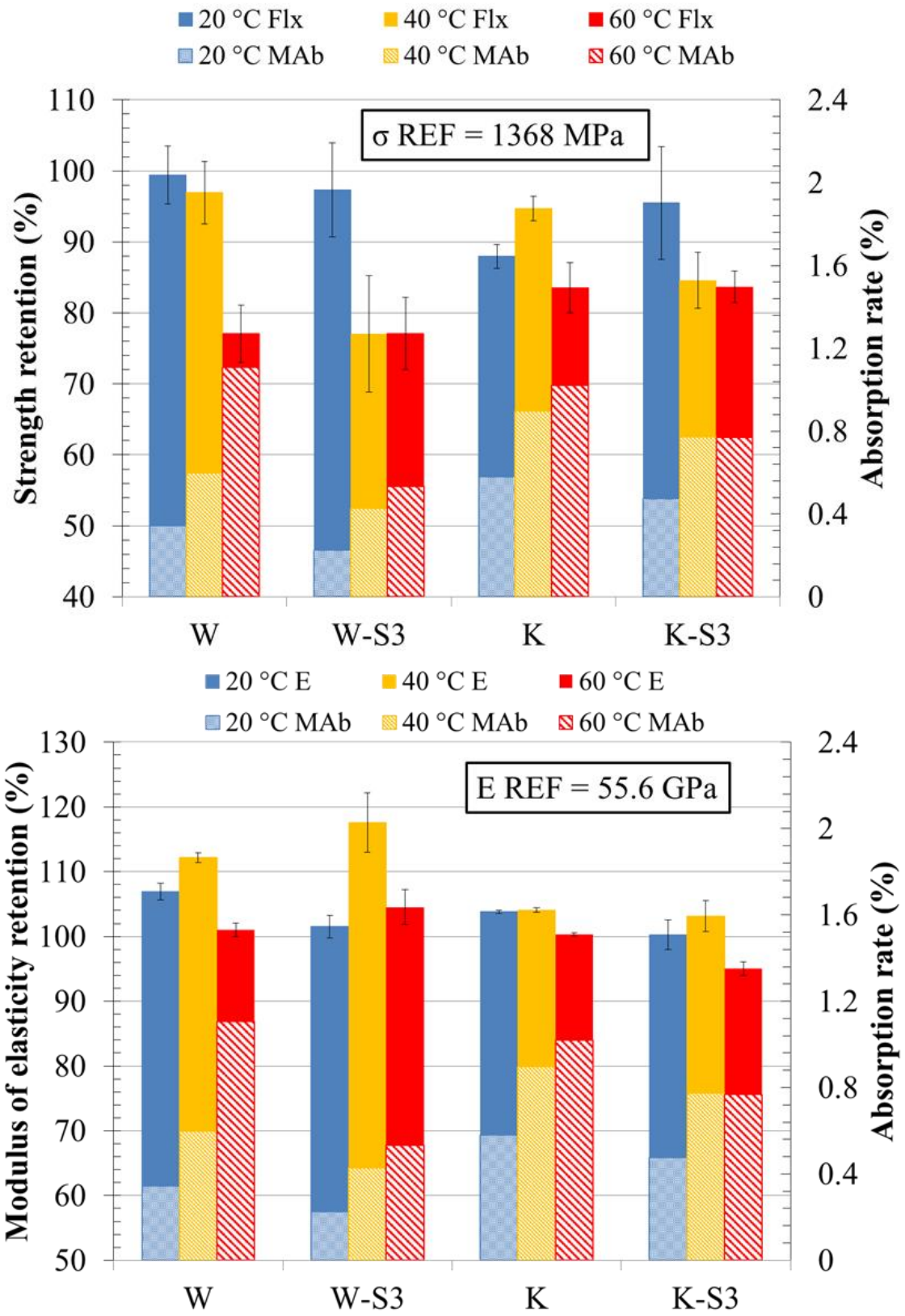

Figure 4. 13: Flexural strength (Flx) and modulus of elasticity (E) are compared to moisture absorption results (MAb) for different conditioning environments after 6480 hr.

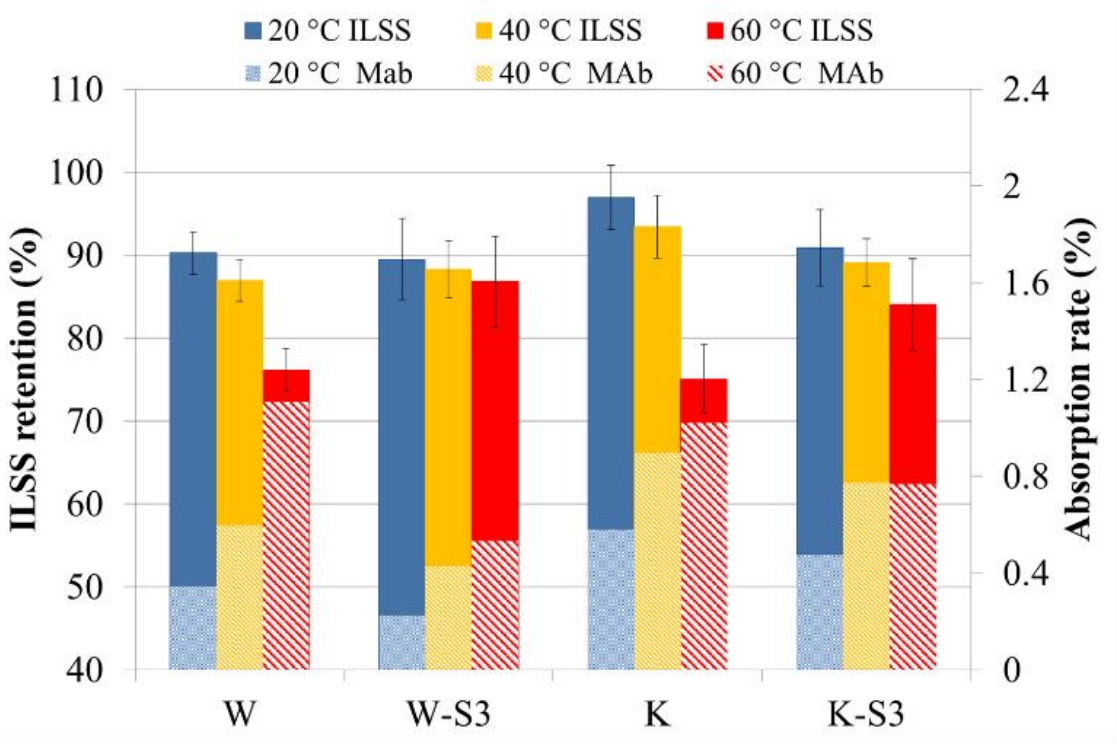

Figure 4. 14: Inter laminar shear strength retention (ILSS) is compared to moisture absorption results (MAb) for different conditioning environments after 6480 hr

It can be noticed that the average flexural strength of all conditioned specimens decreased compared to the reference specimens. In particular, for exposures at 20 and 60°C, the higher the temperature, the lower the flexural strength, which is in line with the finding previously discussed for TNS and MAb tests. Conversely, at 40°C, the application of sustained stress appears to effect strength retention significantly, as the strength of stressed samples was much lower than that of unstressed ones. However, this behaviour was only recorded for flexural tests and the same trend was not observed in TNS and ILSS tests results.

The average values of the flexural modulus of elasticity increased marginally for most of the specimens, with the exception of samples conditioned in water at 40°C for which the flexural stiffness increased more than 10%. The overall higher stiffness could have been caused by post-curing of the matrix during conditioning. This is in line with the results obtained from the direct tension tests as well as the FTIR findings, albeit at lower temperature.

The results from the ILSS tests show that the higher the conditioning temperature, the higher the strength degradation, but also that stressed specimens experienced lower reduction in ILSS than unstressed ones. Such findings are in good agreement with previous tests carried out in this study, suggesting that the increased temperature favoured the ingress of moisture leading to a premature

inter-laminar de-bonding and that the state of stress induced using the test set-up described in Figure.4.2b limited moisture ingress mitigating the reduction in ILSS. Therefore, further tests on bars subjected to different stress distributions (e.g. uniform tension) should be carried out to examine this aspect in more details.

4.5 CONCLUSIONS

The present study investigated the mechanical performance and physical and chemical characteristics of GFRP bars conditioned in different environments with and without sustained stress. The mechanical and micro structural properties were evaluated by direct tension test, flexural tests, inter-laminar shear tests, moisture absorption, SEM-EDX, FTIR, and DMA. On the basis of the discussion presented above, the following conclusions can be drawn:

- Moisture uptake of the tested GFRP bars occurred at a faster rate up to 4600 hr. The different rate of diffusion can be attributed to the moisture absorption via capillaries and micro-cracks in the resin matrix. This mechanism continues until moisture reaches the fibres, which provide a barrier and restrict moisture flow. The tests results also confirmed that diffusion rate during the initial stages is highly dependent on the temperature, and higher temperatures lead to higher absorption rates.
- Unexpectedly, the stressed specimens exhibited lower absorption rate than the unstressed counterparts. This may be attributed to the method that was used to induce the desired strain (i.e. imposing the required curvature via elastic bending) and the closing of micro cracks within the compression zone of the specimens. Further tests on bars subjected to different stress distributions (e.g. uniform tension) should be carried out to examine this aspect in more details.
- The tensile test results clearly show that the tensile strength of the tested GFRP bars was affected by the conditioning environments. In general, higher temperatures and higher levels of sustained stress lead to higher strength degradation. Similar trends were observed for all types of exposure with most of the tensile strength reduction occurring within the first 2000 hr. This can be attributed to the high diffusion of water molecules through the resin matrix outer layer inducing damage to the fibre/resin interface. After 2000 hr exposure, bars embedded in concrete under sustained stress equivalent to 5000 με conditioned in water at 60°C exhibited the higher reduction in strength due to the acceleration of moisture uptake caused by the high temperature and as a result of the higher level of damage in the matrix caused by the sustained stress.

- The reduction in the tensile strength of all conditioned samples subjected to a sustained stress equivalent to 3000 με was within the limits recommended in existing codes for high durability bars. A lower average strength retention was observed only for the specimens subjected to the higher sustained stress equivalent to 5000 με.
- No significant change was observed in the elastic modulus of the tested GFRP bars regardless of the conditioning environment or exposure period. Although a small degree of degradation was observed through SEM and EDX in the outer resin matrix layer and some of the glass fibres closer to the surface of the bar, the observed level of damage was too small to result into an appreciable stiffness reduction.
- The change in flexural properties (e.g. strength, stiffness) was in line with what observed as a result of direct tension tests.
- No significant deterioration was observed through SEM/EDX in the glass fibres. The debonding between fibre/matrix seems to be the main issue affecting the long-term mechanical properties of GFRP bars.
- The EDX scan detected additional elements such as silicon (Si), aluminium (Al), and calcium (Ca) in the interface zone and in the resin matrix. This is attributable to the dissolution of the fibres and leaching of their components into the resin matrix.
- The FTIR analysis showed a significant increase in the amount of hydroxyl groups at the surface of the material. This is an indication of chemical degradation in the resin matrix.

In summary, the long-term mechanical properties of GFRP bars appear to be mainly affected by diffusion of moisture through the resin rich layer and the debonding between the fibre/matrix interfaces due to the dissolution of the saline coupling agents. Therefore, more developmental work could focus on these aspects to improve further the durability of GFRP bars for civil engineering application.

4.6 REFERENCES

1. Nkurunziza G,Debaiky A, Cousin P, Benmokrane B. Durability of GFRP bars: A critical review of the literature. Progress in Structural Engineering and Materials, 2005; 7(4):194-209.
2. Dejke V. Durability of FRP Reinforcement in Concrete. Literature and Experiments. Sweden: Department of Building Materials. Chalmers University of Technology Goteborg, 2001, p. 210.
3. Karbhari V, Chin W, Hunston D, Benmokrane B, Juska T, Morgan R, Lesko J, Sorathia U, Reynaud D. Durability gap analysis for fiber-reinforced polymer composites in civil infrastructure. Journal of composites for construction, 2003; 7(3):238-247.
4. Micelli F, Nanni A. Durability of FRP rods for concrete structures. Construction and Building materials, 2004; 18(7): 491-503.
5. Benmokrane B, Wang P, Ton-That TM. Durability of glass fiber-reinforced polymer reinforcing bars in concrete environment. J Compos Constr, 2002; 6(3):143–153.
6. Chen Y, Davalos J, Ray I, Kim H. Accelerated aging tests for evaluations of durability performance of FRP reinforcing bars for concrete structures. Composite Structures, 2007. 78(1):101-111.
7. Nelson WB. Accelerated testing: statistical models, test plans, and data analysis. John Wiley & Sons; 2009.
8. Bank LC, Gentry TR, Barkatt A. Accelerated Test Methods to Determine the Long-Term Behavior of FRP Composite Structures: Environmental Effects. Journal of Reinforced Plastics and Composites, 1995; 14(6):559-587.
9. Byars E,Waldron P, Dejke V, Demis S, Heddadin S. Durability of FRP in concrete deterioration mechanisms. International Journal of Materials and Product Technology, 2003; 19(1):28-39
10. Benmokrane B, Elgabbas F, Ehab A, ASCE M and Cousin P. Characterization and comparative durability study of glass/vinylester, basalt/vinylester, and basalt/epoxy FRP bars. Journal of Composites for Construction, 2015; 19(6):04015008.
11. Mufti AA, Onofrei M, Benmokrane B, Banthia N, Boulfiza M, Newhook J, Bakht B, Tadros G, Brett P. Report on the studies of GFRP durability in concrete from field demonstration structures. In: Proceedings of the Conference on Composites in Construction. Lyon, Jul, 2005. p.11-13

12. Sawpan MA, Mamun AA, Holdsworth PG. Long-term durability of pultruded polymer composite rebar in concrete environment. Materials & Design, 2014; 57:616-624
13. Robert M, Benmokrane B. Behavior of GFRP reinforcing bars subjected to extreme temperatures. Journal of Composites for Construction, 2009; 14(4):353-60.
14. Bank LC, Gentry TR, Barkatt A, Prian L, Wang F, Mangla SR. Accelerated aging of pultruded glass/vinylester rods. In: Second International Conference on Composites in Infrastructure, Januaray, 1998 (Vol. 2).
15. Robert M, Benmokrane B. Combined effects of saline solution and moist concrete on long-term durability of GFRP reinforcing bars. Construction and Building Materials, 2013; 38:274-84.
16. Fergani H, Di Benedetti M, Guadagnini M, Lynsdale C, Mais C. Long-term performance of GFRP bars under the combined effects of sustained load and severe environments. In: The 8th International Conference on Fibre-Reinforced Polymer (FRP) Composites in Civil Engineering. Hong Kong, 2016.
17. Serbescu A, Guadagnini M, Pilakoutas K. Mechanical characterization of basalt FRP rebars and long-term strength predictive model. Journal of Composites for Construction. 2014; 19(2):04014037.
18. Robert M, Cousin P, Benmokrane B. Durability of GFRP reinforcing bars embedded in moist concrete. Journal of Composites for Construction. 2009; 13(2):66-73.
19. Kamal AS, Boulfiza M. Durability of GFRP rebars in simulated concrete solutions under accelerated aging conditions. Journal of Composites for Construction. 2010; 15(4):473-81.
20. fib Task-group 9.3. FRP Reinforcement in RC Structures. fib Bulletin. 2007; 40, (147).
21. Canadian Standard Association (CSA). Specification for fibre-reinforced polymers. CAN/CSA S807-10. Rexdale, Ontario, Canada; 2010. p 27.
22. ACI 440.3R-04. Guide test methods for fiber-reinforced polymers (FRPs) for reinforcing or strengthening concrete structures, ACI Committee 440, American Concrete Institute, Farmington Hills, Michigan, USA; 2004.
23. Almusallam TH, Al-Salloum YA. Durability of GFRP rebars in concrete beams under sustained loads at severe environments. Journal of composite materials, 2006; 40(7):623-37.

24. Wu G, Dong ZQ, Wang X, Zhu Y, Wu ZS. Prediction of long-term performance and durability of BFRP bars under the combined effect of sustained load and corrosive solutions. Journal of Composites for Construction, 2014; 19(3):04014058.
25. Nkurunziza, G, Benmokrane B, Debaiky A, Masmoudi R, Effect of sustained load and environment on long-term tensile properties of glass fiber-reinforced polymer reinforcing bars. ACI structural journal, 2005. 102(4):615.
26. Wang J, GangaRao H, Liang R, Zhou D, Liu W, Fang Y. Durability of glass fiber-reinforced polymer composites under the combined effects of moisture and sustained loads. Journal of Reinforced Plastics and Composites, 2015; 21:1739-54.
27. Bakis CE. Durability of GFRP reinforcement bars. InAdvances in FRP Composites in Civil Engineering. Berlin:Springer, 2011. p.33-36.
28. Broomfield, PJ. Corrosion of Steel in Concrete: Understanding, Investigation and Repair. London: Chapman & Hall, 1997. p.1-215.
29. Mias C, Guadagnini M, Torres L, Fergani H. Strength of GFRP RC beams after sustained loading. In: Proceedings of FRPRCS-12 & APFIS-15.Conference.Nanjing, 2015.
30. ASTM Standard D4475,2002(2016), "Test Method for Apparent Horizontal Shear Strength of Pultruded Reinforced Plastic Rods By the Short-Beam Method". ASTM International, West Conshohocken, PA.
31. ASTM Standard D 4476, 2003(2014), "Test Method for Flexural Properties of Fiber Reinforced Pultruded Plastic Rods,". ASTM International. West Conshohocken, PA.
32. ASTM Standard D7028,2007(2015),"Test Method for Glass Transition Temperature (DMA Tg) of Polymer Matrix Composites by Dynamic Mechanical Analysis (DMA) ", ASTM International. West Conshohocken, PA.
33. ASTM Standard D570,1998(2010), "Test Method for Water Absorption of Plastics, ", ASTM International. West Conshohocken, PA.
34. Lu Z, Xian G, Li H. Effects of exposure to elevated temperatures and subsequent immersion in water or alkaline solution on the mechanical properties of pultruded BFRP plates. Composites Part B: Engineering, 2015; 77:421-430.
35. Mousa A, Karger-Kocsis J. Cure characteristics of a vinyl ester resin as assessed by FTIR and DSC techniques. Polymer and Polymer Composites. 2000 Jan 1;8(7):455-60.

CHAPTER 5

5 LONG-TERM PERFORMANCE OF GFRP BARS IN CONCRETE ELEMENTS UNDER SUSTAINED LOAD AND ENVIRONMENTAL ACTIONS

ABSTRACT

This chapter presents an experimental study aimed at investigating the long-term tension stiffening and flexural behaviour of concrete elements reinforced with glass fibre reinforced polymer (GFRP) bars subjected to accelerated aging conditions. Six tension stiffening specimens and eight small-scale GFRP RC beams were exposed to different environments and sustained stress levels for 120 and 270 days, respectively. Subsequently, the specimens were tested to failure and their behaviour was compared to that of reference specimens. The test results revealed that stressed specimens conditioned in a wet environment experienced a reduction in tension stiffening response as a result of bond degradation and a reduced stress transfer from the bar to the surrounding concrete. The results also indicate that the accelerated aging conditions affected the overall flexural behaviour and led to higher deflections and larger crack widths. The long-term deformation of elements subjected to a stress level representing typical in-service conditions, however, always complied with the design limits suggested by current guidelines. Higher imposed loads (inducing maximum strain level in the reinforcement of about 5000με) led to both deflections and crack widths in excess of the values recommended at serviceability limit state. Finally, the response of the tested specimens is compared to that predicted according to fib Model Code 2010 and Eurocode 2 and it is shown that both models fail to capture adequately the long-term structural behaviour of stressed GFRP RC specimens conditioned in wet environment.

5.1 INTRODUCTION

The use of fibre reinforced polymer (FRP) bars, and in particular glass FRP (GFRP), as reinforcement in concrete structures to address corrosion-related issues is receiving a great deal of attention and a significant growth in field applications has been recorded in the past few years [1-4]. Despite being recognised as durable reinforcement, however, the work conducted in the past three decades has focused mainly on the short-term behaviour of FRP RC elements [5-12], and very few studies have investigated their long-term structural performance [13,14]. The limited experimental research on this topic, which is often inconclusive, is inadequate to demonstrate the long-term potential benefits of this new class of reinforcement. Experience from field studies is also limited due to the relatively young age of existing field applications. Thus, understanding the long-term performance of FRP RC elements at both serviceability and ultimate limit states is key to enable an optimal and safe design of more sustainable structures and infrastructure. Current design procedures and guidelines for FRP RC elements rely heavily on the outcome of short-term studies [17-20], hence their validity in predicting long-term performance needs to be carefully assessed, especially in terms of service conditions, which often govern the design.

Researchers have suggested modifications to Branson's equation to account for the effect of relatively low stiffness of FRP reinforcement on the effective moment of inertia when calculating short-term deflections of FRP RC elements [7-10,18], or have proposed modifications on the basis of observations on the more fundamental tension stiffening behaviour [11,21-24]. These different approaches have been implemented in current design guidelines for FRP RC (e.g. [25-28]) but have been shown to overestimate tension stiffening and underestimate deflections [29,30]. In addition, there is very limited research examining long-term tension stiffening response [e.g. 31], and no studies have been reported on the combined effects of severe environmental exposure and loading conditions on the long-term tension stiffening and flexural behaviour of GFRP RC members.

Exposure to different chemical environments, moisture, elevated temperatures or temperature variations can all cause degradation of the resin-rich outer layer, thus affecting the bond between bar and concrete, and affect adversely the bond between fibres and resin in the reinforcing bars (i.e. interlaminar shear)[32]. Exposure to ordinary temperature cycles can also lead to bond degradation due to the difference in thermal expansion between the bar and the concrete [33]. All of these environmental conditions would cause a reduction in tension stiffening and affect the performance of GFRP RC members in bending.

This chapter presents part of a multi-scale experimental programme that is aimed at providing a better understanding of the durability of GFRP bars in concrete. Accelerated tests on small and medium-scale bare bar specimens [32] were complemented by accelerated tests on GFRP RC tension ties and small scale beams to examine the long-term bond and flexural behaviour of GFRP RC members under service conditions. Two different levels of sustained stress were considered in this study: 1) a stress inducing a level of strain in the FRP bar equivalent to 3000 με to generate a state of stress in the concrete surrounding the bars that is typical of prescribed service conditions; 2) a stress level inducing a level of strain in the FRP bar equivalent to 5000 με to initiate greater damage in the surrounding concrete and promote a higher degradation rate.

Test results presented in this chapter are used to assess the performance of existing tension stiffening models and predict long-term deflections of GFRP RC members. The outcome of this study will provide important insights into the durability of FRP bars in concrete and inform the development of more reliable design equations to predict the long-term behaviour of FRP RC elements under service conditions, in terms of both deflections and crack width.

5.2 EXPERIMENTAL TEST PROGRAMME

"The author apologies for some repetition in experimental work program as this chapter has been published as journal paper".

This study is part of an extensive experimental programme carried out at the University of Sheffield that is aimed at examining the durability of GFRP bars in concrete members. Typical environmental conditions known to accelerate the degradation processes of GFRP bars in concrete structures were examined in this study, along with the application of given levels of sustained stress. A maximum temperature of 60°C was chosen based on tests recommended in different standards and employed in previous research [26, 34-36]. This level of temperature was found to be high enough to accelerate the degradation of the mechanical properties of the bars, yet still below the glass transition temperature expected for typical pultruded GFRP reinforcement. The length of exposure was also chosen on the basis of previous research employing accelerated tests and it was found to be appropriate to enable the onset and stabilisation of the main degradation processes [35, 36]. Six tension stiffening specimens (TS) and eight simply supported small-scale GFRP RC beams (BM) were exposed to different environments and sustained stress levels and load tested to study their long-term performance. The specimens are designated according to the format XX.ttt.TT°C.E.SS, where XX denotes the specimen typology, ttt, TT°C and E are the exposure time, temperature and environment(a=air, W=water), respectively, while SS represents

the loading condition. For example, TS.120.60°C.W.3k is a tension stiffening specimen, exposed for 120 days to water at 60°C with a sustained load inducing 3000 με in the reinforcement.

Tension stiffening specimens were square in cross-section (100 x 100 mm) and 1100 mm long with an effective bond length, lc, of 500 mm (Figure. 5.1). After casting, these specimens were cured in water at 20°C to minimise the effects of drying shrinkage on the tension stiffening behaviour.

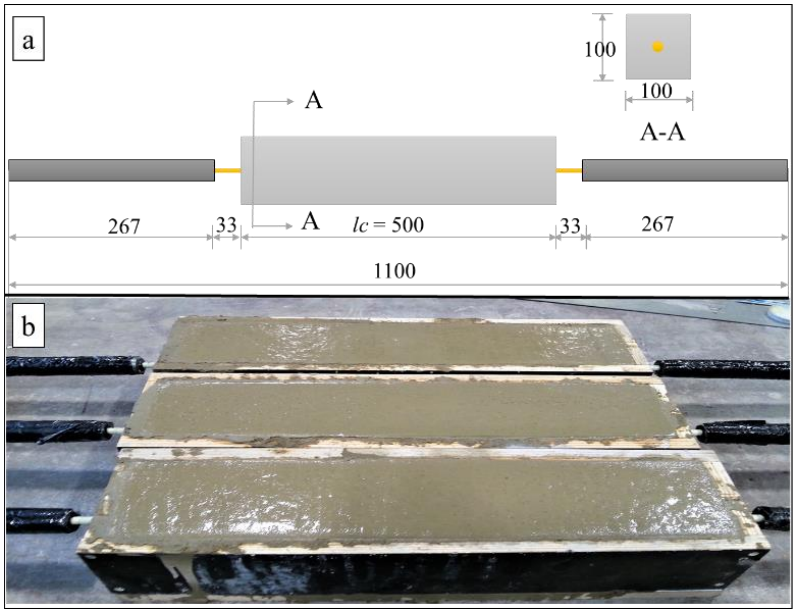

Figure 5. 1 Geometric details of the Tenssion stiffening specimens (all dimensions in mm)

All RC beams were 110 mm wide, 150 mm deep and 1200 mm long, with a clear span of 1000 mm (Figure. 5.2). The longitudinal reinforcement consisted of two ribbed GFRP bars in tension and two sand coated basalt FRP (BFRP) bars in compression. The GFRP bars used in this research were made of continuous longitudinal glass fibres impregnated in vinyl ester resin with a glass fibre content of 75% by weight, whereas the BFRP bars were produced using a vinyl ester resin matrix with an estimated 75% fibre volume fraction. Both bars were manufactured using a pultrusion process and had a nominal diameter of 8mm and 4mm respectively. The BFRP bars were mainly used to ease the building of the cages, and their contribution to ultimate capacity and overall structural behaviour can be considered to be negligible, yet resulting in a completely non-metallic reinforcing solution. Closed GFRP shear links with a rectangular cross section of 4x10mm were used as shear reinforcement over the shear spans (equally spaced at 100 mm), while steel stirrups were placed in proximity of both supports and loading points to prevent local crushing of concrete. No stirrups were provided in the pure bending zone.

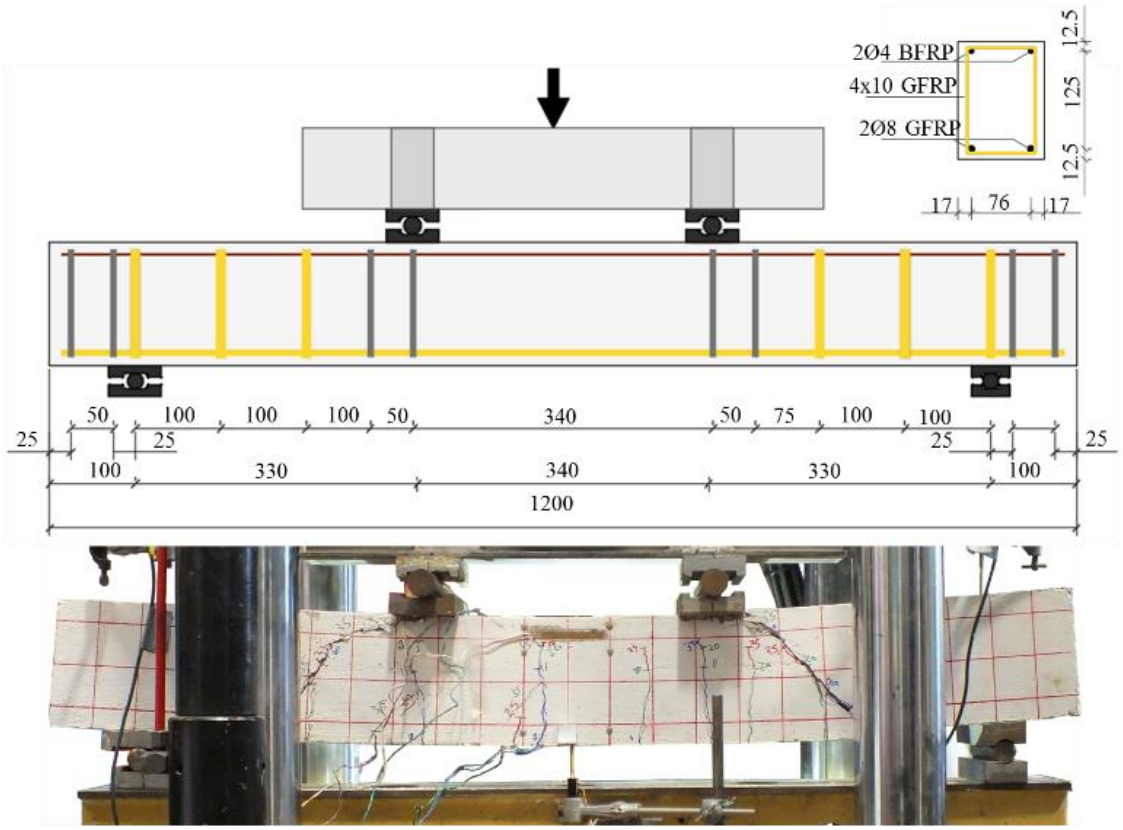

Figure 5. 2: Geometric details and test set-up of the tested FRP RC beams (all dimensions in mm)

Beams and tension stiffening specimens were cast in separate batches using the same mix design consisting of 358 kg/m3 of cement type CEM I, 1000 kg/m3 of coarse aggregate with a maximum size of 10 mm, 817 kg/m3 of sand and a water/ cement ratio of 0.63 and 0.53, respectively. The mechanical properties of the concrete used in this study are summarized in Table 5.1, which include compressive strength f_c, splitting tensile strength f_{ct} and modulus of elasticity E_c measured according to BS EN 12390-1, ASTM C496 and ASTM C469 [37-39], respectively. Concrete cubes and cylinders were cured under the same conditions as the test specimens (i.e., TS, BM) and tested on the same day as the corresponding specimens were tested. Ribbed GFRP bars with a nominal diameter of 8 mm were utilized in this study as tensile reinforcement for both TS and BM specimens.

Table 5. 1: Concrete properties

Sample	Conditioning			f_c		E_C		f_{ct}	
	Environment (RH %)*	Temperature (°C)	Time (days)	Avg (MPa)	St.D	Avg (GPa)	St.D	Avg (MPa)	St.D
BM	RH 80%	20	0	55.0	1.4	33.1	0.4	3.2	0.2
BM	RH 100%	60	270	35.5	3.9	26.2	3.5	2.6	0.5
BM	RH 50%	20	270	50.4	8.4	33.1	2.1	3.0	0.3
TS	RH 80%	20	0	60.5	5.2	33.8	1.0	3.6	0.3
TS	RH 100%	60	120	52.0	6.0	32.7	1.8	3.0	0.1

*RH Relative humidity

Table 5.2 summarizes the average values and associated standard deviations of the rupture tensile strength, f_{fu}, the modulus of elasticity, E_f, and the maximum strain, ε_{fu}, as obtained from uniaxial tension tests carried out on four samples according to ACI 440.3R-04 [34]. Nominal manufacturer values, when available, are provided in brackets.

Table 5. 2: Reinforcement material properties.

Reinforcement			E_f		ε_{fu}		f_{fu}	
Type	Material	Size (mm)	Avg. (GPa)	St.D. (GPa)	Avg. (%)	St.D. (%)	Avg. (MPa)	St.D. (MPa)
Tension	GFRP	Ø8	57.0 (60.0)	1.5	2.8	0.9	1542.0 (1000.0)	28.0
Compression	BFRP	Ø4	44.0	1.0	2.9	_	1285.0	47.0
Shear	GFRP	4x10	28.0	_	1.9	_	720.0	_

The complete test matrix is presented in Table 5.3. Two benchmark beams were unconditioned and unstressed. The remaining six beams were clamped in pairs back to back using an external rigid fixture consisting of transverse steel bolts and steel springs sandwiched between two steel plates as shown in (Figure.5.3-a). The desired sustained load was imposed by compressing the springs of a predetermined amount. A sustained stress inducing a tensile strain of 3000 με was selected as recommended by SLS design code provisions [25], while a higher stress inducing a strain of 5000 με was examined to assess the effect of less stringent serviceability limits. Some of the stressed specimens were submerged in water at 60°C for 270 days to accelerate aging. In addition, two TS specimens were tested as reference, while the remaining were conditioned at 60°C and 100% relative humidity (RH) for 120 days, two of which were also stressed inducing a strain level of about 3000 με in the reinforcement. The desired level of tensile strain in the TS specimens was applied via a spring of adequate stiffness mounted in a stiff pre-tensioning rig as shown in (Figure. 5.3-b). During the conditioning period, the mid-span deformation of the beams was measured periodically using a caliper and demec gauge system. The crack width was measured using a hand-held microscope with a precision of 0.02 mm, whilst the sustained strain in the reinforcement was monitored using strain gauges installed on each of the GFRP bars at mid-span.

Table 5. 3: Specimens designation

Specimen		Conditioning			Applied strain in longitudinal reinforcement (με)
Label	Test	Environment	Temperature (°C)	Time (d)	
TS.REF	TS	Lab	20	0	0
TS.120.60.W	TS	Water	60	120	0
TS.120.60.W.3k	TS	Water	60	120	3000
B.REF	FLX	Lab	20	270	0
BM.270.20.a.3k	FLX	Lab	20	270	3000
BM.270.60.W.3k	FLX	Water	60	270	3000
BM.270.60.W.5k	FLX	Water	60	270	5000

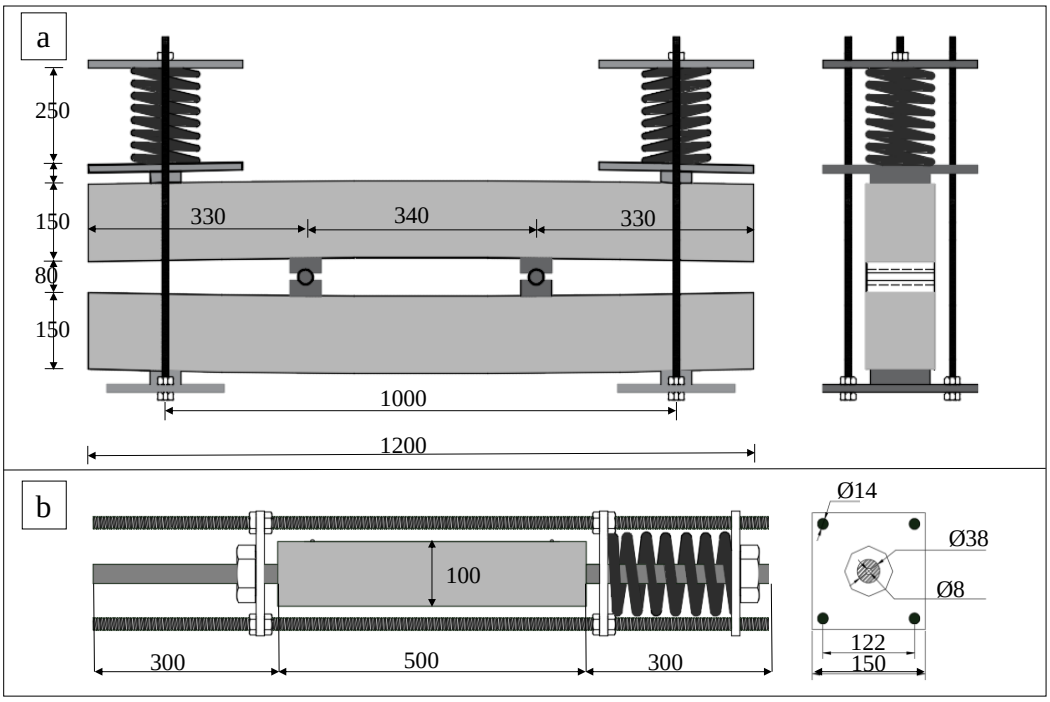

Figure 5. 3: Sustained load for simulating service loading (a) on beams (b) on tension stiffening specimens(all dimensions in mm)

5.2.1 Test set-up and instrumentation

5.2.1.1 Tension stiffening specimens

TS specimens were tested with the set-up shown in Figure. 5.4 using a 1,000 kN ESH universal testing machine in displacement control at a rate of 1 mm/min. Precautions were taken to avoid crushing of the bars in the machine grips. In particular, two threaded steel bars were drilled axially to obtain a hole in the longitudinal direction sufficiently large to accommodate the GFRP bar.

These fixtures were mounted at both ends of the GFRP bars and bonded using epoxy resin. Each threaded steel bars was then embedded in two steel profiles and gripped in the machine (Figure. 5.4. A-A).

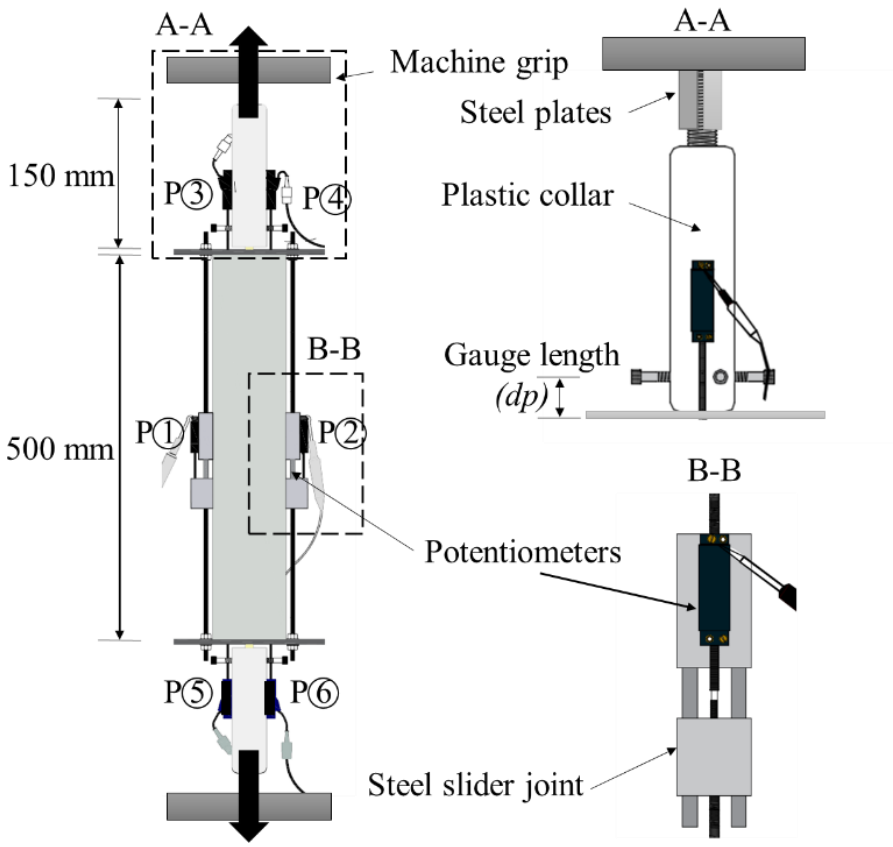

Figure 5. 4: Test set-up for direct tension test

Figure. 5.4 also illustrates the layout of the potentiometers (P1 to P6) used to measure the average concrete deformation (P1 and P2, $dc_{concrete}$) and the average slip between the GFRP bar and the top (P3 and P4, $df_{slip,top}$) and bottom (P5 and P6, $df_{slip,bottom}$) surfaces of the concrete prism. Potentiometers P1 and P2 were placed on two slider joints bolted to the steel plates at both ends of the concrete prism, while potentiometers P3 to P6 were mounted on a plastic collar coaxial to the GFRP bar and fixed to it with three equally-spaced screws at distance *dp* from the end surfaces of the concrete prism. The aforementioned test set-up was instrumental in obtaining the composite strain in the RC member and the stress in the concrete, which are the key parameters governing tension stiffening response.

In addition, crack width and spacing were monitored using Digital Image Correlation (3D-DIC) to gain additional insights into the initiation and development of bond degradation. DIC is a contactless measuring technique for determining full-field deformations on the surface of an

object under loading [40]. In this study, images were acquired with two CMOS digital cameras having a 4272×2848 pixel resolution (Canon EOS 1100D) and equipped with zoom lenses with F-number and focal length of 5.6 and 25 mm, respectively (Canon EF-S 18-55mm f/3.5-5.6 IS II). The cameras were rigidly connected 430 mm apart and mounted on a tripod. The stereo-vision system was positioned at 700 mm from the specimen. A light-emitting diode (LED) lamp was used to illuminate the measurement surface. During the test, the shutter was triggered remotely every 10 seconds by the data acquisition system in order to synchronize the images with point-wise transducers readings. The measured surface was smoothed and whitewashed to create a light background. A black speckle pattern was then spray-painted using a flexible stainless steel stencil. The target diameter of the speckles was approximately 1 mm in order to ensure an optimal speckle size of 4.5 pixels [41,42]

The composite strain ($\varepsilon_{composite}$) is the strain in the portion of the bar originally embedded in concrete and it can be calculated by dividing the total measured elongation by the concrete length l_c. The total elongation is obtained as the concrete deformation (*dc*) plus the slip at the two ends of the prism (*ds*) discounted by the elastic deformation of the bar (df_e) at the two ends of the specimen along *dp* (Eq. 5.1).

$$\varepsilon_{composite} = \frac{Total\ elongation}{Concrete\ length} = \frac{dc+ds_{top}+ds_{bot}-\frac{Q}{A_f E_f}(2*df_e)}{l_c} \quad (5.1)$$

where,

Q is the applied load; A_f is the area of the GFRP bar; and E_f is its modulus of elasticity.

The concrete contribution (σ_c) is the tensile stress carried by the concrete as the applied load (Q) increases. This parameter has been used to evaluate the effect of the bar size on tension stiffening behaviour [43] and it will be employed in this study to assess the concrete tensile performances for different conditioning environments. The concrete contribution (σ_c) can be calculated based on equilibrium and assuming that the reinforcement strain (ε_f) is equal to the composite strain ($\varepsilon_{composite}$) (Eq. 5.2, 5.3, 5.4)

$$Q = Q_C + Q_f \quad (5.2)$$

$$Q_f = E_f . \varepsilon_f . A_f \quad (5.3)$$

$$\sigma_c = \frac{Q - E_f \varepsilon_f A_f}{A_c} \quad (5.4)$$

where,

Q is the applied load and Q_C and Q_f are the forces in the concrete and in the GFRP bar, respectively; and A_c is the area of the cross-section of the concrete prism.

The effect of sustained loading and environmental conditioning on the tension stiffening response will be assessed through the analysis of the tension stiffening performance factor (i_{TFP}) and the bond index.

The tension stiffening performance factor (i_{TFP}) is determined by normalizing the concrete contribution with respect to the tensile cracking strength of the reference sample (f_{cr}) Eq. 5.5.

$$i_{TFP} = \frac{\sigma_c}{f_{cr}} \quad (5.5)$$

The bond index represents the average load carried by the cracked concrete (Q_C) divided by the load carried by the concrete at first crack (Q_{Cr}) [44].

$$bond\ index = \frac{Q_C}{Q_{Cr}} \quad (5.6)$$

5.2.1.2 Analytical model for tension stiffening

The tension stiffening model adopted in *fib* model code 2010 [28], which was originally developed for steel RC, was shown to yield reliable results for the short-term tension stiffening behaviour of GFRP RC members [29]. According to this model, the strain behaviour is calculated in three stages, namely the un-cracked stage, the crack formation stage and the stabilized cracking stage, according to Eq.5.7, Eq. 5.8 and Eq.5.9, respectively.

Stage I (Un-cracked): $$\varepsilon^*_{composite} = \frac{\sigma_c}{E_C} \quad (5.7)$$

Stage II (Crack formation): $$\varepsilon^{*}_{composite} = \frac{\sigma_{fr}.(1-\beta)}{E_f} \quad (5.8)$$

Stage III (Stabilized cracking): $$\varepsilon^{*}_{composite} = \frac{\sigma_f - \beta.\sigma_{fr}}{E_f} \quad (5.9)$$

where,

The maximum bar stress at a crack during stage II (σ_{fr}) can be defined according to Eq. 5.10

$$\sigma_{fr} = \frac{f_{ctm}}{\rho_{f.eff}}\left(1 + \alpha_c \rho_{f.eff}\right) \quad (5.10)$$

where,

σ_f is the stress in the FRP bar at a crack; f_{ctm} is the tensile strength of the concrete; β is an empirical coefficient to assess the mean strain depending on the type of loading and can be either 0.6 for short-term loading or 0.4 for long-term loading; $\rho_{f,eff}$ is the ratio between the cross-sectional area of bar and concrete; and α_c is the ratio between the modulus of elasticity of FRP and concrete.

5.2.1.3 Beams

Four-point bending tests were carried out using the set-up shown in Figure. 5.2. Beams were instrumented with linear variable differential transducers (LVDTs) at mid-span and at the supports to measure the net deflection. The load was applied in displacement control using a universal testing machine (1000 kN-ESH) at a rate of 1 mm/min. Quasi-static incremental loading cycles were carried out at a load inducing a predefined level of strain in the tensile reinforcement, namely 3000 με and 5000 με, before the beams were loaded to failure. Crack widths were also measured at every 5 kN load increment with a crack width microscope.

5.2.1.4 Review of EC2 code to predict deflection

According to Eurocode 2 [45], the total deformations (curvature or deflection) of members subjected to flexure can be calculated by an interpolation between cracked and un-cracked section deformations Eq.5.11, which is conceptually more meaningful to represent the variation of the stiffness along the length of the beam due to the presence of cracking [11,20].

$$\alpha = \zeta.\alpha_{II} + (1-\zeta).\alpha_{I} \quad (5.11)$$

$$\zeta = 1-\beta\left(\frac{M_{cr}}{M}\right)^2 \quad (5.12)$$

where,

α is the considered deformation parameter (e.g. deflection) and the subscripts I and II refer to un-cracked and cracked states, respectively; ζ is a distribution coefficient (accounting for tensioning stiffening response of the RC member at a section); β is a load duration coefficient (1 for short-term loading and 0.5 for sustained or repeated loading); M_{cr} is the cracking moment; and M is the applied moment.

5.2.1.5 Review of EC2 code to predict maximum crack width and spacing

EC2 calculates the maximum crack width and the maximum crack spacing according to Eq. 5.13 and Eq. 5.14, respectively.

$$w_{cr,max} = S_{cr,max}\left(\varepsilon_{fm} - \varepsilon_{cm}\right) \quad (5.13)$$

$$S_{cr,max} = 3.4c + 0.425k_1k_2\emptyset/\rho_{p,eff} \quad (5.14)$$

$$\left(\varepsilon_{fm} - \varepsilon_{cm}\right) = \frac{\sigma_f}{E_f} - \frac{k_t f_{ct,eff}\left(1+\alpha_c\rho_{p,eff}\right)}{E_f\rho_{p,eff}} \geq 0.6\frac{\sigma_f}{E_f} \quad (5.15)$$

Where,

$S_{cr,max}$ is the maximum crack spacing; c is the concrete cover; k_1 is the bond coefficient equal to 0.8 for good bond performance and 1.6 for low bond performance; k_2 is a coefficient depending on the form of the strain distribution (0.5 for bending and 1 for pure tension); ϕ is the diameter of the bar; $\rho_{p,eff}$ is the effective reinforcement ratio, where the effective area of the concrete in tension is calculated according to Eq. 5.16

$$A_{eff} = min\left\{2.5b.(h-d), \frac{b(h-x)}{3}, \frac{bh}{2}\right\} \quad (5.16)$$

Where,

h and *b* are the width and the height of the beam; *d* is the effective depth; and *x* is the neutral axis depth.

The mean differential strain (ε_{fm}-ε_{cm}) can be calculated according to Eq. 5.15 as the difference between the strain in the reinforcement, ε_{fm}, and the mean concrete strain, ε_{cm}, between cracks, which takes into account the tension stiffening effect; the stress in the tension reinforcement, σ_f, is calculated by assuming a cracked section; k_t is a factor depending on the duration of the loading (0.6 for short-term loads and 0.4 for long-term loading); and $f_{ct,eff}$ is the effective concrete tensile strength

5.3 EXPERIMENTAL RESULTS AND DISCUSSION

The experimental results are presented in the following sections and are used to discuss the effect of long-term environmental exposure on the tension stiffening and flexural behaviour of the tested specimens.

5.3.1 Tension stiffening response of GFRP RC specimens

The effect of environmental long-term exposure and sustained stress on the tension stiffening behaviour can be evaluated by analysing the load–strain responses, the cracking behaviour and the concrete contribution.

5.3.1.1 Load–strain responses

Figure. 5.5 presents the load–strain responses measured during the experimental tests for the reference specimens and for those conditioned in water at 60°C for 120 days with and without sustained loading. The composite strains ($\varepsilon_{composite}$) were computed according to Eq. 5.1, and, for comparison purposes, the fully cracked response (unconditioned bare GFRP bar) is also plotted.

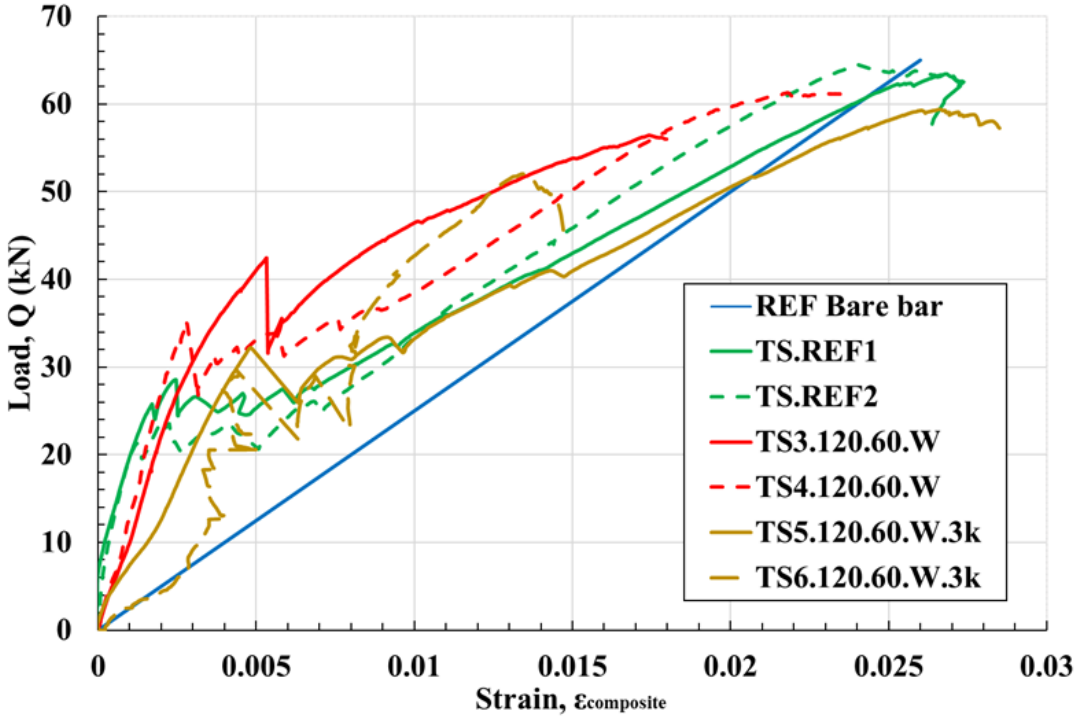

Figure 5. 5: Composite responses against applied load

The graph shows that the unstressed conditioned specimens (TS3.120.60.W and TS4.120.60.W) exhibited significantly higher tension stiffening than the stressed specimens (TS5.120.60.W.3k and TS6.120.60.W.3k). This suggests that, in unstressed specimens, the bond between the bar and the concrete increased, possibly due to the swelling of the bar due to moisture absorption and to the resulting increase in mechanical interlocking and in friction forces at the interface [46].

Figure. 5.6: Extracting the bars from conditioned unstressed specimens

Conversely, specimens conditioned under sustained stress had a relatively lower tension stiffening response after cracking compared to other specimens and an initial softer response up to cracking load. This is supported also by examining the variation of the bond index (β, Eq. 5.6) with increasing $\varepsilon_{composite}$ (Figure. 5.7) and by estimating the tension stiffening as the area under

each curve (A_1, A_2 and A_3). In fact, the observed bond enhancement for unstressed specimens was approximately 40% compared with the references specimens. This confirms the detrimental effect of sustained stress on conditioned samples.

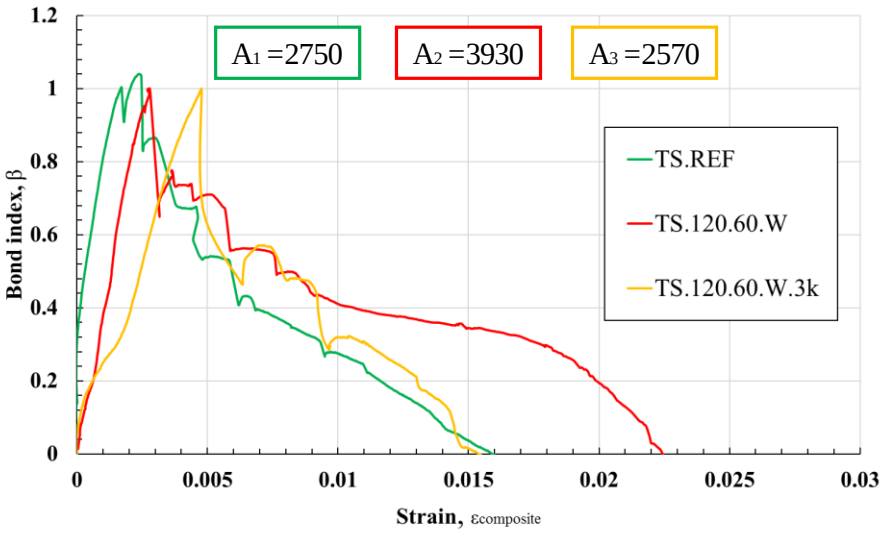

Figure 5. 7: Tension-stiffening bond index response $A_{1,2,3}$ are the area under each curve.

In fact, stressed conditioned samples, despite being exposed to water at 60°C, did not benefit from the moisture absorption and the consequent aforementioned increase of the bond properties, showing a decrease in tension stiffening of approximately 7%. This reduction might be due to the development of micro-cracks as a result of concrete creep and to the deterioration of the resin rich layer of the bars in moist concrete environment, leading to bond degradation and to the consequent slipping of the bar at both ends of the specimens. Evidence of slip between the bar and the concrete was also evident when specimens were subsequently split for closer investigation. Residues of the ribs of the GFRP bar were found encased in the concrete at the two ends of the specimen (Figure. 5.8-a-c), confirming that failure developed at the interface layer between the ribs and the core of the bar.

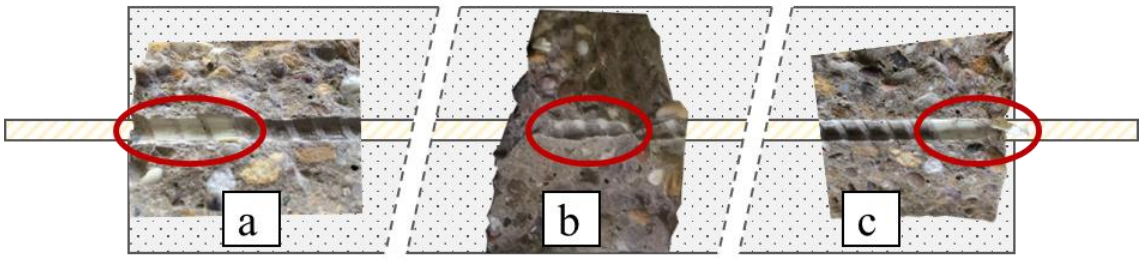

Figure 5. 8: ribs rupture and surface degradation in stressed specimens.

The performance of *fib* 2010 in predicting the short and long-term tension stiffening response of the tested GFRP RC members is presented in Figure. 5.9 (a) and (b) respectively. The bare bar response is also included for reference. While the general trend is well captured, the model significantly underestimates the deformation of both reference and stressed specimens, while it underestimates the tension stiffening behaviour of the unstressed specimens.

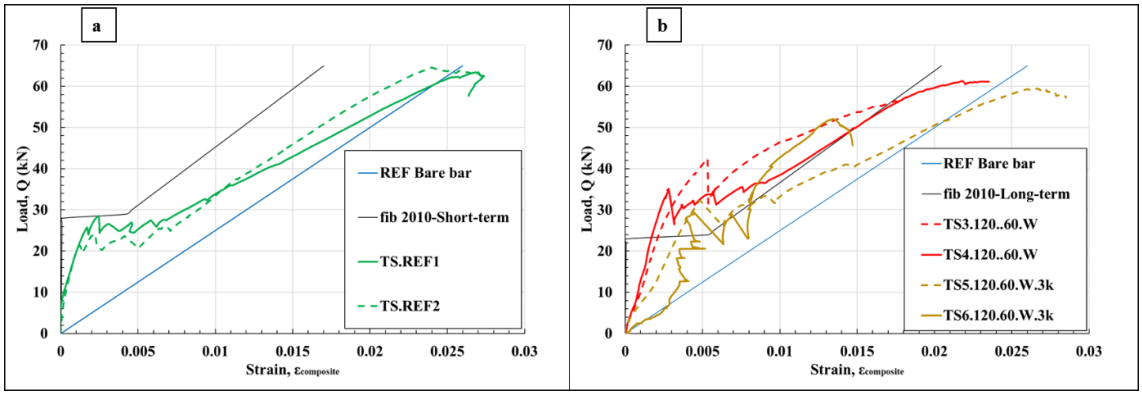

Figure 5. 9: (a) short-term prediction and the corresponding test results for references (b) long-term prediction and the corresponding test results aged specimens

5.3.1.2 Concrete contribution

Figure. 5.10 shows the variation of the tension stiffening performance indexes (i_{TSP}, see Eq.5.5) of both unconditioned and conditioned TS specimens as a function of composite strain ($\varepsilon_{composite}$, Eq. 5.1).

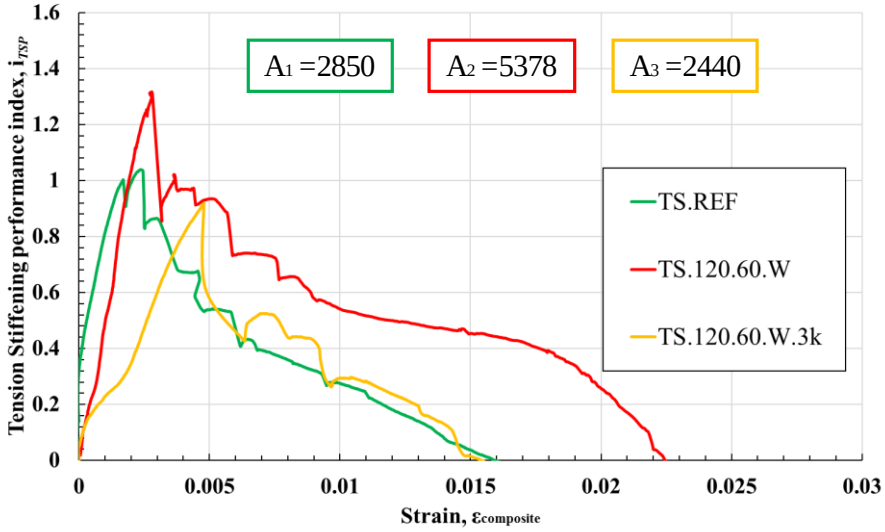

Figure 5. 10: Tension stiffening contribution

The areas under each curve, which are also reported in Figure. 5.10 and are here referred to as the tension stiffening performance values, were calculated and compared to examine the concrete contribution to the overall tensile response. The tension stiffening performance of unstressed specimens conditioned in water at 60°C increased approximately by 88% compared to that of the reference specimens, whereas a decrease of approximately 15% was recorded in the stressed samples. Similarly, the experimental concrete contribution at cracking load, σ_c, calculated according to Eq.5.4 and summarized in Table 5.4, shows on average an increase of approximately 36% for the unstressed specimens and a decrease of approximately 16% for the stressed samples when compared to the control specimens. These results are in line with the observations made above in reference to the bond enhancement found in unstressed samples and the tension stiffening degradation seen in stressed specimens. As evidenced in Figure. 5.8-b, the presence of a sustained load caused local de-bonding along the bar, thus affecting the overall bond and tension stiffening behaviour.

Table 5. 4: Concrete contribution in tensile behaviour

specimens	Concrete contribution at cracking load		$\sigma_c/\sigma_{c\ REF}$
	σ_c	Avg (MPa)	
T.S.REF1	2.0	1.90	1.00
T.S.REF2	1.8		
T.S3.120.60.W	2.7	2.65	1.36
T.S4.120.60.W	2.6		
T.S5.120. 60.W.3k	1.7	1.65	0.84
T.S6.120. 60.W.3k	1.6		

5.3.1.3 Cracking behaviour

Typical crack patterns just before failure are presented in Figure. 5.11, in which cracks can be identified as a sudden increment in the vertical displacement field (i.e. sharp change in colour) captured through DIC. The number associated with each crack represents their order of appearance, while the numbers between cracks are the measured spacing values. Unstressed conditioned specimens exhibited a smaller average crack spacing (60mm) and a higher number of cracks (4) than stressed specimens, characterized by an average crack spacing of 169mm and two primary cracks, and also than reference specimens that had an average crack spacing of 88 mm and three primary cracks. This suggests that the unstressed conditioned specimens had a better bond compared to the others tested specimens and corroborates the observations made

above on bond enhancement in unstressed specimens, which resulted in a more effective stress transfer from the bar to the concrete and consequently in the opening of a higher number of cracks. Conversely, the bond degradation in stressed specimens reduced the stress transferred to the concrete and therefore the number of cracks.

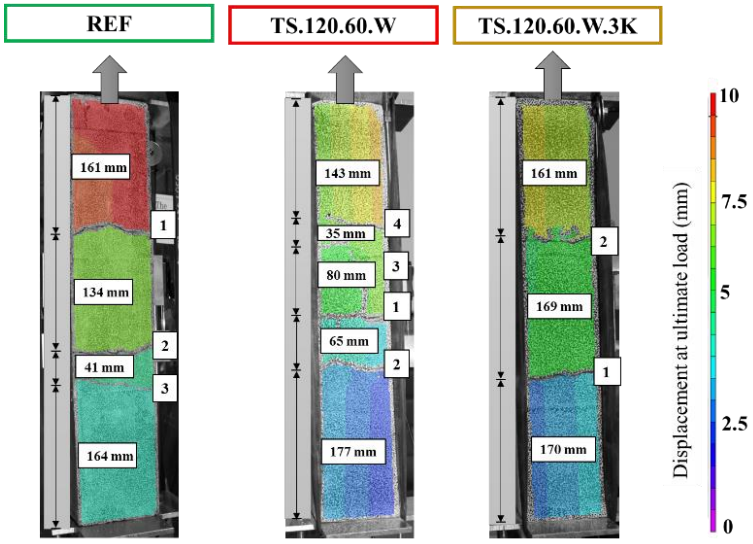

Figure 5. 11: Crack spacing and the crack number according to the appearances

5.3.2 Load test of small-scale GFRP RC beams

The results of four-point bending tests on small-scale GFRP RC beams are discussed below in terms of load-deflection response as well as cracking behaviour. The results from the study on the tensile behaviour of conditioned and stressed GFRP bars embedded in concrete are also used in the following to gain additional insights on the overall performance of GFRP RC elements.

Figure. 5.12 shows typical experimental load–deflection curves for specimens subjected to each type of conditioning and sustained loading, along with the theoretical response obtained by implementing the EC 2 model. It should be noted that the overall experimental deflection shown in the figure also includes the residual deformation due to the application of the first and the second cycle of loading at 3000 and 5000 με for control beam and the residual deformation for conditioned beams due to the applied sustained load (initial offset at zero load). As the design of GFRP RC members is usually controlled by SLS limitations, the test results were compared at service load, which corresponds, as recommended by EC2, to about 35% of the ultimate load (ULS) of BM.REF (shown in the figure with an horizontal solid line). In particular, it was observed that specimens conditioned in water at 60°C and with sustained loading corresponding to 3000 με and 5000 με showed larger deformations (up to 49% and 68%, respectively) than

BM.REF. Such increments may be attributed to the reduction in tension stiffening effect as observed in the direct tension tests previously discussed. While the deflection of the stressed beam conditioned at ambient temperature (BM.270.20.a.3k) is similar to the one of the control beam, a reduction in stiffness was noticed at early stage of loading, which was fully recovered once the load reached about 6 kN. This could be attributed to a local bond degradation between bars and concrete at the crack locations due to creep of concrete over the period that the specimens were subjected to the sustained load. Conversely, beams conditioned in water showed some high initial stiffness at early stage of loading that could be attributed to the self-heling phenomenon typical of concrete in wet conditions.

Figure. 5.12-(a) and Figure. 5.12-(b) show that the EC2 model predicted with a good degree of accuracy the deflections of the control beam and the stressed beam conditioned at ambient temperature up to service load. However, for load levels higher than 30 kN, the model underestimated the deflections, not accounting for the contribution of shear cracks to the total deformation. In addition, despite providing sufficiently accurate predictions at service load for short and long-term conditioning at ambient temperature, the EC2 model significantly underestimated deflection for specimens subjected to long-term conditioning in water at 60°C. It can also be noted that, only beam BM.270.60.W.5k deflected more than the maximum allowable deflection at SLS (taken as *l*/250, or 4 mm) and highlighted in Figure. 5.12 with a vertical solid line.

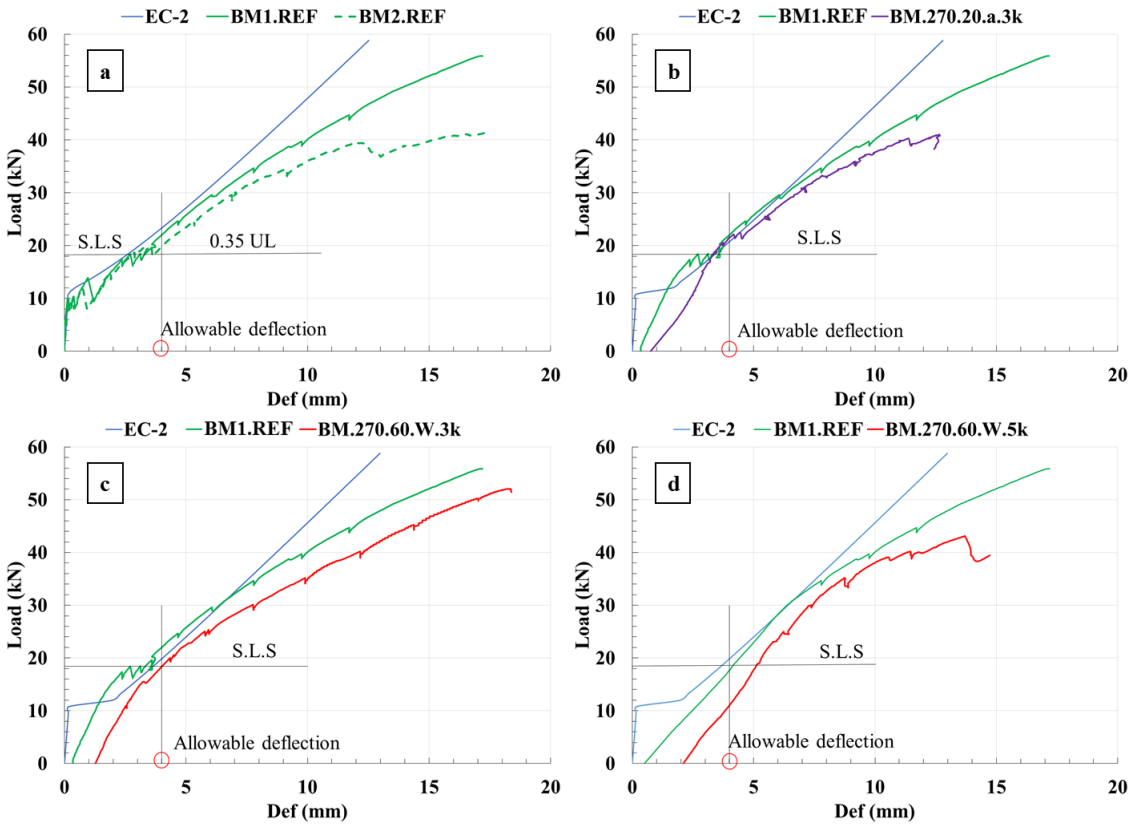

Figure 5. 12: Theoretical and experimental load-deflection curves: (a) Control beams; (b) 3000με stressed beams aged in air; (c) 3000με stressed beams aged in tank; (d) 5000με beams tank

5.3.2.1 Crack spacing

The cracking patterns for all tested beams at SLS and at ULS are shown in Figure.5.13 and Figure.5.14, respectively. Initially, vertical cracks appeared in the pure bending zone as the load reached the cracking level for the reference specimens (un-cracked before testing) and as it exceeded 5 kN for the conditioned specimens (pre-cracked due to imposed sustained stress). As the load approached 20 kN shear cracks begun to form. It was noted that conditioned beams developed fewer secondary cracks than control beams as the bond between GFRP bars and concrete deteriorated during the conditioning process.

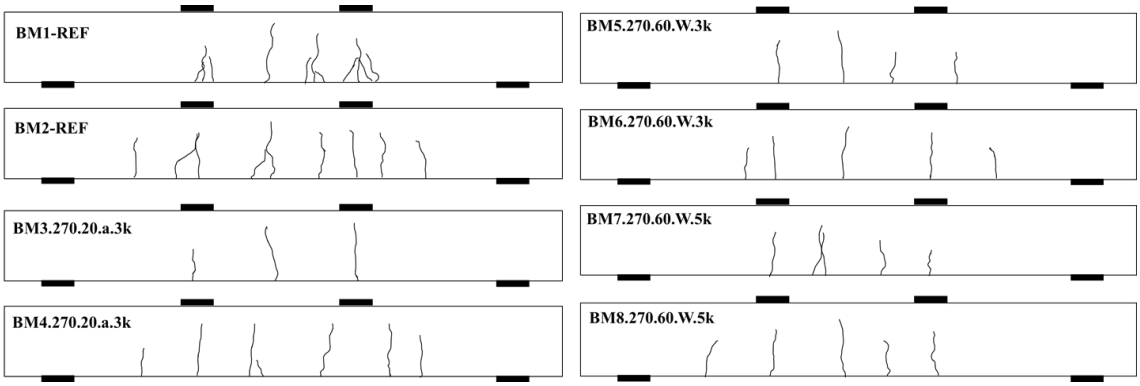

Figure 5. 13: Crack pattern at service load of tested beams

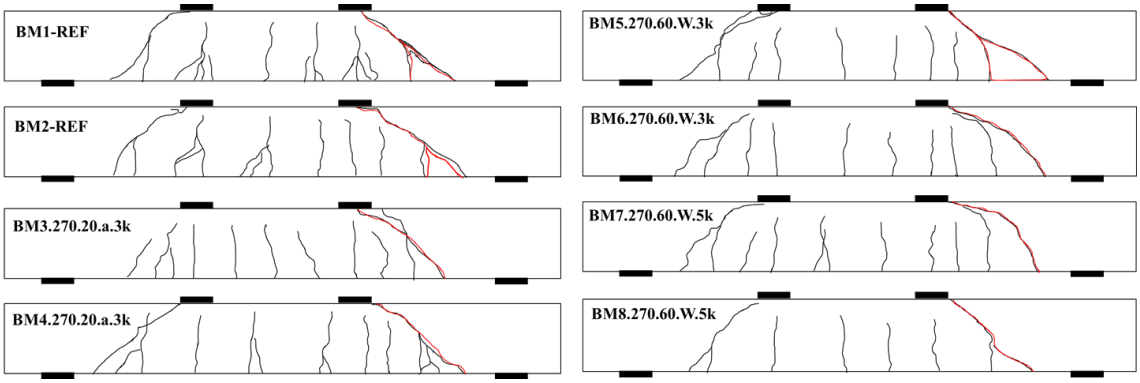

Figure 5. 14: Crack pattern at failure of tested beams the red colour is failure crack.

The number of primary cracks as well as the average and the maximum crack spacing at both SLS and ULS are presented in Table 5.5 along with the theoretical maximum crack spacing values calculated considering both good and poor bond conditions (i.e., k_1=0.8. and k_1=1.6, respectively). The control beams consistently showed the lowest average crack spacing both at SLS and at ULS, confirming the good bond of unconditioned GFRP bars with concrete.

Table 5. 5: Number of cracks and crack spacing of all tested specimens and theoretical crack spacing.

Beam	S.L.S				U.L.S			EC2	
	No.	Spacing			No.	Spacing		Spacing	
		Avg (mm)	Max (mm)	Exp*/Th*		Avg (mm)	Max (mm)	k_1=0.8 (mm)	k_1=1.6 (mm)
BM1.REF	5	78	107	1.1	6	78	107	98	163
BM2.REF	4	93	117	1.1	5	83	108		
BM3.270.60.a.3k	3	172	175	1.1	5	88	88		
BM4.270.60.a.3k	4	129	140	0.8	4	107	128		
BM5.270.60.W.3k	3	126	146	0.9	4	113	146		
BM6.270.60.W.3k	3	158	187	1.1	4	113	147		
BM7.270.60.W.5k	4	103	117	0.7	4	103	117		
BM8.270.60.W.5k	4	119	158	0.9	4	119	158		

Exp* Experimental values, Th* Theoretical values

The effect of sustained stress on crack spacing was variable and difficult to decouple from the influence of the moist alkaline environment at high temperature. In general, the wider crack spacing in stressed beams conditioned in water can be attributed to the reduction in bond strength as result of the skin degradation of the bars. Based on the outcomes of the tension stiffening results, the theoretical value representing good bond is adopted to predict the maximum crack spacing of reference specimens, whereas the one representing poor bond is used in the case of stressed specimens. The crack spacing obtained from EC2 is in good agreement with the test results at SLS. In particular, at SLS, the crack spacing predicted for beams BM4.270.60.a.3k and BM7.270.60.W.5k are slightly overestimated.

5.3.2.2 Crack width

The width of the cracks that developed within the zero shear zone was measured at the height of the longitudinal reinforcement at different load levels using an optical microscope. Figure. 5.15 shows the experimental crack widths for one of the specimens subjected to each type of conditioning environment and sustained loading (solid line) as well as the predicted crack widths according to the EC2 model (dashed lines).

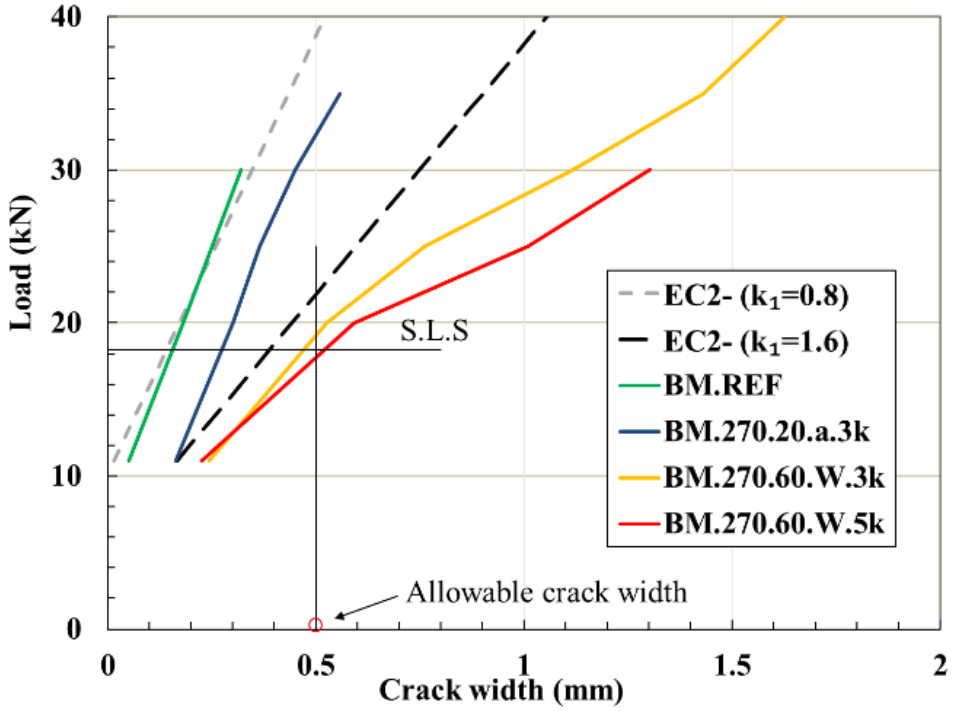

Figure 5. 15: Crack width vs. applied load compared with EC2 model.

In general, crack widths were larger for stressed samples conditioned in water at high temperature. Nonetheless, for all specimens, the maximum measured crack width at SLS always remained within the allowable crack width (i.e. 0.5 mm) according to current guidelines [25-26]. It can be noted that the experimental maximum crack width of the control beam can be accurately predicted by the EC2 approach with a bond coefficient of 0.8, as no onset bond degradation is expected at this stage. However, the model fails to predict accurately the long-term crack widths for stressed specimens, providing conservative values for dry environments while being un-conservative for exposure to wet conditions. Thus, using short-term tests results to predict the long-term cracking response of GFRP RC members and develop service life prediction models can lead to an unsafe design.

5.4 CONCLUSIONS

The experimental data obtained from this research was used to examine the long-term performance of GFRP bars in concrete members and assess the performance of the *fib* and EC2 models for predicting tension stiffening, deflections as well as crack spacing and crack width. The results of this study are summarized below.

- Exposure to severe environment and sustained loading deteriorated the resin rich layer of GFRP bars. This resulted in the bond degradation between concrete and reinforcement and, in turn, reduced tension stiffening and affected the total structural performance of the GFRP RC members. Conversely, exposure to a moist environment without sustained loading did not cause any noticeable bond strength degradation. In fact, the swelling of the GFRP bar, as a result of moisture absorption, increased the mechanical interlocking and the friction forces at the interface between concrete and reinforcement, leading to a stronger bond and to a relatively higher tension stiffening behaviour.
- The *fib* model failed to accurately represent the tension stiffening response of the tested GFRP RC members. In particular, the model underestimated the performance of the unstressed conditioned specimens while, overestimated that reference and stressed conditioned specimens. Additional work is recommended to further improve the accuracy of this model.
- The deformations (deflection and crack width) of the beams subjected to a load that induced strain levels of about 3000με in the GFRP bars remained within the limiting values suggested in current guidelines. Only the beams subjected to a higher sustained load level (equivalent to a strain of 5000 με in the GFRP bars) exhibited deformations exceeding current allowable limits.
- The EC2 models to predict long-term deflection and crack width failed to capture adequately the combined effect of severe environment and sustained loading. In particular, the model predictions were in agreement with the experimental deflection results measured at service load for reference specimens (short-term) and for stressed beams that were conditioned in air (long-term). However, the predicted deformation for stressed beams that were conditioned in water (long-term) was significantly underestimated. In addition, the use of a bond coefficient describing weak bond conditions led to unsafe crack width predictions. More accurate tension stiffening and bond factors representing GFRP RC beams in real application need to be identified.

It should be mentioned that the above conclusions are based on the analysis of test results carried out on a single type of GFRP bar and thus may not directly extend to other types of reinforcement.

5.5 REFERENCES

1. Nkurunziza, G., Debaiky, A., Cousin, P. and Benmokrane, B., (2005). Durability of GFRP bars: a critical review of the literature. *Progress in structural engineering and materials*, *7*(4), pp.194-209.
2. Benmokrane, B. and Mohamed, H.M., (2013), J. Durability issues of FRP for civil infrastructure. In *11th international symposium on fiber reinforced polymers for reinforced concrete structures (FRPRCS11). Guimaraes*.
3. Micelli, F. and Nanni, A., (2004). Durability of FRP rods for concrete structures. *Construction and Building materials*, *18*(7), pp.491-503.
4. Nanni, A., Claure, G., y Basalo, F.J.D.C. and Gooranorimi, O., (2016). Concrete and Composites Pedestrian Bridge. Concrete International, 38(11), pp.57-63.
5. Miàs, C., Torres, L., Turon, A. and Barris, C., (2013). Experimental study of immediate and time-dependent deflections of GFRP reinforced concrete beams. *Composite Structures*, *96*, pp.279-285.
6. Mias, C., Torres, L., Guadagnini, M. and Turon, A., (2015). Short and long-term cracking behaviour of GFRP reinforced concrete beams. *Composites Part B: Engineering*, *77*, pp.223-231.
7. Brown, V. L., and Bartholomew, C. L. (1996). "Long-term deflection of GFRP-reinforced-concrete beams." *Fiber Composites in Infrastructure: Proc., 1st Int. Conf. on Composites in Infrastructures (ICCI'96),* H. Saadatmanesh and M. R. Ehsani, eds., Tucson, AZ, 389–400
8. Pecce, M., Manfredi, G. and Cosenza, E., (2000). Experimental response and code Modelsof GFRP RC beams in bending. *Journal of Composites for Construction*, *4*(4), pp.182-190.
9. Toutanji, H.A. and Saafi, M., (2000). Flexural behavior of concrete beams reinforced with glass fiber-reinforced polymer (GFRP) bars. *ACI structural journal*, *97*(5), pp.712-719.
10. Yost, J.R., Gross, S.P. and Dinehart, D.W., (2003). Effective moment of inertia for glass fiber-reinforced polymer-reinforced concrete beams. *Structural Journal*, *100*(6), pp.732-739.
11. Bischoff, P.H., (2005). Reevaluation of deflection prediction for concrete beams reinforced with steel and fiber reinforced polymer bars. *Journal of Structural Engineering*, *131*(5), pp.752-767.

12. Barris, C., Torres, L., Turon, A., Baena, M. and Catalan, A., (2009). An experimental study of the flexural behaviour of GFRP RC beams and comparison with prediction models. *Composite Structures*, *91*(3), pp.286-295.
13. Almusallam, T.H. and Al-Salloum, Y.A., (2006). Durability of GFRP rebars in concrete beams under sustained loads at severe environments. Journal of composite materials, 40(7), pp.623-637
14. Park, Y., Kim, Y.H. and Lee, S.H., (2014). Long-term flexural behaviors of GFRP reinforced concrete beams exposed to accelerated aging exposure conditions. Polymers, 6(6), pp.1773-1793.
15. Gross, S.P., Yost, J.R. and Stefanski, D.J., (2009). Effect of sustained loads on flexural crack width in concrete beams reinforced with internal FRP reinforcement. Special Publication, 264, pp.13-32.
16. Youssef, T.A., (2010). Time-dependent behaviour of fibre reinforced polymer(FRP) bars and FRP reinforced concrete beams under sustained load (Vol. 72, No. 04).
17. Kassem, C., Farghaly, A.S. and Benmokrane, B., (2011). Evaluation of flexural behavior and serviceability performance of concrete beams reinforced with FRP bars. *Journal of Composites for Construction*, *15*(5), pp.682-695.
18. Benmokrane, B., Chaallal, O. and Masmoudi, R., (1996). Flexural response of concrete beams reinforced with FRP reinforcing bars. *ACI Structural Journal*, *93*(1), pp.46-55.
19. Masmoudi, R., Theriault, M. and Benmokrane, B., (1998). Flexural behavior of concrete beams reinforced with deformed fiber reinforced plastic reinforcing rods. *Structural Journal*, *95*(6), pp.665-676.
20. Barris, C., Torres, L., Baena, M., Pilakoutas, K. and Guadagnini, M., (2012). Serviceability limit state of FRP RC beams. *Advances in Structural Engineering*, *15*(4), pp.653-663.
21. Faza, S. S., and GangaRao, H. V. S. (1992). "Pre- and post-cracking deflection behavior of concrete beams reinforced with fiber-reinforced plastic rebars." *Proc., 1st Int. Conf. on the Use of Advanced Composite Materials in Bridges and Structures (ACMBS-I)*, K. Neale and P. Labossiere, eds., Society for Civil Engineering, Montreal, Canada, 151–160
22. Mota, C., Alminar, S., and Svecova, D. (2006). "Critical review of deflection formulas for FRP-RC members." *J. Compos. Constr.*, *10(3*), 183–194.
23. Razaqpur, A. G., Svecova, D., and Cheung, M. S. (2000). "Rational method for calculating deflection of fiber-reinforced polymer reinforced beams." *ACI Struct. J.*, 97(1), 175–184.

24. Bischoff, B. H., and Scanlon, A. (2007). "Effective moment of inertia for calculating deflections of concrete members containing steel reinforcement and fiber-reinforced polymer reinforcement." *ACI Struct. J.*, 104(1), 68–75.
25. ACI (American Concrete Institute). (2015). Guide for the design and construction of concrete reinforced with FRP bars. *ACI 440.1R-15, Farmington Hills,* MI.
26. Canadian Standards Association, CSA., (2002). Design Construction of Building Components with Fibre-Reinforced Polymers. *CSA S806–02, Canadian Standards Association, Rexdale, Ont., Canada*.
27. Italian National Research Council (CNR). (2006). Guide for the design and construction of concrete structures reinforced with fiber-reinforced polymer bars, *CNR-DT 203/2006, Rome*
28. Model Code, (2010). First complete draft–vol. 1. *fib Bulletin*, (55).
29. Kharal, Z. and Sheikh, S., (2017). Tension Stiffening and Cracking Behavior of Glass Fiber-Reinforced Polymer-Reinforced Concrete. *ACI Structural Journal*, *114*(2), p.299.
30. Bischoff, P.H. and Paixao, R., (2004). Tension stiffening and cracking of concrete reinforced with glass fiber reinforced polymer (GFRP) bars. *Canadian Journal of Civil Engineering*, *31*(4), pp.579-588.
31. Scott, R.H. and Beeby, A.W., (2005). Long-term tension-stiffening effects in concrete. *ACI Structural Journal*, *102*(1), p.31.
32. Fergani, H., Di Benedetti, M., Mias, C., Lynsdale, C. and Guadagnini, M.,(2016). Characterization and durability study of GFRP bars exposed to severe environments and under sustained loads. In *Proceedings The 5th International Conference on Durability of Fibre Reinforced Polymer (FRP) Composites for Construction and Rehabilitation of Structures, Sherbrooke, Canda*
33. Elbadry, M.M., Abdalla, H. and Ghali, A., (2000). Effects of temperature on the behaviour of fiber reinforced polymer reinforced concrete members: experimental studies. *Canadian Journal of Civil Engineering*, *27*(5), pp.993-1004.
34. ACI, A., 2004. 440.3 R-04: Guide Test Methods for Fiber-Reinforced Polymers (FRPs) for Reinforcing or Strengthening Concrete Structures. *American Concrete Institute, Farmington Hills, USA.*
35. Robert, M., Wang, P., Cousin, P. and Benmokrane, B., 2010. Temperature as an accelerating factor for long-term durability testing of FRPs: Should there be any limitations?. *Journal of Composites for Construction*, 14(4), pp.361-367.

36. Davalos, J.F., Chen, Y. and Ray, I., 2012. Long-term durability prediction models for GFRP bars in concrete environment. *Journal of Composite Materials*, 46(16), pp.1899-1914.
37. EN, BS., 2012. 12390-1: Testing hardened concrete Shape, dimensions and other requirements for specimens and moulds. *British Standards Institute, London*.
38. ASTM C496/C496M-11, Standard test method for splitting tensile strength of cylindrical concrete specimens.
39. ASTM C469-94,. Standard Test Method for Static Modulus of Elasticity and Poisson's Ratio of Concrete in Compression. 1994
40. Sutton, M.A., (2013). Computer vision-based, noncontacting deformation measurements in mechanics: a generational transformation. *Applied Mechanics Reviews, 65*(5), p.050802.
41. Zappa, E., Mazzoleni, P. and Matinmanesh, A., (2014). Uncertainty assessment of digital image correlation method in dynamic applications. *Optics and Lasers in Engineering*, *56*, pp.140-151.
42. Di Benedetti, M, Cholostiakow, S, Fergani, H, Zappa. E, Cigada, A, and Guadagnini, M,(2015). 3D-DIC for strain measurement in small scale GFRP RC specimens. *Third Conference on Smart Monitoring,Assessment and Rehabilitation of Civil Structures*, Antalya, Turkey
43. Sooriyaarachchi, H., Pilakoutas, K. and Byars, E., (2005). Tension stiffening behavior of GFRP-reinforced concrete. Special Publication, 230, pp.975-990.
44. Bischoff, P.H., (2001). Effects of shrinkage on tension stiffening and cracking in reinforced concrete. *Canadian Journal of Civil Engineering*, *28*(3), pp.363-374.
45. British Standards Institution, (2004). Eurocode 2: Design of Concrete Structures: Part 1-1: General Rules and Rules for Buildings. British Standards Institution.
46. Fergani, H., Di Benedetti, M., Mias, C., Lynsdale, C. and Guadagnini, M.,(2016). Long-term performance of GFRP bars under the combined effects of sustained load and severe environments. In *Proceedings The 8th International Conference on Fibre-Reinforced Polymer (FRP) Composites in Civil Engineering, Hong Kong, China*

CHAPTER 6

6 DURABILITY AND SERVICE LIFE PREDICTION OF GFRP BARS EMBEDDED IN CONCRETE UNDER SUSTAINED STRESS

6.1 INTRODUCTION

The lack of data on the long-term performance of GFRP bars in concrete structure has resulted in conservative recommendations being generally proposed by the various committees working in the field and adopted in relevant design codes and guidelines [1-4]. The most common approach to account for the long-term performance of the reinforcement at the initial design stages is the use of an environmental reduction factor to limit the long-term design tensile strength of the material, as well as the introduction of maximum allowable levels of sustained stress in the reinforcement [2,3]. The conservative nature of these empirically derived parameters, however, critically affects overall design and can increase significantly the amount of required reinforcement, thus making GFRP bars no longer economically viable in some applications.

A study conducted on several concrete bridges across Canada assessed the status of the GFRP reinforcement used in the deck reported that after 10-13 years, no signs of degradation were observed [5]. A more recent field study carried out on the 'Sierrita de la Cruz Creek' bridge confirmed the good performance of GFRP bars in aggressive environments after fifteen years of service [6] and provided additional evidence of the conservative nature of existing recommendations. This was concluded on the basis of a series of tests, including mechanical testing as well as SEM/EDS, scanning electron microscopy, energy dispersive X-ray spectroscopy, and thermogravimetry [6]. Therefore, more reliable models to predict the long-term performance of GFRP reinforcement in concrete structures are needed to guarantee an optimal use of materials and the development of more sustainable construction processes.

In the past decades, several research studies on the durability of GFRP bars have been carried out and a number of predictive models have been proposed [7-11]. Most of these models were developed on the basis of accelerated tests on bars exposed to artificial alkaline pore solutions or to moisture saturated concrete environments [7-11]. Although all of this research work has assisted in developing a good body of knowledge on the topic, the tested environments used in

these studies were undoubtedly more severe than those that GFRP reinforcement would be exposed to in typical applications and care should be taken when interpreting the results of these studies. In addition, none of the available predictive models takes into account explicitly the effect of sustained stress and thus cannot easily account for different in-service conditions.

In this research, modifications to the predictive model proposed by TG 5.1 (formerly 9.3) of the International Federation for Structural Concrete in Bulletin 40 [12] are proposed to estimate the durability and long-term performance of GFRP bars in concrete. The model builds upon the outcome of the work presented in Chapters 4 and 5 and on the assumptions that the Arrhenius theory can be applied to the degradation mechanisms that occur over the entire range of temperatures considered here and that all deterioration processes are affected to the same degree by a temperature shift.

A new strength retention equation for GFRP bars in concrete is proposed here, along with a new set of environmental reduction factors.

6.1.1 Designing for durability

6.1.1.1 Empirical approaches

Existing design codes/guidelines in Norway, Japan, Canada and USA [1-4] recommend the use of a single strength reduction factor (Eq. 6.1) to determine the long-term design tensile strength of FRP reinforcement and predict the effect of environmental exposure on material properties.

$$f_{fu} = C_E . f^*_{fu} \tag{6.1}$$

where

f_{fu} is design tensile strength, C_E environmental reduction factor and f^*_{fu} the guaranteed tensile strength

In the Norwegian design recommendations (NS3473), the environmental factor ηenv is set to a value of 0.5 for GFRP bars in reinforced concrete structures and there are no provisions to account for different environmental exposures. ACI440.1R-15 recommends the use of an environmental reduction factor of 0.8 or 0.7 for GFRP reinforcement in concrete elements non-exposed (indoor applications) or exposed to the earth and weather, respectively. The Japanese and Canadian guidelines are similar to the Norwegian design recommendation, with only a single environmental reduction factor being specified to account for the durability of GFRP RC elements. Both Canadian and Norwegian design codes and recommendations, also account for the effects of

sustained load through the use of an additional reduction factor and the total reduction can be obtained by multiplying the factors for environmental exposure and sustained load. Table 6.1 shows the strength reduction factors due to environmental exposure and sustained stress as specified in the aforementioned design codes/guidelines [1-4].

Table 6. 1: Environmental reduction factor for GFRP bars in existing design guidelines

Reduction Factor	NS3473 (Norway)	ACI (USA)	CHBDC (Canada)	JSCE (Japan)
Environmental	0.50	0.7-0.8	0.75	0.77
Sustained stress	0.8-1.0	N/A	0.8-1.0	N/A
Environmental and sustained stress	0.4-0.5	0.7-0.8	0.60-0.75	0.77

Based on the outcomes of this research and other studies [1-2], exposure to different environmental conditions (e.g. temperature and moisture) affects the initiation and rate of degradation mechanisms within the GFRP reinforcement, and thus its long-term performance, to different degrees. While different environmental factors are proposed based on the type of fibre used in the reinforcing bar, the use of a single environmental factor cannot capture adequately the effects of real environmental exposure and, although simple to apply, can lead to very conservative long-term predictions [13].

Alternative approaches, based on the implementation of a more theoretical framework, have been proposed by several researchers and technical committees and are discussed below.

6.1.2 Theoretical approaches

6.1.2.1 Byars et al.

The approached proposed by Byars et al. [14] to predict long-term strength retention of FRP bars in RC members provided the initial framework for the work of *fib* TG 9.3 (now T5.1). This approach allows modifying the reduction factor according to the expected in-service environmental conditions and the required design service life.

$$f_{fd} = f_{fk_0}.\eta_{env} \tag{6.2}$$

where,

$f_{fd}$is the design tensile strength value for the target service life of structure, f_{fk_0} is the characteristic tensile strength (short-term test) and $\eta_{env}$is the environmental reduction factor calculated using the following equation:

$$\eta_{env} = \left(1 - \Delta f_{ft,env} . \eta_{mo} . \eta_T . \eta_{SL}\right) \quad (6.3)$$

where,

$\Delta f_{ft,env}$ is the standard reduction of tensile strength due to environmental effects (assumed as 0.5 for GFRP bars after 100 years in concrete under standard exposure conditions), η_{moist} is the correction factor for moisture condition, η_T is the correction factor for temperature and η_{SL} is the correction factor for desired service-life. The suggested values of these correction factors are given in Table 6.2.

Table 6. 2: Correction term for moisture(η_{moist}), mean annual temperature(η_T)and service life (η_{SL})

Correction term	Conditions	Value
η_{moist}	Dry concrete (RH app. 50%)	0.65
	Moist concrete (RH app. 80%)	1
	Saturated concrete (RH app. 100%)	1.5
η_T	Mean annual temperature (°C) <5	0.85
	5< Mean annual temperature (°C) <15	1
	15< Mean annual temperature (°C) <25	1.15
η_{SL}	Service life of 50 years	0.85
	Service life of 100 years	1.0

Although similar in form to Eq. 6.1, the design equation proposed by the authors (Eq. 6.2) is therefore less prescriptive and can easily account for specific in-service conditions. However, the basic values of $\Delta f_{ft,env}$ and η_{moist} were proposed on the basis of conservative assumptions and not on a solid theoretical framework or reliable empirical data. The $\Delta f_{ft,env}$ was assumed to be 0.5 after 100 years in standard exposure conditions with no explanation, while the moisture correction factors were assumed according to ACI 440 recommendations, which were already recognized to require further calibration and improvements [15]. The correction factors for service life n_{SL} simply relies on the assumption that strength reduces linearly with the logarithm of time.

6.1.2.2 *fib* Bulletin 40

In Bulletin 40 [12], TG 9.3 (now T5.1) of *fib* proposed a refine approach to address the issues discussed above. In the refined approach, all of the parameters affecting the long-term durability of FRP bars (i.e. relative humidity, temperature, bar diameter and service life) are incorporated in one factor and the design tensile strength is calculated using the following expression.

$$f_{fd} = f_{fk1000h}[(100 - R_{10})/100]^n/\gamma_f \quad (6.4)$$

where,

f_{fd} is the design tensile strength for the target service life of the structure, $f_{fk1000h}$ is the characteristic tensile strength retention for FRP bars after being exposed to the given test environment for 1000h, R_{10} represents the reduction of tensile strength due to environmental effects per logarithmic decade (in percentage), and the exponent n incorporates factors associated with moisture, temperature services life and diameter correction factor (Eq. 6.5).

$$n = n_{moist} + n_T + n_{SL} + n_d \quad (6.5)$$

where,

n_{moist} is the correction factor for moisture condition, n_T is the correction factor for temperature (similar to [14]), n_{SL} is the correction factor for desired service-life, $n_d$is a term to account for bar diameter.

Although Eq. 6.5 assumes that the effect of all environmental factors can be simply added in a linear manner (i.e. effects are not coupled), a more complex synergistic effect on degradation mechanisms is expected The material safety factor, γ_f, accounts for the variability of the tensile strength. All these factors, as suggested in Bulletin 40, are presented in Table 6.3.

Table 6. 3: Correction term for moisture(n_{moist}), mean annual temperature(n_T), service life (n_{SL}) and (n_d) diameter as proposed in *fib* Bulletin 40 [12].

Correction term	Conditions	Value
n_{moist}	Dry concrete (RH app. 50%)	**-1**
	Moist concrete (RH app. 80%)	**0**
	Saturated concrete (RH app. 100%)	**1**
n_T	Mean annual temperature (°C) <5	**-0.5**
	5< Mean annual temperature (°C) <15	**0**
	15< Mean annual temperature (°C) <25	**0.5**
	25< Mean annual temperature (°C) <35	**1**
n_{SL}	Service life of 1 year	**1**
	Service life of 10 years	**2**
	Service life of 50 years	**2.7**
	Service life of 100 years	**3**
η_d	Bigger than tested	0
	Same as tested	0
	75% of tested	0.5
	50% of tested	1
γ_f	For GFRP materials	1.25

According to Eq. 6.4, the term $[1/(100\text{-}R_{10})/100]^n/\gamma_f$ can be considered as the equivalent to the environmental reduction factor proposed in other design guidelines. R_{10} represents the rate of strength degradation (slope of the strength loss over time in double logarithmic scale) and it plays a critical role in calculating the final value of the environmental reduction factor. In addition, the inclusion of the *n* factor allows to account explicitly for the expected environmental exposure conditions. However, the assumptions considered to formulate this approach still require to be validated against a reliable set of data. As discussed in the following, Weber and Witt (2007) carried out additional work on this model and provided further insights on the theoretical framework [16].

6.1.2.3 Weber and Witt

The approach proposed in Eq. 6.6 and 6.7 [16] is similar to that proposed in Bulletin 40 [12]. The authors also discussed in more depth the theoretical basis of the approach and proposed some adjustments to the correction parameters used in [16] (see Table 6.4).

As stated in [16], the use of an exponential equation to predict the mechanical degradation due to environmental exposure describes best the kinetics of the chemical and physical processes.

$$f_{fd} = \left(\frac{f_{fk1000h}}{\eta_{env}}\right)/\gamma_f \tag{6.6}$$

$$\eta_{env} = 1/(100\% - R_{10})^{n} \quad (6.7)$$

where,

η_{env} is the environmental reduction factor and R_{10} and n are as defined in Eqs. 6.4 and 6.5.

It is worth mentioning that if the value of $f_{fk1000h}$ is not known, the long-term design value can be estimated from the short-term strength value and the use of the following equation for the environmental factor (i.e. shifting the degradation curve by two logarithmic decades):

$$\eta_{env} = 1/(100\% - R_{10})^{n+2} \quad (6.8)$$

Table 6. 4: Correction factors for moisture(n_{moist}), mean annual temperature(n_T), service life (n_{SL}) and (n_d) bar diameter as proposed in Weber and Witt [16]

Correction term	Conditions	Value
n_{moist}	Dry concrete (RH app. 50%)	-1
	Moist concrete (RH app. 80%)	0
	Saturated concrete (RH app. 100%)	1
n_T	Mean annual temperature (0°C)	-0.5
	Mean annual temperature (10°C)	0
	Mean annual temperature (20°C)	1.5
	Mean annual temperature (30°C)	2
n_{SL}	Service life of 1 year	1
	Service life of 10 years	2
	Service life of 50 years	2.7
	Service life of 100 years	3
η_d	half as tested	0.5
	Same as tested	0
	Double	0
γ_f	For GFRP materials	1.25

6.1.2.4 Serbescu et al.

On the basis of additional work carried out at the University of Sheffield [11], the use of two new degradation parameters has been proposed to consider the influences of pH level and degradation onset Eq. 6.9 Table 6.5. The proposed revised approach introduces an extension of Eq. 6.5 as follows:

$$n = n_{moist} + n_T + n_{SL} + n_d + n_{pH} + n_{on} \quad (6.9)$$

In both *fib* Bulletin 40 and Weber and Witt models, the degradation rate (R_{10}) was determined by estimating the slope of the strength loss curve over time in double logarithmic scale generated from short-term test results. The rate is calculated in the period between one to ten years during which is assumed constant

$$R_{10} = \frac{log(f_{1year}) - log(f_{10year})}{log(100000) - log(10000)} \quad (6.10)$$

Conversely, Serbescu et al. 2013 model calculated the rate per logarithmic decade using Eq.6.11 for a period between 0 to 1000hr under the assumption that the rate is constant over time for all different conditions. In addition, the degradation curve is shifted horizontally based on the onset of the bar degradation when exposed to chosen reference environment.

$$R_{10} = 100 - (10^{m}.100)(\%) \quad (6.11)$$

where,

m is the average for different exposure temperatures of the slopes of the degradation curves in double logarithmic graph and can be estimated according to Eq.6.12

$$m = \frac{log(f_{fk0}) - log(f_{fk1000})}{log(1) - log(1000)} \quad (6.12)$$

Table 6. 5: Correction term for pH level (n_{pH}), onset of degradation (n_{on}) proposed by Serbescu et al. [11]

Correction term	Conditions	Value
n_{pH}	7-9	0
	10-12.8	0.5
	>12.8	1
n_{on}	$f_{fk\ ref} = f_{fk0}$	-1.5
	$f_{fk\ ref} \neq f_{fk0}$	$n_{on,opt}$

6.1.2.5 Discussion on theoretical approaches

Although all of the theoretical approaches reviewed above adopt a similar underlying theoretical framework, this is not explicitly embedded throughout and still relies on the use of empirically derived parameters. Byars et al. 2003 [14] adopt a constant strength reduction coefficient for a 100 year service life, whilst a more adaptable degradation rate (R_{10}) concept is introduced in the other approaches. However, R_{10} is determined over different lengths of exposure and this can lead to significant variations in long-term predictions. The factor *n*, which integrates the effect of

individual environmental correction factors ($i.e., n_{moist}, n_T, n_d, n_{SL}$) and is affected by the kinetics of the chemical and physical processes, is used in a different way in [14] and the other approaches to modify long-term strength retention rates. In order to ensure a more consistent design, a more objective approach is required to estimate the effects of environmental exposure and other mechanical and physical degradation mechanisms on the long-term performance of FRP RC elements. For this purpose, a better understanding of the degradation mechanisms and the long-term behaviour of GFRP bars in concrete environment is fundamental. The following sections introduce a more comprehensive framework to assess the long-term strength retention of FRP bars and determine critical environmental factors based on sound theoretical models.

6.2 A NEW FRAMEWORK FOR SERVICE LIFE PREDICTIONS OF GFRP BARS IN FIELD ENVIRONMENTS

Based on the findings of this research and on the information obtained from the literature [12, 1719] two basic assumptions were adopted to predict strength retention of GFRP bars in real applications:

1-The chemical reactions were found to be the driving the degradation process of the GFRP bars in concrete in the presence of moisture. Consequently the rate of the chemical reactions (R) is expected to control the degradation rate as shown in Eqs. 6.13 or 6.14.

$$\text{Chemical reactions rate} = \frac{change\ in\ concentration}{change\ in\ time} = \frac{moles}{sec} \tag{6.13}$$

$$R = K \cdot [A] \tag{6.14}$$

where

R is the chemical reaction rate; *K* is the reaction rate constant [1/sec] [20]; A is the concentration of the reactant [mole]

As previously shown in Chapter 4, the properties of the resin rich layer (i.e., outermost part of the bar), where the deterioration takes place, change over time.

$$\begin{matrix} t = 0 & [A]_0 \\ t = t & [A]_t \end{matrix} \rightarrow \begin{matrix} \Delta[A] = [A]_t - [A]_0 \\ \Delta t = t - 0 \end{matrix}$$

$$R = \frac{-\Delta[A]}{\Delta t} \tag{6.15}$$

By combining Eq. 6.14 and Eq. 6.15 and considering an instantaneous rate, the following can be written:

$$\frac{d[A]}{dt} = -K[A]$$

This equation can be solved for the time interval 0→t

$$\int_{[A]_0}^{[A]_t} \frac{d[A]}{[A]} = -K \int_0^t dt$$

$$ln[A]_t - ln[A]_0 = -Kt \tag{6.16}$$

Potential solutions for Eq. 6.16 are the following equations 6.17 or 6.18. In this research, equation 6.18 was employed to describe the behaviour of strength retention with time

$$ln[A]_t = -Kt + -ln[A]_0$$

$$Y = mt + b \tag{6.17}$$

or

$$[A]_t = [A]_0 e^{-Kt}$$

$$Y = A_0 e^{mt} \tag{6.18}$$

where

K, or *m*, are the reaction rate constants [1/sec]

2-The second assumption is that the reaction rate constant, or the degradation rate of the GFRP bar, can be expressed by the Arrhenius relationship as shown in Eq.6.19:

$$K = m = A \cdot e^{\left(-\frac{E_a}{RT}\right)} \tag{6.19}$$

where

K = rate constant (1/time); A = constant of the material and degradation process; E_a = activation energy; R = universal gas constant; and T = temperature in Kelvin.

The primary assumption of Arrhenius principle is that the single dominant degradation mechanism of the material will not change with time and temperature during the exposure, but the rate of degradation will be accelerated with the increase in temperature [10, 21, 22].

6.2.1 Detailed steps and prediction of strength retention

The steps required to obtain strength retention predictions for the different environmental conditions examined in the experimental study are discussed in detail in the following. The design tensile strength after exposure (f_{fd}) will be determined as a function of the initial tensile strength (f_{fk_0}) through the implementation of a model (Eq. 6.20) similar to that proposed by Byars et al. in [14].

$$f_{fd} = f_{fk_0} * \eta_{env} \tag{6.20}$$

where,

η_{env} is the environmental strength reduction according to Eq.6.21; (f_{fk_0}) is the initial tensile strength; (f_{fd}) is the predicted (design) tensile strength

$$\eta_{env} = (1 - (n_{sl} + n_{onset} + n_T + n_{moist} + n_{sus}).R_{10}) \tag{6.21}$$

where,

n_{sl} is the desired service-life time parameter, which assumes that an increase in time causes an increase in deterioration of the bar; The n_{onset} parameter corresponds to the starting time of degradation of GFRP materials in the reference environment; n_T is the time shifting factor due to exposure to different temperatures; n_{moist} is the term for moisture condition, taken as defined in Bulletin 40 [12]; n_{sus} is the proposed correction factor for the desired sustained stress. The value of; n_{Tsus} was proposed based on the degradation curves that best fit the behaviour of the stressed specimens. The proposed values for all degradation parameters (n) are tabulated in Table 6.6, and are discussed in detail in the following.

Table 6. 6. Degradation parameters adopted in this model

Degradation parameter	Range	Value
Service life (n_{sl})	25 year	5.30
	50	5.64
	100	5.94
Moisture RH (n_{moist})	Saturated (100%)	0
	Moist (80%)	0.5
	Dry (50%)	1
Temperature (n_T)	To be calculated n_T = (log(onset time reference temperature)-log(onset time /TSF))	
Sustained Stress (n_{su})	non	0.0
	Gives 3000με	-0.15
Onset (n_{onset})	Be provided	-3.13 for the GFRP bar tested in this research programme

In order to estimate the strength degradation rate (R_{10}), a master curve describing the behaviour of the reference specimens is required (i,e., specimens exposed to the reference environment - taken in this work as moist concrete at 20°C). This curve can be constructed not only utilizing short-term test results but also data obtained at higher temperatures. This is possible as a result of the Arrhenius principle assumptions, according to which the degradation mechanisms do not change in time, but their degradation rate changes with temperature. As a result, the degradation curves at 20°C, 40°C, 60°C would be represented by three straight lines on the log-log scale. Such lines are characterised by the same slope (same degradation mechanism) but are shifted by a specific amount (different degradation rate) (Fig. 6.1).

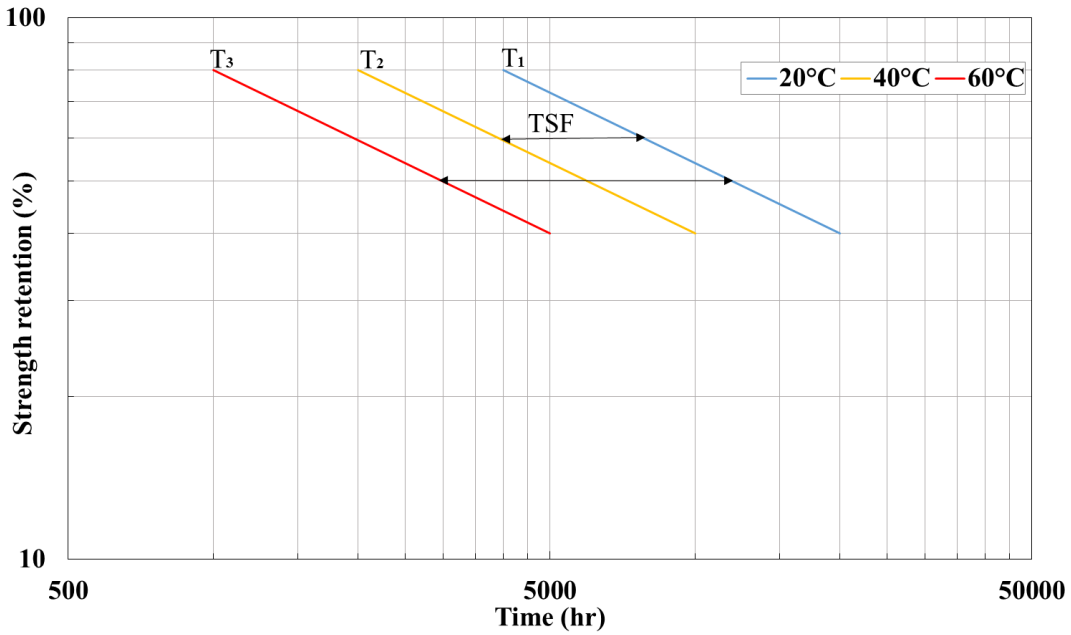

Figure 6. 1: The time shift between curves for different temperature exposure.

Based on Eq. 6.19, Eq. 6.22 can be used to calculate the time shift factor (TSF) for two different exposure temperatures.

$$TSF = \frac{t_1}{t_2} = \frac{{}^{c}/_{k_1}}{{}^{c}/_{k_2}} = \frac{A.e^{-\frac{E_a}{RT_2}}}{A.e^{-\frac{E_a}{RT_1}}} = e^{\frac{E_a}{R}\left(\frac{1}{T_1}-\frac{1}{T_2}\right)} \quad (6.22)$$

The calculation of the degradation coefficient (*m*) (step 1) is required for the estimation of the activation energy (E_a) (step 2) which, in turn, is necessary to solve Eq.6.22. Once all data are shifted, the master curve can be defined (step 3) and the degradation rate (R_{10}) calculated (step 4).

6.2.1.1 Step1 - Degradation coefficient

The average tensile strength of the specimens conditioned at 20°C, 40°C and 60°C for 1000, 2000 and 6480 hr were calculated as a percentage of the value calculated for the unconditioned samples (strength retention). The experimental strength retention was plotted over time and the following equation (see also Eq. 6.18) was used to determine value of the reaction rate constant *m* (Figure.6.2).

$$Y = A_0 e^{mt}$$

where,

Y is strength retention in %; A_0 initial strength retention in %; *t* exposure time; and m=$\frac{1}{k}$, as expressed in Eq. 6.17.

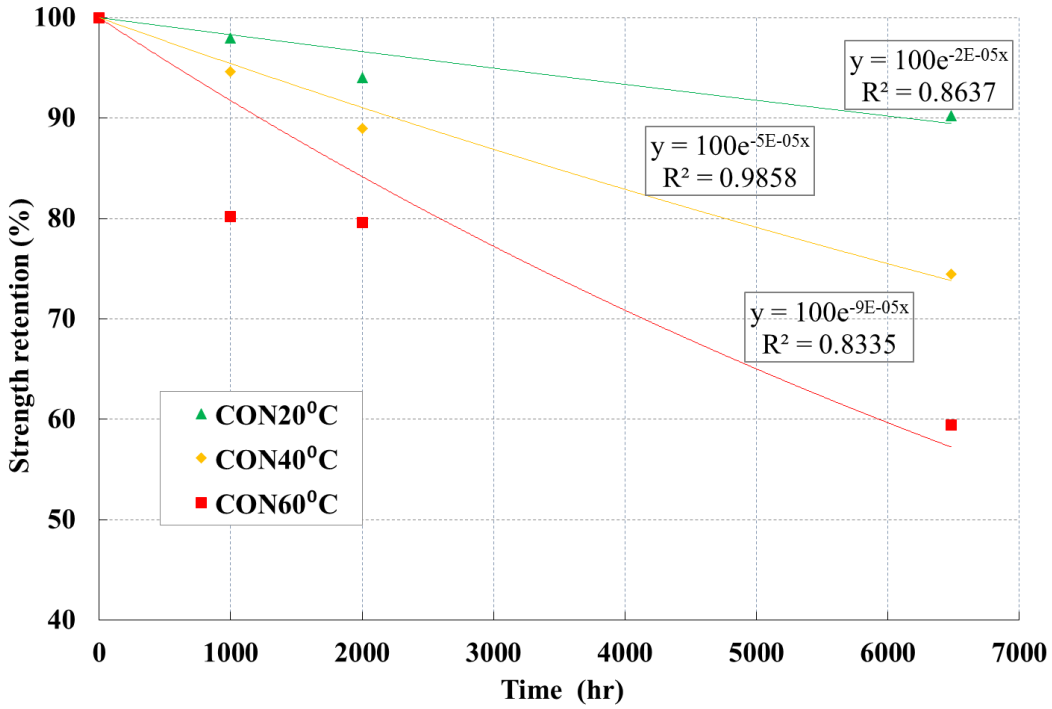

Figure 6. 2: Strength retention for the three considered temperatures.

For each set of data, the curves with the best correlation coefficient (R^2 with a minimum value of 0.80 [10]) were used (see Table 6.7).

Table 6. 7: Degradation coefficients

Temperature (°C)	GFRP bars in moist concrete	
	m	R^2
20	-2E-05	0.86
40	-5E-05	0.98
60	-9E-05	0.83

6.2.1.2 Step 2 - Activation energy

The Arrhenius relationship can be rewritten as shown below

$$K = A \cdot e^{\left(-\frac{E_a}{RT}\right)}$$

$$\frac{1}{K} = \frac{1}{A} \cdot e^{\left(-\frac{E_a}{RT}\right)} \tag{6.23}$$

$$ln\left(\frac{1}{K}\right) = \frac{E_a}{R} \cdot \frac{1}{T} - ln(A) \tag{6.24}$$

In Eq. 6.24, the activation energy (E_a) is isolated and can be estimated as the slope of the curves in the Arrhenius plot (Figure.6.3). The graph in Figure 6.3 was obtained by using the regression

equations determined in Step 1 (Figure 6.2) to evaluate the time at which target strength retention values (i.e., 50%, 60%, 70%, 80% and 90%) are achieved for all conditioning temperatures. The natural logarithm of this time-to-strength-retention is plotted against the reciprocal of the temperature and a linear regression is used to interpolate the data referring to specimens characterised by the same retention rate. The regression coefficients (E_a/R) and correlation coefficients (R^2) are presented in Table 6.8. The high values of R^2 and the parallelism of the curves (the slopes of the curves E_a/R are equal) confirm that the Arrhenius principle can be applied to predict the strength retention of GFRP bars in concrete environments.

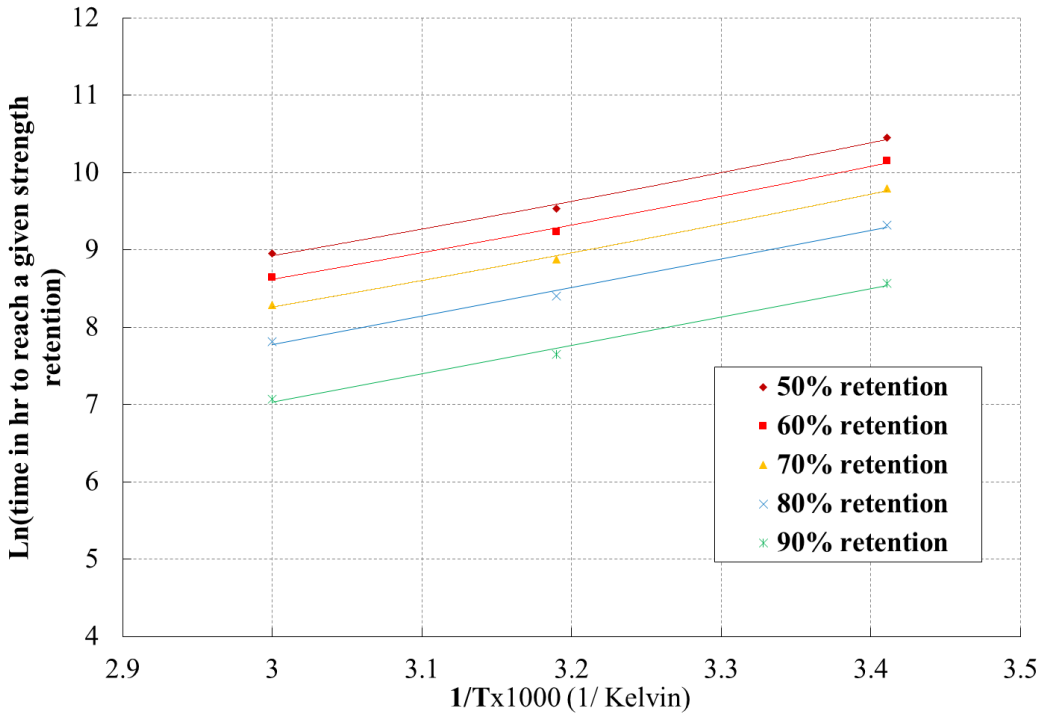

Figure 6. 3: Arrhenius plots of tensile strength degradation for GFRP bars exposed to moist concrete.

Table 6. 8: Coefficients of Regression Equations for Arrhenius Plots

Tensile strength retention (%)	GFRP bars in moist concrete	
	E_a/R (J/mole)	R^2
50	3672	0.99
60	3672	0.99
70	3762	0.99
80	3762	0.99
90	3762	0.99

Note *R*: gas constant = 8.134 (J/mole·K)

6.2.1.3 Step 3 - Extrapolation

Using the activation energy coefficient in Eq.6.22, the time shift factors (TSF) were calculated and used to shift the experimental results obtained at 40°C and 60°C according to Eq. 6.25.

$$t^*_{@T_1} = TSF_{T_2 \to T_1} \cdot t_{@T_2} \tag{6.25}$$

where

$t^*_{@T_1}$ is the equivalent time to reach the given strength retention at T_1; $t_{@T_2}$ is the actual exposure time to reach the same strength retention at T_2.

The master curves was obtained by regression analysis considering all reference and shifted data. The regression equation was then used to extrapolate the onset of degradation and the residual strength of the 100 years for the references environment (Figure. 6.4).

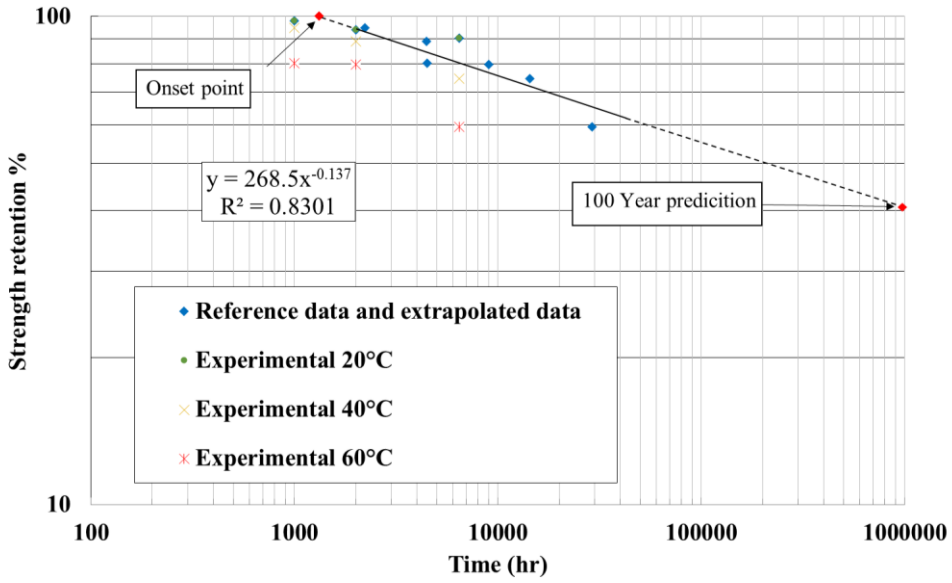

Figure 6. 4: Constructed master curve for reference environments.

6.2.1.4 Step 4 - Degradation rate

The degradation rate (R_{10}) in the double logarithmic scale used to represent the strength retention corresponds to the change of residual strength (%) over one decade. Taking into account the assumption that degradation follows chemical reaction behaviour [23], it is proposed to calculate R_{10} as a weighted average of the R_{10} for each decade from onset till 100 years Eq. 6.26.

$$R_{10} = \sum_{i=1}^{3} w_i . R_{10_i} \quad (6.26)$$

where,

i is the number of decades; w_i is the weight associated with the *i*-th decade; in the most typical case degradation occurs over 3 decades and the weighting can be taken as w_1=0.5; w_2=0.3and w_3= 0.2.

The master curve and predefined parameters (i.e., (*Ea/R*), R_{10}; n_{onset}) were obtained for the GFRP bars examined in this study at reference conditions (i.e., embedded in unstressed moist concrete at 20°C) (Figure. 6.5). Thus, the predicted strength retention for other environmental exposures and loading conditions can be obtained using Eq. 6.20, 6.21 and Table 6.6.

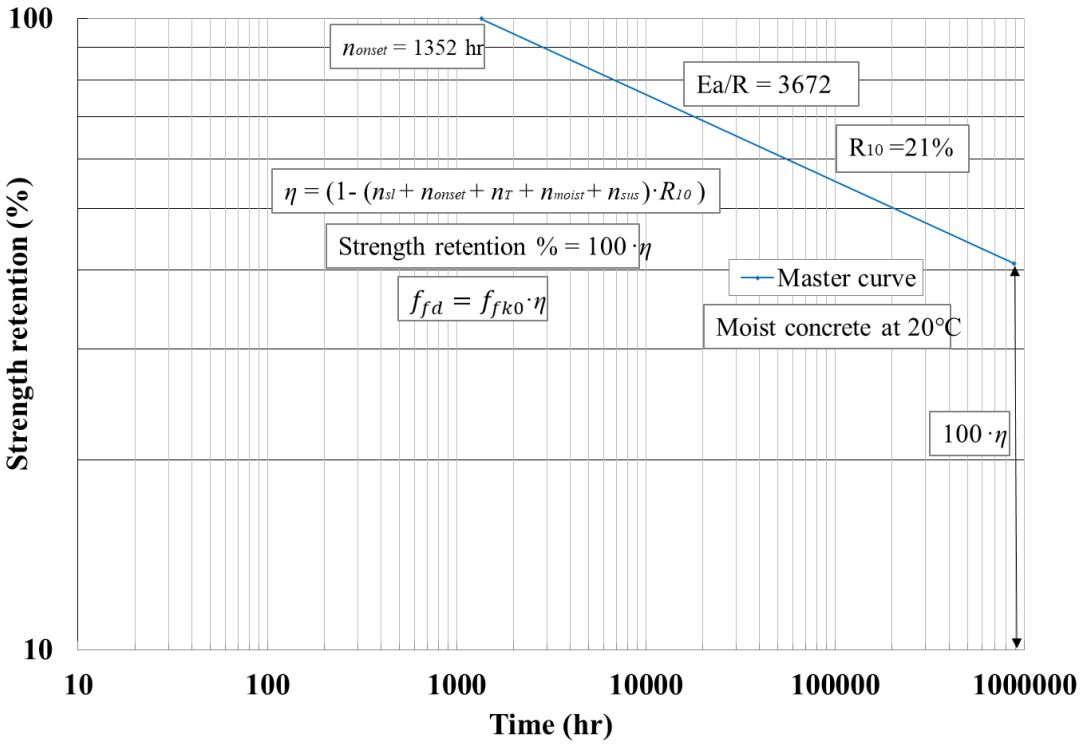

Figure 6. 5: Proposed model plot with obtained parameters for tested GFRP bar.

6.2.2 Discussion on the proposed approach

The environmental reduction factor used in the proposed methodology (Eq. 6.21) is determined in a similar manner to that prosed by Byars *et al.* [14] but introduces the use of an explicit strength degradation rate (Eq. 6.26). In addition, the effect of sustained stress, which highly affects the long term performances of GFRP reinforcement in real applications, is included through the use of a newly proposed sustained stress correction factor. Furthermore, a new method is proposed to estimate the degradation onset of an FRP bar at reference environment as well as other environments. Finally, as the effect of temperature on the physical and mechanical properties of an FRP bar is a function of several parameters, such as type of resin matrix, degree of bar curing, and fibre volume fraction, it is proposed that the temperature correction factor (n_T) be estimated accurately for each type of bar according to equation Eq. 6.27.

$$n_T = log(t_{0_{REF}}) - log\left(\frac{t_{0_{REF}}}{TSF_{T_2 \rightarrow T_{REF}}}\right) \tag{6.27}$$

where

$t_{0_{REF}}$ is the time of onset degradation for the GFRP bar at reference condition; $TSF_{T_2 \rightarrow T_{REF}}$ is time shift factor between considered temperature and reference temperature.

T_{REF} is the reference temperature taken as 20°C.

6.2.3 Application of the new approach

The new methodology discussed above was successfully implemented to predict the long-term strength retention of the GFRP bars embedded in wet concrete and conditioned at different temperature levels (Figure 6.6) as part of this research programme. As shown in Figure 6.6, more conservative predictions are given by the model for both 20°C and 40°C conditioning. This can be mainly attributed to the adopted method for calculating the rate of degradation (R_{10}), which is highly skewed by the higher degradation observed at 60°C conditioning.

Conservative prediction of strength retention for stressed specimens were also obtained for specimens subjected to sustained stress (Figure 6.7). This can be attributed to the negligible effects of the chosen values of imposed sustained stress (equivalent to typical in-service conditions) during the conditioning time. It is worth mentioning that the predicted strength retention values obtained by utilising the proposed methodology and the correction factor in Table 6.6 are almost identical to those obtained by constructing master curves based on the experimental test results (Figure. 6.8).

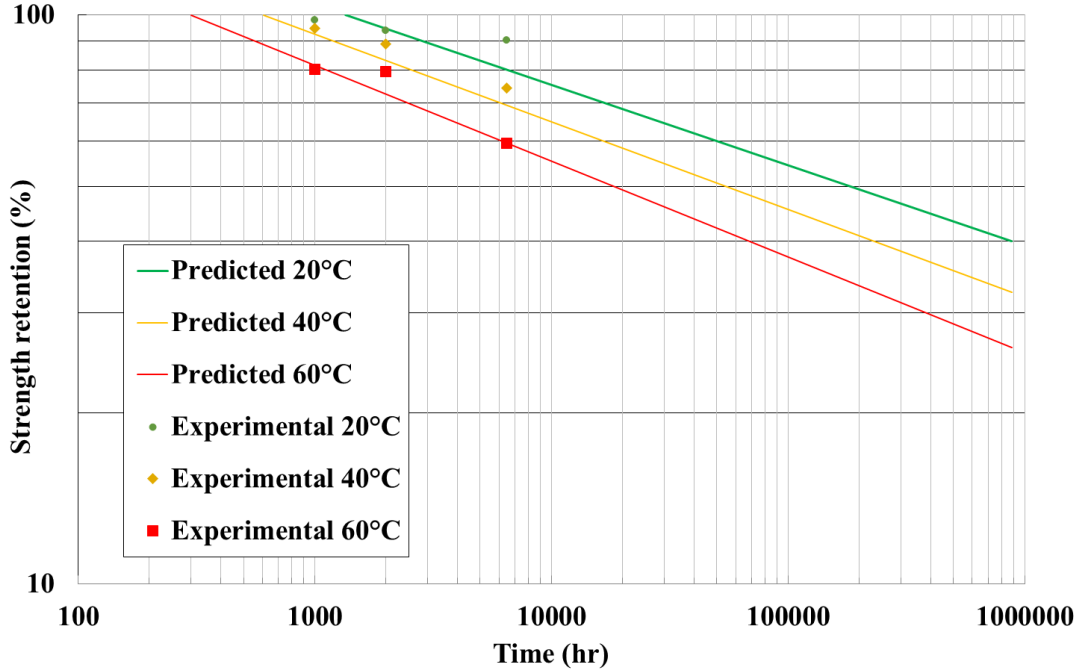

Figure 6. 6: Predicted strength retention of bars in various environments compared with the experimental results of this study.

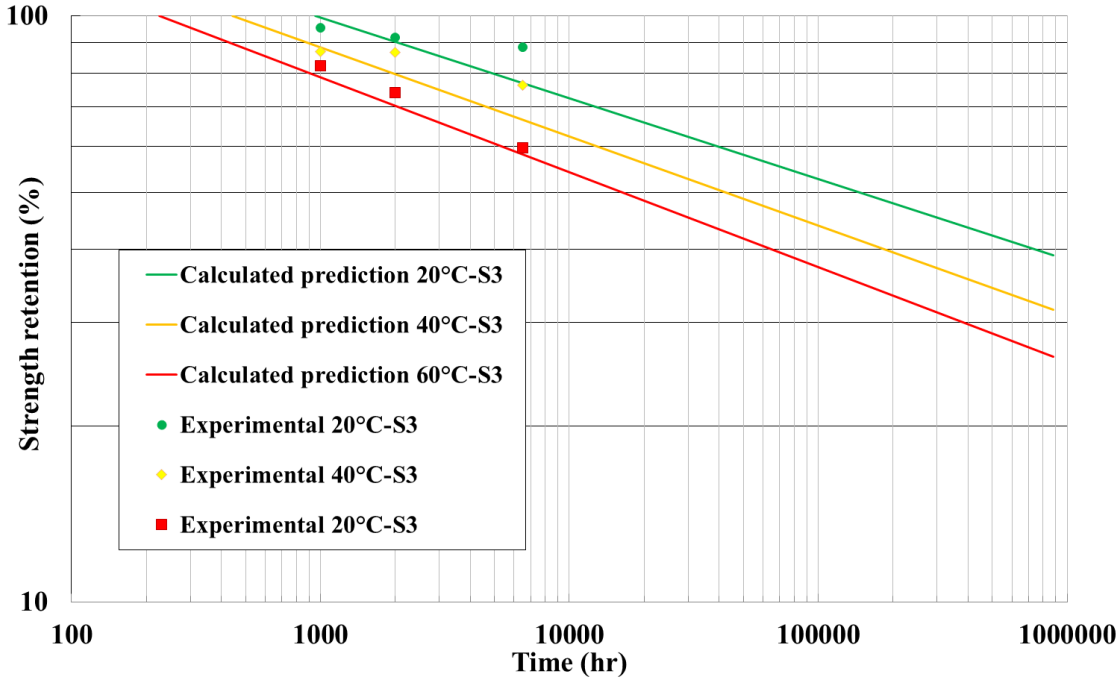

Figure 6. 7: Predicted strength retention of stressed bars embedded in moist concrete at various temperatures and compared with the experimental results of this study.

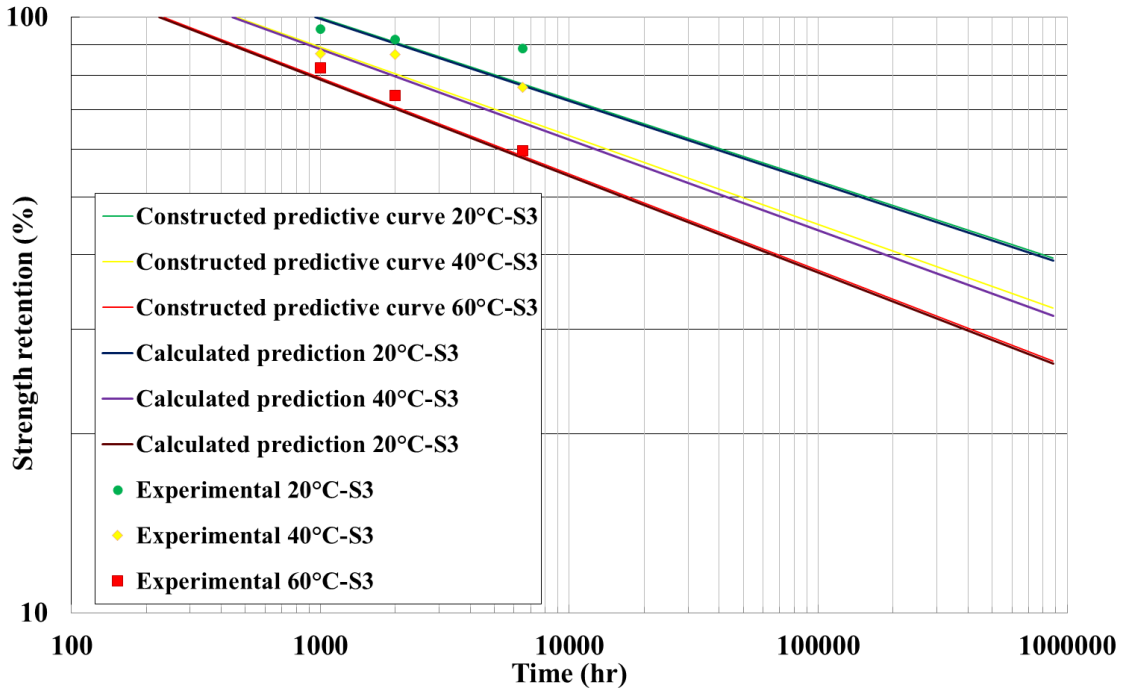

Figure 6. 8: Predicted strength retention of stressed bars embedded in moist concrete using analytical procedure and constructing master curve based on experimental tests result of this study.

6.2.4 New model validation

The methodology developed in this study to predict the long-term strength retention of GFRP bars was validated against results of other studies on GFRP bars exposed to real concrete environment [7, 10, 21, 24]. Master curves were produced by utilising test results at different exposure temperatures from previous research and using the proposed model as shown in Figures 6.9, 6.10, 6.11 and 6.12. Taking into account the large variety of tested GFRP materials, bar sizes, concrete properties and concrete cover, the proposed approach provides reasonably good predictions. In detail, the suggested procedure approximate more accurately the degradation experienced by the specimens subjected to high temperature (60°C), whilst it provides more conservative estimates at lower temperatures (20°C and 40°C). This can be attributed to the fact that the specimens at these temperature levels may require longer exposure time to achieve a given degradation. Tests at additional temperature levels may be needed to achieve higher reliability in the determination of appropriate TSF and improve prediction at all temperature levels.

Finally, the advantage of the proposed approach is that it can be easily implemented using predefined degradation parameters (E_a/R, n_{onset}, R_{10}), or the latter can be obtained by performing regression analyses on short-term test results.

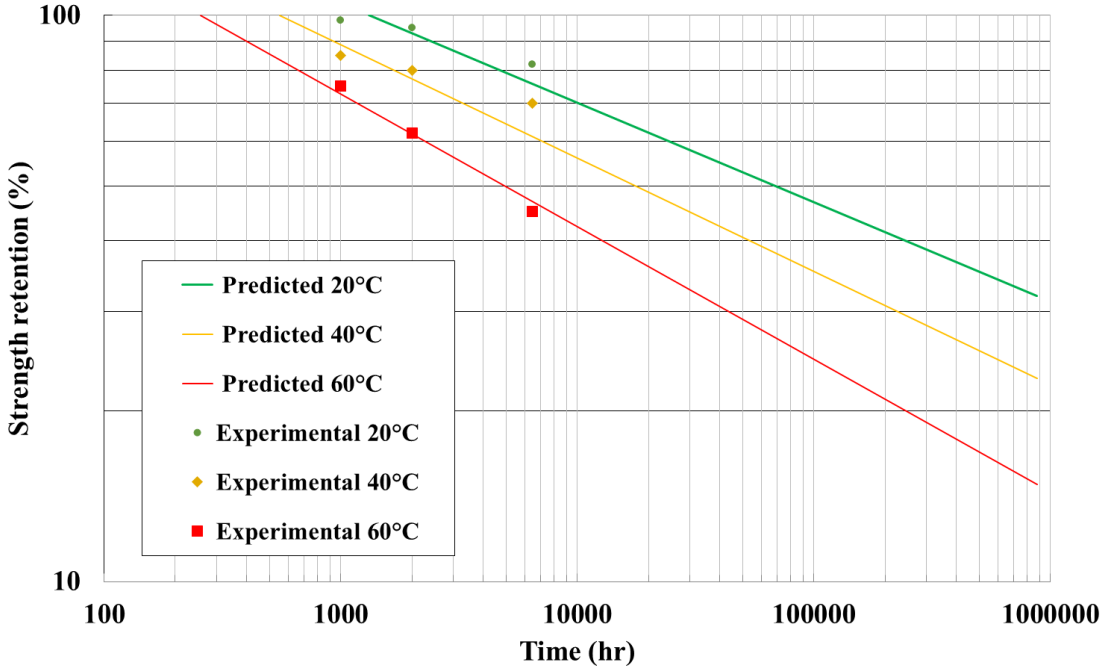

Figure 6. 9: Validation of suggested model using the experimental test results of Davalos et al. [21].

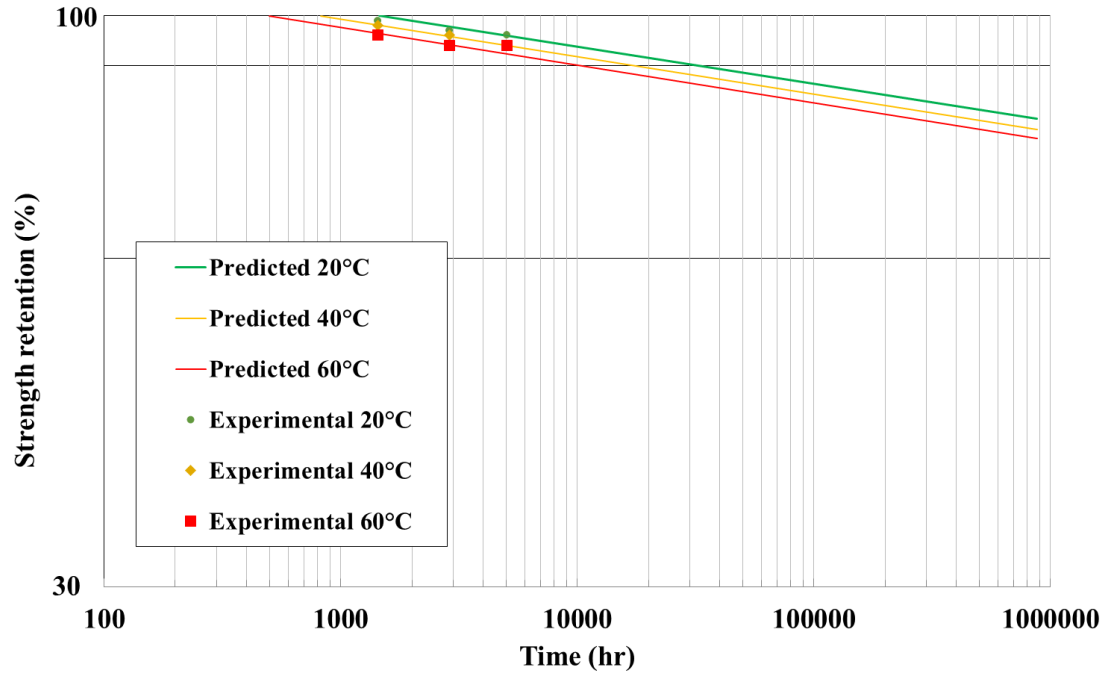

Figure 6. 10: Validation of suggested model using the experimental test results of Rebert and Benmokrane [10].

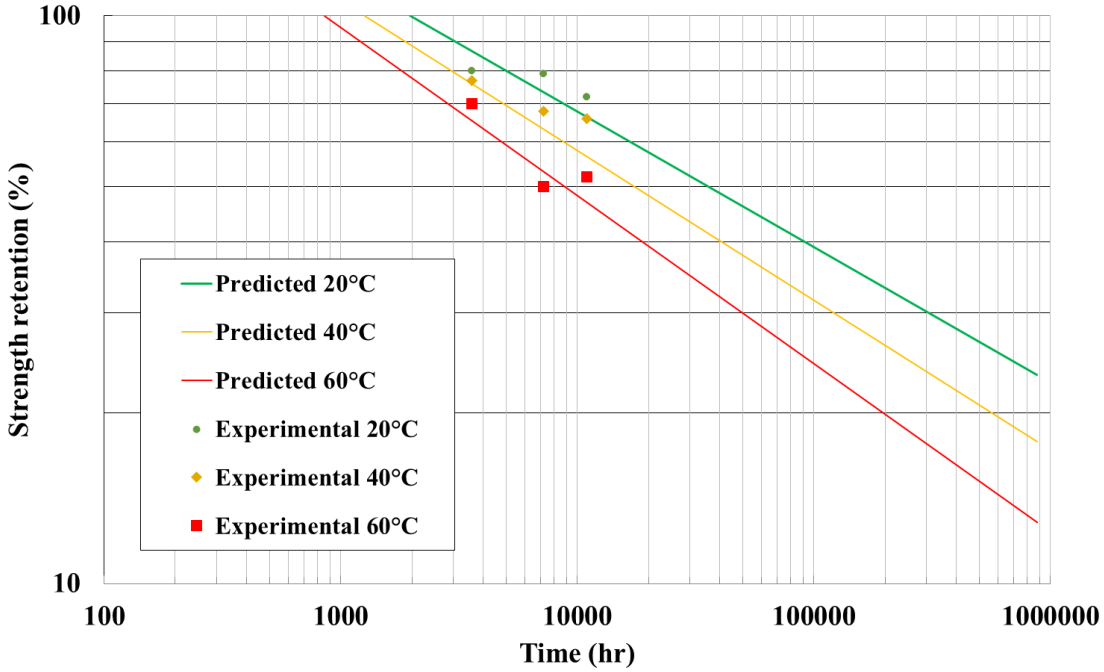

Figure 6. 11: Validation of suggested model using the experimental test results of El-Hassan et al. [24].

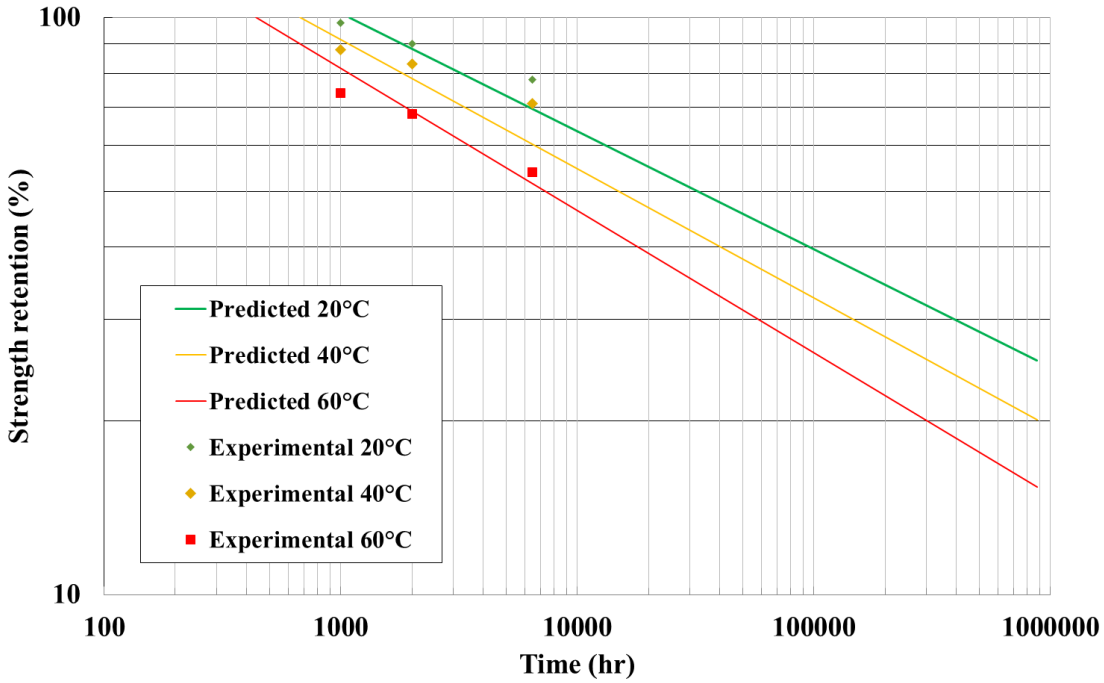

Figure 6. 12: Validation of suggested model using the experimental test results of Dejke and Tepfer [7].

6.2.5 Comparison to current predictive models

The performance of the proposed model was also compared with that of other models discussed in section 6.2. On the basis of the experimental data generated in this study, Figures 6.13, 6.14, 6.15 present the comparison of tensile strength retention prediction between the proposed model and the model included in *fib* Bulletin 40 [12] as well as those proposed by Weber and Witt [16] and Serbescu et al. [11], respectively. All curves obtained by the new approach for the different temperature levels approximate well the experimental values. Indeed, the predicted tensile strength retention at all different services life time ware overall less conservative than predicted by the other models.

It should be kept in mind that changes in deterioration mechanisms over time at high temperatures can sometimes create complications in the application of the Arrhenius temperature degradation relationship, thereby affecting the accuracy of predictions. This needs to be taken into account when determining the temperature correction parameter.

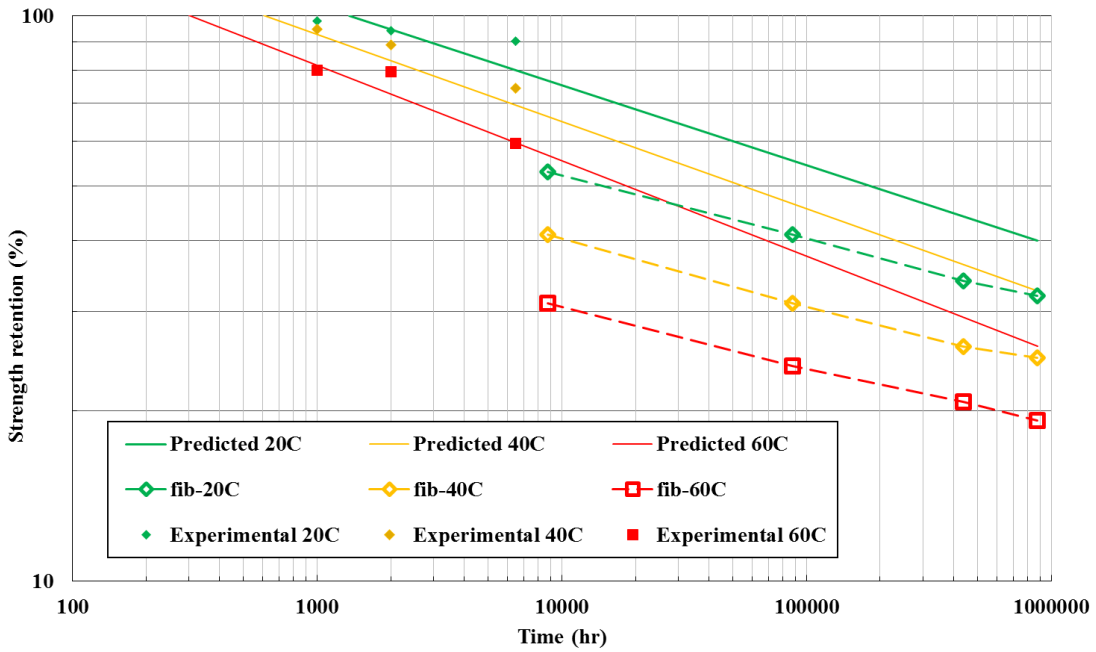

Figure 6. 13: Predicted strength retention of GFRP bars vs and *fib* Bulletin 40 [12].

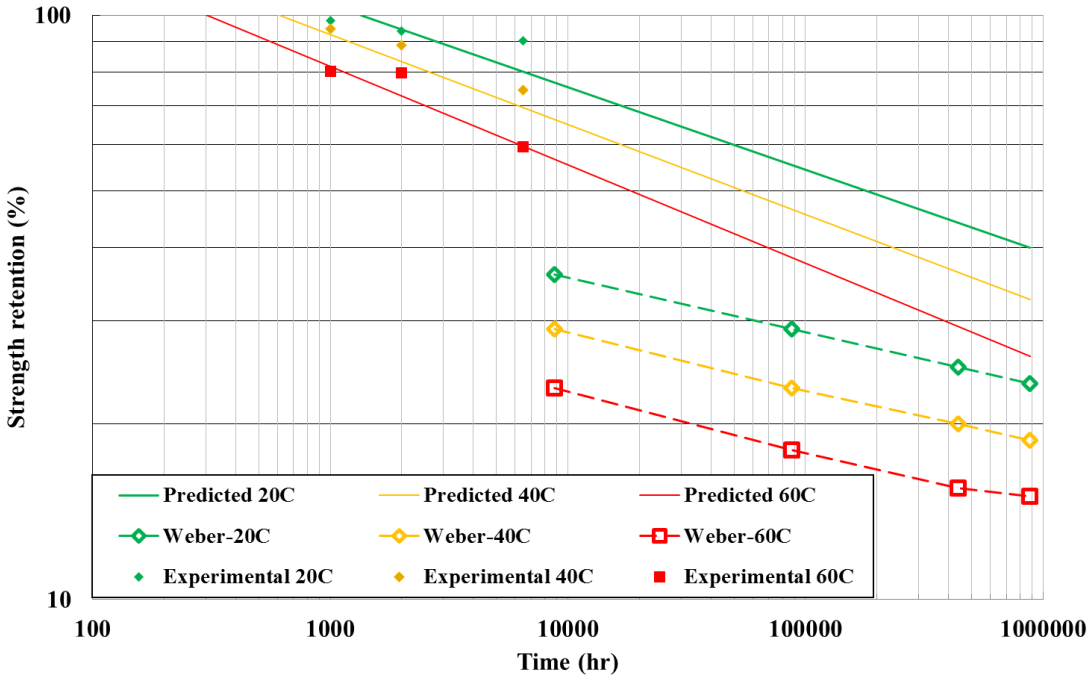

Figure 6. 14: Predicted strength retention of GFRP bars vs Weber and Witt [14].

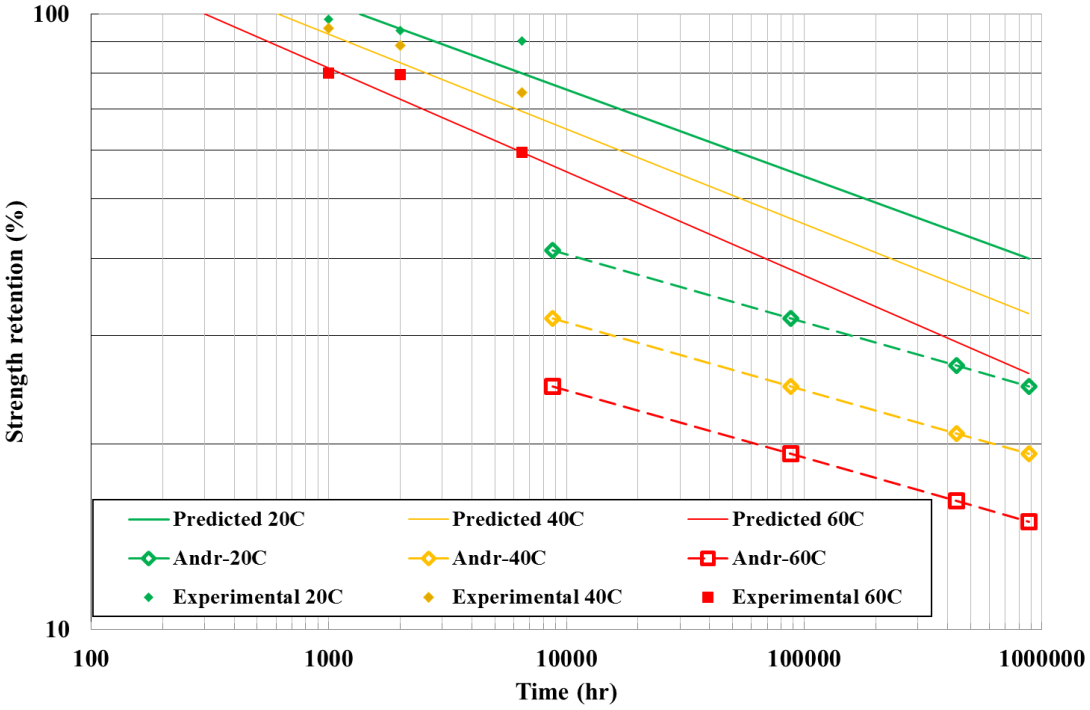

Figure 6. 15: Predicted strength retention of GFRP bars vs Serbescu et al. [11].

6.2.6 Current environmental reduction factors and proposed tensile strength retention values

As discussed in Section 6.2, current design approaches recommend the use of a single environmental reduction factor and do not allow to account explicitly for the effect of significant environmental parameters such as moisture, temperature, alkali environment and exposure time.

The above limitations were investigated and addressed in this study to yield a more flexible design framework and new degradation parameters were proposed to account for different environmental exposure conditions in a more objective manner. The environmental reduction factors η_{env} for different combined exposure conditions were calculated and shown in Table 6.9 and compared with the environmental reduction factors specified in current design codes/guidelines (see Table 6.1). By using the suggested parameters, the design strength of GFRP bars can be adjusted according to the expected environmental exposure and in-service conditions.

The effect of sustained stress is also included explicitly in the proposed model through the use of a separate degradation parameter and its effects are also summarised in Table 6.9 for a typical in-service sustained stress level of 14% (equivalent to an imposed strain of about 3000με) as recommended in ACI440.R-15. As confirmed by the experimental tests carried out in this study, the application of sustained stress accelerates the environmental attack and degradation processes at an early stage of conditioning and affects long-term residual strength.

It is worth pointing out that, with the exception of the Norwegian design recommendations, the environmental reduction factors used by current design codes and guidelines seem to overestimate the long-term residual properties, especially for high temperature regions and under saturated or wet conditions. This can potentially lead to unconservative design solutions and shorter-than-required service life in extreme environments. In addition, the use of a more flexible framework can enable the development of optimal design solutions for GFRP RC structures depending on specific in-service conditions or can account for future changes in environmental exposures (e.g. due to climate change) or loading conditions (e.g. due to change of use, increase of service loads).

Table 6. 9: Environmental reduction factor η_{env} for different combined exposure conditions and sustained stress

n_{sl}		n_{onset}	n_T		n_{moist}		n_{sus}		η_{env}	η_{env}
Design life (year)	Value	Value	Temp (°C)	Value	RH (%)	Value	Loading % ULS	Value	Unstressed	Stressed
50	5.64	3.13	10	-0.19	50	-1	14	-0.15	0.74	0.71
			20	0					0.70	0.67
			40	0.35					0.63	0.60
			60	0.65					0.57	0.54
100	5.94	3.13	10	-0.19	50	-1	14	-0.15	0.68	0.65
			20	0					0.64	0.61
			40	0.35					0.57	0.54
			60	0.65					0.51	0.48
50	5.64	3.13	10	-0.19	80	-0.5	14	-0.15	0.64	0.61
			20	0					0.60	0.57
			40	0.35					0.53	0.50
			60	0.65					0.47	0.44
100	5.94	3.13	10	-0.19	80	-0.5	14	-0.15	0.58	0.55
			20	0					0.54	0.51
			40	0.35					0.47	0.44
			60	0.65					0.41	0.38
50	5.64	3.13	10	-0.19	100	0	14	-0.15	0.54	0.51
			20	0					0.50	0.47
			40	0.35					0.43	0.40
			60	0.65					0.37	0.34
100	5.94	3.13	10	-0.19	100	0	14	-0.15	0.48	0.45
			20	0					0.44	0.41
			40	0.35					0.37	0.34
			60	0.65					0.31	0.28

6.3 CONCLUSIONS

The newly developed framework presented here is based on the model proposed in *fib* Bulletin 40 and the implementation of a TSF concept. The framework accounts for the effects of exposure temperature, moisture, and service time and extends previous models to include the effect of sustained stress. On the basis of the experimental work presented in Chapters 4 and 5, and under the assumption that Arrhenius theory is valid for the entire range of temperatures examined as part of this study, a modified strength retention equation for GFRP bars in concrete has been

developed and proposed, along with a revised set of environmental reduction factors. The outcomes of this study are summarised below:

- The environmental reduction factors currently recommended in existing codes and guidelines do not reflect the genuine effects of continued environmental exposure, combined with a sustained load, in various applications.
- The most significant cause of GFRP bar degradation in concrete is chemical reactions, which tends to be accelerated by a range of physical processes.
- The chemical reaction or degradation rate of the GFRP bar in concrete can be expressed by the Arrhenius relationship.
- The effects of sustained stress was incorporate as an explicit environmental reduction factor and a correction value was proposed.
- The temperature correction factor should account for variation in chemical compositions and manufacturing processes of different GFRP bars. An approach for estimating temperature correction factors using the activation energy of a specific composite was proposed.
- The predicted long-term behaviour curves provided by the proposed approach agree reasonably well with the experimental test results obtained from this study as well as other studies available in the literature.
- The predicted strength loss behaviour at low temperature ranges was slightly overestimated. Longer exposure time, or the use of test data at additional temperature levels, are recommended to obtain more accurate TSF and long-term predictions for low levels of temperature.
- The environmental reduction factors recommended in current codes and guidelines can potentially lead to unconservative design solutions and shorter-than-required service life in extreme environments.
- The use of the proposed framework can enable the development of optimal design solutions for GFRP RC structures depending on specific in-service conditions or can account for future changes in environmental exposures (e.g. due to climate change) or loading conditions (e.g. due to change of use, increase of service loads).

6.4 REFERENCES

1. Norway Standard NS 3473 (1998), Norwegian Council for Building Standardization, Norway.
2. ACI ,(2006), Guide for the Design and Construction of Concrete Reinforced with FRP Bars, *American Concrete Institute, Committee 440*. Farmington Hills, MI, USA.
3. CHBDC ,(2006), Canadian Highway Bridge Design Code, *Canadian Standards Association International*, Toronto, Ontario, Canada.
4. JSCE ,(1997), Recommendation for Design and Construction of Concrete Structures Using Continuous Fiber Reinforcing Materials, *Research Committee on Continuous Fiber Reinforcing Materials*, Japan Society of Civil Engineers, Tokyo, 325 p.
5. Mufti, A.A., Newhook, J., Benmokrane, B., Tadros, G. and Vogel, H.M., (2011). Durability of GFRP rods in field demonstration projects across Canada. *In Proc., 4th Int. Conf. on Durability & Sustainability of Fibre Reinforced Polymer (FRP) Composites for Construction and Rehabilitation of Structures (CDCC2011) (pp. 27-35)*. Quebec City.Canada
6. Gooranorimi O, Bradberry T, Nanni.A,(2017). Durability of GFRP reinforcement in built structures: a 15-year old concrete bridge deck. *In Proceedings The 5th International Conference on Durability of Fibre Reinforced Polymer (FRP) Composites for Construction and Rehabilitation of Structures*, Sherbrooke, Canda
7. Dejke, V. and Tepfers, R., (2001),. Durability and service life prediction of GFRP for concrete reinforcement. *In Proc., 5th Int. Conf. on Fiber-Reinforced Plastics for Reinforced Concrete Structures (FRPRCS-5)* (Vol. 1, pp. 505-516). London: Thomas Telford.
8. Bank, L.C., Gentry, T.R. and Barkatt, A., (1995). Accelerated test methods to determine the long-term behavior of FRP composite structures: environmental effects. *Journal of Reinforced Plastics and Composites*, 14(6), pp.559-587.
9. Chen, Y., Davalos, J.F., Ray, I. and Kim, H.Y., (2007). Accelerated aging tests for evaluations of durability performance of FRP reinforcing bars for concrete structures. *Composite Structures*, 78(1), pp.101-111.
10. Robert, M. and Benmokrane, B., (2013). Combined effects of saline solution and moist concrete on long-term durability of GFRP reinforcing bars. *Construction and Building Materials*, 38, pp.274-284.

11. Serbescu, A., Guadagnini, M. and Pilakoutas, K., (2014). Mechanical characterization of basalt FRP rebars and long-term strength predictive model. *Journal of Composites for Construction*, 19(2), p.04014037.
12. *fib* Bulletin 40, (2007). FRP reinforcement in RC structures. Technical report.
13. Huang, J.,(2013). Safe Use of GFRP Bar in RC Structures in Europe . *11th international symposium on fibre reinforced polymers for reinforced concrete structures (FRPRCS-11)*
14. Byars, E.A., Waldron, P., Dejke, V., Demis, S. and Heddadin, S., (2003). Durability of FRP in concrete–current specifications and a new approach. *International Journal of Materials and Product Technology*, 19(1-2), pp.40-52.
15. American Concrete Institute (2000), "Guide for the Design and Construction of Concrete Reinforced with FRP Bars", Committee 440,
16. Weber, A. and Witt, C., (2007). Durability Design for FRP-Rebars. In *Proceedings of the Third International Conference on durability and field applications of fibre reinforced polymer (FRP) composites for construction, Quebec City (Quebec) Canada, May* (pp. 22-24).
17. Nkurunziza, G., Debaiky, A., Cousin, P. and Benmokrane, B., (2005). Durability of GFRP bars: a critical review of the literature. *Progress in structural engineering and materials*, 7(4), pp.194-209.
18. Nanni, A., Claure, G., De Caso y Basalo, F.J,. and Gooranorimi, O., (2016). Concrete and Composites Pedestrian Bridge. Concrete International, 38(11), pp.57-63.
19. Sawpan, M.A., Mamun A., and Holdsworth,P.PG, (2014)'Long term durability of pultruded polymer composite rebar in concrete environment', *Materials & Design*, 57,2014, 616-624
20. Espenson, J.H., 1995. Chemical kinetics and reaction mechanisms (Vol. 102). New York: McGraw-Hill.
21. Davalos, J.F., Chen, Y. and Ray, I., (2012). Long-term durability prediction models for GFRP bars in concrete environment. *Journal of Composite Materials*, 46(16), pp.1899-1914.
22. Carra, G. and Carvelli, V., (2015). Long-term bending performance and service life prediction of pultruded Glass Fibre Reinforced Polymer composites. Composite Structures, 127, pp.308-315.
23. Brown, T.L., LeMay Jr, H.E. and Bursten, B.E., (2006). Chemical kinetics. *Reactions in the Solid State*, 22, p.130.

24. El-Hassan, H., El-Maaddawy, T., Al-Sallamin, A. and Al-Saidy, A., (2017). Performance evaluation and microstructural characterization of GFRP bars in seawater-contaminated concrete. *Construction and Building Materials*, 147, pp.66-78.

CHAPTER 7

7 CONCLUSIONS AND RECOMMENDATIONS FOR FUTURE WORK

7.1 CONCLUSIONS

The main purpose of this research project was to develop a more in-depth understanding of the degradation mechanisms that affect long-term performance of GFRP bars reinforcement in concrete. A large experimental programme including both mechanical and physical material characterisation was completed as part of this study on GFRP bars exposed to different environments and mechanical conditioning. Tests on small-scale structural elements exposed to different environments were also carried out. Based on the insights gained during this work and the extensive set of complementary experimental data, a model capable of predicting the long-term residual strength of GFRP reinforcement in concrete exposed to different environments was developed. All of the objectives set out in Chapter 1 were achieved and the main conclusions are summarised below.

7.1.1 From the literature review:

- The long-term bond behaviour plays a critical role in the long-term performance of GFRP reinforced concrete structures.
- Several degradation mechanisms can affect long-term performance of GFRP bars in concrete. The most significant degradation mechanisms identified involve the free hydroxide ions (OH^-) attacking the polymer matrix and the disassembling of the long molecular chains by hydrolysis reaction, promoting the ingress of more water molecules (H_2O) and OH^- ions. These, in turn, can break the polymer-polymer chain secondary bond, creating localised voids and ultimately affecting the physical and mechanical properties of the GFRP matrix (i.e. causing plasticization). In addition, direct contact with water molecules can also lead to the degradation of glass fibres through the dissolution process.
- Different studies showed varied, and sometime contrasting, results on strength and bond performance of GFRP bars in concrete. This is mainly due to the differences in material composition and properties of GFRP bars and in the different test methods used for assessment, which have not yet been standardised. In addition, the long-term bond

behaviour of GFRP bars is highly affected by the surface geometry of the GFRP bar and transverse properties of the rich resin outer layer of the bar.

- Applying sustained stress on GFRP RC members results in bond degradation that can significantly affect long-term performance.
- A decrease in the long-term performance of the bars can affect the long-term performance of GFRP RC structures causing larger than allowable deflections and crack widths.
- The design of GFRP RC members is often controlled by limiting deflection and crack width at service loads (i.e. serviceability limit state - SLS).
- Previous studies on GFRP RC beams exposed to tropical weathering conditions reported higher deflection and wider crack width compared to control beams kept under ambient conditions.
- Recent field studies carried out on several existing GFRP RC structures have shown that, after more than fifteen years of service, the GFRP bars used for these concrete structures showed no obvious signs of degradation.
- There is no standard method to determine the durability of GFRP bars in concrete structures other than that proposed by the Canadian standards. Each research group has designed their own experimental procedure to transform or translate the data obtained under accelerated conditions and to develop their prediction model for GFRP deterioration in a concrete environment.
- There is an urgent need to develop a holistic prediction model that can reliably assess the long-term durability performance of GFRP bars in concrete exposed to different in-service environments.

7.1.2 Long-term performance of GFRP subjected to different environmental exposures and sustained stress

- The tests results show that there is significant tensile strength degradation when GFRP bars are subjected to elevated temperature and alkaline environments, while no significant change was observed in the elastic modulus of the tested GFRP bars, regardless of the conditioning environment or exposure period. Strength reduction of up to 41% was observed for the specimens exposed to 60°C after 6480 hr.
- The change in flexural properties of GFRP bars (e.g. strength, stiffness) tested in a three point configuration after conditioning was in line with the observations resulting from the direct tension tests.

- ILSS experimental outcomes showed that the higher the conditioning temperature, the higher the strength degradation. It was observed, however, that the reduction in ILSS was lower in stressed than in unstressed specimens. This phenomenon could be attributed to the method used to stress the samples in this research (i.e., bending, Figure. 6.1) which, by reducing the number of open pores in the portion of the bar in compression, limited moisture uptake in stressed samples.
- Although the SEM images showed that moisture and alkaline deterioration take place, not only in the resin matrix and glass fibre, but also at the interface between the fibre and the resin matrix, no significant degradation was observed through SEM in the glass fibres. The debonding between fibre/matrix and resin matrix deterioration seems to be the main issue affecting the long-term mechanical properties of GFRP bars.
- FTIR analyses showed a considerable increase in the number of hydroxyl groups at the surface of the material. This is an indication of chemical degradation in the resin matrix.
- The outer rich-resin layer of GFRP bars in concrete structures plays a crucial role in the bond between concrete and rebar, and since the surfaces of the GFRP bars were highly affected by moist alkaline environments, this indicates that degradation of the outer layer of GFRP bars in moist concrete applications should be adequately considered.

7.1.3 Long-term performance of GFRP RC members under loading condition and various environmental exposures

- Exposure to wet environments at elevated temperatures and sustained loading deteriorated the resin-rich layer of the GFRP bars, resulting in degradation of the bond between the concrete and the reinforcement and, in turn, reducing the tension stiffening and the overall structural performance of the GFRP RC members. Conversely, exposure to a moist environment without sustained loading did not cause bond strength degradation. In fact, the swelling of the GFRP bar, as a result of moisture absorption, seems to have increased the mechanical interlocking and the friction forces at the interface between concrete and reinforcement, leading to a stronger bond and to a relatively higher tension stiffening behaviour.
- Environmental exposure had a significant effect on the structural degradation of concrete beams reinforced with GFRP.
- The beams stressed with an allowable level of sustained stress (resulting in a strain level of about 3000με) exhibited deflections and maximum crack widths within the

recommended code limits for SLS. On the contrary, the beams stressed with a level of load equivalent to an imposed strain of 5000 με exceeded the recommended SLS limits for both deflection and crack width.

- The EC2 models to predict long-term deflection and crack width failed to describe the combined effect of severe environment and sustained loading. It should be noted, however, that these models have been developed for steel RC elements and, although based on fundamental principles that can be applied to both FRP and steel RC elements, the long term effects on material properties and bond between reinforcement and concrete need to be reassessed.

7.1.4 Long-term tensile strength prediction model

- GFRP bars exhibited better long-term performance in a dry concrete environment than in a moist concrete environment. Therefore, the environmental reduction factors currently recommended in existing codes and guidelines can be applied and would be safe in field applications where structural elements are exposed to dry conditions, but can often lead to very conservative solutions. Whereas, for a GFRP RC member continuously subjected to moist environments, the environmental degradation would increase dramatically, and the factors recommended in current codes and guidelines would require more calibration to produce a safe design.
- The total reduction factor for durability design should account for to the different levels of exposure to temperature, relative humidity and sustained load.
- The newly developed framework presented here is based on the model proposed in *fib* Bulletin 40 and the implementation of a TSF concept. It was assumed that the chemical reaction or degradation rate of the GFRP bar in concrete at different temperature exposure could be represented by the Arrhenius relationship. By utilising this approach, it is possible to convert the exposure time in accelerated conditions to time in real applications. The effects of sustained stress were incorporated as an explicit environmental reduction factor and a correction value was proposed.
- An approach for estimating temperature correction factors using the activation energy of a specific composite was proposed.
- The predicted long-term behaviour curves provided by the proposed approach agree reasonably well with the experimental test results obtained from this study as well as other studies available in the literature.

- The environmental reduction factors recommended in current codes and guidelines can potentially lead to unconservative design solutions and shorter-than-required service life in extreme environments.
- The use of the proposed framework can enable the development of optimal design solutions for GFRP RC structures depending on specific in-service conditions or can account for future changes in environmental exposures (e.g. due to climate change) or loading conditions (e.g. due to change of use, increase of service loads).

7.2 RECOMMENDATIONS FOR FUTURE RESEARCH

Based on both the experimental and analytical work carried out as part of this study, a series of recommendations for future research are given below:

- The effect of long-term hygrothermal aging on the chemical structure and mechanical properties of the resin matrix should be examined in more depth. Additional work should be carried out also on the characterisation of the saline coupling agents of the fibre/matrix interfaces.
- The time required to reach the onset of degradation and the activation energy required for this process are key parameters for the prediction of long-term performances of GFRP bars. A more reliable methodology to determine these parameters should be developed to ensure more accurate TSF. This methodology should comprise a full chemical and microstructure characterisation at different temperatures and exposure conditions (e.g. FTIR, SEM).
- The bond deterioration of GFRP bars under sustained stress subjected to different environmental conditions require further investigation in order to provide a safe design.
- Other types of bond test method should be used on GFRP RC members to represent the actual state, such as flexural bond tests to examine long-term bond performances of GFRP bars in concrete.
- A safety factor for bond strength should be developed to take into account the deterioration of bond strength with time, which should then be used for the design of GFRP RC structures.
- More investigation is required to assess the long-term effects of other types of environmental conditioning, such as low and sub-zero temperatures, freeze thaw cycles and elevated temperatures on the long-term performance of full-scale GFRP RC elements.

- The effects of creep and fatigue should be incorporated into long-term predictive models to obtain more reliable estimates of expected service life.

APPENDIX I

MECHANICAL CHARACTERISATION TESTS

1. Tensile strength data for GFRP bars

This section presents additional data obtained from direct tension tests result presented in Chapter 4. This data includes load strain-strain diagrams, Modulus of elasticity graphs, summary of tests result and failure modes pictures of all controlled bars as well as the conditioned ones.

Tensile properties of references specimens (REF)

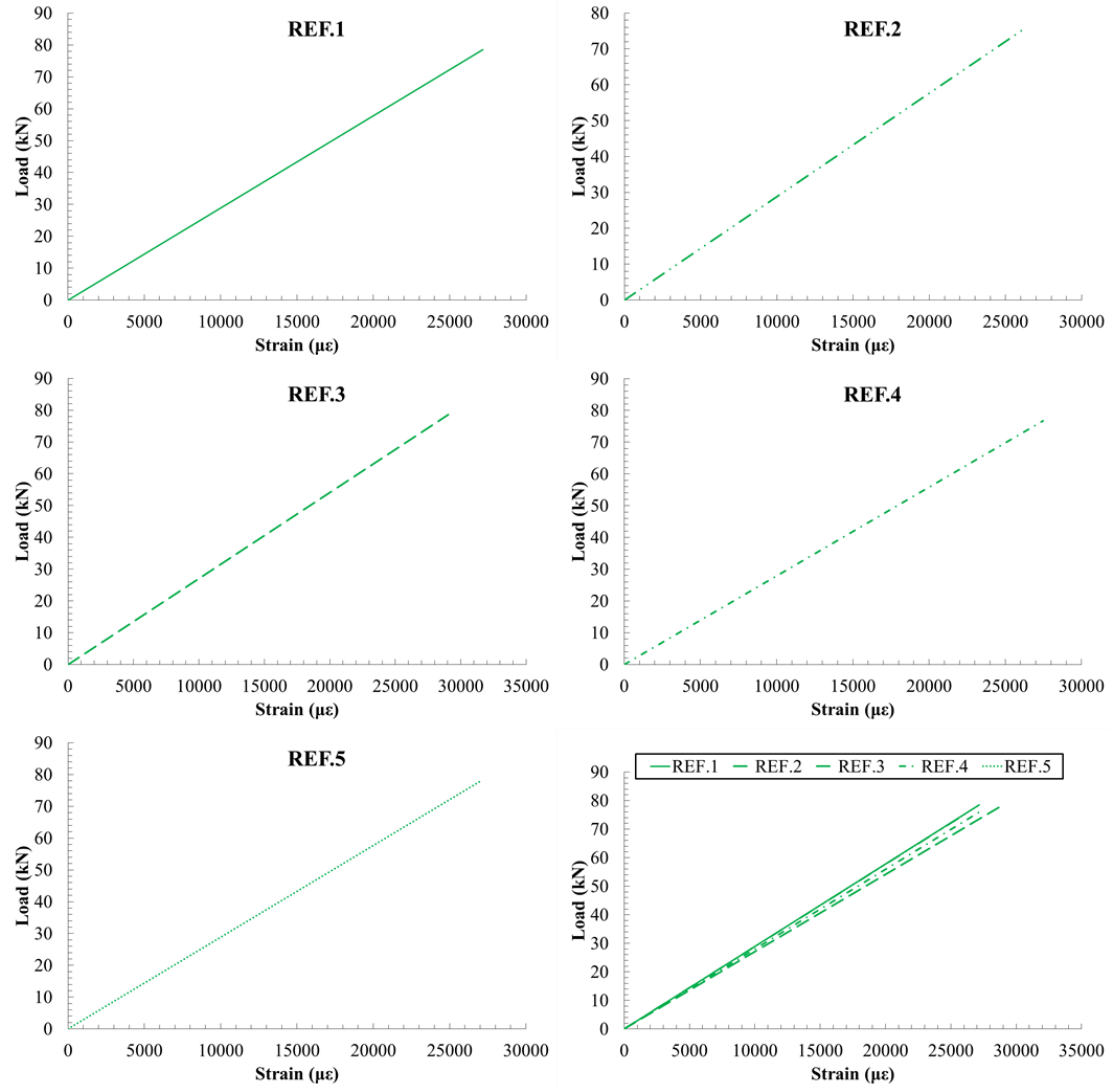

Figure.I.1 Load-strain of references specimens (REF)

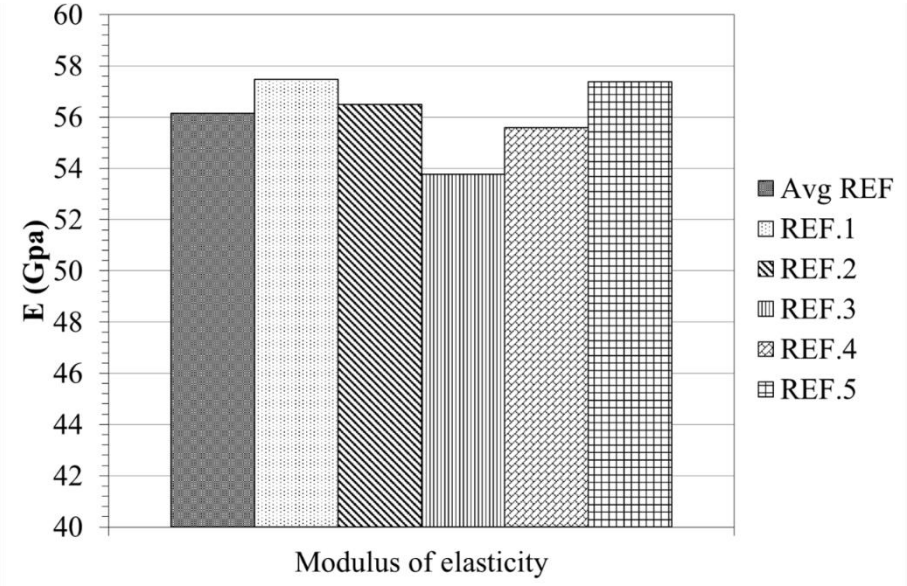

Figure.I.2: Modulus of elasticity for control specimens

Table I.1: A summary of tensile test results of concrete specimen (REF)

Specimens	P_{max} (kN)	E (GPa)	σ_{max} (MPa)	ε_{max}	note
REF.1	78.8	57.4	1568	0.027	
REF.2	75.3	56.4	1499	0.026	
REF.3	78.5	53.7	1562	0.029	
REF.4	76.7	55.5	1526	0.027	
REF.5	78.0	57.3	1552	0.027	
Average	77.5	56.1	1541	0.027	
std	1.4	1.52	28	0.0009	
%STD	1.8	2.7	1.8	3.4	
min	75.3	53.7	1499	0.026	
max	78.8	57.4	1568	0.029	

Tensile properties of concrete specimens

(M-CON-20°C-42d)

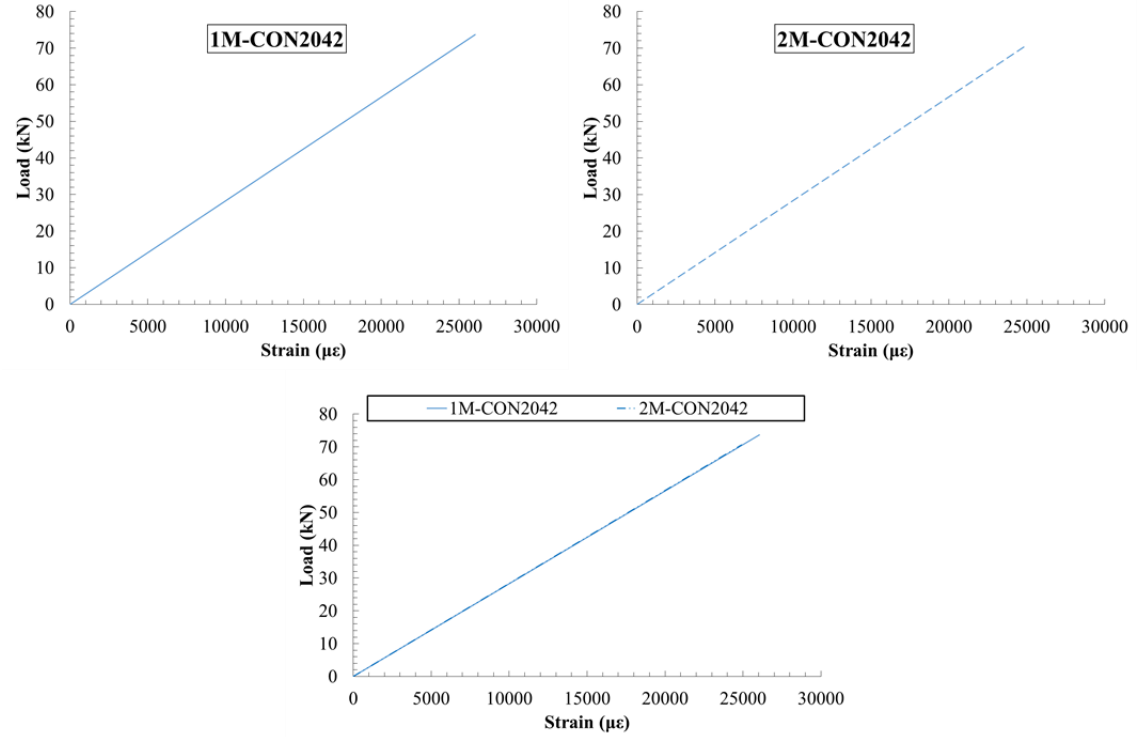

Figure.I.3 Load-strain of concrete specimens (M-CON-20°C-42d)

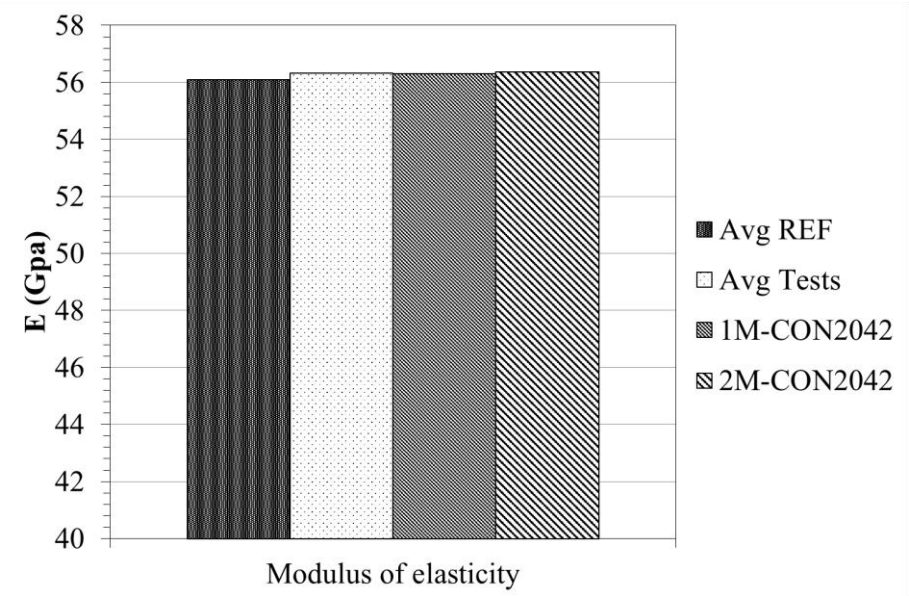

Figure.I.4: Modulus of elasticity for concrete specimens (M-CON-20°C-42d)

Table I.2: A summary of tensile test results of concrete specimen (M-CON-20°C-42d)

Specimens	P_{max} (kN)	E (GPa)	σ_{max} (MPa)	ε_{max}	note
1M-CON2042	73.7	56.3	1466	0.026	
2M-CON2042	70.5	56.3	1403	0.024	
3M-CON2042	76.5		1522		
average	75.1	56.3	1463	0.025	
std	2.9	3.9	59.3	0.80	
%STD	3.9	1.0	4.0	0.003	
min	70.5	56.3	1403	0.024	
max	76.5	56.3	1522	0.026	

(M-CON-40°C-42d)

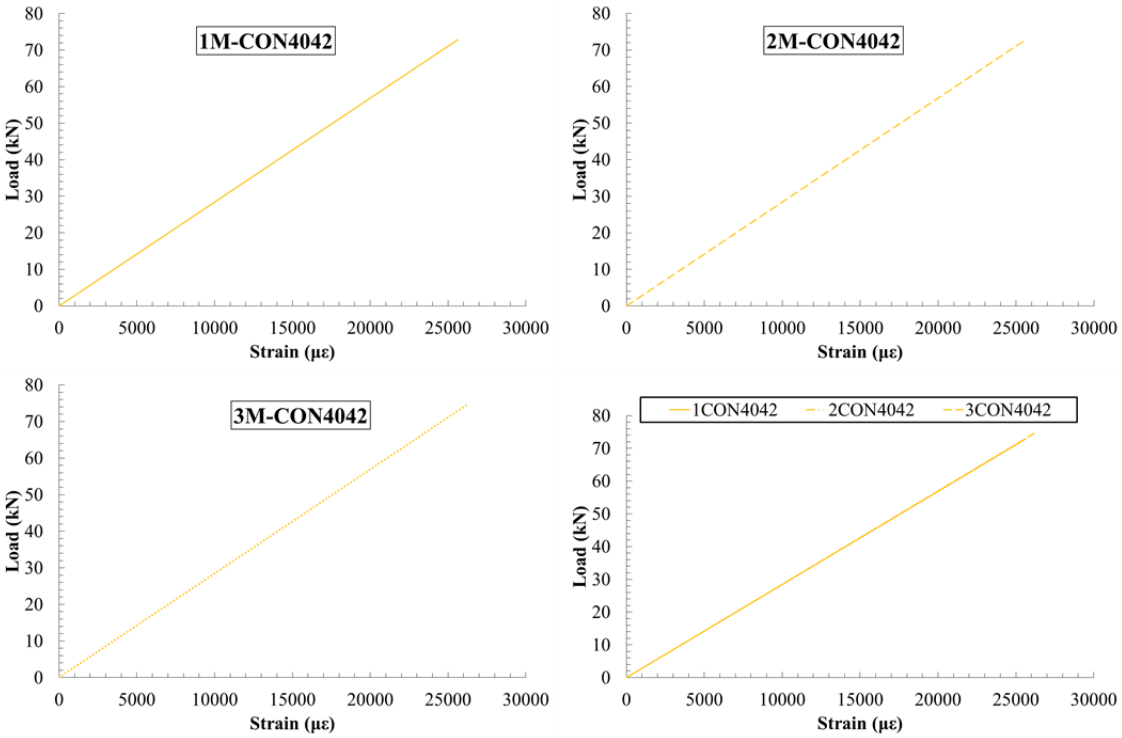

Figure.I.5 Load-strain of concrete specimens (M-CON-40°C-42d)

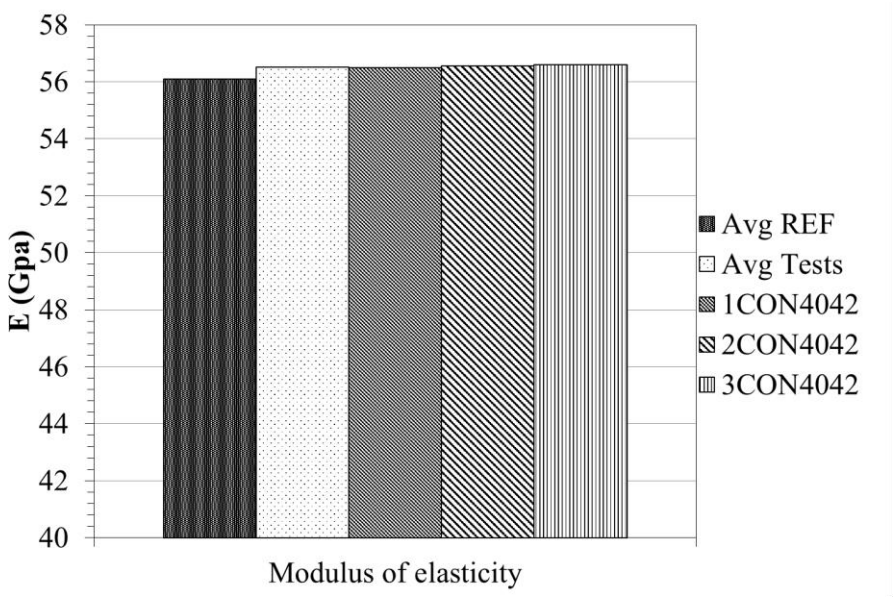

Figure.I.6: Modulus of elasticity for concrete specimens (M-CON-40°C-42d)

Table I.3: A summary of tensile test results of concrete specimen (M-CON-40°C-42d)

Specimens	P_{max} (kN)	E (GPa)	σ_{max} (MPa)	ε_{max}	note
1CON4042	72.8	56.4	1448	0.025	
2CON4042	72.6	56.5	1444	0.025	
3CON4042	74.5	56.6	1482	0.026	
average	73.3	56.5	1458	0.025	
std	1.0	0.05	20	0.0003	
%STD	1.4	0.10	1.42	1.34	
min	72.6	56.4	1444	0.025	
max	74.5	56.6	1482	0.026	

(M-CON-60°C-42d)

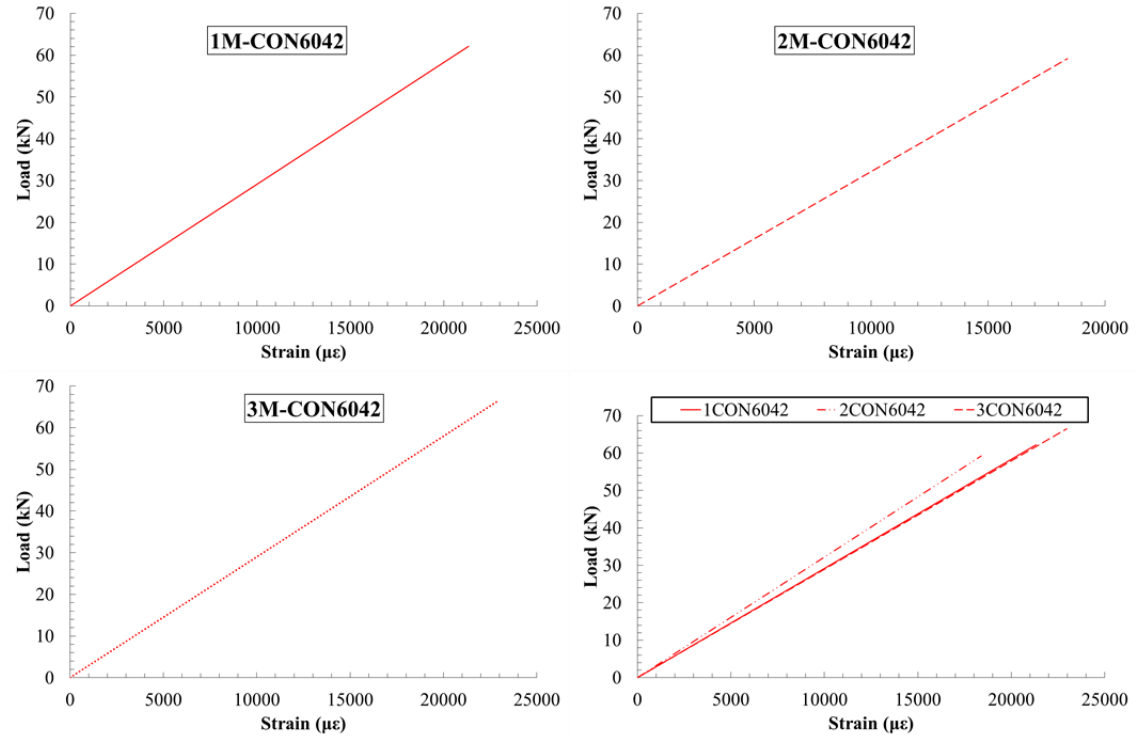

Figure.I.7 Load-strain of concrete specimens (M-CON-60°C-42d)

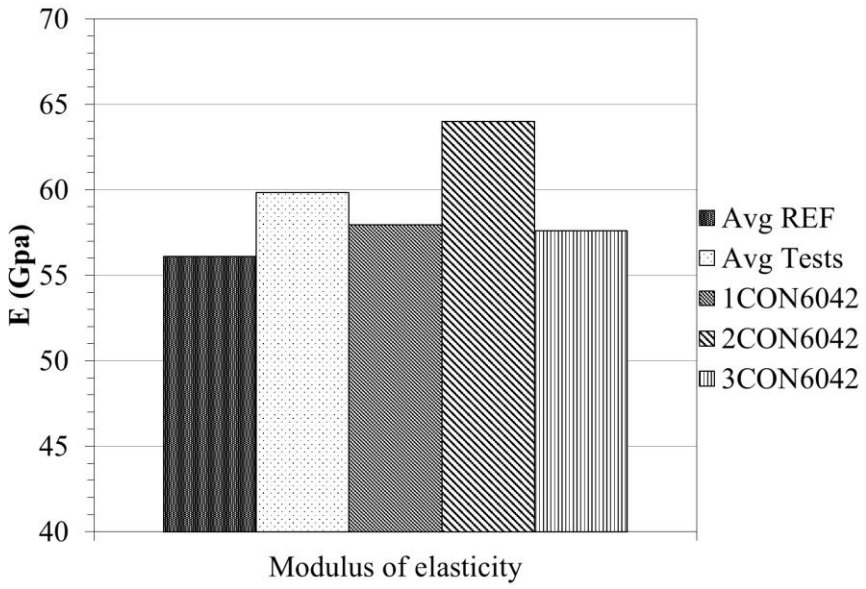

Figure.I.8: Modulus of elasticity for concrete specimens (M-CON-40°C-42d)

Table I.4: A summary of tensile test results of concrete specimen (M-CON-60°C-42d)

Specimens	P_{max} (kN)	E (GPa)	σ_{max} (MPa)	ε_{max}	note
1CON6042	62.1	57.9	1235	0.021	
2CON6042	59.1	64.0	1176	0.018	
3CON6042	66.5	57.5	1322	0.022	
average	62.6	59.8	1244	0.019	
std	3.6	3.6	73	0.002	
%STD	5.9	6.0	5.9	11.69	
min	59.1	57.5	1176	0.018	
max	66.5	64.0	1322	0.022	

(M-CON-20°C-90d)

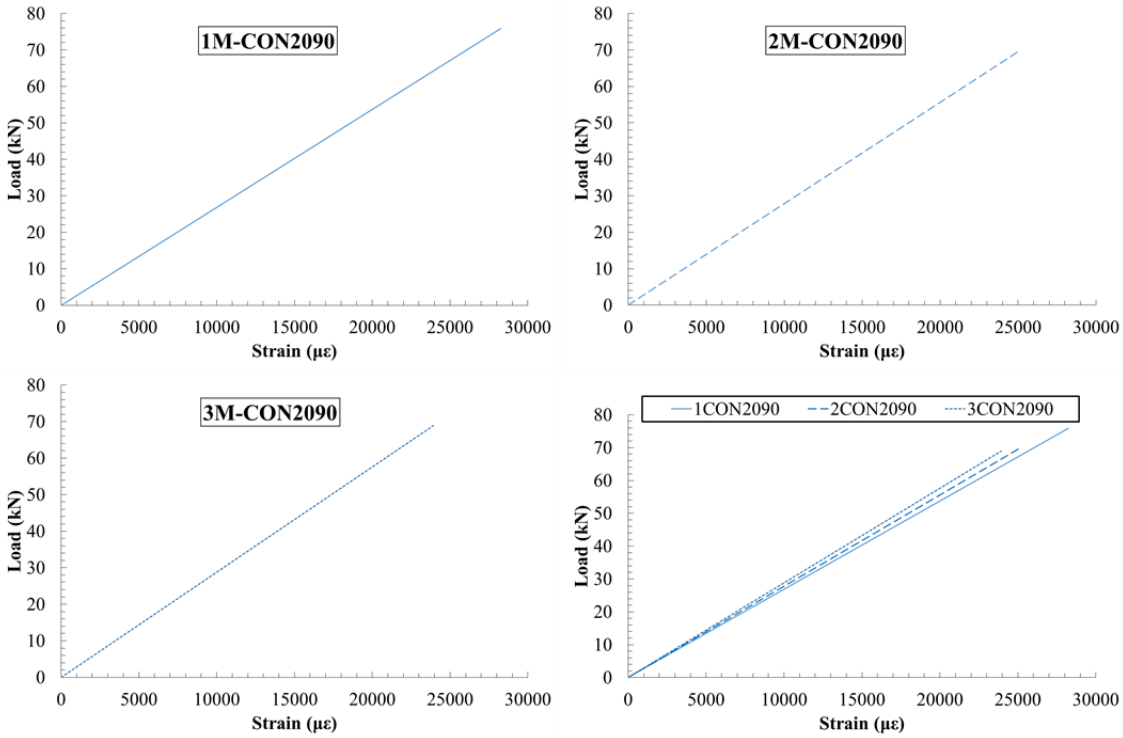

Figure.I.9 Load-strain of concrete specimens (M-CON-20°C-90d)

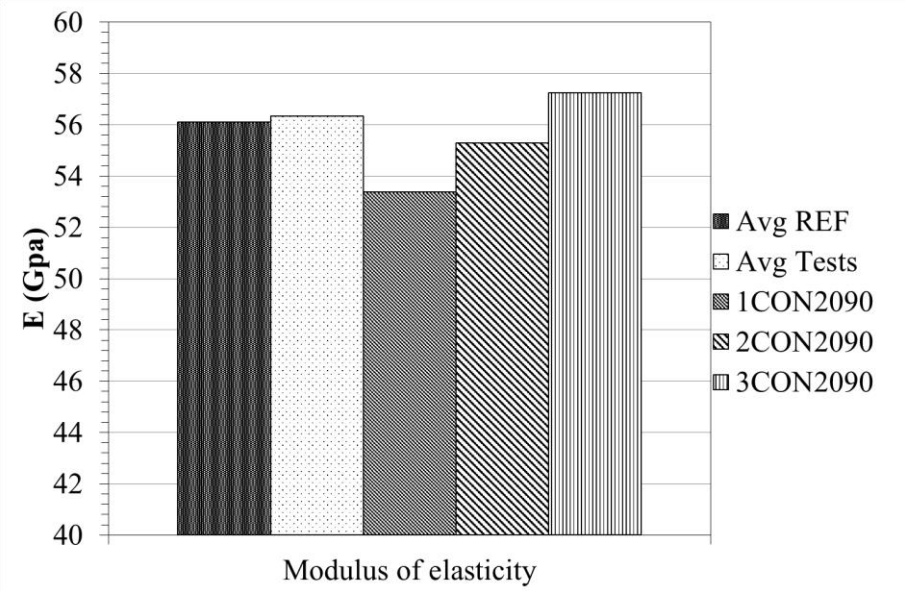

Figure.I.10: Modulus of elasticity for concrete specimens (M-CON-20°C-90d)

Table I.5: A summary of tensile test results of concrete specimen (M-CON-20°C-90d)

Specimens	**P_{max} (kN)**	**E (GPa)**	**σ_{max} (MPa)**	**ε_{max}**	**note**
1CON2090	75.8	53	1508	0.028	
2CON2090	69.6	55	1386	0.025	
3CON2090	68.8	57	1370	0.023	
average	71.4	55	1421	0.025	
std	3.8	1.9	75	0.002	
%STD	5.3	3.4	5.3	8.69	
min	68.8	53.	1370	0.023	
max	75.8	57	1508	0.028	

(M-CON-40°C-90d)

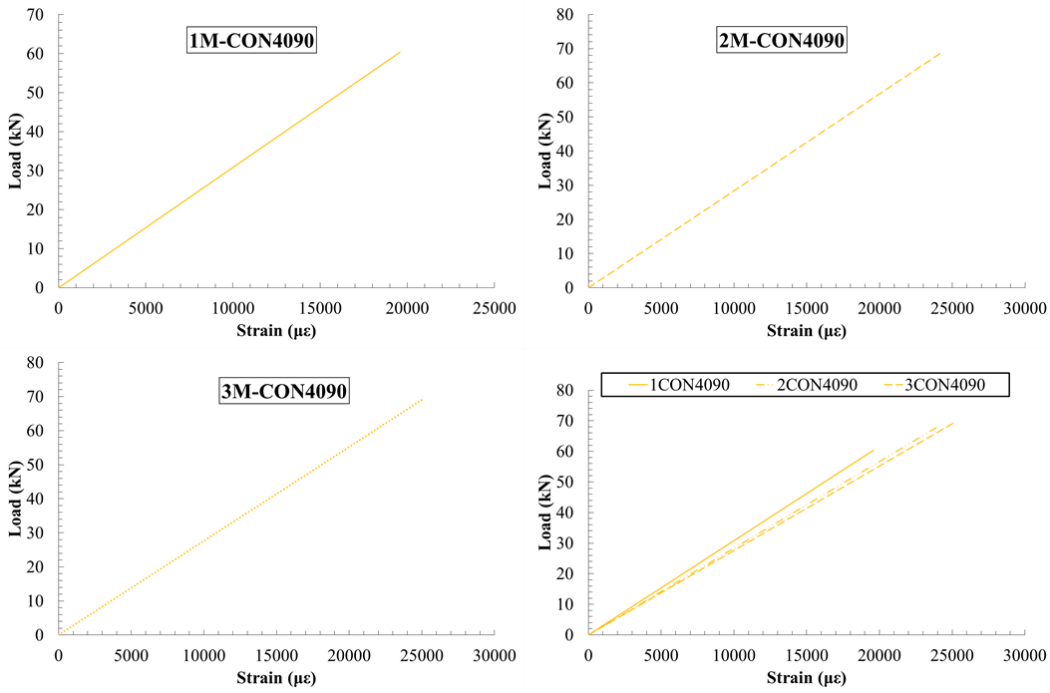

Figure.I.11 Load-strain of concrete specimens (M-CON-40°C-90d)

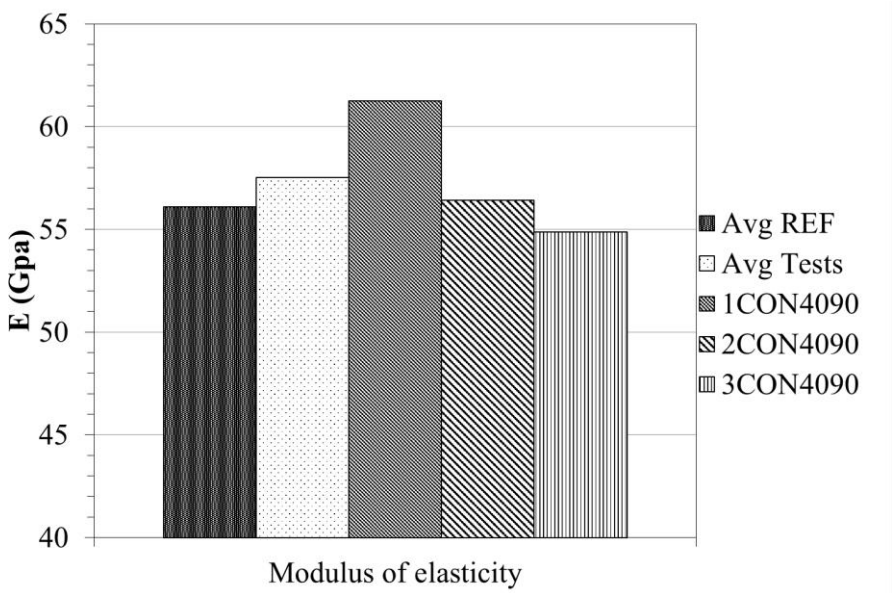

Figure.I.12: Modulus of elasticity for concrete specimens (M-CON-40°C-90d)

Table I.6: A summary of tensile test results of concrete specimen (M-CON-40°C-90d)

Specimens	P_{max} (kN)	E (GPa)	σ_{max} (MPa)	ε_{max}	note
1CON4090	60.3	61.2	1200	0.019	
2CON4090	68.4	56.4	1362	0.024	
3CON4090	69.3	54.8	1379	0.025	
average	68.9	57.5	1370	0.024	
std	0.6	1.0	12.2	0.0007	
%STD	0.8	1.8	0.89	2.84	
min	60.3	54.8	1200	0.019	
max	69.3	61.2	1379	0.025	

(M-CON-60°C-90d)

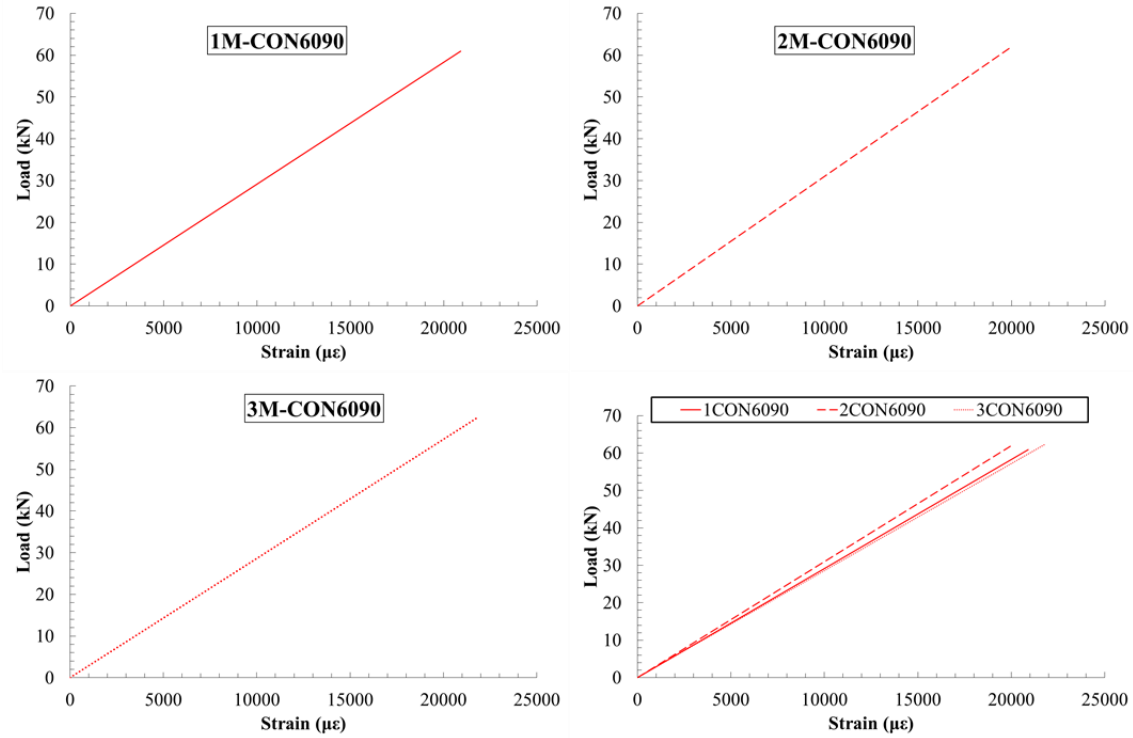

Figure.I.13 Load-strain of concrete specimens (M-CON-60°C-90d)

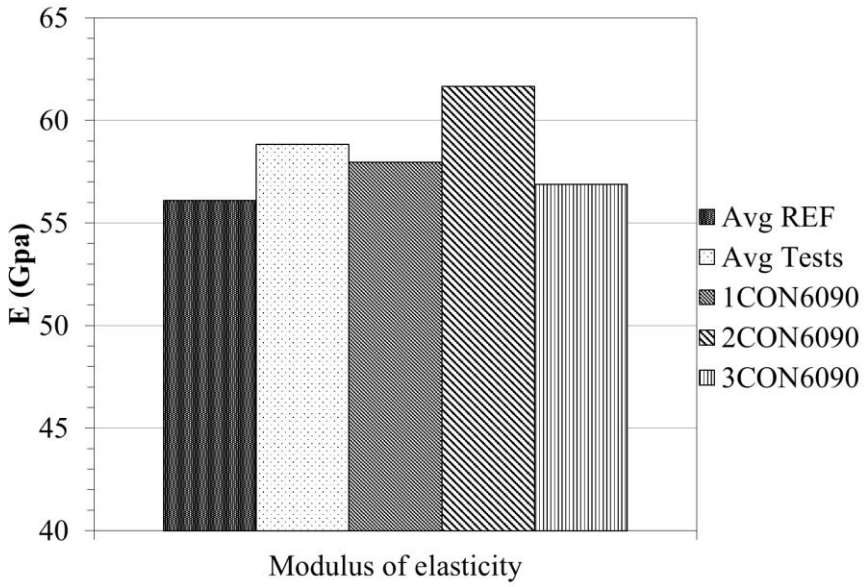

Figure.I.14: Modulus of elasticity for concrete specimens (M-CON-60°C-90d)

Table I.7: A summary of tensile test results of concrete specimen (M-CON-60°C-90d)

Specimens	P_{max} (kN)	E (GPa)	σ_{max} (MPa)	ε_{max}	note
1CON6090	60.9	57.9	1211	0.020	
2CON6090	61.8	61.6	1229	0.019	
3CON6090	62.3	56.8	1240	0.021	
average	61.7	58.8	1227	0.020	
std	0.7	2.5	14.6	0.0009	
%STD	1.2	4.2	1.2	4.50	
min	60.9	56.8	1211	0.019	
max	62.3	61.6	1240	0.021	

(M-CON-20°C-270d)

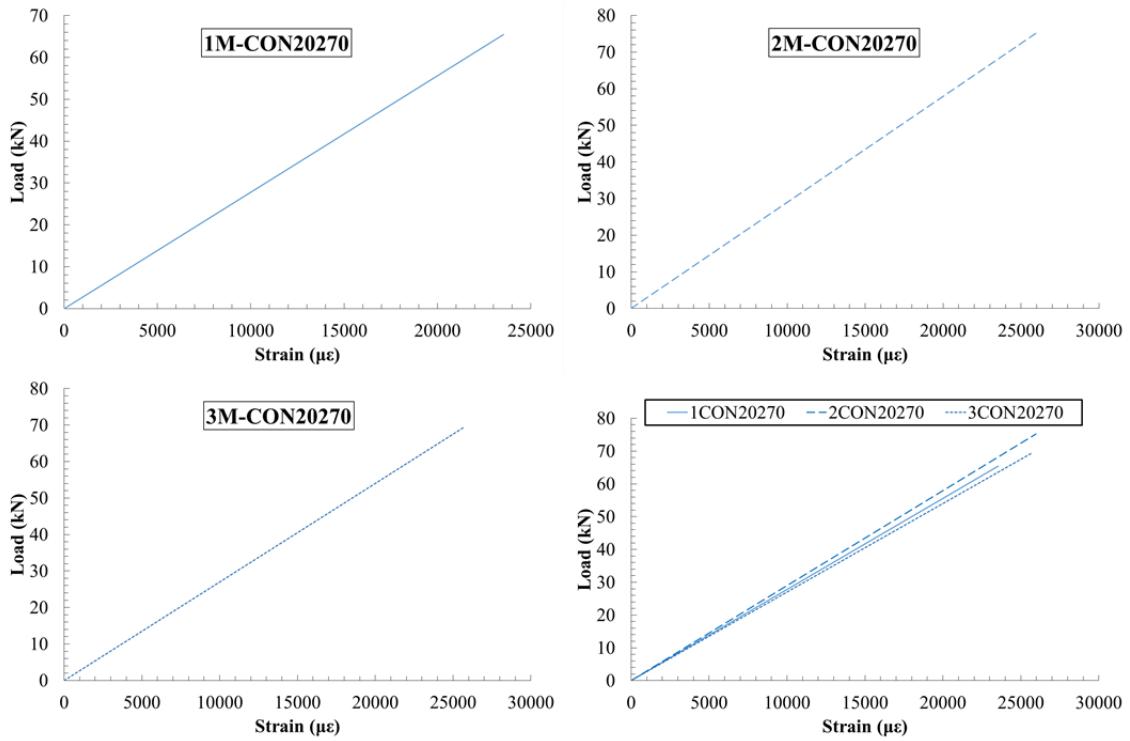

Figure.I.15 Load-strain of concrete specimens (M-CON-20°C-270d)

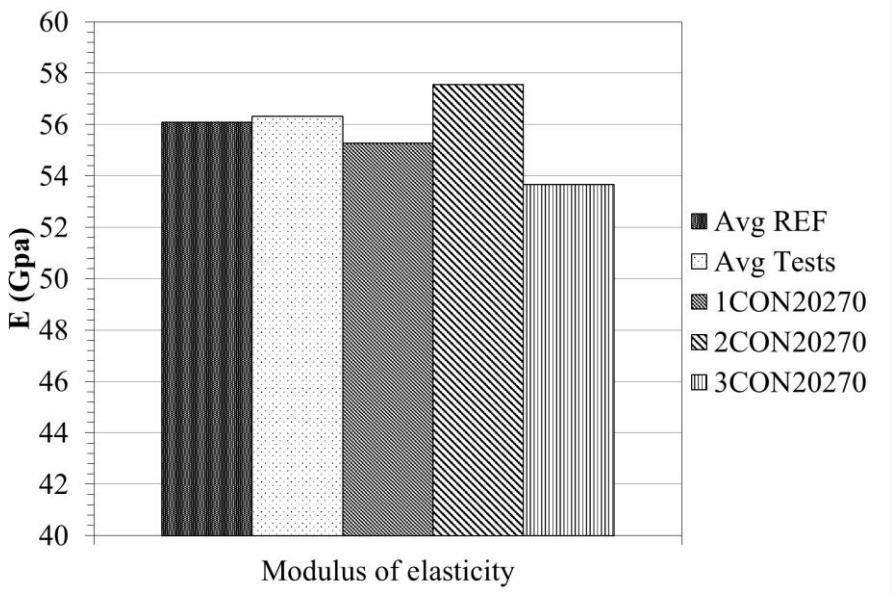

Figure.I.16: Modulus of elasticity for concrete specimens (M-CON-20°C-270d)

Table I.8: A summary of tensile test results of concrete specimen (M-CON-20°C-270d)

Specimens	P_{max} (kN)	E (GPa)	σ_{max} (MPa)	ε_{max}	note
1CON20270	65.4	55.2	1305	0.02	
2CON20270	75.1	57.5	1500	0.03	
3CON20270	69.3	53.6	1380	0.03	
average	70.0	55.5	1390	0.03	
std	4.9	1.9	0.10	0.00	
%STD	7.0	3.5	7.00	5.33	
min	65.4	53.6	1300	0.02	
max	75.1	57.5	1500	0.03	

(M-CON-40°C-270d)

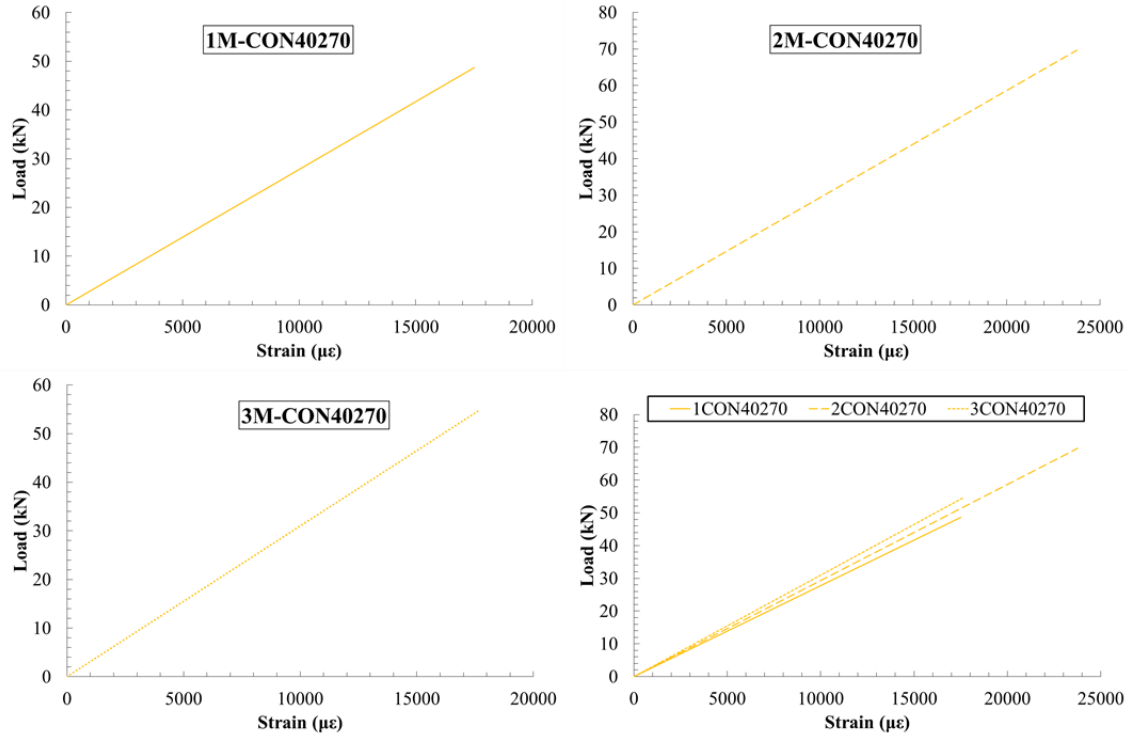

Figure.I.17 Load-strain of concrete specimens (M-CON-40°C-270d)

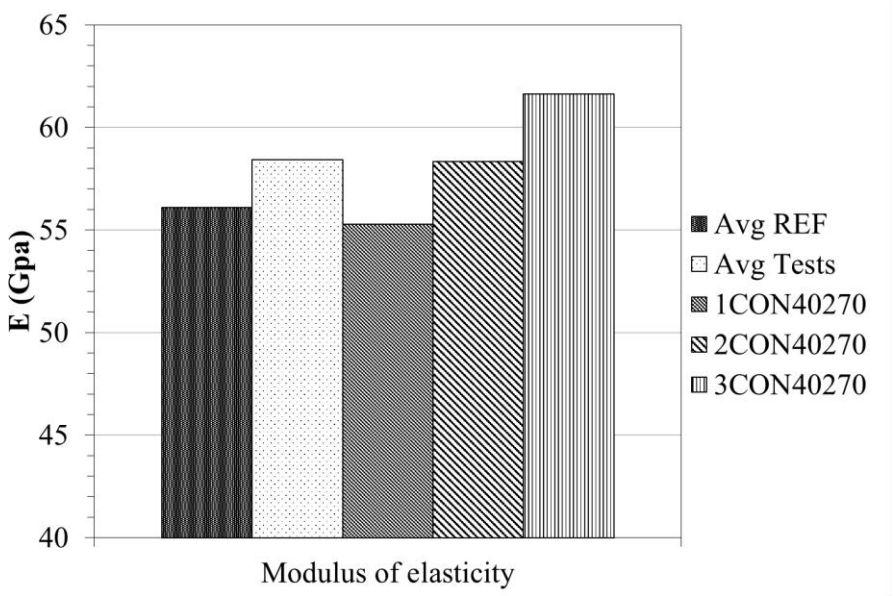

Figure.I.18: Modulus of elasticity for concrete specimens (M-CON-40°C-270d)

Table I.9: A summary of tensile test results of concrete specimen (M-CON-40°C-270d)

Specimens	P_{max} (kN)	E (GPa)	σ_{max} (MPa)	ε_{max}	note
1CON40270	48.6	55.2	970	0.018	
2CON40270	69.7	58.3	1390	0.024	
3CON40270	54.7	61.6	1090	0.018	
average	57.7	58.4	1150	0.020	
std	10.8	3.1	0.22	0.004	
%STD	18.7	5.4	18.74	18.129	
min	48.6	55.2	970	0.018	
max	69.7	61.6	1390	0.024	

(M-CON-60°C-270d)

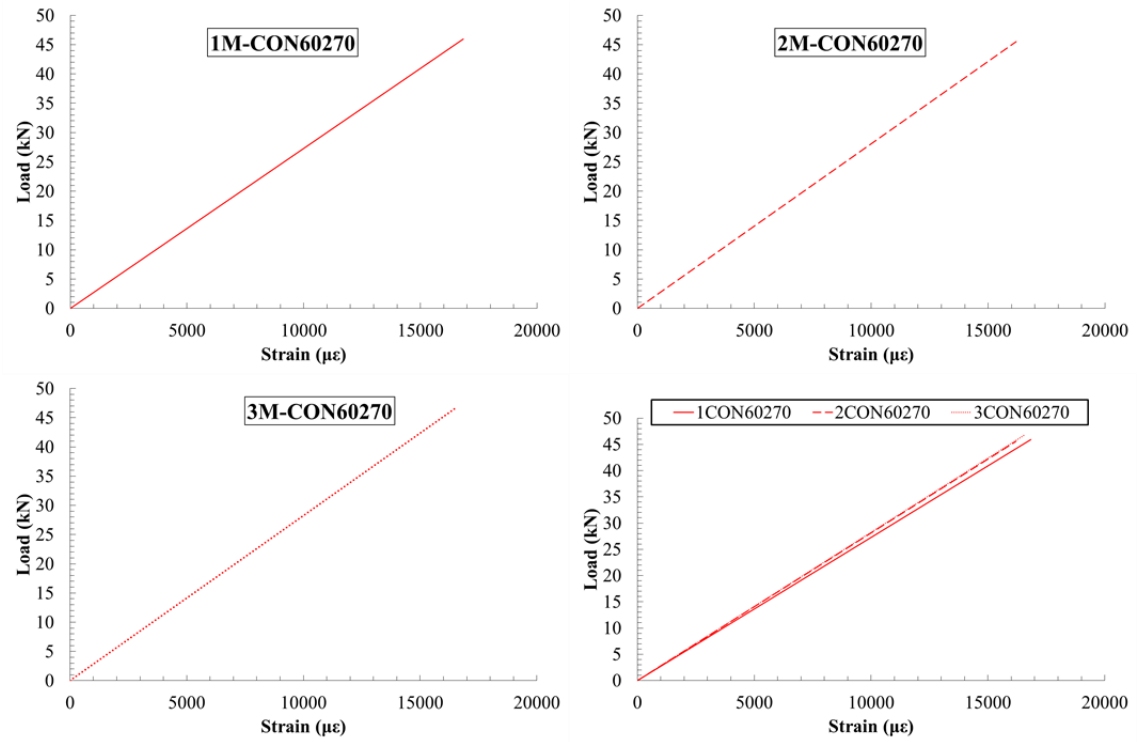

Figure.I.19 Load-strain of concrete specimens (M-CON-60°C-270d)

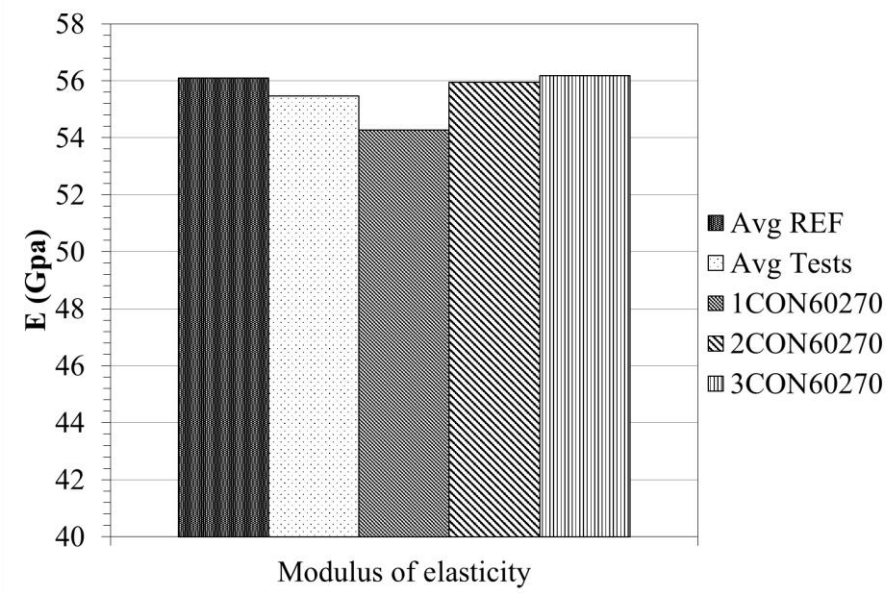

Figure.I.20: Modulus of elasticity for concrete specimens (M-CON-60°C-270d)

Table I.10: A summary of tensile test results of concrete specimen (M-CON-60°C-270d)

Specimens	P_{max} (kN)	E (GPa)	σ_{max} (MPa)	ε_{max}	note
1CON60270	45.9	54.2	914	0.017	
2CON60270	45.5	55.9	906	0.016	
3CON60270	46.8	56.1	932	0.017	
average	46.1	55.4	9170	0.017	
std	0.6	1.0	0.013	0.0003	
%STD	1.4	1.8	1.4	1.9	
min	45.5	54.2	906	0.016	
max	46.8	56.1	932	0.017	

(M-CON-20°C-42d-S3)

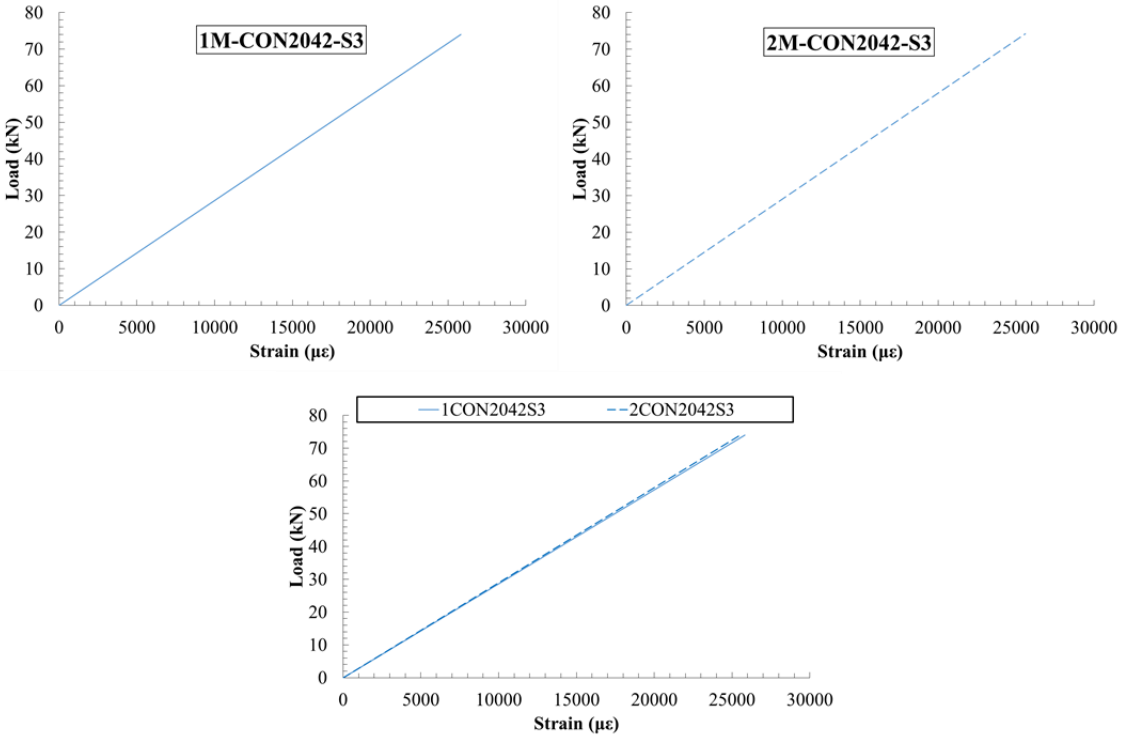

Figure.I.21 Load-strain of concrete specimens (M-CON-20°C-42d-S3)

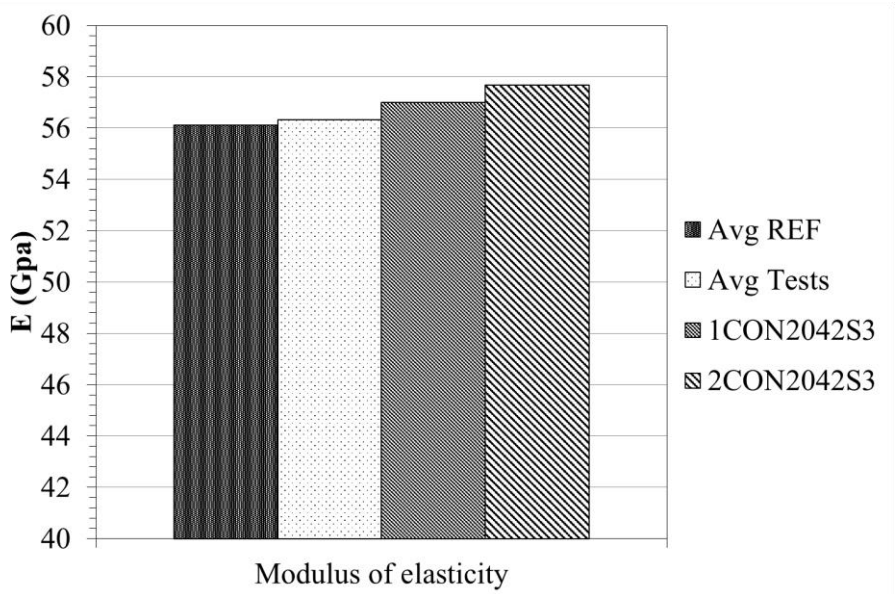

Figure.I.22: Modulus of elasticity for concrete specimens (M-CON-20°C-42d-S3)

Table I.11: A summary of tensile test results of concrete specimen (M-CON-20°C-42d)

Specimens	P_{max} (kN)	E (GPa)	σ_{max} (MPa)	ε_{max}	note
1CON2042S3	74.0	57.0	1471	0.026	
2CON2042S3	74.22	57.6	1475	0.025	
3CON2042S3					
average	74.1	57.3	1473	0.025	
std	0.1		3.0		
%STD	0.2		0.2		
min	74.0	57	1471	0.025	
max	74.2	57.6	1475	0.026	

(M-CON-40°C-42d-S3)

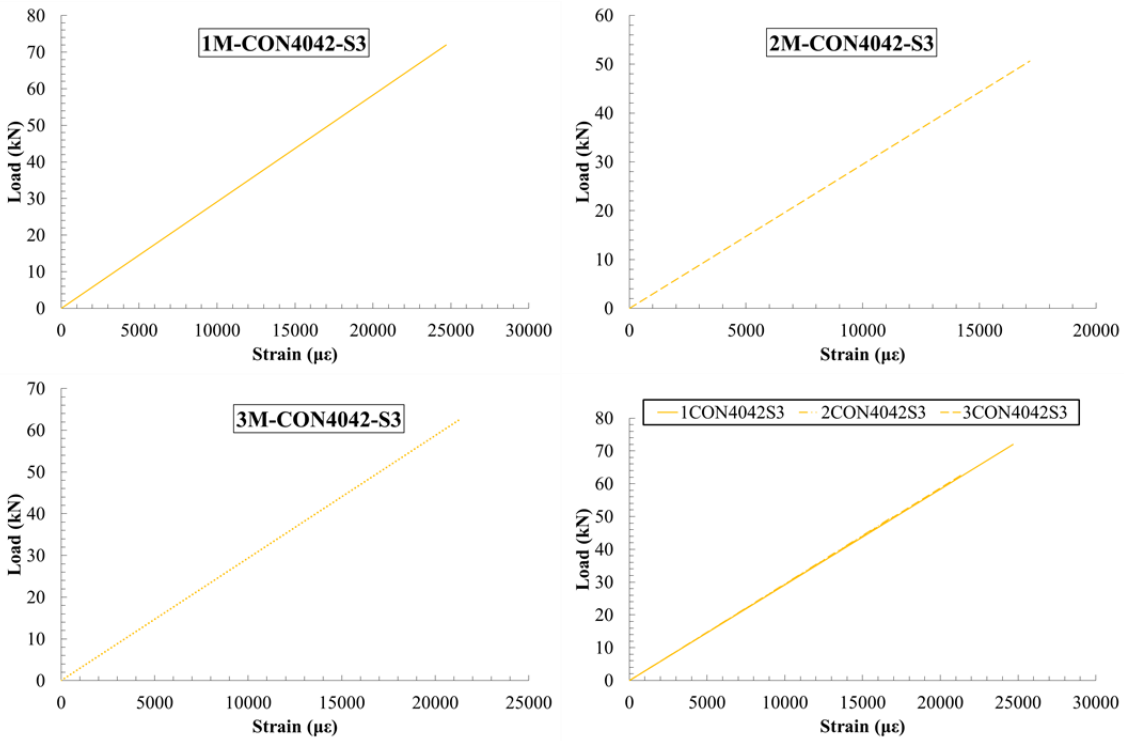

Figure.I.23 Load-strain of concrete specimens (M-CON-40°C-42d)

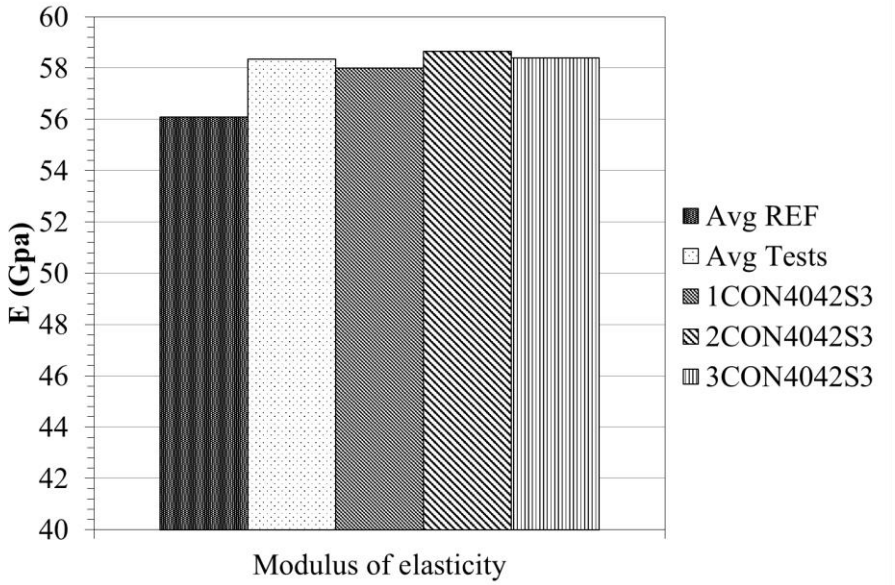

Figure.I.24: Modulus of elasticity for concrete specimens (M-CON-40°C-42d-S3)

Table I.12: A summary of tensile test results of concrete specimen (M-CON-40°C-42d-S3)

Specimens	P_{max} (kN)	E (GPa)	σ_{max} (MPa)	ε_{max}	note
1CON4042S3	72.0	58.0	1431	0.019	
2CON4042S3	50.6	58.6	1006	0.017	
3CON4042S3	62.6	58.3	1246	0.021	
average	67.3	58.3	1228	0.019	
std	10.7	0.3	213	0.002	
%STD	15.9	0.5	17	10.94	
min	50.6	58.0	1006	0.017	
max	72.0	58.6	1431	0.021	

(M-CON-60°C-42d-S3)

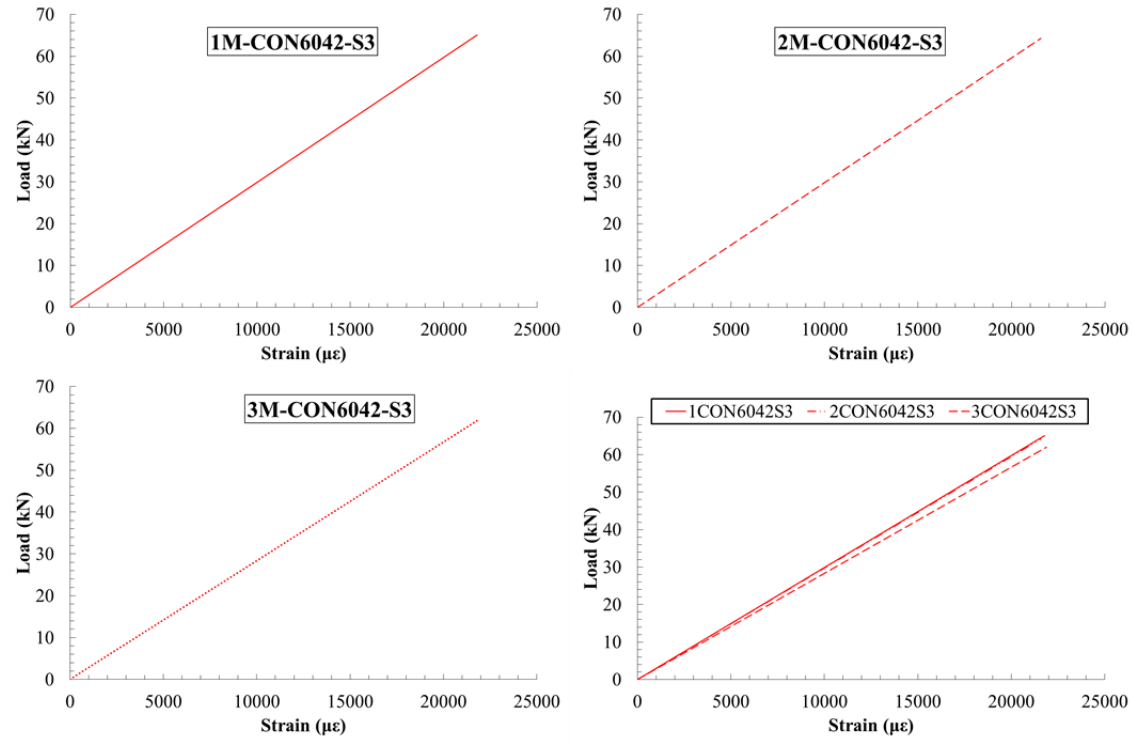

Figure.I.25 Load-strain of concrete specimens (M-CON-60°C-42d-S3)

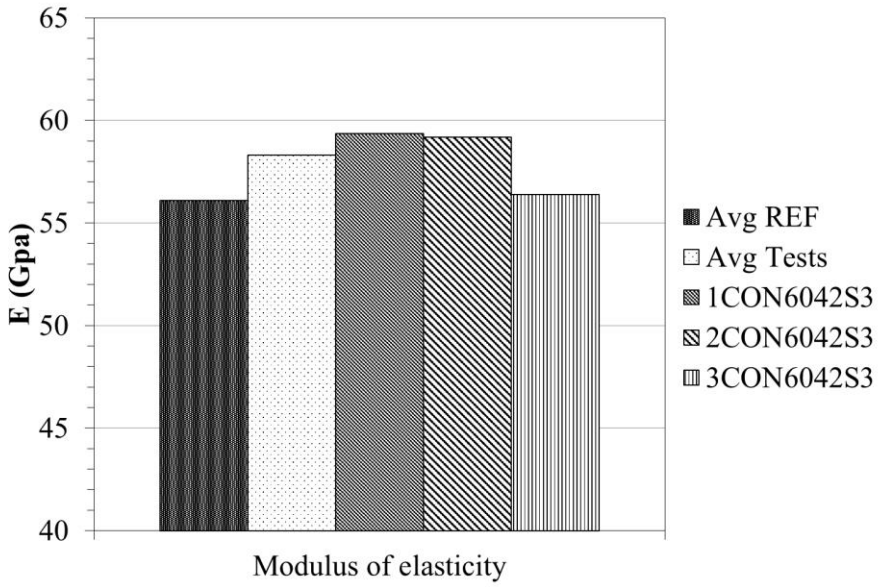

Figure.I.26: Modulus of elasticity for concrete specimens (M-CON-40°C-42d-S3)

Table I.13: A summary of tensile test results of concrete specimen (M-CON-60°C-42d-S3)

Specimens	P_{max} (kN)	E (GPa)	σ_{max} (MPa)	ε_{max}	note
1CON6042S3	65.0	59.3	1293	.021	
2CON6042S3	64.2	59.1	1276	.021	
3CON6042S3	62.0	56.3	1233	.021	
average	63.7	58.3	1267	.021	
std	1.5	1.6	31	0.0001	
%STD	2.4	2.8	2.4	0.70	
min	62.0	56.3	1233	.021	
max	65.0	59.3	1293	.021	

(M-CON-60°C-42d-S5)

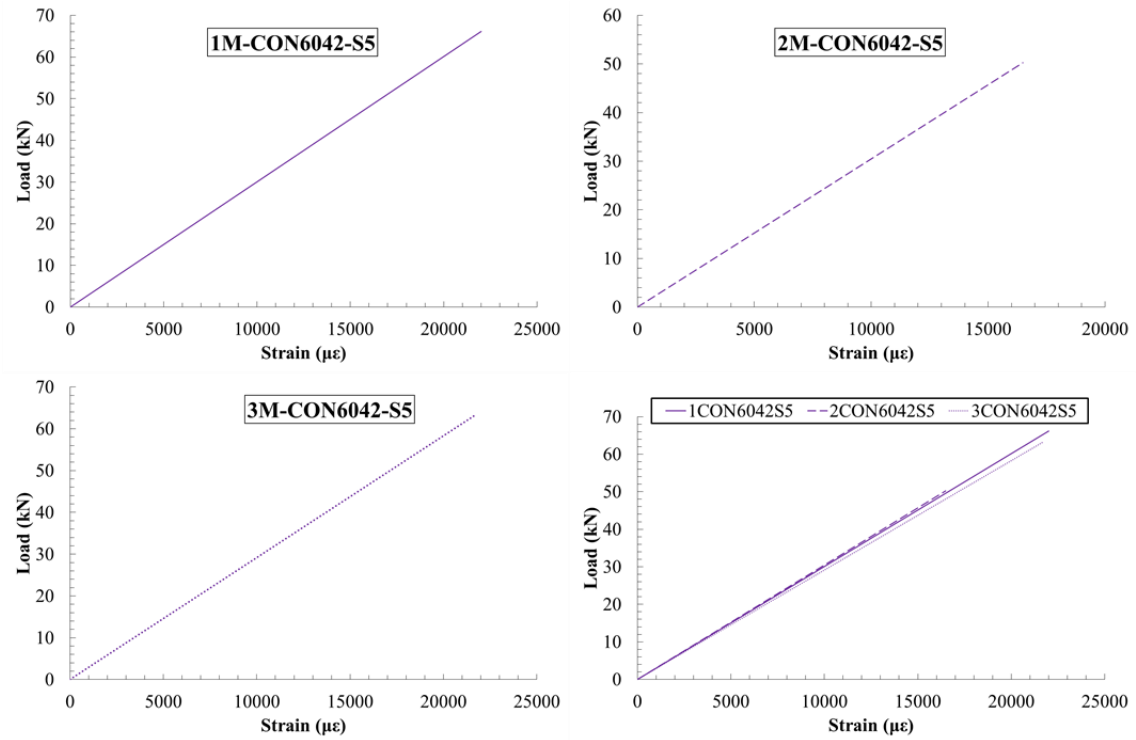

Figure.I.27 Load-strain of concrete specimens (M-CON-60°C-42d-S5)

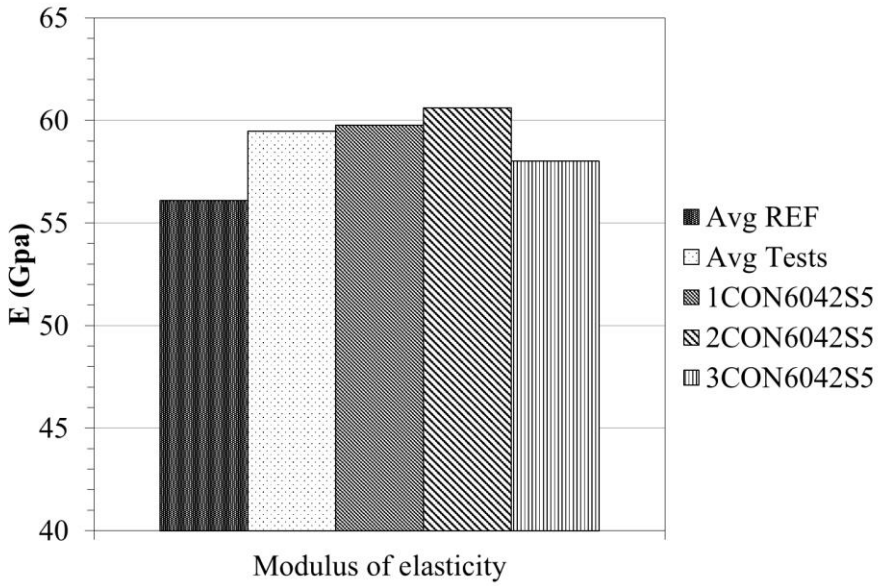

Figure.I.28: Modulus of elasticity for concrete specimens (M-CON-40°C-42d-S5)

Table I.14: A summary of tensile test results of concrete specimen (M-CON-60°C-42d-S5)

Specimens	P_{max} (kN)	E (GPa)	σ_{max} (MPa)	ε_{max}	note
1CON6042S5	66.1	59.7	1314	0.022	
2CON6042S5	50.2	60.6	999	0.016	
3CON6042S5	63.2	58.0	1257	0.021	
average	59.8	59.4	1190	.020	
std	8.4	1.3	167	0.003	
%STD	14.1	2.2	14	15.41	
min	50.2	58.0	999	0.016	
max	66.1	60.6	1314	0.022	

(M-CON-20°C-90d-S3)

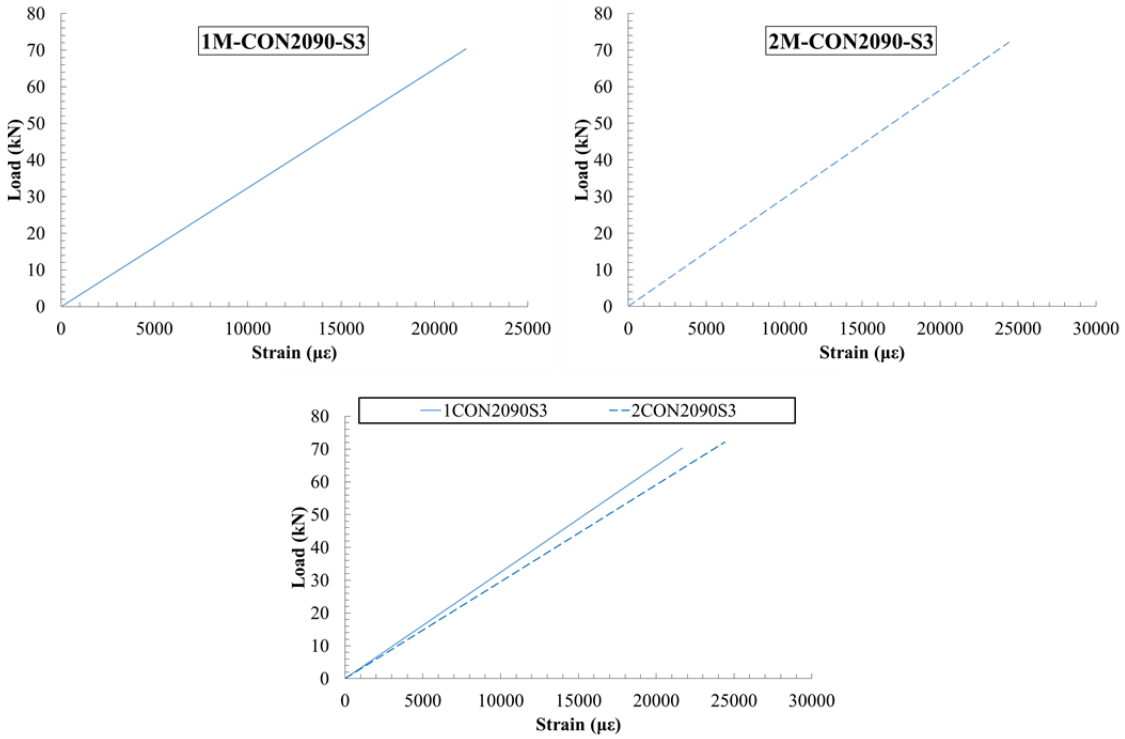

Figure.I.29 Load-strain of concrete specimens (M-CON-20°C-90d-S3)

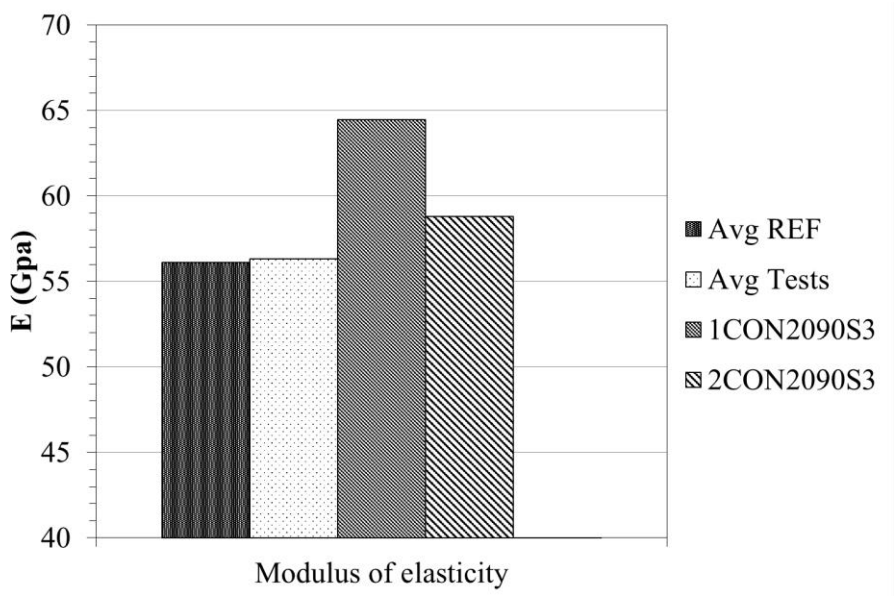

Figure.I.30: Modulus of elasticity for concrete specimens (M-CON-20°C-90d-S3)

Table I.15: A summary of tensile test results of concrete specimen (M-CON-20°C-90d-S3)

Specimens	P_{max} (kN)	E (GPa)	σ_{max} (MPa)	ε_{max}	note
1CON2090S3	70.2	64.4	1398	0.022	
2CON2090S3	72.1	58.8	1436	0.024	
3CON2090S3					
average	71.2	61.6	417	0.023	
std	1.3	4.0	0.02	0.002	
%STD	1.8	6.4	1.8	8.38	
min	70.2	58.8	1398	0.022	
max	72.1	64.4	1436	0.024	

(M-CON-40°C-90d-S3)

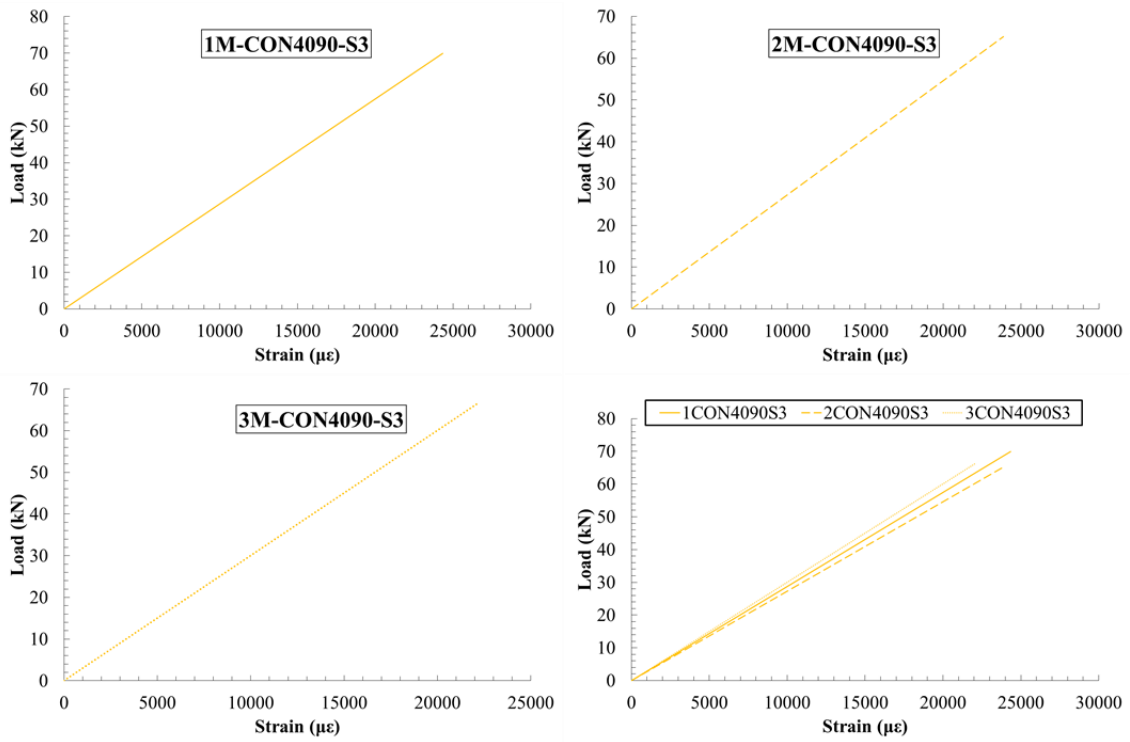

Figure.I.31 Load-strain of concrete specimens (M-CON-40°C-90d-S3)

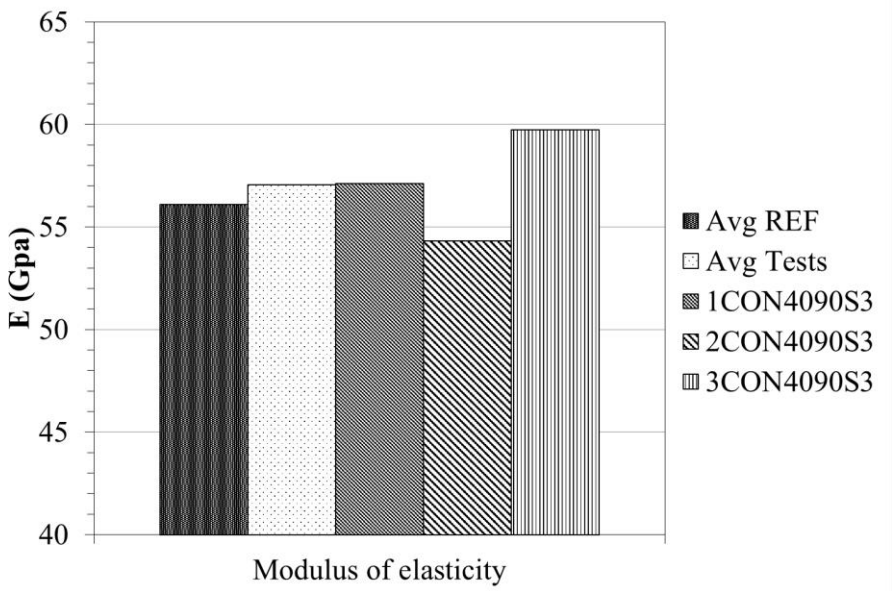

Figure.I.32: Modulus of elasticity for concrete specimens (M-CON-40°C-90d-S3)

Table I.16: A summary of tensile test results of concrete specimen (M-CON-40°C-90d-S3)

Specimens	P_{max} (kN)	E (GPa)	σ_{max} (MPa)	ε_{max}	note
1CON4090S3	69.8	57.1	1390	0.024	
2CON4090S3	65.1	54.3	1297	0.024	
3CON4090S3	66.4	59.7	1321	0.022	
average	67.149	57.0	1336	0.023	
std	2.439	2.6	0.04	0.001	
%STD	3.633	4.7	3.6	4.988	
min	65.169	54.3	1297	0.022	
max	69.874	59.7	1390	0.024	

(M-CON-60°C-90d-S3)

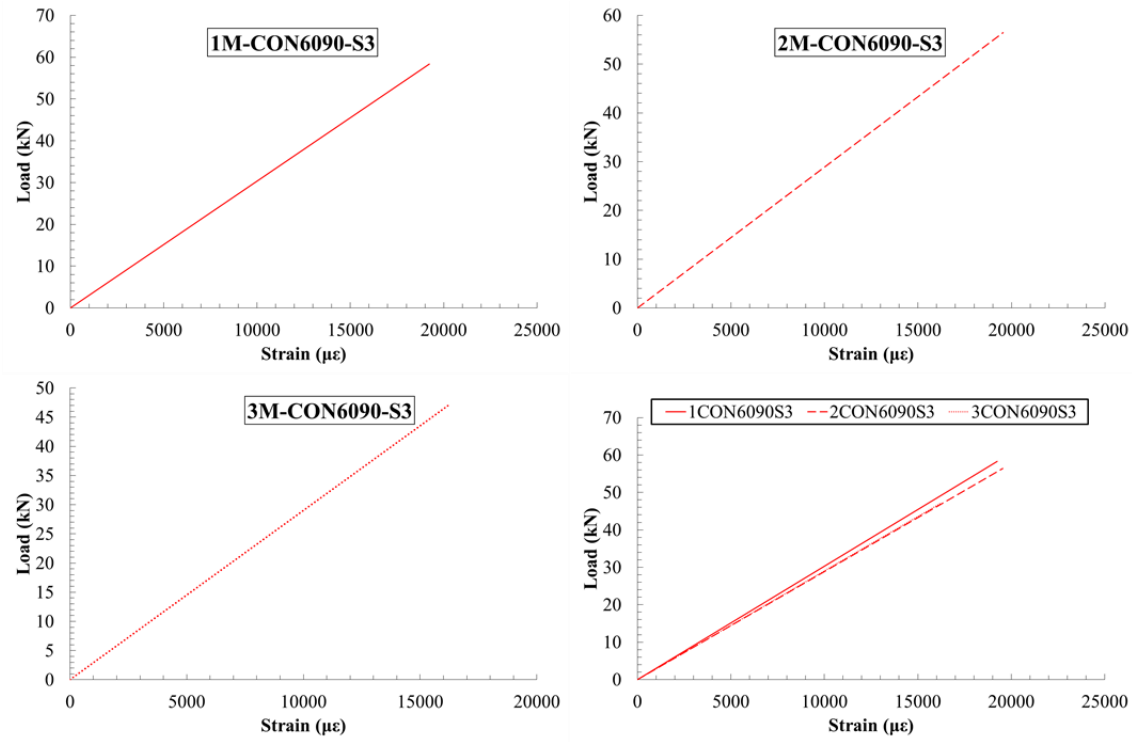

Figure.I.33 Load-strain of concrete specimens (M-CON-60°C-90d-S3)

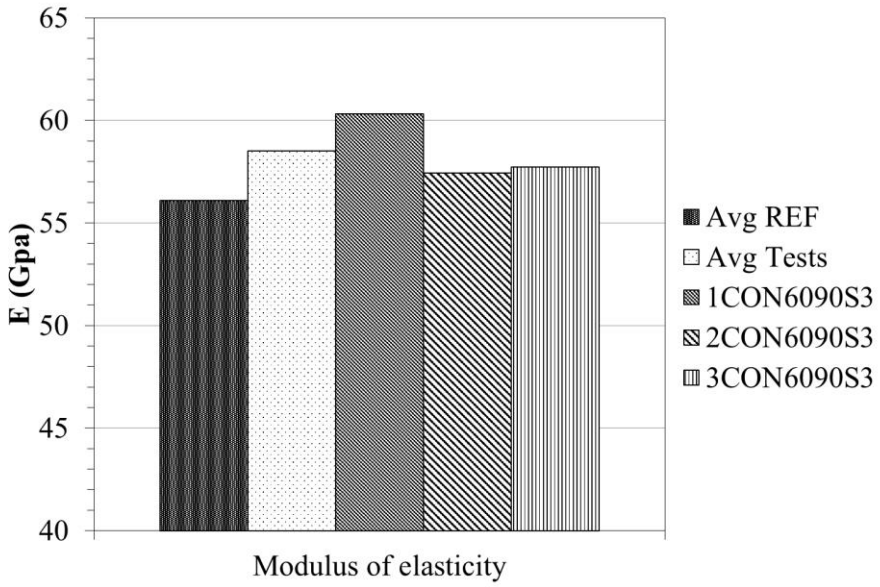

Figure.I.34: Modulus of elasticity for concrete specimens (M-CON-60°C-90d-S3)

Table I.17: A summary of tensile test results of concrete specimen (M-CON-60°C-90d-S3)

Specimens	P_{max} (kN)	E (GPa)	σ_{max} (MPa)	ε_{max}	note
1CON6090S3	58.3	60.3	1161	0.019	
2CON6090S3	56.4	57.4	1123	0.020	
3CON6090S3	47.1	57.7	937	0.016	
average	53.9	58.4	1073	0.018	
std	6.0	1.5	0.1	0.002	
%STD	11.1	2.7	11.1	9.996	
min	47.1	57.4	937	0.016	
max	58.3	60.3	1161	0.020	

(M-CON-60°C-90d-S5)

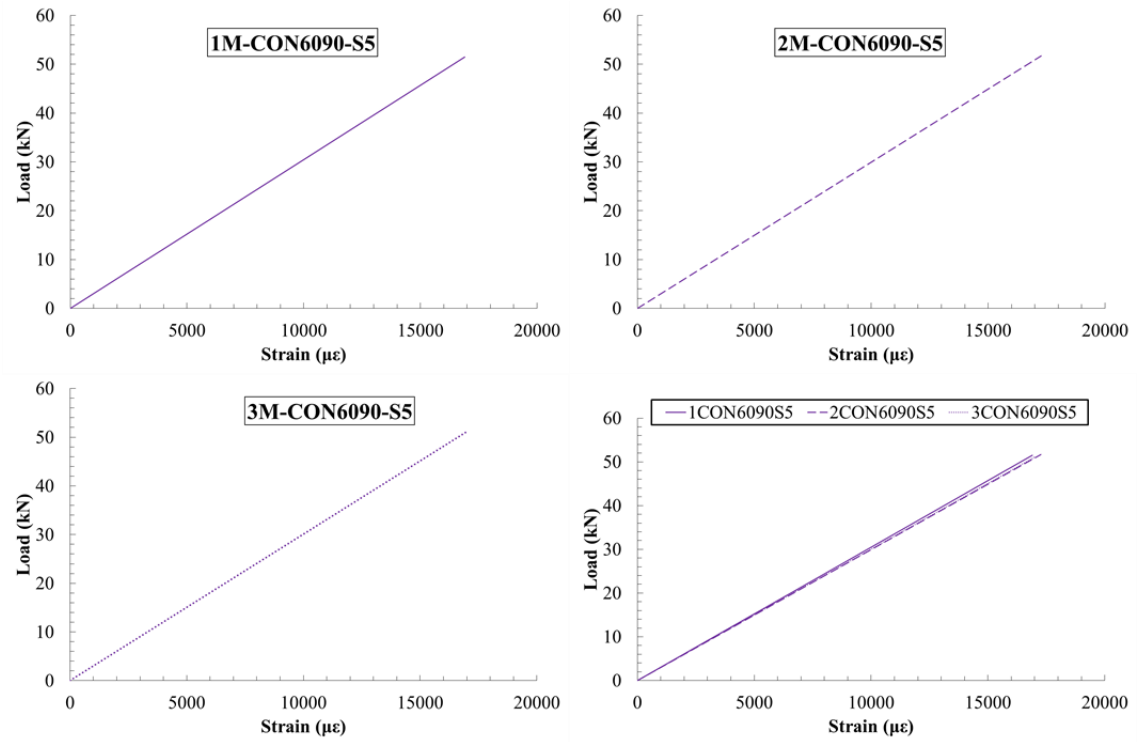

Figure.I.35 Load-strain of concrete specimens (M-CON-60°C-90d-S5)

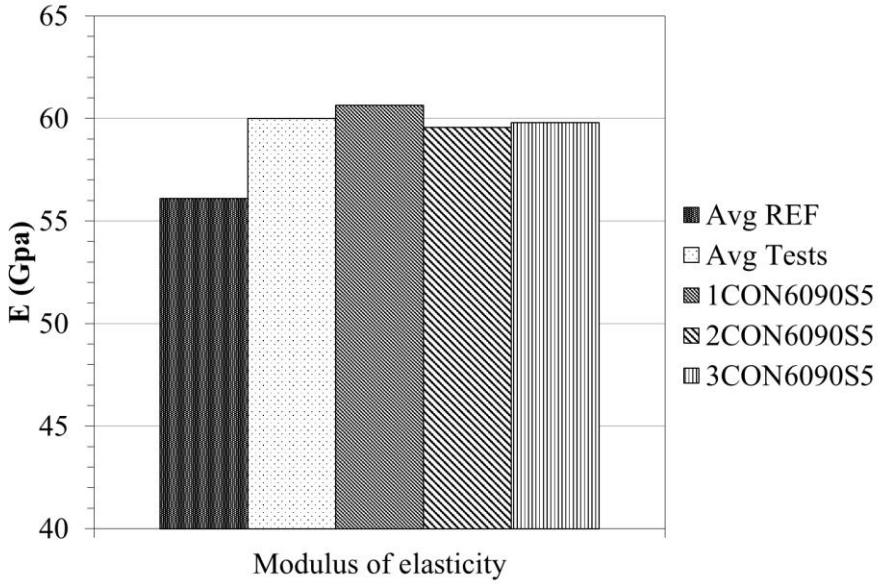

Figure.I.36: Modulus of elasticity for concrete specimens (M-CON-60°C-90d-S5)

Table I.18: A summary of tensile test results of concrete specimen (M-CON-60°C-90d-S5)

Specimens	P_{max} (kN)	E (GPa)	σ_{max} (MPa)	ε_{max}	note
1CON6090S5	51.5	60.6	1025	0.017	
2CON6090S5	51.7	59.5	1029	0.017	
3CON6090S5	51.0	59.7	1016	0.017	
average	51.4	59.9	1023	0.017	
std	0.3	0.5	0.01	0.001	
%STD	0.6	0.9	0.6	1.137	
min	51.0	59.5	1016	0.017	
max	51.7	60.6	1029	0.017	

(M-CON-20°C-270d-S3)

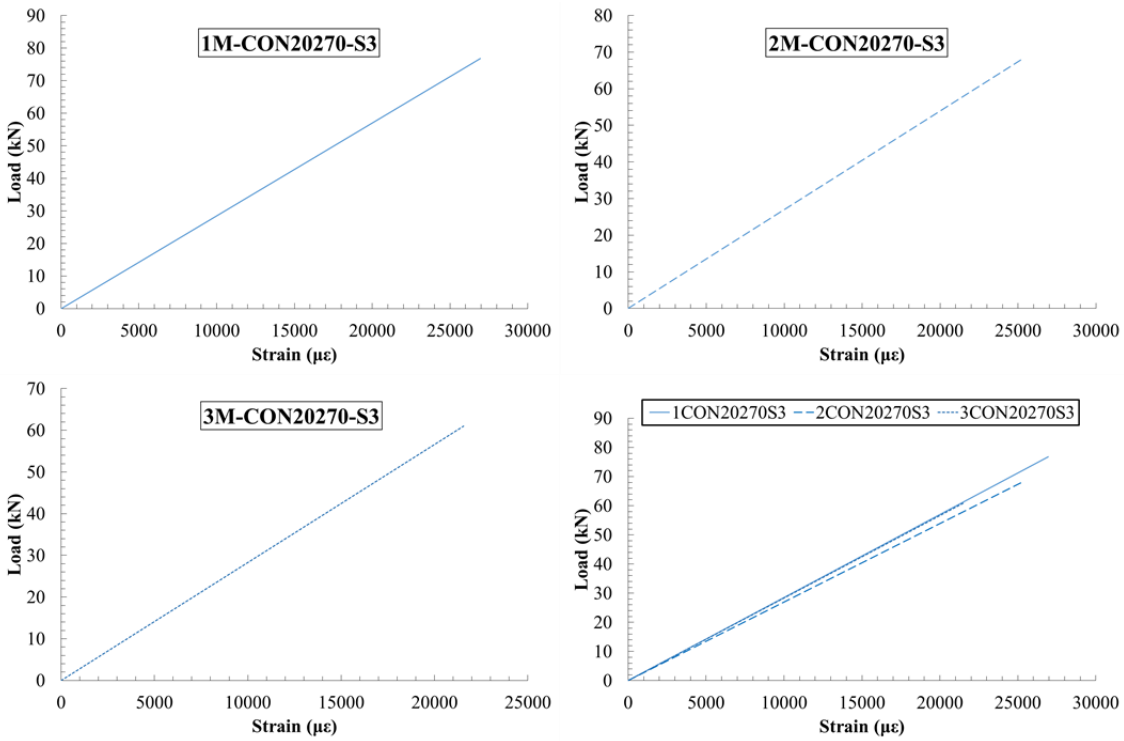

Figure.I.37 Load-strain of concrete specimens (M-CON-20°C-270d-S3)

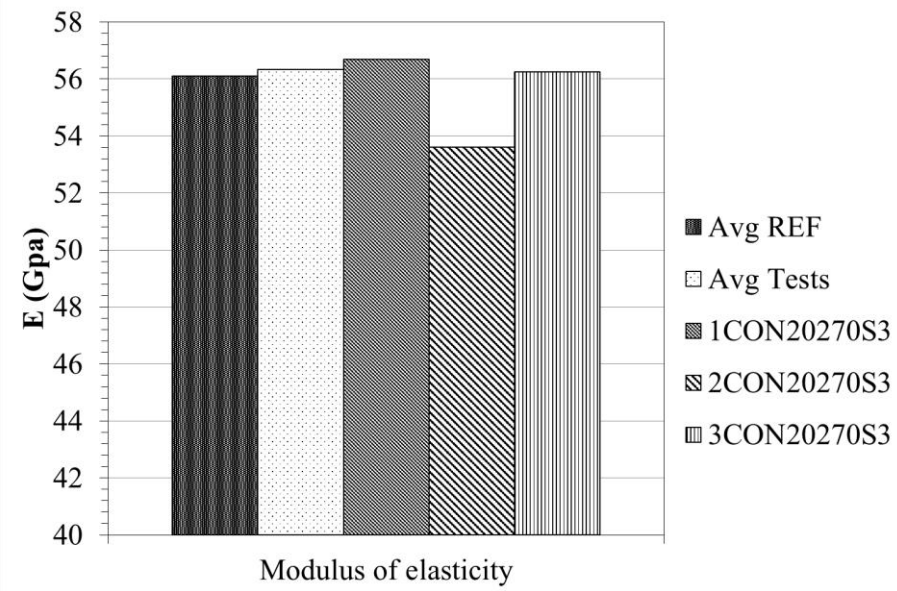

Figure.I.138: Modulus of elasticity for concrete specimens (M-CON-20°C-270d-S3)

Table I.19: A summary of tensile test results of concrete specimen (M-CON-20°C-270S3)

Specimens	P_{max} (kN)	E (GPa)	σ_{max} (MPa)	ε_{max}	note
1CON20270-S3	76.8	56.6	1528	0.026	
2CON20270-S3	68.1	53.5	1355	0.025	
3CON20270-S3	60.9	56.2	1213	0.021	
average	68.6	55.5	1365	0.024	
std	7.9	1.6	158	.0002	
%STD	11.5	3.0	11.5	11.21	
min	60.9	53.5	1213	0.021	
max	76.8	56.6	1528	0.026	

(M-CON-40°C-270d-S3)

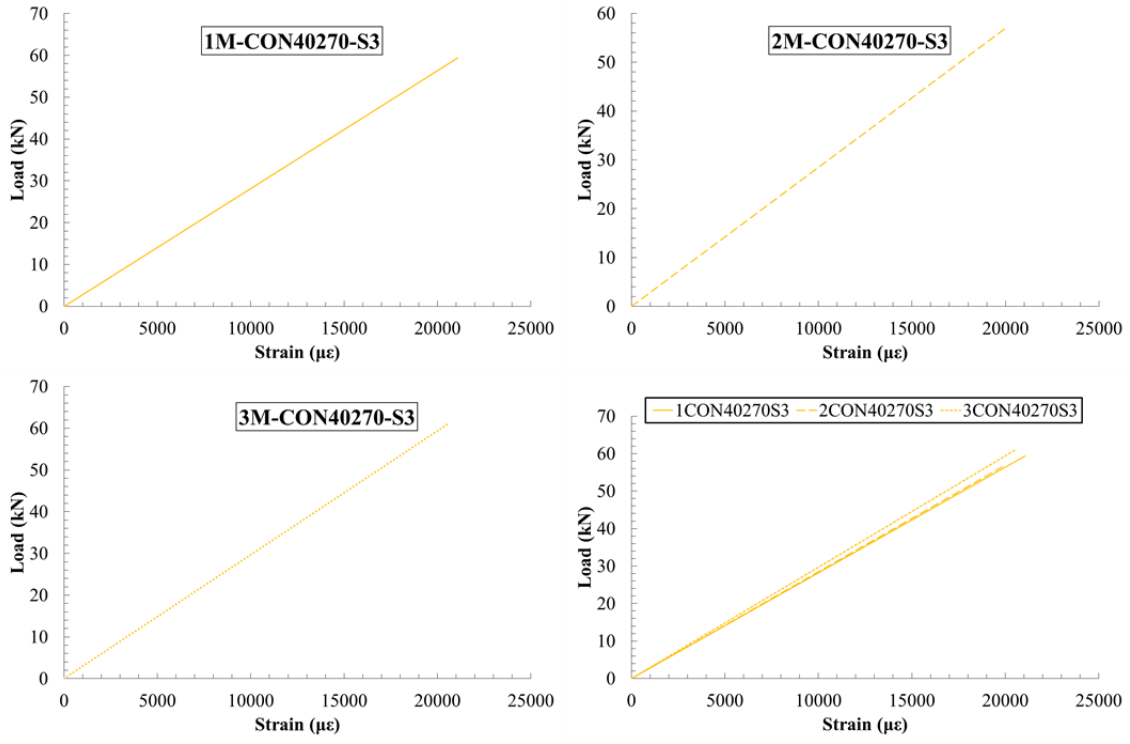

Figure.I.39 Load-strain of concrete specimens (M-CON-40°C-270d-S3)

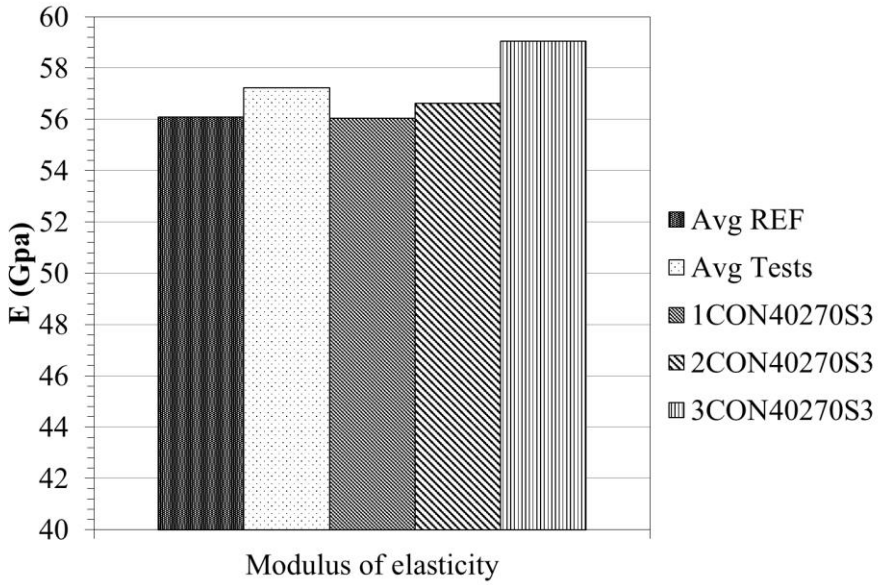

Figure.I.40: Modulus of elasticity for concrete specimens (M-CON-40°C-270d-S3)

Table I.20: A summary of tensile test results of concrete specimen (M-CON-40°C-270d-S3)

Specimens	P_{max} (kN)	E (GPa)	σ_{max} (MPa)	ε_{max}	note
1CON40270S3	59.3	56.0	1181	0.021	
2CON40270S3	56.9	56.6	1132	0.020	
3CON40270S3	61.1	59.0	1217	0.021	
average	59.1	57.2	1177	0.021	
std	2.1	1.5	42.5	0.001	
%STD	3.6	2.7	3.6	2.636	
min	56.9	56.0	1132	0.020	
max	61.1	59.0	1217	0.021	

(M-CON-60°C-270d-S3)

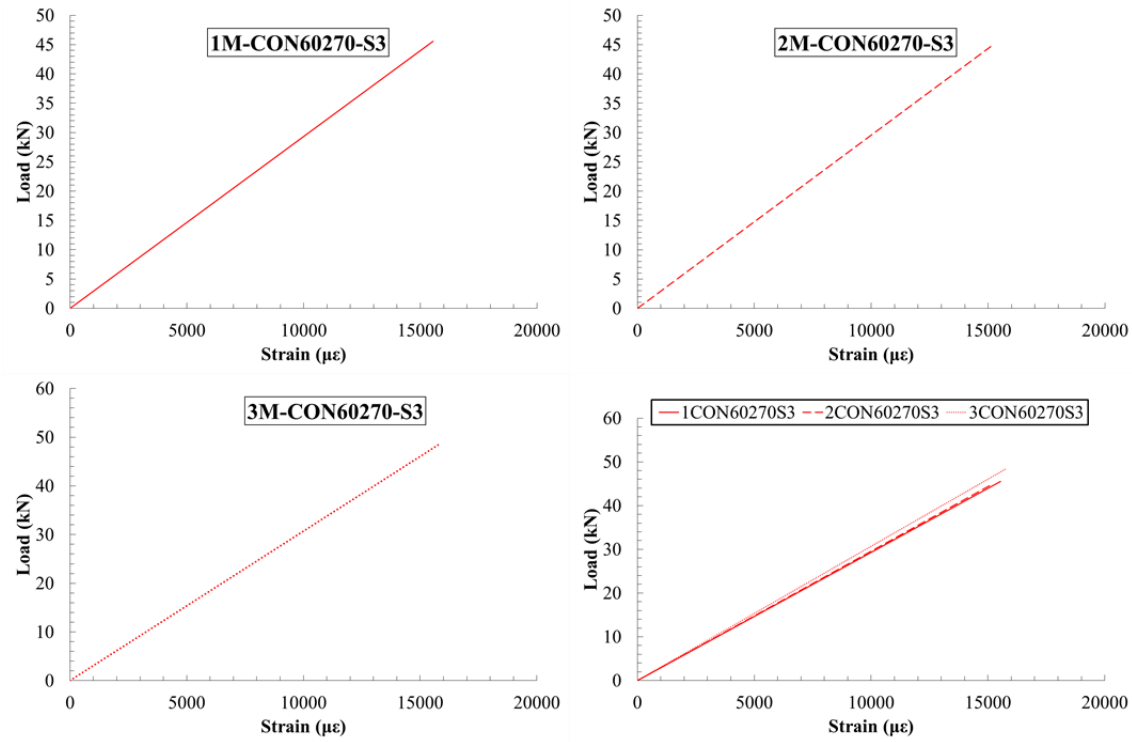

Figure.I.41 Load-strain of concrete specimens (M-CON-60°C-270d-S3)

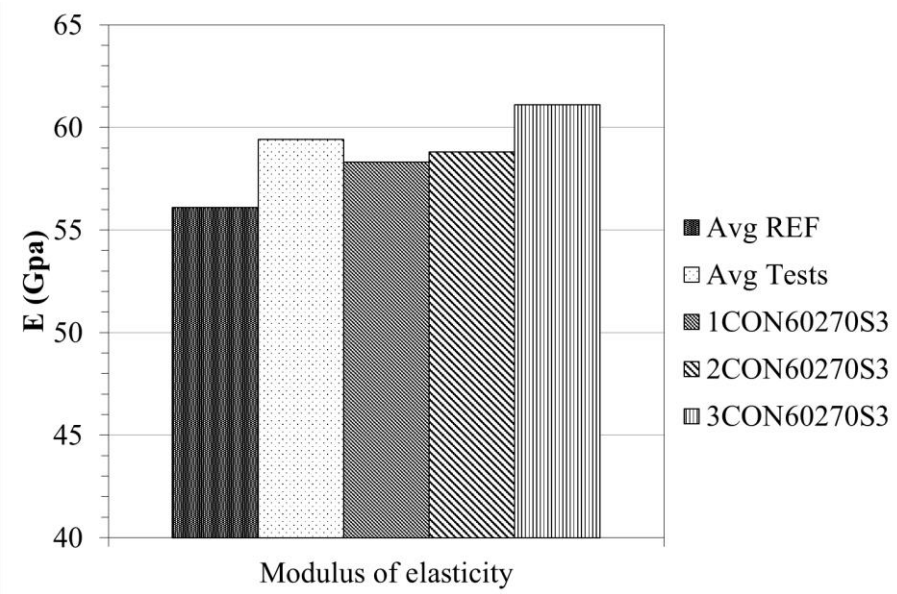

Figure.I.42: Modulus of elasticity for concrete specimens (M-CON-60°C-270d-S3)

Table I.21: A summary of tensile test results of concrete specimen (M-CON-60°C-270S3)

Specimens	P_{max} (kN)	E (GPa)	σ_{max} (MPa)	ε_{max}	note
1CON60270S3	45.5	58.3	906	0.016	
2CON60270S3	44.6	58.8	889	0.015	
3CON60270S3	48.4	61.1	964	0.016	
average	46.2	59.4	919	0.015	
std	1.9	1.4	39.2	0.000	
%STD	4.2	2.5	4.2	2.1	
min	44.6	58.3	889	0.015	
max	48.4	61.1	964	0.016	

(M-CON-60°C-270d-S5)

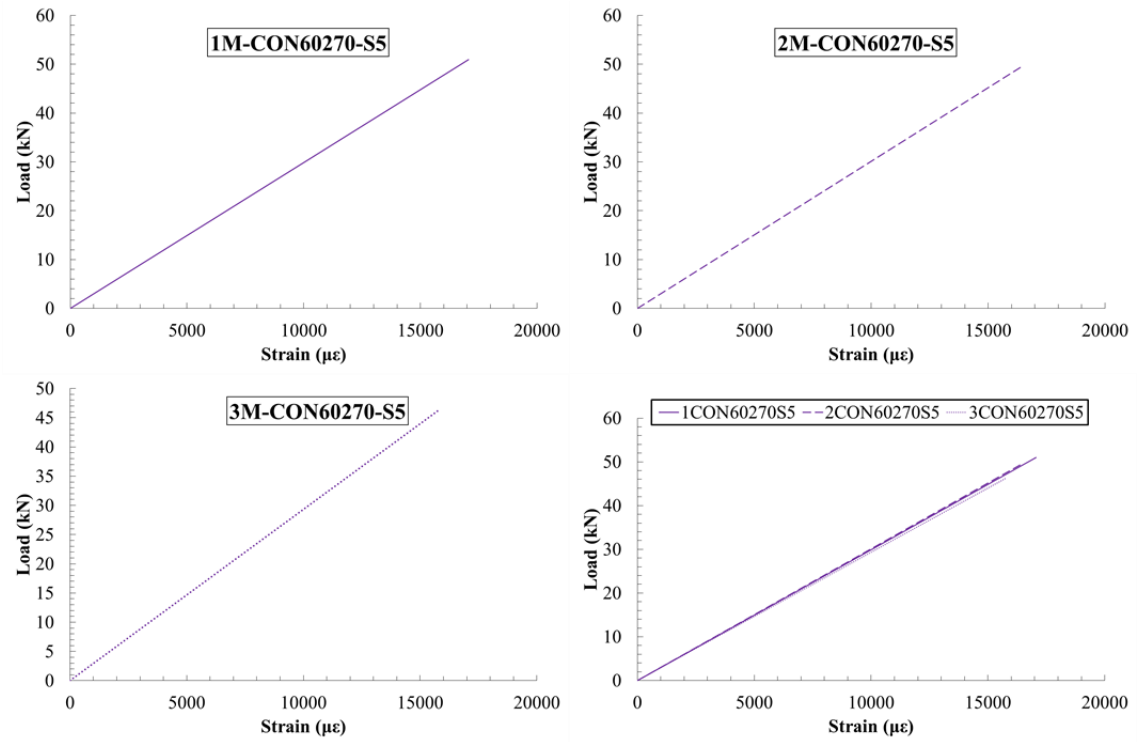

Figure.I.43 Load-strain of concrete specimens (M-CON-60°C-270d-S5)

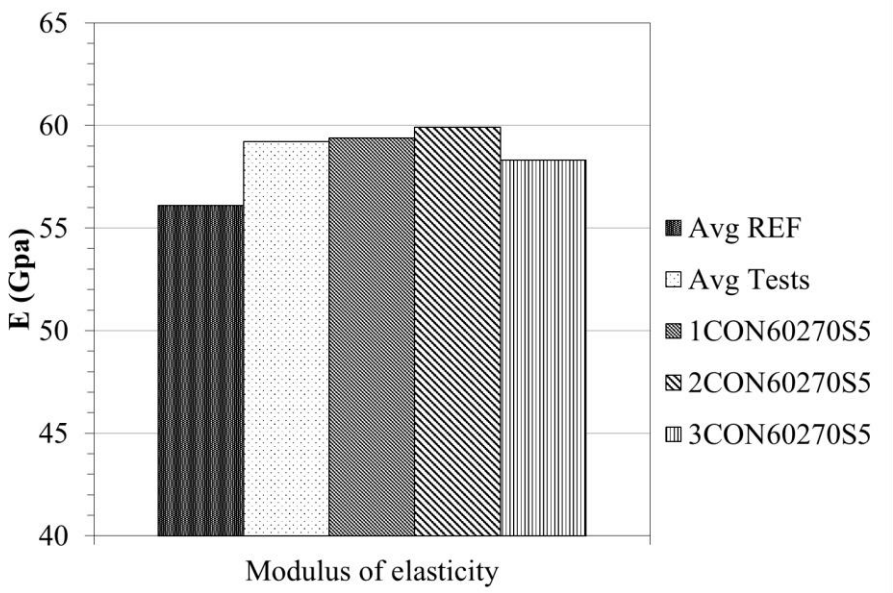

Figure.I.44: Modulus of elasticity for concrete specimens (M-CON-60°C-270d-S5)

Table I.22: A summary of tensile test results of concrete specimen (M-CON-60°C-270S5)

Specimens	P_{max} (kN)	E (GPa)	σ_{max} (MPa)	ε_{max}	note
1CON60270S5	50.9	59.4	1013	0.016	
2CON60270S5	49.3	59.9	981	0.015	
3CON60270S5	46.2	58.3	920	0.016	
average	48.8	59.2	971	0.016	
std	2.3	0.8	47.3	0.001	
%STD	4.8	1.3	4.8	3.899	
min	46.2	58.3	920.5	0.016	
max	50.9	59.9	1013.8	0.017	

(CON-Air-270d)

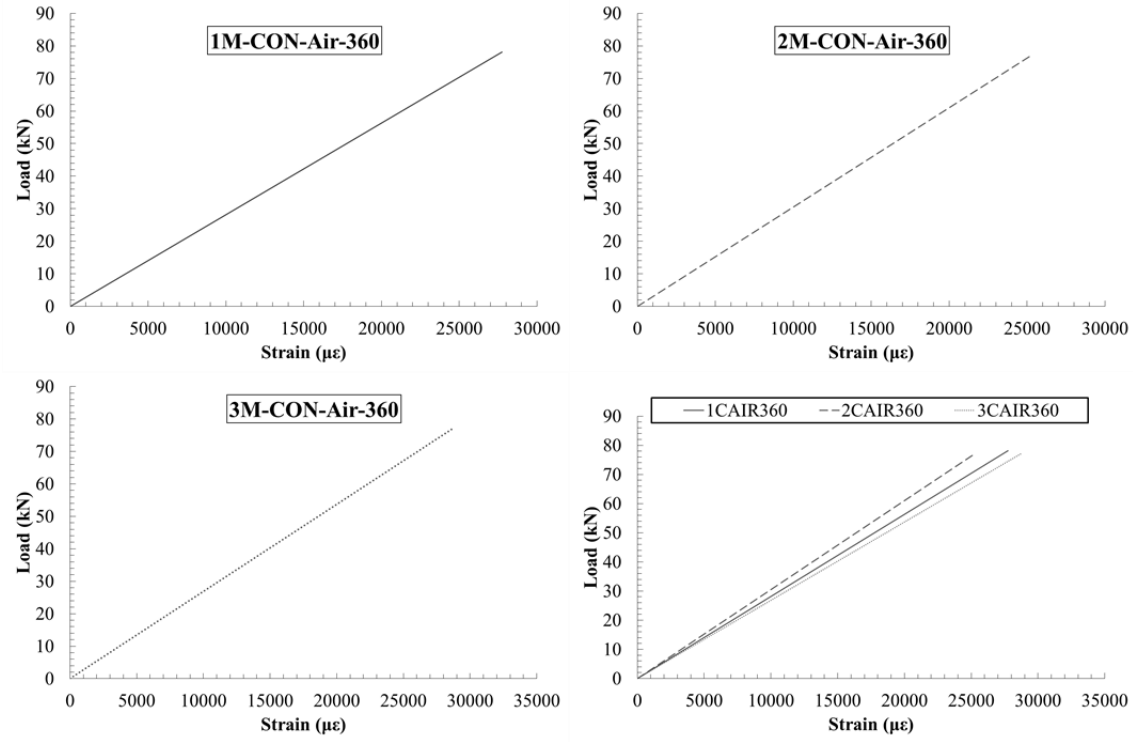

Figure.I.45 Load-strain of concrete specimens (CON-Air-360d)

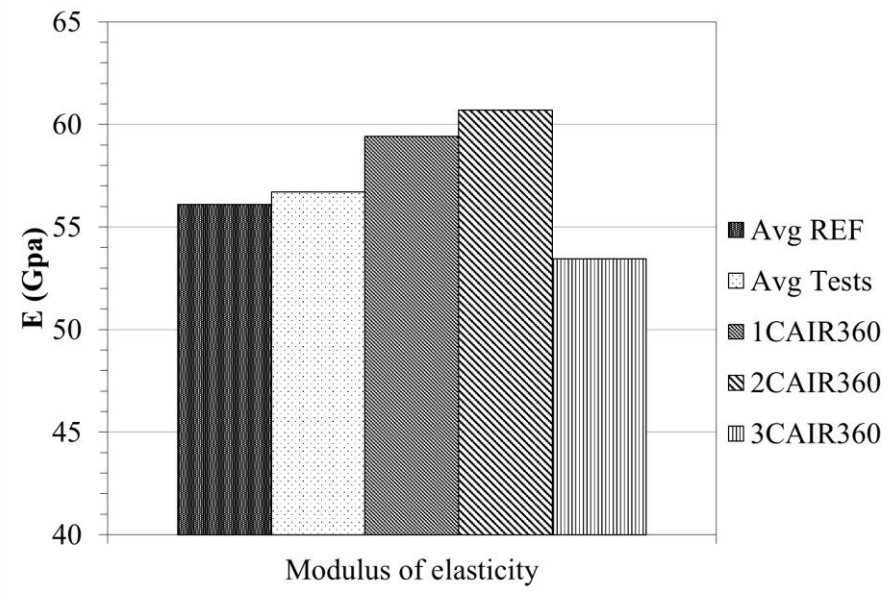

Figure.I.46: Modulus of elasticity for concrete specimens (CON-Air-3600d)

Table I.23: A summary of tensile test results of concrete specimen (CON-Air-360d)

Specimens	P_{max} (kN)	E (GPa)	σ_{max} (MPa)	ε_{max}	note
1CAIR360	78.1	55.9	1554	0.028	
2CAIR360	77.0	60.6	1532	0.025	
3CAIR360	77.1	53.4	1535	0.029	
average	77.4	56.7	1540	0.027	
std	0.6	3.6	12.1	0.002	
%STD	0.7	6.4	0.7	6.6	
min	77.0	53.4	1532	0.025	
max	78.1	60.6	1554	0.029	

(K-20°C-42d)

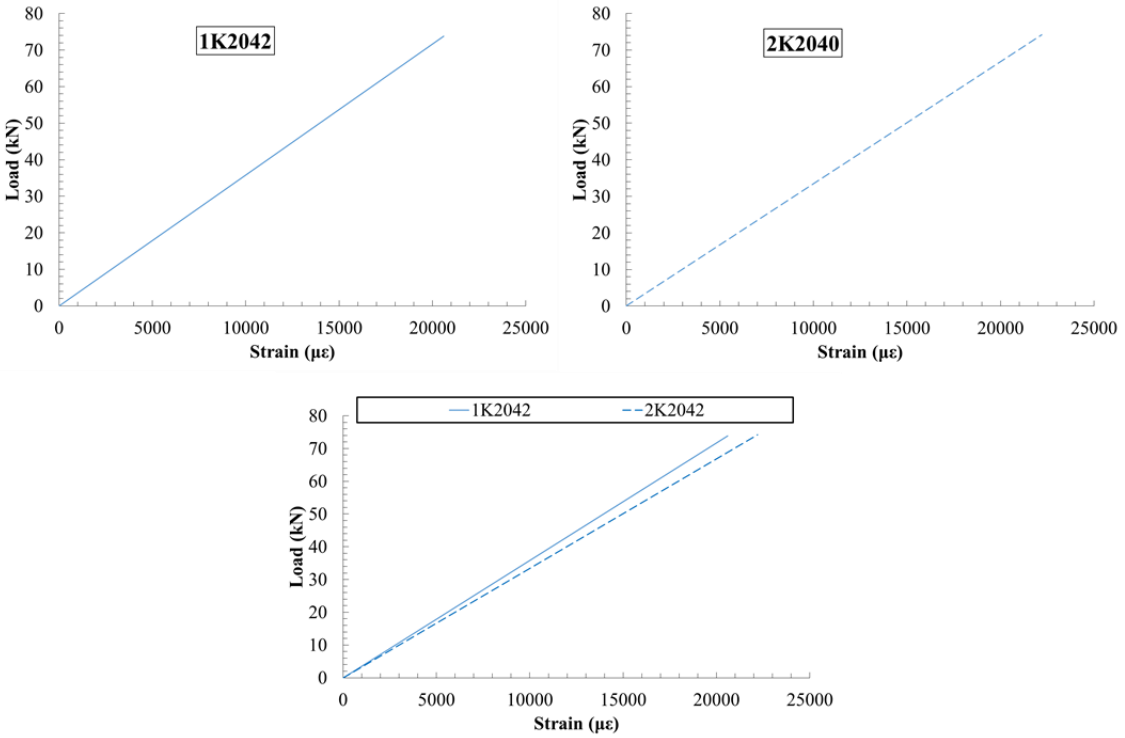

Figure.I.47 Load-strain of concrete specimens (K-20°C-42d)

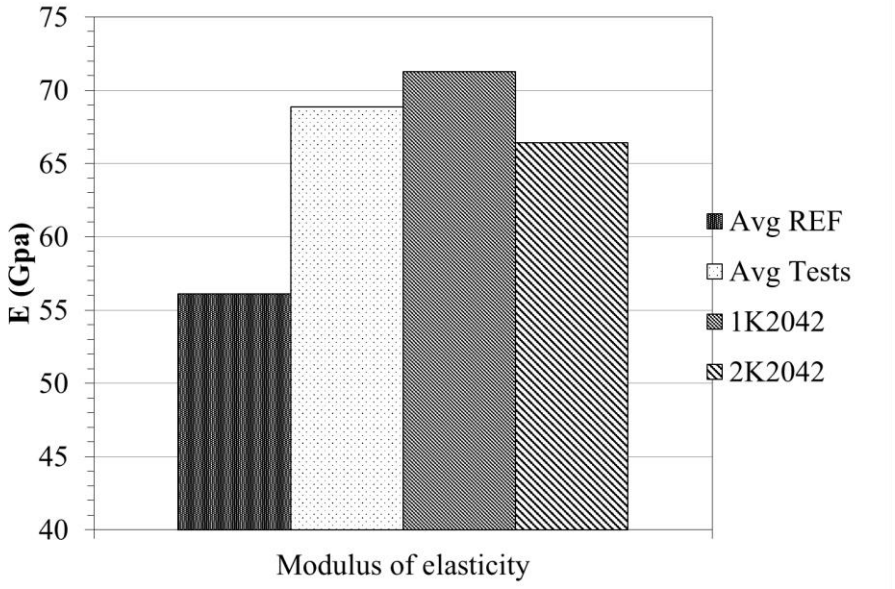

Figure.I.48: Modulus of elasticity for concrete specimens (K-20°C-42d)

Table I.24: A summary of tensile test results of concrete specimen (K-20°C-42d)

Specimens	P_{max} (kN)	E (GPa)	σ_{max} (MPa)	ε_{max}	note
1K2042	73.8	71.2	1469	0.021	
2K2042	74.1	66.4	1475	0.022	
3K2042	74.0				
average	73.9	68.8	1472	0.021	
std	0.2	0.003	0.01	0.001	
%STD	0.3	0.005	0.3	5.2	
min	73.8	66.4	1469	0.021	
max	74.1	71.2	1475	0.022	

(K-20°C-42d)

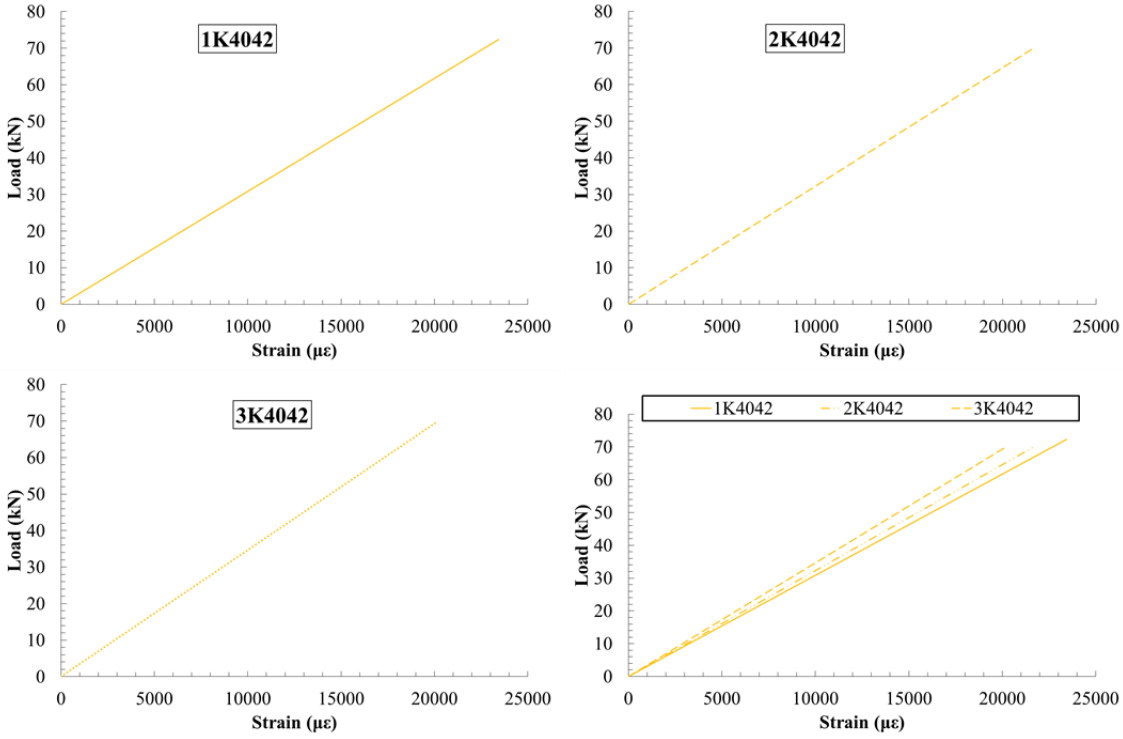

Figure.I.49 Load-strain of concrete specimens (K-20°C-42d)

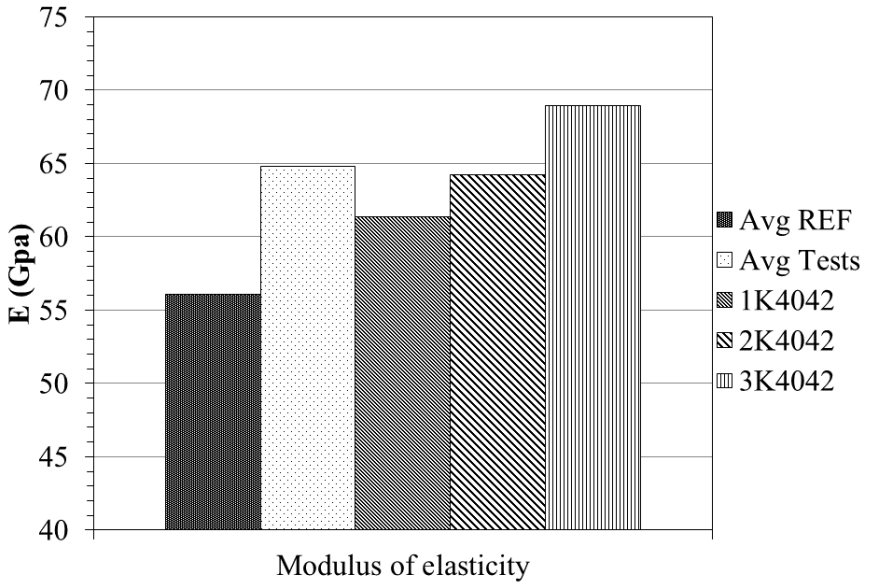

Figure.I.50: Modulus of elasticity for concrete specimens (K-20°C-42d)

Table I.25: A summary of tensile test results of concrete specimen (K-40°C-42d)

Specimens	P_{max} (kN)	E (GPa)	σ_{max} (MPa)	ε_{max}	note
1K4042	72.3	61.3	1439	0.023	
2K4042	70.1	64.2	1396	0.022	
3K4042	69.8	68.9	1389	0.020	
average	70.7	64.8	1408	0.022	
std	1.3	0.004	0.02	0.002	
%STD	1.9	0.006	1.9	7.552	
min	69.8	61.3	1389	0.020	
max	72.3	68.9	1439	0.023	

(K-60°C-42d)

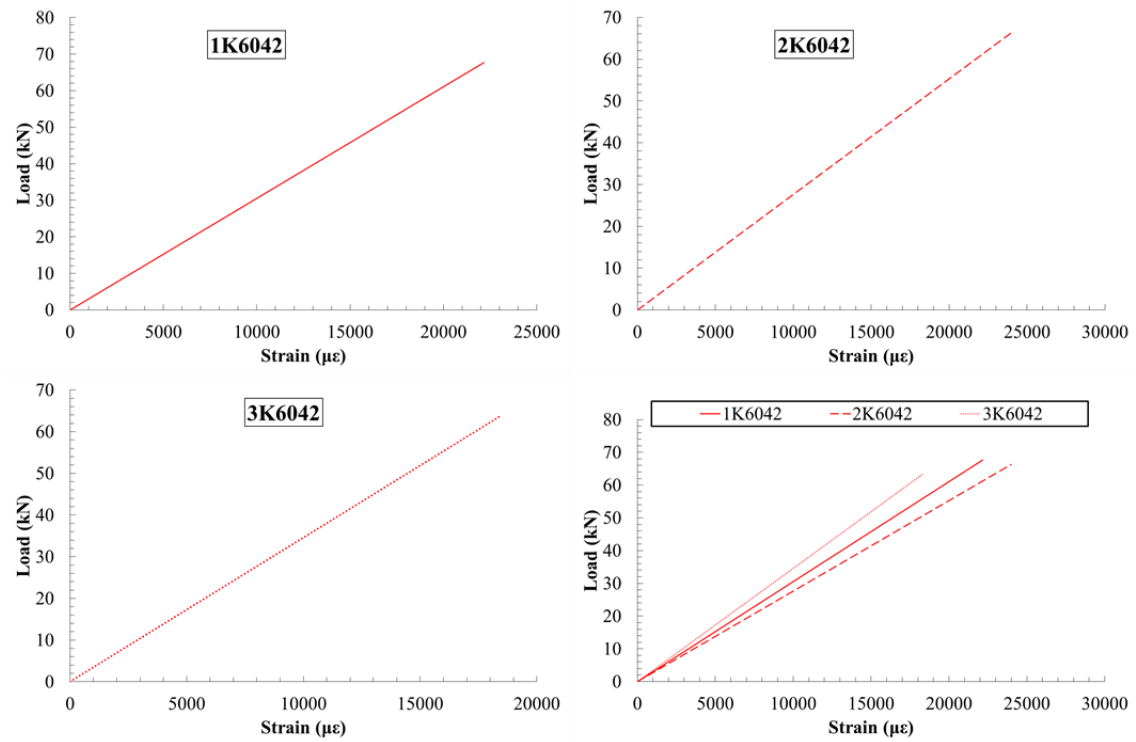

Figure.I.51 Load-strain of concrete specimens (K-60°C-42d)

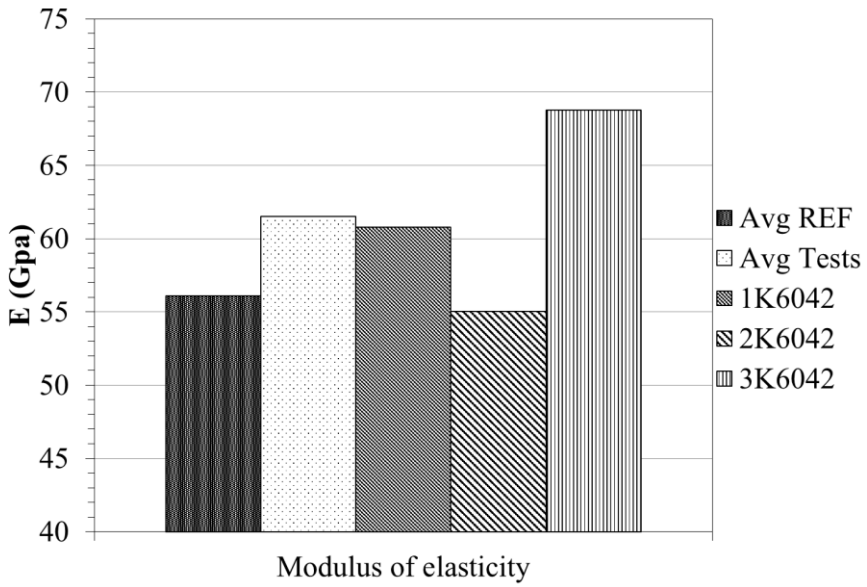

Figure.I.52: Modulus of elasticity for concrete specimens (K-60°C-42d)

Table I.26: A summary of tensile test results of concrete specimen (K-60°C-42d)

Specimens	P_{max} (kN)	E (GPa)	σ_{max} (MPa)	ε_{max}	note
1K6042	67.6	60.7	1347	0.022	
2K6042	66.3	55.0	1320	0.024	
3K6042	63.5	68.7	1265	0.018	
average	65.8	61.5	1310	0.022	
std	2.0	0.007	0.04	0.003	
%STD	3.1	0.01	3.1	13.2	
min	63.5	55.0	1265	0.018	
max	67.6	68.7	1347	0.024	

(K-60°C-42d-S3)

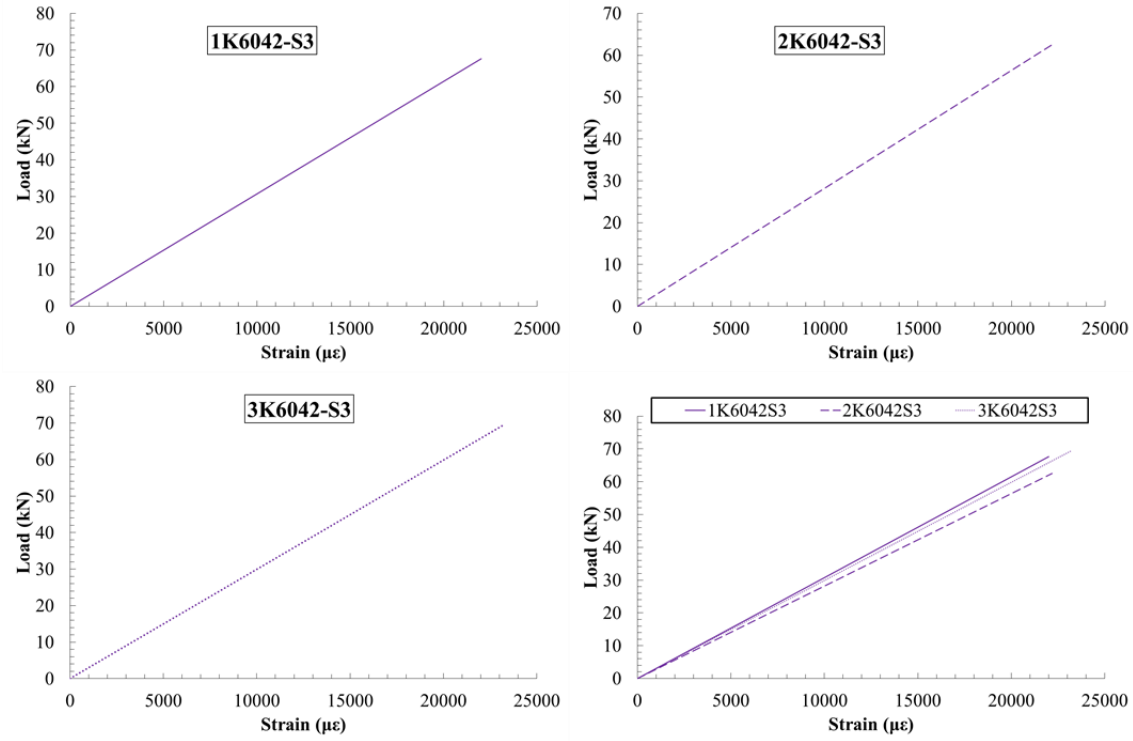

Figure.I.53 Load-strain of concrete specimens (K-60°C-42d-S3)

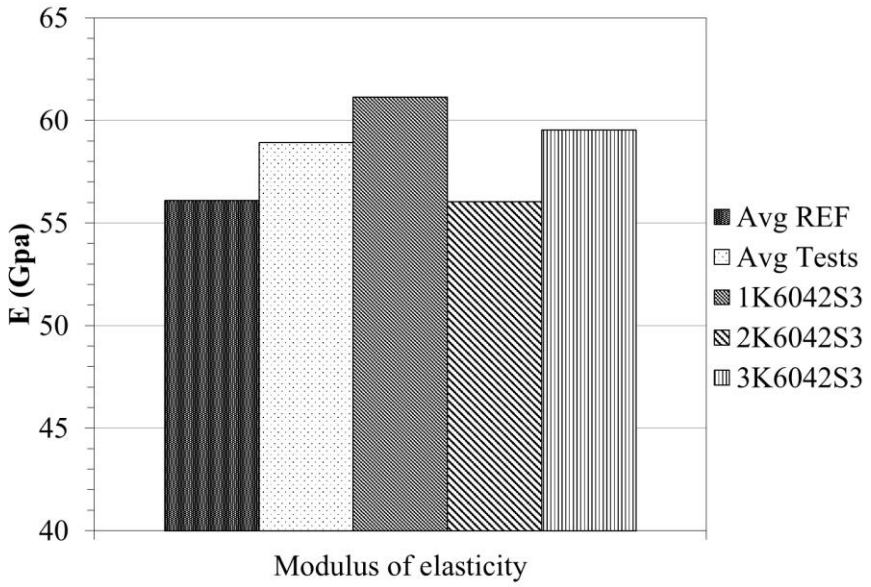

Figure.I.54: Modulus of elasticity for concrete specimens (K-60°C-42d-S3)

Table I.27: A summary of tensile test results of concrete specimen (K-60°C-42d-S3)

Specimens	P_{max} (kN)	E (GPa)	σ_{max} (MPa)	ε_{max}	note
1K6042S3	67.6	61.1	1353	0.022	
2K6042S3	62.5	56.0	1244	0.022	
3K6042S3	69.6	59.5	1385	0.023	
average	66.6	58.9	1327	0.023	
std	3.6	2.6	0.07	0.001	
%STD	5.4	4.4	5.5	2.8	
min	62.5	56.0	1244	0.022	
max	69.6	61.1	1385	0.023	

(K-20°C-90d)

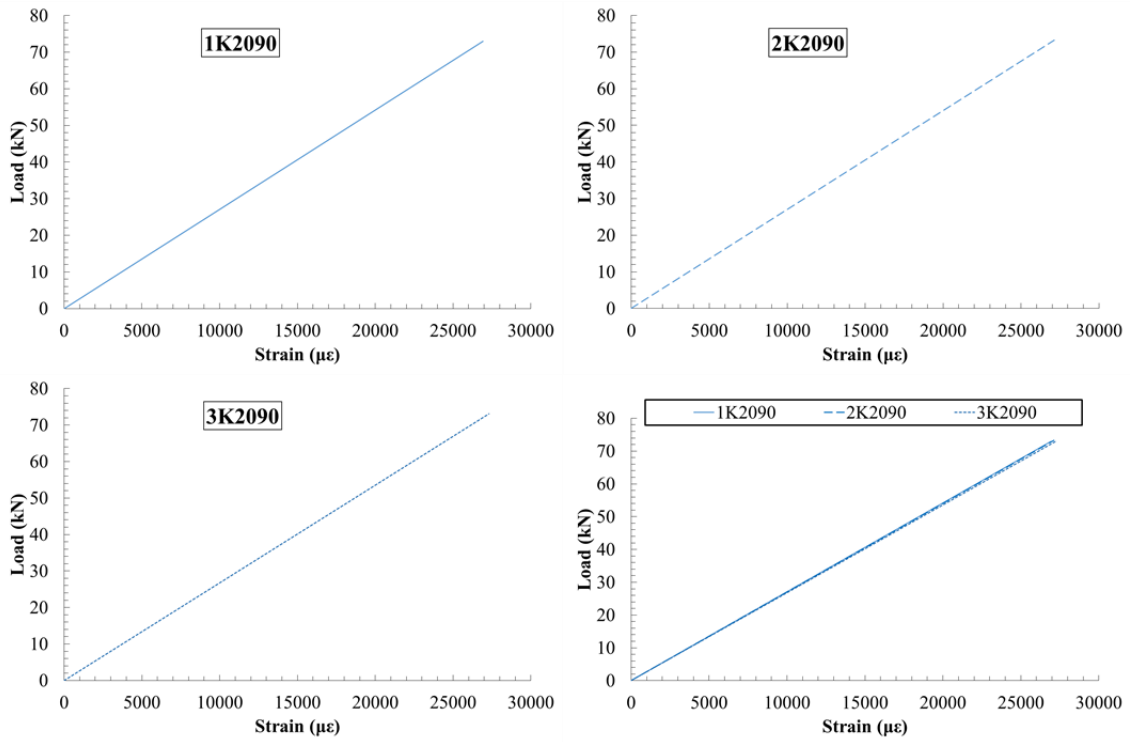

Figure.I.55 Load-strain of concrete specimens (K-20°C-90d)

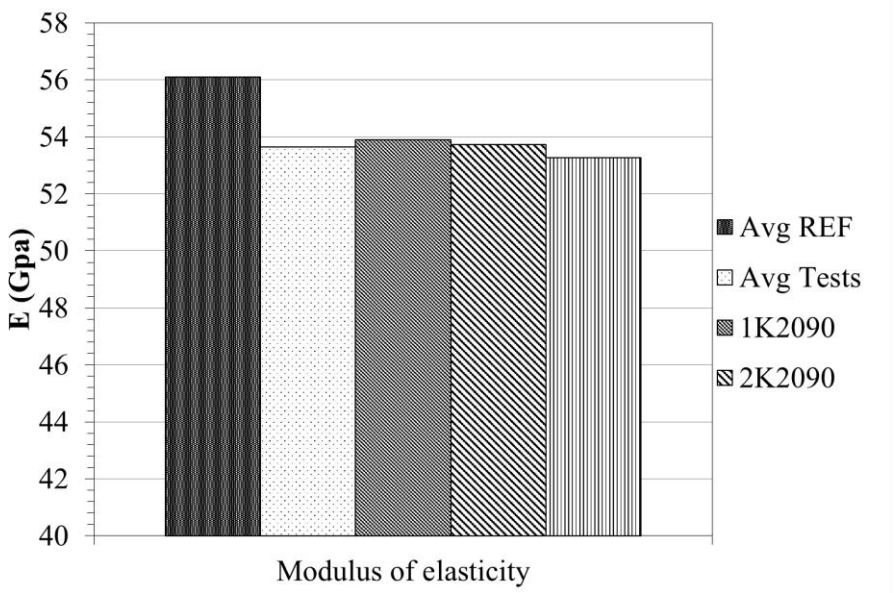

Figure.I.56: Modulus of elasticity for concrete specimens (K-20°C-90d)

Table I.28: A summary of tensile test results of concrete specimen (K-20°C-90d)

Specimens	P_{max} (kN)	E (GPa)	σ_{max} (MPa)	ε_{max}	note
1K2090	72.9	53.9	1452	0.027	
2K2090	73.2	53.7	1458	0.027	
3K2090	73.1	53.2	1455	0.027	
average	66.6	53.6	1455	0.027	
std	0.1	0.3	0.003	0.000	
%STD	0.2	0.6	0.219	0.703	
min	72.9	53.2	1452	0.027	
max	73.2	53.9	1458	0.027	

(K-40°C-90d)

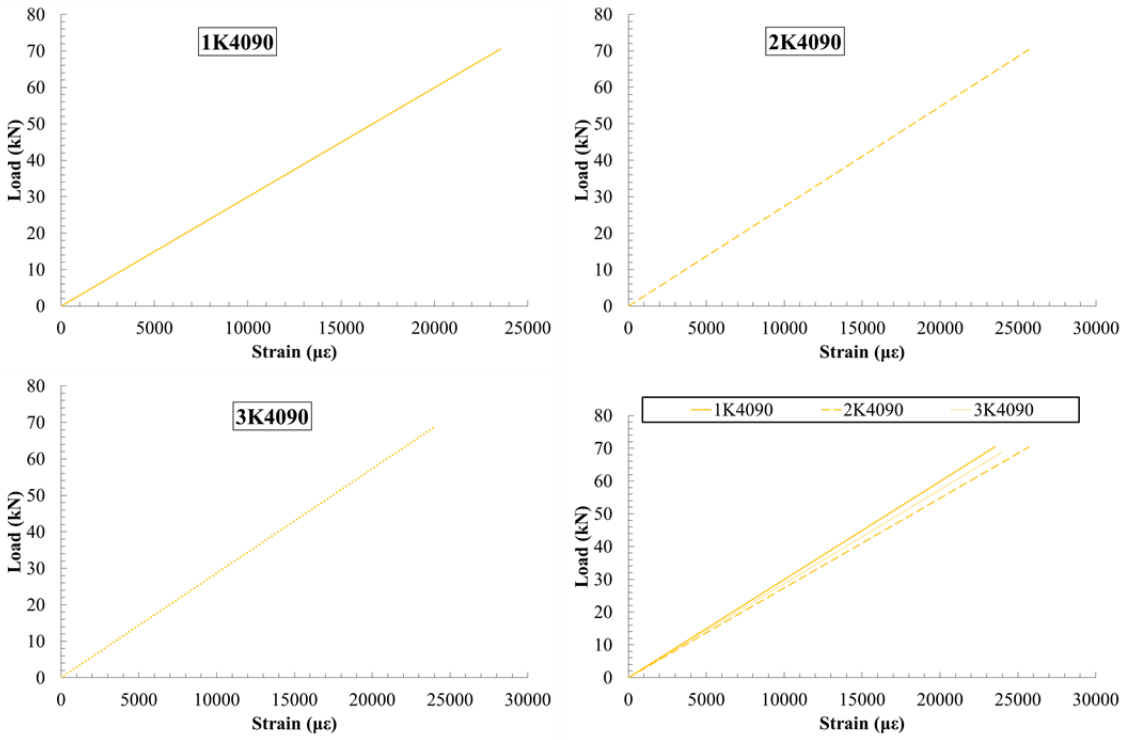

Figure.I.57 Load-strain of concrete specimens (K-40°C-90d)

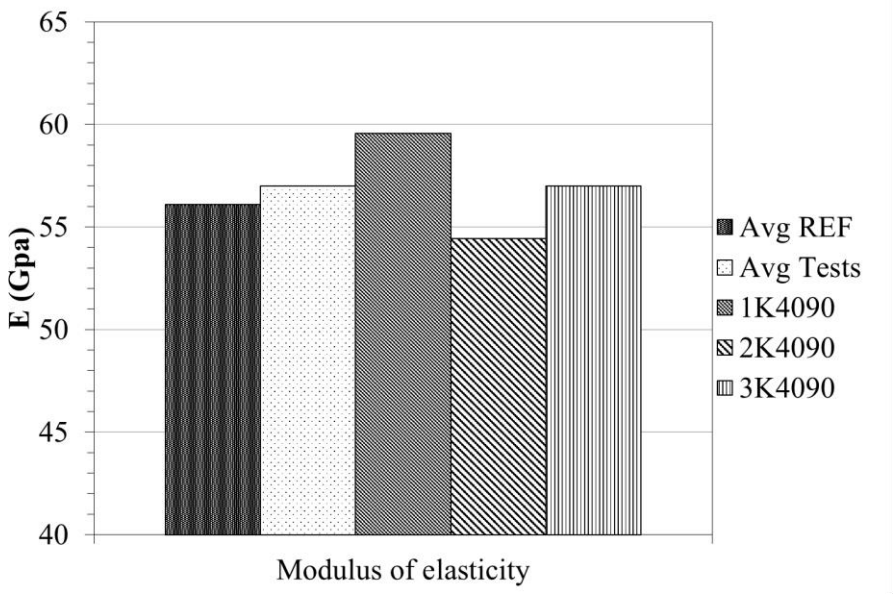

Figure.I.58: Modulus of elasticity for concrete specimens (K-40°C-90d)

Table I.29: A summary of tensile test results of concrete specimen (K-40°C-90d)

Specimens	P_{max} (kN)	E (GPa)	σ_{max} (MPa)	ε_{max}	note
1K4090	70.5	59.5	1403	0.024	
2K4090	70.3	54.4	1399	0.026	
3K4090	68.7	56.9	1368	0.024	
average	66.6	56.9	1.390	0.024	
std	0.9	2.5	0.019	0.001	
%STD	1.4	4.5	1.3	4.6	
min	68.7	54.4	1368	0.024	
max	70.5	59.5	1403	0.026	

(K-60°C-90d)

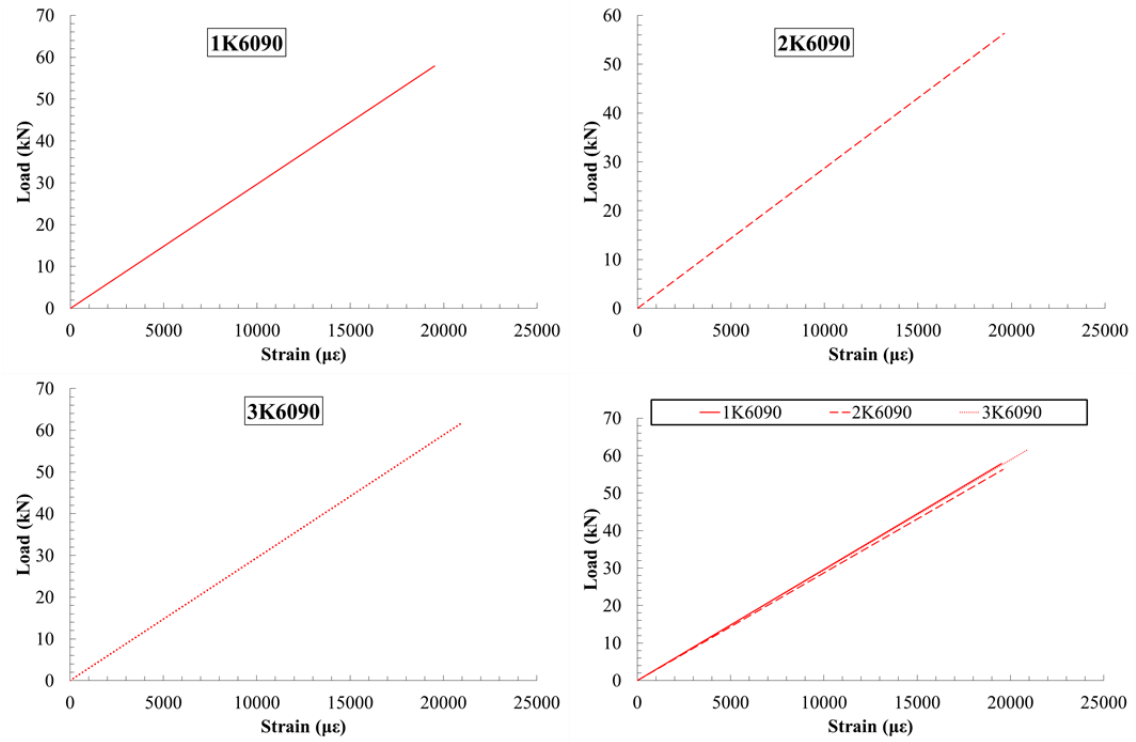

Figure.I.59: Load-strain of concrete specimens (K-60°C-90d)

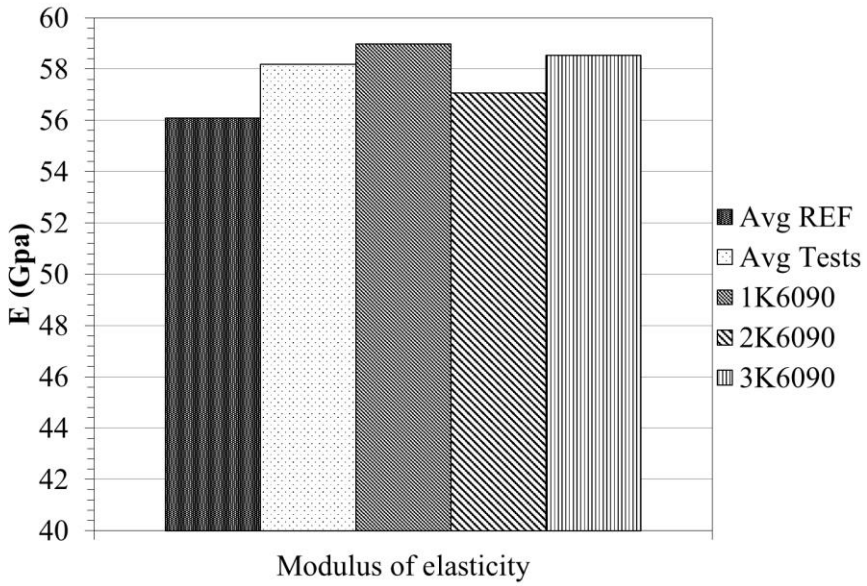

Figure.I.60: Modulus of elasticity for concrete specimens (K-60°C-90d)

Table I.30: A summary of tensile test results of concrete specimen (K-60°C-90d)

Specimens	P_{max} (kN)	E (GPa)	σ_{max} (MPa)	ε_{max}	note
1K6090	57.8	58.9	1151	0.020	
2K6090	56.2	57.0	1120	0.020	
3K6090	61.4	58.5	1223	0.021	
average	66.6	58.1	1165	0.020	
std	2.6	0.9	0.053	0.001	
%STD	4.0	1.7	4.5	3.8	
min	56.2	57.0	1120	0.020	
max	61.4	58.9	1223	0.021	

(K-60°C-90d-S3)

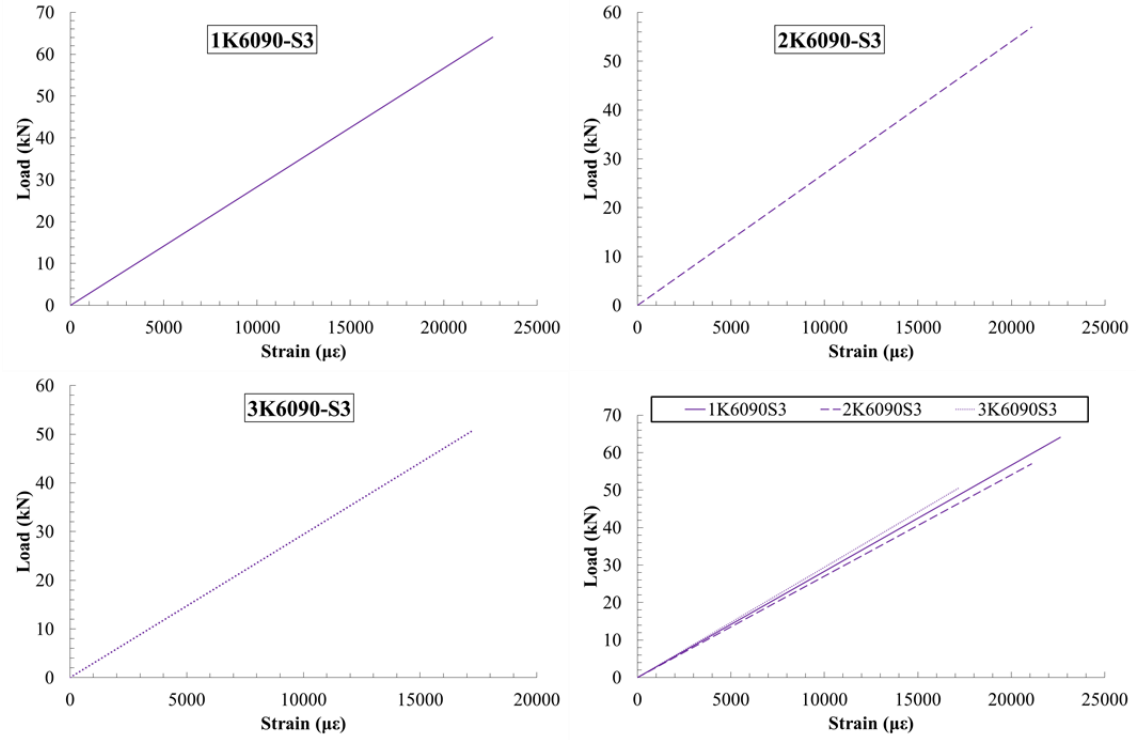

Figure.I.61 Load-strain of concrete specimens (K-60°C-90d-S3)

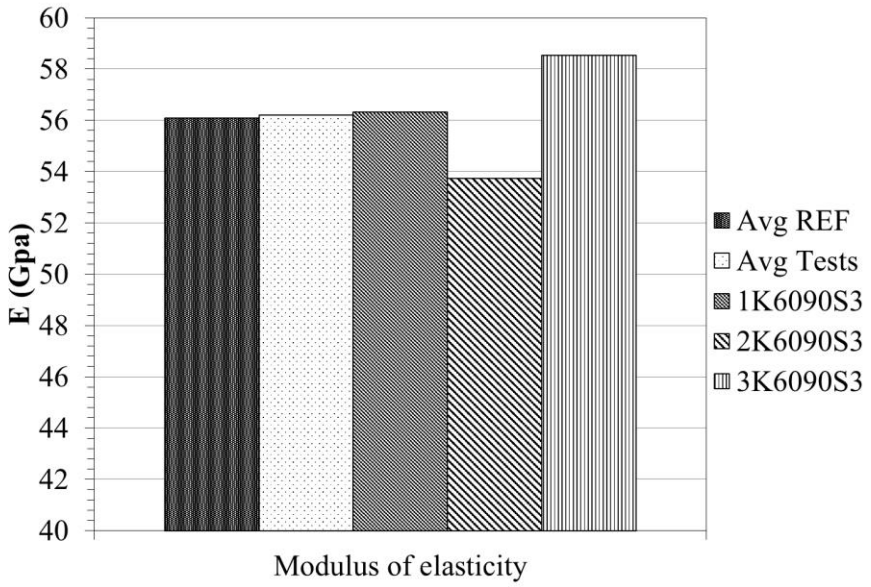

Figure.I.62: Modulus of elasticity for concrete specimens (K-60°C-90d-S3)

Table I.31: A summary of tensile test results of concrete specimen (K-60°C-90d-S3)

Specimens	P_{max} (kN)	E (GPa)	σ_{max} (MPa)	ε_{max}	note
1K6090S3	64.0	56.3	1151	0.020	
2K6090S3	56.9	53.7	1120	0.021	
3K6090S3	50.7	58.5	1223	0.021	
average	66.6	56.1	1165	0.021	
std	6.6	2.4	0.05	0.000	
%STD	10.0	4.2	4.5	1.1	
min	50.7	53.7	1120	0.020	
max	64.0	58.5	1223	0.021	

(K-20, 40, 60°C-270d)

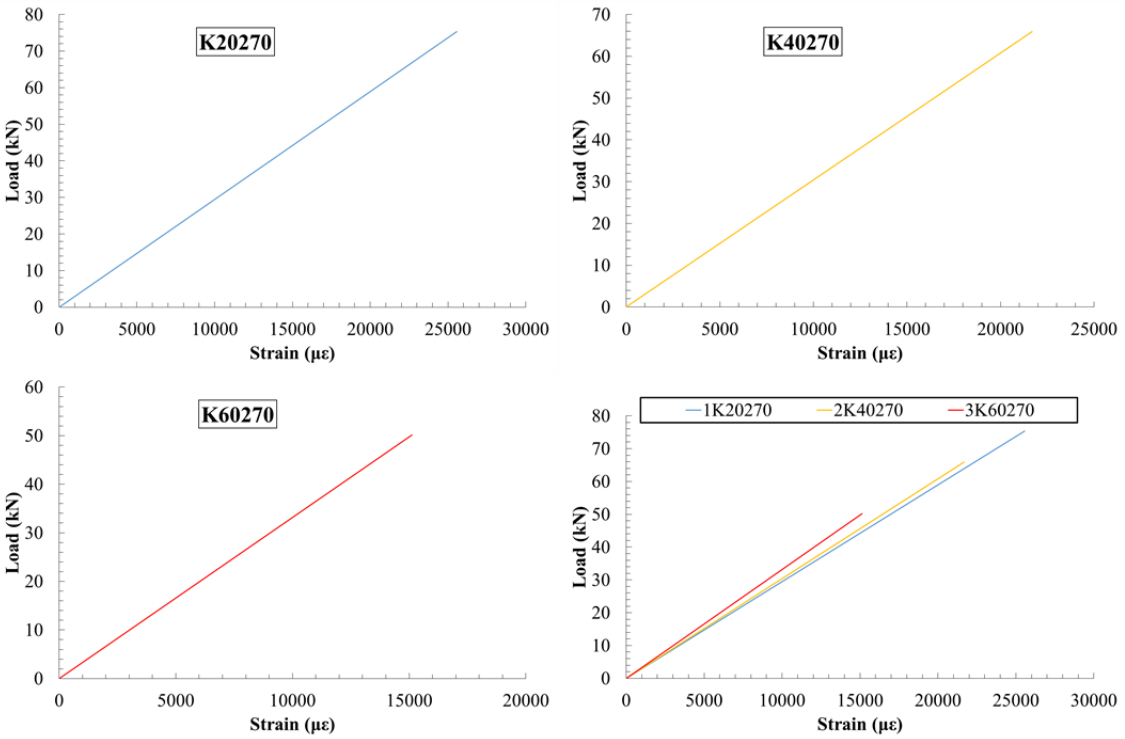

Figure.I.63 Load-strain of concrete specimens (K-20, 40, 60°C-90d)

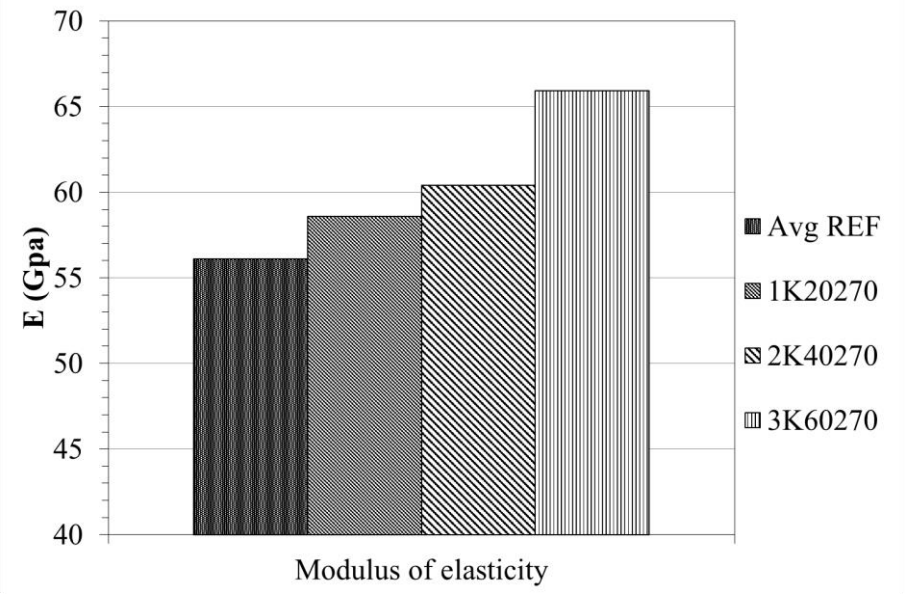

Figure.I.64: Modulus of elasticity for concrete specimens (K-20, 40, 60°C-90d)

Table I.32: A summary of tensile test results of concrete specimen (K-60°C-90d-S3)

Specimens	P_{max} (kN)	E (GPa)	σ_{max} (MPa)	ε_{max}	note
1K20270	75.3	58.5	1498	0.025	
2K40270	65.8	60.4	1310	0.021	
3K60270	50.1	65.9	997	0.015	

Test setup and failure mode for tested bars

The pictures presented below show the tests set up and failure mode of tested bars.

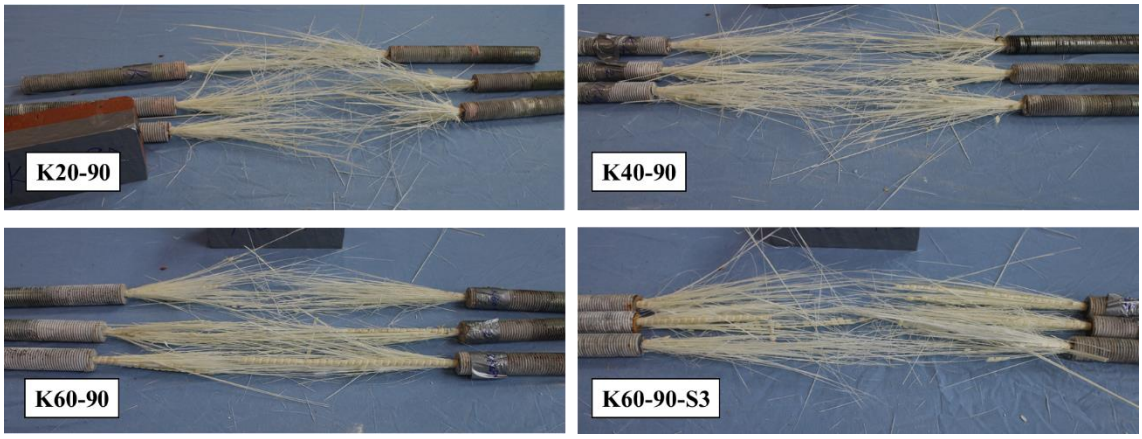

2. Interlaminar shear strength (ILSS) data for GFRP bars

This section presents the ILSS data including the load-displacement curves of tests bars on three point tests and the images of tests set up and failure mode.

ILSS (REF)

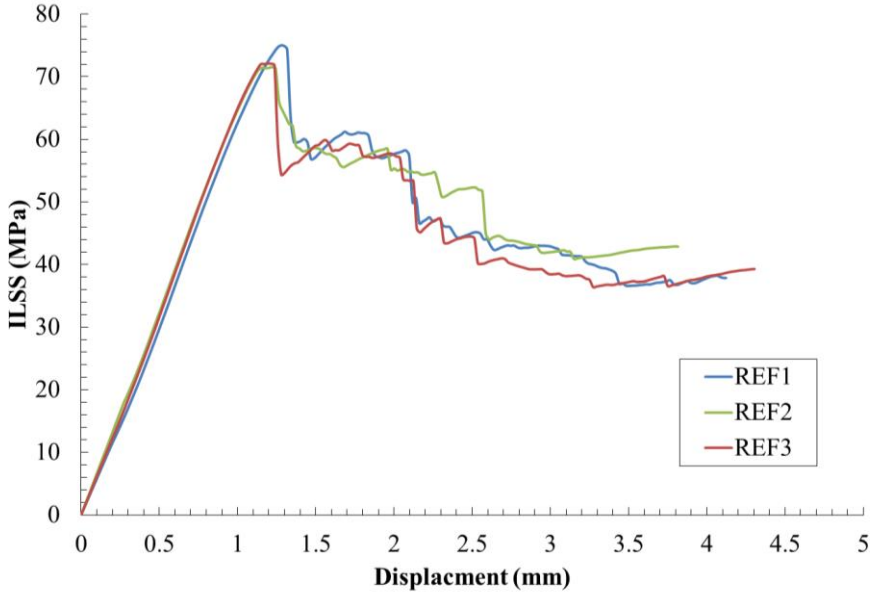

Figure.I.65 Stress-displacement of GFRP bars specimens (REF)

Table I.33: A summary of ILSS test results of GFRP bars specimens (REF)

SAMPLES	ILSS (MPa)	Avg	SLOP	Avg
160K	74.98		67.28	
260K	71.53	72.87	66.57	67.39
360K	72.09		68.33	
St	1.85			
cov	2.54			

ILSS (20360W)

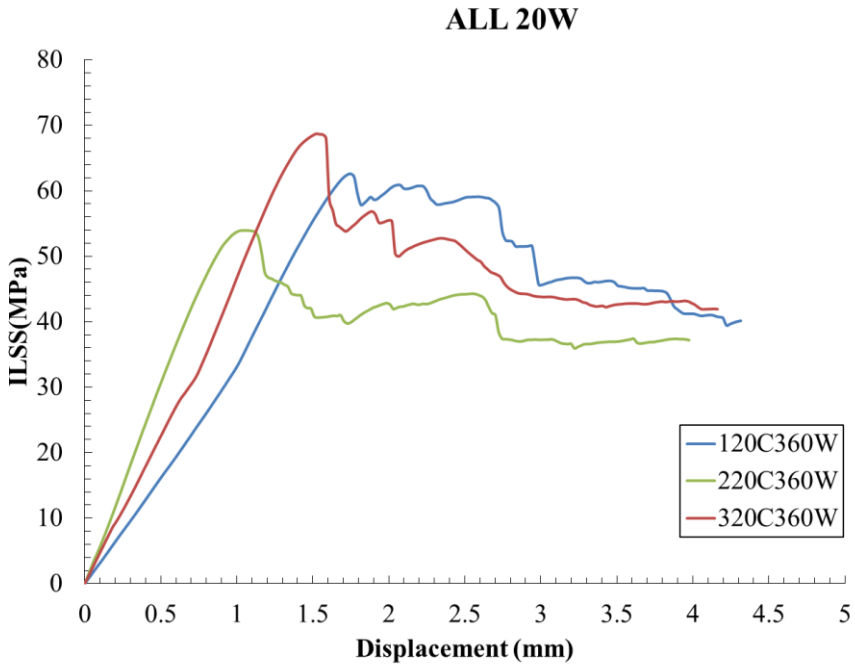

Figure.I.66 Stress-displacement of GFRP bars specimens (20360W)

Table I.34: A summary of ILSS test results of GFRP bars specimens (20360W)

SAMPLES	ILSS (MPa)	Avg	SLOP	Avg
120W	62.59		40.06	
220W	63.94	65.74	41.15	43.85
320W	68.70		50.34	
St	3.21			
cov	4.89			

ILSS (40360W)

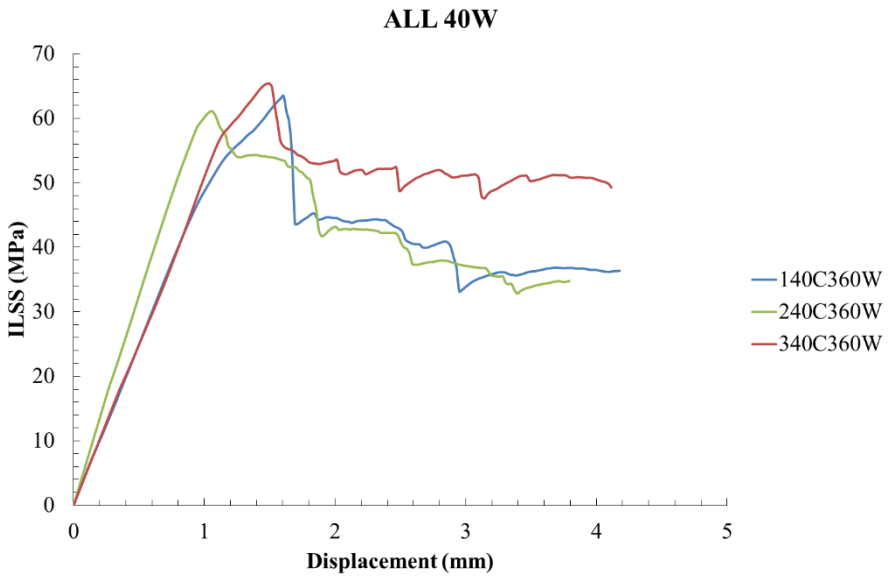

Figure.I.67 Stress-displacement of GFRP bars specimens (40360W)

Table I.35: A summary of ILSS test results of GFRP bars specimens (40360W)

SAMPLES	ILSS (MPa)	Avg	SLOP	Avg
140W	63.46		49.54	
240W	61.14	63.34	63.03	53.98
340W	65.43		49.39	
St	2.15			
cov	3.39			

(60360W)

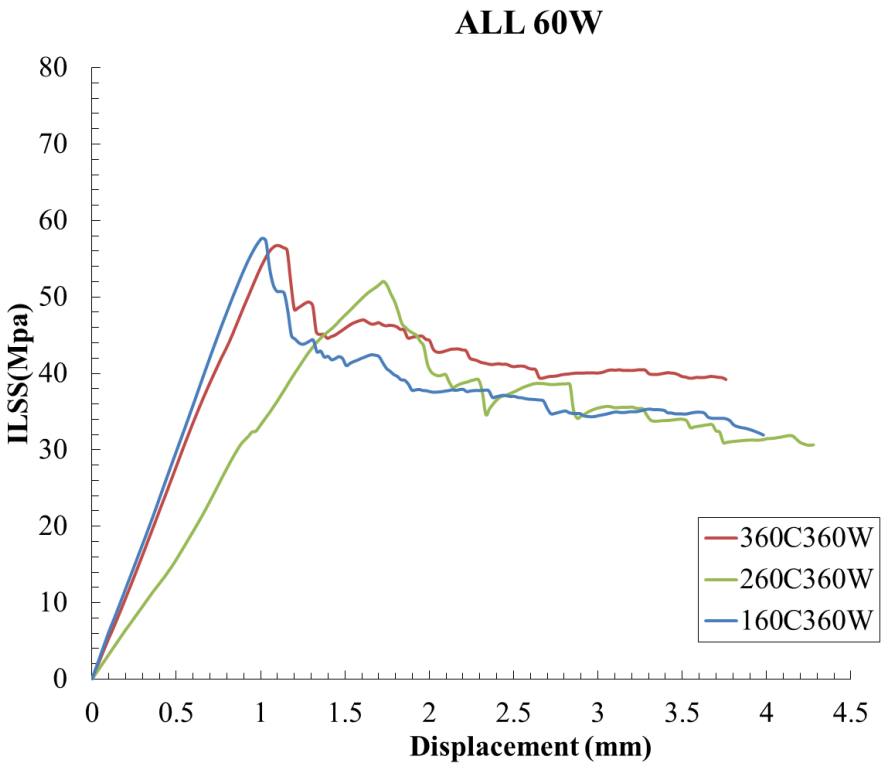

Figure.I.68 Stress-displacement of GFRP bars specimens (60360W)

Table I.36: A summary of ILSS test results of GFRP bars specimens (60360W)

SAMPLES	ILSS (MPa)	Avg	SLOP	Avg
160W	57.70	55.49	60.82	50.96
260W	52.04		35.05	
360W	56.73		57.00	
St	3.02			
cov	5.45			

(20360WS3)

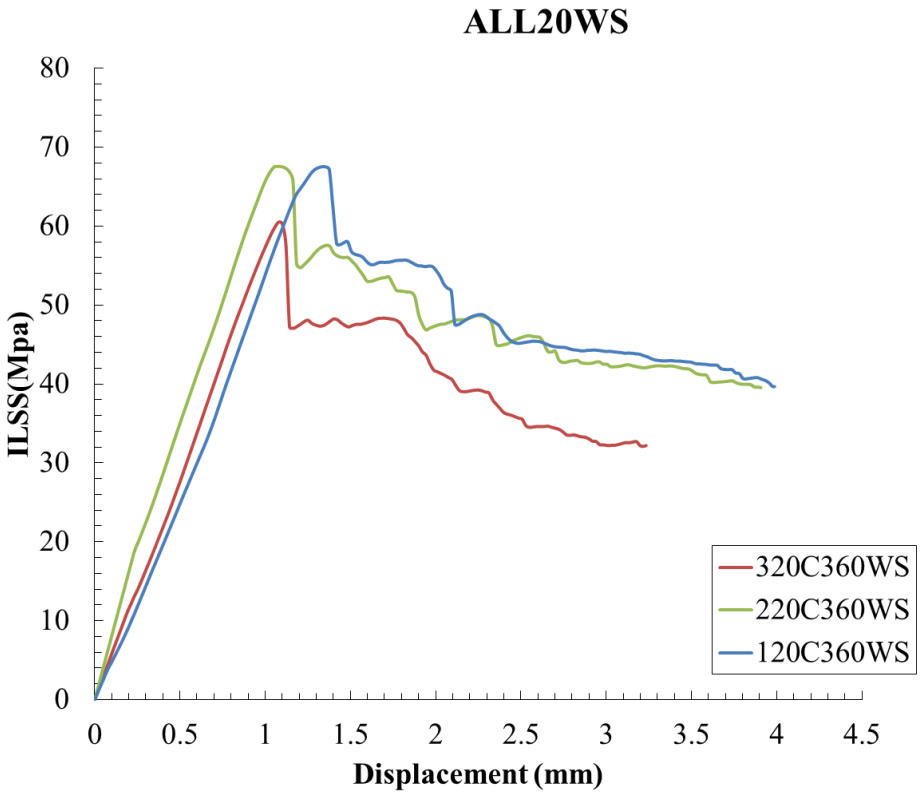

Figure.I.69 Stress-displacement of GFRP bars specimens (20360WS)

Table I.37: A summary of ILSS test results of GFRP bars specimens (20360WS)

SAMPLES	ILSS (MPa)	Avg	SLOP	Avg
120WS	67.53		55.31	
220WS	65.56	65.19	61.99	57.40
320WS	62.50		54.89	
St	2.54			
cov	3.89			

(40360WS)

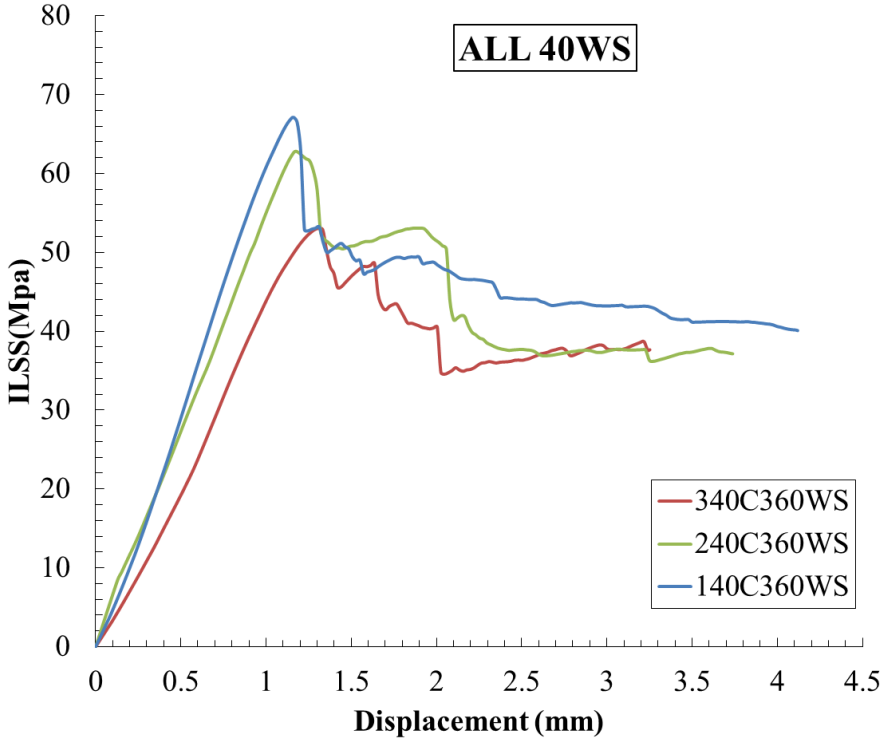

Figure.I.70 Stress-displacement of GFRP bars specimens (40360WS)

Table I.38: A summary of ILSS test results of GFRP bars specimens (40360WS)

SAMPLES	ILSS (MPa)	Avg	SLOP	Avg
140W	67.13		63.11	
240W	62.79	64.33	48.17	50.90
340W	63.07		41.42	
St	2.43			
cov	3.78			

(60360WS)

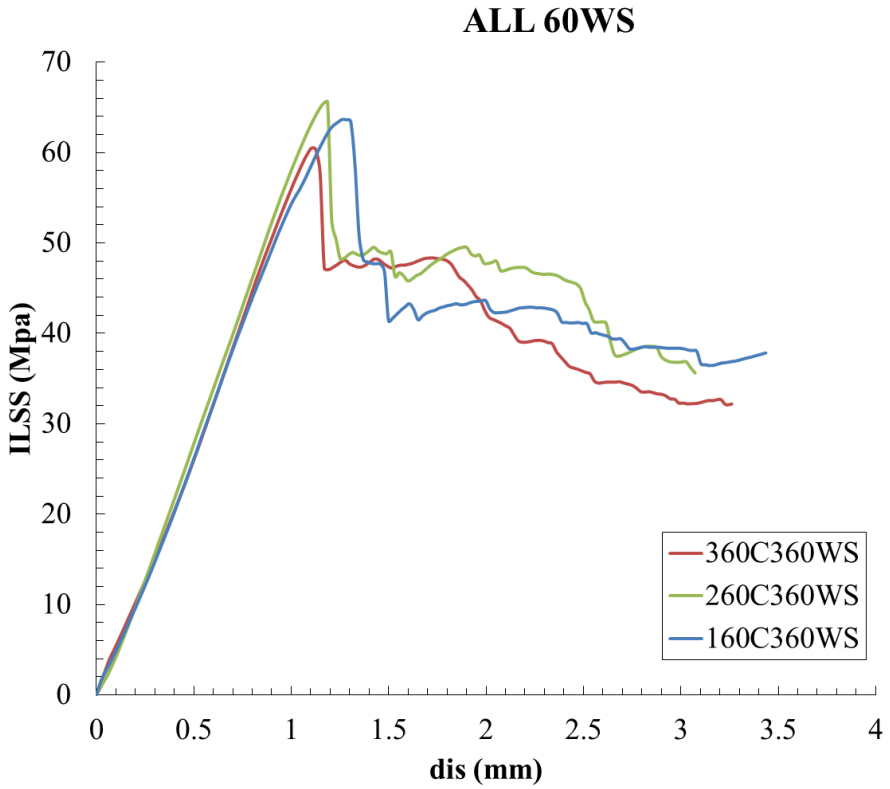

Figure.I.71 Stress-displacement of GFRP bars specimens (60360WS)

Table I.39: A summary of ILSS test results of GFRP bars specimens (60360WS)

SAMPLES	ILSS (MPa)	Avg	SLOP	Avg
160WS	63.66		55.45	
260WS	65.59	63.25	60.35	57.13
360WS	60.50		55.59	
St	2.57			
cov	4.07			

(20360K)

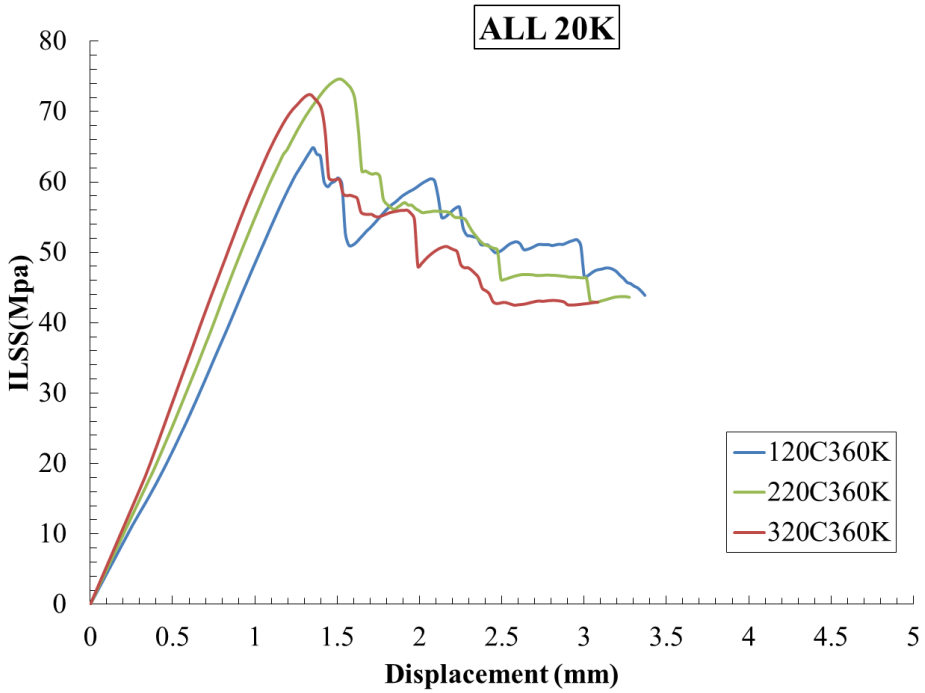

Figure.I.72 Stress-displacement of GFRP bars specimens (20360K)

Table I.40: A summary of ILSS test results of GFRP bars specimens (20360K)

SAMPLES	ILSS (MPa)	Avg	SLOP	Avg
120K	66.87		52.07	
220K	72.63	70.62	56.04	56.62
320K	72.37		61.76	
St	3.25			
cov	4.60			

(40360K)

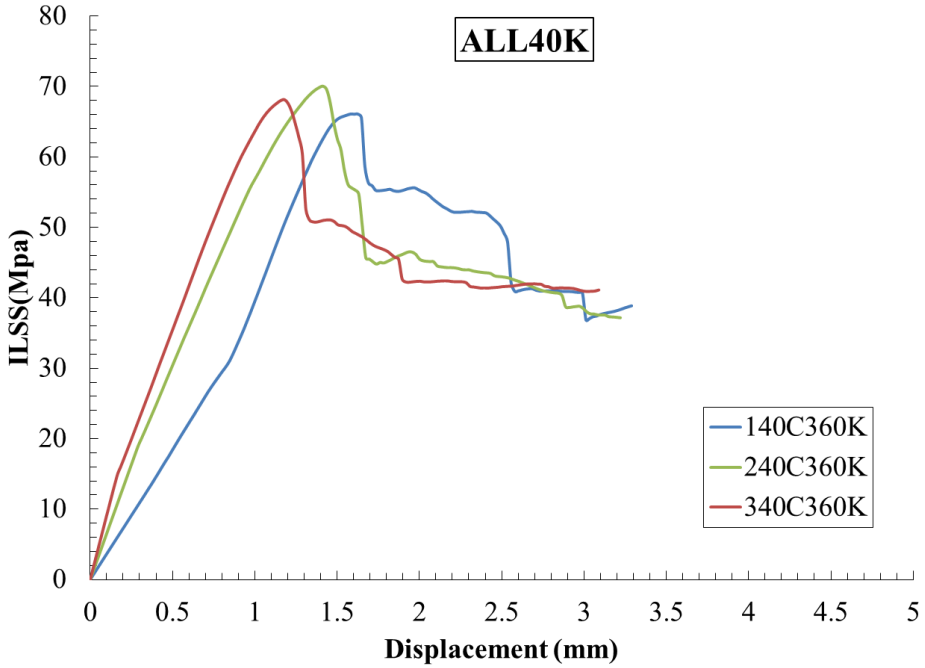

Figure.I.73 Stress-displacement of GFRP bars specimens (40360K)

Table I.41: A summary of ILSS test results of GFRP bars specimens (40360K)

SAMPLES	ILSS (MPa)	Avg	SLOP	Avg
140K	66.10		57.06	
240K	70.04	68.09	52.39	56.50
340K	68.13		60.06	
St	1.97			
cov	2.89			

(60360K)

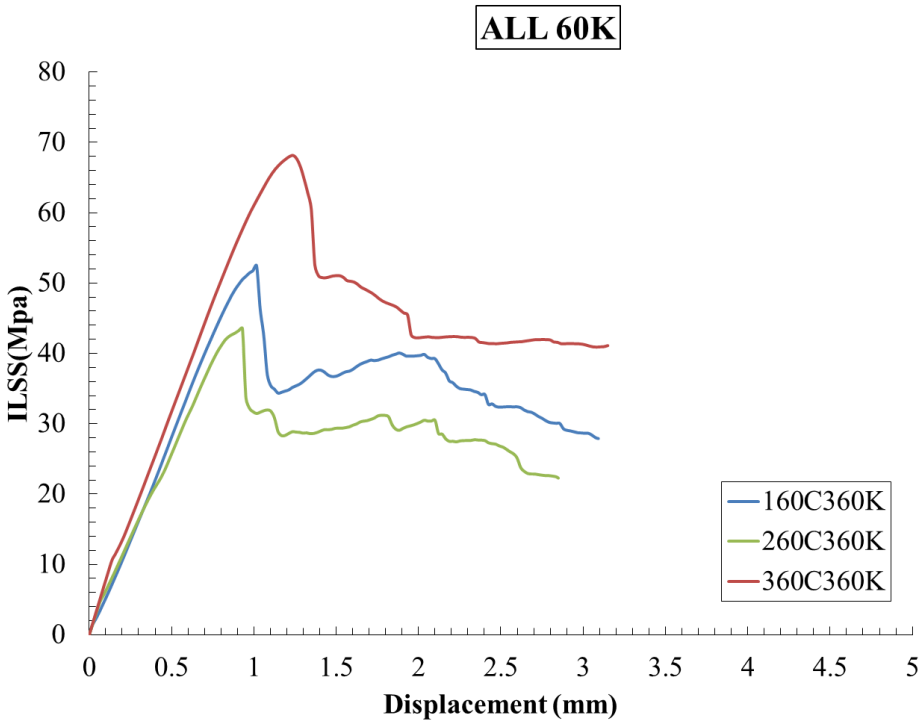

Figure.I.74 Stress-displacement of GFRP bars specimens (60360K)

Table I.42: A summary of ILSS test results of GFRP bars specimens (60360K)

SAMPLES	ILSS (MPa)	Avg	SLOP	Avg
160K	52.45		59.07	
260K	53.55	54.71	49.30	54.85
360K	58.13		56.17	
St	3.01			
cov	5.50			

(20360KS)

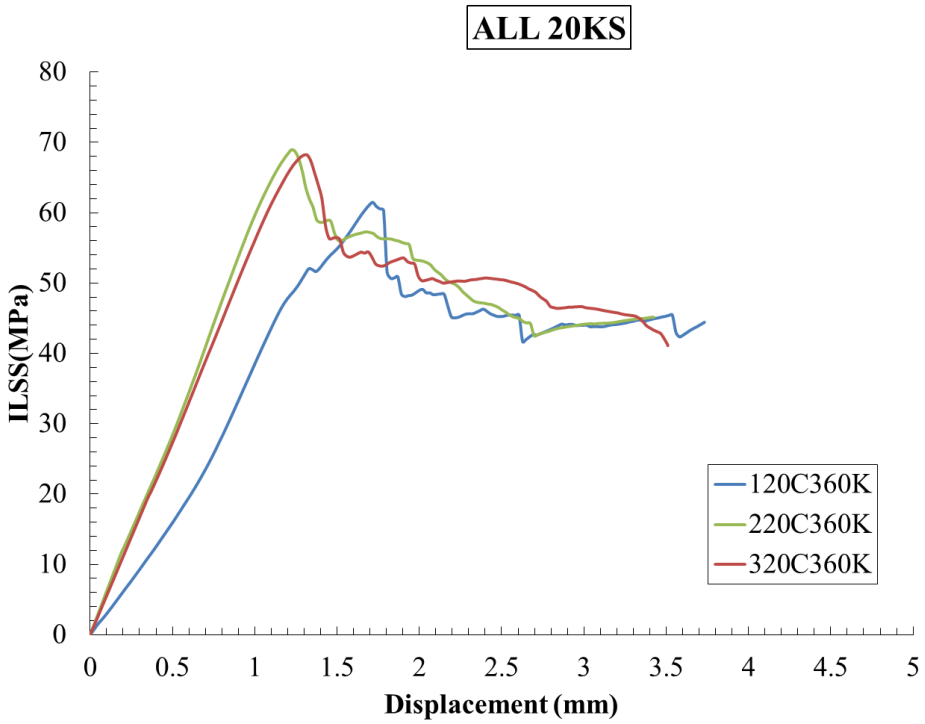

Figure.I.75 Stress-displacement of GFRP bars specimens (20360KS)

Table I.43: A summary of ILSS test results of GFRP bars specimens (20360KS)

SAMPLES	ILSS (MPa)	Avg	SLOP	Avg
120K	61.47		45.55	
220K	68.95	66.21	59.82	53.28
320K	68.20		54.48	
St	4.12			
cov	6.22			

(40360KS)

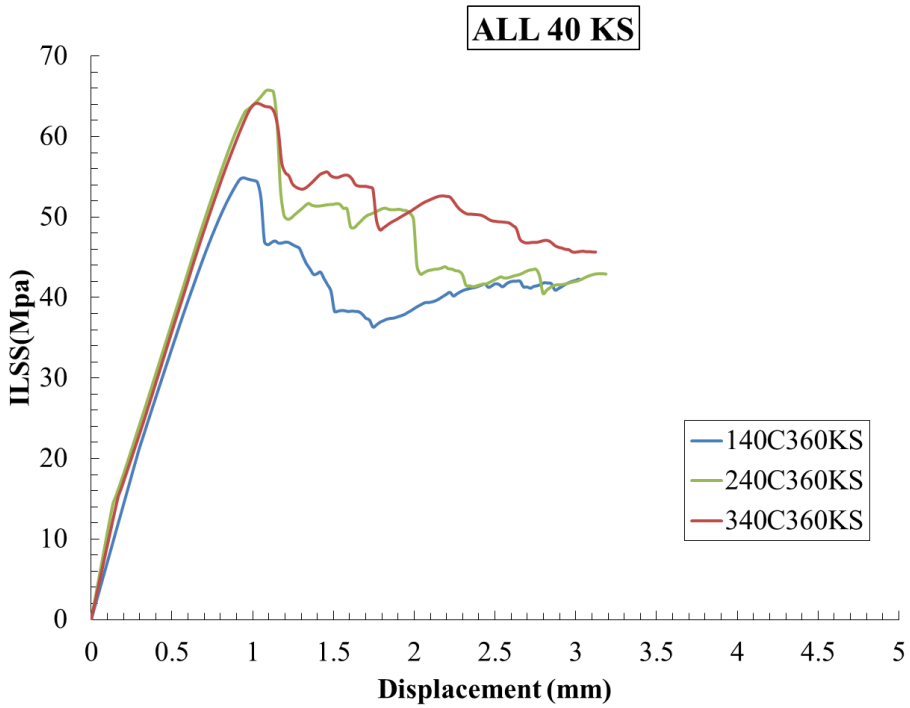

Figure.I.76 Stress-displacement of GFRP bars specimens (40360KS)

Table I.44: A summary of ILSS test results of GFRP bars specimens (40360KS)

SAMPLES	ILSS (MPa)	Avg	SLOP	Avg
140KS	54.88		27.83	
240KS	65.74	64.94	59.67	59.32
340KS	64.14		58.97	
St	1.13			
cov	1.74			

(60360KS)

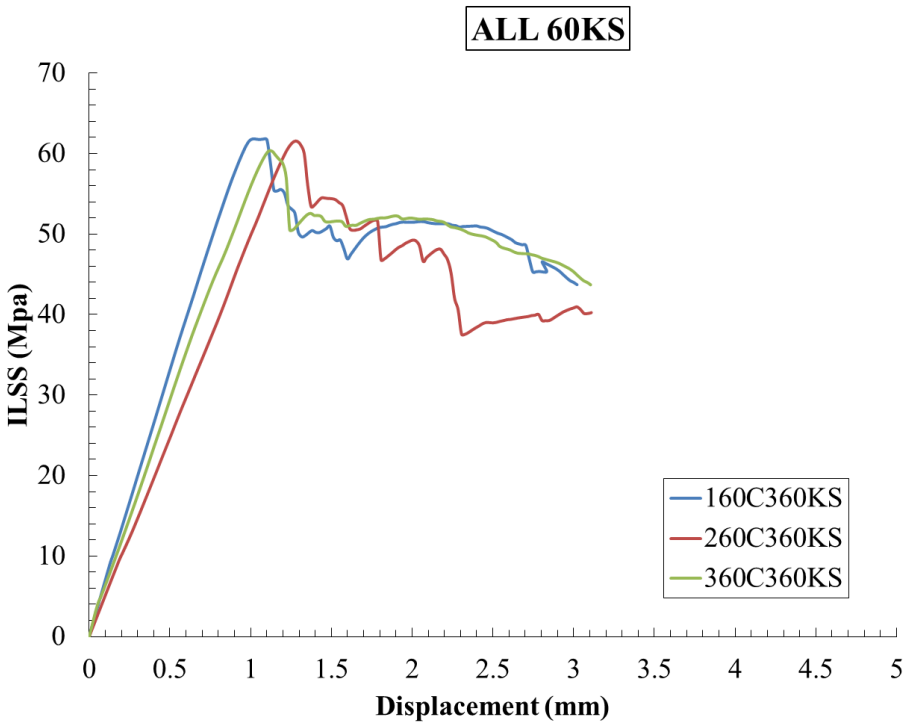

Figure.I.77 Stress-displacement of GFRP bars specimens (60360KS)

Table I.45: A summary of ILSS test results of GFRP bars specimens (60360KS)

SAMPLES	ILSS (MPa)	Avg	SLOP	Avg
160K	61.82	61.22	65.52	56.99
260K	61.52		49.29	
360K	60.31		56.16	
St	0.79			
cov	1.30			

Failure mode and test set up for GFRP bars

The following pictures presented shows the tests set up and failure mode of tested bars.

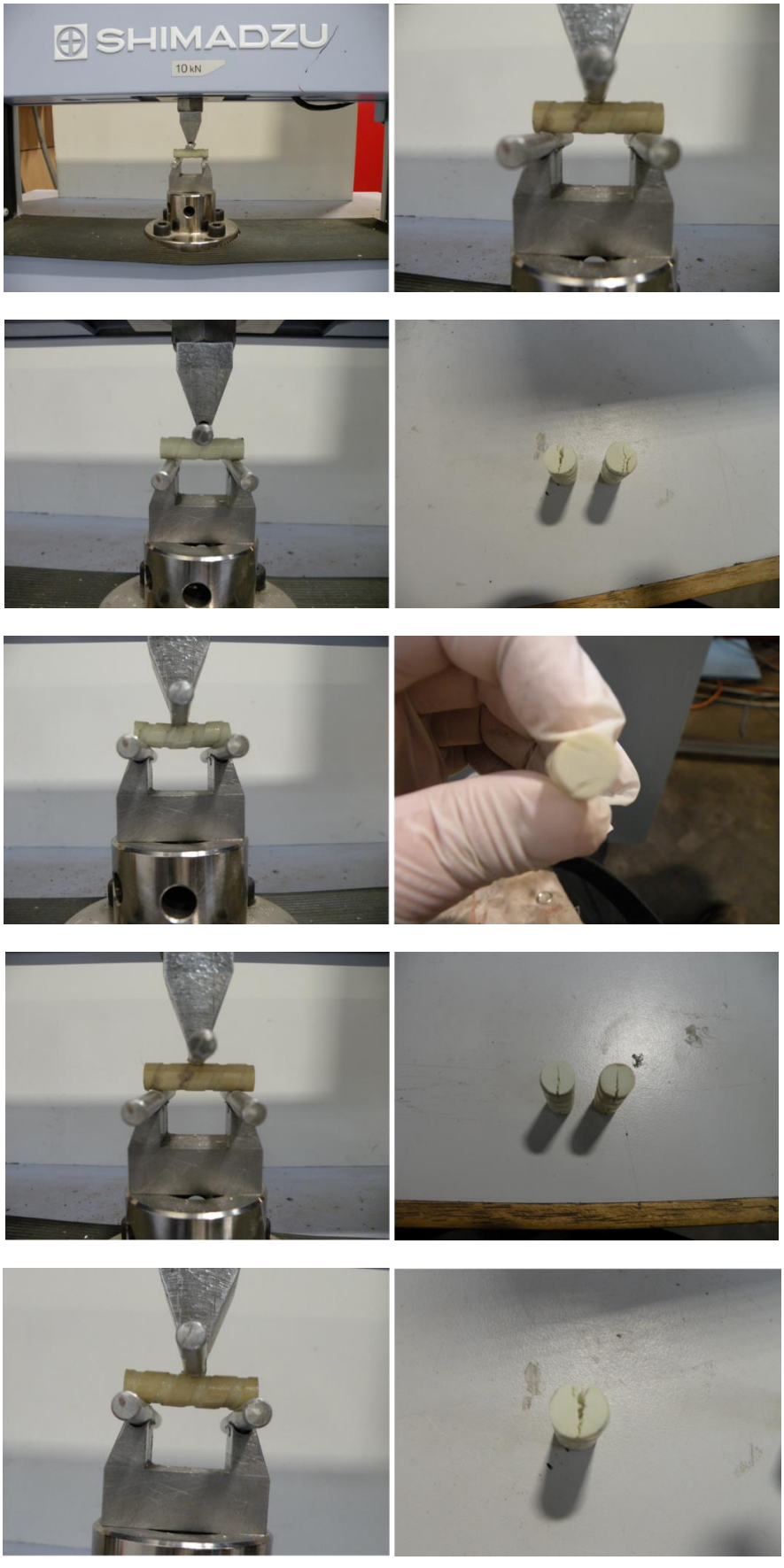
SHIMADZU
10 kN

3. Flexural properties data for GFRP bars

This section presents the flexural properties data of conditioned and unconditioned GFRP bars. The data is including the flexural strength and modulus of elasticity of tested bars attached with pictures of failure made and tests set up

(REF)

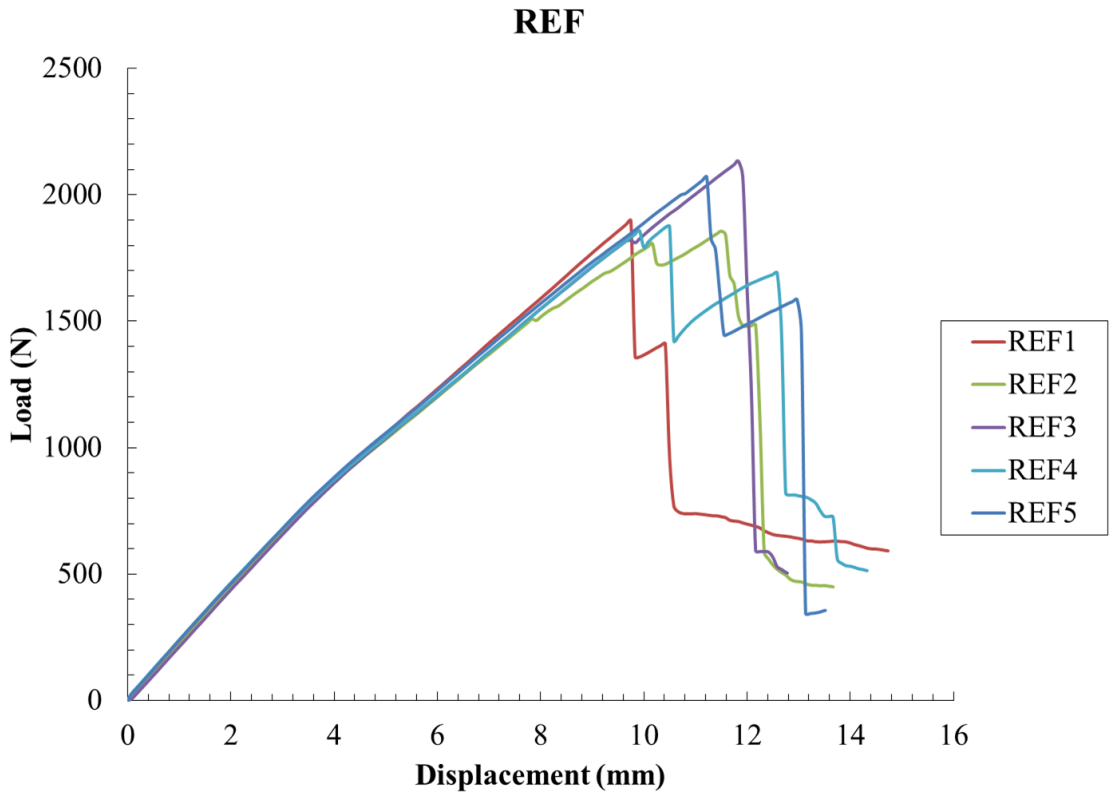

Figure.I.78 Load-displacement of tested GFRP bars in three point test (REF)

Table I.45: A summary of Flexural properties of tested GFRP bars specimens (REF)

sample	E (GPa)	Avg	σ (MPa)	Avg	ε	Avg
REF1	56.91		1321.09		0.025	
REF2	54.80		1291.99		0.029	
REF3	55.23	55.67	1484.32	1368.67	0.029	0.028
REF4	55.26		1305.07		0.025	
REF5	56.17		1440.89		0.029	
std	0.85	stdv	87.72	stdv	0.002	
cov	1.53	cov	6.41	cov	7.088	

(30, 40, 60°C360W)

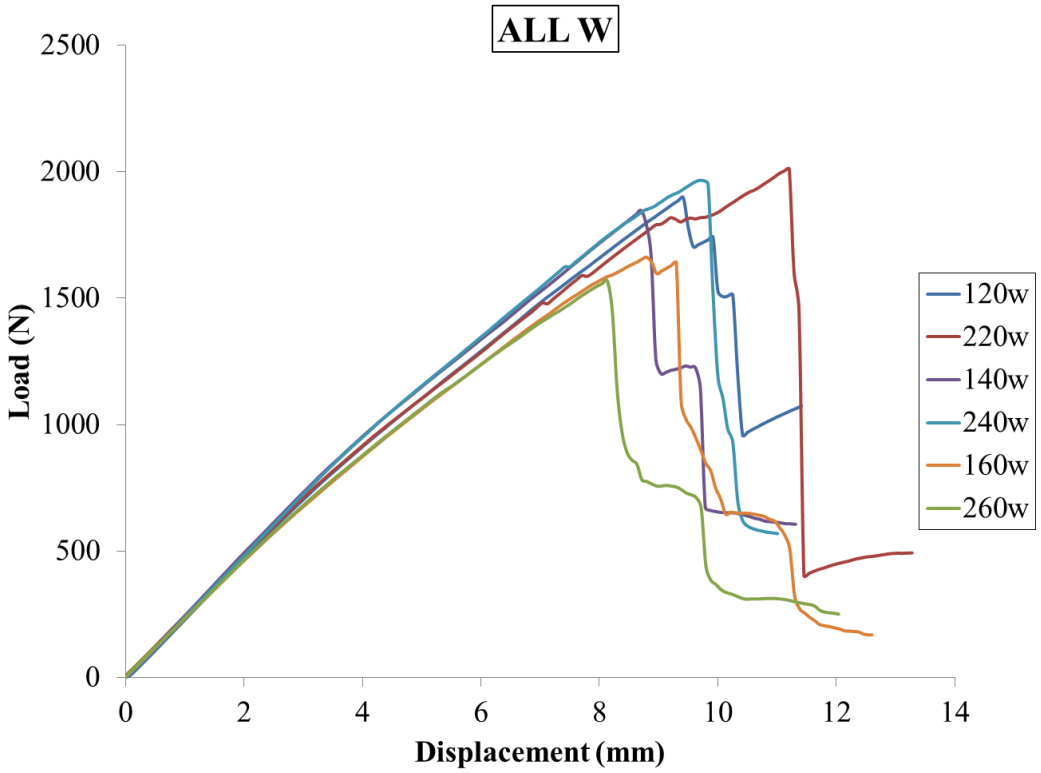

Figure.I.79 Load-displacement of tested GFRP bars in three point test (20,40, 60°C-360W)

(20360W)

Table I.46: A summary of Flexural properties of tested GFRP bars specimens (20360W)

sample	E (GPa)	Avg	σ (MPa)	Avg	ε	Avg
120w	60.0	59.5	1320	1360	0.029	0.031
220w	59.0		1399		0.033	
	std	0.7	std	55		
	cov	1.3	cov	4.0		

(40360W)

Table I.47: A summary of Flexural properties of tested GFRP bars specimens (40360W)

sample	E (GPa)	Avg	σ (MPa)	Avg	ε	Avg
140w	62.1	62.4	1285	1326	0.029	0.029
240w	62.7		1367		0.028	
	std	0.4	std	58		
	cov	0.7	cov	4.3		

(60360W)

Table I.48: A summary of Flexural properties of tested GFRP bars specimens (60360W)

sample	E (GPa)	Avg	σ (MPa)	Avg	ε	Avg
160w	56.6	56.2	1156	1124	0.032	0.031
260w	55.8		1092		0.031	
	std	0.57	std	45.5		
	cov	1.02	cov	4.0		

(30, 40, 60°C360WS)

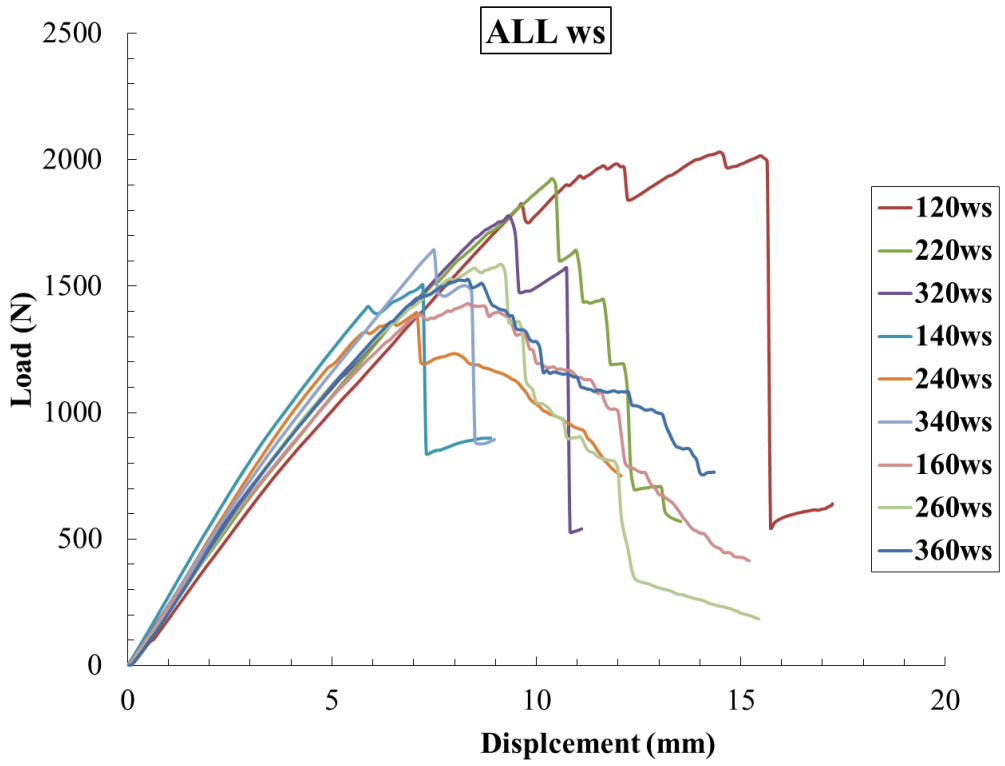

Figure.I.80 Load-displacement of tested GFRP bars in three point test (20, 40, 60°C-360WS)

(20360WS)

Table I.49: A summary of Flexural properties of tested GFRP bars specimens (20360WS)

sample	E (GPa)	Avg	σ (MPa)	Avg	ε	Avg
120ws	55.5		1414		0.043	
220ws	56.5	56.5	1341	1331	0.034	0.035
320ws	57.4		1239		0.028	
	std	0.98	std	88.1		
	cov	1.74	cov	6.6		

(40360WS)

Table I.50: A summary of Flexural properties of tested GFRP bars specimens (40360WS)

sample	E (GPa)	Avg	σ (MPa)	Avg	ε	Avg
140ws	68.8		1047		0.023	
240ws	63.0	65.4	971	1054	0.031	0.025
340ws	64.4		1143		0.023	
	std	3.028	std	86.6		
	cov	4.625	cov	8.2		

(60360WS)

Table I.51: A summary of Flexural properties of tested GFRP bars specimens (60360WS)

sample	E (GPa)	Avg	σ (MPa)	Avg	ε	Avg
160ws	56.4		997		0.038	
260ws	58.6	58.2	1103	1054	0.039	0.038
360ws	59.5		1063		0.037	
	std	1.5	std	53.6		
	cov	2.6	cov	5.0		

(20, 40, 60°C360K)

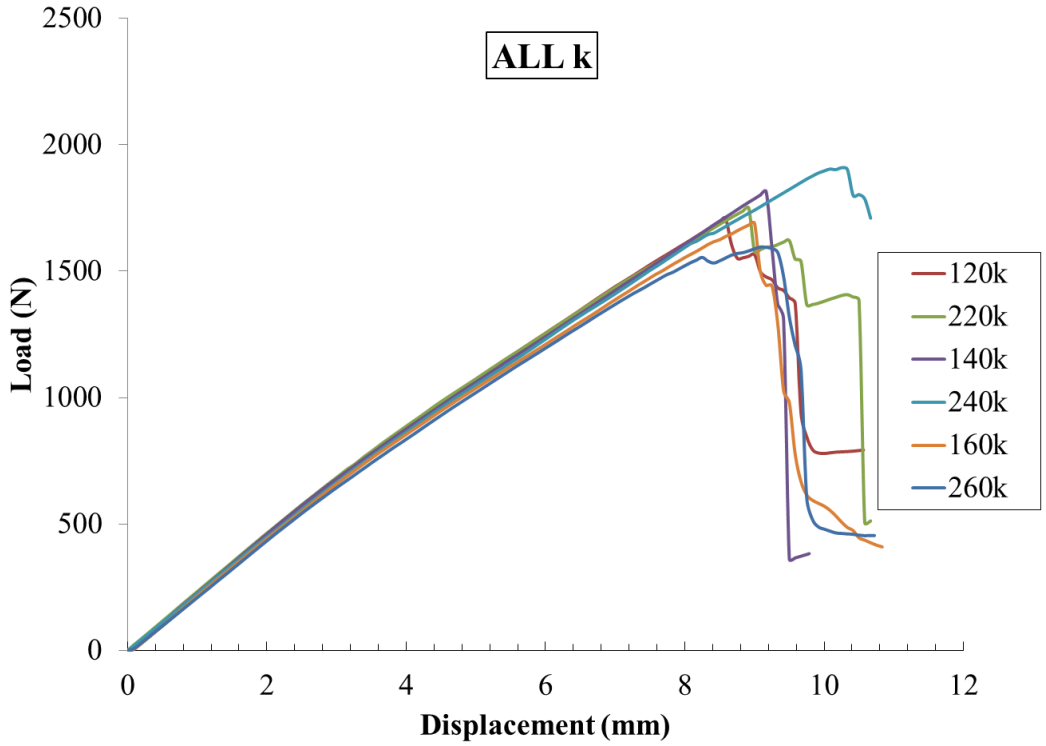

Figure.I.81 Load-displacement of tested GFRP bars in three point test (20, 40, 60°C-360K)

(20360K)

Table I.52: A summary of Flexural properties of tested GFRP bars specimens (20360K)

sample	E (GPa)	Avg	σ (MPa)	Avg	ε	Avg
120K	57.9	57.8	1189	1203	0.028	0.028
220K	57.7		1218		0.028	
	std	0.139	std	20.4		
	cov	0.240	cov	1.6		

(40360K)

Table I.53: A summary of Flexural properties of tested GFRP bars specimens (40360K)

sample	E (GPa)	Avg	σ (MPa)	AVA	ε	avaε
140K	58.0	57.9	1263	1296	0.025	0.029
240K	57.7		1328		0.033	
	std	0.2	std	46.3		
	cov	0.3	cov	3.5		

(60360K)

Table I.54: A summary of Flexural properties of tested GFRP bars specimens (60360K)

sample	E (GPa)	Avg	σ (MPa)	Avg	ε	Avg
160K	55.7	55.8	1176	1143	0.030	0.029
260K	55.9		1110		0.027	
	std	0.1	std	46.3		
	cov	0.2	cov	4.0		

(20, 40, 60°C360KS)

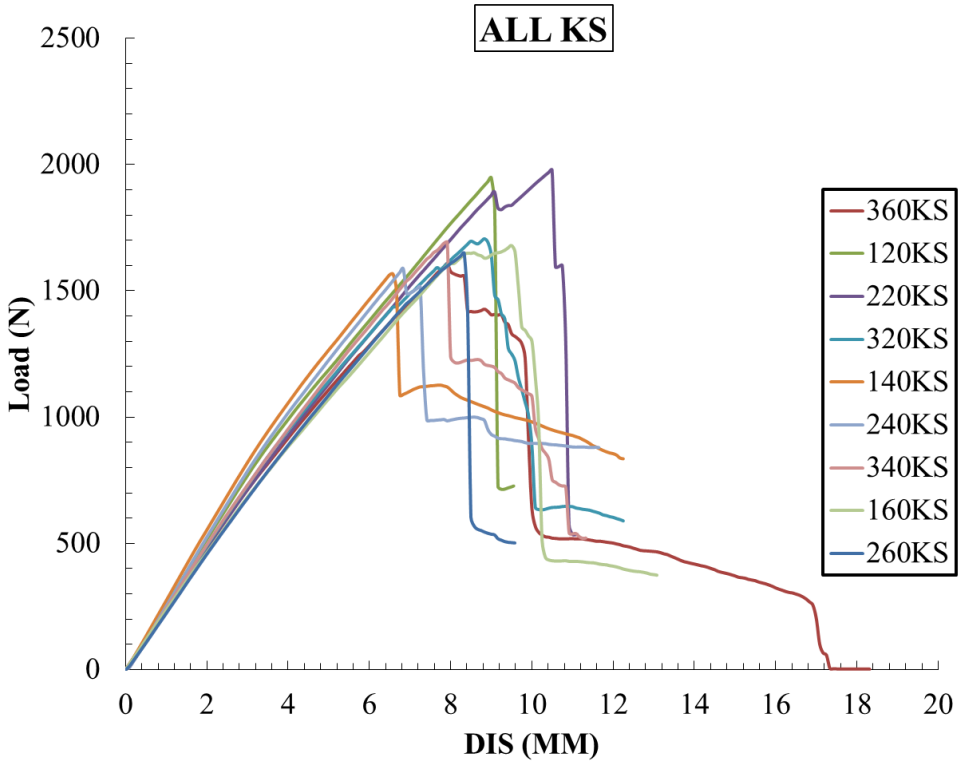

Figure.I.82 Load-displacement of tested GFRP bars in three point test (20, 40, 60°C-360KS)

(20360KS)

Table I.55: A summary of Flexural properties of tested GFRP bars specimens (20360K)

sample	E (GPa)	Avg	σ (MPa)	Avg	ε	Avg
120KS	57.2		1355		0.025	
220KS	55.1	55.8	1377	1306	0.029	0.028
320KS	55.0		1187		0.031	
	std	1.2	std	103.8		
	cov	**2.2**	**cov**	**7.9**		

(40360KS)

Table I.56: A summary of Flexural properties of tested GFRP bars specimens (40360K)

sample	E (GPa)	Avg	σ (MPa)	Avg	ε	Avg
140KS	56.8		1189		0.031	
240KS	59.0	57.4	1105	1157	0.030	0.030
340KS	56.4		1177		0.029	
	std	1.3	std	45.8		
	cov	2.3	cov	3.9		

(60360KS)

Table I.57: A summary of Flexural properties of tested GFRP bars specimens (40360K)

sample	E (GPa)	Avg	σ (MPa)	Avg	ε	Avg
160KS	52.2		1168.9		0.034	
260KS	53.2	52.9	1147.8	1145	0.025	0.035
360KS	53.2		1118.5		0.046	
	std	0.5	std	25.3		
	cov	1.0	cov	2.2		

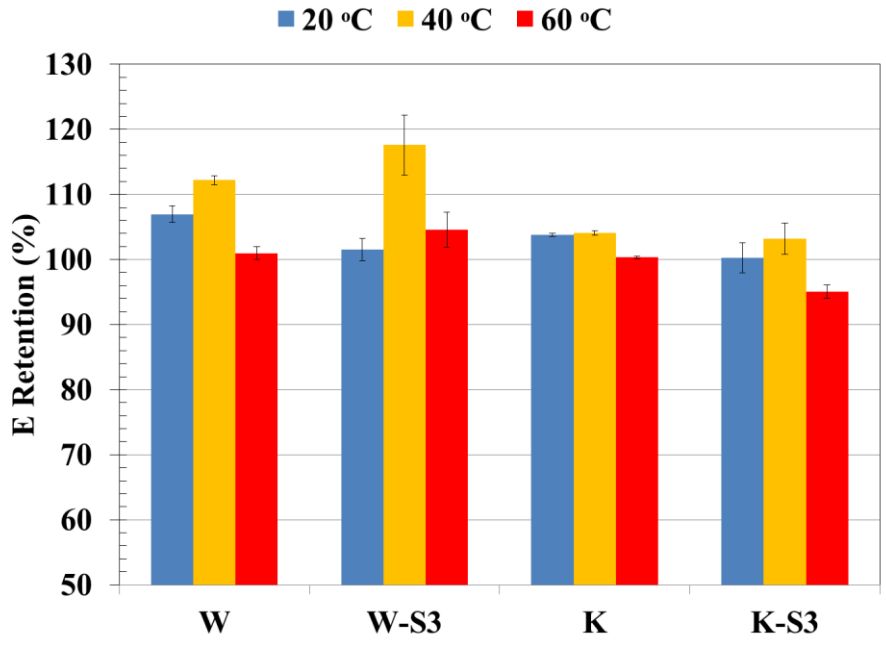

Figure.I.83 Modulus of elasticity (E) of tested GFRP bars conditioned in water and alkaline solution at 20, 40, 60°C for I year.

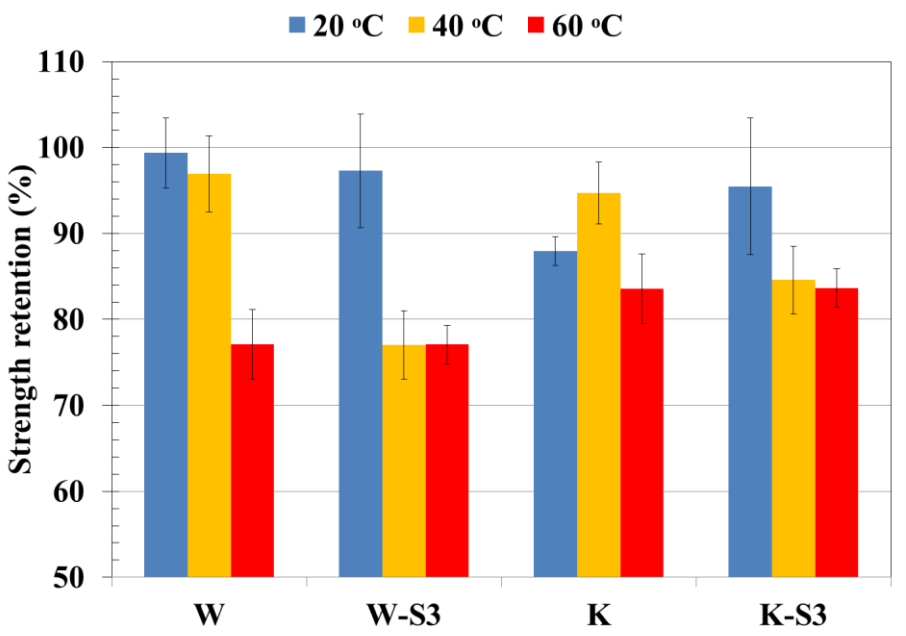

Figure.I.83 Flexural strength of tested GFRP bars conditioned in water and alkaline solution at 20, 40, 60°C for I year.

Failure mode and test set up for GFRP bars under three point test

The following pictures presented shows the tests set up and failure mode of tested bars.

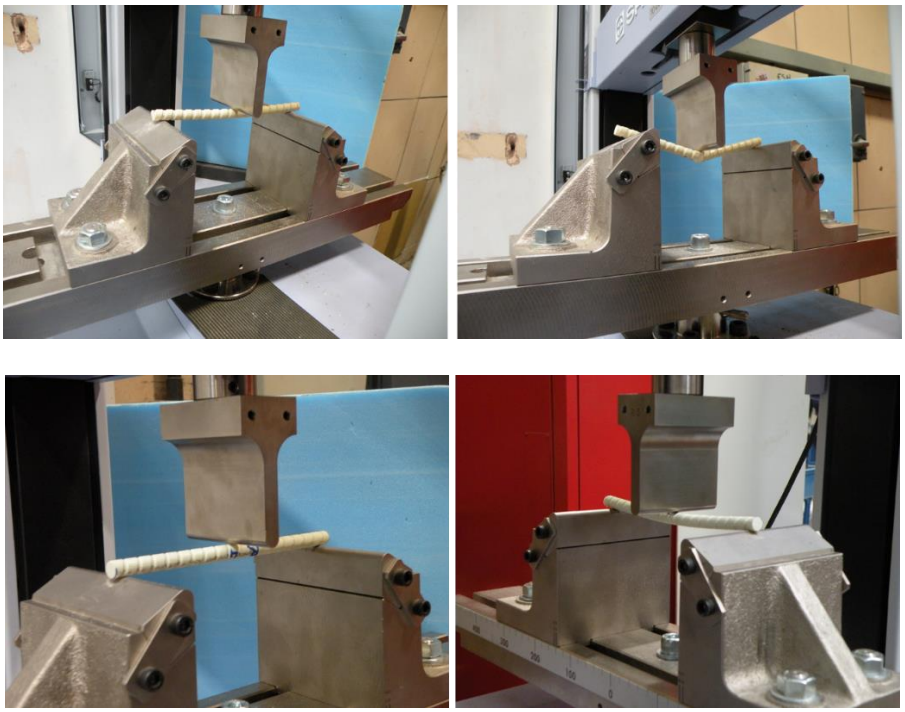

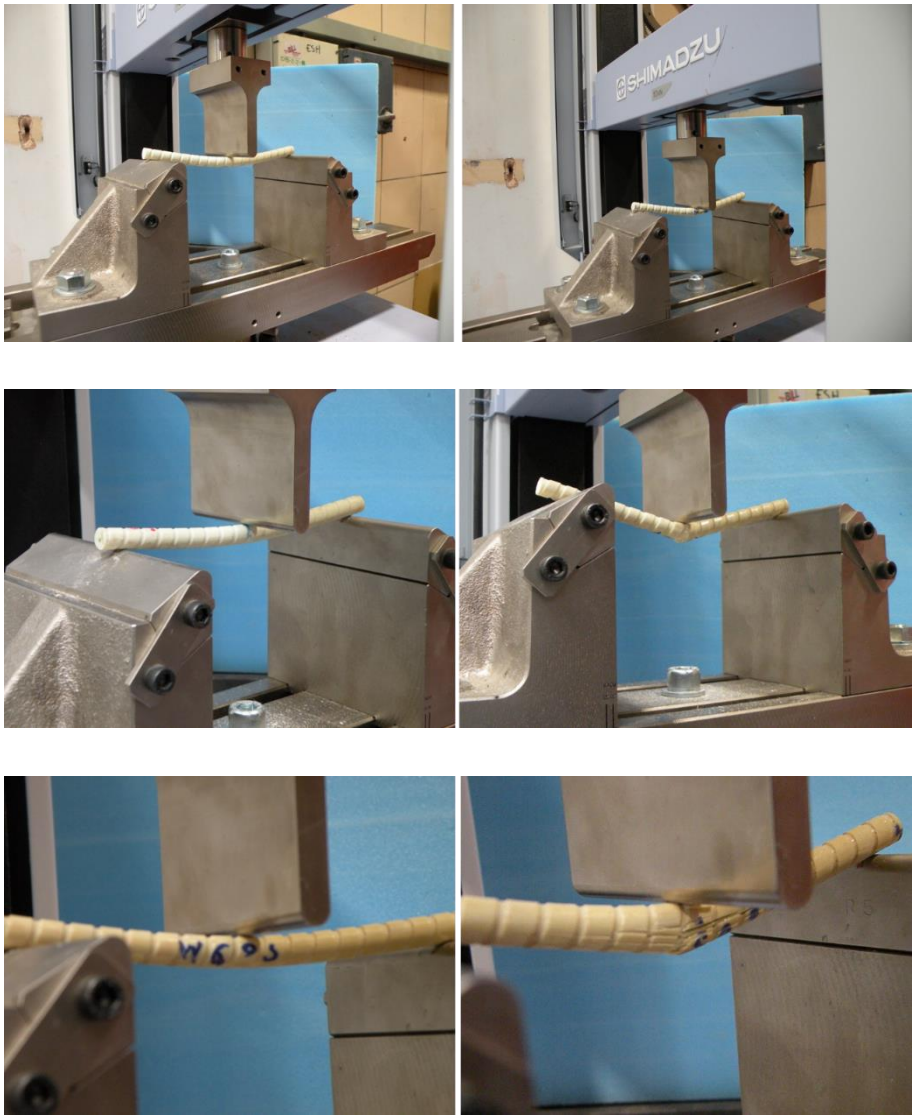
SHIMADZU
W6 D3

APPENDIX II

PHYSICAL AND CHEMICAL ANALYSIS AND MEASURED PROPERTIES

1. Moisture absorption data for GFRP bars

This section presents additional data obtained from gain weight tests. This data includes absorption rate-time diagrams for GFRP bars in different solution at different level of temperature, summary of measurement data and the pictures of examined specimens for both conditioned ones with and without stress.

Specimens are immersed in tap water (W)

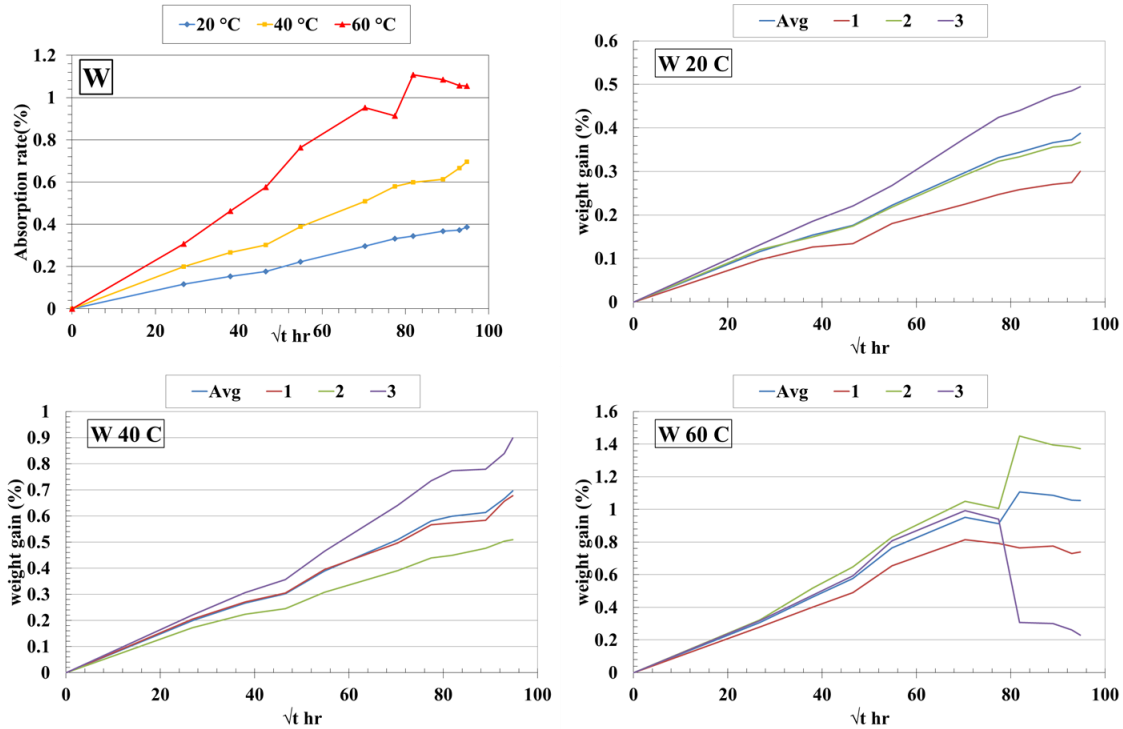

Figure.II.1 Absorption rate of specimens conditioned in water (W)

Table II.1: A summary of weight gain test results of GFRP specimen (Water 20°C)

Time $(\sqrt{t})$	Moisture gain			
	ava	**1**	**2**	**3**
0.00	0.00	0.00	0.00	0.00
26.84	0.12	0.10	0.12	0.13
37.95	0.15	0.13	0.15	0.19
46.48	0.18	0.13	0.17	0.22
54.77	0.22	0.18	0.22	0.27
70.31	0.30	0.22	0.29	0.38
77.45	0.33	0.25	0.32	0.42
81.85	0.34	0.26	0.33	0.44
88.99	0.37	0.27	0.36	0.47
92.95	0.37	0.27	0.36	0.49
94.74	0.39	0.30	0.37	0.49

Table II.2: A summary of weight gain test results of GFRP specimen (Water 40°C)

Time $(\sqrt{t})$	Moisture gain			
	ava	**1**	**2**	**3**
0.00	0.00	0.00	0.00	0.00
26.84	0.20	0.20	0.17	0.22
37.95	0.27	0.27	0.22	0.31
46.48	0.30	0.30	0.24	0.36
54.77	0.39	0.40	0.31	0.46
70.31	0.51	0.50	0.39	0.64
77.45	0.58	0.57	0.44	0.73
81.85	0.60	0.57	0.45	0.77
88.99	0.61	0.58	0.48	0.78
92.95	0.67	0.66	0.50	0.84
94.74	0.70	0.68	0.51	0.90

Table II.3: A summary of weight gain test results of GFRP specimen (Water 60°C)

Time $(\sqrt{t})$	Moisture gain			
	ava	**1**	**2**	**3**
0	0.00	0.00	0.00	0.00
26.84	0.31	0.28	0.32	0.32
37.95	0.46	0.40	0.52	0.47
46.48	0.58	0.49	0.65	0.59
54.77	0.76	0.65	0.83	0.81
70.31	0.95	0.82	1.05	0.99
77.45	0.91	0.79	1.01	0.94
81.85	1.11	0.76	1.45	0.31
88.99	1.09	0.78	1.40	0.30
92.95	1.06	0.73	1.38	0.26
94.74	1.05	0.74	1.37	0.23

Specimens are immersed in tap water (W-S)

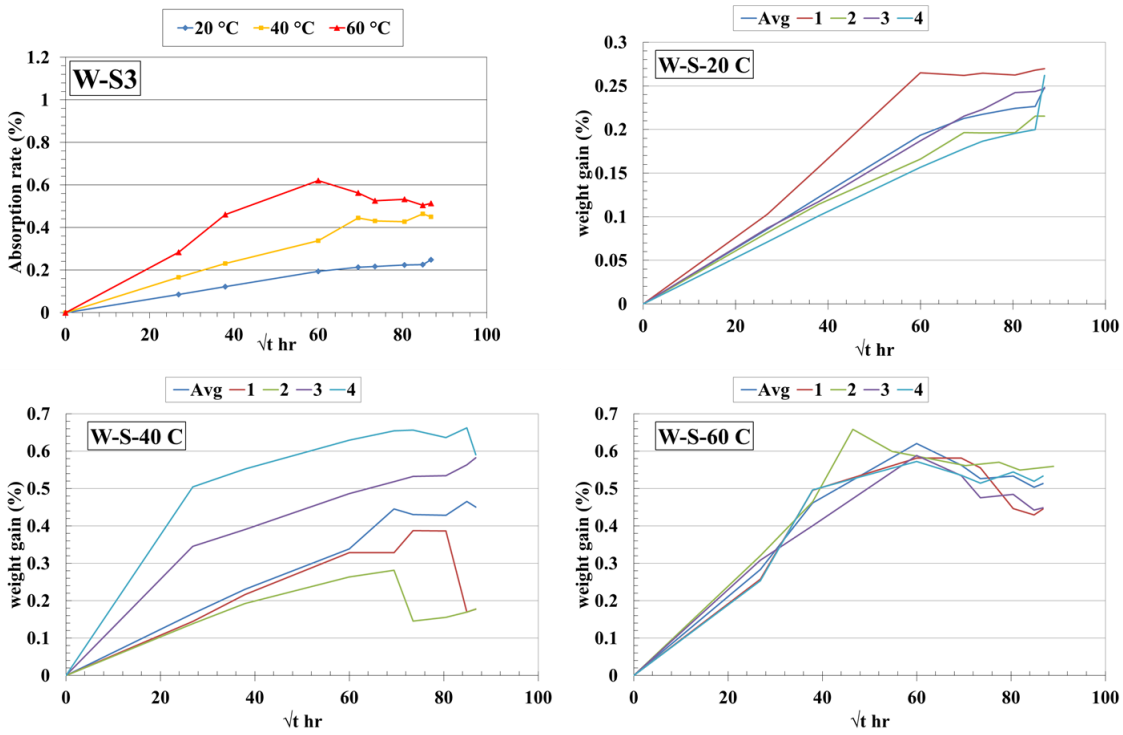

Figure.II.2 Absorption rate of specimens conditioned in water (W)

Table II.4: A summary of weight gain test results of GFRP specimen (Water-S3-20°C)

Time $(\sqrt{t})$	Moisture gain				
	ava	1	2	3	4
0.00	0.00	0.00	0.00	0.00	0.00
26.84	0.09	0.10	0.08	0.09	0.07
37.95	0.12	0.16	0.11	0.12	0.10
60.00	0.19	0.26	0.17	0.19	0.16
69.45	0.21	0.26	0.20	0.22	0.18
73.48	0.22	0.26	0.20	0.22	0.19
80.49	0.22	0.26	0.20	0.24	0.20
84.85	0.23	0.27	0.22	0.24	0.20
86.81	0.25	0.27	0.22	0.25	0.26

Table II.5: A summary of weight gain test results of GFRP specimen (Water-S3-40°C)

Time $(\sqrt{t})$	Moisture gain				
	ava	**1**	**2**	**3**	**4**
0.00	0.00	0.00	0.00	0.00	0.00
26.84	0.17	0.14	0.14	0.35	0.50
37.95	0.23	0.22	0.19	0.39	0.55
60.00	0.34	0.33	0.26	0.49	0.63
69.45	0.45	0.33	0.28	0.52	0.65
73.48	0.43	0.39	0.15	0.53	0.66
80.49	0.43	0.39	0.16	0.53	0.64
84.85	0.47	0.17	0.17	0.56	0.66
86.81	0.45	0.18	0.18	0.58	0.59

Table II.6: A summary of weight gain test results of GFRP specimen (Water –S3-60°C)

Time $(\sqrt{t})$	Moisture gain				
	ava	**1**	**2**	**3**	**4**
0.00	0.00	0.00	0.00	0.00	0.00
26.84	0.28	0.26	0.32	0.31	0.25
37.95	0.46	0.50	0.46	0.40	0.50
60.00	0.62	0.58	0.66	0.59	0.57
69.45	0.56	0.58	0.60	0.53	0.54
73.48	0.53	0.56	0.56	0.48	0.51
80.49	0.53	0.45	0.57	0.48	0.54
84.85	0.50	0.43	0.55	0.44	0.52
86.81	0.51	0.45	0.56	0.45	0.53

Specimens are immersed in alkaline solution (K)

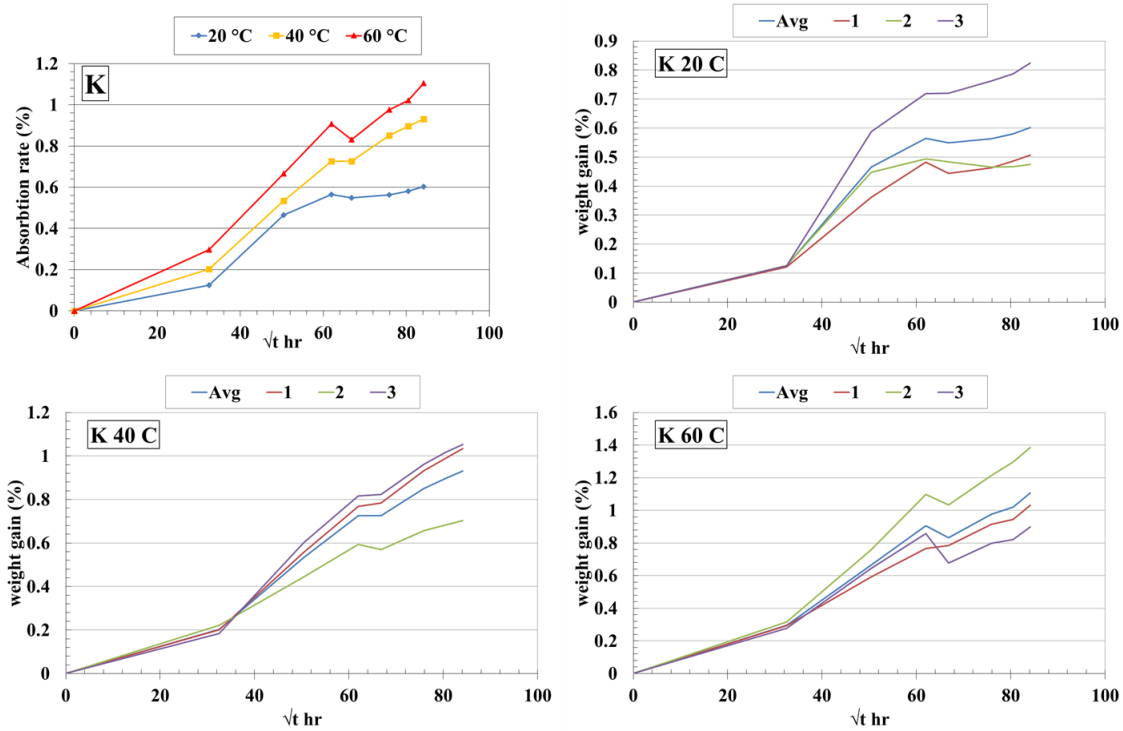

Figure.II.3 Absorption rate of specimens conditioned in alkaline solution (K)

Table II.7: A summary of weight gain test results of GFRP specimen (alkaline solution 20°C)

Time $(\sqrt{t})$	Moisture gain			
	ava	1	2	3
0.00	0.00	0.00	0.00	0.00
32.50	0.12	0.12	0.13	0.13
50.44	0.47	0.36	0.45	0.59
61.96	0.56	0.48	0.49	0.72
66.81	0.55	0.44	0.48	0.72
75.89	0.56	0.46	0.47	0.76
80.49	0.58	0.49	0.47	0.79
84.14	0.60	0.51	0.47	0.82

Table II.8: A summary of weight gain test results of GFRP specimen (alkaline solution 40°C)

Time $(\sqrt{t})$	Moisture gain			
	ava	1	2	3
0.00	0.00	0.00	0.00	0.00
32.50	0.20	0.20	0.22	0.18
50.44	0.53	0.56	0.44	0.60
61.96	0.73	0.77	0.59	0.82
66.81	0.73	0.78	0.57	0.82
75.89	0.85	0.93	0.66	0.96
80.49	0.90	0.99	0.68	1.02
84.14	0.93	1.03	0.70	1.05

Table II.9: A summary of weight gain test results of GFRP specimen (alkaline solution 60°C)

Time $(\sqrt{t})$	Moisture gain			
	ava	1	2	3
0.00	0.00	0.00	0.00	0.00
32.50	0.30	0.29	0.32	0.28
50.44	0.67	0.59	0.76	0.64
61.96	0.91	0.77	1.10	0.86
66.81	0.83	0.78	1.03	0.68
75.89	0.98	0.92	1.21	0.80
80.49	1.02	0.94	1.30	0.82
84.14	1.11	1.03	1.39	0.90

Specimens are immersed in alkaline solution (K-S)

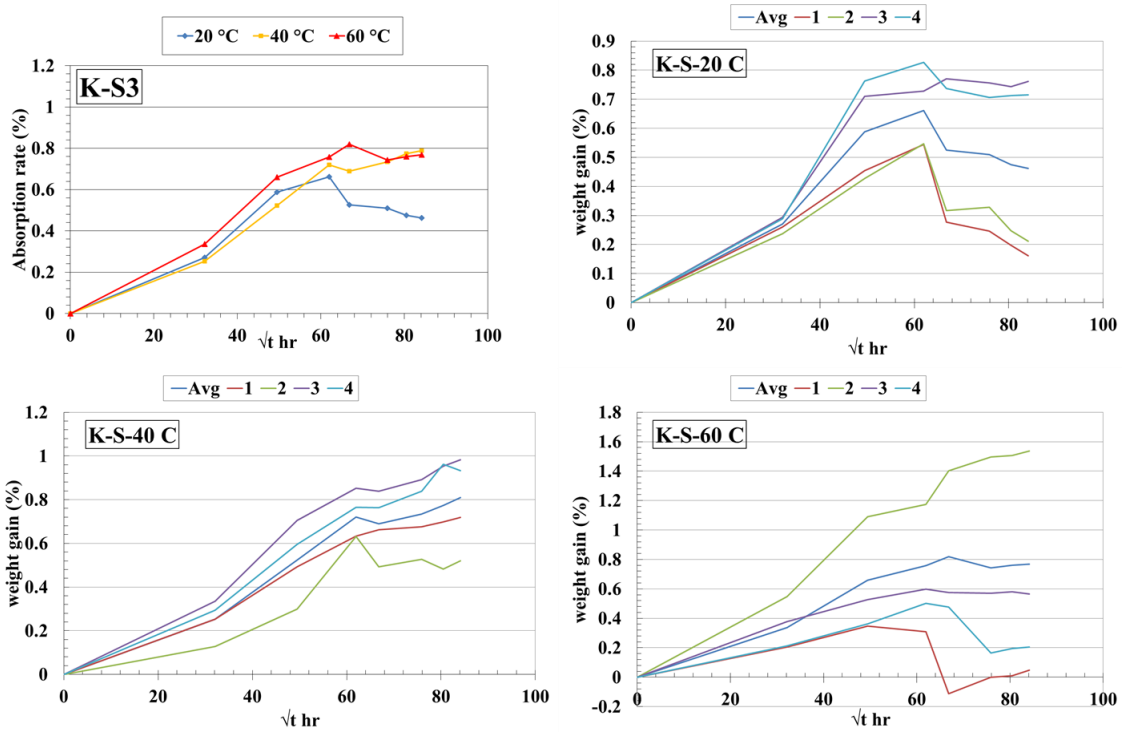

Figure.II.4 Absorption rate of specimens conditioned in water (K-S)

Table II.10: A summary of weight gain test results of GFRP specimen (alkaline solution S3-20°C)

Time $(\sqrt{t})$	Moisture gain				
	ava	1	2	3	4
0.00	0.00	0.00	0.00	0.00	0.00
32.12	0.27	0.26	0.24	0.29	0.29
49.48	0.59	0.45	0.43	0.71	0.76
61.96	0.66	0.54	0.55	0.73	0.83
66.81	0.53	0.28	0.32	0.77	0.74
75.89	0.51	0.25	0.33	0.76	0.71
80.49	0.48	0.20	0.25	0.74	0.71
84.14	0.46	0.16	0.21	0.76	0.72

Table II.11: A summary of weight gain test results of GFRP specimen (alkaline solution -S3-40°C)

Time $(\sqrt{t})$	Moisture gain				
	ava	**1**	**2**	**3**	**4**
0.00	0.00	0.00	0.00	0.00	0.00
32.12	0.25	0.25	0.13	0.33	0.29
49.48	0.52	0.49	0.30	0.71	0.59
61.96	0.72	0.63	0.63	0.85	0.76
66.81	0.69	0.66	0.49	0.84	0.76
75.89	0.73	0.68	0.53	0.89	0.84
80.49	0.77	0.70	0.48	0.95	0.96
84.14	0.81	0.72	0.52	0.98	0.93

Table II.12: A summary of weight gain test results of GFRP specimen (alkaline solution –S3-60°C)

Time $(\sqrt{t})$	Moisture gain				
	ava	**1**	**2**	**3**	**4**
0.00	0.00	0.00	0.00	0.00	0.00
32.12	0.34	0.21	0.55	0.38	0.21
49.48	0.66	0.35	1.09	0.53	0.36
61.96	0.76	0.31	1.17	0.60	0.50
66.81	0.82	-0.11	1.40	0.58	0.48
75.89	0.74	0.00	1.50	0.57	0.16
80.49	0.76	0.01	1.50	0.58	0.19
84.14	0.77	0.05	1.54	0.56	0.20

Photographs for tests specimens

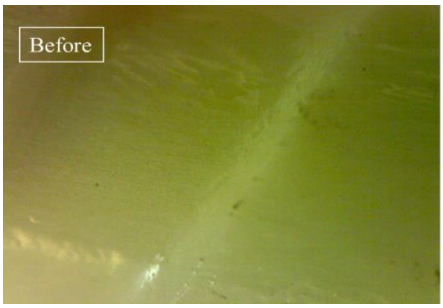

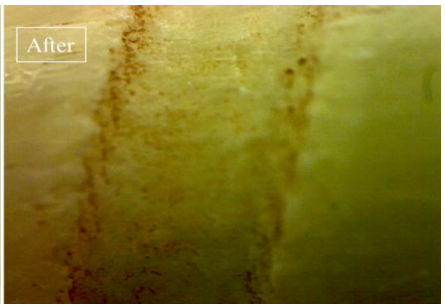

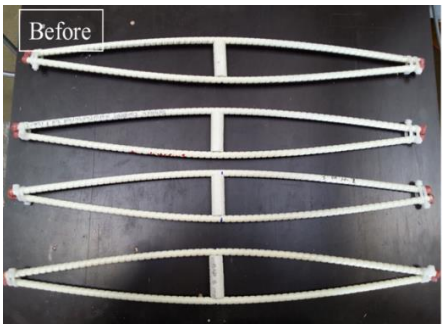

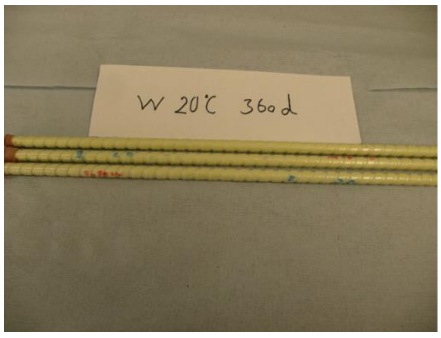

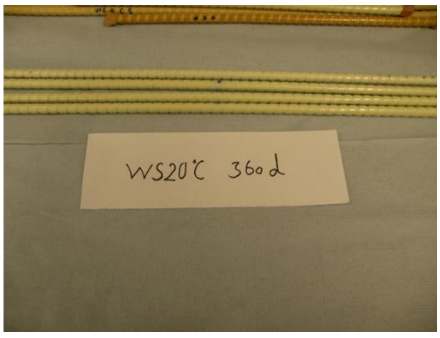

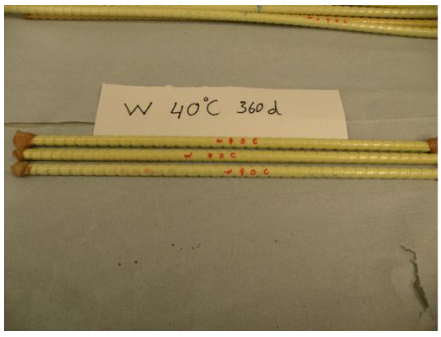

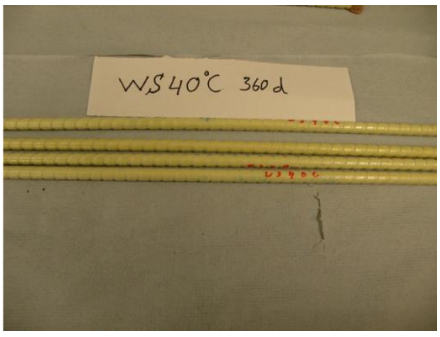

2. Dynamic mechanical analysis (DMA) data for GFRP bars

This section presents additional data obtained from DMA analysis to measure the change in Tg Glass transitions temperature. This data includes melting points diagrams for GFRP bars in different methods (i.e., Storage modulus and Tan Delta approaches). The tests carried out on both control and conditioned specimens.

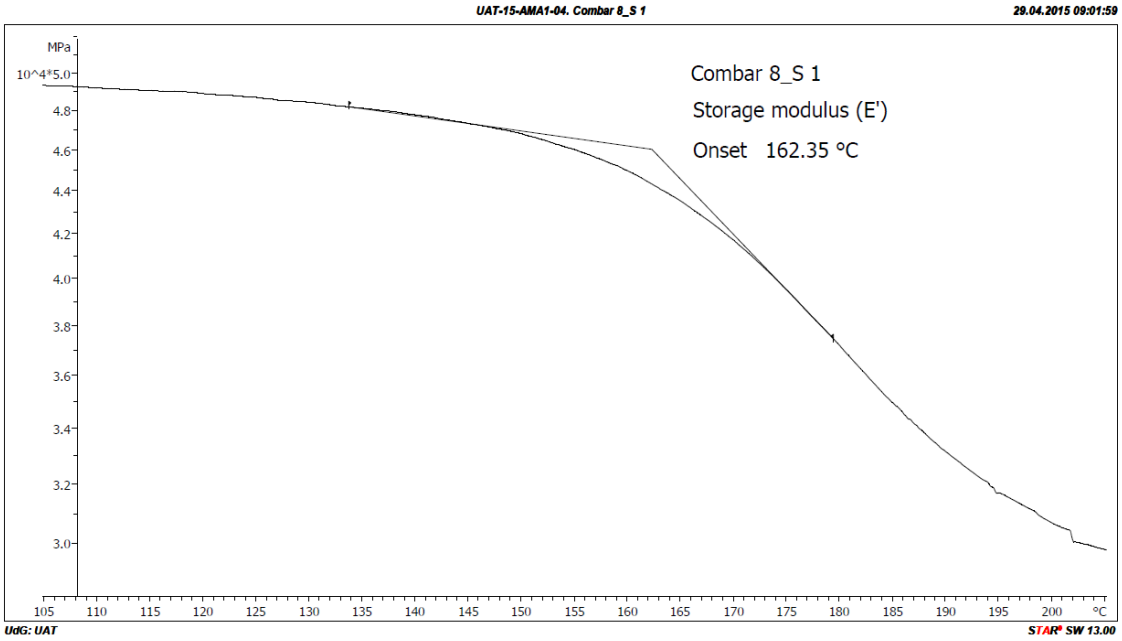

Figure.II.5 Tg of control specimens (1) by strong modulus.

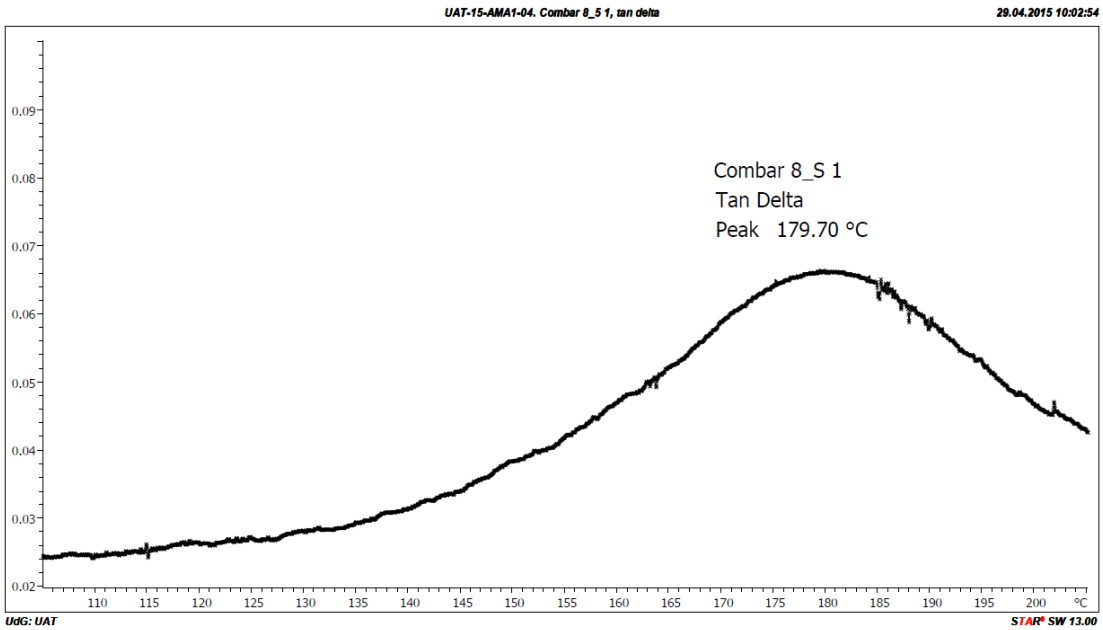

Figure.II.6 Tg of control specimens (1) by tan delta.

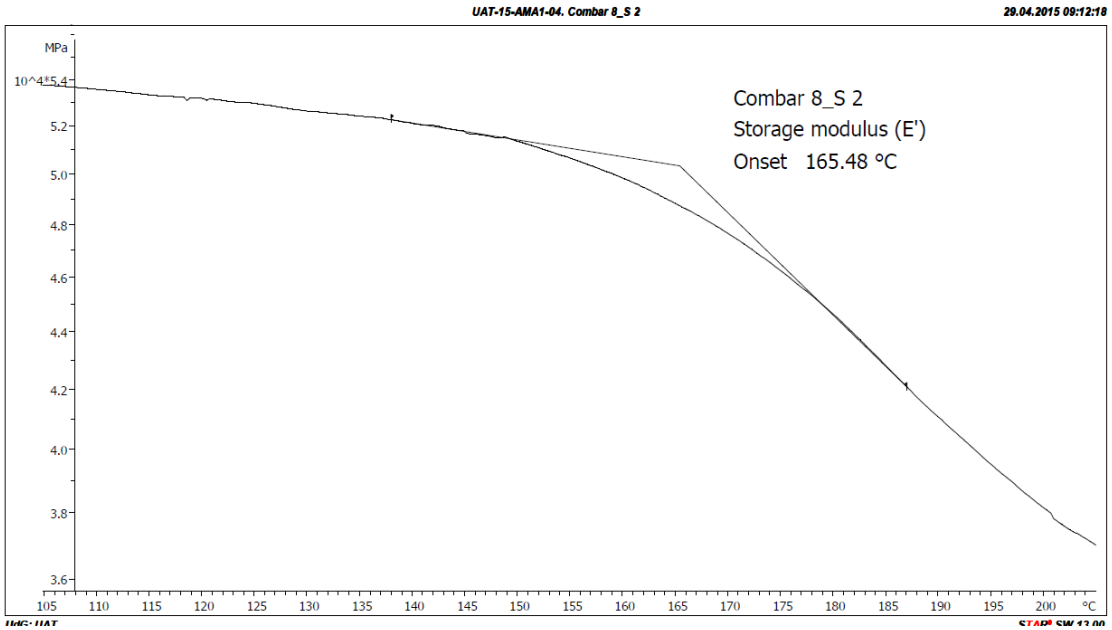

Figure.II.7 Tg of control specimens (2) by strong modulus.

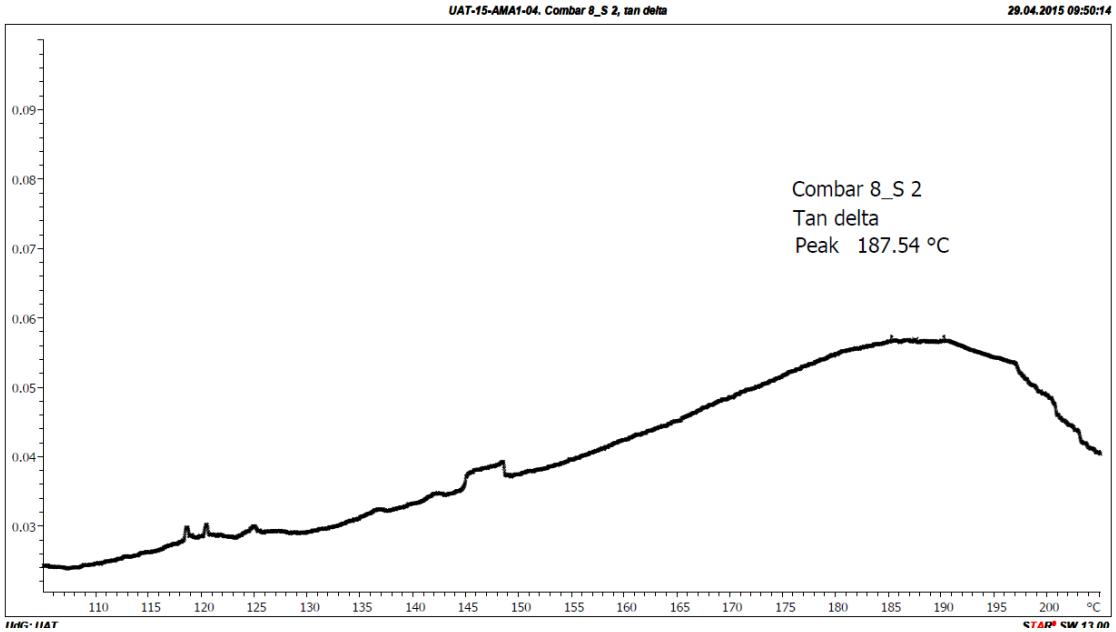

Figure.II.8 Tg of control specimens (2)by tan delta.

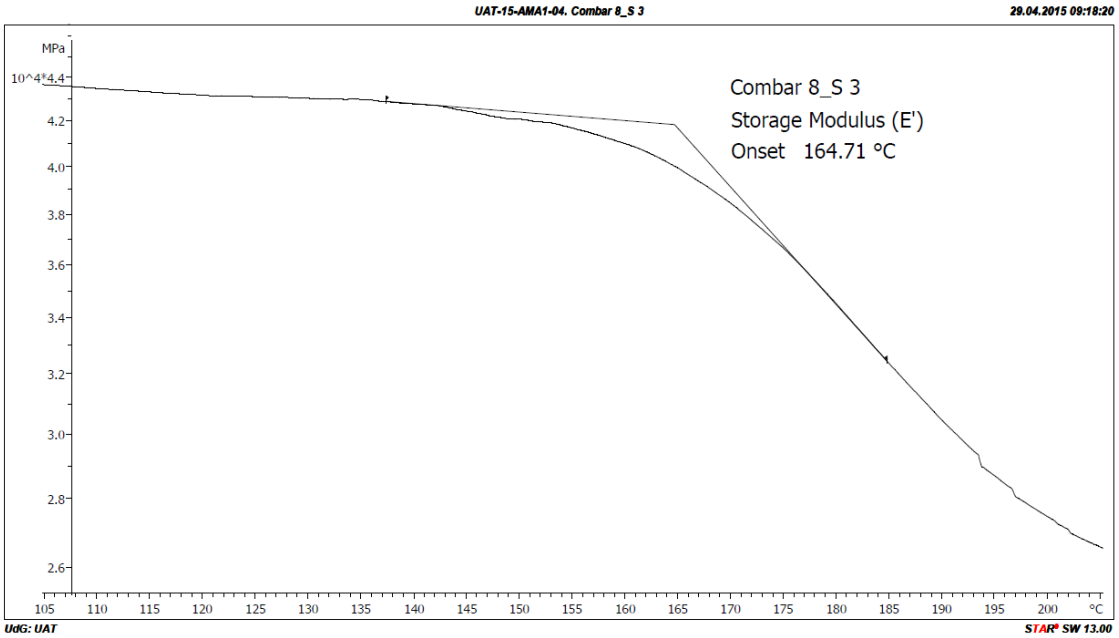

Figure.II.9 Tg of control specimens by strong modulus.

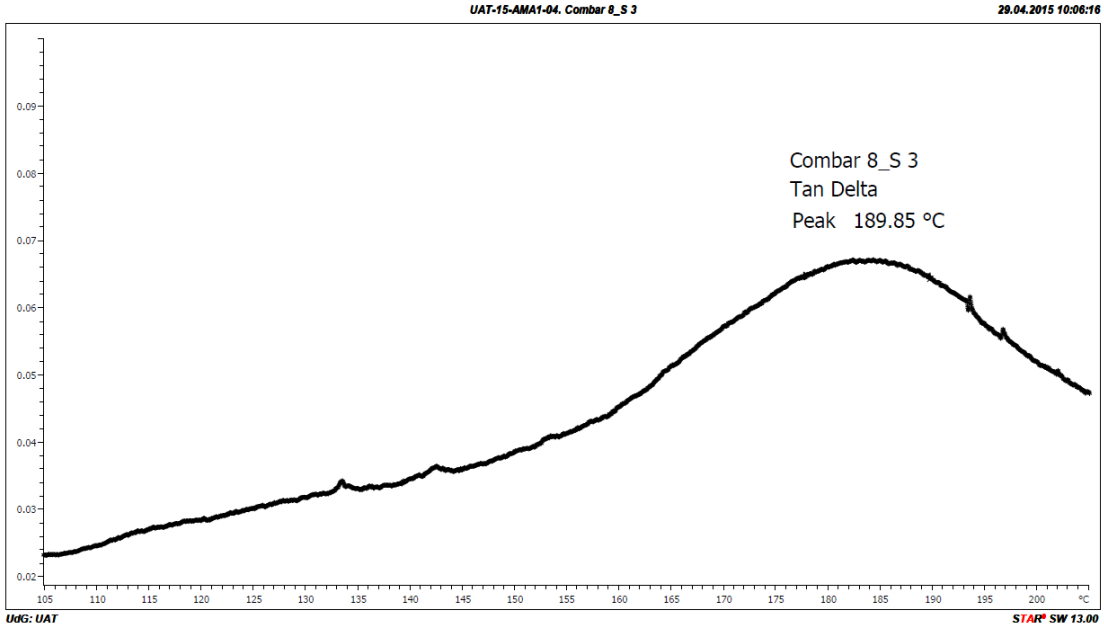

Figure.II.10 Tg of control (3) specimens by tan delta.

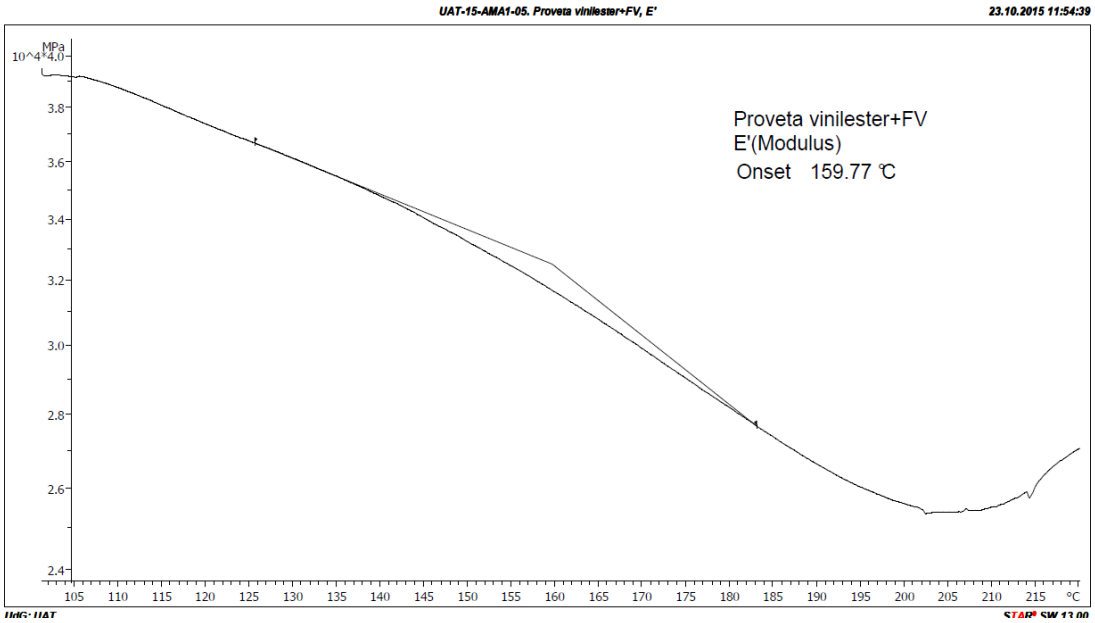

Figure.II.11 Tg of control specimens by strong modulus.

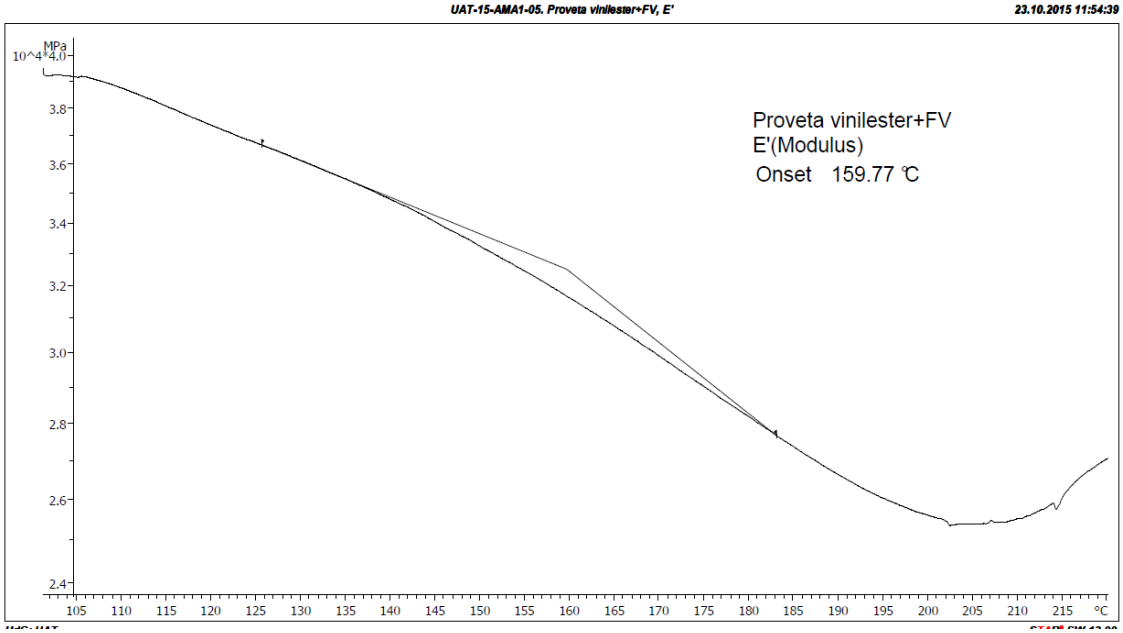

Figure.II.12 Tg of conditioned specimens by strong modulus.

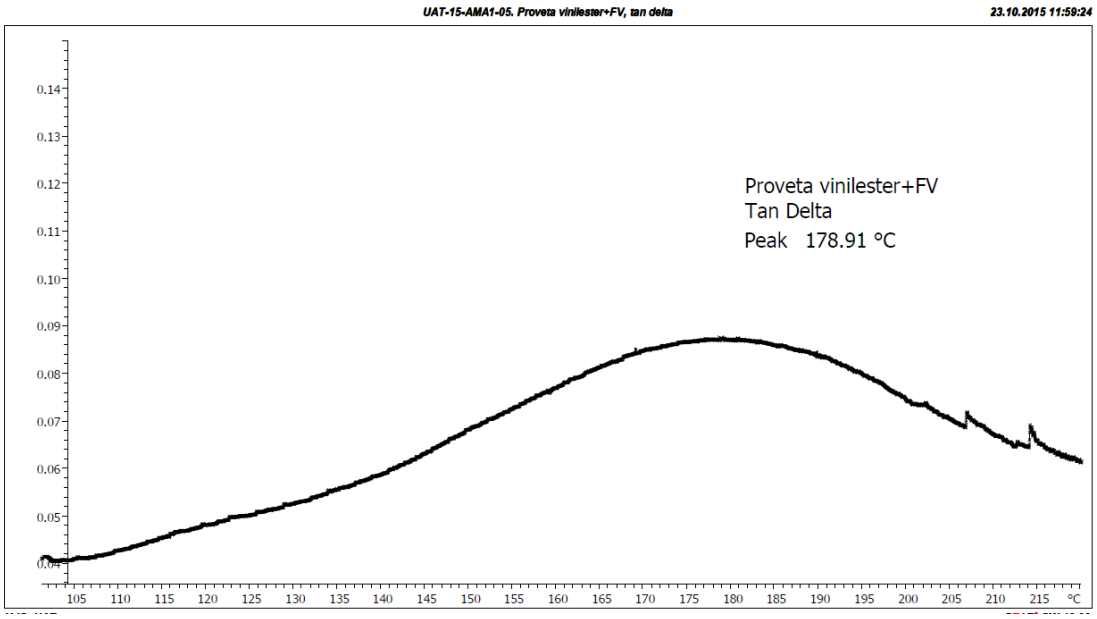

Figure.II.13 Tg of conditioned specimens by tan delta.

Photographs for test setup specimens

Figure.II.14: Tg test setup

3 Scanning electron microscope (SEM) images for GFRP bars

This section presents additional images obtained from SEM technique to assess the change in microstructure of control and conditioned samples.

Figure.II.15: SEM specimens at different conditions and time

Figure.II.16: SEM specimens at different conditions and time

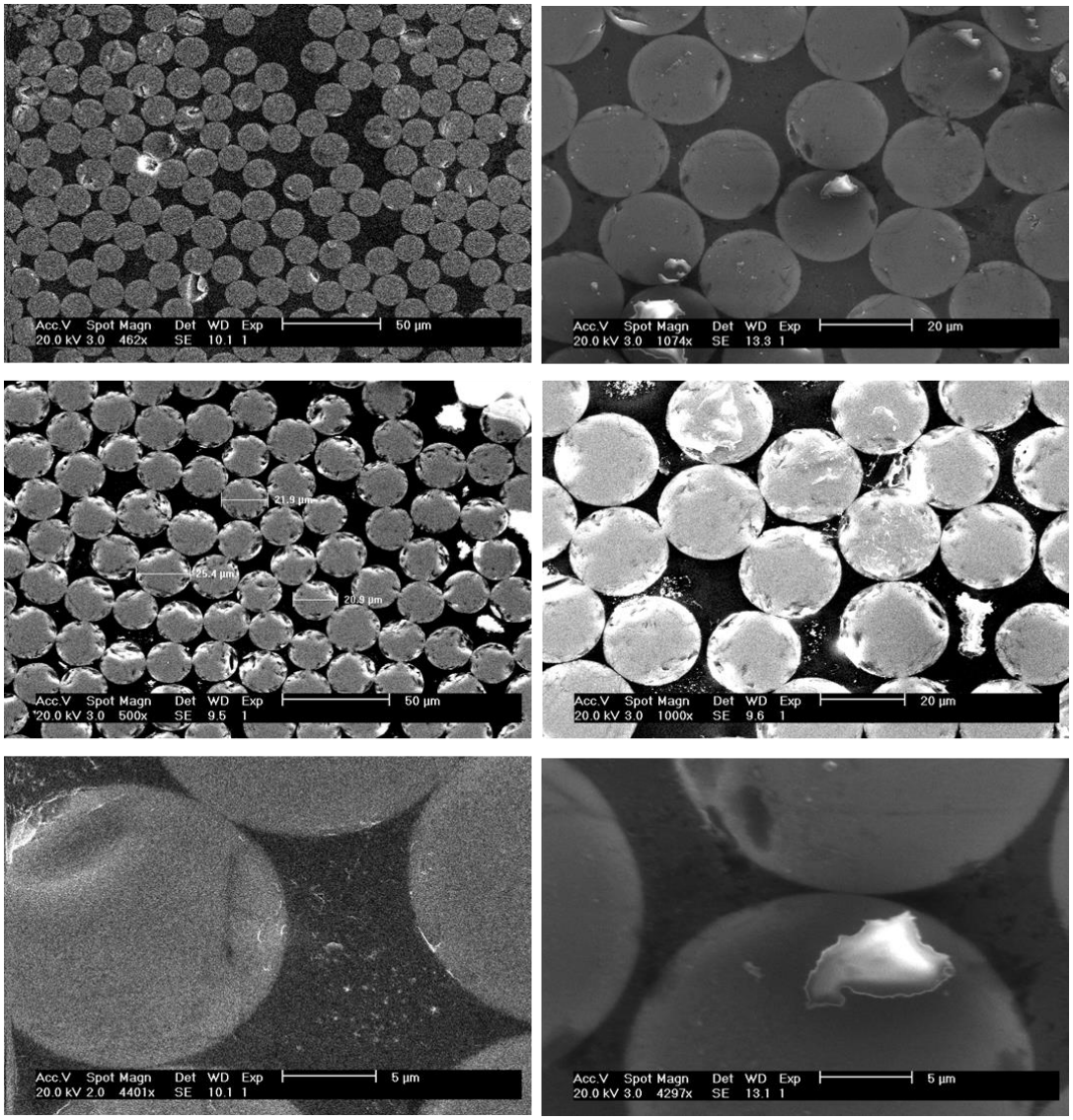

Figure.II.17: SEM images of the cross-sections of control specimens

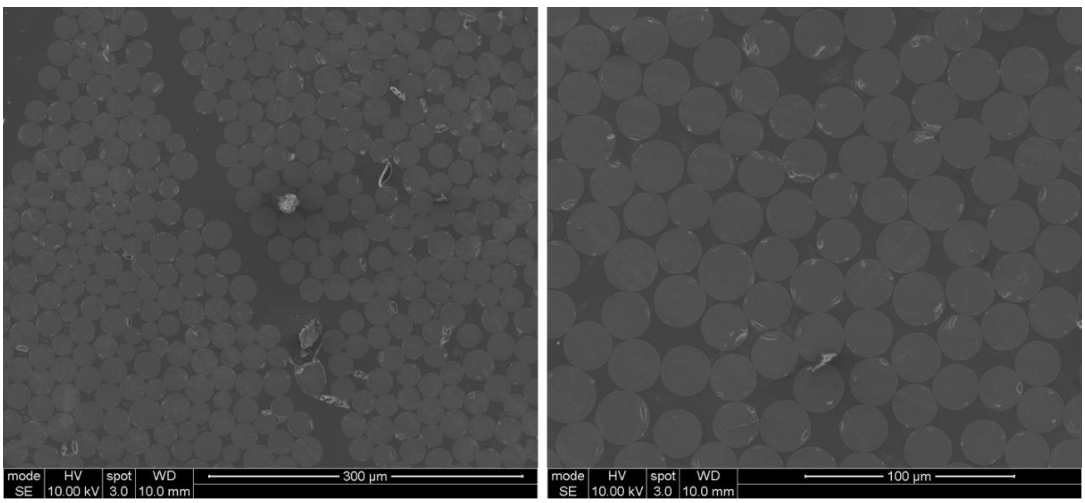

Figure.II.18: SEM images of the cross-sections of control specimens

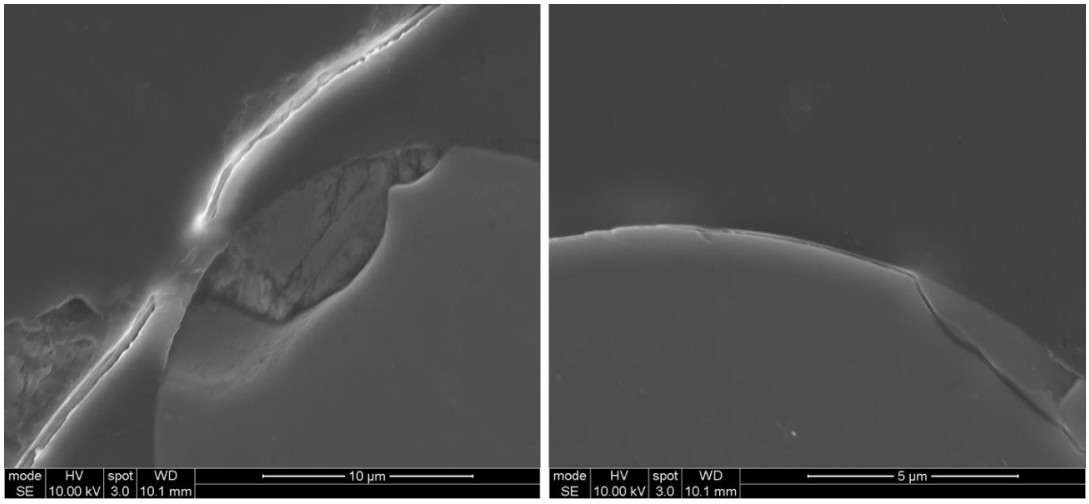

Figure.II.19: SEM images of the cross-sections of control specimen conditioned in water at 60°C for 1 year

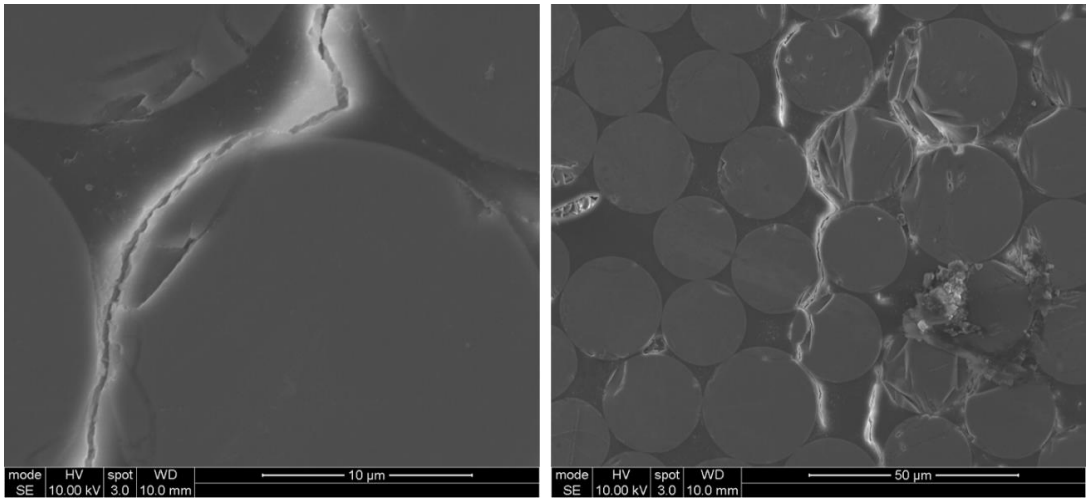

Figure.II.20: SEM images of the cross-sections of specimen conditioned in water under stress at 60°C for

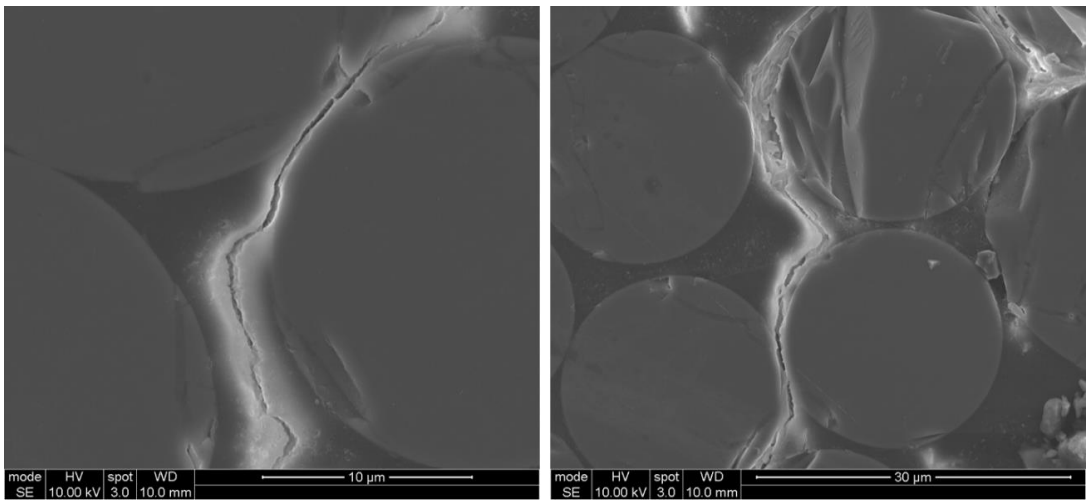

Figure.II.21: SEM images of the cross-sections of specimen conditioned in water under stress at 60°C for 1 year

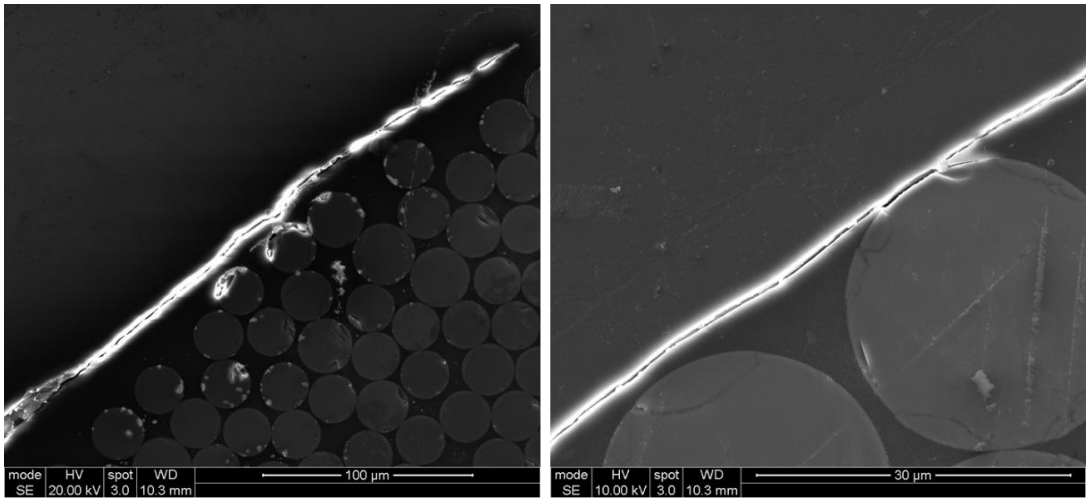

Figure.II.22: SEM images of the cross-sections of specimen conditioned in water at 60°C for 1 year

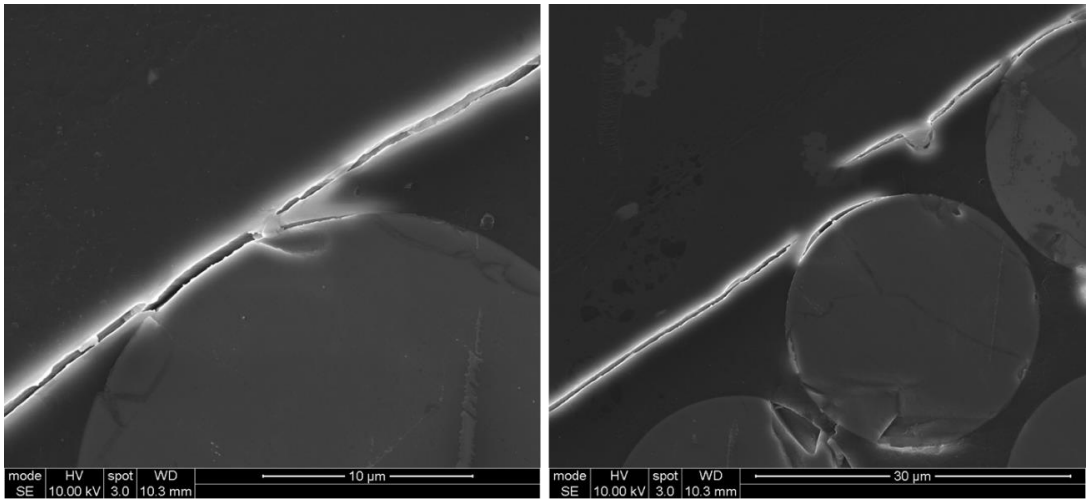

Figure.II.23: SEM images of the cross-sections of specimen conditioned in water at 60°C for 1 year

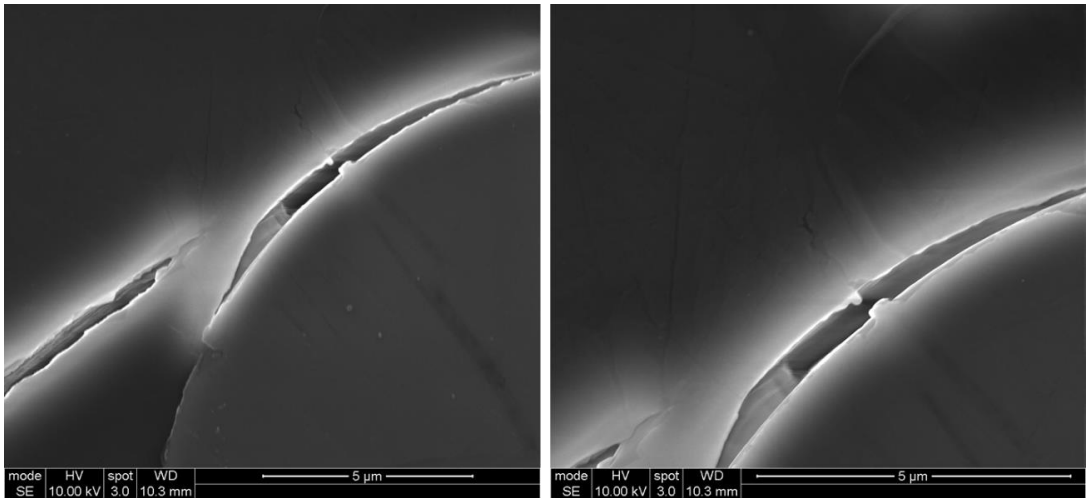

Figure.II.24: SEM images of the cross-sections of specimen conditioned in water at 60°C for 1 year

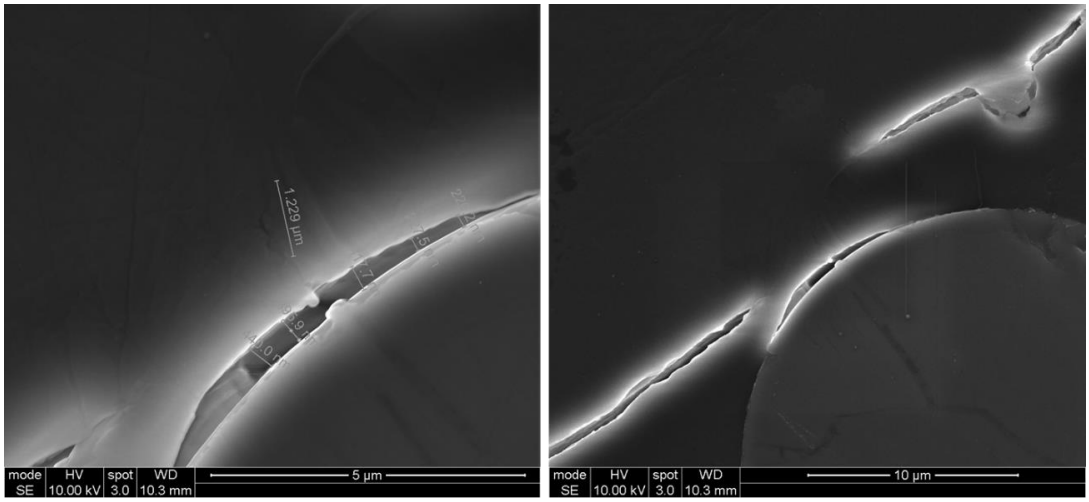

Figure.II.25: SEM images of the cross-sections of specimen conditioned in water at 60°C for 1 year

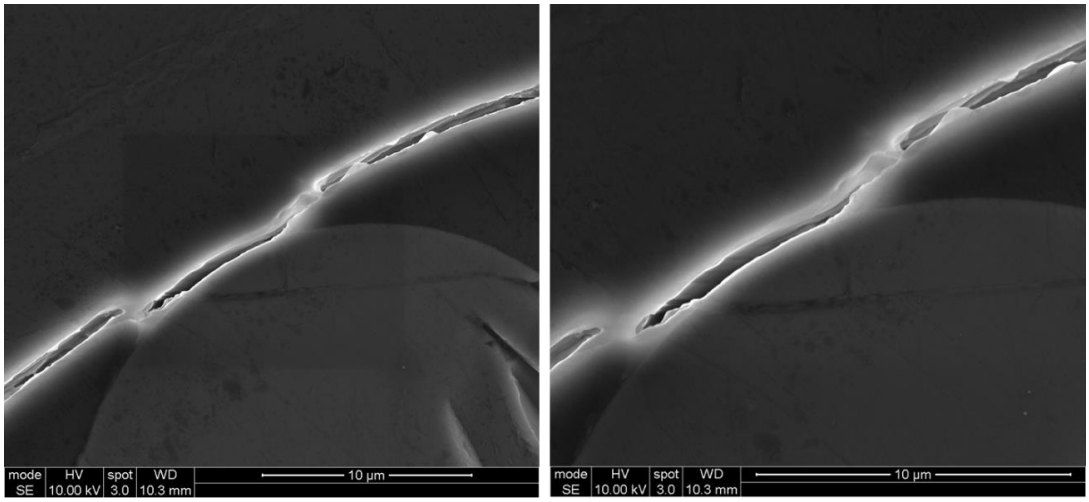

Figure.II.26: SEM images of the cross-sections of specimen conditioned in water at 60°C for 1 year

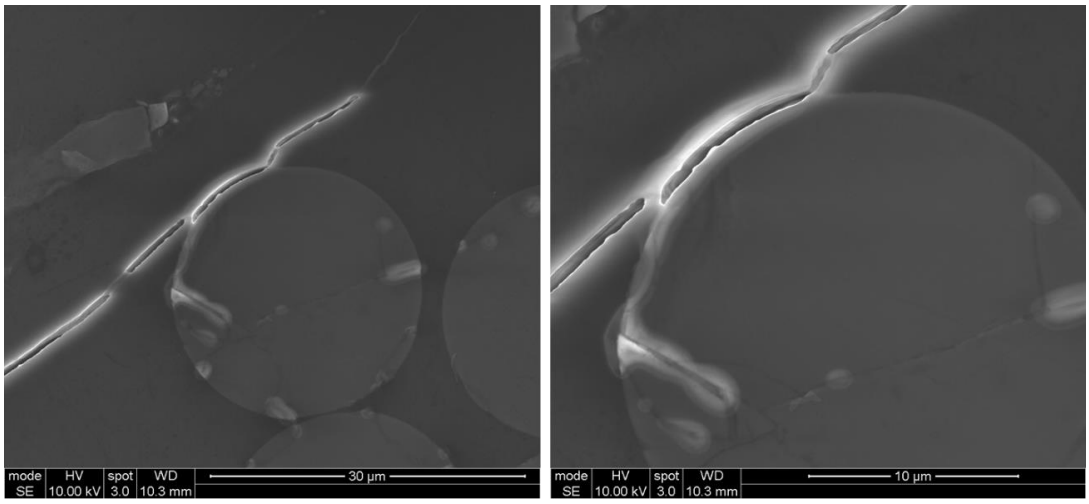

Figure.II.27: SEM images of the cross-sections of specimen conditioned in water at 60°C for 1 year

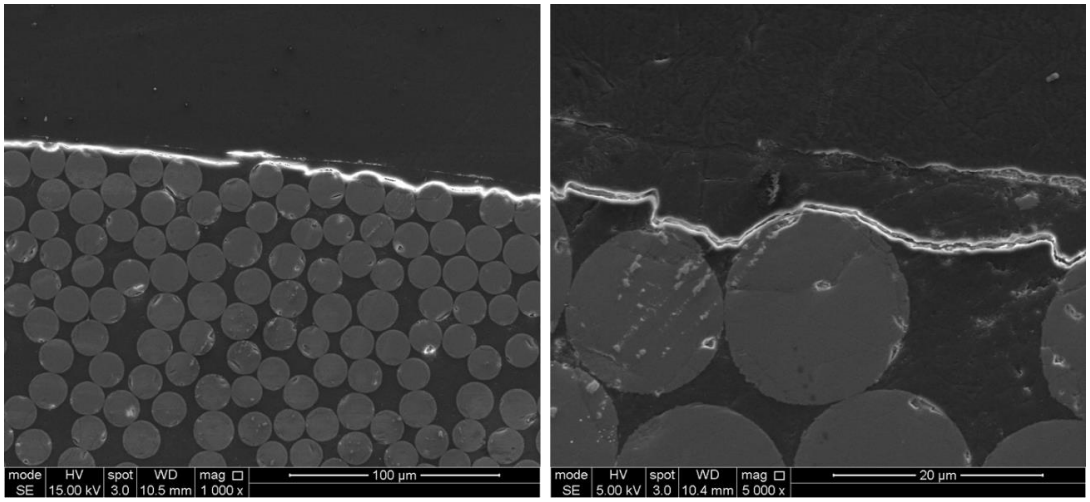

Figure.II.28: SEM images of the cross-sections of specimen conditioned in alkaline solution at 60°C for 1 year

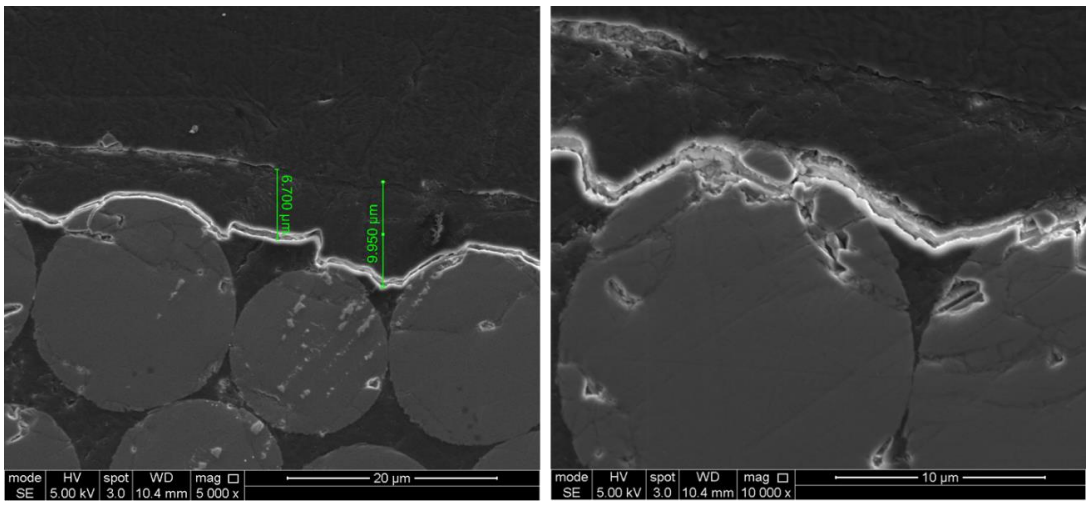

Figure.II.29: SEM images of the cross-sections of specimen conditioned in alkaline solution at 60°C for 1 year

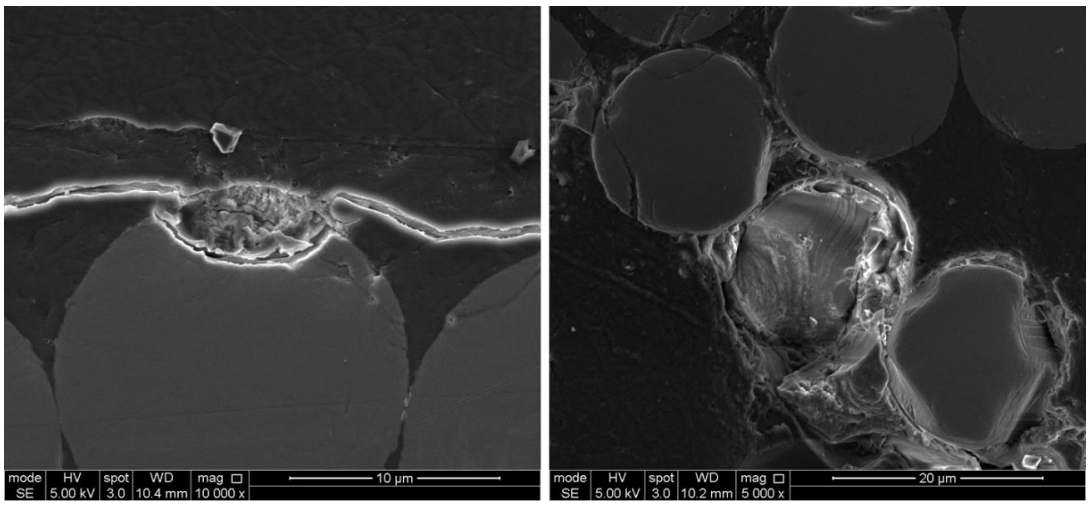

Figure.II.30: SEM images of the cross-sections of specimen conditioned in alkaline solution at 60°C for 1 year

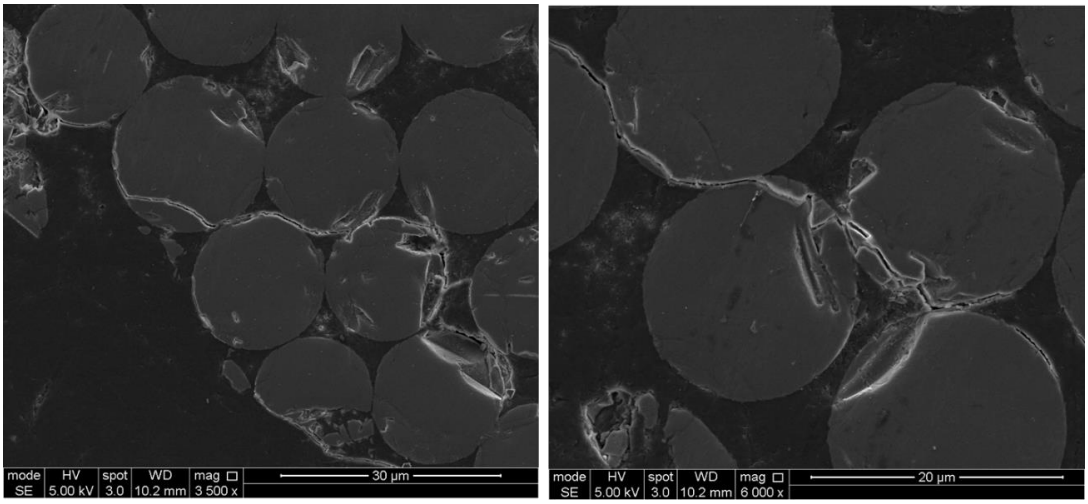

Figure.II.31: SEM images of the cross-sections of specimen conditioned in alkaline solution under stress at 60°C for 1 year

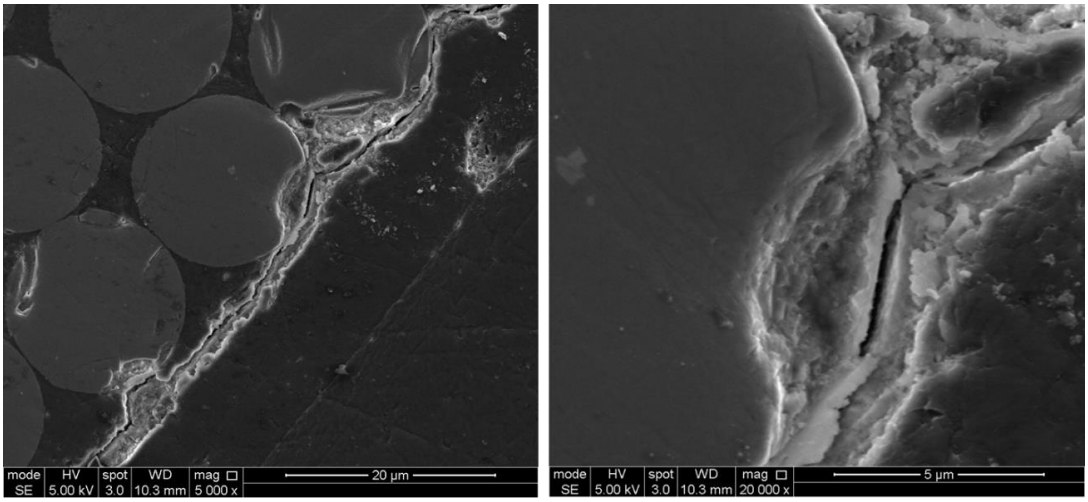

Figure.II.32: SEM images of the cross-sections of specimen conditioned in alkaline solution under stress at 60°C for 1 year

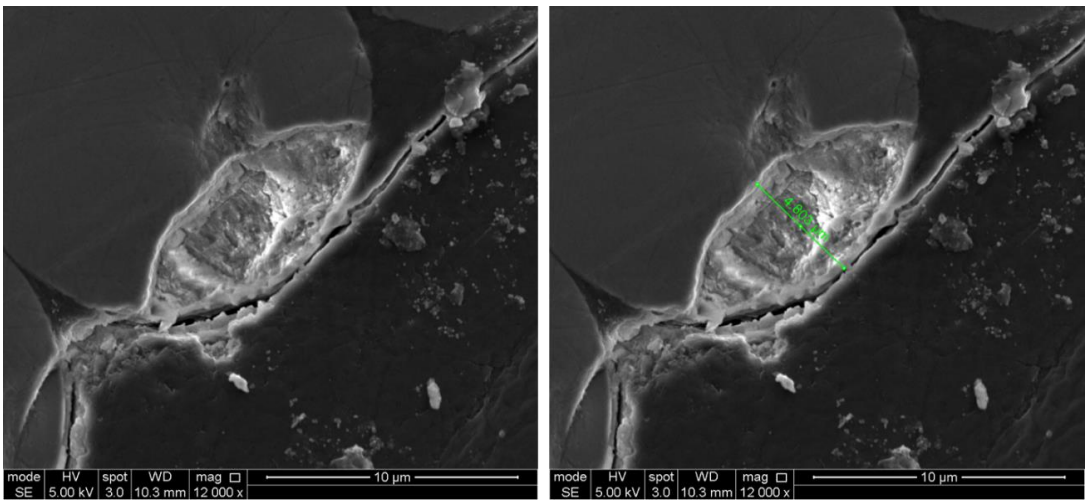

Figure.II.33: SEM images of the cross-sections of specimen conditioned in alkaline solution at 60°C for 1 year

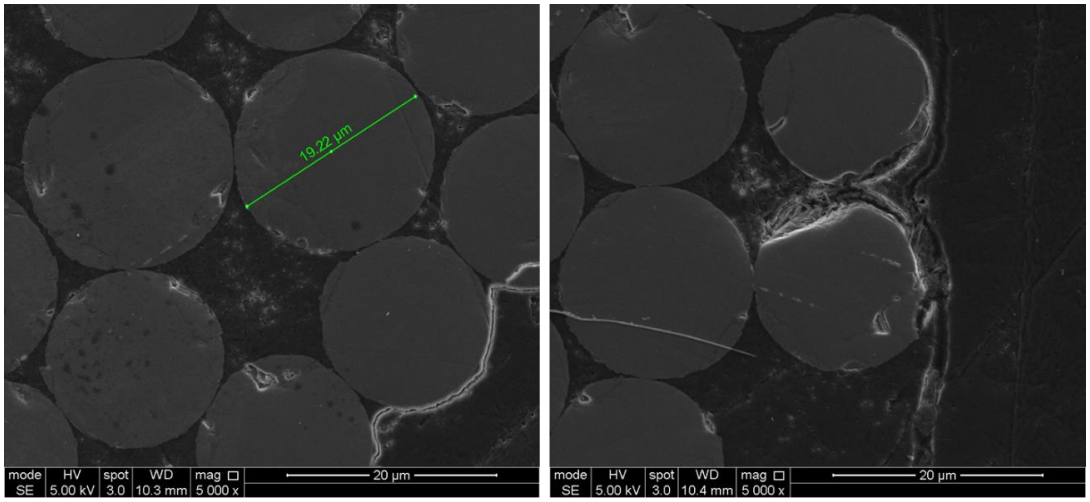

Figure.II.34: SEM images of the cross-sections of specimen conditioned in alkaline solution at 60°C for 1 year

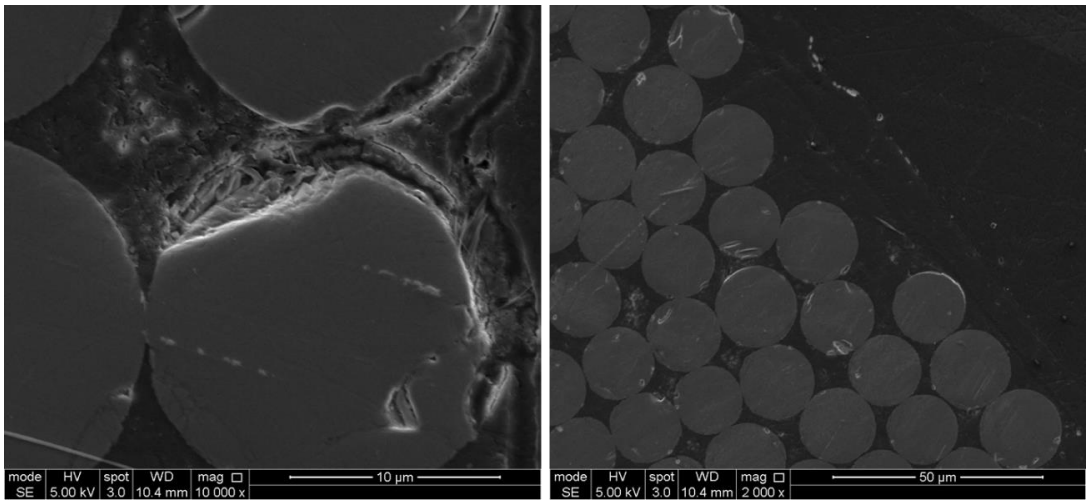

Figure.II.35: SEM images of the cross-sections of specimen conditioned in alkaline solution at 60°C for 1 year

4 Fourier Transform Infrared (FTIR) Spectroscopy for GFRP bars

This part presents data the interpretation of FTIR result obtained to investigate the change in chemical composition of rich resin matrix (vinyl ester) for control and conditioned samples.

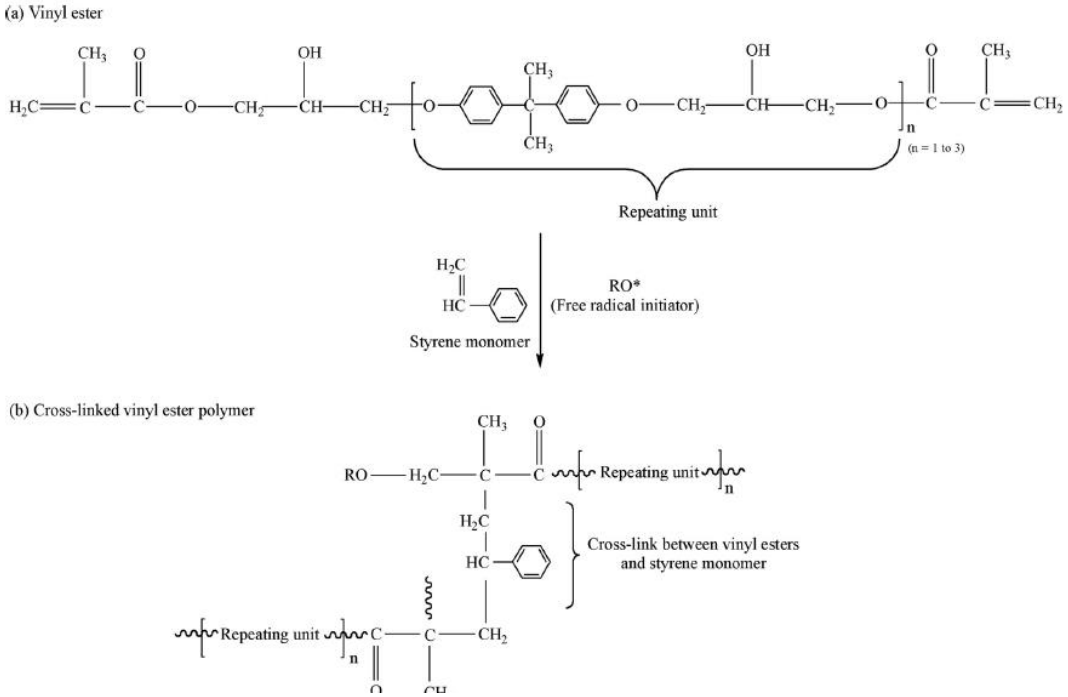

Figure.II.36: polymer ester chain of Vinyl ester

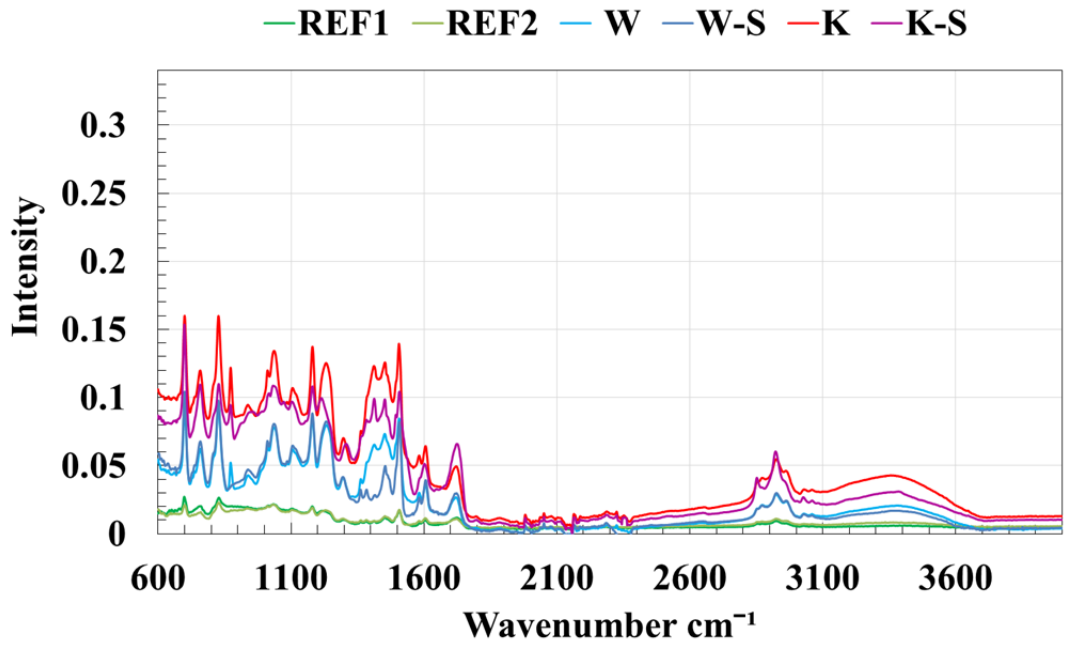

Figure.II.37: FTIR spectra for the resin matrix on the surface of GFRP bars

Table II.13: A summary of the peaks of conditioned and control specimens (outer layer).

Possible Assignment	REF1	W	W-S	K	K-S
OH-stretching vibration	3403	3394	3402	3356	3386
C-H stretching vibration	3029	3029	3027	3029	3026
C=O stretching	1724	1720	1723	1721	1724
C=C stretching vibration	1605	1606	1605	1606	1602
Aromatic ring stretch	1508	1507	1507	1506	1508
CH2 bend band	1454	1453	1454	1453	1453
CH3 bend band	1411	1413	1414	1412	1414
CH2 and CH3 scissor	1383	1363	1384	1378	1385
C-O stretch	1297	1295	1310	1297	1307
C—O—C stretching	1160	1165	1180	1180	1180
C=C stretch	936	938	936	938	946
Aromatic ring stretch or CH2 rocking	760	759	759	759	758

Table II.14: the peaks and possible band according to previous research.

FT-IR transmittance peaks of the alkaline aged and control GFRP rebars.

Possible assignment	Transmittance peak (cm^{-1})
OH stretching vibrations	3400
C—H stretch of the benzene ring	3026
CH, CH_2 and CH_3 stretch	2960/2927/2871
C =O stretch	1722
Aromatic ring stretch	1605/1581/1506
Aromatic ring stretch	1448
CH_2 and CH_3 scissor	1380
C—O stretch	1295
C—CO—C stretch	1160
C =C stretch	920
Aromatic ring stretch or CH_2 rocking	755

Table II.15: Band ratios results for FTIR analysis on the outer surface of the samples

REF **CURING INDEX**

OH/C-H	C=O/C-H	C-O/C-H	C=C/CH	CH2/C-H	CH3/C-H	C-CO-C/CH	C=C/CH
1.05	2.07	1.78	1.49	1.63	1.29	3.52	3.45

W

OH/C-H	C=O/C-H	C-O/C-H	C=C/CH	CH2/C-H	CH3/C-H	C-CO-C/CH	C=C/CH
1.40	1.82	2.80	2.46	1.96	1.43	5.84	2.91

W-S

OH/C-H	C=O/C-H	C-O/C-H	C=C/CH	CH2/C-H	CH3/C-H	C-CO-C/CH	C=C/CH
1.16	2.09	2.93	2.73	2.10	1.46	6.22	3.32

K

OH/C-H	C=O/C-H	C-O/C-H	C=C/CH	CH2/C-H	CH3/C-H	C-CO-C/CH	C=C/CH
1.32	1.52	2.16	1.97	1.68	1.26	4.22	2.89

K-S

OH/C-H	C=O/C-H	C-O/C-H	C=C/CH	CH2/C-H	CH3/C-H	C-CO-C/CH	C=C/CH
1.156	2.46	2.46	1.86	2.20	1.26	4.06	3.36

The FTIR tests result shows the hydrolysis of the ester linkages and it was clearer in unstressed samples.

The stressed samples has lower chemical interaction than unstressed samples.

The reduction in C=O confirmed the hydrolysis reaction as the end of Vinyl ester chain were breaked

Alkaline solution were more aggressive than water and cause more the breakage in ester chain of the tested specimens as result of more OH ions in alkaline

Curing index were increase as more repeating unite were connected to horizontal chain

The samples conditioned in Water has more C=C bond than the samples conditioned in alkaline because has less breakage in original chain and the residual C=C higher.

CH2-CH3 were increase as repeating units connected to horizontal chain

Oxidation reaction also were observed and C-O were increased by both hydrolysis reaction and oxidation reaction.

Stressed samples have higher C-O that may be because the stress open the path for oxygen and more penetration of oxygen inside

For the samples extracted for inside the bars there is no hydrolysis reaction observed but there is oxidation reaction take place.

The tests result show also curing index increase which is need more research in atomic level which is not my field

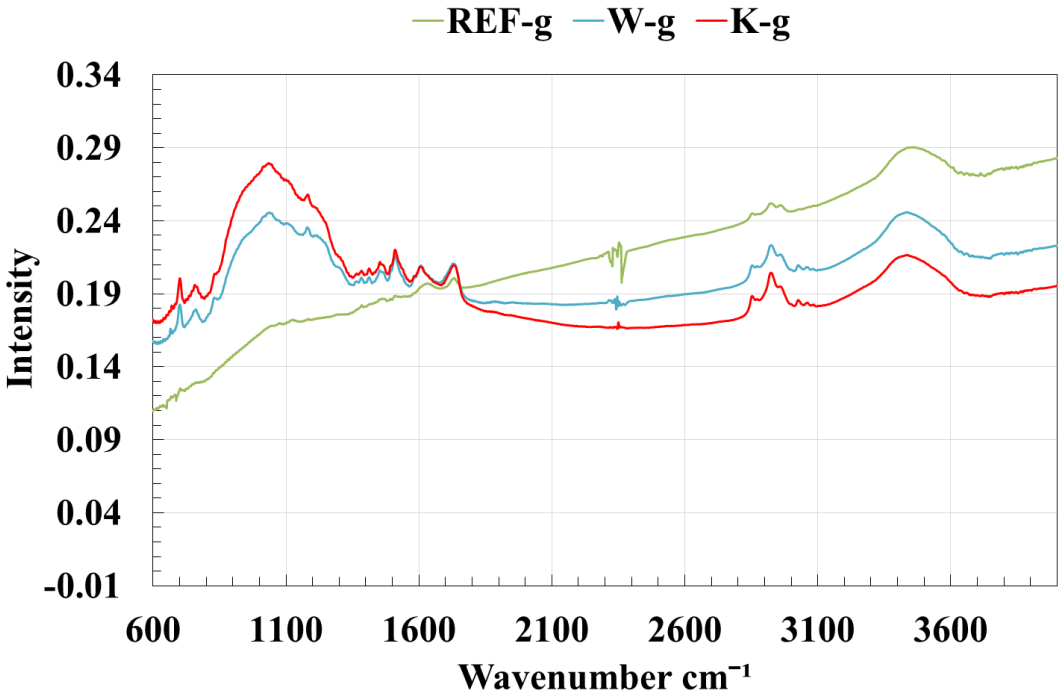

Figure.II.38: FTIR spectra for the core of GFRP bars

Table II.16: Band ratios results for FTIR analysis on the inner layer of the samples

REF-g			**CURING INDEX**				
OH/C-H	C=O/C-H	C-O/C-H	C=C/CH	CH2/C-H	CH3/C-H	C-CO-C/CH	C=C/CH
1.16	0.57	0.70	0.79	1.01	0.98	0.69	0.61

W-g							
OH/C-H	C=O/C-H	C-O/C-H	C=C/CH	CH2/C-H	CH3/C-H	C-CO-C/CH	C=C/CH
1.12	0.57	1.00	0.98	1.07	1.00	1.12	1.07

K-g							
OH/C-H	C=O/C-H	C-O/C-H	C=C/CH	CH2/C-H	CH3/C-H	C-CO-C/CH	C=C/CH
1.12	0.57	1.18	1.11	1.10	1.00	1.38	1.41

5 Energy dispersive X-Ray analysis (EDX) for GFRP bars

This part illustrated the EDX analysis obtained to provide the chemical elemental identification and quantitative the chemical composition of GFRP bars. The following unused data were apart of analysis data that used to indicate any chemical change in chemical composition of rich resin matrix (vinyl ester) and in glass fiber for control and conditioned samples.

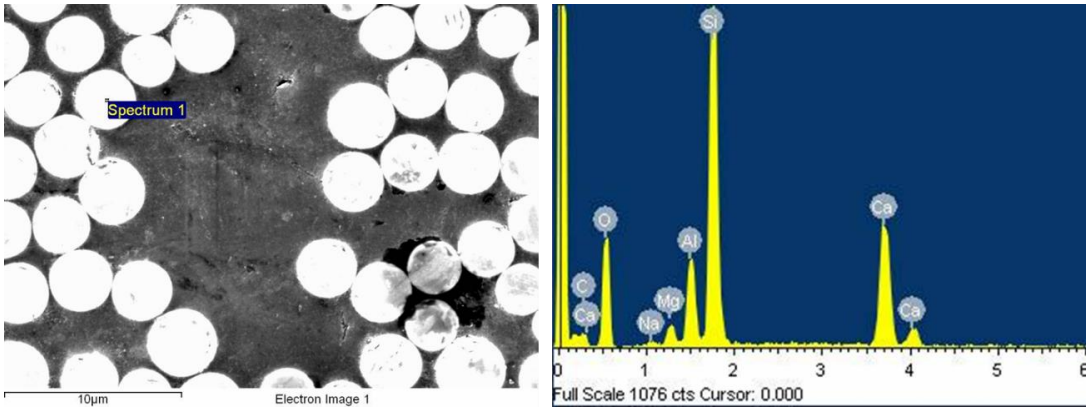

Figure.II.39: Results of EDX scans for specimens contol specimens (fibres).

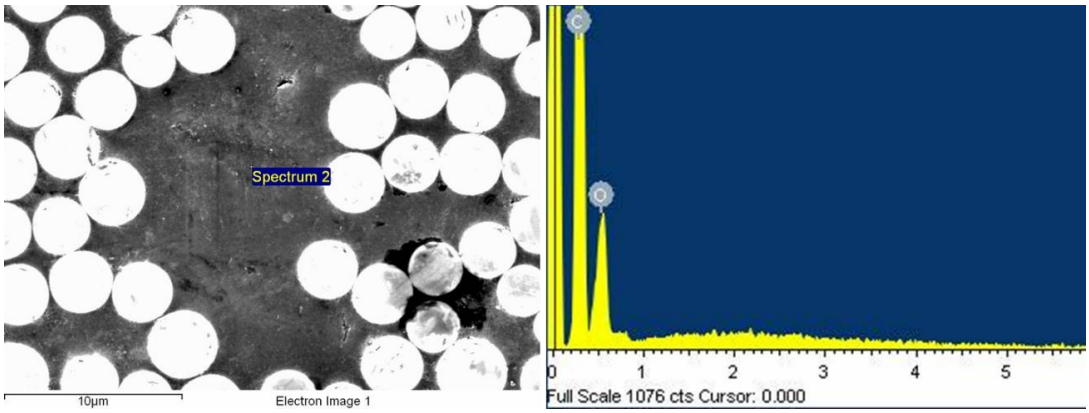

Figure.II.40: Results of EDX scans for specimens contol specimens (matrix).

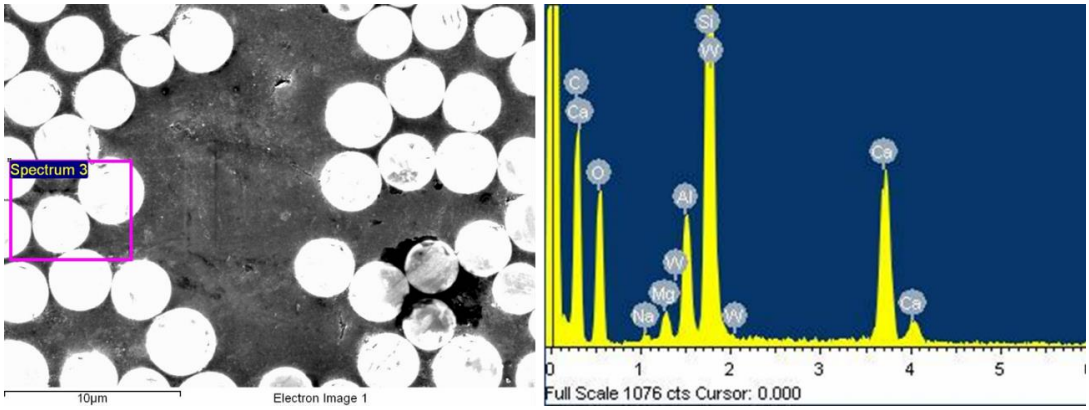

Figure.II.41: Results of EDX scans for specimens contol specimens (area).

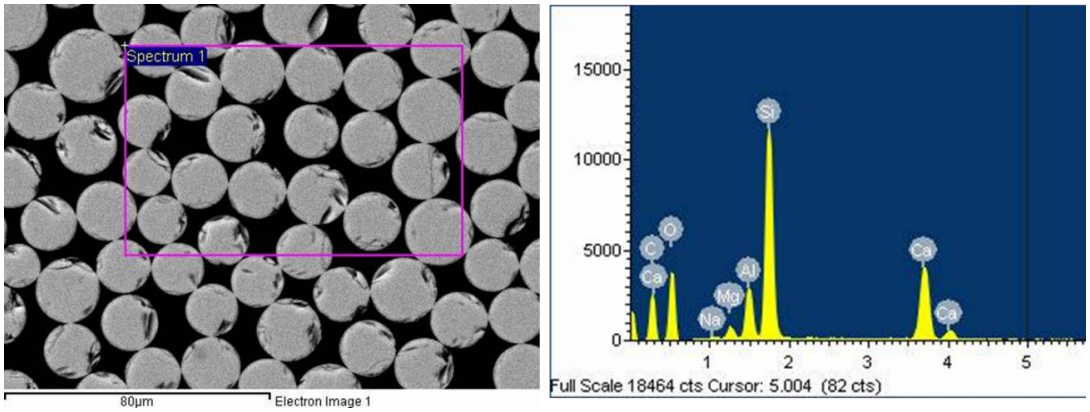

Figure.II.42: Results of EDX scans for specimens contol specimens (area).

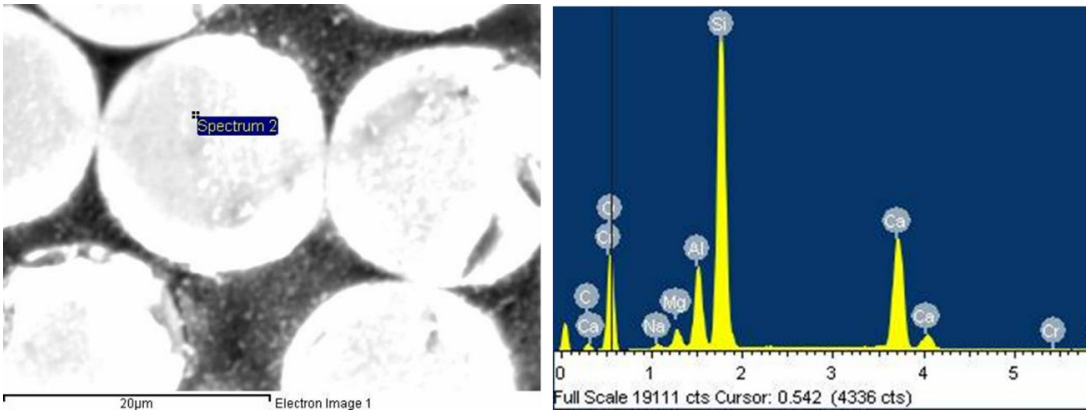

Figure.II.43: Results of EDX scans for specimens contol specimens (area).

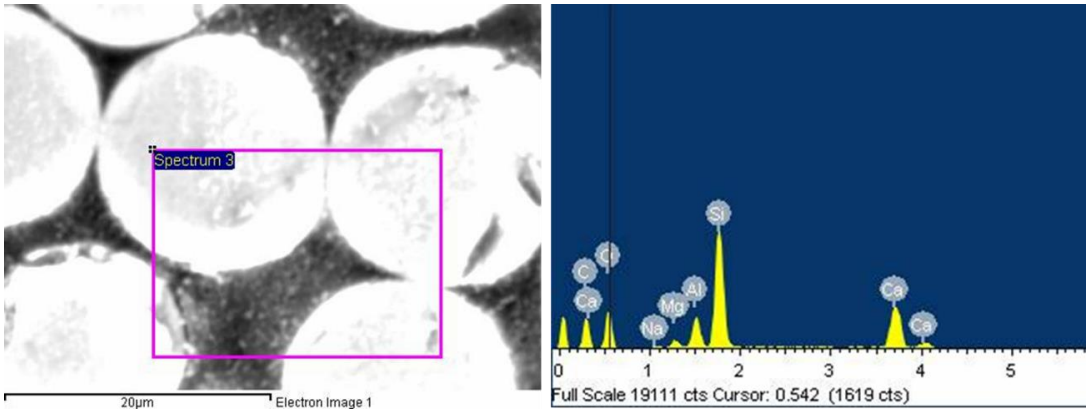

Figure.II.44: Results of EDX scans for specimens contol specimens (area).

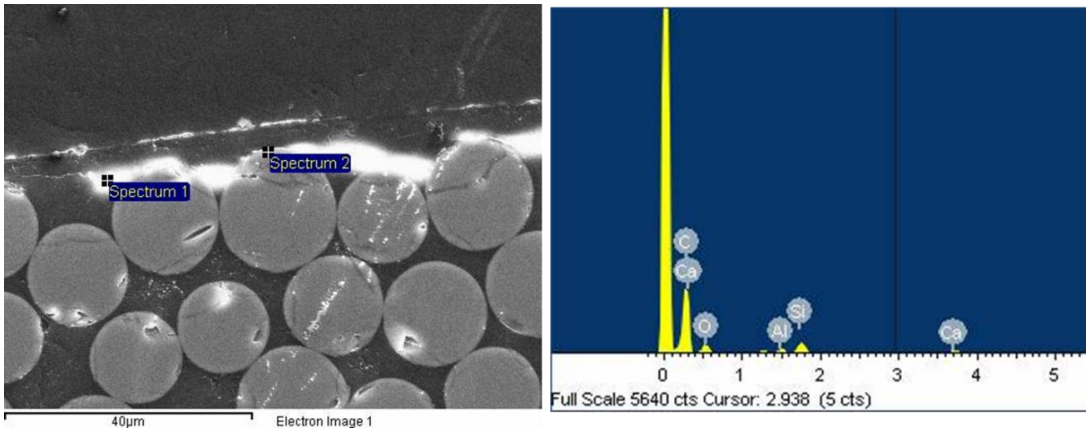

Figure.II.45: Results of EDX scans for specimens specimens conditioned in water at 60°C for 8760 hr (spectrum 1)

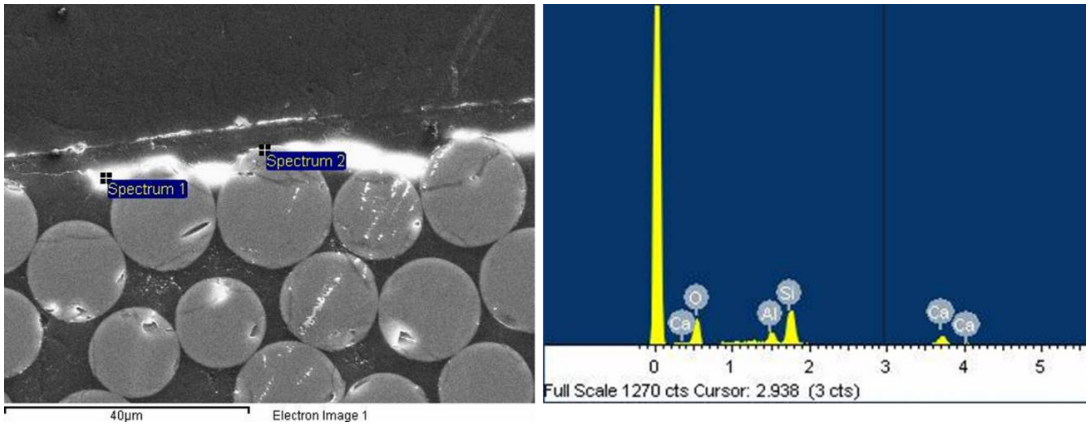

Figure.II.46: Results of EDX scans for specimens specimens conditioned in water at 60°C for 8760 hr (spectrum 2)

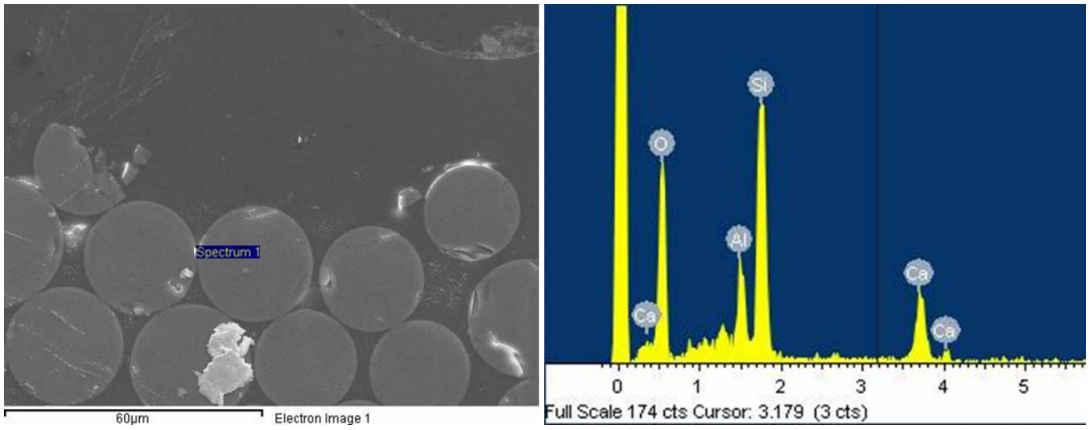

Figure.II.47: Results of EDX scans for specimens specimens conditioned in water at 60°C for 8760 hr

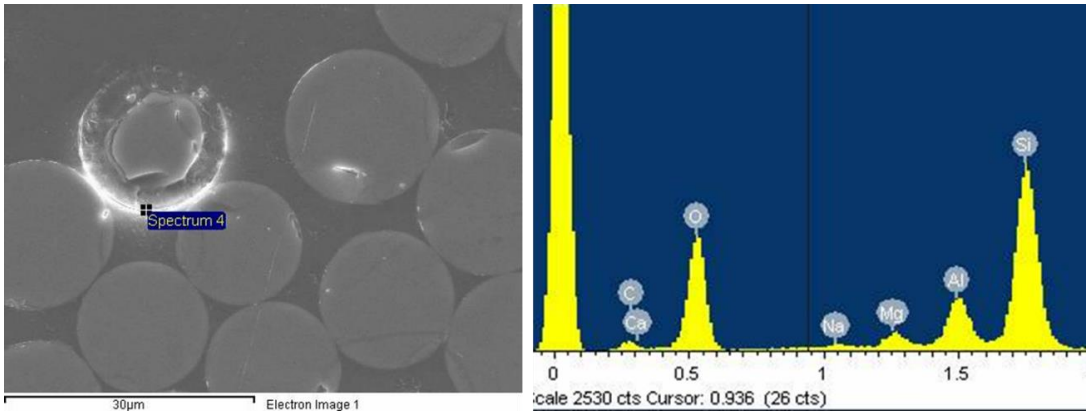

Figure.II.48: Results of EDX scans for specimens specimen conditioned alkaline solution at 60°C for 8760 hr.

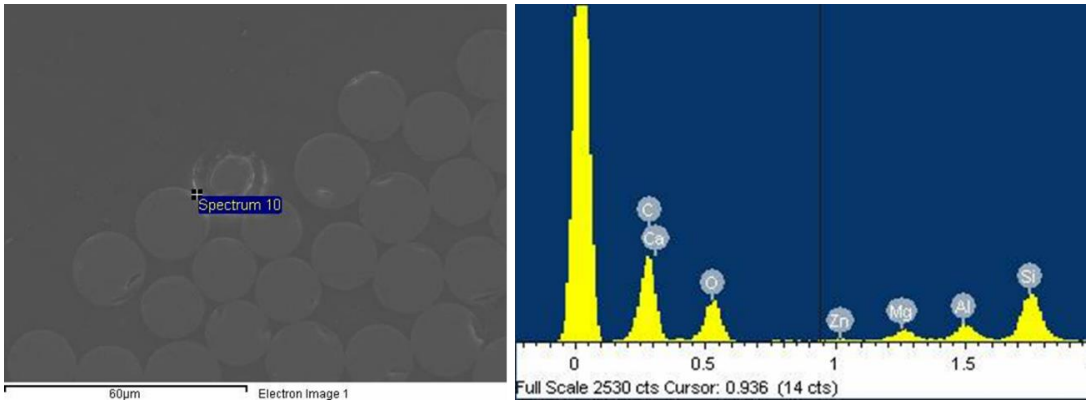

Figure.II.49: Results of EDX scans for specimens specimen conditioned alkaline solution at 60°C for 8760 hr.

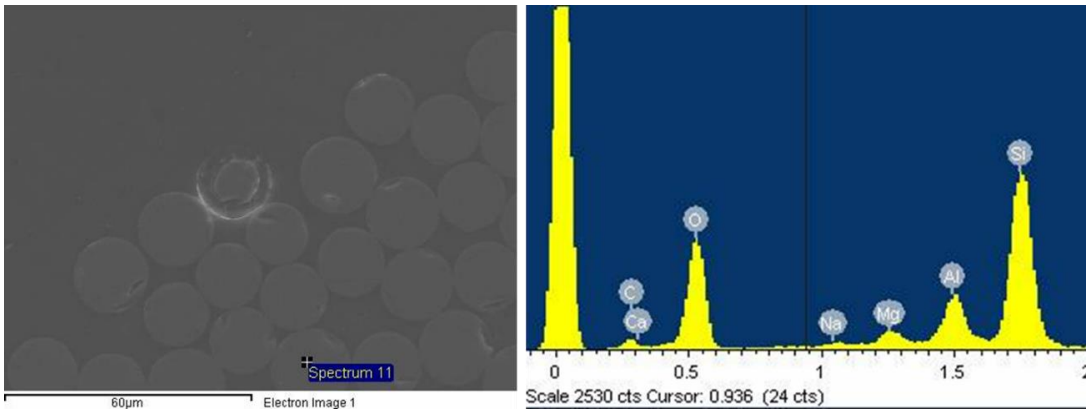

Figure.II.50: Results of EDX scans for specimens specimen conditioned alkaline solution at 60°C for 8760 hr.

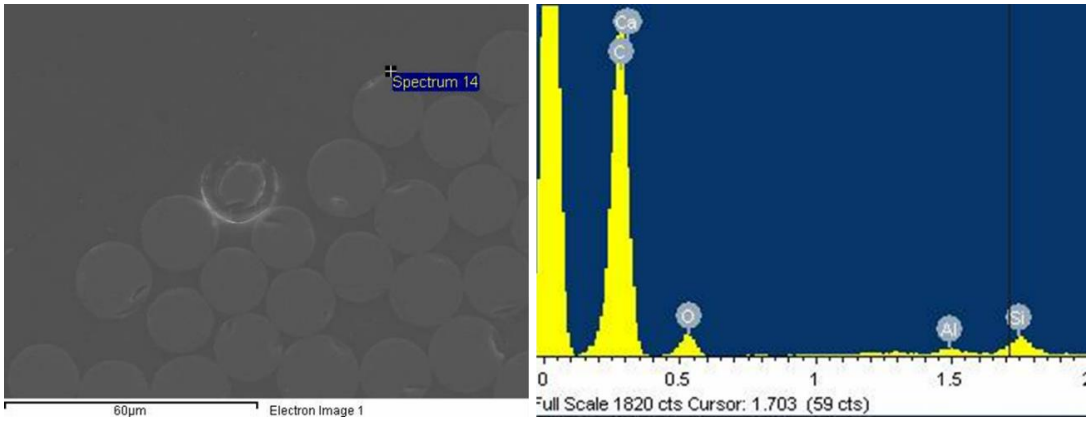

Figure.II.51: Results of EDX scans for specimens specimen conditioned alkaline solution at 60°C for 8760 hr.

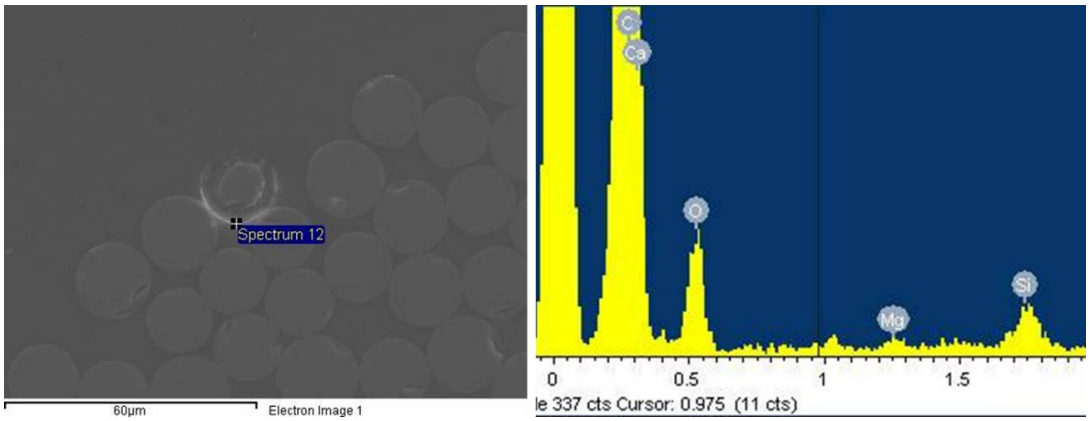

Figure.II.52: Results of EDX scans for specimens specimen conditioned alkaline solution at 60°C for 8760 hr.

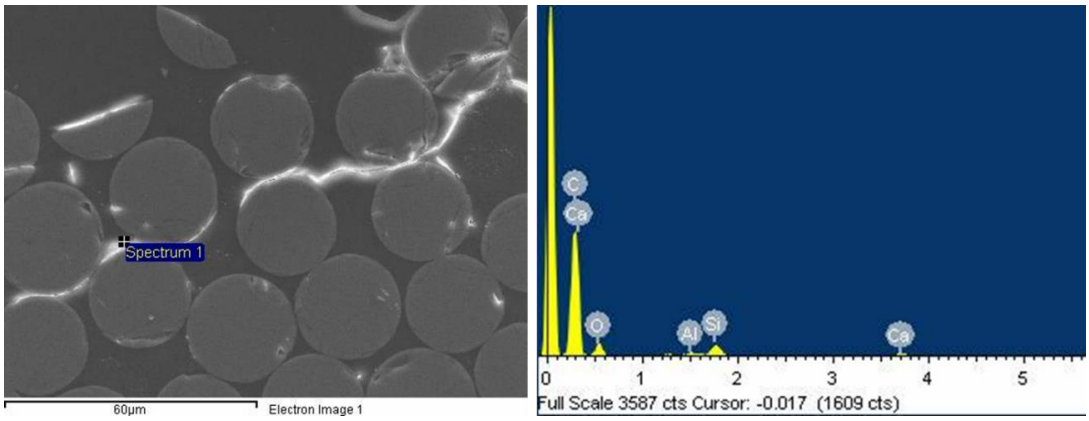

Figure.II.53: Results of EDX scans for specimens specimen conditioned alkaline solution at 60°C for 8760 hr.

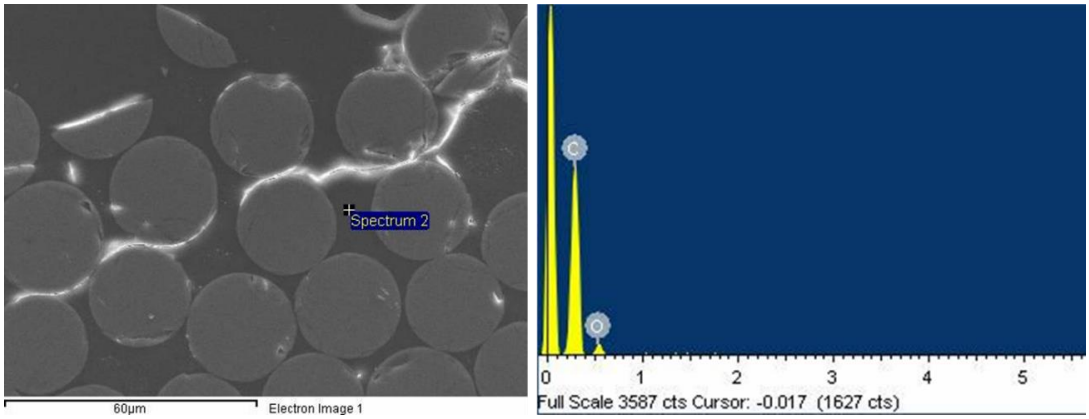

Figure.II.54: Results of EDX scans for specimens specimen conditioned alkaline solution at 60°C for 8760 hr.

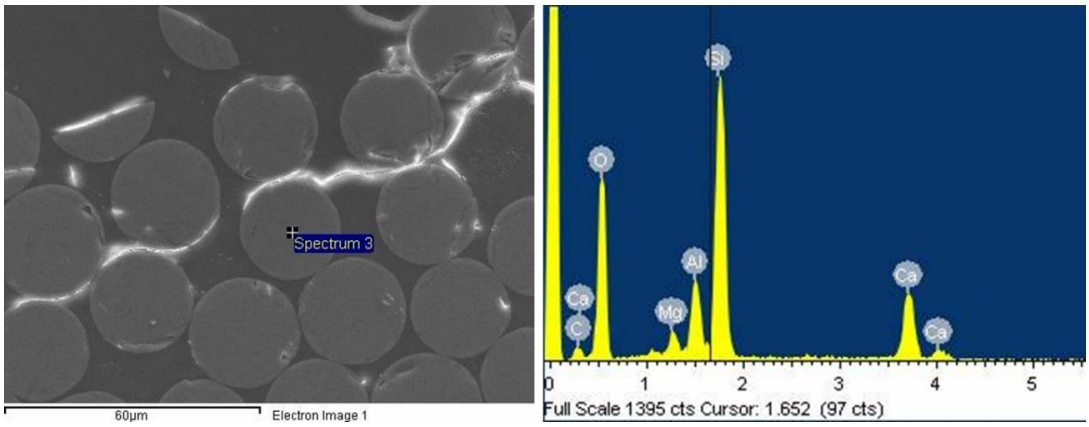

Figure.II.55: Results of EDX scans for specimens specimen conditioned alkaline solution at 60°C for 8760 hr.

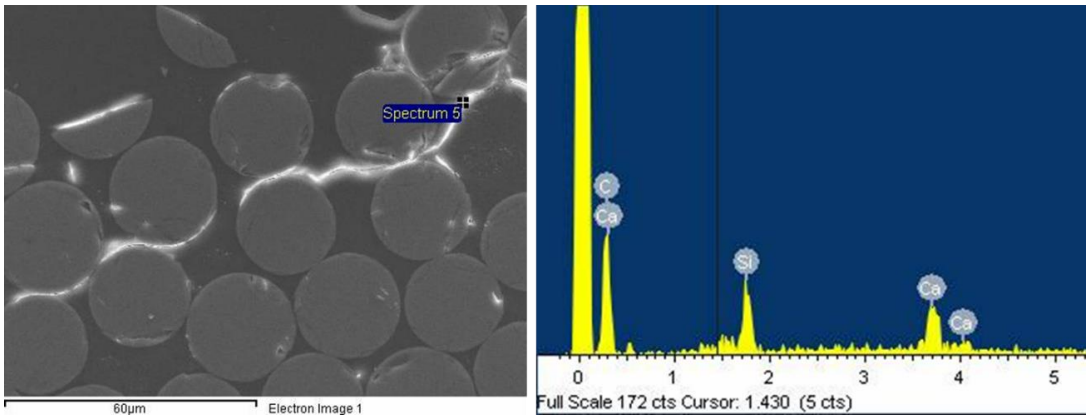

Figure.II.56: Results of EDX scans for specimens specimen conditioned alkaline solution at 60°C for 8760 hr.

APPENDIX III

LONG-TERM STRUCTURAL PERFORMANCE OF GFRP RC CONCRETE ELEMENTS

1. Flexural response behaviour

This section presents additional data obtained from flexural behaviour tests. This data includes the design calculation, monitoring during conditioning time, Shrinkage study, cracking measurement and Load- flexural responses diagrams for GFRP RC beams in different aging conditions.

Beams

Concrete mix

Ready mix Concrete

Casting day is 14/10/2014

Starting time 10:30 am

Finishing time 12.15 am

The detailed concrete mixes proportion supplied by Lafarge Tarmac Company for flexural test is presented in the following tables:

Table III.1: Lafarge Tarmac mix design

Target Concrete compressive strength(MPa)	Slump (mm)	Size of coarse aggregate (mm)	Mass per unit volume (kg/m^3)			
			Natural aggregates	sand	CEM I 52.5 Cement	WATER
40	180	10	1041	777	349	190

The average of slump test was 181 mm

The compressive strength of concrete was measured for 7 days and 28 days as shown in the following tables:

Table III.2: Compressive strength of Lafarge Tarmac mix design

Specimen ID	Dimension mm	Mass (kg)	Density(kg/m^3)	Load at failure(kN)	Stress(MPa) At 7 days	Stress(MPa) At 28 days
FT C 1	150X150X150	8.305	2460	958.7	42.16	
FT C 2	150X150X150	8.243	2442	874.9	38.87	
FT C 3	150X150X150	8.231	2438	938.2	41.69	
FT C 4	150X150X150	7.841	2323	1201.4		53.39
FT C 5	150X150X150	8.311	2462	1248.8		55.5
FT C 6	150X150X150					

Table III.3: Compressive strength of Lafarge Tarmac mix design at the day of testing

ID	Conditions	Data of casting	Data of testing	D*h (mm)	Mass (kg)	Failure (kN)	Stress (MPa) 7 days	Stress (MPa) 28 days
1	W.60 °C	14/10/14	1/3/2016	50 *100	437.6	54.2		27.6
2	W.60 °C	14/10/14	1/3/2016	50 *100	437.4	45		22.91
3	W.60 °C	14/10/14	1/3/2016	50 *100	430	55.6	32 CUBE	28.3
4	AIR	14/10/14	1/3/2016	50 *100	434	58.8		29.9
5	AIR	14/10/14	1/3/2016	50 *100	435	68		34.62
6	AIR	14/10/14	1/3/2016	50 *100	443	90	45 CUBE	46

Design calculations for GFRP reinforced beam

Assumption Compression mode failure

D=150-10-4-4=132mm

$A_f=4^2*\pi*2=100.53mm^2$

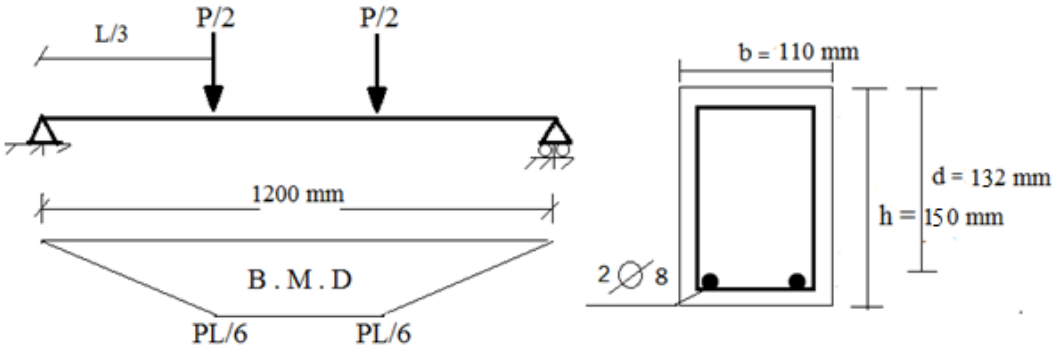

Figure.III.1 Specimen geometry and four point test

A_f : Area of FRP bars

$\rho = \frac{Af}{bd} = \frac{100.531}{110*132} = .0076$

ρ : reinforcement ratio

Calculation the stress in GFRP reinforcement from ACI 440 Equation 8-4d

$F_f = \sqrt[2]{\frac{(E_f \in_{cu})^2}{4} + \frac{0.85*\beta 1*F_c}{\rho_f}} * E_f \in_{cu} - 0.5 E_f \in_{cu} \leq F_{fu}$

$\beta 1 = .76$ from ACI 440

$E_f = 61000 \frac{N}{mm^2}$

$F_c = 55\ MP_a$

$F_{fu} = 1290\ \frac{N}{mm^2}$

$F_f = \sqrt[2]{\frac{(61*.003)^2}{4} + \frac{0.85*.76*.055}{.0076} * (61 * .003)} - (.5*.003*61)$

$F_f = 837\ \frac{N}{mm^2}$ which is < $1290\ \frac{N}{mm^2}$ OK

Calculate ρ_{fb} from ACI440 Equation (8-3)

$\rho_{fb} = .85* \beta 1* \frac{F_c}{Ffu} * \frac{E_f \in_{cu}}{E_f \in_{cu} + Ffu}$

$\rho_{fb} = .85*.76* \frac{55}{1290} * \frac{61000*.003}{(61000*.003)+1290} = .0034$

$1.4* \rho_{fb} = 0.00479 \quad \rho > 1.4* \rho_{fb}$

$M_n = \rho* F_f (1-0.59* \frac{\rho* Ff}{F_c}) bd^2$

$M_n = .0076*837*(1-0.59* \frac{.0076*837}{55})*110*132^2 = 12.5$ KN.m

$M_n = 11.36$ KN.m

$M = \frac{PL}{6}$

$11.36 = \frac{P*1}{6}$

$\frac{P}{2} = 34.08$ KN

For 30% of F_{fu}

$M_n = .0076*387*(1-0.59* \frac{.0076*387}{55})*110*132^2$

$M_n = 5.45$ KN.m

$M = \frac{PL}{6}$

$5.25 = \frac{P*1}{6}$

$\frac{P}{2} = 15.75$ KN

For 50 % of F_{fu}

$M_n = .0076*645*(1-0.59* \frac{.0076*645}{55})*110*132^2 = 8.9$ KN.m

$M_n = 8.9$ KN.m

$M = \frac{PL}{6}$

$\frac{P}{2}$= 26.7 KN

Minimum reinforcements:

$A_{min} = 1.8\frac{\sqrt[3]{F_c}}{Ffu} bd$

Load application, conditioning and monitoring

Figure.III.2 sustained load application

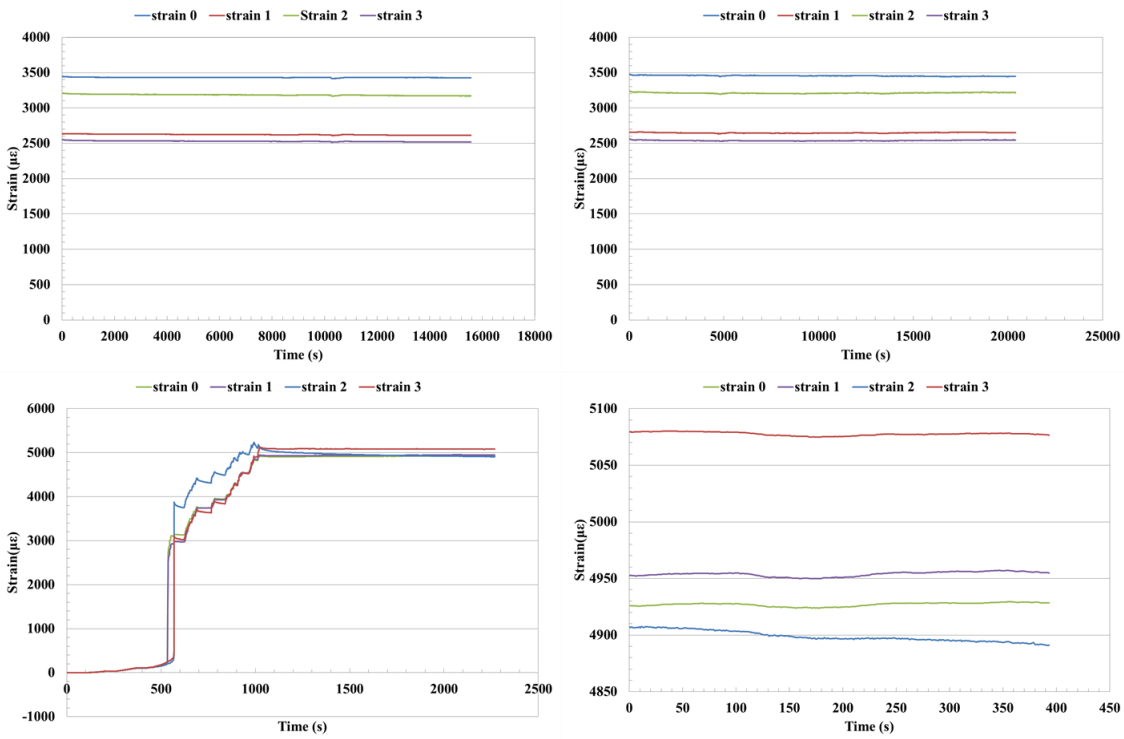

Figure.III.3 sustained strain application in GFRP bars and monitoring before conditioning

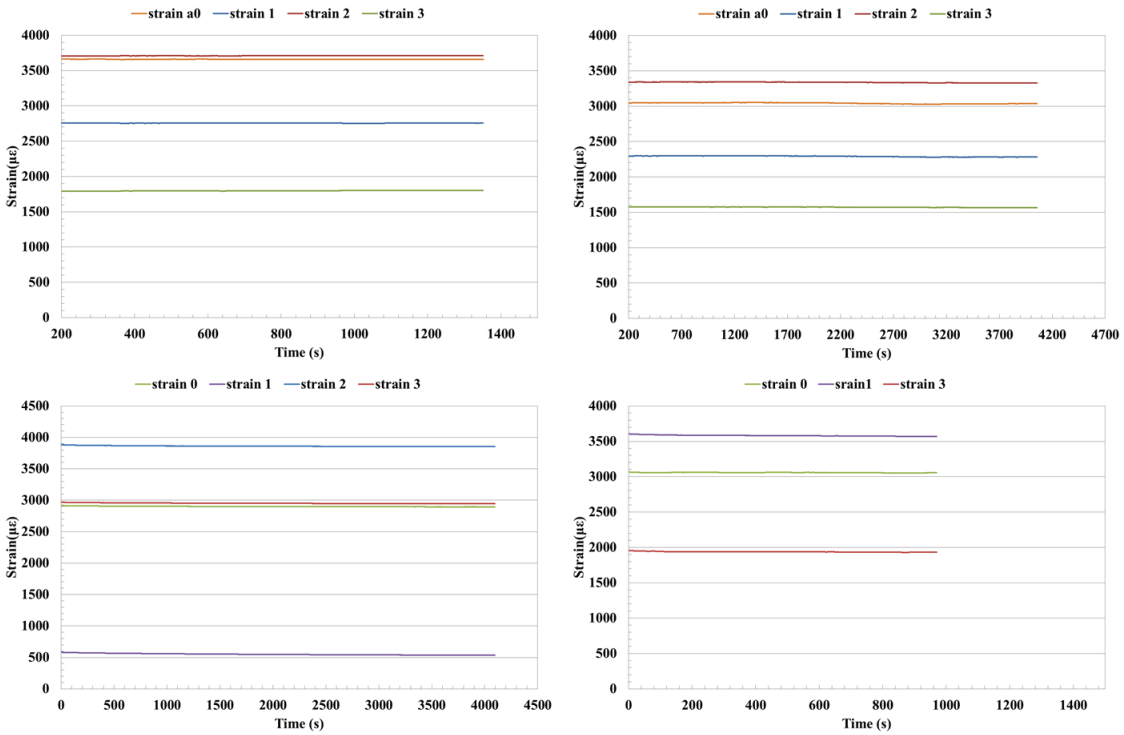

Figure.III.4 sustained strain monitoring during conditioning

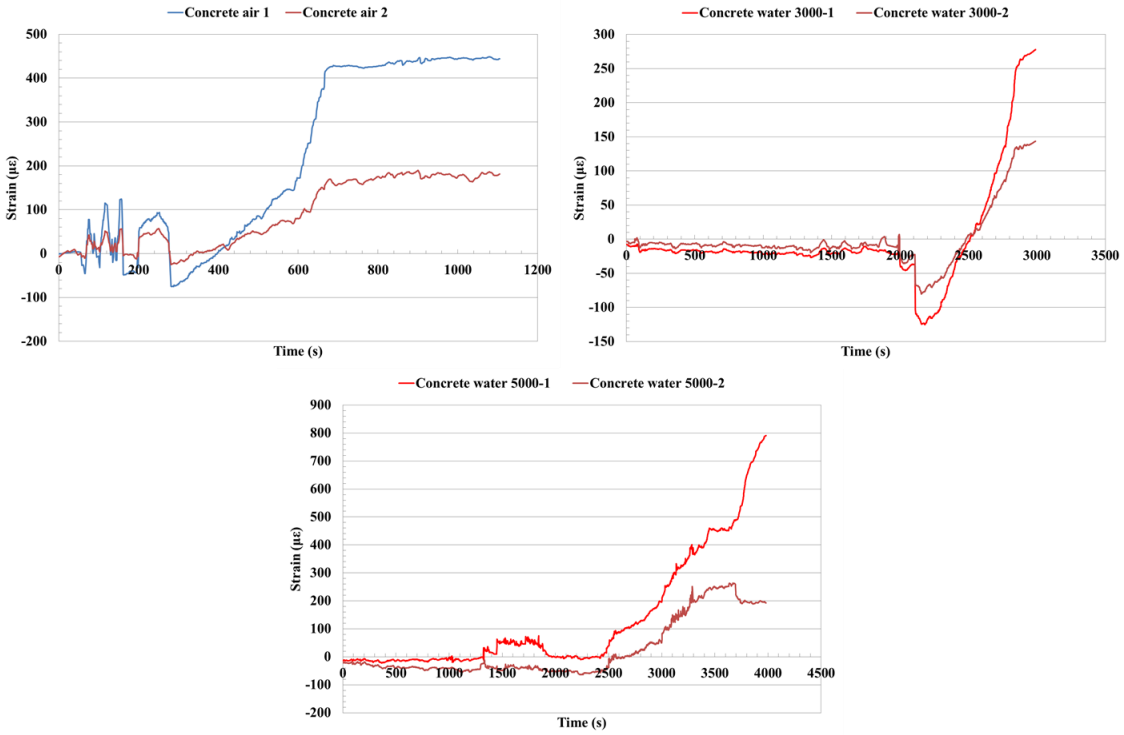

Figure.III.5 sustained strain on concrete monitoring before conditioning

Deflection and cracking monitoring:

Deflection and cracking monitoring:

Deflection

Deflection measurements

B-a-3K-270

Measurement at mid span 71.7 mm second measurement 71.48 mm

Left side 66.30 mm second measurement 67.12 mm

Right side 63.83 mm second measurement 61.71 mm

Spring length 220 mm

Table III.4: Deflection measurement

side L 1 :	181.38- 181.86	side R 1 :	179.73 179.69
side L 2 :	181.20 182.52	side R 2 :	181.18 182.16
side L3:	181.53 181.9	side R 3:	180.91 181.76
side L 4 :	181.50 181.74	side R4 :	180.9 180.29

Cracking monitoring

Table III.5: Cracking monitoring

LOAD KN	Crack 1	Crack 2	Crack 3	Crack 4	Crack 5	Date
3000 με	0.4 mm	0.4mm	0.36 mm	0.4 mm	0.36	30/03/15
	0.44	0.34	0.34	0.34		29/04/15

B-W6-3K-270

Measurement at mid span 71.19 mm second measurement 71.07 mm after undoes 70.51 mm

Left side 68.30 mm second measurement 69 mm after undo 68.28 mm

Right side 62.63 mm second measurement 60.99 mm after undo 61.18 mm

Spring length 220 mm

Table III.6: Deflection measurement

side L 1 :	182.32 184	side R 1 :	185.73 187
side L 2 :	183.25 184	side R 2 :	181.2 183
side L3:	182.53 184	side R 3:	180.93 181
side L 4 :	181.50 184	side R4 :	181.9 184

Cracking monitoring

Table III.7: Cracking monitoring

LOAD KN	Crack 1	Crack 2	Crack 3	Crack 4	Crack 5	Date
3000 με	0.4 mm	0.4mm	0.4 mm	0.36 mm	0.4	30/03/15

B-W6-5K-270

Measurements at mid span 69.41mm after 71.31mm 71.08 mm after undo 70.80mm

1- 72.48 mm , 62.64 mm 53.38 mm after undo 63.68 mm

2- 66.54 mm, 56.91 mm 59.5mm 62.31 mm

Spring length 220 mm

Table III.8: Deflection measurement

side L 1 : 153.9mm 155mm	side R 1 : 164.4 mm 166 mm
side L 2 : 167.5 mm 170mm	side R 2 : 155.7mm 158 mm
side L3: 159.7mm 163 mm	side R 3: 160 mm 162mm
side L 4 : 162.8mm 164 mm	side R4 : 159.2 mm 162 mm

Cracking monitoring

Table III.9: Compressive strength of Lafarge Tarmac mix design at the day of testing

LOAD KN	Crack 1	Crack 2	Crack 3	Crack 4	Crack 5	Date
5000 με	0.44 mm	0.34 mm	0.5 mm	0.34 mm		30/03/15

Shrinkage measurement

After conditioning the specimens were employed for shrinkage study the data were used to determine the residual deformation.

Figure.III.6 the specimens after 9 months of conditioning

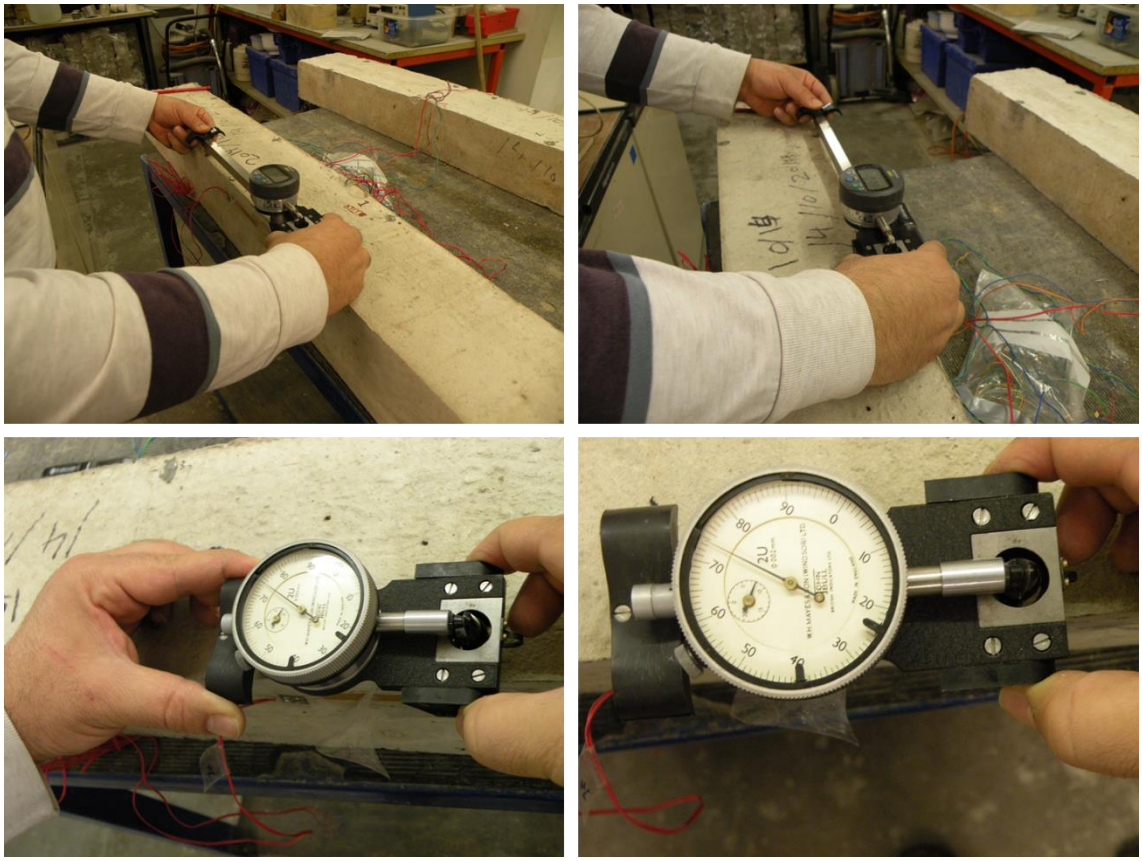

Figure.III.7 shrinkage measurement using demec gauge and demec points

Beams in air

Table III 10: shrinkage measurement beam in lab beam 1 tension side

B1	**Tension**			
Time (hr)	O1b1t (με)	o2b1t (με)	o3b1t (με)	AV (με)
24	-5.28	-10.56	-13.2	-9.68
48	-7.92	-10.56	-7.92	-8.8
72	-5.28	-7.92	-5.28	-6.16
96	-5.28	-7.92	-2.64	-5.28

Table III 11: shrinkage measurement beam in lab beam1compression side

B1	**Compression**			
Time (hr)	O1b1t (με)	o2b1t (με)	o3b1t (με)	AV (με)
24	-13.2	-15.84	-5.28	-11.44
48	-21.12	-18.48	-5.28	-14.96
72	-15.84	-15.84	-2.64	-11.44
96	-15.84	-15.84	-2.64	-11.44

Table III 12: shrinkage measurement beam in lab beam 2 tension side

B1	**Tension**			
Time (hr)	O1b1t (με)	o2b1t (με)	o3b1t (με)	AV (με)
24	-13.2	-13.2	-15.84	-14.08
48	-13.2	-21.12	-10.56	-14.96
72	-13.2	-18.48	-13.2	-14.96
96	-13.2	-21.12	-7.92	-14.08

Table III 13: shrinkage measurement beam in lab beam1compression side

B1	**Compression**			
Time (hr)	O1b1t (με)	o2b1t (με)	o3b1t (με)	AV (με)
24	-13.2	-13.2	-15.84	-14.08
48	-23.76	-2.64	-10.56	-12.32
72	-18.48	2.64	-5.28	-7.04
96	-21.12	5.28	-7.92	-7.92

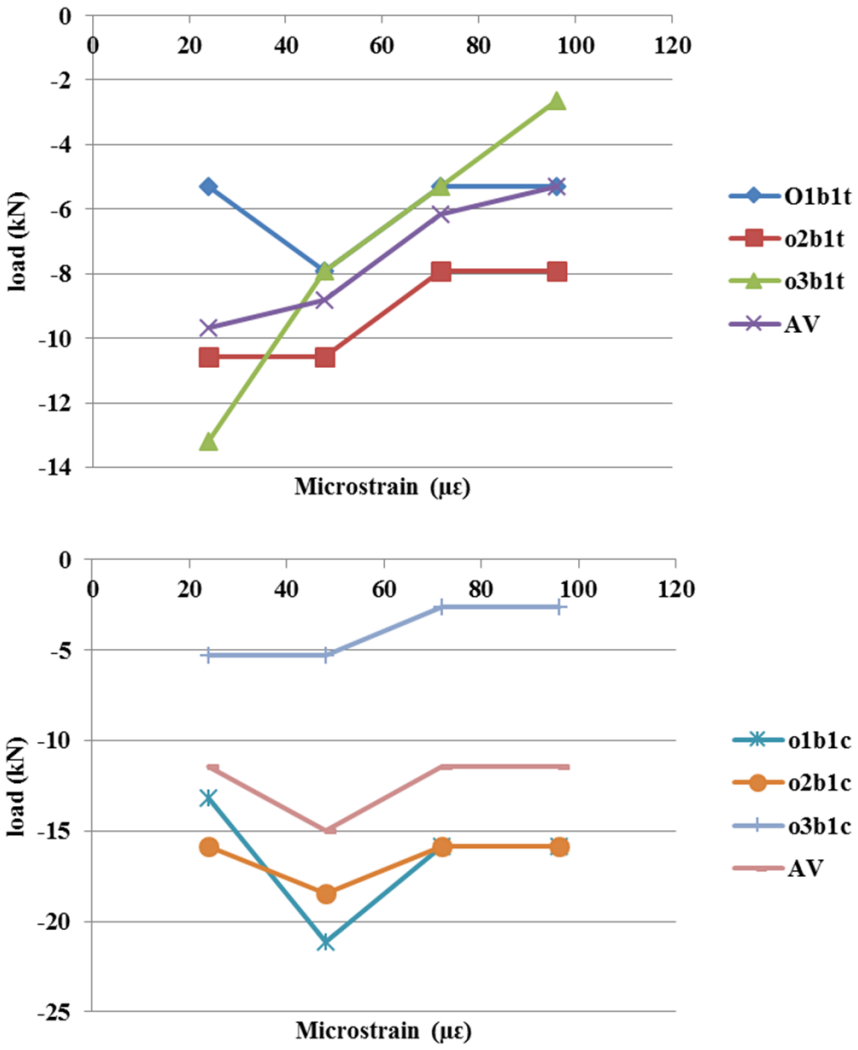

Figure.III.8: strain changing with time beam 1

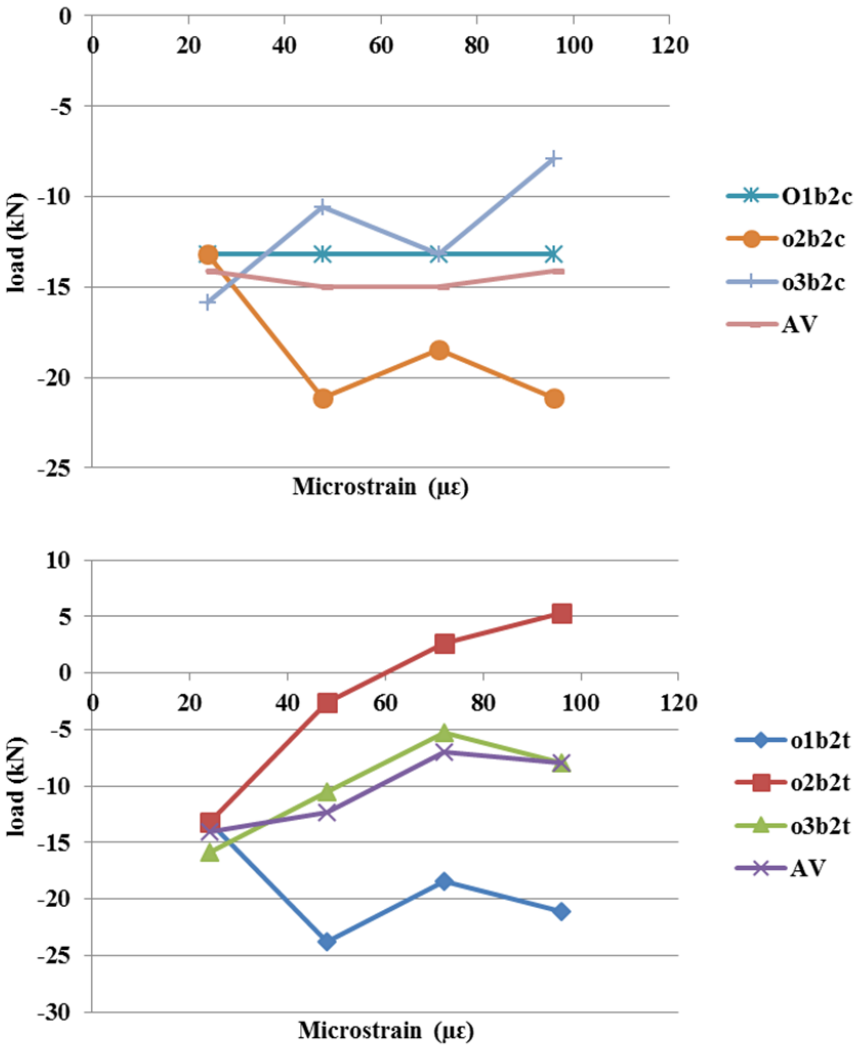

Figure.III.9: strain changing with time beam 2

Table III 14: shrinkage measurement stressed beam at 3000 (με) conditioned in water at 60°C beam 1 tension side

B1	**TEN**			
Time (hr)	O1b1t (με)	o2b1t (με)	o3b1t (με)	AV (με)
24	21.12	44.88	39.6	35.2
48	31.68	63.36	63.36	52.8
72	39.6	84.48	73.92	66
96	44.88	89.76	87.12	73.92
120	55.44	108.24	95.04	86.24
144	60.72	126.72	102.96	96.8
168	63.36	137.28	110.88	103.84
192	71.28	142.56	126.72	113.52
216	76.56	145.2	132	117.92
264	79.2	158.4	139.92	125.84

Table III 15: shrinkage measurement stressed beam at 3000 (με) conditioned in water at 60°C beam 1 compression side

B1	**COMP**			
Time (hr)	O1b1t (με)	o2b1t (με)	o3b1t (με)	AV (με)
24	-7.92	-7.92	-13.2	-9.68
48	-5.28	-2.64	-5.28	-4.4
72	0	2.64	-2.64	0.0
96	-2.64	7.92	2.64	2.64
120	0	18.48	15.84	11.44
144	7.92	29.04	18.48	18.48
168	5.28	34.32	21.12	20.24
192	7.92	36.96	31.68	25.52
216	13.2	42.24	36.96	30.8
264	18.48	47.52	36.96	34.32

Table III 16: shrinkage measurement stressed beam at 3000 (με) conditioned in water at 60°C beam 2 Tension side

B1	**TEN**			
Time (hr)	O1b1t (με)	o2b1t (με)	o3b1t (με)	AV (με)
24	-18.48	-18.48	-39.6	-25.52
48	-13.2	-7.92	-36.96	-19.36
72	-7.92	-2.64	-34.32	-14.96
96	0.0	10.56	-26.4	-5.28
120	13.2	23.76	-21.12	5.28
144	18.48	34.32	-15.84	12.32
168	21.12	36.96	-10.56	15.84
192	26.4	42.24	-5.28	21.12
216	34.32	50.16	-2.64	27.28
264	39.6	55.44	5.28	33.44

Table III 17: shrinkage measurement stressed beam at 3000 (με) conditioned in water at 60°C beam 2 compression side

B1	**COMP**			
Time (hr)	O1b1t (με)	o2b1t (με)	o3b1t (με)	AV (με)
24	21.12	44.88	44.88	36.96
48	36.96	60.72	66	54.56
72	52.8	76.56	73.92	67.76
96	66	89.76	87.12	80.96
120	76.56	105.6	100.32	94.16
144	87.12	116.16	110.88	104.72
168	95.04	121.44	118.8	111.76
192	100.32	129.36	126.72	118.8
216	110.88	142.56	137.28	130.24
264	121.44	147.84	142.56	137.28

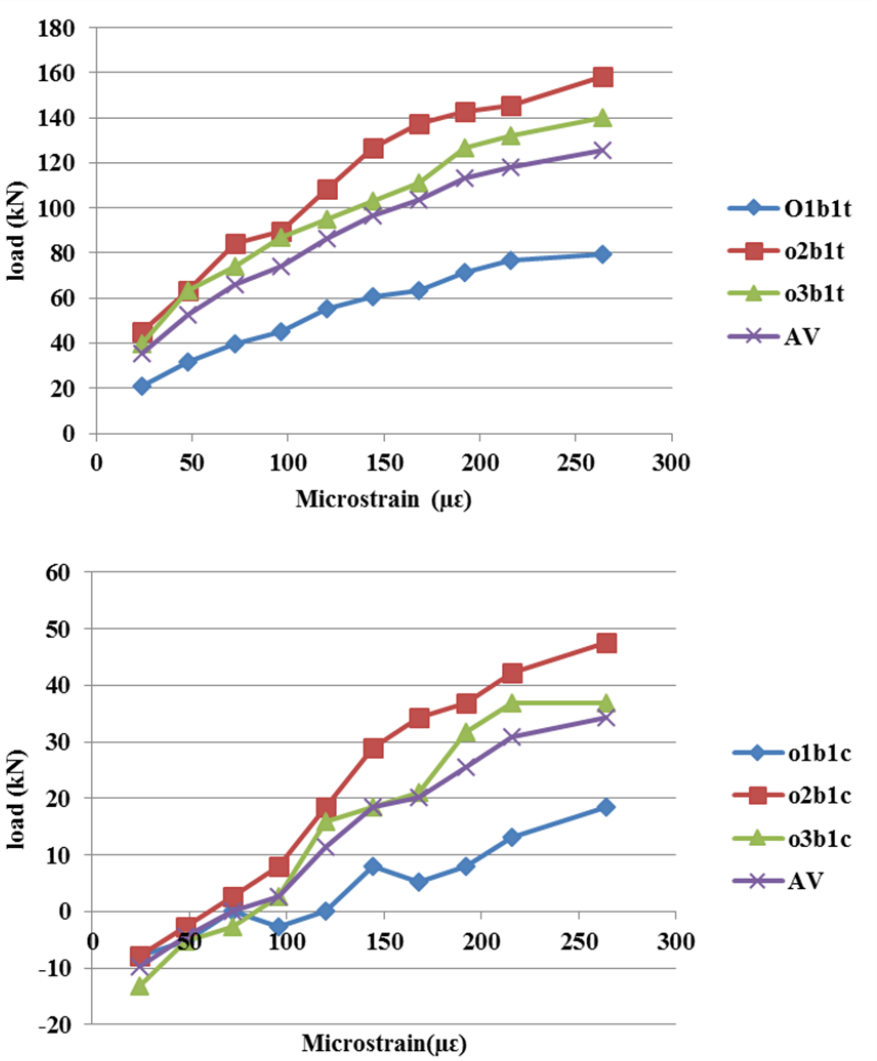

Figure.III.10: strain changing with time for stressed beam at 3000 (με) conditioned in water at 60°C beam 1

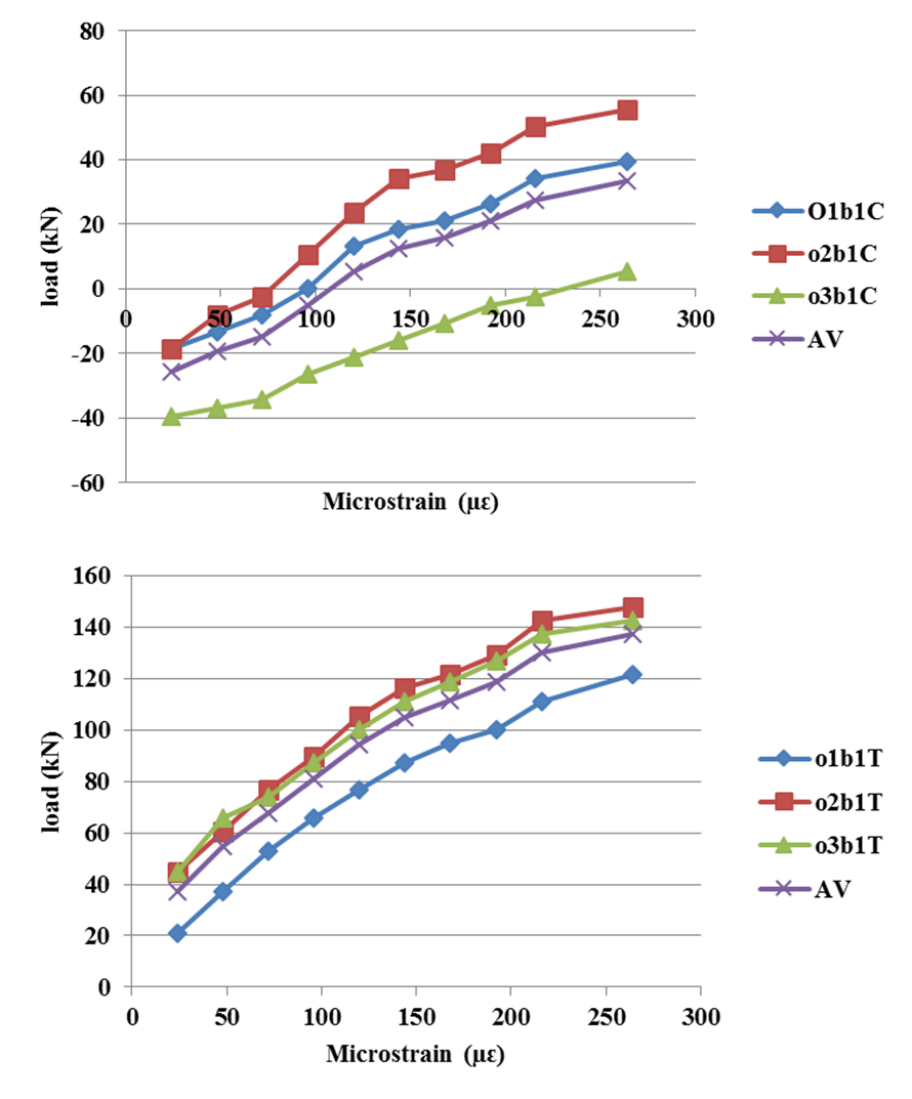

Figure.III.11: strain changing with time for stressed beam at 3000 (με) conditioned in water at 60°C beam 2

Table III 18: shrinkage measurement stressed beam at 5000 (με) conditioned in water at 60°C beam 1 tension side

B1	**TEN**			
Time (hr)	O1b1t (με)	o2b1t (με)	o3b1t (με)	AV (με)
24	15.84	21.12	21.12	19.36
48	36.96	52.8	50.16	46.64
72	52.8	68.64	66	62.48
96	63.36	84.48	71.28	73.04
120	89.76	105.6	102.96	99.44
144	100.32	121.44	118.8	113.52
168	110.88	139.92	126.72	125.84
192	121.44	147.84	139.92	136.4
216	134.64	163.68	142.56	146.96
264	145.2	174.24	150.48	156.64

Table III 19: shrinkage measurement stressed beam at 5000 (με) conditioned in water at 60°C beam 1 compression side

B1	**COMP**			
Time (hr)	O1b1t (με)	o2b1t (με)	o3b1t (με)	AV (με)
24	-23.76	-29.04	-23.76	-25.52
48	-15.84	-15.84	-13.2	-14.96
72	-15.84	-15.84	-13.2	-14.96
96	-13.2	-15.84	-10.56	-13.2
120	-5.28	-2.64	7.92	0
144	-2.64	0	5.28	0.88
168	0	18.48	2.64	7.04
192	10.56	7.92	10.56	9.68
216	21.12	15.84	13.2	16.72
264	18.48	18.48	13.2	16.72

Table III 20: shrinkage measurement stressed beam at 5000 (με) conditioned in water at 60°C beam 2 Tension side

B1	**TEN**			
Time (hr)	O1b1t (με)	o2b1t (με)	o3b1t (με)	AV (με)
24	-7.92	-15.84	-26.4	-16.72
48	-7.92	-7.92	-18.48	-11.44
72	0	-2.64	-18.48	-7.04
96	5.28	-5.28	-13.2	-4.4
120	23.76	21.12	23.76	22.88
144	26.4	23.76	29.04	26.4
168	26.4	29.04	33	29.48
192	34.32	34.32	39.6	36.08
216	39.6	36.96	44.88	40.48
264	36.96	44.88	52.8	44.88

Table III 21: shrinkage measurement stressed beam at 5000 (με) conditioned in water at 60°C beam 2 compression side

B1	COMP			
Time (hr)	O1b1t (με)	o2b1t (με)	o3b1t (με)	AV (με)
24	15.84	15.84	21.12	17.6
48	29.04	29.04	47.52	35.2
72	42.24	44.88	60.72	49.28
96	60.72	58.08	71.28	63.36
120	87.12	73.92	102.96	88.00
144	100.32	92.4	110.88	101.2
168	113.52	95.04	124.08	110.88
192	118.8	110.88	134.64	121.44
216	134.64	108.24	153.12	132
264	142.56	124.08	158.4	141.68

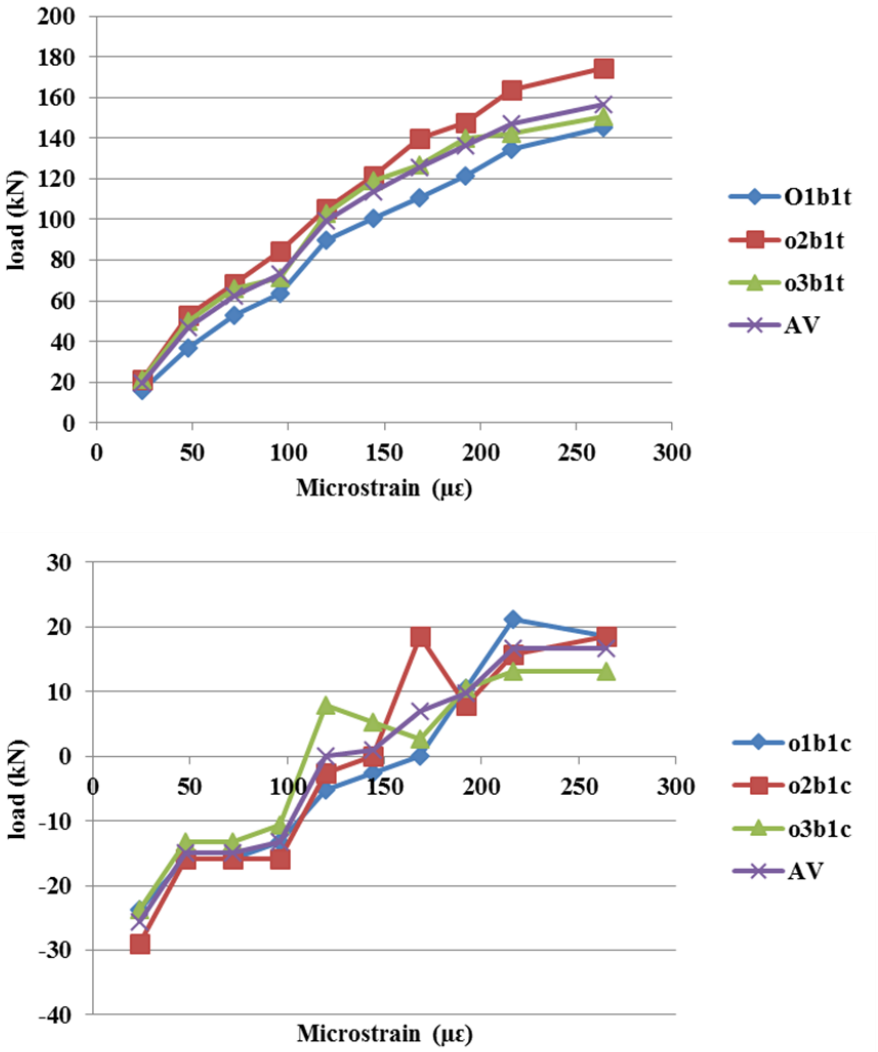

Figure.III.12: strain changing with time for stressed beam at 5000 (με) conditioned in water at 60°C beam 1

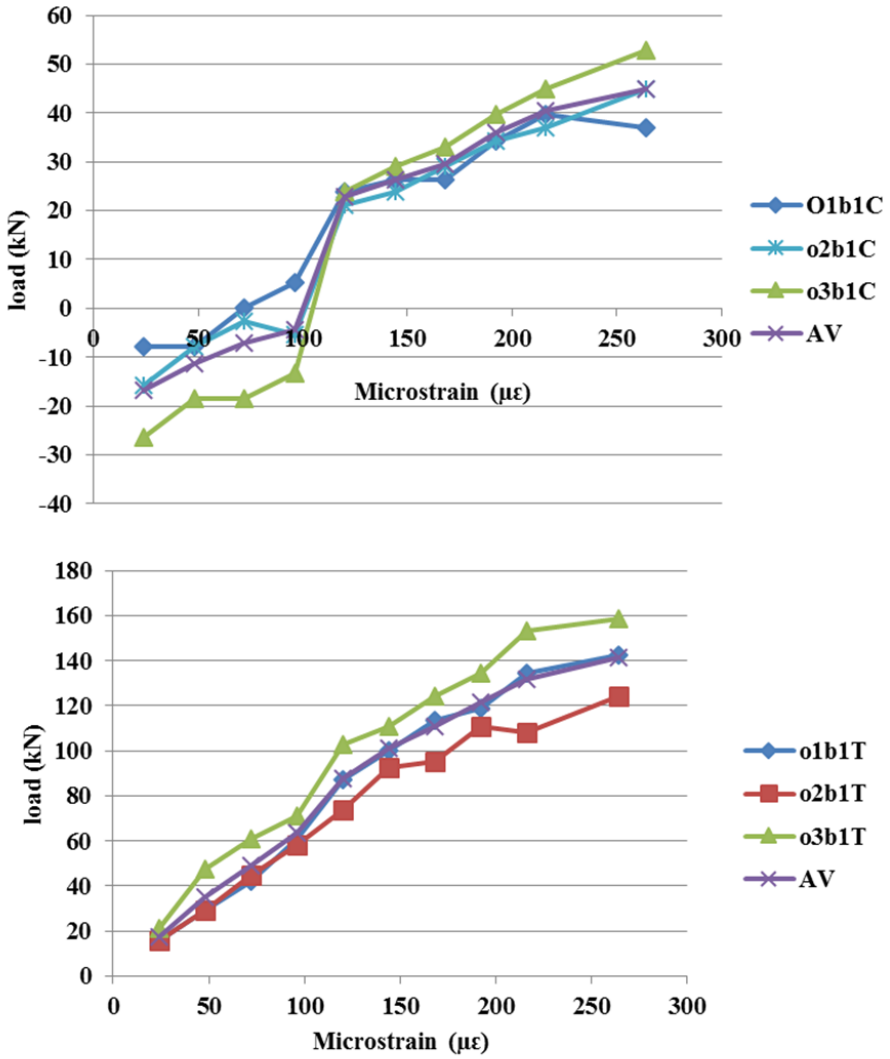

Figure.III.13: strain changing with time for stressed beam at 3000 (με) conditioned in water at 60°C beam 2 compression side beam 1

Shrinkage calibration

The shrinkage for reinforced concrete member conditioned without stress also has been measured to correct the deformations (dummy specimen)

Table III 22: shrinkage measurement GFRP RC conditioned in water at 60°C

Dummy specimen	
Time (hr)	Strain (με)
24	-84.48
48	-73.92
72	-81.84
96	-87.12
120	-100.32
144	-113.52
168	-116.16
192	-124.08
216	-126.72
264	-137.28

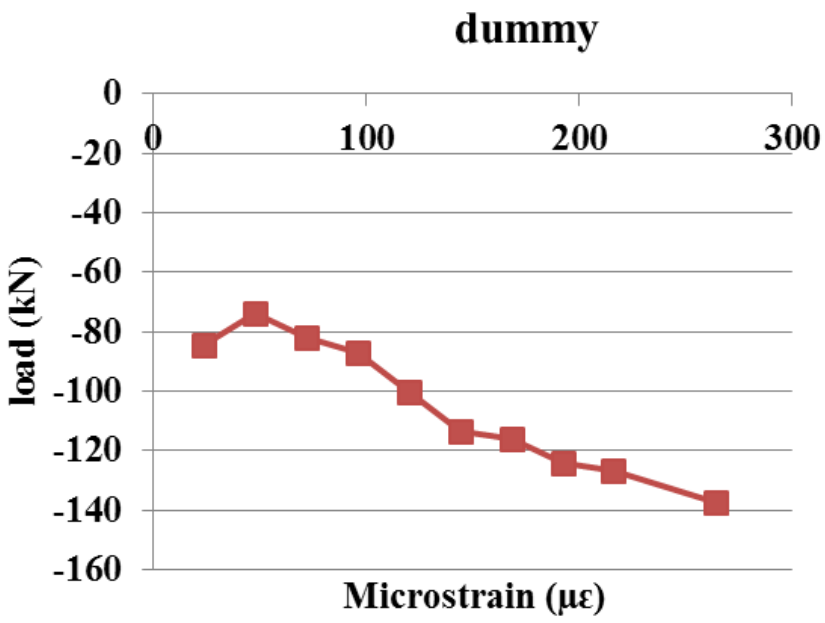

Figure.III.14: strain changing with time for specimen conditioned in water at 60°

Teste setup and date acquisitions

Test set-up

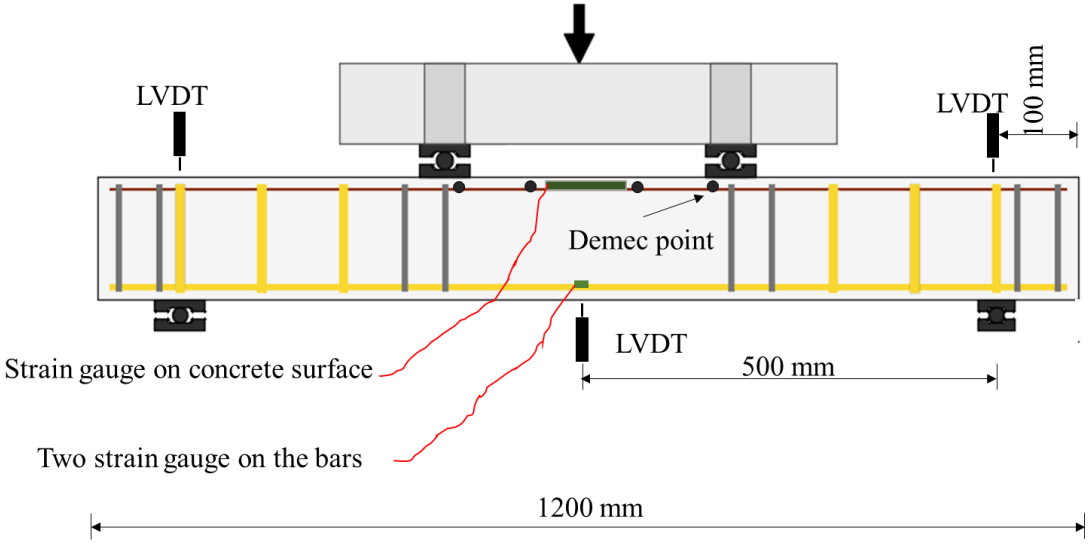

Figure.III.15: flexural test set-up

Cracking width measurement

Cracks widths were measured at the level of reinforcements using mobile optical microscope

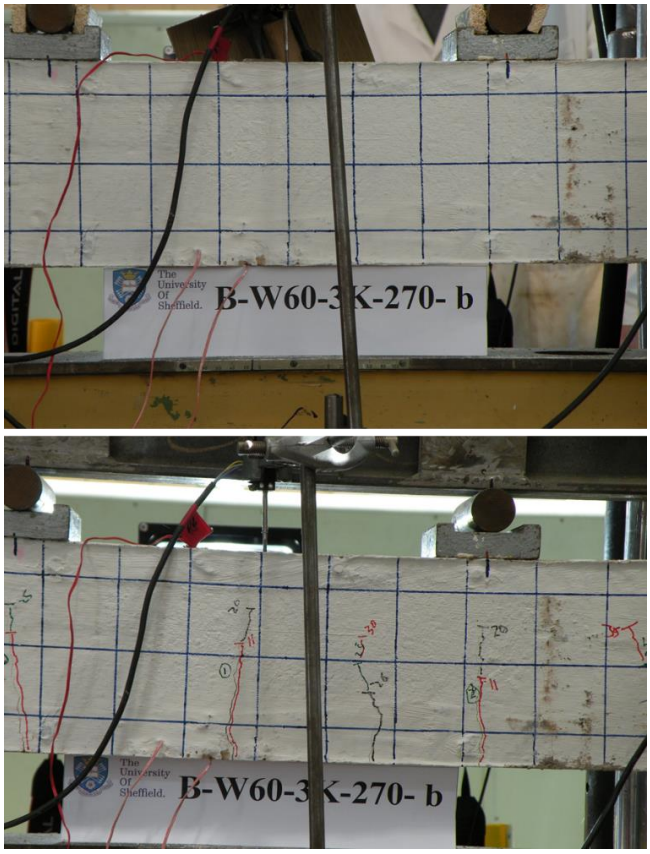

Figure.III.16: cracking monitoring and measurement

Table III 23: crack width measurement of beam B-a-3k-a crack 1

	11 KN	20 KN	25 KN	30KN	35KN
First	1.06	2	2.2	2.33	2.84
Second	1.03	1.98	2.31	2.6	3.42
Third	0.91	1.91	2.25	2.58	3.15
Avg	1.08	1.96	2.25	2.50	3.13
width	0.27	0.49	0.57	0.63	0.79

Table III 24: crack width measurement of beam B-a-3k-a crack 2

	11 KN	20 KN	25 KN	30KN	35KN
First	6.95	1.52	1.66	1.98	2.37
Second	8.04	1.44	1.72	1.99	2.44
Third	6.99	1.50	1.86	2.11	2.52
Avg	7.32	1.49	1.75	2.02	2.44
width	0.19	0.38	0.44	0.51	0.62

Table III 25: crack width measurement of beam B-a-3k-b crack 1

	11 KN	20 KN	25 KN	30KN	35KN
First	6.32	1.24	1.47	1.84	2.43
Second	6.45	1.15	1.49	1.65	2.10
Third	6.34	1.15	1.34	1.83	2.06
Avg	6.37	1.18	1.43	1.78	2.19
width	0.16	0.30	0.36	0.45	0.56

Table III 26: crack width measurement of beam B-a-3k-b crack 2

	11 KN	20 KN	25 KN	30KN	35KN
First	0.97	1.68	2.10	2.30	2.80
Second	1.08	1.66	2.20	2.20	2.60
Third	1.12	1.72	2.20	2.40	2.80
Avg	1.06	1.69	2.17	2.30	2.73
width	0.27	0.43	0.55	0.58	0.69

Table III 27: crack width measurement of beam B-W-3k-a crack 1

	11 KN	20 KN	25 KN	30KN	35KN	40kN
First	5.42	1.65	2.29	3.11	4.18	3.99
Second	5.95	1.48	2.22	3.22	3.99	4.49
Third	7.91	1.56	2.26	2.92	3.65	4.66
Avg	6.43	1.56	2.25	3.08	3.94	4.38
width	0.16	0.40	0.57	0.78	1.00	1.11

Table III 28: crack width measurement of beam B-W-3k-a crack 2

	11 KN	20 KN	25 KN	30KN	35KN	40kN
First	3.60	0.94	1.49	1.93	2.55	3.14
Second	3.50	1.10	1.47	2.05	2.56	2.93
Third	4.01	1.03	1.55	1.95	2.57	3.14
Avg	3.70	1.02	1.50	1.98	2.56	3.07
width	0.09	0.26	0.38	0.50	0.65	0.78

Table III 29: crack width measurement of beam B-W-3k-b crack 1

	11 KN	20 KN	25 KN	30KN	35KN	40kN
First	6.22	1.52	2.11	2.98	3.50	3.91
Second	5.54	1.57	2.10	2.82	3.44	4.21
Third	6.22	1.75	2.21	2.92	3.61	4.32
Avg	5.99	1.62	2.14	2.91	3.52	4.15
width	0.15	0.41	0.54	0.74	0.89	1.05

Table III 30: crack width measurement of beam B-W-3k-b crack 2

	11 KN	20 KN	25 KN	30KN	35KN	40kN
First	8.10	1.42	1.94	2.70	3.16	3.91
Second	7.27	1.59	2.09	2.58	3.17	3.60
Third	8.02	1.56	2.23	2.72	3.12	3.90
Avg	7.80	1.52	2.09	2.67	3.15	3.80
width	0.20	0.39	0.53	0.68	0.80	0.97

Table III 31: crack width measurement of beam B-W-5k-a crack 1

	11 KN	20 KN	25 KN	30KN	35KN	40kN
First	3.07	4.53	5.17	5.18	8.44	9.60
Second	3.06	5.19	4.85	5.86	8.02	10.54
Third	3.06	4.98	4.97	6.39	8.75	10.12
Avg	3.06	4.90	5.00	5.81	8.40	10.09
width	0.08	0.12	0.13	0.15	0.21	0.26

Table III 32: crack width measurement of beam B-W-5k-a crack 2

	11 KN	20 KN	25 KN	30KN	35KN	40kN
First	3.70	0.93	1.55	2.08	2.51	3.19
Second	3.70	1.12	1.47	2.00	2.37	3.55
Third	3.98	1.05	1.59	1.94	2.50	3.21
Avg	3.79	1.03	1.54	2.01	2.46	3.32
width	0.10	0.26	0.39	0.51	0.62	0.84

Table III 33: crack width measurement of beam B-W-5k-b crack 1

	11 KN	20 KN	25 KN	30KN
First	8.49	2.30	4.25	4.96
Second	8.45	2.41	3.80	5.19
Third	9.64	1.97	3.86	5.24
Avg	8.86	2.23	3.97	5.13
width	0.23	0.57	1.01	1.30

Table III 34: crack width measurement of beam B-W-5k-b crack 2

	11 KN	20 KN	25 KN	30KN
First	3.40	1.28	2.03	3.99
Second	4.30	1.36	2.37	4.90
Third	4.10	1.25	1.97	5.15
Avg	3.93	1.30	2.12	4.68
width	0.10	0.33	0.54	1.19

Table III 35: Average crack width of control beams

Load	**REF1**	**REF2**
11	0.04	0.08
20	0.18	0.2
25	0.25	0.36
30	0.32	0.4

Carking measurement images

The following images show how the cracks widths were measured by optical microscope. The cracks widths were determined and calculated using twist software. Three location of cracks were chosen to measure the cracks widths at different level of load.

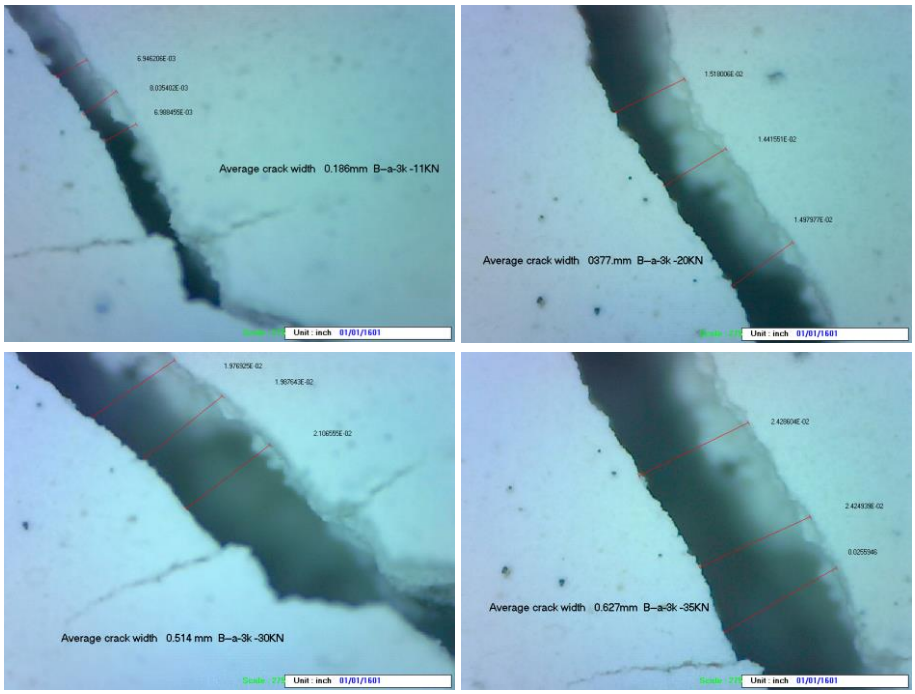

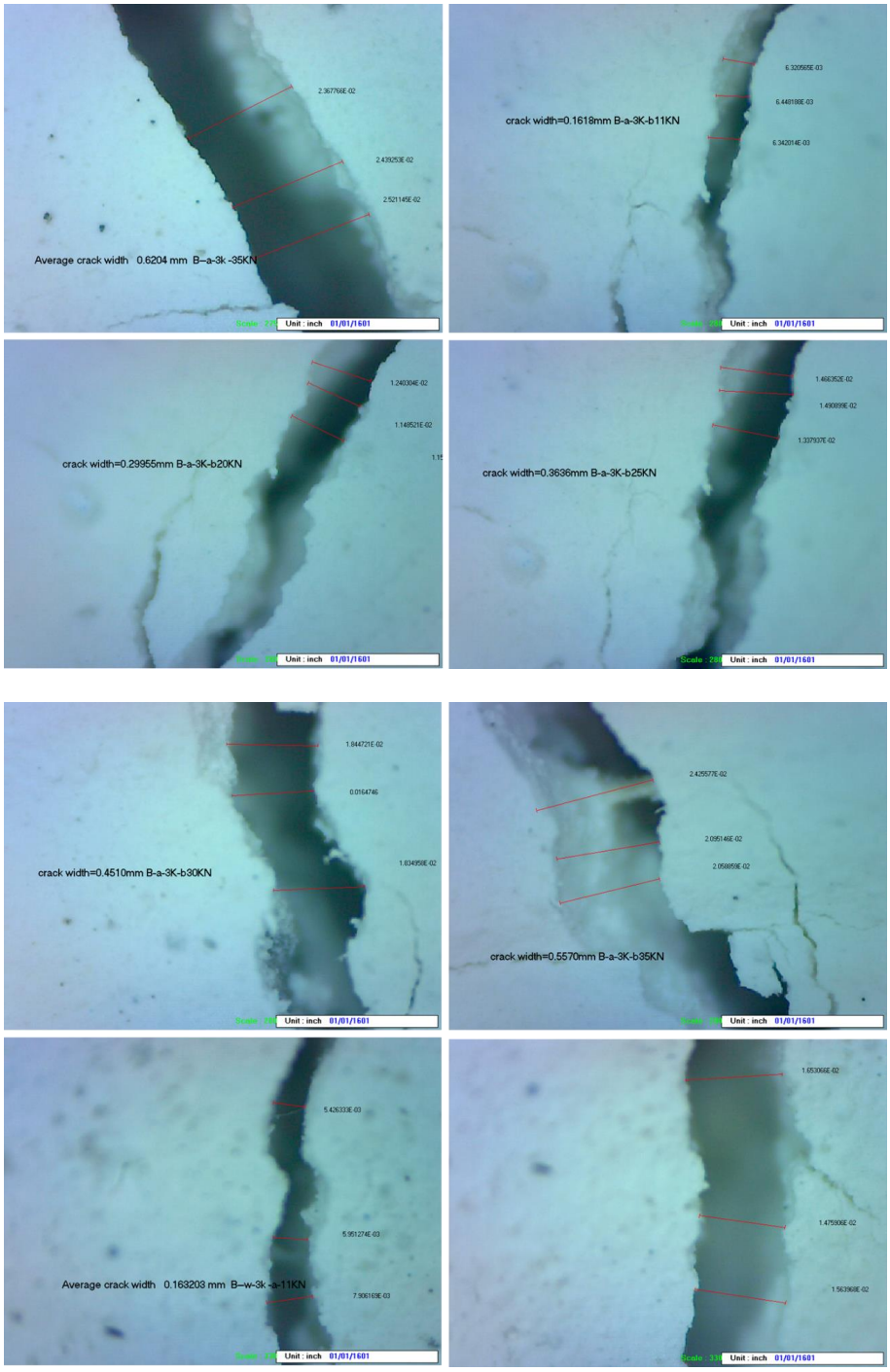
Average crack width 0.6204 mm B–a-3k -35KN
crack width=0.1618mm B-a-3K-b11KN
crack width=0.29955mm B-a-3K-b20KN
crack width=0.3636mm B-a-3K-b25KN
crack width=0.4510mm B-a-3K-b30KN
crack width=0.5570mm B-a-3K-b35KN
Average crack width 0.163203 mm B–w-3k -a-11KN

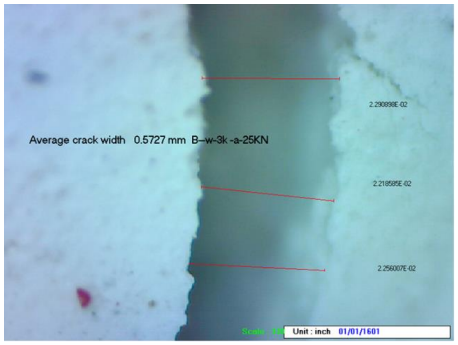
Average crack width 0.5727 mm B–w-3k -a-25KN
Unit : inch 01/01/1601

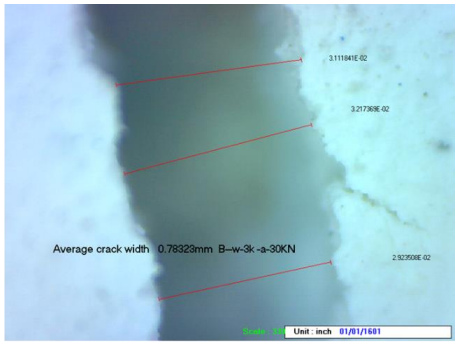
Average crack width 0.78323mm B–w-3k -a-30KN
Unit : inch 01/01/1601


Average crack width 1mm B–w-3k -a-35KN
Unit : inch 01/01/1601

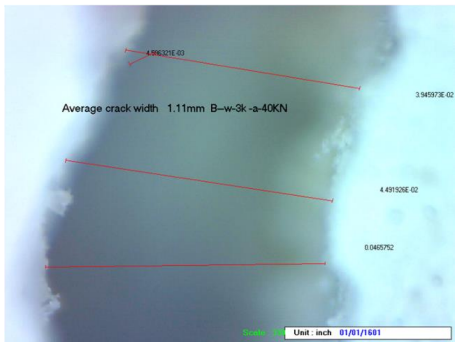
Average crack width 1.11mm B–w-3k -a-40KN
Unit : inch 01/01/1601

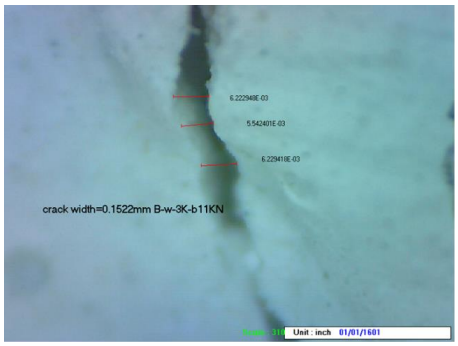
crack width=0.1522mm B-w-3K-b11KN
Unit : inch 01/01/1601

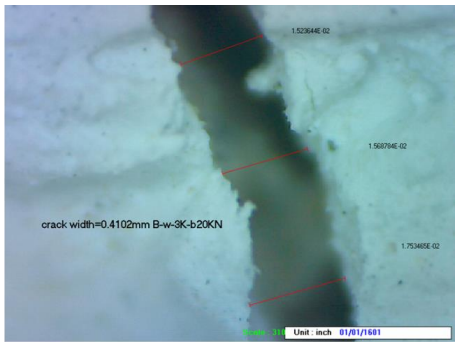
crack width=0.4102mm B-w-3K-b20KN
Unit : inch 01/01/1601

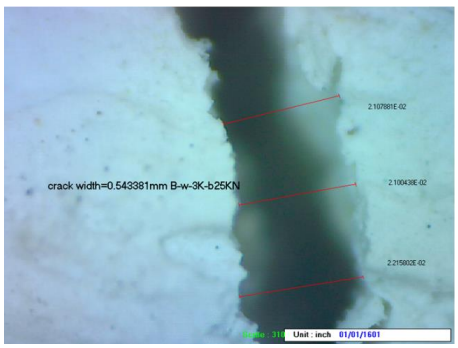
crack width=0.543381mm B-w-3K-b25KN
Unit : inch 01/01/1601

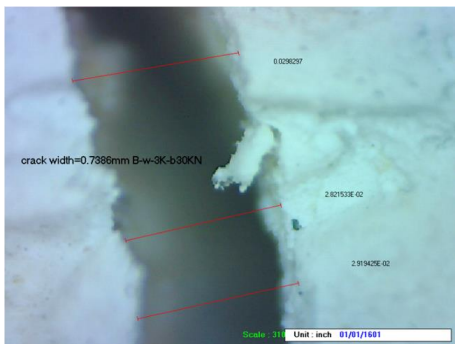
crack width=0.7386mm B-w-3K-b30KN
Unit : inch 01/01/1601

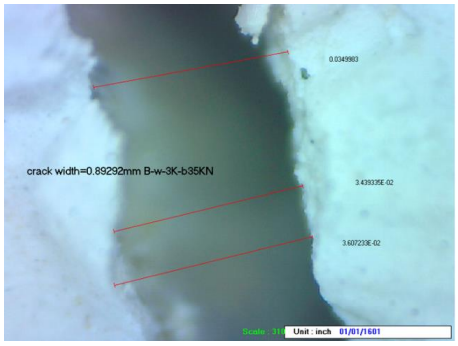
crack width=0.89292mm B-w-3K-b35KN
Unit : inch 01/01/1601

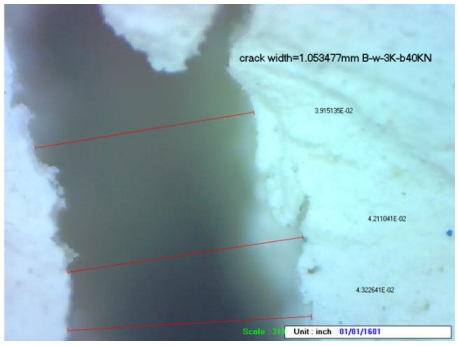
crack width=1.053477mm B-w-3K-b40KN
Unit : inch 01/01/1601

Strain in the flexural reinforcing GFRP bars

Control beams

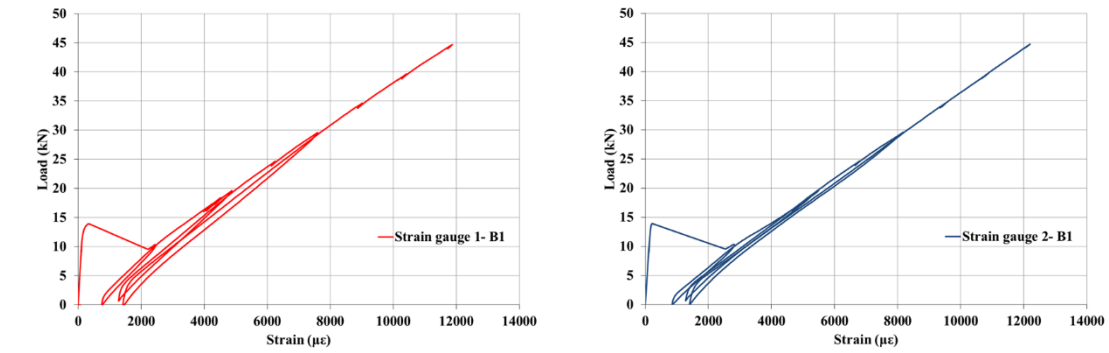

Figure.III.17: Strain in main reinforcement in control beam1

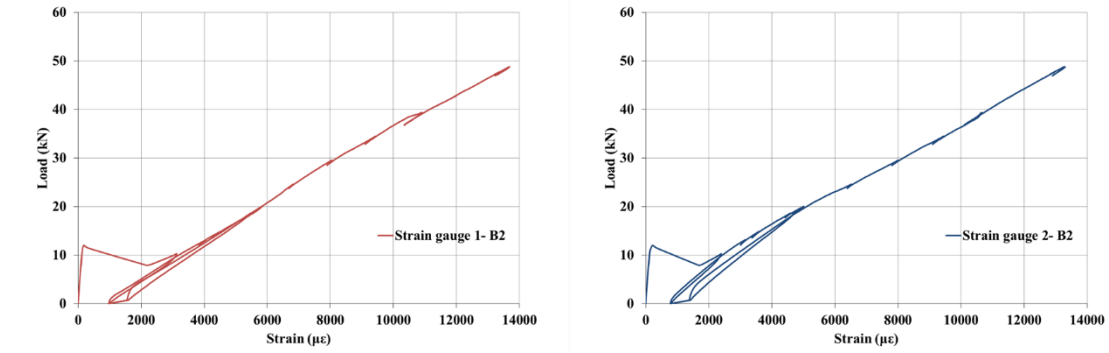

Figure.III.18: Strain in main reinforcements in control beam2

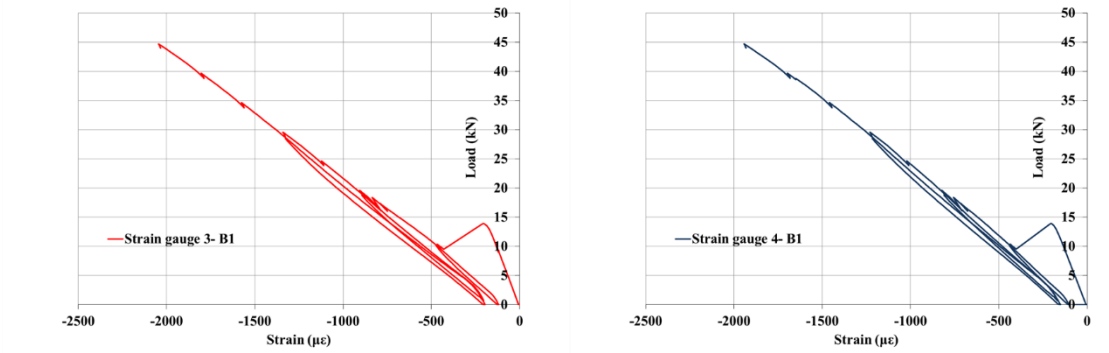

Figure.III.19: Strain in concrete in control beam1

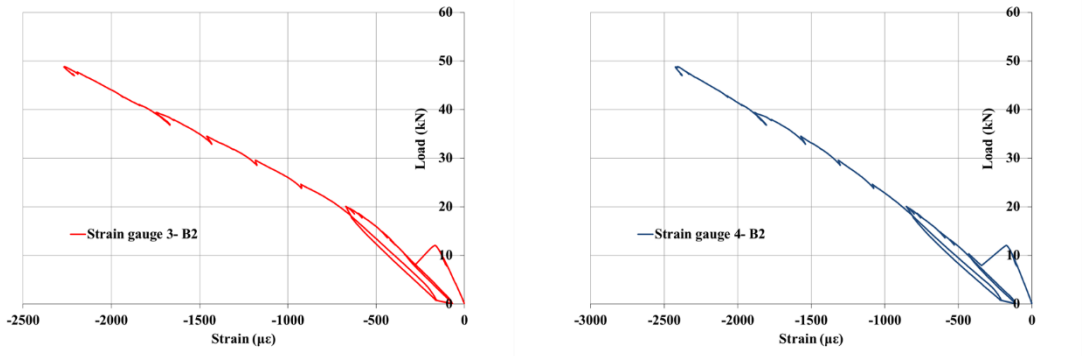

Figure.III.20: Strain in concrete in control beam2

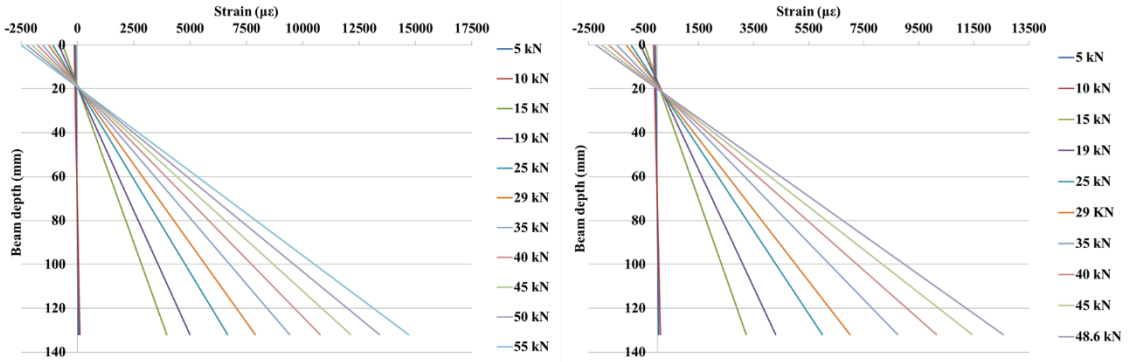

Figure.III.21: strain distribution in cross section of reference beams.

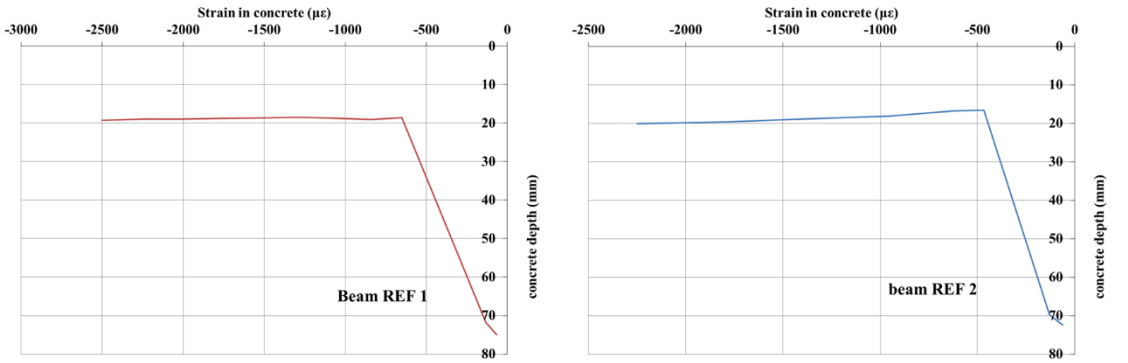

Figure.III.22: Neutral axis of reference beams.

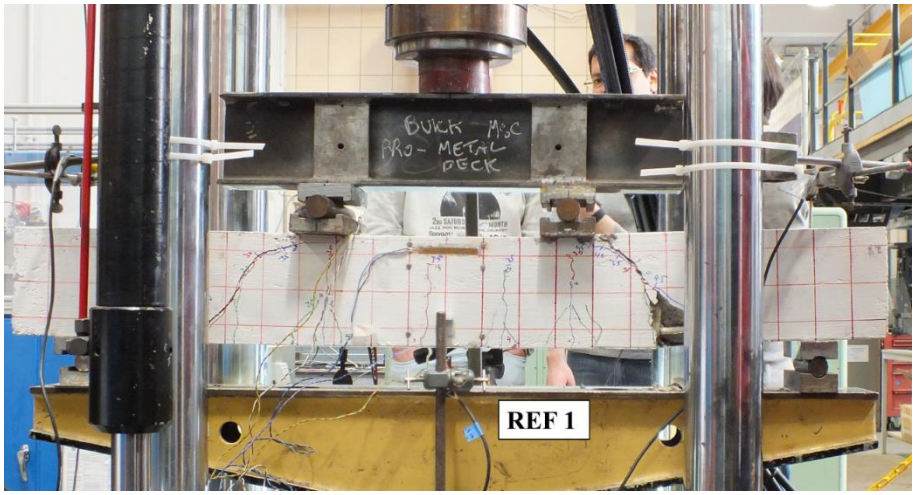

Figure.III.23: Crack pattern and failure mode of reference beam 1.

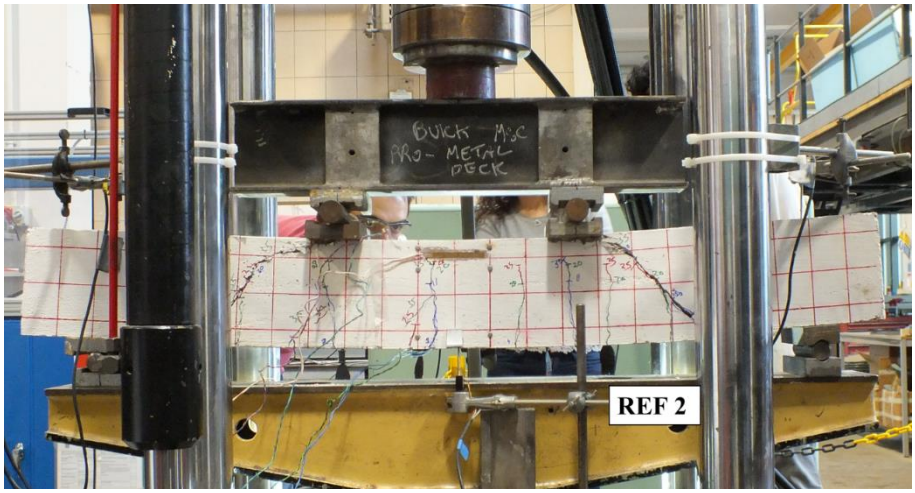

Figure.III.24: Crack pattern and failure mode of reference beam 2.

Beams stressed and stored in lab

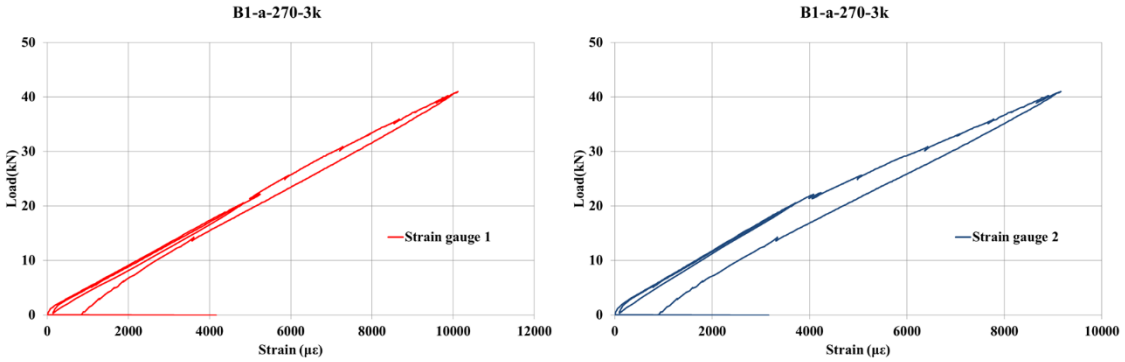

Figure.III.25: Strain in main reinforcement in beam stressed and stored in lab conditions (B1-a-270d-3k)

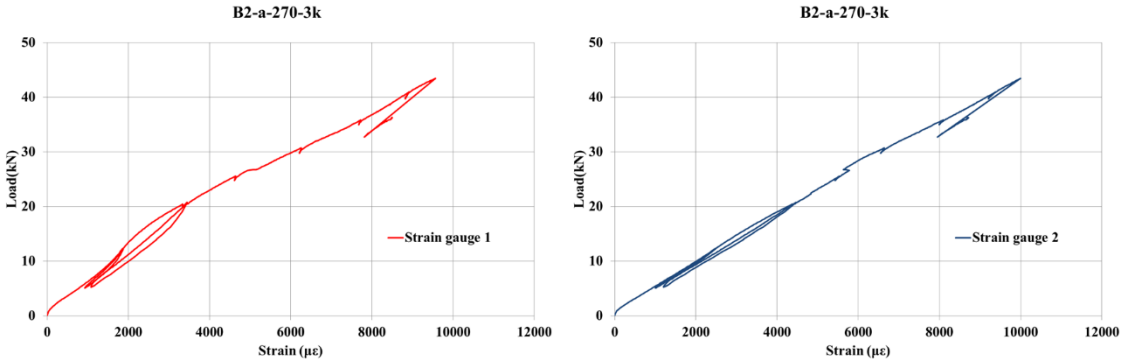

Figure.III.26: Strain in main reinforcement in beam stressed and stored in lab conditions (B2-a-270d-3k)

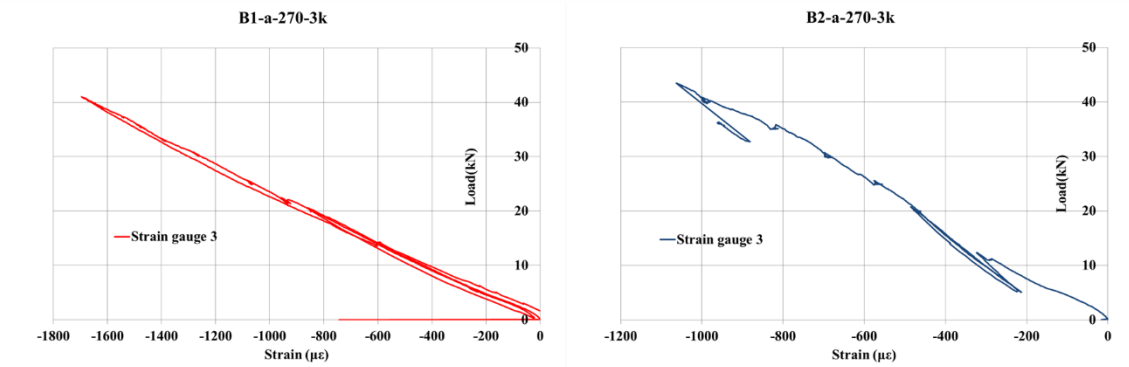

Figure.III.27: Strain at concrete surface in beams stressed and conditioned in lab environment (B1, B2-a-270d-3k)

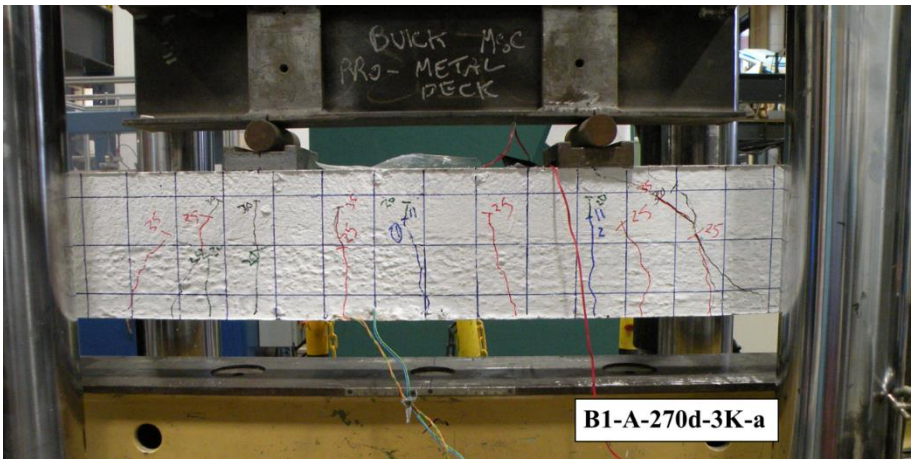

Figure.III.28: Crack pattern and failure mode of beam1 loaded and stored in lab.

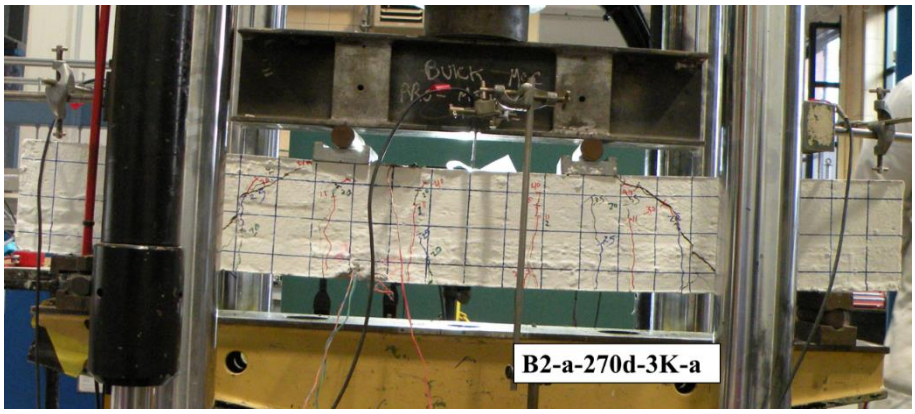

Figure.III.29: Crack pattern and failure mode of beam1 loaded and stored in lab.

Beams stressed at level gives 3000 με and conditioned in water at 60°C

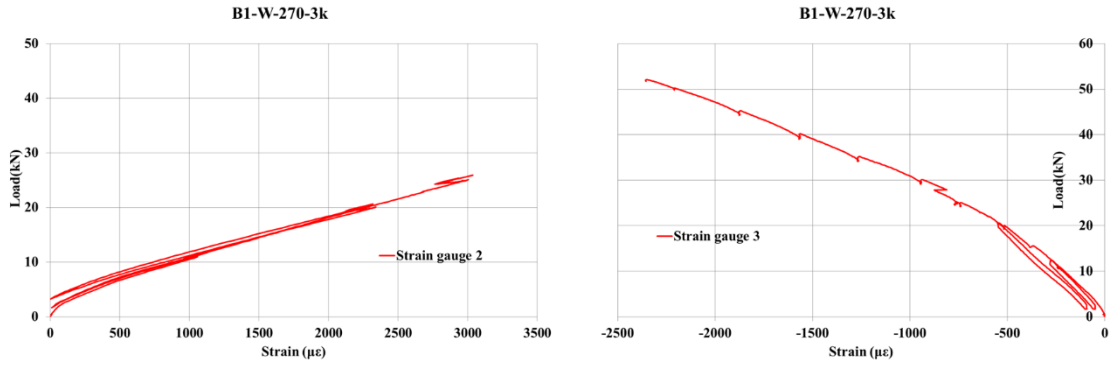

Figure.III.30: Strain in main reinforcement and at concrete zone in beam stressed and conditioned in water at 60°C (B1-W-270d-3k)

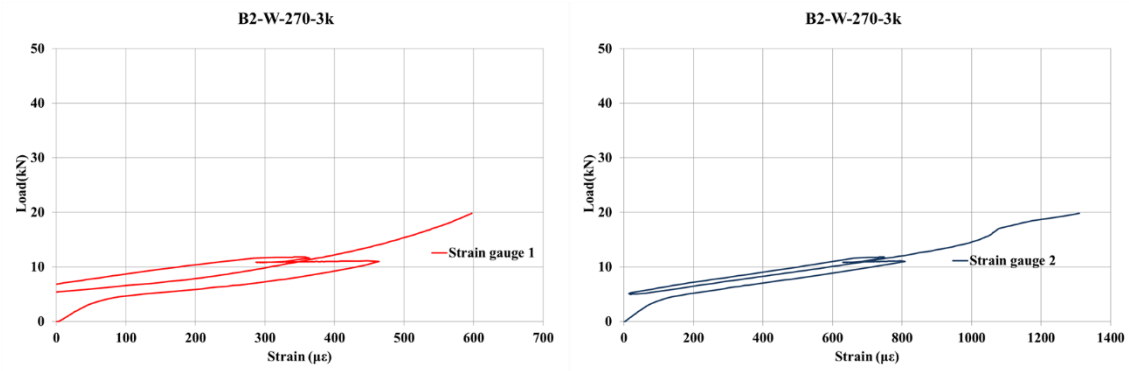

Figure.III.31: Strain in main reinforcement in beam stressed and conditioned in water at 60°C (B2-W-270d-3k)

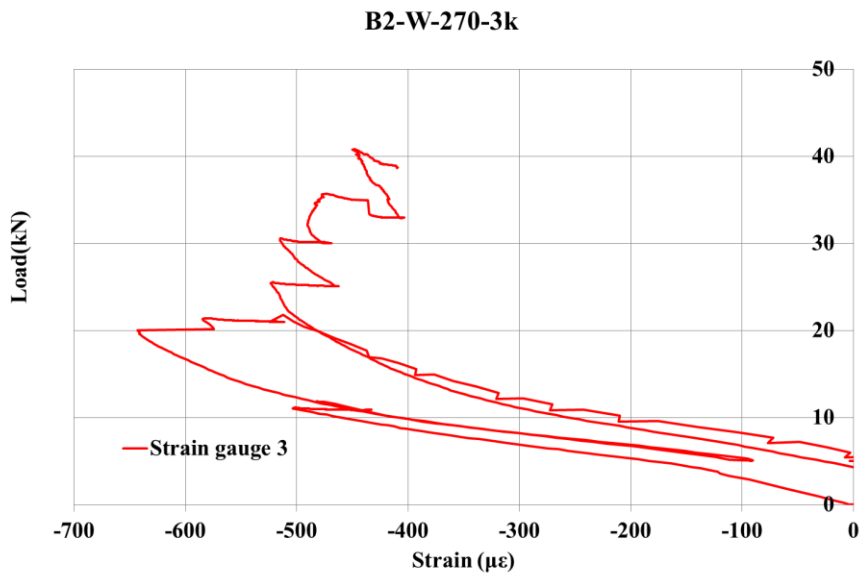

Figure.III.32: Strain in concrete surface in beam stressed and conditioned in water at 60°C (B2-W-270-3k)

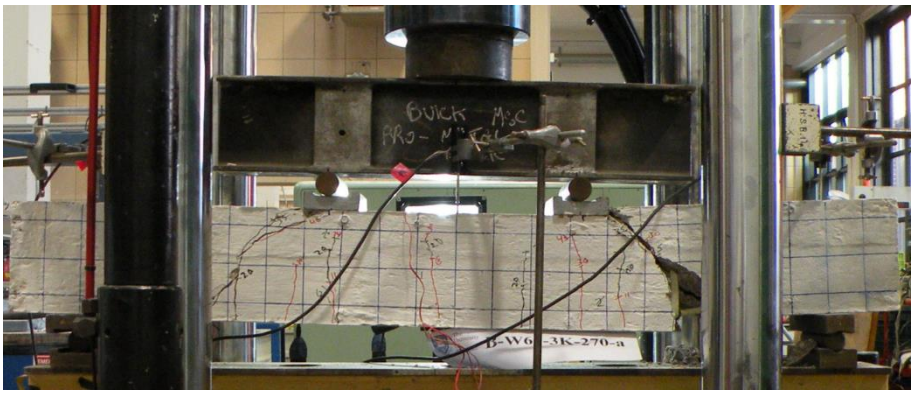

Figure.III.33: Crack pattern and failure mode of beam1 loaded and stored in conditioned in water at 60°C (B1-W-270d-3k.

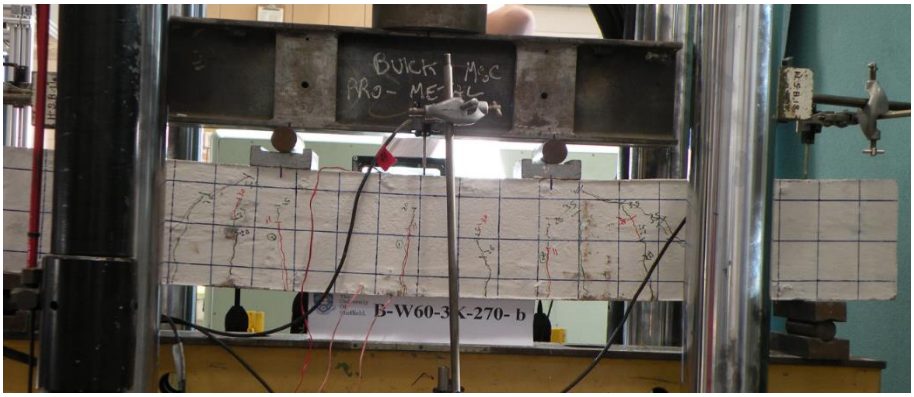

Figure.III.34: Crack pattern and failure mode of beam1 loaded and stored in conditioned in water at 60°C (B1-W-270d-3k.

Beams stressed at level gives 5000 με and conditioned in water at 60°C

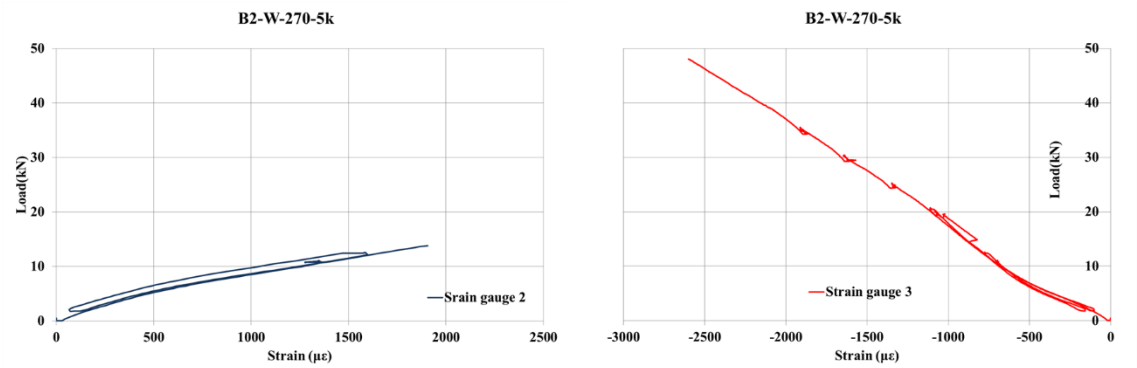

Figure.III.35: Strain in main reinforcement and at concrete zone in beam stressed and conditioned in water at 60°C (B2-W-270d-5k)

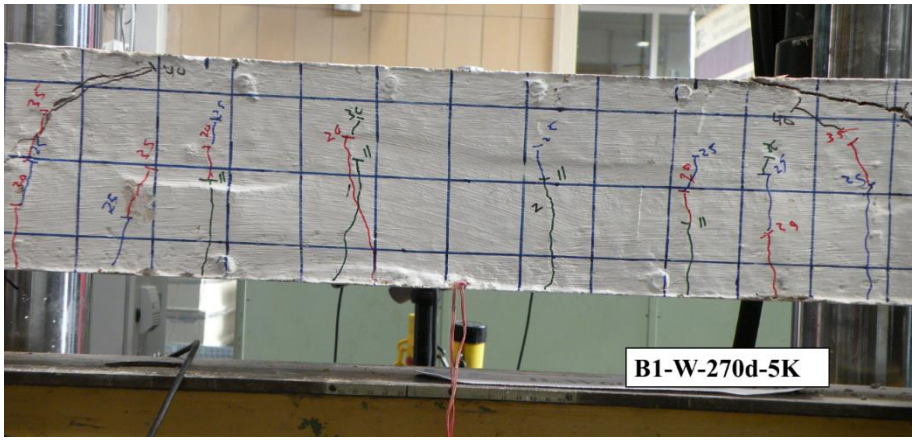

Figure.III.36: Crack pattern and failure mode of beam1 loaded and stored in conditioned in water at 60°C (B1-W-270d-5k).

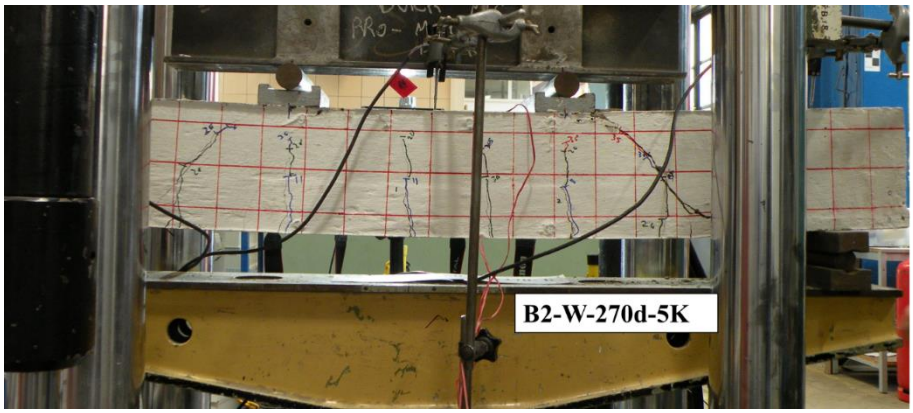

Figure.III.37: Crack pattern and failure mode of beam1 loaded and stored in conditioned in water at 60°C (B2-W-270d-5k).